DURATION OF EARTHQUAKE GROUND MOTION: INFLUENCE ON STRUCTURAL COLLAPSE RISK AND INTEGRATION IN DESIGN AND ASSESSMENT PRACTICE

A DISSERTATION
SUBMITTED TO THE DEPARTMENT OF CIVIL AND ENVIRONMENTAL ENGINEERING
AND THE COMMITTEE ON GRADUATE STUDIES
OF STANFORD UNIVERSITY
IN PARTIAL FULFILLMENT OF THE REQUIREMENTS
FOR THE DEGREE OF
DOCTOR OF PHILOSOPHY

Reagan Chandramohan
August 2016

This dissertation is online at: http://purl.stanford.edu/fg920pt3240

I certify that I have read this dissertation and that, in my opinion, it is fully adequate in scope and quality as a dissertation for the degree of Doctor of Philosophy.

Gregory Deierlein, Primary Adviser

I certify that I have read this dissertation and that, in my opinion, it is fully adequate in scope and quality as a dissertation for the degree of Doctor of Philosophy.

Jack Baker

I certify that I have read this dissertation and that, in my opinion, it is fully adequate in scope and quality as a dissertation for the degree of Doctor of Philosophy.

Eduardo Miranda

Approved for the Stanford University Committee on Graduate Studies.

Patricia J. Gumport, Vice Provost for Graduate Education

This signature page was generated electronically upon submission of this dissertation in electronic format. An original signed hard copy of the signature page is on file in University Archives.

Abstract

Amplitude, frequency content, and duration are widely recognized as the key characteristics of earthquake ground motions that influence structural response. Yet, in current structural design and assessment practice, ground motions are often explicitly characterized by just their pseudo acceleration response spectra—which quantify their amplitude and frequency content—while duration is commonly relegated to implicit, qualitative consideration. This study evaluates the need to explicitly consider duration, in addition to response spectra, in structural design and assessment.

The influence of duration on structural collapse capacity is investigated by numerically simulating the response of structures under short and long duration ground motions. Realistic nonlinear structural models that incorporate the in-cycle and cyclic deterioration of the strength and stiffness of structural components, and the destabilizing $P-\Delta$ effect of gravity loads, are employed to successfully detect the effect of duration. Long duration ground motions from recent large magnitude earthquakes, like the 2008 Wenchuan (China, M_W 7.9), 2010 Maule (Chile, M_W 8.8), and 2011 Tohoku (Japan, M_W 9.0) earthquakes, are used in the analyses. The effect of response spectral shape is controlled for by selecting sets of short and long duration ground motions with similar response spectra, and by employing appropriate statistical tools to post-process the analysis results. Significant duration, Ds, is identified as the duration metric best suited for use in structural design and assessment, since it is amenable to incorporation in a vector intensity measure alongside the response spectrum, and is an efficient predictor of structural collapse capacity. Response spectral shape and duration are together shown to be capable of explaining around 80 % to

85 % of the variance in the collapse intensities of ground motions used to analyze 51 reinforced concrete moment frame buildings. Response spectral shape or duration alone, are capable of explaining a significantly smaller fraction of the variance in the collapse intensities. This highlights the need to explicitly consider both response spectra and duration in structural design and assessment, and indicates that the additional consideration of other ground motion characteristics is likely to produce diminishing returns.

A procedure based on the generalized conditional intensity measure (GCIM) framework is developed to compute source-specific conditional probability distributions of the durations of the ground motions anticipated at a site. Commonly used ground motion databases—like the PEER NGA-West2 database—are currently dominated by short duration ground motions, since many more low and moderate magnitude earthquakes ($6.0 < M_W < 7.5$) have been recorded in recent history than large magnitude interface earthquakes ($M_W \sim 9.0$). Selecting records from the PEER NGA-West2 database without explicitly considering duration is, therefore, shown to result in the unconservative underestimation of structural collapse risk at sites located near active subduction zones, that are susceptible to long duration ground motions from large magnitude interface earthquakes. For example, selecting records from the PEER NGA-West2 database to explicitly match only conditional spectrum targets, and not duration targets, is shown underestimate the mean annual frequency of collapse of an eight-story reinforced concrete moment frame building by 29 % when located in Seattle (Washington) and 59 % when located in Eugene (Oregon). A relatively small influence of duration is observed at San Francisco (California), which is likely to experience short to moderate duration ground motions from shallow crustal earthquakes. The prevalent practice of implicitly accounting for duration using causal parameters like rupture mechanism, earthquake magnitude, source-to-site distance, and site Vs_{30}, is shown to result in the selection of records that poorly match conditional spectrum and duration targets, thereby producing biased collapse risk estimates.

Strategies are proposed to explicitly consider duration, in addition to response spectral shape, in the analysis procedures contained in the following standards for

structural performance assessment and design: (*i*) the FEMA P-58 seismic performance assessment methodology; (*ii*) the FEMA P695 methodology to quantify seismic performance factors; and (*iii*) the ASCE 7-16 seismic design provisions. The effect of duration is incorporated in multiple stripe analysis (MSA) by selecting records to match duration targets, in addition to conditional spectrum targets, at each intensity level. A structural reliability framework incorporating response spectral shape (quantified by a scalar parameter called S_aRatio) and duration (quantified by Ds), is developed to compute a hazard-consistent collapse fragility curve by post-processing the results of an incremental dynamic analysis (IDA) conducted using a generic record set. The procedure first involves defining a failure surface by fitting a multiple linear regression model to the computed ground motion collapse intensities using S_aRatio and Ds as predictors. The probability of collapse at an intensity level is then computed by integrating the site-specific target distributions of S_aRatio and Ds conditional on that intensity level, over the failure domain. A simplified method is additionally developed to efficiently compute just the hazard-consistent median collapse capacity.

The effects of response spectral shape and duration are incorporated in ASCE 7-16's equivalent lateral force procedure by developing site and structural system-specific adjustment factors for the design base shear. These adjustment factors are computed based on the site-specific conditional median S_aRatio and Ds targets and the sensitivity of the structure to the effects of response spectral shape and duration. The use of these adjustment factors ensures a more uniform distribution of structural collapse risk over different geographical regions, and between different structural systems. Sample calculations indicate that a 1 s reinforced concrete moment frame building in San Francisco would need to be designed to a base shear that is 43 % higher than the value used in current practice to maintain parity with a similar structure designed at a reference site, chosen here to be Los Angeles (California). A similar structure in Eugene would need to be designed to a base shear that is 67 % higher. ASCE 7-16's nonlinear response history analysis procedure requires analyzing structures at the risk-target maximum considered earthquake (MCE_R) intensity level, at which a significant effect of duration on peak story drift ratio is unlikely to be observed. Hence, the imposed acceptance criteria are unlikely to reliably capture the

effect of duration. It is, therefore, recommended that the selected records be scaled to an MCE_R level modified by a duration adjustment factor, analogous to the one developed for the equivalent lateral load procedure.

The explicit central difference time integration scheme is proposed as a robust and efficient alternative to commonly used implicit schemes, like the Newmark average acceleration scheme, which often suffer from numerical non-convergence issues when used to simulate the dynamic response of nonlinear structural models, especially when simulating response under long duration ground motions. Its robustness stems from its non-iterative nature, while its efficiency is a consequence of the requirement to factorize a linear combination of only the mass and damping matrices at each time step. The use of a constant damping matrix, therefore, ensures that the matrix factorization needs to be performed just once for the entire analysis. It is shown to be more efficient than implicit schemes when conducting IDA in parallel, despite the limit on the maximum time step imposed by its stability criterion. Its benefits are believed to outweigh a few additional steps involved during model creation, including the assignment of mass to all degrees of freedom. Finally, efficient parallel algorithms are developed to conduct MSA and IDA on multi-core computers and distributed parallel clusters, to enable the use of these otherwise computationally intensive analysis techniques in research and practice.

Acknowledgements

First and foremost, I am sincerely grateful to both my advisors: Prof. Greg Deierlein and Prof. Jack Baker, for their patient and dedicated efforts to guide my progress as I worked through this dissertation. Their insightful comments and feedback at every juncture; their balanced emphasis both on broad objectives, as well as fine details; their composed and clear-headed counsel when research hit roadblocks; their patience when subjected to barrages of (often naïve) questions, all made research seem a lot easier than I have heard it should be. In addition to being fine teachers, accomplished researchers, and excellent mentors, they are two of the nicest people I have known. Among the number of useful lessons I have learnt from them, although most are related to conducting quality research, by far the most valuable has been the importance of being a kind, respectful, and humble individual.

I would like to thank all my professors at Stanford University for the roles they played in aiding my transformation from a wide-eyed graduate student to a confident young researcher. I am especially grateful to Prof. Eduardo Miranda and Prof. Kincho Law for going out of their way to guide me through my research work and provide helpful advice when required. I would consider myself fortunate if some of their exuberance and enthusiasm rubbed off on me in the time I spent with them in the classroom. Thanks also to Prof. Anne Kiremidjian and Prof. Greg Beroza for their constructive feedback on this dissertation. The quality feedback provided by Brendon Bradley, Julian Bommer, and Frank McKenna on various chapters of this dissertation is also acknowledged. Special thanks to Frank McKenna for his prompt

help and guidance whenever needed, in conducting the structural response simulations that form the foundation of this study, using OpenSees. I extend my gratitude to Wenhao Chen, Meera Raghunandan, Abbie Liel, Anirudh Rao, Curt Haselton, Jen Foschaar, Steve Kramer, Jeff Bayless, and Christine Goulet, for being kind enough to share their research data in the form of OpenSees models, Matlab scripts, ground motions, etc., which made a large portion of this research work possible. I also take this opportunity to acknowledge the sources of funding that enabled this study, including the Stanford School of Engineering, the Stanford Department of Civil and Environmental Engineering, the John A. Blume Earthquake Engineering Research Center, the Stanford Office of the Vice Provost for Graduate Education, and the Pacific Earthquake Engineering Research Center.

I am thankful for the companionship and camaraderie of all my friends at the Blume Center, including Cristian Acevedo, *Prof.* Matt Bandelt, Nenad Bijelic, *Prof.* Henry Burton, Luis Ceferino, Tim Frank, Abhineet Gupta, Ezra Jampole, *Prof.* David Lallemant, Maryia Markhvida, Isamar Rosa, Andy Seifried, Shrey Shahi, Beliz Ugurhan, and many others. I will always cherish our long conversations in the corridors and during the Blume Center happy hours. I thank Racquel Hagen, Jill Filice, Kim Vonner, Brenda Sampson, and other administrative staff for their timely help and support at every stage. I will also treasure the merry company of Devadas Mallya and Greeshma Yellareddy over these last few years. I thank them for constantly reminding me not to take myself (or anything) too seriously. Finally, and most importantly, I am extremely grateful to Prabha Mallya for her inspiration and support through this long, winding journey. She was my window into a colorful and exciting world that does not revolve around earthquakes.

Contents

List of Tables

List of Figures

List of Procedures/Algorithms

Chapter 1

Introduction

1.1 Background and motivation

1.1.1 Motivation to study the influence of duration on structural response

The widespread deployment of strong motion recording stations over the last few decades in high seismic regions around the world, has made a large number of ground motions recorded from recent earthquakes available for use in structural engineering practice and research. As postulated by Gutenberg and Richter (1944), however, lower magnitude crustal earthquakes have occurred much more frequently than larger magnitude subduction earthquakes within this time frame. As a result, commonly used record sets like the FEMA P695 far-field set (FEMA 2009b, Appendix A) and the PEER Transportation sets (Baker et al. 2011, Chapter 3); and ground motion databases like the PEER NGA-West2 database (Ancheta et al. 2014), are dominated by relatively short duration ground motions recorded from low and moderate magnitude ($6.0 < M_W < 7.5$) shallow crustal earthquakes. This is evident from Figure 1.1, where the 5–75 % significant durations (Trifunac and Brady 1975), Ds_{5-75}, of the records in these sets and intense records from the PEER NGA-West2 database are compared to the durations of ground motions anticipated in Seattle from an interface

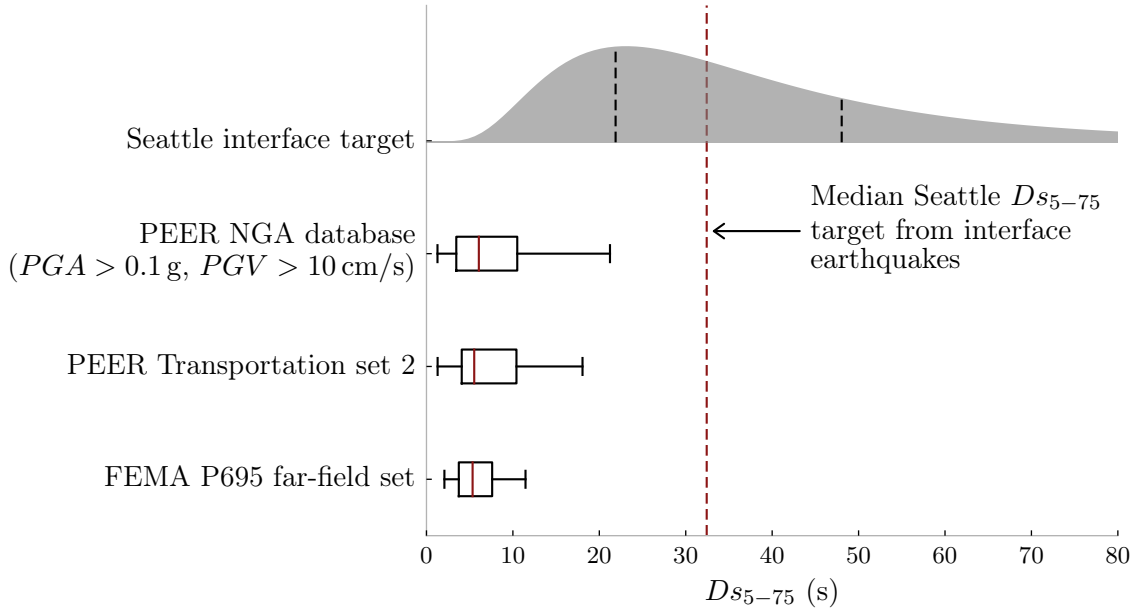

Figure 1.1: Comparison of the 5–75 % significant durations, Ds_{5-75}, of the ground motions in commonly used record sets, and intense ground motions in the PEER NGA-West2 database, to the target Ds_{5-75} distribution corresponding to interface earthquakes, conditional on the 2 % in 50 year exceedance probability of $S_a(1\,\text{s})$ at Seattle.

earthquake in the Cascadia subduction zone (the computation of target conditional distributions of ground motion duration is described in Chapters 4 and 5). The reliance on these short duration ground motions when formulating seismic design provisions, in conjunction with an emphasis on the seismic hazard in coastal California, which is controlled by such low and moderate magnitude crustal earthquakes, has likely introduced a short duration bias in our seismic design philosophy. Such a short duration bias could potentially permit the development of new structural designs that possess lower margins of safety against collapse than intended, in sites located near active subduction zones (e.g., the US Pacific Northwest, Mexico, Chile, Japan), which are susceptible to long duration ground motions. The distinction being made here between short and long duration ground motions is illustrated in Figure 1.2.

The predominant use of cyclic loading protocols for component testing, that attempt to simulate the response of structures under short duration ground motions produced by low and moderate magnitude earthquakes, is a prime example of the

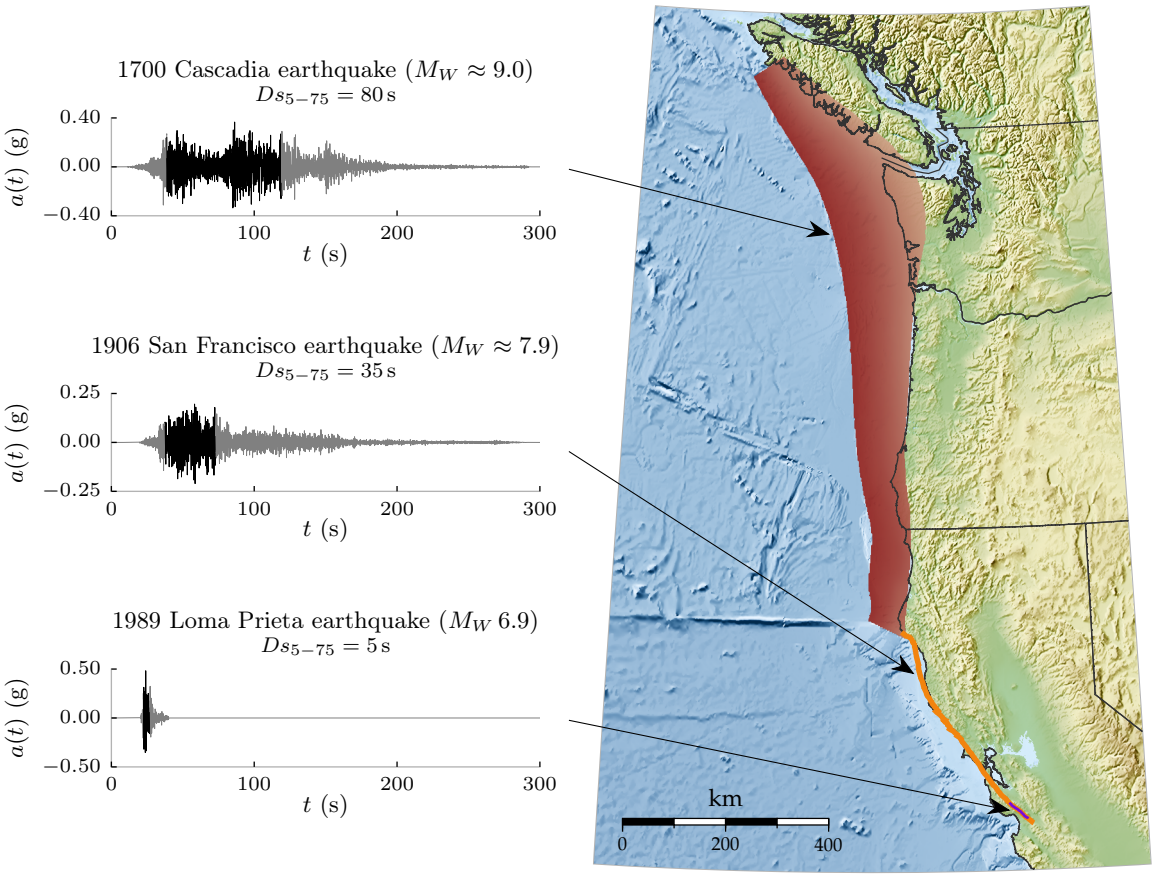

Figure 1.2: Map of the extents of the fault ruptures and representative ground motions produced by three prominent historical earthquakes in Western USA. The area of the Cascadia subduction zone that ruptured during the 1700 Cascadia earthquake was obtained from Satake et al. (2003); the depicted extent of the rupture along the San Andreas fault from the 1906 San Francisco earthquake was obtained from Wald et al. (1993) and Thatcher et al. (1997). Since recorded ground motions from the 1700 Cascadia ($M_W \approx 9.0$) and 1906 San Francisco ($M_W \approx 7.9$) earthquakes are not available, typical ground motions recorded from other earthquakes of comparable magnitude, viz., the 2011 Tohoku (Japan, M_W 9.0) and 2008 Wenchuan (China, M_W 7.9) earthquakes respectively, are shown instead. The portions of the accelerograms shaded in black are the intervals used to compute their 5–75 % significant durations, Ds_{5-75}.

aforementioned implicit short duration bias (ATC 1992, Chapters 4 and C.4; SAC 1997, Appendix E; Krawinkler et al. 2001). Studies such as Takemura and Kawashima (1997), FEMA (2009a), and Krawinkler (2009) have indicated that structural components generally exhibit different hysteretic behaviors depending on the nature of the imposed loading protocol. This suggests that the hysteretic response of structural components under long duration loading protocols—of the type recently developed by Bazaez and Dusicka (2016)—will generally be different compared to their behavior under short duration loading protocols. These observations highlight the need for additional research to accurately characterize the influence of duration on structural response, and if found to be significant, to develop strategies to explicitly consider it in structural design and assessment. The approximate method recently proposed by Liel et al. (2015), to embed the anticipated effect of duration in the computation of site-specific, risk-targeted maximum considered earthquake (MCE_R) (ASCE 2016, § 11.4.3) values, represents an attempt to address this shortcoming in the current seismic design provisions. Finally, the extensive dataset of long duration ground motions recorded from recent large magnitude earthquakes, like the 2008 Wenchuan (China, M_W 7.9), 2010 Maule (Chile, M_W 8.8), and 2011 Tohoku (Japan, M_W 9.0) earthquakes, provides a fresh opportunity to revisit the study of duration without having to rely on simulated long duration ground motions.

Clues to the potential for ground motion duration to influence the capacity of structures can be obtained from an examination of the fatigue-life relation. The nature of cyclic loading imposed on structures by relatively intense ground motions that induce deformations which extend into the inelastic range, typically falls under the low-cycle fatigue regime. Low-cycle fatigue in metallic materials is traditionally characterized by the strain-life curve depicted in Figure 1.3, also known as the Coffin-Manson relation (Manson 1953; Coffin 1954). The strain-life curve, which is usually determined experimentally, posits a decreasing linear relation in log-space between the plastic strain induced in the material at each load reversal, and the average number of reversals of the same amplitude required to cause failure. An alternative interpretation of the strain-life curve is that fewer cycles of larger amplitude, and a larger number of cycles of lower amplitude are both equally capable of

causing material failure. The strain-life curve is, however, derived strictly for small components under constant-amplitude cyclic loads, and is not directly applicable to larger civil engineering structures subjected to variable-amplitude earthquake loads. Drawing a qualitative parallel, however, provides reason to believe that long duration earthquake ground motions would be capable of causing structural collapse at lower intensity levels compared to short duration ground motions. Studies as early as Husid (1967) (pp. 137–138) have alluded to this possibility. This effect of ground motion duration can be readily captured using relatively simple structural models that employ non-simulated collapse modes, typically consisting of a cycle counting scheme in conjunction with some variant of Miner's rule (Miner 1945). Capturing the effect of duration using structural models that explicitly simulate dominant collapse modes, however, requires the use of sophisticated finite element models that are capable of capturing the cyclic fatigue behavior of structural components on a macroscopic scale (Krawinkler and Zohrei 1983). The attribution of the brittle fractures observed in a number of beam-column joints in steel moment frame buildings after the 1994 Northridge (USA, M_W 6.7) and 1995 Kobe (Japan, M_W 6.9) earthquakes, to the inadequate fatigue resistance and fracture toughness of the beam flange to column flange welds (FEMA 2000, § 1.2), highlights the potential of fatigue-related damage modes to influence structural behavior under earthquakes. EERI (2012) and Mantawy and Anderson (2015) have also alluded to the increased likelihood of observing fatigue-related structural damage under long duration ground motions produced by large magnitude earthquakes. This effect of duration is what is implicitly implied by the common intuitive observation made by reconnaissance teams following earthquakes that a structure would probably have collapsed if the ground motion had lasted just a little longer (Jennings et al. 1971; Cornell 1997).

A list of global cities with populations greater than 1000, located closer than 200 km from the plate interface of an active subduction zone, was compiled to obtain an estimate of the total number of people likely to benefit from research into the impact of long duration ground motions on structural collapse risk. The population data for all cities was obtained from the GeoNames geographical database (Wick and Boutreux 2016), and the geometries of about 85 % of all subduction zones

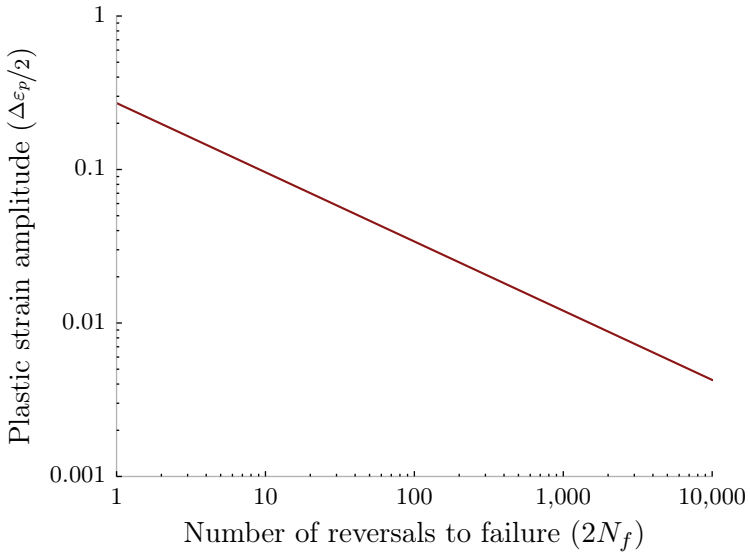

Figure 1.3: Typical strain-life curve characterizing the number of reversals (twice the number of cycles) to failure under zero-mean, constant-amplitude, cyclic loading to different plastic strain amplitudes.

worldwide were obtained from USGS Slab model database (Hayes et al. 2012).* A subset of these cities with populations greater than 100,000, and the geometries of the considered subduction zones, are plotted in Figure 1.4. The list of cities likely to experience long duration ground motions includes heavily populated cities like Mexico City (Mexico), Jakarta (Indonesia), Tokyo (Japan), Taipei (Taiwan), Lima (Peru), and Santiago (Chile). Cities near Central Asian and European subduction zones, including densely populated centers located near the Himalayan thrust zone, unfortunately could not be considered since these subduction zones were absent from the USGS Slab model database. The total population of the compiled list of cities was computed to be approximately 337 million. Hence, research into the detrimental effects of long duration ground motions has the potential to benefit more than 337 million of the world's population.

*Thanks to Anirudh Rao for directing me to these data sources.

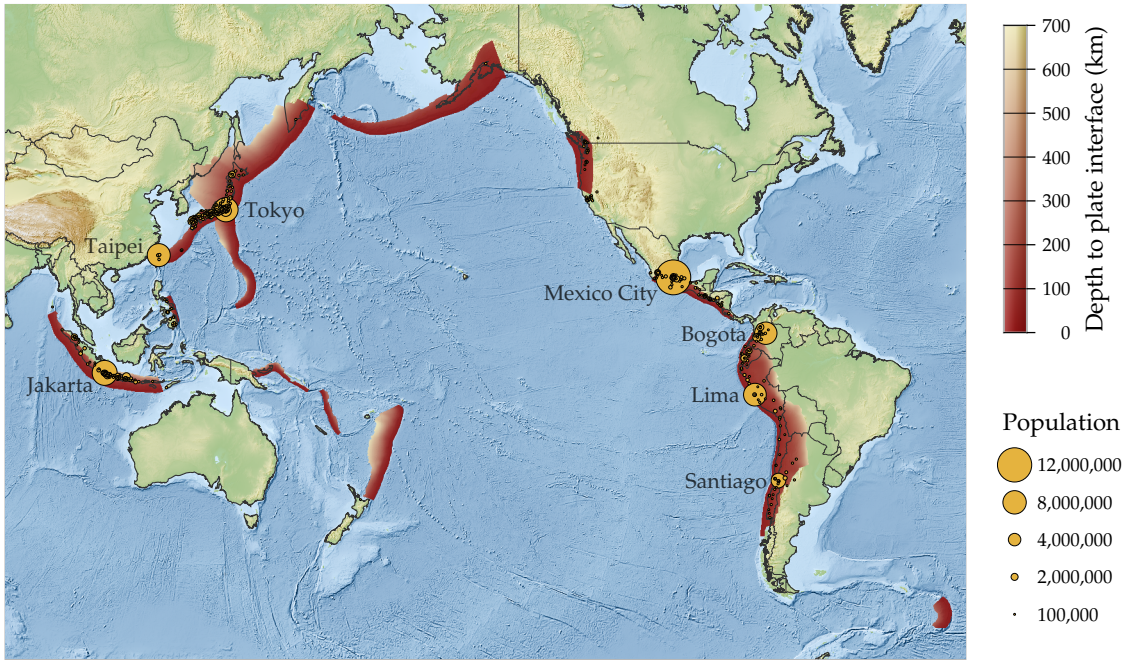

Figure 1.4: A subset of the cities used to compute the total global population exposed to long duration ground motions is plotted using yellow circles with diameters proportional to their populations. Only those cities with populations greater than 100,000, located closer than 200 km to the plate interface of the subduction zones present in the USGS Slab model database, are plotted. Cities with populations above 4,000,000 are labeled. The considered subduction zones are plotted in red.

1.1.2 Definition of ground motion duration

The *duration* of an earthquake accelerogram typically refers only to the duration of strong ground motion contained within the accelerogram, that can be considered to be of engineering importance. Upon employing this definition to infer the duration of the accelerogram plotted in Figure 1.5, it is immediately evident that the entire length of the accelerogram: 125 s, is probably not the best measure of its duration, since *strong* ground motion is limited to a shorter interval from approximately 25 s to 80 s. Early studies (e.g., Veletsos and Newmark 1960; Housner 1965) relied on visual inspection to distinguish this interval of *strong* ground motion. Recognizing the ambiguity of this approach, researchers have since developed a number of wide and varied precise mathematical methods to define the duration of *strong* ground motion—of engineering relevance—contained within an accelerogram (Bommer and Martinez-Pereira 1999). Commonly employed definitions include (*i*) *bracketed duration*: the time elapsed between the first and last excursions of the accelerogram above a specified acceleration threshold, e.g., 0.05 g (Ambraseys and Sarma 1967; Bolt 1973); and (*ii*) *significant duration*: the time interval over which a specific percentage range, e.g., 5–75 %, 5–95 %, of the integral $\int_0^{t_{max}} a^2(t)dt$ is accumulated, where $a(t)$ represents the ground acceleration at time t, and t_{max} represents the length of the accelerogram (Trifunac and Brady 1975). While these metrics correspond to the canonical definition of ground motion duration, other duration metrics that are only implicitly correlated to the duration of strong ground motion, and may not even possess units of time, have also been proposed. $I_D = \frac{\int_0^{t_{max}} a^2(t)dt}{PGA \times PGV}$, for example, is a dimensionless duration metric proposed by Cosenza and Manfredi (1997). Although the form and nature of a duration metric do influence its usability in structural design and assessment, a more important criterion is its correlation to key structural demands.

1.1.3 Factors influencing ground motion duration

The duration of an earthquake ground motion is primarily dependent on the duration of source rupture (Esteva and Rosenblueth 1964; Hanks and McGuire 1981; Kempton and Stewart 2006). Larger magnitude earthquakes typically rupture longer

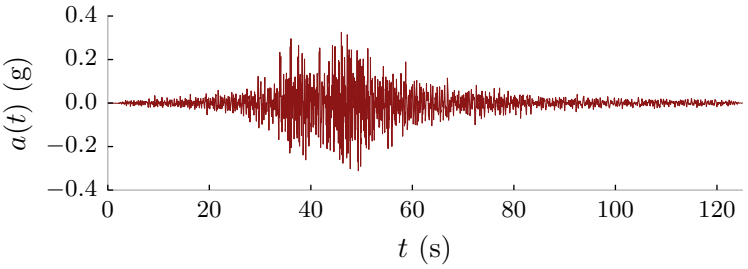

Figure 1.5: An accelerogram recorded from the 2010 Maule (Chile) earthquake at the Llolleo station.

segments of faults at approximately constant average rupture velocities (Dobry et al. 1978; Trifunac and Novikova 1995; Somerville et al. 1999), thereby producing ground motions of longer durations. The extents of the fault ruptures from three prominent historical earthquakes in Western USA: the 1700 Cascadia earthquake ($M_W \approx 9.0$), 1906 San Francisco earthquake ($M_W \approx 7.9$), and 1989 Loma Prieta earthquake (M_W 6.9), are plotted in Figure 1.2, along with representative ground motions they produced. Since recorded ground motions from the 1700 Cascadia and 1906 San Francisco earthquakes are not available, representative ground motions produced by other earthquakes of comparable magnitude: the 2011 Tohoku (Japan, M_W 9.0) and 2008 Wenchuan (China, M_W 7.9) earthquakes, are plotted corresponding to them instead. The increase in ground motion duration with earthquake magnitude is evident from Figure 1.2. While it is common knowledge that large magnitude subduction earthquakes typically produce long duration ground motions, it is worth noting that $M_W \sim 8.0$ crustal earthquakes are also capable of producing reasonably long duration ground motions. In addition to the length of rupture, the direction of rupture propagation with respect to the hypocenter and the presence of asperities at the fault interface can also influence the source rupture duration, and thereby, the durations of the produced ground motions.

Ground motion duration increases with distance from the source due to the scattering and dispersion of seismic waves, and the difference in the arrival times of waves propagating at different velocities and traversing different paths (Esteva and Rosenblueth 1964; Trifunac and Brady 1975; Novikova and Trifunac 1994; Stein and

Wysession 2003, § 2.8; Boore and Thompson 2014). Ground motion duration also depends on local site conditions, with longer duration ground motions typically observed at sites with softer soils due to repeated seismic wave reflections within the soft soil layer (Trifunac and Brady 1975; Dobry et al. 1978; Novikova and Trifunac 1994). The dependence of duration on source-to-site distance and site soil conditions is, however, much smaller compared to its dependence on earthquake magnitude. Sedimentary basins are expected to significantly amplify the durations of ground motions (in addition to their low frequency energy content) at sites located atop them by trapping seismic waves that enter them at an oblique angle (Marafi et al. 2017). The canonical example of this phenomenon is the amplification of the durations of ground motions at sites in Mexico City located atop the bed of the ancient Lake Texcoco, during the 1985 Mexico City earthquake (Anderson et al. 1986; Kawase and Aki 1989; Chávez-García and Bard 1994; Reinoso and Ordaz 2001). Studies like Somerville et al. (1997), Bommer and Martinez-Pereira (1999), and Singh et al. (1999) have additionally observed a dependence on near-fault rupture directivity, with ground motions of shorter duration (and larger amplitude) observed at forward directivity sites. Statistical analyses conducted by Kempton and Stewart (2006) have, however, found only a small effect of rupture directivity on duration, depending on the metric used to quantify duration.

1.1.4 Review of previous studies that investigated the influence of duration on structural response

Amplitude, frequency content, and duration have been widely recognized as the key ground motion characteristics that influence structural response since the inception of modern earthquake engineering (Jennings et al. 1968; Trifunac and Hudson 1971; Housner and Jennings 1977; Dobry et al. 1978). Of the three, amplitude and frequency content are conveniently quantified by the pseudo acceleration response spectrum, which has been universally adopted by the engineering community as the primary basis for structural design and assessment. Duration, on the other hand, has received considerably lesser attention. Early studies that postulated an influence of

ground motion duration on structural response were based solely on theoretical considerations and observational evidence, since numerical simulation and experimental testing capabilities were still at their infancy (e.g., Housner 1975; Trifunac and Westermo 1977; Dobry et al. 1978; McGuire and Barnhard 1979). These studies directed the attention of the engineering community towards duration and triggered the development of a number of metrics to quantify duration, also based purely on theoretical grounds (e.g., Ambraseys and Sarma 1967; Page et al. 1972; Bolt 1973; Housner 1975; Trifunac and Brady 1975; Saragoni 1977; McCann and Shah 1979; Vanmarcke and Lai 1980), some of which enjoy widespread use to date. A number of subsequent studies like Kawashima and Aizawa (1986), Xie and Zhang (1988), Kawashima and Aizawa (1989), Cosenza and Manfredi (1997), Bommer and Martinez-Pereira (1999), Hancock and Bommer (2005), Taflampas et al. (2009), Wang et al. (2015), and Marafi et al. (2016) have proposed additional duration metrics, although most of them have enjoyed lesser traction compared to the metrics that were developed earlier. Some studies like Bolt (1973), Trifunac and Westermo (1977), and Montejo and Kowalsky (2008) have proposed the use of frequency-dependent metrics to characterize duration, in a manner analogous to how the response spectrum represents a frequency-dependent measure of ground motion intensity. Many of these duration metrics are summarized in Bommer and Martinez-Pereira (1999).

A number of studies have attempted to assess the influence of ground motion duration on structural response over the last few decades, adopting a wide range of approaches. Studies like Vanmarcke and Lai (1980), Jeong and Iwan (1988), Zembaty (1988), Peng et al. (1989), Sánchez-Carratalá and Ferrer (2004), and Bora et al. (2014) employed stochastic methods rooted in random vibration theory in their investigations. Others like Housner (1956), Zahrah and Hall (1984), Fajfar and Vidic (1994), Sucuoğlu and Nurtuğ (1995), Krawinkler (1997), Chai et al. (1998), Chai and Fajfar (2000), Manfredi (2001), Malhotra (2002), Chou and Uang (2003), Kunnath and Chai (2004), Chai (2005), Teran-Gilmore and Simon-Velazquez (2008), Nicknam et al. (2010), and Alıcı and Sucuoğlu (2016) followed the school of thought that the energy transmitted to a structure by a ground motion—or alternatively the hysteretic energy dissipated by a structure—represents a fundamental measure of structural damage.

Hence, they employed energy-based metrics, often computed from the response of single-degree-of-freedom oscillators, to quantify the cumulative damage potential of a ground motion. Since ground motion duration is closely related to these energy-based metrics, these studies could be considered indirect investigations into the effect of duration. Studies like Mahin (1980), Oyarzo-Vera and Chouw (2008), Das and Gupta (2010), Iervolino et al. (2014), Raghunandan et al. (2014), Goda (2015), Jeon et al. (2015), Tesfamariam and Goda (2015), Iervolino et al. (2016), and Jalayer and Ebrahimian (2016) characterized damage aggregated over multiple earthquake shocks, including a main shock and one or more aftershocks. This too could be considered an indirect means to examine the influence of duration, which is closely related to the total accumulated damage.

One of the earliest studies to employ nonlinear dynamic analyses to investigate the effect of duration on structural response was Clough et al. (1965). This study assessed the effect of duration on the peak lateral displacements, member ductility demands, and column axial forces by analyzing a nonlinear model of a 20-story building using sections of an accelerogram recorded from the 1940 El Centro earthquake, of different lengths, and scaled to different intensities. A number of other studies, including Mahin (1980), Kennedy et al. (1984), Sewell (1992), Rahnama and Manuel (1996), Sewell et al. (1996), Cornell (1997), Tremblay (1998), Reinoso et al. (2000), Bommer et al. (2004), Lindt and Goh (2004), Ruiz-García and Miranda (2005), Iervolino et al. (2006), Hancock and Bommer (2007), Montejo and Kowalsky (2008), Oyarzo-Vera and Chouw (2008), Lin et al. (2010), Barbosa et al. (2012), Sarieddine and Lin (2013), Barbosa et al. (2014), Ou et al. (2014), Romney et al. (2014), Hou and Qu (2015), and Mantawy and Anderson (2015), have since employed nonlinear dynamic analyses to assess the influence of duration on structural demands. Takizawa and Jennings (1980), Xie and Zhang (1988), Bernal (1992), Ibarra and Krawinkler (2005), Raghunandan and Liel (2013), Raghunandan et al. (2015), and Marafi et al. (2016) conducted analyses on structural models capable of simulating structural collapse to study the effect of duration on structural collapse capacity. Many of these studies are summarized in Hancock and Bommer (2006). Lignos et al. (2011), Mohammed et al. (2015), and Galanis et al. (2016) have supplemented nonlinear dynamic analyses with

experimental investigations of the response of structures under long duration ground motions. The conclusions reached by each of these studies were found to depend on (*i*) the nature of ground motions used; (*ii*) the metrics used to quantify duration; (*iii*) the characteristics of the structural models employed; and (*iv*) the structural demand parameters considered. The broad consensus that can be drawn from this wide body of research is that ground motion duration generally does not affect peak demands, like peak story drifts and peak member forces, but significantly influences cumulative damage metrics, like total dissipated hysteretic energy and accumulated plastic strain. Studies that simulated structural collapse also found an effect of duration on collapse capacity, or the capacity of a structure to resist structural collapse, as typically quantified by a collapse fragility curve.

This study extends previous research on the topic by accounting for the following key criteria, deemed necessary to adequately capture the effect of duration:

(*i*) Use structural models that incorporate the in-cycle and cyclic deterioration of structural strength and stiffness (FEMA 2009a), and the destabilizing $P-\Delta$ effect of gravity loads.

(*ii*) Use long duration ground motions recorded from large magnitude earthquakes, like the recent 2008 Wenchuan (China, M_W 7.9), 2010 Maule (Chile, M_W 8.8), and 2011 Tohoku (Japan, M_W 9.0) earthquakes. Most earlier studies either relied on simulated long duration records, or used shorter duration records recorded from lower magnitude earthquakes.

(*iii*) Adequately control for the effect of response spectral shape to prevent it from confounding the observations.

(*iv*) Identify and use effective and efficient (as defined by Luco and Cornell 2007) metrics to quantify ground motion duration.

(*v*) Investigate the effect of duration on structural collapse risk by combining the results of structural collapse simulations with a measure of the site-specific seismic hazard that includes a description of the durations of the anticipated ground motions.

Structural collapse risk estimation is a key ingredient in building design code calibration and performance assessment methodologies. Assessing the impact of duration on structural collapse risk, therefore, is a necessary first step in evaluating the need to consider duration in structural design and assessment.

1.1.5 Treatment of duration in current standards for structural performance assessment and design

Peak structural deformations and peak member forces currently form the basis for acceptance criteria used in the design of new buildings (e.g., Eurocode 2004, § 4.3, § 4.4; PEER TBI 2010, § 8.6, § 8.7; LATBSDC 2014, § 3.5.4; ASCE 2016, § 12.12.1, § 16.2.4) and the evaluation of existing buildings (e.g., ASCE 2013, § 7.5). Transient peaks of demands like story drift ratio and floor acceleration are also most commonly used to define component fragility curves in modern structural performance assessment methodologies (e.g., FEMA 2012c, § 2.3). As discussed in § 1.1.4, however, a large majority of prior research has found little or no effect of duration on peak demands. Cumulative damage metrics, on which a significant influence of duration has been observed, currently find no place in design and assessment practice. Ground motion duration has, therefore, been relegated to implicit, qualitative consideration in most standards for structural performance assessment and design employed in practice today (e.g., Eurocode 2004; FEMA 2012b; ASCE 2013; ASCE 2016).

The effect of duration on the capacity of soils to resist seismic loads, on the other hand, is far more pronounced and widely acknowledged by the geotechnical engineering community. Duration has been shown to influence the liquefaction potential of soils (Seed and Idriss 1982; Youd et al. 2001; Sideras and Kramer 2012), the lateral spread displacements resulting from liquefaction (Rauch and Martin 2000), and the stability and displacement of slopes (Bray et al. 1998; Travasarou et al. 2004). Ground motion duration is, therefore, given more prominent consideration in the design and assessment of geotechnical systems than structural systems. The effect of duration is commonly considered in liquefaction assessments by adjusting the capacity of the soil to resist cyclic loads by a magnitude scaling factor (Seed and Idriss 1982).

Probabilistic seismic hazard analysis (PSHA) (Cornell 1968; Kramer 1996, § 4.4; McGuire 2004) forms the foundation of current structural design and assessment practice. PSHA is used to characterize the frequency with which any given intensity of ground motion—usually quantified by $S_a(T_1)$, the pseudo spectral acceleration at the fundamental elastic modal period of the structure—is exceeded at a site. Seismic hazard deaggregation calculations (McGuire 1995) then permit the determination of the earthquake scenario (defined by rupture mechanism, magnitude, source-to-site distance, etc.) that is most likely to cause the exceedance of a given $S_a(T_1)$ value at the site. The earthquake scenario that controls the exceedance of a specific target ground motion intensity level is commonly used as the basis for implicitly considering duration in a number of standards for structural design and assessment. The HAZUS loss assessment methodology, for example, approximately accounts for the effect of duration by modifying the effective damping factor used to adjust the demand response spectrum, based on the magnitude of the controlling earthquake scenario (FEMA 2012a, § 5.6.2.1). Procedures to select ground motions for use in response history analysis procedures frequently advocate the selection of records to match a target conditional spectrum (Abrahamson and Al Atik 2010; Jayaram et al. 2011b)—or alternatively a conditional mean spectrum (Baker et al. 2011)—to explicitly account for the response spectral shapes of the ground motions anticipated at the site. They, however, seldom recommend the selection of records whose durations explicitly match those of the ground motions anticipated at the site. Instead, they advocate the selection of records whose causal parameters match those that define the controlling earthquake scenario (e.g., Eurocode 2004, § 3.2.3; FEMA 2012b, § 4.4.2; ASCE 2013, § 2.4.2.2; ASCE 2016, § 16.2.2), with the expectation that this would result in the selection of records of approximately appropriate durations. Recent studies like Tarbali and Bradley (2016) have, however, demonstrated the potential for selecting records with durations that do not adequately represent the site-specific seismic hazard when using such indirect means to account for duration. The ground motion selection guidelines proposed by a number of standards are summarized in NIST (2011) (Chapter 3). Shome et al. (1998), Bommer and Acevedo (2004), Beyer and Bommer (2007), Katsanos et al. (2010), and NIST (2011) (Chapter 5) discuss some of the finer details

associated with ground motion selection and scaling, and reflect the current state of knowledge. Static analysis procedures like the equivalent lateral force (ELF) procedure described in (ASCE 2016, § 12.8), on the other hand, recommend the use of lateral load profiles that represent the intensity of anticipated ground motions, but account for neither their response spectral shapes nor their durations.

1.2 Objectives

The first objective of this study is to **quantify the influence of ground motion duration on structural collapse capacity**. Accomplishing this task additionally requires the achievement of the following sub-objectives:

(*i*) Evaluate commonly used duration metrics and identify ones that are well suited for use in structural design and assessment. The suitability of a duration metric is defined by the feasibility of incorporating it alongside the response spectrum in a vector intensity measure, and its efficiency in predicting a ground motion's collapse intensity.

(*ii*) Study the sensitivity of the effect of duration to key structural characteristics, and thereby help identify classes of structures that are more vulnerable to long duration ground motions than others.

(*iii*) Study the physical mechanisms that drive the observed influence of duration on structural collapse capacity. The effect of duration is often qualitatively attributed to cyclic deterioration in strength and stiffness and the ratcheting of drifts, accentuated by the $P-\Delta$ effect; the underlying mechanism by which long duration ground motions influence structural collapse by ratcheting are, however, less clearly understood.

The second objective is to **quantify the influence of duration on structural collapse risk** at sites located in different tectonic regimes, and to use the results to evaluate the need to explicitly consider duration in structural design and assessment. This again additionally requires the achievement of the following sub-objectives:

(*i*) Develop a procedure to characterize the seismic hazard at a site in terms of the probability distributions of the durations of the anticipated ground motions.

(*ii*) Evaluate the effectiveness of the current practice of implicitly accounting for duration by selecting records for response history analysis to match target ranges of causal parameters like rupture mechanism, magnitude, source-to-site distance, and site Vs_{30} (the time-averaged shear wave velocity of the top 30 m of the soil profile).

The third and final objective is to **develop strategies to explicitly consider duration in standards for structural performance assessment and design**, alongside response spectral shape, if duration is found to have a significant effect on structural collapse risk. The development of strategies to incorporate duration in a standard is to be accompanied by comparative nonlinear dynamic analyses that demonstrate the benefits of the proposed modifications to the standard.

1.3 Scope

The influence of duration on structural collapse capacity is investigated by conducting numerical simulations of the dynamic response of structures under ground motions of different durations. The effect of duration is captured using realistic, deteriorating nonlinear structural models that incorporate the destabilizing $P-\Delta$ effect of gravity loads. Peak story drift ratio and collapse capacity are the only two structural demands whose sensitivity to ground motion duration is investigated, since they form the basis for current structural design and assessment practice. Duration is not expected to significantly influence peak floor accelerations and peak floor velocities, which are commonly used to characterize damage to non-structural components; hence they are not considered in this study. Although duration is intuitively expected to influence cumulative damage metrics, they too are not considered, since they are seldom explicitly used in design and assessment practice. The cumulative hysteretic energy dissipated by a structural component is, instead, indirectly used by the phenomenological model employed to simulate its hysteretic behavior, to algorithmically degrade

its strength and stiffness over successive cycles, thereby manifesting itself in the form of amplified deformations under intense, long duration ground motions. The influence of duration is investigated using predominantly ductile reinforced concrete moment frames, although the effects on some steel moment frames and braced frames are also studied. No experimental tests are conducted as part of this study; although, the hysteretic models employed in the numerical simulations have been calibrated to results from previously conducted experimental tests. Numerical convergence issues associated with the simulation of structural response under long duration ground motions are investigated, and recommendations are made to circumvent the problem.

The influence of duration is investigated by comparing the response of structures under short and long duration ground motions, while adequately controlling for the anticipated effect of response spectral shape using careful record selection and appropriate post-processing of the analysis results using statistical tools. Only those long duration ground motions produced by large magnitude earthquakes involving long ruptures, recorded on sites with relatively firm soils, are considered. Narrow-band, long duration ground motions produced by the resonance of sedimentary basins are not considered since it was perceived that their unique nature may require parameters beyond just duration and response spectra to adequately characterize their effects on structural response. Additionally, traditional ground motion prediction models cannot yet adequately account for these basin effects, rendering it difficult to accurately characterize the seismic hazard at sites likely to experience such ground motions. Although physics-based ground motion simulation tools have been successfully employed to predict ground motions at sites located atop sedimentary basins (Frankel 2000; Pitarka 2004; Frankel et al. 2007; Olsen et al. 2008), they were not considered in this study.

The generalized conditional intensity measure (GCIM) framework (Bradley 2010) is adopted to characterize the probability distributions of the durations of the anticipated ground motions. The GCIM framework extends the concept of a conditional spectrum to compute conditional distributions of intensity measures other than just response spectral ordinates, like duration. Investigations into the effect of duration on structural collapse risk are limited to three sites located in Seattle (Washington),

Eugene (Oregon), and San Francisco (California), since the seismic hazard at these sites can be considered representative of a large number of other sites in Western USA. The seismic hazard at Eugene is dominated by interface earthquakes in the Cascadia subduction zone, while the hazard at San Francisco is dominated by earthquakes on nearby crustal faults like the San Andreas and Hayward faults. The seismic hazard at Seattle, however, receives contributions from interface and in-slab earthquakes from the Cascadia subduction zone, as well as crustal earthquakes from the adjacent Seattle fault zone.

Finally, strategies are proposed to incorporate the effect of duration into the following standards for structural performance assessment and design:

(*i*) the FEMA P-58 seismic performance assessment methodology (FEMA 2012b);

(*ii*) the FEMA P695 methodology to quantify seismic performance factors (FEMA 2009b); and

(*iii*) the ASCE 7-16 seismic design provisions (ASCE 2016).

More specifically, methods are developed to account for the effect of duration, alongside response spectral shape, in multiple stripe analysis (MSA) (Jalayer 2003, Chapter 4), incremental dynamic analysis (IDA) (Vamvatsikos and Cornell 2002), and ASCE 7-16's equivalent lateral force (ELF) (ASCE 2016, § 12.8) and nonlinear response history analysis (NLRHA) (ASCE 2016, Chapter 16) procedures.

1.4 Organization

The research conducted as part of this study is documented over Chapters 2 to 7, and the results of the study are summarized in Chapter 8. Each of the six body chapters is written in the format of a typical journal paper, beginning with *Abstract* and *Introduction* sections, and ending in a *Conclusion* section, to simplify the process of future submission to journals. The use of this format necessitated the replication of some background and introductory material over multiple chapters, to enable each chapter to stand alone, with minimal references across chapters. The section sign: §

in singular and §§ in plural, is frequently used to refer to specific sections within this document and other cited references using a compact notation.

Chapter 2 describes the use of spectrally equivalent long and short duration record sets to quantify the influence of ground motion duration on the collapse capacity of a five-story steel moment frame building. A number of commonly used duration metrics are compared to identify the ones that are well suited for use in structural design and assessment. The sensitivity of the effect of duration to key parameters of a reinforced concrete bridge pier model is then studied.

Chapter 3 examines the physical mechanisms that cause the observed effect of duration on the collapse capacity of the same steel moment frame building analyzed in Chapter 2. The cyclic deterioration of structural strength and stiffness and the gradual ratcheting of drifts, accentuated by the $P-\Delta$ effect, are shown to represent the two major mechanisms by which duration influences structural response. The relative contributions of the two mechanisms to the total observed effect of duration are quantified. A response parameter called the *ratcheting interval* is defined and used to explain the larger potential for long duration ground motions to cause structural collapse by ratcheting.

Chapter 4 describes a procedure based on the GCIM framework, to compute probability distributions of the durations of the ground motions anticipated at a site. Hazard-consistent collapse risk estimates of an eight-story reinforced concrete moment frame building are obtained by analyzing it using ground motions selected to match duration and response spectrum targets, computed at three sites in Western USA: Seattle (Washington), Eugene (Oregon), and San Francisco (California). The bias in the estimated structural collapse risk when using ground motions from the PEER NGA-West2 database, selected to match only hazard-consistent response spectrum targets, is then quantified at all three sites. This bias quantifies the consequence of ignoring duration when selecting records for structural collapse risk estimation. The effectiveness of ground motion selection procedures that implicitly account for duration using causal parameters is also examined.

Chapter 5 develops a structural reliability framework to compute a hazard-consistent collapse fragility curve by post-processing the results of an IDA conducted using a

generic record set, thereby eliminating its biggest shortcoming, and making it a competitive alternative to MSA. The hazard-consistent collapse fragility curve of the same eight-story reinforced concrete moment frame building analyzed in Chapter 4, computed using the reliability framework, is shown to compare well with the fragility curve obtained by conducting MSA using hazard-consistent ground motions, at Seattle, Eugene, and San Francisco. A simplified procedure that allows the efficient computation of just the hazard-consistent median collapse capacity, is also developed.

Chapter 6 proposes strategies to explicitly consider the effect of duration, alongside response spectral shape, in the following standards for structural performance assessment and design: (*i*) the FEMA P-58 seismic performance assessment methodology (procedures to estimate collapse capacity and demands given collapse has not occurred); (*ii*) the FEMA P695 methodology to quantify seismic performance factors; and (*iii*) the ASCE 7-16 seismic design provisions (ELF and NLRHA procedures).

Chapter 7 proposes the use of the explicit central difference numerical time integration scheme as a robust and efficient alternative to commonly used implicit schemes, like the Newmark average acceleration scheme, for nonlinear response history analysis. It is demonstrated to be robust against numerical non-convergence issues that most implicit schemes frequently suffer from, especially when structures are analyzed under long duration ground motions. It is also shown to be more efficient than implicit schemes when used to conduct structural collapse simulations, despite the limit on the maximum time step imposed by its stability criterion. The few additional steps required during model creation, including the assignment of mass to all degrees of freedom, are shown to be outweighed by improved performance in terms of robustness and efficiency. Efficient parallel algorithms to conduct MSA and IDA on multi-core computers and distributed parallel clusters are then developed.

In summary, Chapters 2, 3 and 7 address the first stated objective of quantifying the influence of duration on structural collapse capacity. Chapters 4 and 5 tackle the second objective of assessing the impact of duration on structural collapse risk by combining the observed influence of duration on structural collapse capacity with the seismic hazard at a few representative sites. Chapter 6 finally distils the results from Chapters 2 to 5 into succinct strategies by which the effect of duration can be

incorporated in structural design and assessment standards.

Chapter 2

Quantifying the influence of ground motion duration on structural collapse capacity using spectrally equivalent records

Adapted from Chandramohan, R., J. W. Baker, and G. G. Deierlein (2016). "Quantifying the influence of ground motion duration on structural collapse capacity using spectrally equivalent records". *Earthquake Spectra* **32** (2), pp. 927–950. DOI: 10.1193/122813EQS298MR2.

2.1 Abstract

This study examines the influence of ground motion duration on the collapse capacities of a modern, five-story steel moment frame and a reinforced concrete bridge pier. The effect of duration is isolated from the effects of ground motion amplitude and response spectral shape by assembling sets of "spectrally equivalent", long and short duration records, and employing them in comparative non-linear dynamic analyses. For the modern steel moment frame, the estimated median collapse capacity is 29 %

lower when using the long duration set, as compared to the short duration set. For the concrete bridge pier, the collapse capacity is 17 % lower. A comparison of commonly used duration metrics indicates that significant duration is the most suitable metric to characterize ground motion duration for structural analysis. Sensitivity analyses to structural model parameters indicate that structures with high deformation capacities and rapid rates of cyclic deterioration are the most sensitive to duration.

2.2 Introduction

The influence of ground motion duration on structural demands is a topic that has been researched extensively in the literature. As summarized in Hancock and Bommer (2006), previous studies have drawn different conclusions depending on the structural demand parameters they considered. The few that considered only peak structural deformations (e.g., Sarieddine and Lin 2013) generally found duration to have little effect. Most others studies (e.g., Cornell 1997; Bommer et al. 2004; Iervolino et al. 2006; Hancock and Bommer 2007; Oyarzo-Vera and Chouw 2008; Raghunandan and Liel 2013) found that although duration does not influence peak deformations, it does influence cumulative damage indices. Current seismic design standards and loading protocols for component testing do not explicitly account for the effects of duration. ASCE (2010) attempts to do so, implicitly, by specifying that accelerograms to be used for structural analysis should be chosen from earthquakes having magnitudes consistent with those that control the risk-targeted maximum considered earthquake (MCE_R) (ASCE 2010) ground motion. Even alternative performance-based evaluation methodologies (e.g., PEER TBI 2010; FEMA 2012b) do not have a well-defined framework for incorporating the effects of ground motion duration, apart from qualitative ground motion selection.

This study aims to highlight the importance of considering duration when selecting ground motions for structural response analysis, with particular emphasis on evaluating structural collapse. Structural collapse capacity is an important metric used to calibrate seismic design codes, whose main aim is to ensure safety against collapse (ASCE 2010). Collapse is also an important limit state in performance-based loss

evaluation (Moehle and Deierlein 2004). Evaluating the influence of ground motion duration on collapse capacity requires numerical models that accurately characterize structural behavior at large non-linear deformations. Ideally, such models should incorporate the in-cycle and cyclic deterioration of strength and stiffness of structural components (Ibarra et al. 2005), as well as the destabilizing $P-\Delta$ effects of gravity loads (Gupta and Krawinkler 2000). Many prior studies (e.g., Iervolino et al. 2006; Hancock and Bommer 2007; Oyarzo-Vera and Chouw 2008; Sarieddine and Lin 2013) employed numerical models that did not incorporate all these features, and hence, may not provide a comprehensive assessment of the influence of duration on collapse safety. By incorporating deterioration and $P-\Delta$ effects, this study provides an informative assessment of the effect of duration, including analyses to evaluate the sensitivity of the observed effect of duration to model parameters.

A number of other studies (e.g., Zahrah and Hall 1984; Sucuoğlu and Nurtuğ 1995; Krawinkler 1997; Chai and Fajfar 2000; Malhotra 2002; Kunnath and Chai 2004) have identified total dissipated hysteretic energy as an indicator of structural damage, and considered ground motion duration to act as a proxy for this demand measure. They have also attempted to quantify the damage potential of accelerograms based on the hysteretic energy dissipated by single-degree-of-freedom oscillators. In this study, structural damage is not explicitly quantified in terms of the dissipated hysteretic energy, but the cumulative hysteretic energy dissipated by each plastic hinge is used to cyclically degrade its strength and stiffness after each inelastic excursion, such that damage is manifested in the form of larger structural deformations under intense, long duration ground motions, eventually leading to structural collapse.

In addition to the issues associated with the reliable modeling of deterioration, three challenges that have hampered studies on the influence of ground motion duration on structural response are (*i*) the scarcity of long duration ground motions, (*ii*) the difficulty in isolating the effect of duration from other ground motion characteristics, such as amplitude and frequency content, and (*iii*) the lack of consensus on an effective ground motion duration metric that relates to structural behavior. The first challenge has been addressed in some previous studies (e.g., Mahin 1980; Xie and Zhang 1988; Rahnama and Manuel 1996; Tremblay 1998; Raghunandan and Liel

2013; Sarieddine and Lin 2013) through the use of artificially simulated, long duration accelerograms. In this study, the scarcity of available ground motions has been addressed by collecting and utilizing long duration ground motions recorded from recent large magnitude earthquakes, most notably the 2008 Wenchuan (China), 2010 Maule (Chile), and 2011 Tohoku (Japan) earthquakes. The second challenge of isolating the effect of duration from other ground motion characteristics has been previously addressed by Hancock and Bommer (2007), Montejo and Kowalsky (2008), and Ou et al. (2014) by modifying the spectral content of recorded accelerograms to have similar response spectra. Sideras and Kramer (2012) used stochastically simulated accelerograms having similar amplitude and frequency characteristics, but different durations. This study employs spectrally equivalent, long and short duration record sets, with unmodified spectral content, to isolate and quantify the influence of duration. The third challenge is addressed by analyzing several ground motion duration metrics to identify the one that is best suited for selecting ground motions to use in non-linear collapse analyses.

2.3 Ground motion selection and collapse capacity estimation

The collapse capacity of a structure can be treated as a random variable, defined as the intensity of ground excitation that causes structural collapse. Its cumulative distribution function, known as a collapse fragility curve, relates ground motion intensity to the probability of collapse. Calculation of collapse capacity requires a non-linear structural model that can accurately simulate response from the initiation of inelasticity up to the onset of collapse at large deformations. The non-linear response is evaluated by scaling ground motions to different intensity levels, the distributions of whose characteristics (such as frequency content, duration, and pulse-like characteristics) at each intensity level, match their respective predicted distributions corresponding to the site-specific seismic hazard. When a different set of ground motions is used at each intensity level, the procedure is referred to as multiple stripe analysis

(Jalayer 2003). This is in contrast to incremental dynamic analysis (IDA), whereby a single set of ground motions is scaled to different intensity levels (Vamvatsikos and Cornell 2002). Multiple stripe analysis is generally preferred for building-specific applications since it captures site-specific hazard conditions. In this study, however, IDA is employed for the purposes of comparative collapse analyses using two sets of spectrally equivalent ground motions with different durations. Ground motion intensity is defined by the 5 % damped pseudo spectral acceleration at the fundamental period of the structure, $S_a(T_1, 5\,\%)$.

The frequency content of a ground motion is commonly characterized by its response spectral shape, whose influence on predicted collapse capacity has been demonstrated in previous studies (e.g., Baker and Cornell 2006b; Haselton et al. 2011a). This study evaluates whether ground motion duration influences structural collapse capacity as well, thereby warranting consideration during record selection for collapse analysis, in addition to response spectral shape. Bradley (2010) has proposed a framework to determine the predicted distribution of duration at a site, conditional on a chosen intensity level. This conditional distribution of duration can be computed using seismic hazard deaggregation information, a ground motion prediction equation for duration (e.g., Abrahamson and Silva 1996; Kempton and Stewart 2006; Bommer et al. 2009), and information on the correlation between the residuals (epsilon values per Baker and Cornell 2005) of duration and response spectral ordinates (e.g., Bradley 2011).

The selected ground motions are used as input to non-linear dynamic structural analyses, where the collapse limit state is defined by the unbounded increase in peak global deformations, above a pre-defined threshold (Haselton and Deierlein 2008). The probability of collapse at each intensity level is computed as the fraction of ground motions causing collapse at that intensity level. The collapse fragility curve is then determined by fitting a lognormal cumulative distribution function to these data points using a maximum likelihood approach.

2.4 Creation of record sets

A major component of this study entailed assembling a set of long duration ground motions from earthquake recordings. Significant duration (Ds_{5-75}) was used to characterize ground motion duration since it has been widely used in the literature, and preliminary studies by the authors (Foschaar et al. 2011) indicated it to be the preferred metric for this kind of analysis. The significant duration of a ground motion is defined as the time interval over which a specific percentage range of the following integral is accumulated:

$$\int_0^{t_{max}} a^2(t)dt \tag{2.1}$$

where $a(t)$ represents the ground acceleration and t_{max} represents the length of the record. As shown in Figure 2.1, the 5–75 % qualifier on significant duration refers to the percentages of the integral defined in Equation (2.1), over which the significant duration is defined. It is later demonstrated that the choice of Ds_{5-75} for selecting records does not significantly influence the final results, though significant duration is shown to be a more robust and convenient predictor of the effect of duration on structural collapse than other metrics.

To assemble the long duration record set, approximately 2000 horizontal record pairs were collected from the following large magnitude earthquakes: 1974 Lima (Peru), 1985 Valparaiso (Chile), 1985 Michoacan (Mexico), 2003 Hokkaido (Japan), 2010 Maule (Chile), and 2011 Tohoku (Japan). They were baseline corrected and filtered using the recommendations of Boore (2005) and Boore and Bommer (2005). Record pairs from the following large magnitude events in the PEER NGA-West2 database (Ancheta et al. 2013) were also included in the collection: 1992 Landers (USA), 1999 Kocaeli (Turkey), 2008 Wenchuan (China), and 2010 El Mayor Cucapah (USA). Since the selected ground motions were to be used for collapse analyses requiring fairly high intensities, record pairs with geometric mean peak ground acceleration (PGA) smaller than 0.1 g or geometric mean peak ground velocity (PGV) smaller than 10 cm/s were screened out. From the resulting database, long duration record pairs were identified as those with Ds_{5-75} of at least one of the two components greater

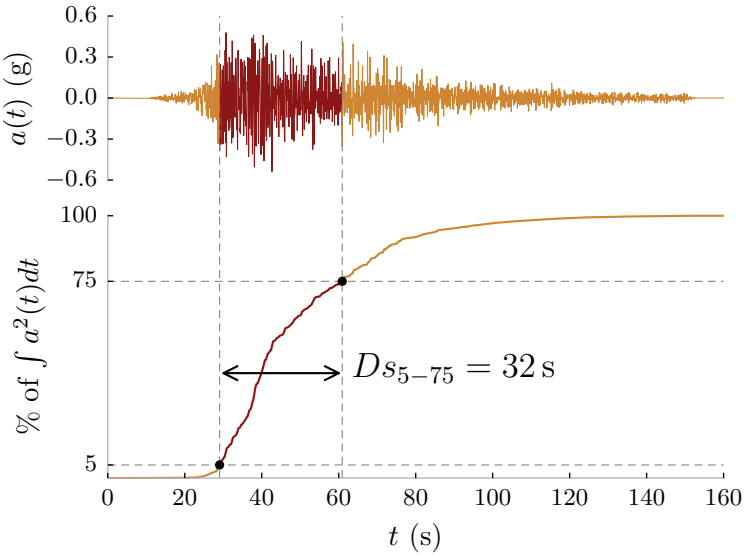

Figure 2.1: Computation of the 5–75 % significant duration (Ds_{5-75}) of a ground motion.

than 25 s. The 25 s threshold was decided after reviewing a histogram of Ds_{5-75} of all available records, striking a balance between being long enough to observe an effect of duration, but not so long as to result in too small of a set. The threshold was applied to the Ds_{5-75} of individual components rather than the geometric mean Ds_{5-75} of both components since doing so would have screened out some viable long duration records. Long duration records from soft soil sites were also screened out since it was felt that soft soil records have unique characteristics that would require selection criteria beyond response spectral shape to maintain parity between long and short duration record pairs. Finally, to avoid having any single event dominate the record set, the number of record pairs selected from any event was limited to 25. This process resulted in the creation of a long duration record set containing 73 record pairs, with a geometric mean of 42 s. As a point of reference, 42 s corresponds to the predicted median Ds_{5-75} for a magnitude 9.1 earthquake, at a source distance of 100 km, using Abrahamson and Silva (1996). The distribution of Ds_{5-75} for this long duration set is shown in the upper portion of Figure 2.2. As summarized in Table 2.1, ground motions are included from 10 earthquakes, and records from the 2011 Tohoku and 2008 Wenchuan earthquakes constitute over half of the set.

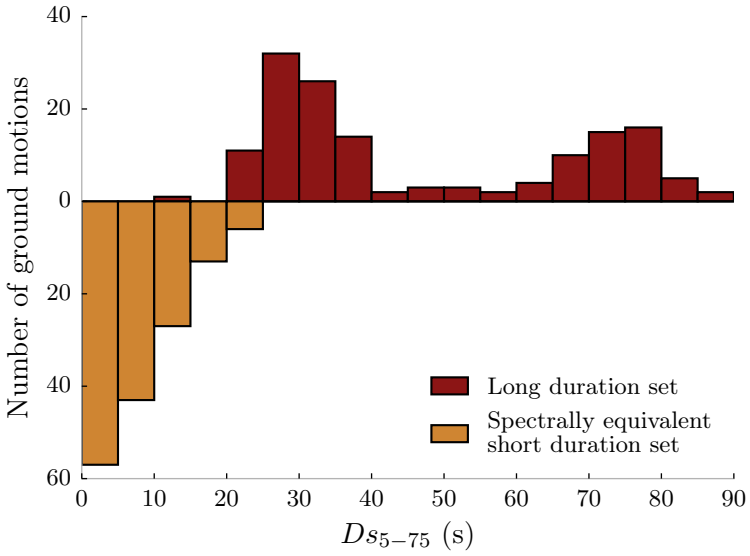

Figure 2.2: Distribution of Ds_{5-75} of the records in the spectrally equivalent, long and short duration record sets.

Table 2.1: Summary of the number of record pairs from each earthquake in the long duration record set.

Earthquake	**Magnitude**	**Number of record pairs**
1974 Lima (Peru)	8.1	2
1985 Valparaiso (Chile)	7.8	4
1985 Michoacan (Mexico)	8.0	4
1992 Landers (USA)	7.3	3
1999 Kocaeli (Turkey)	7.5	2
2003 Hokkaido (Japan)	8.3	6
2008 Wenchuan (China)	7.9	16
2010 Maule (Chile)	8.8	8
2010 El Mayor Cucapah (USA)	7.2	3
2011 Tohoku (Japan)	9.0	25

A companion short duration record set was assembled to serve as a control group. For each of the 146 individual records in the long duration set, a corresponding record with Ds_{5-75} smaller than 25 s and a closely matching response spectrum was chosen from the PEER NGA-West2 database. To find a short duration record with a response spectrum closely matching that of a given long duration record, the target response spectrum of the long duration record was discretized at periods from 0.05 s to 6.00 s, at intervals of 0.05 s, to obtain 120 spectral ordinates, L_1, L_2, L_3, ..., L_{120}, with mean $\bar{L}$. The corresponding response spectral ordinates, S_1, S_2, S_3, ..., S_{120} with mean $\bar{S}$, were calculated for all records from the PEER NGA-West2 database that belonged to a horizontal record pair, both of whose components had Ds_{5-75} lesser than 25 s. The spectral ordinates of each short duration record were then scaled by a factor $k = \bar{L}/\bar{S}$, such that the mean of the spectral ordinates of the scaled record ($k\bar{S}$) was equal that of the long duration record ($\bar{L}$). A constraint of $k \leq 5$ was imposed to avoid the scaling of low intensity records by large factors. The sum of squared errors (SSE) used to quantify the error between the two response spectra was then computed as

$$SSE = \sum_{i=1}^{120} (L_i - kS_i)^2 \tag{2.2}$$

Among all candidate short duration records that had not already been selected, the one with the lowest sum of squared errors was chosen. Figure 2.3 shows a comparison of the response spectra and time histories of one such spectrally equivalent, long and short duration record pair. This resulted in the creation of a short duration set with a geometric mean Ds_{5-75} of 6 s, with each of the 146 records having a spectrally equivalent match in the long duration set. As a point of reference, 6 s is the predicted median Ds_{5-75} for a magnitude 6.4 earthquake, at a source distance of 50 km, using Abrahamson and Silva (1996). The distribution of Ds_{5-75} for the short duration set is shown in the lower portion of Figure 2.2. By selecting these with matching spectral shapes, it is hypothesized that variations in the collapse capacity estimated using the two record sets can be attributed to the difference in their ground motion durations. It is later verified that the adopted selection procedure did not introduce any significant biases with respect to other ground motion characteristics

that may influence the calculated collapse capacity as well. Detailed information about the two record sets is available in a digital appendix to this paper: http://purl.stanford.edu/gq974qw0332.

2.5 Non-linear dynamic analysis of a steel moment frame model

A modern, five-story steel special moment frame, based on an actual building located in San Francisco (also used in FEMA 2014), was modeled and analyzed to assess the influence of duration. A schematic of the two-dimensional model, which was analyzed using OpenSees rev. 5184 (McKenna et al. 2006), is shown in Figure 2.4. The beams and columns of the frame were modeled using linear elastic elements, with zero-length plastic hinges located at the ends of each column and the reduced beam section (RBS) cuts near the ends of each beam. The hysteretic behavior of the plastic hinges was modeled using the Modified Ibarra-Medina-Krawinkler bilinear model that includes a post-peak negative stiffness branch of the backbone curve to capture in-cycle deterioration, as well as an algorithm that cyclically deteriorates strength and stiffness based on the cumulative hysteretic energy dissipated (Ibarra et al. 2005). Finite panel zones were modeled, with their shear deformations represented by a trilinear backbone curve. The contribution of the adjacent gravity system to the destabilizing $P - \Delta$ effect was modeled using a pin-connected leaning column. The calculated fundamental period of the structure is 1.6 s.

During each analysis, the peak story drift ratio (SDR, calculated as the maximum lateral story drift ratio over all the stories and the entire duration of shaking) was monitored, and an unbounded increase in peak SDR, above a threshold of 0.10 rad, was used as an indication of structural collapse. Numerical time integration was performed using the explicit central difference scheme, since it was found to be more robust than implicit numerical integration schemes, which sometimes failed to converge.

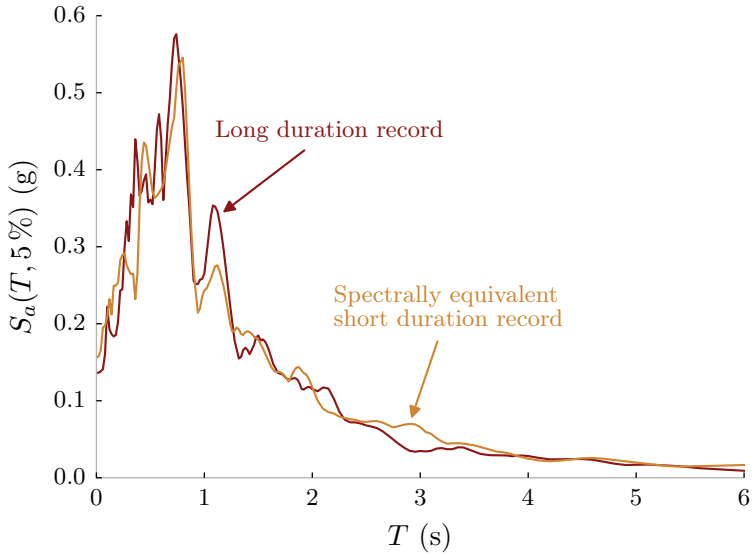

(a)

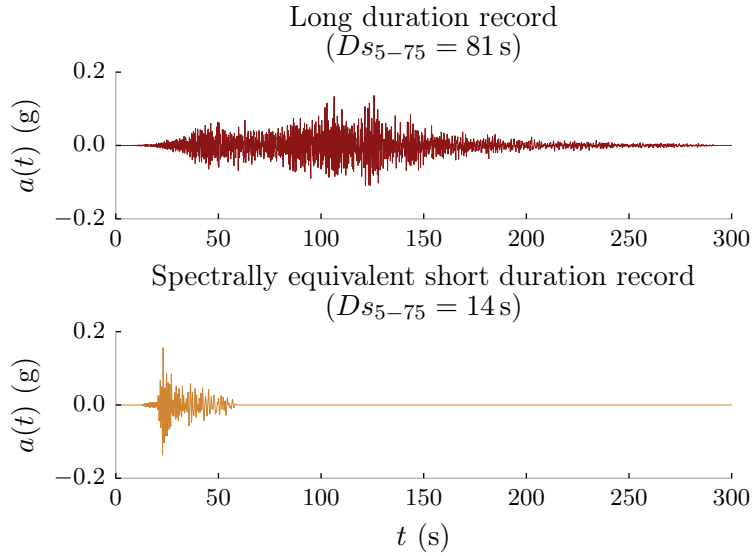

(b)

Figure 2.3: Comparison of the (a) response spectra and (b) time histories of a spectrally equivalent, long and short duration record pair. The long duration record is from the 2011 Tohoku earthquake, recorded at the Kaminoyama (YMT011) station. The short duration record is from the 2004 Chuetsu earthquake, recorded at the Joetsu City (65019) station, scaled by a factor of 0.74.

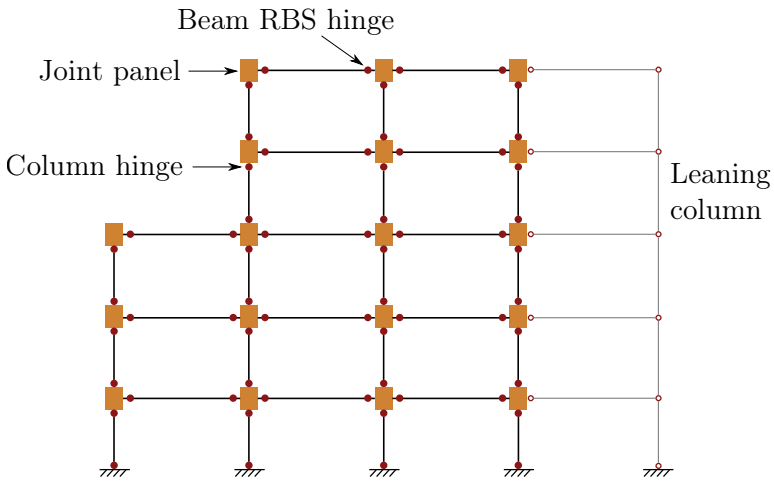

Figure 2.4: Schematic of the five-story steel special moment frame model.

The collapse fragility curves resulting from incremental dynamic analyses conducted using the spectrally equivalent, short and long duration record sets are shown in Figure 2.5. The median collapse capacities estimated using the short and long duration record sets are 0.92 g and 0.65 g, respectively. Since the record sets are spectrally equivalent, the 29 % decrease in estimated median collapse capacity is attributed to the difference in ground motion durations. The estimated probability of collapse at the MCE_R level ($S_a(1.6\,\text{s}, 5\,\%) = 0.41\,\text{g}$ in this case) is about seven times larger using the long duration set than the short duration set (collapse probability of 11 % using the long duration set vs. 1.4 % using the short duration set). When integrated with the seismic hazard curve corresponding to the location of the building in San Francisco, the mean annual frequencies of collapse computed using the short and long duration record sets are 0.92×10^{-4} and 2.8×10^{-4} respectively, indicating a three-fold increase in collapse risk when using the long duration set. Although it is unrealistic to expect ground motions like those contained in the long duration record set in San Francisco, these numbers serve to illustrate how collapse risk can be influenced by ground motion duration.

The geometric means of the IDA curves for both record sets, relating peak SDR to ground motion intensity, are plotted in Figure 2.6. The curves begin to diverge

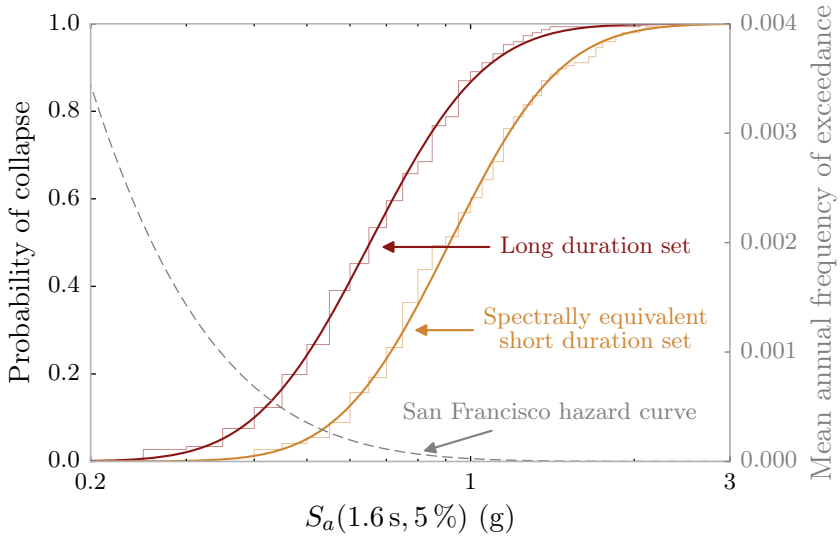

Figure 2.5: Collapse fragility curves estimated using the spectrally equivalent long and short duration record sets, and the hazard curve corresponding to the location of the building in San Francisco.

at a peak SDR value of about 0.03 rad, which coincides with the point where the steel beam hinges reach their peak strengths and begin to strain-soften. This trend has also been observed by the authors in other structural models analyzed in related research (though not presented here), indicating that the influence of ground motion duration on peak SDR is observed only at intensity levels large enough to produce non-linear deformations that extend into the post-peak softening range of inelastic response. This observation helps reconcile the results of this study with the those of many previous studies summarized in Hancock and Bommer (2006), which used numerical models that did not incorporate deterioration and $P-\Delta$ effects, and hence, found no influence of duration on peak deformation demands. An important implication of this is that although long duration ground motions predict lower collapse capacities, the effect of duration on peak global deformations will not be detected when analyzing new building designs at or below $\mathrm{MCE_R}$ intensities ($\mathrm{MCE_R}$ level in this case is $S_a(1.6\,\mathrm{s}, 5\,\%) = 0.41\,\mathrm{g}$), as is standard practice when non-linear analyses are used for building design (Deierlein et al. 2010; PEER TBI 2010). Therefore, methods that consider the influence of ground motion duration on collapse safety will

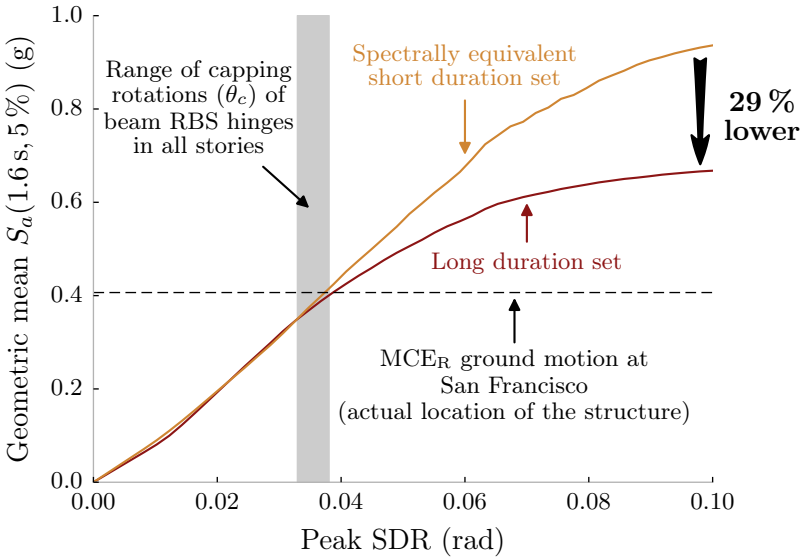

Figure 2.6: Geometric mean curves of the spectrally equivalent, long and short duration record sets.

need to go beyond analyses using ground motions scaled to MCE$_\mathrm{R}$ intensities. Either non-linear analyses will need to be conducted at higher ground motion intensities, where duration-sensitive structural deterioration and $P-\Delta$ effects are captured, or alternatively, adjustment factors for design strength and/or ductility requirements may need to be applied to maintain sufficient margins of safety against collapse, at sites where long duration ground motions are expected.

Shown in Figure 2.7 is a log-log plot of the collapse capacity, $S_a(1.6\,\mathrm{s}, 5\,\%)$, versus Ds_{5-75}, for each ground motion. Although the decreasing trend in collapse capacity with Ds_{5-75} is evident from the plot, this representation of the data does not utilize information about the spectral equivalence of corresponding long and short duration record pairs. Therefore, an alternative representation of the data, in terms of two new parameters: *Collapse Capacity Ratio* and Ds_{5-75} *Ratio* is presented. *Collapse Capacity Ratio* or *CCR* of a spectrally equivalent record pair is defined as the ratio of the collapse capacities produced by the long and short duration records constituting the pair. Similarly, the Ds_{5-75} *Ratio* of a spectrally equivalent record pair is defined as the ratio of the Ds_{5-75} of the long and short duration records. As

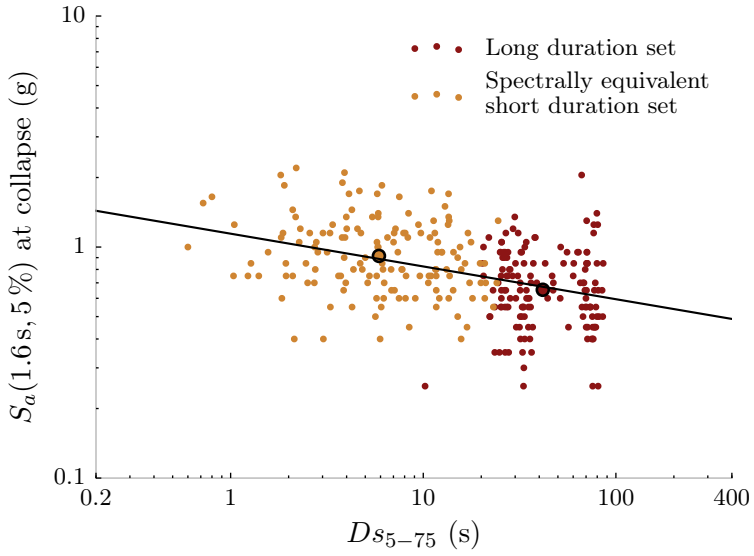

Figure 2.7: Log-log plot of collapse capacity vs. Ds_{5-75} (the two large circles represent the geometric mean collapse capacity and geometric mean Ds_{5-75} of all ground motions in the corresponding set).

shown in Figure 2.8, plotting $\ln(CCR)$ against $\ln(Ds_{5-75}\ Ratio)$ for all 146 spectrally equivalent record pairs confirms that within each spectrally equivalent record pair, on average, the longer the duration of one ground motion with respect to the other, the lower the collapse capacity it predicts. As illustrated by the values highlighted in the figure, a ground motion with 2 times the duration of another predicts a 10 % lower collapse capacity on average. Similarly, a ground motion with 30 times the duration of another predicts a 50 % lower collapse capacity on average.

A few other observations can be made from the plot in Figure 2.8. The p-value (Kutner et al. 2005) of the slope of the least squares regression line (from a 1-sided t-test) is 1.0×10^{-8}. This low p-value indicates that the influence of duration on collapse capacity is statistically significant. The y-intercept of the least squares regression line is 1.08, with a p-value of 0.35 (from a 2-sided t-test). This large p-value implies that if two records have identical spectral shapes and durations represented by Ds_{5-75}, they predict the same collapse capacity on average. This indicates that there were no statistically significant biases introduced during the record selection process with respect to other unaccounted ground motion characteristics that could

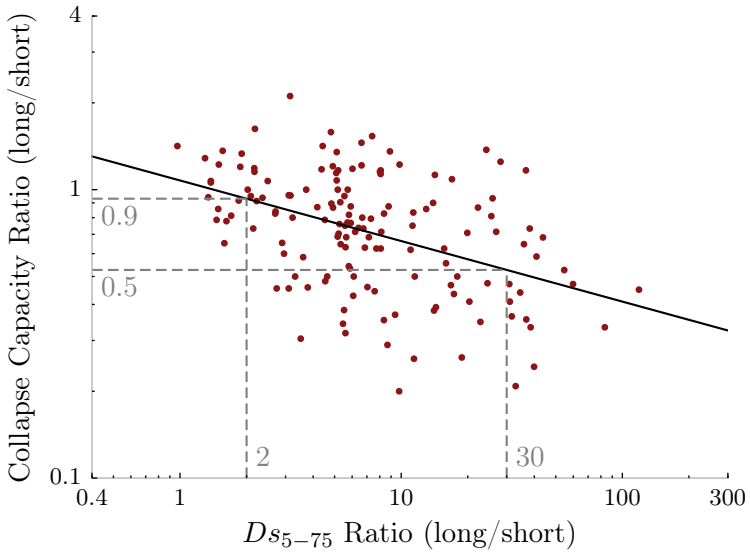

Figure 2.8: Log-log plot of *Collapse Capacity Ratio* vs. Ds_{5-75} *Ratio* with the least squares regression line.

influence collapse capacity. The coefficient of determination (R^2) from the regression analysis is 0.20, which implies that taking into account the Ds_{5-75} of the ground motions decreased the variance in $\ln(CCR)$ by 20 %. This R^2 statistic is a measure of the efficiency of Ds_{5-75} in predicting $\ln(CCR)$ and is used to compare the efficiencies of alternative duration metrics.

2.6 Analysis of duration metrics

A number of metrics exist, other than Ds_{5-75}, that could be used to quantify ground motion duration (Bommer and Martinez-Pereira 1999). This study considers the following, which are evaluated relative to Ds_{5-75}:

- **5–95 % significant duration (Ds_{5-95})**: The time interval over which 5 % to 95 % of the integral $\int_0^{t_{max}} a^2(t)dt$ is accumulated (Trifunac and Brady 1975).
- **0.05 g bracketed duration ($Db_{0.05}$)**: The time elapsed between the first and last excursions of the accelerogram above a threshold of ±0.05 g (Bolt 1973).

Higher or lower thresholds may be used, however, 0.05 g is judged to be a reasonable value for evaluating ground motions that cause damage to engineered structures.

- **Arias intensity (I_A)** $= \frac{\pi}{2g}\int_0^{t_{max}} a^2(t)dt$: A measure of the energy contained in the accelerogram and a hybrid metric of duration and intensity (Arias 1970). It is expected to be correlated to the duration of strong shaking since it involves integration over time (Kayen and Mitchell 1997).

- **Cumulative absolute velocity (CAV)** $= \int_0^{t_{max}} |a(t)|dt$: Another hybrid metric (Benjamin 1988) that is expected to be more correlated to the duration of an accelerogram than its intensity, when compared to Arias intensity, since it involves integration of a lower power of $a(t)$ over time.

- $I_D = \frac{\int_0^{t_{max}} a^2(t)dt}{PGA \times PGV}$: A dimensionless metric of duration proposed by Cosenza and Manfredi (1997), computed as the integral of $a^2(t)$ normalized by the peak ground acceleration and velocity.

A duration metric is considered efficient (Luco and Cornell 2007) if it produces a large decrease in the variance of $\ln CCR$, i.e., produces a large R^2 statistic in a regression analysis similar to the one presented in the previous section. In fact, any ground motion metric that results in a significant decrease in the variance of $\ln CCR$ could be considered an efficient predictor of collapse capacity. This motivates the consideration of hybrid metrics like I_A and CAV.

The efficiencies of the duration metrics defined above are compared by plotting $\ln CCR$ against $\ln Duration\ Ratio$ or $\ln DR$, similar to Figure 2.8. There is, however, some ambiguity in the definition of a few of the duration metrics defined above when records are scaled to cause structural collapse. This ambiguity arises because the $Db_{0.05}$, I_A, and CAV of a ground motion change as it is scaled. Thus, in this context, the duration measure is not unique, and could, for example, refer to either the duration of the original ground motion, or of the ground motion scaled to the collapse intensity, following IDA procedure. Both interpretations are considered in the following comparison.

The R^2 statistics for the duration metrics are summarized in Table 2.2, where values for $Db_{0.05}$, CAV, and I_A are reported both for the original and scaled ground motions. The values in the first (Ds_{5-75} *set*) column are for the record sets discussed previously; values in the other columns are for alternative record sets that are discussed below. In the "Ds_{5-75} *set*" column, all duration metrics computed from the unscaled ground motions have R^2 values between 0.13 and 0.20, and the regression analyses exhibit similar decreasing trends between $\ln CCR$ and $\ln DR$, as observed for the Ds_{5-75} data in Figure 2.8. The $Db_{0.05}$, CAV, and I_A metrics computed from the scaled ground motions (shaded rows in Table 2.2), however, do not share this trend. For the scaled CAV and I_A, $\ln CCR$ is found to increase, rather than decrease, with $\ln DR$. Figure 2.9 shows the different regression lines obtained when I_A is computed from the original and scaled records. This difference is due to the inherent positive correlation of these scaled duration metrics to the estimated collapse capacity. By definition, $Db_{0.05}$, CAV, and I_A increase as the ground motion is scaled up, so if a ground motion is scaled up by a factor x ($x > 1$), CAV increases by a factor of x, I_A increases by a factor of x^2, and $Db_{0.05}$ increases, though in a less predictable manner. This variation in the duration metrics with scaling, coupled with the fact that the short duration records need to be scaled to higher intensities to cause structural collapse than the long duration records, is the cause of the inconsistent trends. Apart from their self-fulfilling correlation to the estimated collapse capacity, duration metrics that are influenced by scaling pose the more obvious problems of having ambiguous values. One could imagine, for example, that if durations were defined at the scaled collapse intensity, then the duration metrics would be structure-dependent and determinable only after conducting an IDA. Thus, duration metrics that do not vary with scaling, such as significant duration and I_D, are better suited than others to analysis applications where ground motions are routinely scaled, such as conducting IDA.

The results discussed thus far are based on pairs of long and short duration ground motions that were chosen based on their Ds_{5-75} values. To verify that the results were not biased by this initial selection, the same analyses were repeated using long and short duration record sets of roughly the same size, chosen using $Db_{0.05}$ and

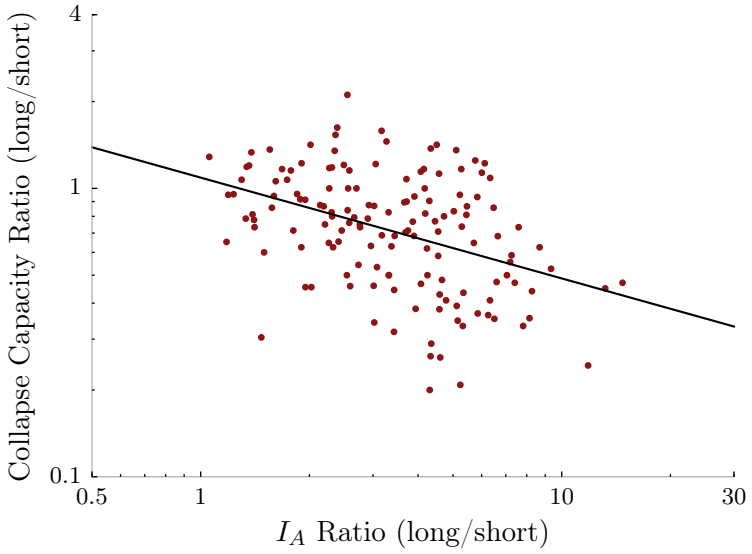

(a)

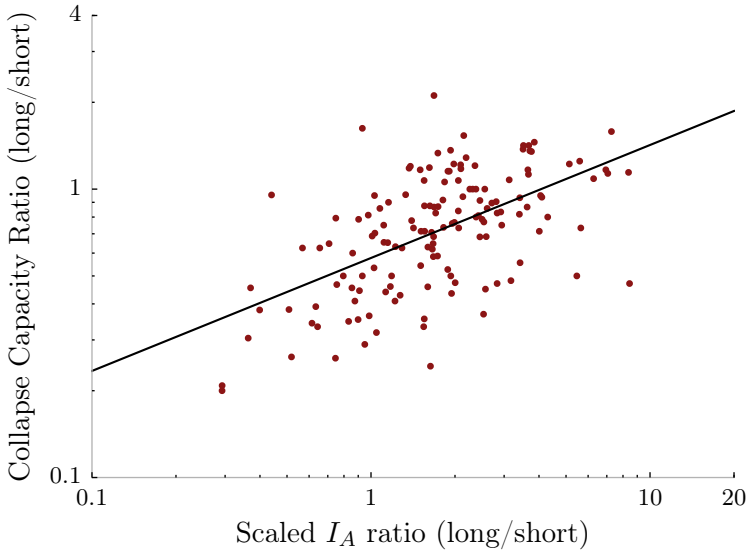

(b)

Figure 2.9: Log-log plots of *Collapse Capacity Ratio* vs. *Duration Ratio*, with least squares regression lines, where duration is represented by Arias intensity computed (a) from the original ground motion and (b) when scaled to the collapse intensity.

Table 2.2: Summary of R^2 statistics for all considered duration metrics computed using three long duration record sets chosen based on Ds_{5-75}, Ds_{5-95}, and $Db_{0.05}$ and their corresponding spectrally equivalent, short duration record sets.

Duration Metric	**R^2 statistic**		
	Ds_{5-75} set	**Ds_{5-95} set**	**$Db_{0.05}$ set**
5–75 % significant duration (Ds_{5-75})	0.20	0.18	0.09
5–95 % significant duration (Ds_{5-95})	0.16	0.16	0.06
0.05 g bracketed duration ($Db_{0.05}$)	0.13	0.19	0.08
I_D (Cosenza and Manfredi 1997)	0.17	0.16	0.10
Cumulative absolute velocity (CAV)	0.20	0.18	0.09
Arias intensity (I_A)	0.17	0.17	0.06
$Db_{0.05}$ when scaled to cause collapse	0.09	0.05	0.04
CAV when scaled to cause collapse	0.01	0.00	0.04
I_A when scaled to cause collapse	0.32	0.20	0.33

Ds_{5-95} to distinguish long from short records. Records with $Db_{0.05}$ greater than 55 s or Ds_{5-95} greater than 45 s were identified as long duration records. Proceeding in the same manner as before, the record sets were selected, IDAs were conducted, and regression analyses were carried out for $\ln CCR$ against $\ln DR$, for all the duration metrics. The trends from the two sets of analyses were found to be similar to those shown previously in Figures 2.8 and 2.9, and the R^2 statistics are summarized in the last two columns of Table 2.2. Although the specific values of the R^2 statistics are different for the three sets (Ds_{5-75}, Ds_{5-95}, and $Db_{0.05}$), the trends between duration metrics within each set are similar.

Scalar intensity measures (IMs), such as CAV, I_A, and source magnitude, which implicitly incorporate information about the amplitude and duration of a ground motion, are often used in geotechnical earthquake engineering to assess the deformation and liquefaction potential of soil deposits (Kayen and Mitchell 1997; Kramer and Mitchell 2006; Sideras and Kramer 2012). For structural analysis and performance assessment, however, a more explicit description of the site hazard in terms of a vector of response spectral ordinates is preferred since the wide range of engineering demand parameters (EDPs) considered for different structures, are each sensitive to different components of the vector. This vector IM is used to define a target response

spectrum, such as a conditional spectrum, which quantifies a target intensity and response spectral shape for selecting ground motions. Where a duration metric is to be added to this vector IM, it should provide non-redundant information that is not already quantified by the other components of the vector. It should, therefore, be independent of ground motion intensity. Among the duration metrics described above, a statistical analysis of records collected for this study confirm that $Db_{0.05}$, CAV, and I_A are all strongly correlated to common IMs like PGA, PGV, and $S_a(1\,\text{s}, 5\,\%)$. This lack of independence implies that they would not be effective duration metrics to add to a vector IM.

To further explore the suitability of alternative duration metrics, three additional long duration record sets based on I_D, CAV, and I_A were developed. An analysis of the selected records revealed that screening ground motions using CAV and I_A can lead to the unintended selection of ground motions with large acceleration values over a short time interval, i.e., ground motions with large CAV and I_A values, but small durations of strong shaking. In addition, certain duration metrics can lead to the selection of ground motions with biased spectral shapes. This is illustrated in Figure 2.10, where the geometric mean response spectra of all six long duration sets, created by screening using the six duration metrics, are compared. The response spectra are all normalized to have $S_a(1.6\,\text{s}, 5\,\%) = 1\,\text{g}$, and are plotted against two common benchmark ground motion sets: the FEMA P695 far-field set (FEMA 2009b) and PEER Transportation set 2 (Baker et al. 2011). The record sets screened using I_D, CAV, and I_A (Figure 2.10a) are observed to have significantly different spectral shapes, when compared to the benchmark sets and the record sets screened using Ds_{5-75}, Ds_{5-95}, and $Ds_{0.05}$ (Figure 2.10b).

Finally, a qualitative comparison of the considered duration metrics is summarized in Table 2.3, where the metrics are judged according to several practical criteria. Based on this comparison, significant duration is identified as the preferred duration metric for use in ground motion selection for structural performance assessment. The choice between 5–75 % and 5–95 % significant duration is less clear, though in the case of the structural models considered in this study, the authors found 5–75 % significant duration to be slightly more robust since it consistently produced higher

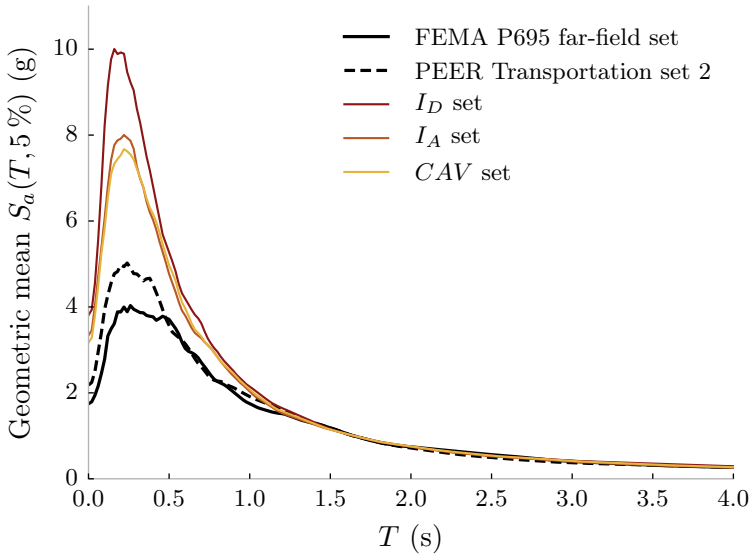

(a)

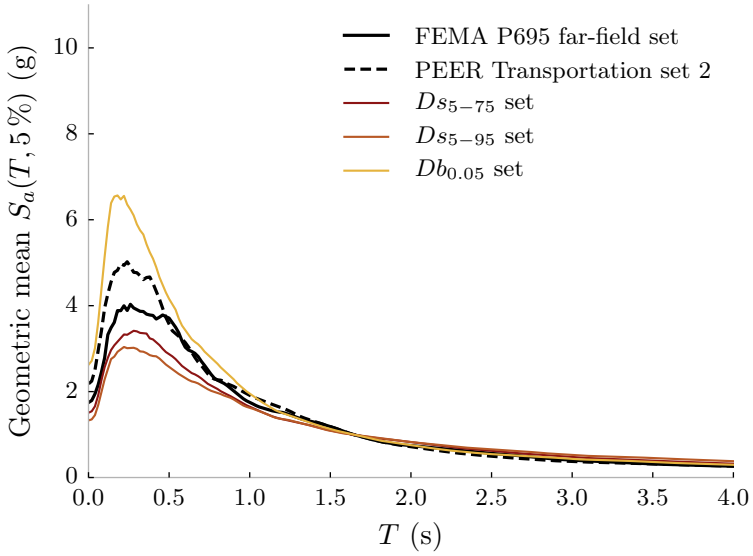

(b)

Figure 2.10: Comparison of the geometric mean response spectra of the long duration sets screened using all six duration metrics, to those of benchmark ground motion sets, scaled to have $S_a(1.6\,\text{s}, 5\,\%) = 1\,\text{g}$.

Table 2.3: Comparison of the characteristics of the duration metrics considered.

Desired characteristic	**Significant duration**	I_D	**Bracketed duration**	**Cumulative absolute velocity**	**Arias intensity**
Is not strongly correlated to common intensity measures	✓	✓	✗	✗	✗
Is not a hybrid metric of intensity and duration	✓	✓	✓	✗	✗
Is unaffected by scaling	✓	✓	✗	✗	✗
Is an efficient predictor of structural collapse capacity (R^2 statistic from Table 2.2 is not too low)	✓	✓	✓	✓	✓
All ground motions with large values of the metric actually have long intervals of strong shaking	✓	✓	✓	✗	✗
Ground motions with large values of the metric do not have unusual spectral shapes	✓	✗	✓	✗	✗

R^2 values in Table 2.2. As noted by Kempton and Stewart (2006), since 5–75 % significant duration is correlated to the duration of body wave arrivals alone, and 5–95 % significant duration is also influenced by the later surface wave arrivals, the choice between the two is expected to be structure dependent. Nevertheless, the procedure developed in this study can be used to assess the efficiency of any other duration metric in predicting structural collapse capacity.

2.7 Sensitivity analysis of the effect of duration to the parameters of a reinforced concrete bridge pier model

To investigate the interaction of structural characteristics with the effect of ground motion duration, a bridge pier structure was employed, since in contrast to the larger steel frame model, its fewer degrees of freedom facilitated systematic variation of structural model parameters. The base model is of a reinforced concrete bridge pier that was previously tested as part of the Concrete Column Blind Prediction Contest (PEER 2010a). The structure was modeled in OpenSees rev. 5184 (McKenna et al. 2006) using a linear elastic element connected to the base through a zero-length plastic hinge, following the Modified Ibarra-Medina-Krawinkler peak-oriented hysteretic model (Ibarra et al. 2005). Similar to the bilinear hysteretic model used in the five-story moment frame model, the peak-oriented model combines a post-peak negative stiffness branch of the backbone curve to capture in-cycle strain-softening and a cyclic model to capture strength and stiffness deterioration based on the cumulative hysteretic energy dissipated. The destabilizing $P-\Delta$ effect of gravity loads was incorporated in the model. A schematic of the model is shown in Figure 2.11a. The parameters of the model were calibrated to experimental measurements, the results of which are compared in Figure 2.11b. Its fundamental period is 1.2 s.

The spectrally equivalent, long and short duration record sets chosen based on Ds_{5-75} were used to conduct IDA on the base model. Collapse was indicated by an unbounded increase in peak chord rotations, above a threshold of 0.16 rad. The percentage decrease in the median collapse capacity estimated by the long duration set, with respect to the short duration set, is 17 %. This is in contrast to a decrease of 29 % reported previously for the moment frame.

To examine how the response of the bridge pier would vary depending on design parameters that control its strength, stiffness, or deformation capacity, the sensitivity of the effect of duration to two model parameters is examined. The two model

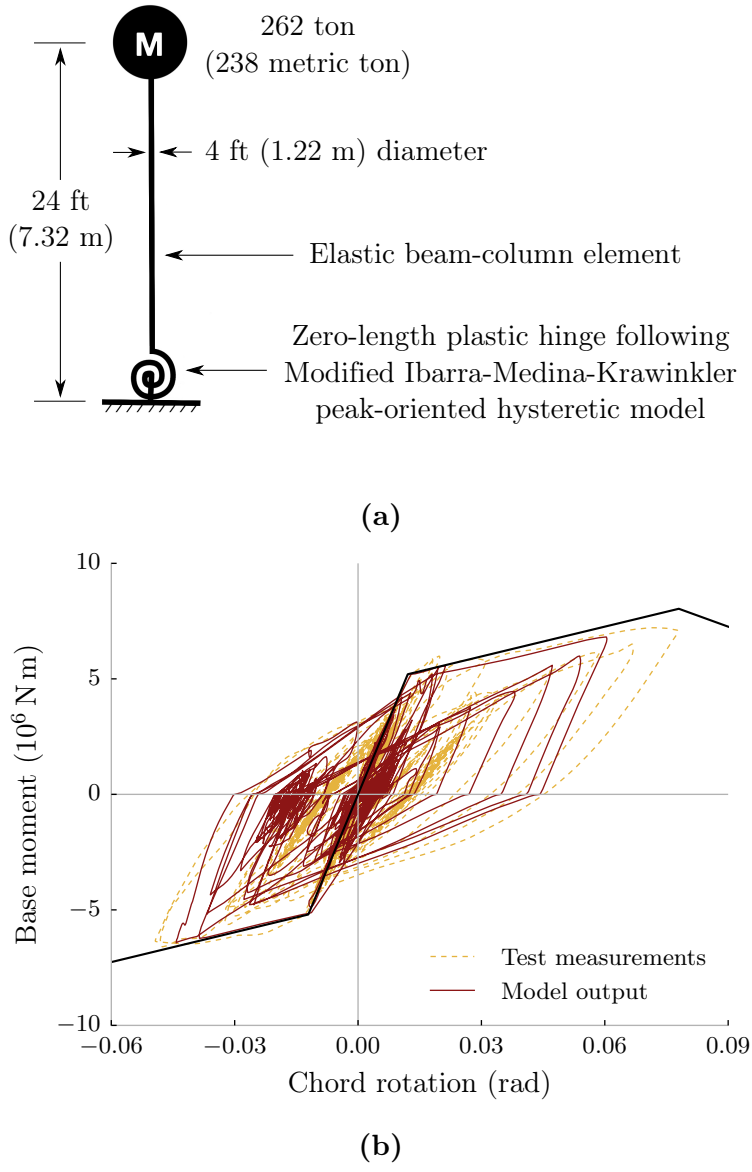

Figure 2.11: Reinforced concrete bridge pier: (a) Model schematic. (b) Calibration of model to test measurements.

parameters are γ and θ_p, both of which are expected to influence the cyclic deterioration and collapse response. The first parameter, γ, is a dimensionless factor used to define the rate of cyclic deterioration in the structure. The deterioration algorithm of the Modified Ibarra-Medina-Krawinkler hysteretic model first defines the reference hysteretic energy dissipation capacity of the structure, E_t, as

$$E_t = \gamma M_y \theta_y \tag{2.3}$$

where M_y is the yield moment and θ_y is the yield chord rotation of the structure. Thereafter, the structure's strength is deteriorated after every hysteretic excursion according to

$$M_i = (1 - \beta_i) M_{i-1} \tag{2.4}$$

$$\beta_i = \left(\frac{E_i}{E_t - \sum_{j=1}^{i} E_j} \right)^c \tag{2.5}$$

where E_i is the hysteretic energy dissipated in the i^{th} excursion, M_i is the deteriorated strength after the i^{th} excursion, and c is an exponent, commonly set to 1. The larger the value of γ, the larger the reference hysteretic energy dissipation capacity of the structure, and therefore, the slower the rate of deterioration. The second parameter, θ_p, is the plastic chord rotational capacity of the structure measured from the yield point to the peak point. The larger the value of θ_p, the more ductile the structure. The ranges over which γ and θ_p were varied in this study are based on the ranges of observed values of each parameter in a reinforced concrete column calibration study by Haselton et al. (2008).

The effect of duration in all subsequent analyses is quantified by the percentage decrease in median collapse capacity estimated by the long duration set, with respect to the short duration set. The variation of this difference in median collapse capacity with γ, with all other model parameters held constant, is plotted in Figure 2.12a. As shown, the value of γ for the base model is equal to 120, representing a well-confined, ductile bridge column. For lower values of γ, the influence of duration is more pronounced, with the difference in median collapse capacity increasing from 17 % for the

base model up to almost 33 % for columns with lower energy dissipation capacities. Under increasing γ, the difference in median collapse capacity tends to saturate at about 8 %. This reduced effect of duration with high γ is intuitively expected, and is consistent with many previous studies on duration that used numerical models that did not incorporate deterioration, and hence, observed little or no effect of duration. The residual reduction in median collapse capacity of about 8 % is presumably due to cyclic ratcheting effects, where the structure ultimately fails at large drifts by $P-\Delta$ effects. This so-called ratcheting effect has been observed previously by Gupta and Krawinkler (2000), and is expected to abet the collapse of a structure subjected to long duration shaking. This trend with energy dissipation appears to differ from that of a recently published study by Raghunandan and Liel (2013), the reasons for which are not obvious. The two studies are, however, not directly comparable due to differences in ground motion selection methodology, and the use of inelastic rather than elastic spectra as the ground motion intensity measure. The apparent differences point to a need for further understanding of the role of cyclic deterioration and collapse assessment methodology on the observed effect of duration.

The interaction of cyclic deterioration and duration of loading on collapse is further illustrated in Figure 2.13. Figures 2.13a and 2.13b compare the hysteretic response of the base model (with $\gamma = 120$) under typical short and long duration ground motions respectively, scaled to the onset of collapse. Since the structure subjected to the long duration ground motion experiences a larger number of hysteretic cycles, it deteriorates more, and thus, collapses at a lower ground motion intensity when compared to the short duration ground motion. Figure 2.13c shows the hysteretic response of the model with lesser energy dissipation capacity (with $\gamma = 40$) under the same long duration ground motion as Figure 2.13b. Comparing Figures 2.13b and 2.13c, the model that deteriorates faster leads to collapse at an even lower intensity.

The variation in the difference in median collapse capacity with θ_p is plotted in Figure 2.12b. Interestingly, here there is a near linear increase in the difference in median collapse capacity with increasing rotational capacity. This again follows intuition since a non-ductile structure (with low θ_p) would collapse soon after yielding,

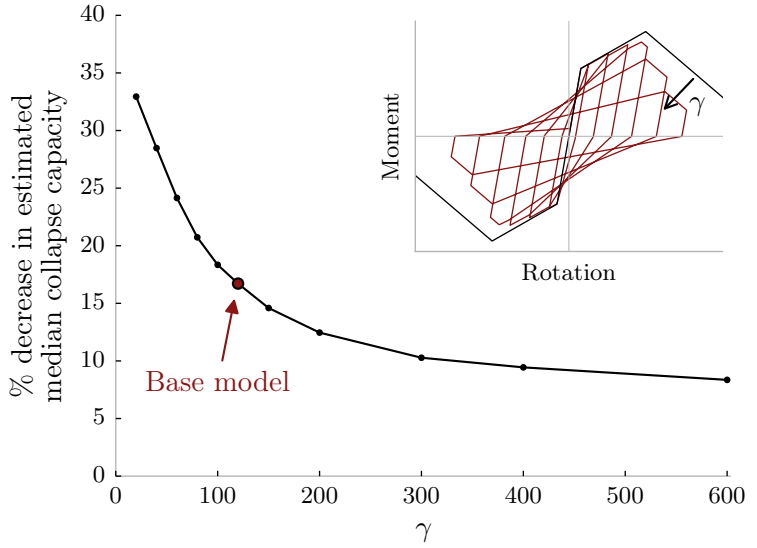

(a)

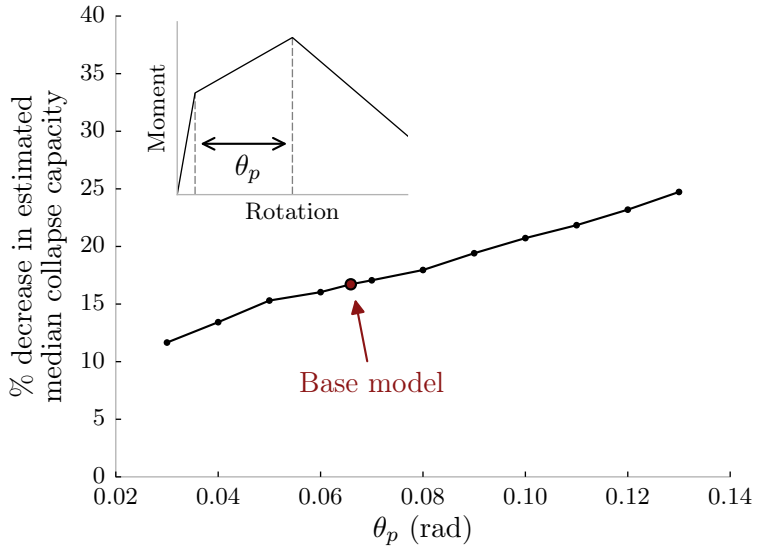

(b)

Figure 2.12: Sensitivity of the percentage decrease in median collapse capacity estimated by the long duration set, with respect to the short duration set, to (a) γ: parameter controlling the rate of deterioration, and (b) θ_p: the plastic rotational capacity from yield to capping.

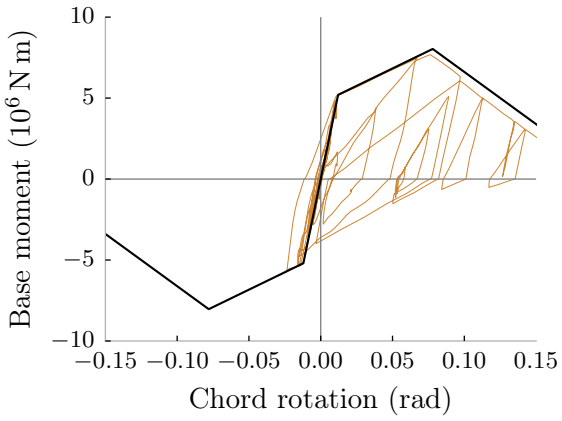

(a)

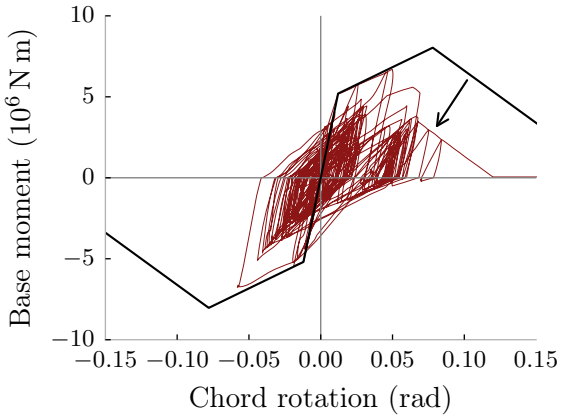

(b)

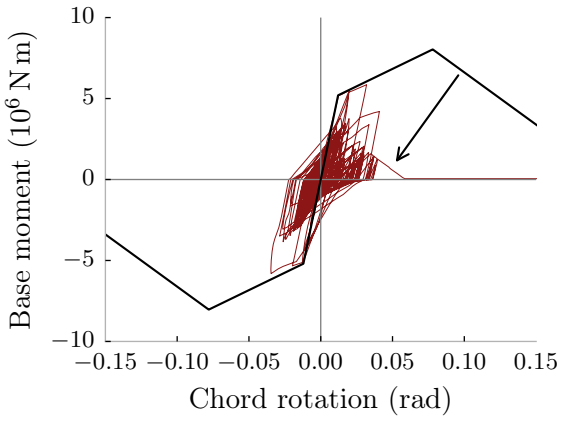

(c)

Figure 2.13: Hysteresis plots of the bridge pier chord rotation for (a) the base model (with $\gamma = 120$) under a short duration ground motion, (b) the base model (with $\gamma = 120$) under a long duration ground motion, and (c) a model with $\gamma = 40$ under same long duration ground motion, when scaled to the onset of collapse.

without much cyclic degradation, thus negating the influence of ground motion duration on collapse capacity. This result is consistent with the findings of Raghunandan and Liel (2013), suggesting that ground motion duration can have a more significant effect on modern, ductile structures than older, non-ductile structures.

2.8 Conclusion

Ground motion duration was found to exert a significant influence on structural collapse capacity. This effect was observable using numerical models that accurately characterized structural behavior at large non-linear deformations, including the in-cycle and cyclic deterioration of strength and stiffness of structural components, and destabilizing $P - \Delta$ effects. The effect of duration was isolated from the effects of other ground motion characteristics using "spectrally equivalent" sets of long and short duration records. A set of high intensity, long duration records from large magnitude earthquakes, including the 2011 Tohoku (Japan), 2010 Maule (Chile), and 2008 Wenchuan (China) earthquakes, was assembled. Each long duration record was paired with a spectrally equivalent short duration record. Each set contains 146 records, and the geometric mean 5–75 % significant duration of the short and long duration record sets are 6 s and 42 s, respectively.

Non-linear dynamic analyses of a five-story steel special moment frame revealed a 29 % decrease in median collapse capacity estimated by the long duration set, compared to the short duration set. Using the seismic hazard information for the building site, this was found to correspond to a three-fold increase in the estimated mean annual frequency of collapse, and a seven-fold increase in the probability of collapse at the MCE_R intensity. Statistics analyzing the spectrally equivalent record pairs indicated that the larger the difference in their durations, the lower the collapse capacity predicted by the long duration record with respect to the short duration record. Non-linear analyses of a ductile concrete bridge pier model showed a 17 % reduction in median collapse capacity estimated by the long duration set, compared to the short duration set. The reduction in collapse capacity with increasing ground

motion duration is in contrast to many previous studies that found little or no influence of duration on peak deformations, suggesting that the models employed in these prior studies may not have fully captured the deterioration of structural strength and stiffness, and/or the destabilizing $P - \Delta$ effect of gravity loads. The structures in these studies also may not have been deformed far enough into the inelastic range for them to experience significant deterioration and consequent destabilization. Parametric studies demonstrated how the influence of duration depends on ductility and deterioration parameters of the structural model. Structures exhibiting rapid cyclic deterioration and with greater deformation capacity were found to be more sensitive to duration.

The effect of duration on peak global deformations was only observed at intensity levels large enough to produce non-linear deformations that extend into the post-peak range of the plastic hinges (at story drift ratios on the order of 0.03 rad for the steel moment frame). For new structural designs, this is likely to only occur above the MCE_R intensity level. Therefore, for modern code-conforming structures, analyses conducted at or below the MCE_R level are not expected to detect ground motion duration effects. This is in spite of the fact that under more intense ground motions, longer duration shaking can reduce the collapse capacity. This raises concerns since the current practice of assessing structures by non-linear dynamic analyses at MCE_R intensities, using predominantly short duration ground motions, may lead to designs with lower margins against collapse in locations where long duration ground motions can be expected.

A comparison of duration metrics found significant duration to be the preferred duration metric for use in ground motion selection for structural performance assessment. Although 5–75 % significant duration was found to be slightly more robust than 5–95 % significant duration for the considered structural model, they both appear to be effective. A key consideration in this choice was that significant duration tends to be uncorrelated to ground motion intensity and response spectral shape, and thus, is convenient to consider as an additional independent parameter in vector seismic hazard analysis. The procedure developed here can also be used to assess the efficiency of any other duration metric in predicting structural collapse capacity.

This study highlights the need to consider ground motion duration, in addition to intensity and response spectral shape, in regions where significant hazard due to long duration shaking exists, such as locations susceptible to large magnitude, subduction zone earthquakes. Further research is warranted to assess the influence of duration on seismic risk, based on a complete characterization of the seismic hazard in such regions, including the durations of anticipated ground motions.

Chapter 3

Physical mechanisms underlying the influence of ground motion duration on structural collapse capacity

Adapted from Chandramohan, R., J. W. Baker, and G. G. Deierlein (2017). "Physical mechanisms underlying the influence of ground motion duration on structural collapse capacity". *16th World Conference on Earthquake Engineering*. Santiago, Chile.

3.1 Abstract

This study explores the physical mechanisms by which the duration of strong ground motion influences structural response. While a number of previous studies have found that ground motion duration influences only cumulative damage indices, and not peak structural deformations, a few recent studies that employed realistic, deteriorating structural models were able to demonstrate the effect of duration on peak deformations and structural collapse capacity. These recent studies were, however, empirical in nature and did not fully explore the reasons behind the observed effects

of duration. Many of the previous studies qualitatively attributed the effects to the cyclic deterioration of strength and stiffness of the structural components, which represents just one mechanism by which duration exerts its influence. In contrast, the present study shows that the gradual ratcheting of drifts, accentuated by the destabilizing $P-\Delta$ effect, is an equally important mechanism by which duration influences structural response. The relative contributions of the two mechanisms—cyclic deterioration and ratcheting—to the observed influence of duration on the collapse capacity of a five-story steel moment frame building, are quantified by conducting incremental dynamic analysis (IDA) using spectrally equivalent sets of long and short duration ground motions. The use of spectrally equivalent ground motions allows controlling for the effect of response spectral shape. A response parameter called the ratcheting interval is defined and used to explain the larger potential for a long duration ground motion to cause structural collapse, when compared to a spectrally equivalent short duration ground motion scaled to the same intensity level. These findings shed light on the interaction between structural model characteristics and the observed influence of ground motion duration on structural response. In addition, they highlight the importance of using models that capture both cyclic deterioration and the $P-\Delta$ effect to reliably account for the effect of ground motion duration when assessing structural collapse risk.

3.2 Introduction

A number of past and recent research efforts have focused on analyzing the influence of ground motion duration on structural response (Hancock and Bommer 2006). As expected, many of them found duration to be strongly correlated to cumulative damage metrics like total dissipated hysteretic energy and accumulated plastic strain. Since a number of these studies employed simplistic, non-deteriorating structural models, however, they did not observe any effect of duration on peak structural deformations (e.g., Cornell 1997; Bommer et al. 2004; Iervolino et al. 2006; Hancock and Bommer 2007; Oyarzo-Vera and Chouw 2008; Raghunandan and Liel 2013; Barbosa et al. 2014; Hou and Qu 2015; Mantawy and Anderson 2015). In light of these findings, and

the prevalent use of acceptance criteria for structural design and assessment based on peak structural deformations, ground motion duration is not explicitly considered in current structural design and assessment standards (e.g., PEER TBI 2010; NIST 2011; ASCE 2016).

Recent studies by the authors and others, using more realistic structural models that simulate structural behavior at large nonlinear deformations more accurately, have, however, demonstrated that duration does influence peak structural deformations (e.g., Raghunandan and Liel 2013; Chapter 2/ Chandramohan et al. 2016b). This effect of duration was observed at ground motion intensities large enough to produce significant inelastic deformations, thereby manifesting itself as a reduction in the collapse capacity of a structure when analyzed under long duration ground motions. These observations are, however, empirical in nature, and do not examine the physical mechanisms underlying the observed effect of duration. While most studies qualitatively attribute the effect of duration to the deterioration in strength and stiffness of structural components under cyclic loading (e.g., Bommer et al. 2004; Beyer and Bommer 2007; Chapter 2/Chandramohan et al. 2016b; Marafi et al. 2016), few have examined the contributions of other mechanisms or attempted to quantify their relative contributions.

The objective of this study is to obtain a deeper understanding of the reasons underlying the observed influence of ground motion duration on structural collapse capacity, i.e., the physical mechanisms that enable long duration ground motions to cause structural collapse at lower intensity levels than short duration ground motions. While structural deterioration is definitely expected to be an important factor, the gradual ratcheting of drifts, exacerbated by the destabilizing $P-\Delta$ effect of gravity loads (Gupta and Krawinkler 2000), has also been observed to play a significant role. Although ASCE 41-13 (ASCE 2013, p. 98), Chapter 2/Chandramohan et al. (2016b), Mahin (1980), Takizawa and Jennings (1980), Hancock and Bommer (2006), PEER (2010b) (p. 2-34), and ASCE (2013) (p. 98) have previously alluded to the possible amplification of deformations under long duration ground motions due to the $P-\Delta$ effect, the actual mechanism by which long duration ground motions influence structural collapse by ratcheting has not yet been investigated. This study

quantifies the relative contributions of deterioration and ratcheting to the sensitivity of a ductile five-story steel moment frame building to ground motion duration. The effect of duration on the collapse capacity of the structure is quantified using sets of spectrally equivalent long and short duration ground motions, which help control for the effect of response spectral shape (Chapter 2/Chandramohan et al. 2016b). The relative contribution of each physical mechanism is evaluated by analyzing a series of different permutations of the original structural model. A response parameter called the *ratcheting interval*, computed from a smoothed story drift ratio (SDR) time history, is introduced and employed to explain the larger potential for a long duration ground motion to cause structural collapse by ratcheting, when compared to a spectrally equivalent short duration ground motion scaled to the same intensity level.

3.3 Steel moment frame model

A ductile five-story steel moment frame building, located in San Francisco, and previously analyzed in Chapter 2/Chandramohan et al. (2016b) and FEMA (2014), was chosen to demonstrate the contributions of the deterioration and ratcheting mechanisms to the observed effect of duration on structural collapse capacity. The frame was designed with strong columns and relatively weak beams with RBS hinges, as illustrated in Figure 3.1. The large strong-column-weak-beam ratio ensures sufficient engagement of all stories under earthquake excitation, without forming any story mechanisms, i.e., without any localization of plastic deformation at only a few stories. Consequently, structural collapse always occurs in the same sidesway collapse mechanism involving all stories, irrespective of whether it is caused by a short or long duration ground motion. Controlling the collapse mechanism in this manner helped prevent any differences in the collapse mechanism when analyzing the structure under long and short duration ground motions, from confounding the results. Results obtained using this structure are also expected to be representative of other modern, code-conforming structures.

A two-dimensional centerline model of the structure was created and analyzed

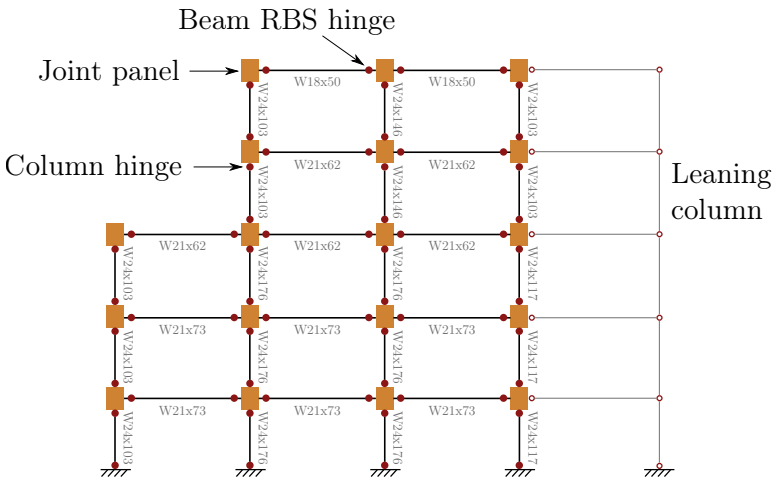

Figure 3.1: Schematic of the numerical model of the five-story steel special moment frame building.

using OpenSees rev. 5184 (McKenna et al. 2006). A schematic of this model is illustrated in Figure 3.1. Each story of the structure is 3.96 m tall, and each bay is 8.84 m wide. The beams and columns were modeled using linear elastic elements, with all the inelastic deformation concentrated in zero-length plastic hinges located at the RBS hinges on each beam, and at the ends of each column. The hysteretic behavior of the plastic hinges was modeled using the bilinear Ibarra-Medina-Krawinkler hysteretic model (Ibarra et al. 2005), modified as per the recommendations of Lignos and Krawinkler (2012). This model incorporates (*i*) a post-capping negative stiffness branch of the backbone curve to capture in-cycle deterioration; and (*ii*) an algorithm to cyclically deteriorate both strength and stiffness based on the cumulative hysteretic energy dissipated. The parameters of the model were computed using the equations proposed by Lignos and Krawinkler (2011). The hysteretic shear behavior of the finite panel zones was modeled using a trilinear backbone curve, whose parameters were computed using the equations described in FEMA (2000). Geometric nonlinearity was modeled using a small-displacement, linear $P-\Delta$ formulation, and the contribution of the adjacent gravity frame to the destabilizing $P-\Delta$ effect was captured using a pin-connected leaning column. A linear viscous damping ratio of 2 % of

critical was assigned to the linear elastic elements only, as recommended by Charney (2008). The elastic fundamental period of the structure is 1.64 s. All response history analyses of the structure were carried out using the explicit central difference time integration scheme, since it was found to be more robust and efficient than implicit time integration schemes, which sometimes failed to converge (Chapter 7).

3.4 Spectrally equivalent long and short duration record sets

This study employs 5–75 % significant duration (Ds_{5-75}) (Trifunac and Brady 1975) to quantify the duration of strong shaking contained in an accelerogram. This metric was shown to be better suited than other duration metrics to guide the selection of ground motions for structural collapse capacity estimation, in a previous study by the authors (Chapter 2/Chandramohan et al. 2016b). It is defined as the time interval over which 5 % to 75 % of the integral $\int_0^{t_{max}} a^2(t)dt$ is accumulated, where $a(t)$ represents the ground acceleration at time t, and t_{max} represents the length of the accelerogram.

The FEMA P695 (FEMA 2009b) far-field record set consists of 22 orthogonal pairs of horizontal ground motions (44 individual components) recorded from shallow crustal earthquakes. Since all 44 records in this set are of relatively short duration (with $Ds_{5-75} < 25$ s), it will henceforth be referred to as the short duration set. Corresponding to each individual ground motion in the short duration set, a companion long duration ground motion (with $Ds_{5-75} > 25$ s) with a closely matching response spectral shape was selected to form a spectrally equivalent long duration set. These long duration ground motions were selected from a database consisting of more than 4000 ground motions recorded from large magnitude earthquakes like 2010 Maule (Chile), 2011 Tohoku (Japan), and 2008 Wenchuan (China). A procedure similar to the one described in Chapter 2/Chandramohan et al. (2016b) was followed to find the long duration record from the database with the closest matching response spectral

shape, while imposing an upper limit of 5.0 on the intensity scaling factor. The response spectra and acceleration time histories of one of the spectrally equivalent long and short duration record pairs are plotted in Figure 3.2; histograms of the durations of the ground motions in the two sets are plotted in Figure 3.3. Detailed information regarding the short and long duration record sets, including response spectra and time series plots, is provided in Appendix A. Since the records in the two sets are selected to have equivalent response spectra, it is assumed that any observed differences in the response of a structure analyzed using them can be attributed to the difference in their durations. It was shown in Chapter 2/Chandramohan et al. (2016b) that this record selection procedure does not introduce any significant biases with respect to other ground motion characteristics that may influence structural response.

3.5 Relative contributions of cyclic deterioration and the $P-\Delta$ effect to the observed influence of duration

The long and short duration record sets were each used to estimate the median collapse capacity of the steel moment frame building by conducting incremental dynamic analysis (IDA) (Vamvatsikos and Cornell 2002). This entails incrementally scaling each ground motion to higher intensity levels until it causes structural collapse, which is indicated by the unbounded increase in the story drift ratio (SDR) at any story above a threshold of 0.10. The lowest $S_a(1.64\,\mathrm{s})$ value that a ground motion needs to be scaled to, to cause structural collapse, is called its *collapse intensity*; where $S_a(1.64\,\mathrm{s})$ represents the 5 % damped pseudo spectral acceleration at the elastic fundamental period of the structure. The median collapse capacity of the structure is then estimated as the geometric mean of the collapse intensities of all the ground motions in a set, assuming the structural collapse capacity follows a lognormal distribution. The median collapse capacity of the structure was estimated as 0.98 g using the short duration set and 0.71 g using the long duration set. The lower median collapse capacity estimated the long duration records implies that they are inherently

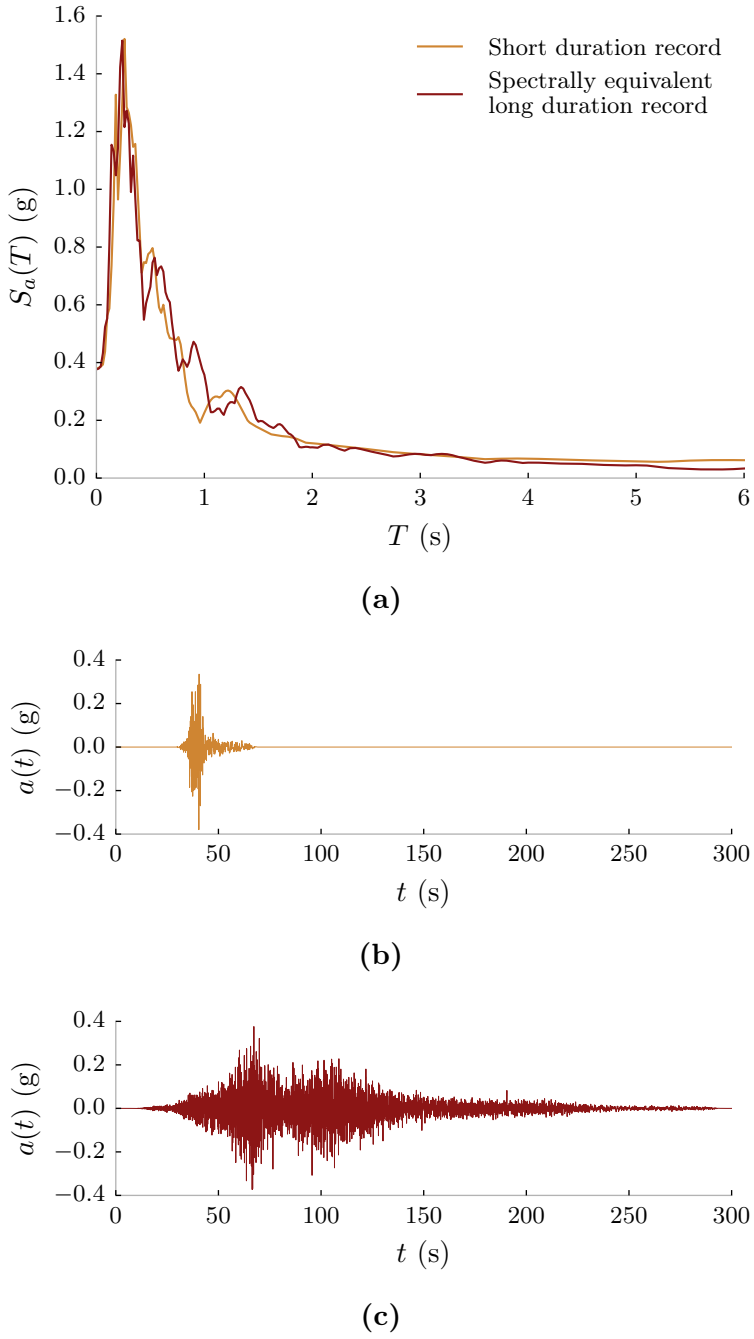

Figure 3.2: Comparison of the (a) response spectra and acceleration time histories of the (b) short and (c) long duration ground motions constituting one of the 44 spectrally equivalent record pairs. The short duration ground motion is from the 1979 Imperial Valley (USA) earthquake, recorded at the El Centro Array #11 station, and has a Ds_{5-75} of 5 s. The long duration ground motion is from the 2011 Tohoku (Japan) earthquake, recorded at the Nagawa (AOMH17) station, scaled by a factor of 2.76, and has a Ds_{5-75} of 53 s.

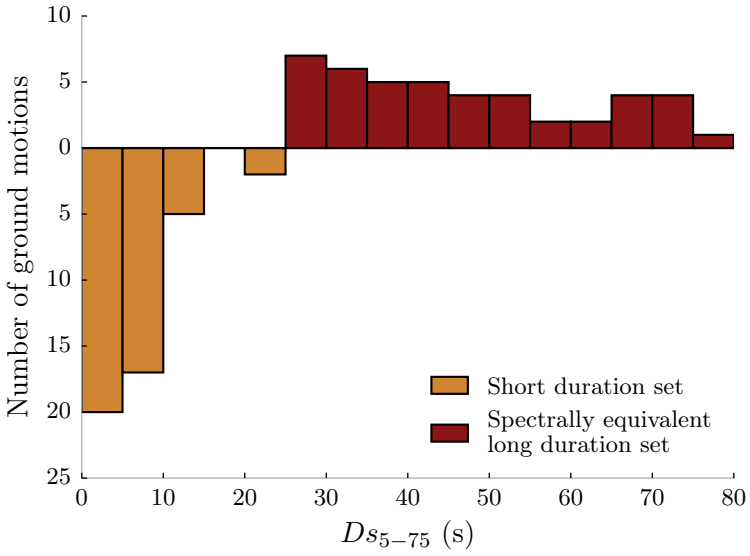

Figure 3.3: Histograms of the 5–75 % significant durations (Ds_{5-75}) of the ground motions in the spectrally equivalent long and short duration record sets.

more damaging than the short duration records. Since the two sets are spectrally equivalent, the 28 % difference in estimated median collapse capacity is a measure of the influence of ground motion duration on structural collapse capacity.

The characteristics of the structural model that enabled the effect of duration to be observed were identified by repeating the analysis using various permutations of the structural model. To assess the contribution of cyclic deterioration to the observed effect of duration, a modified version of the structural model was re-analyzed with the cyclic deterioration of the strength and stiffness of all the plastic hinges disabled. The effect of duration on structural collapse capacity in these analyses was reduced to 18 % from the original 28 %. This residual effect of duration alludes to the existence of mechanisms other than cyclic deterioration by which duration influences structural response. The contribution of the $P-\Delta$ effect was investigated next by repeating the analysis using a version of the structural model with cyclic deterioration enabled, but the $P-\Delta$ effect disabled. The influence of duration on structural collapse capacity was computed to be 17 % in this case, which is nearly equal to the value obtained when only cyclic deterioration was disabled, implying that both cyclic deterioration

and the $P-\Delta$ effect contribute nearly equally to the observed influence of duration on the steel moment frame building. Finally, when both cyclic deterioration and the $P-\Delta$ effect are disabled, the effect of duration is reduced to $-1\,\%$, which is very close to zero. This implies that cyclic deterioration and the $P-\Delta$ effect are the two major contributors to the observed effect of duration, and that both their contributions are equally significant. Ignoring either of the two characteristics when modeling a structure could, therefore, result in inaccurate structural collapse risk estimates. It is worth noting that for the analyses conducted on structural models with the $P-\Delta$ effect disabled, the IDA curves do not flatten, i.e., collapse by dynamic instability is not simulated at or below a peak SDR of 0.10. Nonetheless, the collapse peak SDR threshold of 0.10 is still enforced to maintain consistency with the other cases. The median collapse capacities computed using each record set for all four structural model permutations discussed above, are summarized in Table 3.1. The reason why the deterioration in component strength and stiffness over subsequent inelastic cycles could enable longer duration ground motions to cause structural collapse when scaled to lower intensities, is fairly obvious. The reason why modeling the $P-\Delta$ effect should produce a similar result is, however, not as intuitive. It is hypothesized that the $P-\Delta$ effect enables long duration ground motions to cause structural collapse by ratcheting.

3.6 Effect of duration explained by the ratcheting collapse mechanism

Ratcheting is a mode of sidesway collapse observed in ductile structures, whereby an initial inelastic excursion in one direction, concentrated in one or more stories, produces amplified $P-\Delta$ moments in that direction. These $P-\Delta$ moments encourage further inelastic deformation to occur in the same direction under continued ground excitation, thereby producing even larger $P-\Delta$ moments, which finally lead to dynamic instability and sidesway collapse. Structural collapse by ratcheting can, therefore, be broadly viewed as a two-stage process: (i) the creation of an initial

Table 3.1: Summary of the median collapse capacities of the steel moment frame building estimated using the two spectrally equivalent record sets for all considered structural model permutations. The effect of duration is computed for each case as the percentage decrease in the median collapse capacity estimated using the long duration set, with respect to the short duration set.

Structural model incorporates		**Median collapse capacity estimated using**		**Percentage decrease in median collapse capacity**
Deterioration	**$P-\Delta$ effect**	**Short duration set** (g)	**Long duration set** (g)	
✓	✓	0.98	0.71	28
	✓	1.02	0.84	18
✓		1.15	0.95	17
		1.23	1.24	−1

inelastic excursion, whose magnitude is primarily a function of the ground motion intensity; and (*ii*) the subsequent gradual amplification of drifts due to the $P-\Delta$ moments, which is primarily a function of the duration of strong shaking following the initial excursion. Short duration ground motions cause structural collapse at relatively large ground motion intensities since they rely on large initial inelastic excursions to cause dynamic instability. Long duration ground motions, on the other hand, are able to cause structural collapse at lower ground motion intensities since the smaller initial inelastic excursions produced at these lower intensities are gradually amplified by ratcheting until the eventual onset of dynamic instability later in the time series. A response parameter called the *ratcheting interval* is defined below and used to illustrate this phenomenon.

The ratcheting interval is computed from the SDR time history at the story where the collapse threshold is first exceeded. Hence, it is computable only when the ground motion is scaled at or above its collapse intensity. The SDR time history is first smoothed using the locally weighted scatterplot smoothing (LOWESS) (Cleveland

1979) technique as demonstrated in Figures 3.4a, 3.4b, and 3.4c. The ratcheting interval is then computed as the time elapsed from the last point where the smoothed SDR time history exceeds a threshold of 0.01 until the first point where the actual SDR time history exceeds the collapse threshold of 0.10. It is an approximate measure of the time interval over which drifts are amplified by ratcheting before sidesway collapse due to dynamic instability occurs. Smoothed and thresholded SDR time histories computed from all the long and short duration ground motions, scaled to their respective collapse intensities, are plotted in Figure 3.5a. Histograms of the ratcheting intervals computed from these smoothed time histories are plotted in Figure 3.5b. The long duration ground motions are observed to exhibit longer ratcheting intervals (median of 22 s) on average, when compared to the short duration ground motions (median of 8 s), implying that the ratcheting collapse mode is more dominant under the long duration ground motions when they are each scaled to their respective collapse intensities. It is worth noting that the ground motion collapse intensities were estimated to a precision of 0.01 g when conducting IDA, and longer ratcheting intervals may have been computed for some ground motions if their collapse intensities were estimated to a finer precision. This is not, however, expected to significantly influence the obtained results.

As demonstrated in Figure 3.4, when the long duration ground motions are scaled above their respective collapse intensities, the ratcheting intervals they produce tend to decrease. Therefore, as they are incrementally scaled above their collapse intensities, the mode of collapse they trigger transitions closer to what was observed under the short duration ground motions. The decreasing trend in the median ratcheting intervals produced by the long and short duration records as they are scaled above their collapse intensities, is evident from Figure 3.6. The reason why the median ratcheting interval produced by the long duration records oscillates and saturates beyond a geometric mean $S_a(1.64\,\text{s})$ of about 1.00 g, is discussed later. The median was chosen over the geometric mean to summarize the ratcheting intervals, since it is not affected in instances when ground motions produce a ratcheting interval of 0 s. Ground motions that did not cause structural collapse when scaled to certain intensity levels above their collapse intensities, by a phenomenon called resurrection

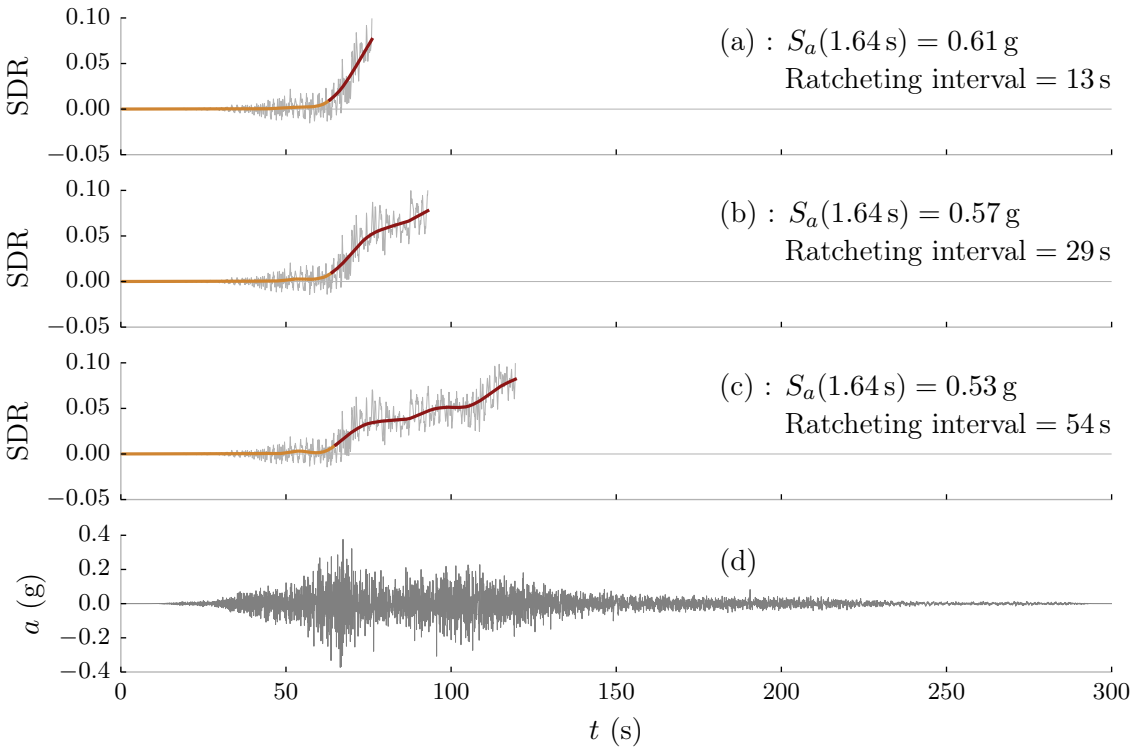

Figure 3.4: Smoothed time histories of the SDR at the fifth story, under the long duration ground motion from the 2011 Tohoku (Japan) earthquake, recorded at the Nagawa (AOMH17) station, scaled to (c) its collapse intensity level: $S_a(1.64\,\mathrm{s}) = 0.53\,\mathrm{g}$, and two higher intensity levels: (b) 0.57 g and (a) 0.61 g. The parts of the smoothed SDR time histories used to compute the ratcheting interval are plotted in red. The original accelerogram, scaled by a factor of 2.76 (the scale factor used during record selection), is plotted in (d).

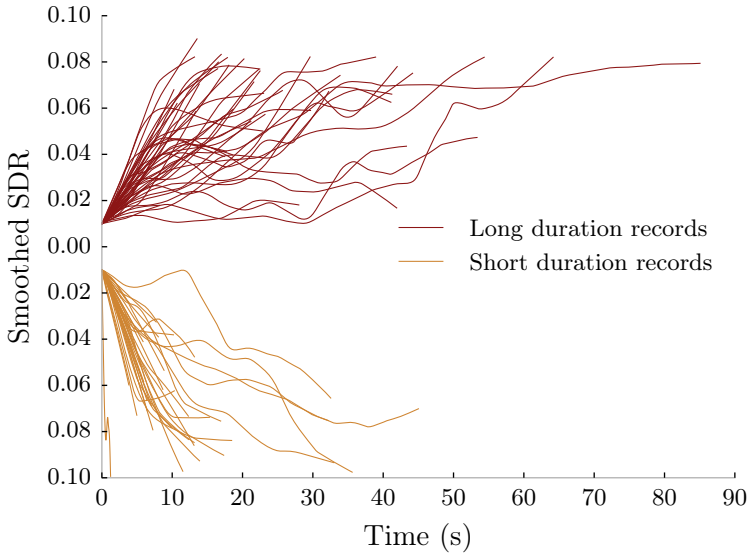

(a)

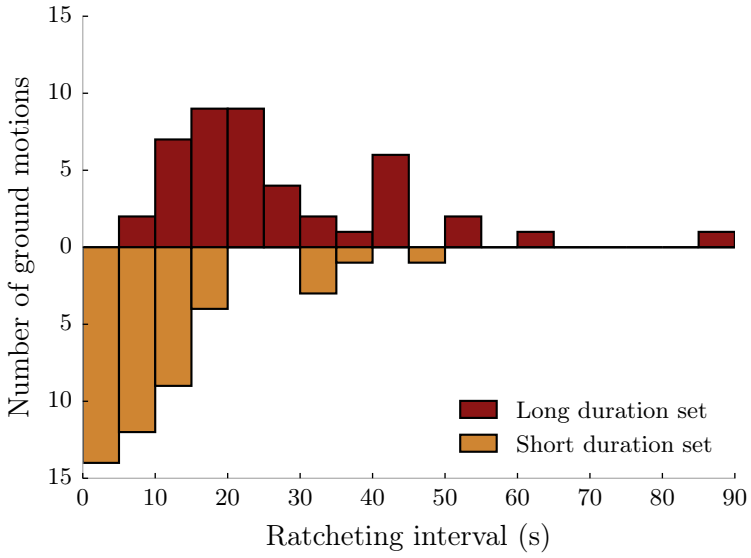

(b)

Figure 3.5: (a) Smoothed SDR time histories at the controlling story under all ground motion from the two sets scaled to their respective collapse intensities, plotted from the last point the smoothed time history exceeds a threshold of 0.01, until the first point the actual SDR time history exceeds the collapse threshold of 0.10; and (b) histograms of the ratcheting intervals computed from these smoothed and thresholded SDR time histories.

(Vamvatsikos and Cornell 2002), were excluded from the computation of the median ratcheting interval at that intensity level. When the long duration records are scaled such that their geometric mean $S_a(1.64\,\text{s})$ value is close to 0.98 g: the geometric mean collapse intensity of the short duration records, they produce a median ratcheting interval almost equal to that produced by the short duration records scaled to their respective collapse intensities. In other words, at this intensity level, both long and short duration ground motions trigger similar modes of collapse. Therefore, as the long duration records are scaled above their collapse intensities, the initial inelastic excursions they produce become large enough to cause structural collapse due to dynamic instability earlier in the time series, in a manner similar to the short duration ground motions. The remaining duration of strong shaking contained in the long duration accelerograms represents their unused, redundant potential to cause structural collapse by ratcheting. This helps explain why a long duration ground motion is more likely to cause structural collapse than a short duration ground motion with a similar response spectral shape, scaled to the same intensity level, as observed previously in Chapter 2/Chandramohan et al. (2016b) and Chapter 4/Chandramohan et al. (2016a).

The reason why the median ratcheting interval produced by the long duration ground motions oscillates and saturates beyond a geometric mean $S_a(1.64\,\text{s})$ of about 1.00 g, is demonstrated using a representative long duration ground motion in Figure 3.7. The expected decrease in ratcheting interval is observed as it is scaled from its collapse intensity of $S_a(1.64\,\text{s}) = 0.76$ g to 0.96 g. When scaled up to 1.18 g though, the ratcheting interval increases since an earlier inelastic excursion has now grown large enough to initiate the ratcheting of drifts until eventual collapse. This phenomenon is responsible for the oscillations in the median ratcheting interval produced by the long duration ground motions, observed in Figure 3.6. As the ground motion is scaled up to 1.52 g, which is twice the collapse intensity level, the ratcheting interval decreases again, as expected. The ratcheting interval does not decrease much below 18 s as it is scaled further above 1.52 g, however, because of the unique nature of the initial portion of the long duration accelerogram, depicted in Figure 3.7e. The gradual ramp in the amplitude of successive ground acceleration cycles over a duration of

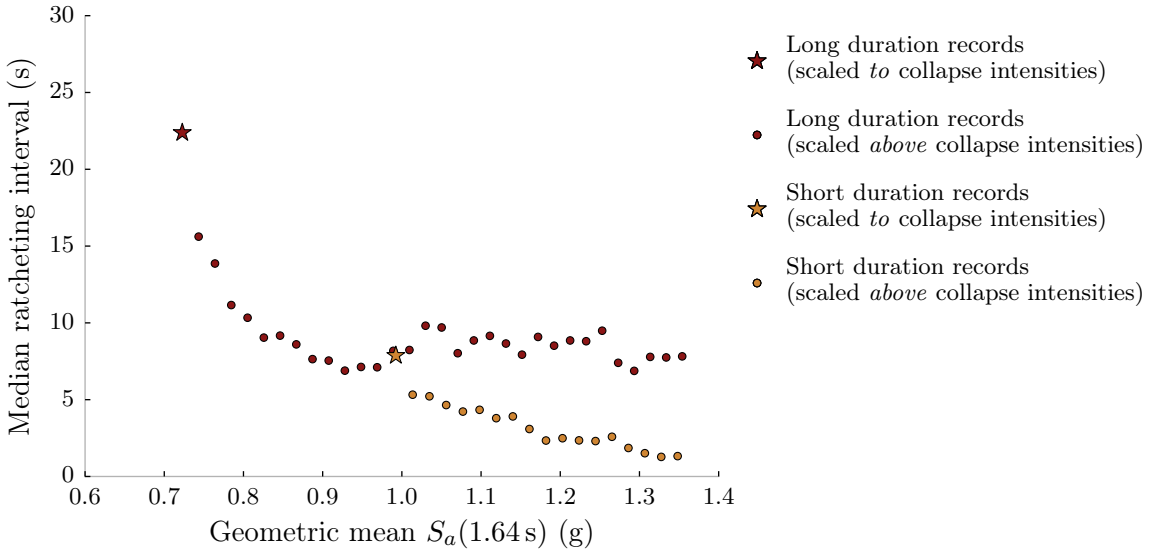

Figure 3.6: The median ratcheting intervals produced by the long and short duration records are plotted against their respective geometric mean collapse intensities as stars. The median ratcheting intervals produced by the records in both sets as they are incrementally scaled above their collapse intensities, are plotted as circles.

about 20 s ensures that the smaller initial cycles are not capable of producing inelastic excursions large enough to initiate ratcheting. This is the reason why the median ratcheting interval of the long duration ground motions saturate at around 10 s, and do not approach 0 s like the short duration ground motions.

3.7 Conclusion

The cyclic deterioration in strength and stiffness of structural components and the ratcheting of drifts due to the $P-\Delta$ effect were shown to be the two major mechanisms by which ground motion duration exerts an influence on the collapse capacity of a ductile five-story steel moment frame building. The relative contributions of these two mechanisms to the total observed effect of duration were quantified by conducting incremental dynamic analysis on several permutations of a numerical model of the steel moment frame building, using spectrally equivalent long and short duration record sets. These record sets allowed assessing the influence of duration on structural

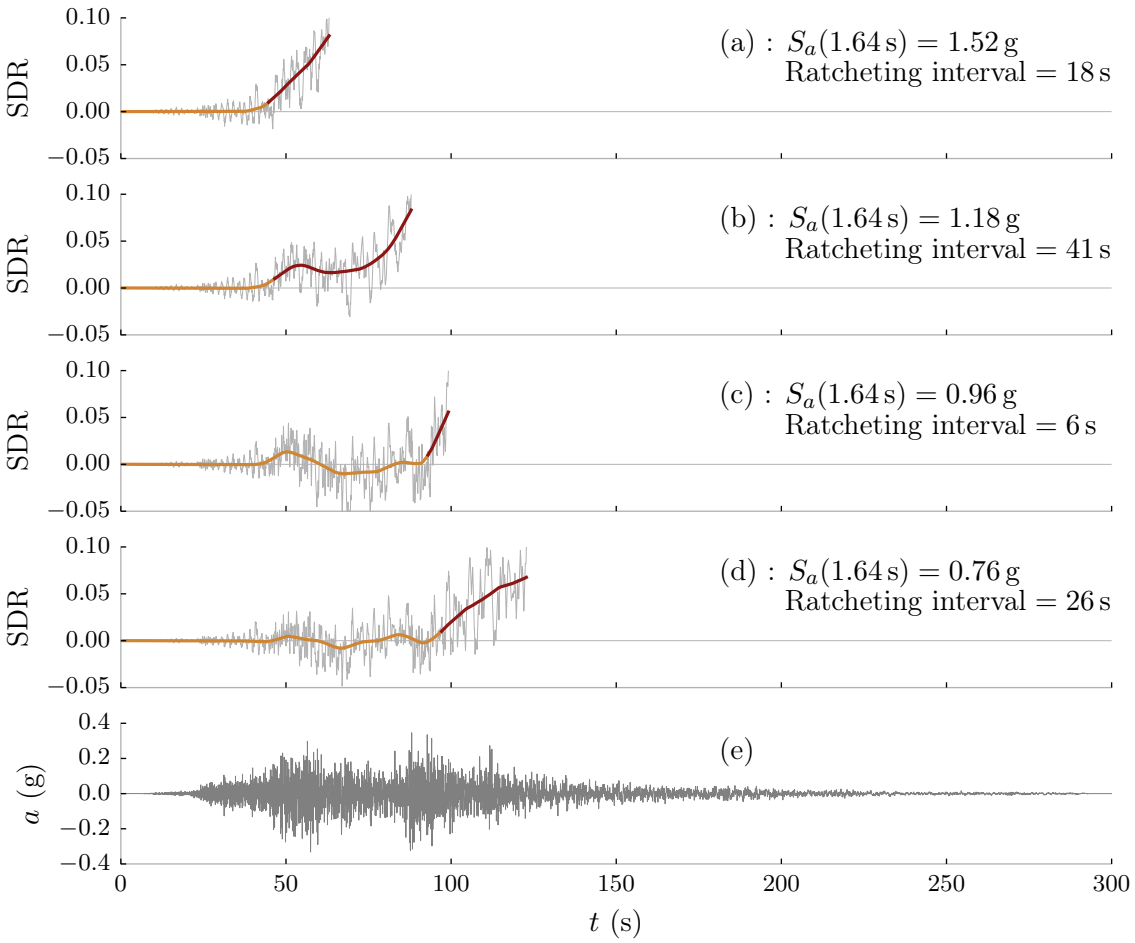

Figure 3.7: Smoothed time histories of the SDR at the fifth story, under the long duration ground motion from the 2011 Tohoku (Japan) earthquake, recorded at the Kakunodate (AKT014) station, scaled to (d) its collapse intensity level: $S_a(1.64\,\mathrm{s}) = 0.76\,\mathrm{g}$, and three higher intensity levels: (c) 0.96 g, (b) 1.18 g and (a) 1.52 g. The parts of the smoothed SDR time histories used to compute the ratcheting interval are plotted in red. The original accelerogram, scaled by a factor of 5.00 (the scale factor used during record selection), is plotted in (e).

collapse capacity while controlling for the effect of response spectral shape. The analysis revealed that both mechanisms contributed almost equally to the observed effect of duration. A response parameter called the ratcheting interval was defined and used to describe how the gradual ratcheting of drifts due to $P-\Delta$ moments can enable a long duration ground motion to cause structural collapse when scaled to a lower intensity level, compared to a short duration ground motion with a similar response spectral shape.

These findings highlight the importance of using structural models that incorporate both cyclic deterioration and the $P-\Delta$ effect, in conjunction with ground motions of durations that closely represent the seismic hazard at the site, to accurately estimate structural collapse risk. While modeling the $P-\Delta$ effect is relatively straightforward and fairly commonplace, accounting for cyclic deterioration poses a few additional challenges. The modified Ibarra-Medina-Krawinkler hysteretic model employed in this study adopts a phenomenological approach to modeling the strength and stiffness deterioration of structural components. For the analyzed steel moment frame, this entails simulating a number of deterioration modes like local flange and web buckling, lateral-torsional buckling, and crack initiation and propagation until fracture (Krawinkler and Zohrei 1983; Deierlein et al. 2010), using a phenomenological deterioration algorithm. Owing to the complexity of this behavior, the model parameters controlling component deterioration are associated with a relatively large degree of uncertainty (Lignos and Krawinkler 2011). This motivates the need to develop and use more realistic physics-based models that explicitly simulate the dominant modes of deterioration. Efforts to calibrate the Ibarra-Medina-Krawinkler hysteretic model, undertaken by Lignos and Krawinkler (2011), used measurements from experimental tests that employed cyclic loading protocols derived predominantly from short duration ground motions (Bazaez and Dusicka 2016). Structural components are, however, expected to exhibit different hysteretic behavior under loading protocols developed to simulate long duration ground motions (FEMA 2009a; Krawinkler 2009; Bazaez and Dusicka 2016). The observation that structural collapse under long duration ground motions occurs predominantly by the gradual, unidirectional ratcheting of drifts, also suggests that long duration cyclic loading protocols used to calibrate and validate

analysis models should consider unsymmetrical loading response. Hence, the applicability of the equations developed to predict median model parameters as functions of member characteristics, when simulating structural response under long duration ground motions, requires further investigation.

Chapter 4

Impact of hazard-consistent ground motion duration in structural collapse risk assessment

Adapted from Chandramohan, R., J. W. Baker, and G. G. Deierlein (2016). "Impact of hazard-consistent ground motion duration in structural collapse risk assessment". *Earthquake Engineering & Structural Dynamics* **45** (8), pp. 1357–1379. DOI: 10.1002/eqe.2711.

4.1 Abstract

This study evaluates the effect of considering ground motion duration when selecting hazard-consistent ground motions for structural collapse risk assessment. A procedure to compute source-specific probability distributions of the durations of ground motions anticipated at a site, based on the generalized conditional intensity measure (GCIM) framework, is developed. Targets are computed for three sites in Western USA, located in distinct tectonic settings: Seattle, Eugene, and San Francisco. The effect of considering duration when estimating the collapse risk of a ductile reinforced concrete moment frame building, designed for a site in Seattle, is quantified by conducting multiple stripe analyses using groups of ground motions selected using

different procedures. The mean annual frequency of collapse ($\lambda_{collapse}$) in Seattle is found to be underestimated by 29 % when using typical-duration ground motions from the PEER NGA-West2 database. The effect of duration is even more important in sites like Eugene ($\lambda_{collapse}$ underestimated by 59 %), where the seismic hazard is dominated by large magnitude interface earthquakes, and less important in sites like San Francisco ($\lambda_{collapse}$ underestimated by 7 %), where the seismic hazard is dominated by crustal earthquakes. Ground motion selection procedures that employ causal parameters like magnitude, distance, and Vs_{30} as surrogates for ground motion duration are also evaluated. These procedures are found to produce poor fits to the duration and response spectrum targets due to the limited number of records that satisfy typical constraints imposed on the ranges of the causal parameters. As a consequence, ground motions selected based on causal parameters are found to overestimate $\lambda_{collapse}$ by 53 %.

4.2 Introduction

Several questions related to the significance of the duration of strong ground motion often arise when considering the performance of buildings in regions susceptible to large magnitude earthquakes ($M_W \sim 9.0$). By how much does ground motion duration affect the collapse safety of buildings subjected to large magnitude earthquakes? How might one incorporate ground motion duration into seismic hazard analysis and structural collapse risk assessment? These questions and related issues are examined through illustrated assessments of buildings located at three sites in Western USA with distinct seismic hazards: Seattle (Washington), Eugene (Oregon), and San Francisco (California).

A recent study by Chapter 2/Chandramohan et al. (2016b) demonstrated that the probability of structural collapse is larger under a long duration ground motion than a short duration ground motion with an equivalent response spectrum. This finding corroborates investigations by Raghunandan and Liel (2013), but is in contrast to most other previous studies (e.g., Bommer et al. 2004; Hancock and Bommer 2006; Iervolino et al. 2006; Hancock and Bommer 2007), which concluded that ground

motion duration does not influence peak structural deformations. A number of these studies did not fully quantify the effect of duration due to one or more of the following factors: (*i*) they used structural models that did not adequately capture deterioration in strength and stiffness, and the destabilizing effect of gravity loads ($P-\Delta$ effects); (*ii*) they used predominantly short duration ground motions from shallow crustal earthquakes; (*iii*) they used duration metrics that were not strongly correlated to structural demands; and (*iv*) they incompletely accounted for the effect of response spectral shape. Lindt and Goh (2004) successfully observed an influence of duration on structural collapse risk by using cumulative damage metrics to define non-simulated collapse criteria, despite using simplistic, non-degrading, single-degree-of-freedom structural models. Although Chapter 2/Chandramohan et al. (2016b) found ground motion duration to be an important predictor of structural collapse capacity, they did not quantify the duration of ground motion anticipated at any specific site. In this regard, this paper extends previous studies by integrating the seismic hazard characterization of duration with structural collapse risk assessment.

The importance of selecting earthquake ground motions that are representative of the site-specific seismic hazard, has been highlighted by a number of studies (Bommer et al. 2000; Bommer and Acevedo 2004; Katsanos et al. 2010). This implies that the characteristics of the selected ground motions should match the characteristics of the ground motions anticipated at the site. A number of documents and standards have been developed to provide guidelines to select representative site-specific ground motions; however, most of them explicitly consider only the response spectra of the selected ground motions. While the response spectrum of a ground motion quantifies its amplitude and frequency content, it is only weakly related to the duration of strong shaking contained in it. Ground motion response spectra have been shown to be well correlated to important structural demand parameters such as peak structural deformations and structural collapse capacity (Shome et al. 1998; Baker and Cornell 2006b; FEMA 2009b), thus justifying their widespread use in seismic hazard and risk assessment as a primary ground motion intensity measure. This paper evaluates the impact of matching ground motion duration targets, in addition to response spectrum targets, when selecting site-specific ground motions for structural collapse

risk assessment.

NIST (2011) summarizes a number of guidelines for selecting ground motions that are representative of the site seismic hazard. PEER TBI (2010) and ASCE (2016) require the assessment of structural performance at the risk-targeted maximum considered earthquake (MCE_R) ground motion intensity level. They recommend the selection of ground motions, whose response spectra are approximately representative of the site seismic hazard, by scaling them such that the mean of their response spectra lies above the MCE_R response spectrum at the site. Alternatively, they provide the option of using the conditional mean spectrum (Baker 2011), which provides a more accurate representation of the site seismic hazard, as a target response spectrum. In addition to response spectra, these standards attempt to implicitly ensure that other characteristics of the selected ground motions, such as duration and pulse-like characteristics, are approximately representative of the site seismic hazard by recommending the selection of ground motions whose causal parameters, such as magnitude, source-to-site distance, and source mechanism, reflect the MCE_R site hazard.

The actual ground motion selection and modification procedure employed in a given situation depends on the type and objective of the analysis to be conducted. Since ground motions serve as the critical link between seismic hazard analysis and structural demand analysis, obtaining accurate structural response estimates requires the explicit consideration of the joint probability distribution of the response spectral ordinates and durations of the selected ground motions (Buratti et al. 2011; Jayaram et al. 2011b). This paper outlines a procedure to compute the probability distribution of the durations of ground motions anticipated at a site, conditional on the exceedance of a primary ground motion intensity measure. The procedure is similar to the one used by Iervolino et al. (2010) to compute conditional distributions of the Cosenza and Manfredi index, I_D (Cosenza and Manfredi 1997), but extends upon it in a number of ways, as described below. The proposed procedure recommends computing different conditional distributions of ground motion duration for each type of seismic source that contributes to the site seismic hazard, e.g., interface, in-slab, and crustal earthquakes, at each considered hazard level. The computation procedure is based

on the generalized conditional intensity measure (GCIM) framework (Bradley 2010). The conditional distributions of duration are computed using seismic hazard deaggregation (McGuire 1995) results, a ground motion prediction equation for duration (e.g., Abrahamson and Silva 1996; Kempton and Stewart 2006; Bommer et al. 2009), and a model for the correlation coefficient between the total residuals, or ε-values, of duration and the chosen primary ground motion intensity measure (e.g., Bradley 2011). These source-specific conditional distributions of duration are then used in conjunction with source-specific conditional spectra (CS) (Abrahamson and Al Atik 2010; Baker 2011; Lin et al. 2013b) as targets to select appropriate proportions of hazard-consistent ground motions corresponding to each type of seismic source.

The potential for sites in Western USA to experience long duration ground motions stems mainly from large magnitude interface earthquakes in the Cascadia subduction zone. Source-specific target distributions of duration and response spectra are computed at three representative sites in Western USA—Seattle (Washington), Eugene (Oregon), and San Francisco (California)—with different levels of contribution to their seismic hazard from interface, in-slab, and crustal earthquakes. The collapse risk of an eight-story reinforced concrete moment frame building located in Seattle is estimated by conducting multiple stripe analysis using three groups of ground motion sets: (*i*) *CS and duration* group selected to match response spectrum and duration targets; (*ii*) *CS only* control group selected to match response spectrum targets only; and (*iii*) *CS and causal parameters* group selected to match response spectrum targets and deaggregated ranges of earthquake causal parameters like magnitude and source-to-site distance. The multiple stripe analysis technique (Jalayer 2003) is chosen to conduct the analyses since it allows the use of different sets of hazard-consistent ground motions at different intensity levels. Finally, the bootstrap method (Efron and Tibshirani 1994) is proposed to quantify the uncertainty in the collapse risk estimates. It is used here to estimate the sampling distribution and standard error of the difference between the mean annual frequency of collapse, $\lambda_{collapse}$, estimated using two alternative groups of ground motion sets. The difference between the $\lambda_{collapse}$ values estimated using the *CS and duration* and *CS only* groups is used to quantify the significance of considering ground motion duration when selecting ground motions

for collapse risk estimation. The difference between the $\lambda_{collapse}$ values estimated using the *CS and causal parameters* and *CS and duration* groups is used to assess the suitability of ground motion selection procedures that employ earthquake causal parameters to implicitly capture the effect of ground motion duration.

4.3 Computation of source-specific target distributions of duration

The proposed procedure to compute the source-specific target distribution of duration at a specific hazard level is based on the GCIM framework (Bradley 2010). The GCIM framework is a generalization of the conditional spectrum (Abrahamson and Al Atik 2010; Baker 2011; Lin et al. 2013b) that allows consideration of a general set of ground motion intensity measures, beyond only response spectral ordinates. The procedure begins with the choice of (*i*) an amplitude-based conditioning ground motion intensity measure, which is quantified by probabilistic seismic hazard analysis (PSHA) (Kramer 1996; McGuire 2004), and (*ii*) a metric to quantify ground motion duration. In this study, the 5 % damped pseudo spectral acceleration, $S_a(T^*)$, is used as the conditioning intensity measure, which is consistent with current structural design practice in the USA. The conditioning period, T^*, is a period of vibration that is representative of the dynamic behavior of the structure under consideration, usually chosen as the fundamental elastic modal period of the structure. Ground motion duration is quantified by significant duration (Trifunac and Brady 1975), Ds, since it was previously identified to be a good predictor of structural collapse capacity (Chapter 2/Chandramohan et al. 2016b), and it can be readily estimated using previously published prediction equations. The significant duration of a ground motion is defined as the time interval over which a specific percentage range of the integral $\int_0^{t_{max}} a^2(t)dt$ is accumulated, where $a(t)$ represents the ground acceleration at time t, and t_{max} represents the length of the accelerogram. 5–75 % significant duration, Ds_{5-75}, is used in this paper, and its computation is illustrated in Figure 4.1. Although $S_a(T^*)$ and Ds_{5-75} are used here, the described procedure is general and

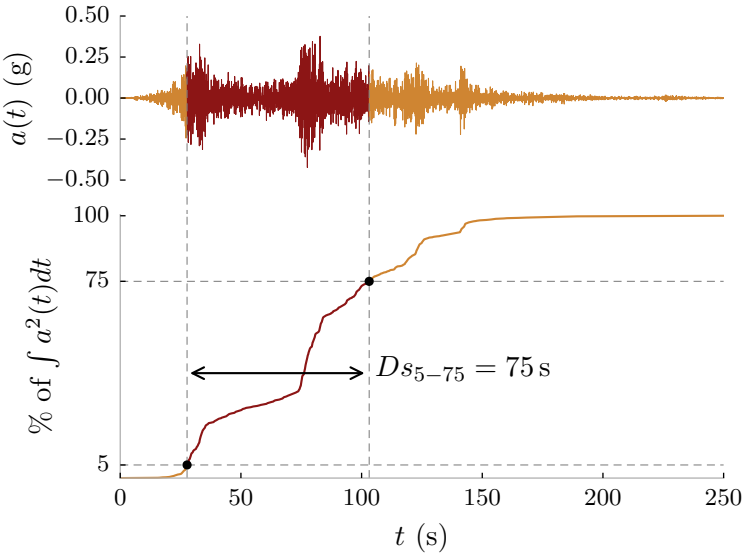

Figure 4.1: (Top) East-West component of the accelerogram recorded from the 2011 Tohoku (Japan) earthquake at the Sakunami station (station code: MYG014), and (Bottom) the normalized, cumulative integral of $a^2(t)$ illustrating the computation of 5–75 % significant duration of the accelerogram.

can be used with any combination of conditioning intensity measure and duration metric.

Note that it is infeasible to use traditional PSHA to obtain a hazard curve that describes the mean annual frequency of exceedance of significant duration, as is typically done for amplitude-based intensity measures like S_a, because significant duration increases with distance from the seismic source. Therefore, extremely long duration ground motions originating from a number of distant sources can contribute significantly to the seismic duration hazard at a site, although they have low spectral acceleration values and are not of engineering consequence. This is one motivation behind computing target distributions of duration, conditional on the exceedance of a primary, amplitude-based ground motion intensity measure.

4.3.1 Target computation procedure

To compute the source-specific conditional distribution of duration, the $S_a(T^*)$ value corresponding to the chosen hazard level is first obtained from the standard hazard curve. Seismic hazard deaggregation is then used to find the earthquake scenarios that are most likely to cause the exceedance of that $S_a(T^*)$ value at the site, defined by the following parameters: (i) source type, ST_i (e.g., interface, in-slab, or crustal), (ii) magnitude, M_i, (iii) source-to-site distance, R_i, (iv) other causal parameters, $\boldsymbol{\Theta}_i$ (e.g., Vs_{30}: the average shear wave velocity of the top 30 m of the soil profile, faulting mechanism, and basin depth), (v) total residual or ε-value for $S_a(T^*)$, ε_i, and (vi) deaggregation weight, p_i, where the subscript i denotes the i^{th} contributing earthquake scenario. A prediction equation for significant duration (e.g., Abrahamson and Silva 1996; Kempton and Stewart 2006; Bommer et al. 2009) is then used to compute the mean, μ, and standard deviation, σ, of the natural logarithm of the significant duration of the ground motions anticipated at the site from each contributing earthquake scenario, as functions of its M, R, and $\boldsymbol{\Theta}$:

$$\mu_{\ln Ds(i)} = f(M_i, R_i, \boldsymbol{\Theta}_i) \tag{4.1a}$$

$$\sigma_{\ln Ds(i)} = g(M_i, R_i, \boldsymbol{\Theta}_i) \tag{4.1b}$$

where $f()$ and $g()$ denote functions defined by the prediction equation. The logarithm of significant duration is used since many prediction equations have found it to be lognormally distributed for a given earthquake scenario (Abrahamson and Silva 1996; Kempton and Stewart 2006; Bommer et al. 2009). The conditional distribution of significant duration for each contributing earthquake scenario is then computed using Equations (4.2a) and (4.2b), which require a model for the correlation coefficient, $\rho(T^*)$, between the ε-values from the predictions of the logarithms of $S_a(T^*)$ and Ds (e.g., Bradley 2011).

$$\mu_{\ln Ds(i)\,|\,\ln S_a(T^*)} = \mu_{\ln Ds(i)} + \rho(T^*)\varepsilon_i\sigma_{\ln Ds(i)} \tag{4.2a}$$

$$\sigma_{\ln Ds(i)\,|\,\ln S_a(T^*)} = \sigma_{\ln Ds(i)}\sqrt{1-\rho(T^*)^2} \tag{4.2b}$$

The relative contribution to the total site seismic hazard from each type of seismic source is computed by summing the deaggregation weights corresponding to all contributing earthquake scenarios from that type of seismic source, using Equation (4.3),

$$\bar{p}_{(st)} = \sum_{ST_i=st} p_i \tag{4.3}$$

where ST is a random variable and st represents a specific source type, e.g., interface, in-slab, or crustal. Source-specific conditional distributions of significant duration are then computed for each seismic source type, st, as a weighted average of the conditional distributions of significant duration for all contributing earthquake scenarios from that type of seismic source, using Equations (4.4a) and (4.4b).

$$\mu_{\ln Ds(st)\,|\,\ln S_a(T^*)} = \sum_{ST_i=st} \frac{p_i}{\bar{p}_{(st)}} \left[\mu_{\ln Ds(i)\,|\,\ln S_a(T^*)}\right] \tag{4.4a}$$

$$\sigma_{\ln Ds(st)\,|\,\ln S_a(T^*)} = \sqrt{\sum_{ST_i=st} \frac{p_i}{\bar{p}_{(st)}} \left[\sigma^2_{\ln Ds(i)\,|\,\ln S_a(T^*)} + \left(\mu_{\ln Ds(i)\,|\,\ln S_a(T^*)} - \mu_{\ln Ds(st)\,|\,\ln S_a(T^*)}\right)^2\right]} \tag{4.4b}$$

These equations are similar to the ones proposed by Lin et al. (2013a) to compute conditional spectra, except in this case, separate target distributions are computed for each type of seismic source. The motivation for doing this will be illustrated in § 4.4.3. Note that although the inputs to Equations (4.4a) and (4.4b) are the means and standard deviations of lognormal distributions, the aggregate source-specific conditional distributions are not necessarily lognormal. They are, however, approximated here as lognormal distributions for practical reasons. Source-specific conditional spectra can be similarly computed using appropriate prediction equations and models for the correlation coefficient between response spectral ordinates.

To select a set of hazard-consistent ground motions at the chosen hazard level, the fraction of ground motions selected to match the target Ds_{5-75} distribution and conditional spectrum corresponding to each type of seismic source should be equal to the $\bar{p}_{(st)}$ value computed for that type of seismic source using Equation (4.3). Several algorithms have been proposed to select ground motions whose characteristics match

a given joint distribution of ground motion intensity measures (Jayaram et al. 2011b; Bradley 2012).

4.3.2 Prediction models for significant duration

Three prediction equations for significant duration are considered in this study: Abrahamson and Silva (1996), Kempton and Stewart (2006), and Bommer et al. (2009). These prediction equations were all developed for crustal earthquakes using the PEER NGA-West database (Ancheta et al. 2013), with Bommer et al. having the largest maximum usable magnitude of 7.9. The authors are currently unaware of any significant duration prediction equations for large magnitude interface earthquakes and deep in-slab earthquakes. Nevertheless, since large magnitude interface earthquakes in the Cascadia subduction zone are the focus of this study ($8.6 \leq M_W \leq 9.3$ as per Petersen et al. (2014)), the ability of the three models to predict durations of ground motions produced by large magnitude interface earthquakes, above their maximum usable magnitude limits, was investigated.

The variation, with magnitude, of the median Ds_{5-75} predicted by the three models, at a rock site and source-to-site distances of 10 km and 80 km, are plotted in Figure 4.2. Predictions extrapolated beyond the maximum usable magnitude of each model are plotted using a dashed line. Ds_{5-75} is seen to increase with both earthquake magnitude and source-to-site distance but is typically more sensitive to changes in magnitude than distance. The predictions of the three models are found to agree well until a magnitude of about 7.5, above which they diverge. Notably, at magnitudes above 7.9, Bommer et al. is found to predict longer duration ground motions at shorter distances, indicated by the crossing of the $Distance = 10$ km and $Distance = 80$ km curves, which is contrary to expectations based on wave propagation physics, thus making it unsuitable for use with the large magnitude earthquakes considered in this study. The predictions of the Abrahamson and Silva, and Kempton and Stewart models were found to be consistent with the durations of ground motions produced by recent large magnitude interface earthquakes from a qualitative comparison, thus supporting their use in this study, especially given the absence of any alternatives.

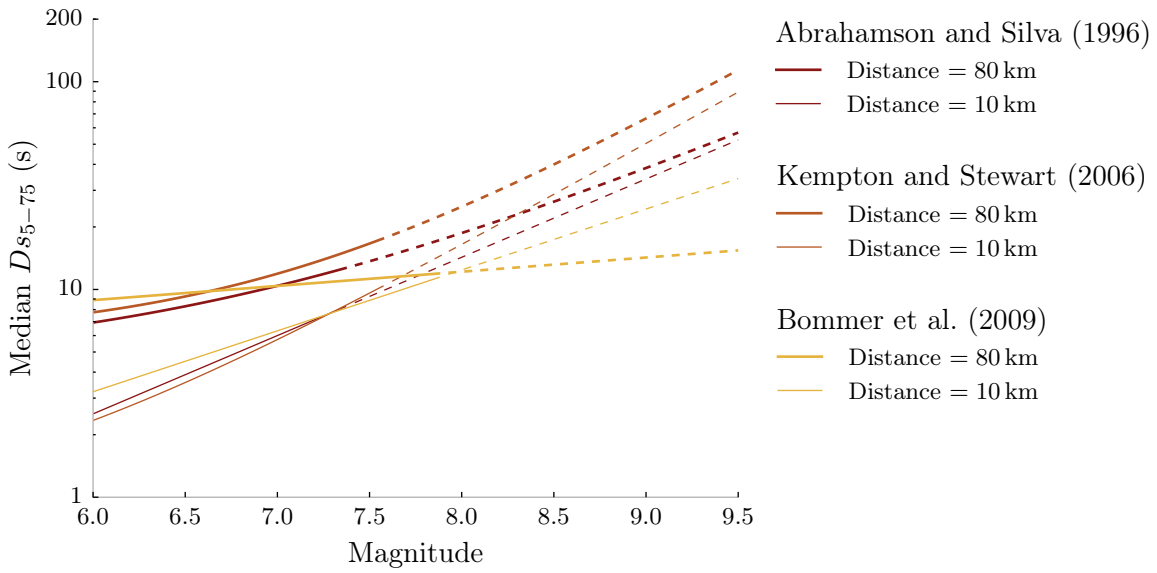

Figure 4.2: Comparison of the three prediction equations for significant duration. Durations predicted by extrapolating the models above their range of calibrated magnitudes are plotted using a dashed line.

Among the two, Kempton and Stewart consistently predicts longer duration ground motions than Abrahamson and Silva. The Abrahamson and Silva equation is used in the calculations presented in § 4.4, and the collapse risk assessments in § 4.5, to conservatively demonstrate the effect of ground motion duration; the effect would be even larger if the Kempton and Stewart model were used instead.

The only available model for the correlation coefficient between the ε-values of $S_a(T^*)$ and Ds_{5-75} was also developed for crustal earthquakes using the PEER NGA-West database (Bradley 2011). The model predicts small negative correlation coefficients for periods shorter than 2.1 s, and small positive correlation coefficients for periods longer than 2.1 s. While the properties of these models are believed to be reasonable for the calculations presented below, there is need for additional studies to verify the application of these models to interface and in-slab earthquakes.

4.4 Analysis of source-specific targets computed for Western USA

The procedure outlined in § 4.3 was used to compute source-specific target distributions of Ds_{5-75}, conditional on the 2 % in 50 year exceedance probability of $S_a(1\,\mathrm{s})$, for Western USA. Seismic hazard deaggregation results were obtained from the USGS (Petersen et al. 2008; USGS 2008). The duration prediction models discussed above were used in the computations, assuming a rock site with $Vs_{30} = 760\,\mathrm{m/s}$. Maps of the percentage contribution to the seismic hazard from interface earthquakes, and the conditional median target Ds_{5-75} of ground motions produced by interface earthquakes in the Cascadia subduction zone, for locations that have non-zero contributions to their seismic hazard from interface earthquakes, are shown in Figures 4.3a and 4.3b respectively. A map of the $S_a(1\,\mathrm{s})$ values that are exceeded with a probability of 2 % in 50 years is shown in Figure 4.3c.

In Figure 4.3b, the conditional median target Ds_{5-75} of ground motions produced by interface earthquakes is seen to increase from around 30 s near the Pacific coast to around 45 s at distances about 600 km inland, due to the increase in predicted Ds_{5-75} with distance from the Cascadia subduction zone. As seen in Figure 4.3a, this increase in target duration is, however, accompanied by a corresponding decrease in the percentage contribution to the total seismic hazard from interface earthquakes, from almost 100 % near the Pacific coast to 0 % at distances around 600 km inland. Localized drops in the percentage contribution from interface earthquakes are also observed around seismically active crustal faults near Seattle, Southern Oregon, and Northern California. The $S_a(1\,\mathrm{s})$ value corresponding to a 2 % probability of exceedance in 50 years decreases from values greater than 0.6 g near the Pacific coast to below 0.2 g at distances around 300 km inland. Therefore, although longer duration ground motions are expected at larger distances from the Cascadia subduction zone, the relative contribution of these long duration ground motions produced by interface earthquakes to the total seismic hazard, as well as the expected intensity of these ground motions, decreases with distance. As a result, ground motion duration

is an important consideration for structural performance assessment only at sites located near the Cascadia subduction zone. The exact magnitude of the importance, however, depends on parameters like the conditioning period and the intensity level, as discussed in § 4.4.2.

4.4.1 Targets at three representative sites

Three sites located in Seattle, Eugene, and San Francisco were chosen to illustrate how proximity to different types of seismic sources can influence the site seismic hazard. The sites are located in different tectonic settings with varying levels of contribution to their seismic hazard from different types of seismic sources, as shown in Figure 4.4. San Francisco's seismic hazard comes almost entirely from crustal faults, including the San Andreas, Hayward, and San Gregorio faults. Eugene, on the other hand, is adjacent to the Cascadia subduction zone and distant from seismically active crustal faults; hence the subduction zone is the dominant contributor to its seismic hazard. Seattle's seismic hazard is affected by both the Cascadia subduction zone and the Seattle fault zone, which is a network of crustal faults under the city.

The Cascadia subduction zone is a source of both interface and in-slab earthquakes. The large magnitude interface earthquakes are caused by relative motion between the subducting Juan de Fuca plate, and the over-riding North American plate. The 2014 USGS national seismic hazard maps (Petersen et al. 2014) consider future interface earthquakes of magnitude as large as 9.3 in the Cascadia subduction zone. The 1700 Cascadia earthquake was an interface earthquake of estimated magnitude 9.0. In-slab earthquakes are deep earthquakes caused by ruptures within the subducting Juan de Fuca plate as it sinks into the mantle, at depths of 35 km to 70 km (Petersen et al. 2014). Although in-slab earthquakes are of smaller magnitude than interface earthquakes, they are much more frequent. The 2001 Nisqually earthquake was an in-slab earthquake of magnitude 6.8.

Seismic hazard deaggregation plots, conditional on the 2 % in 50 year exceedance

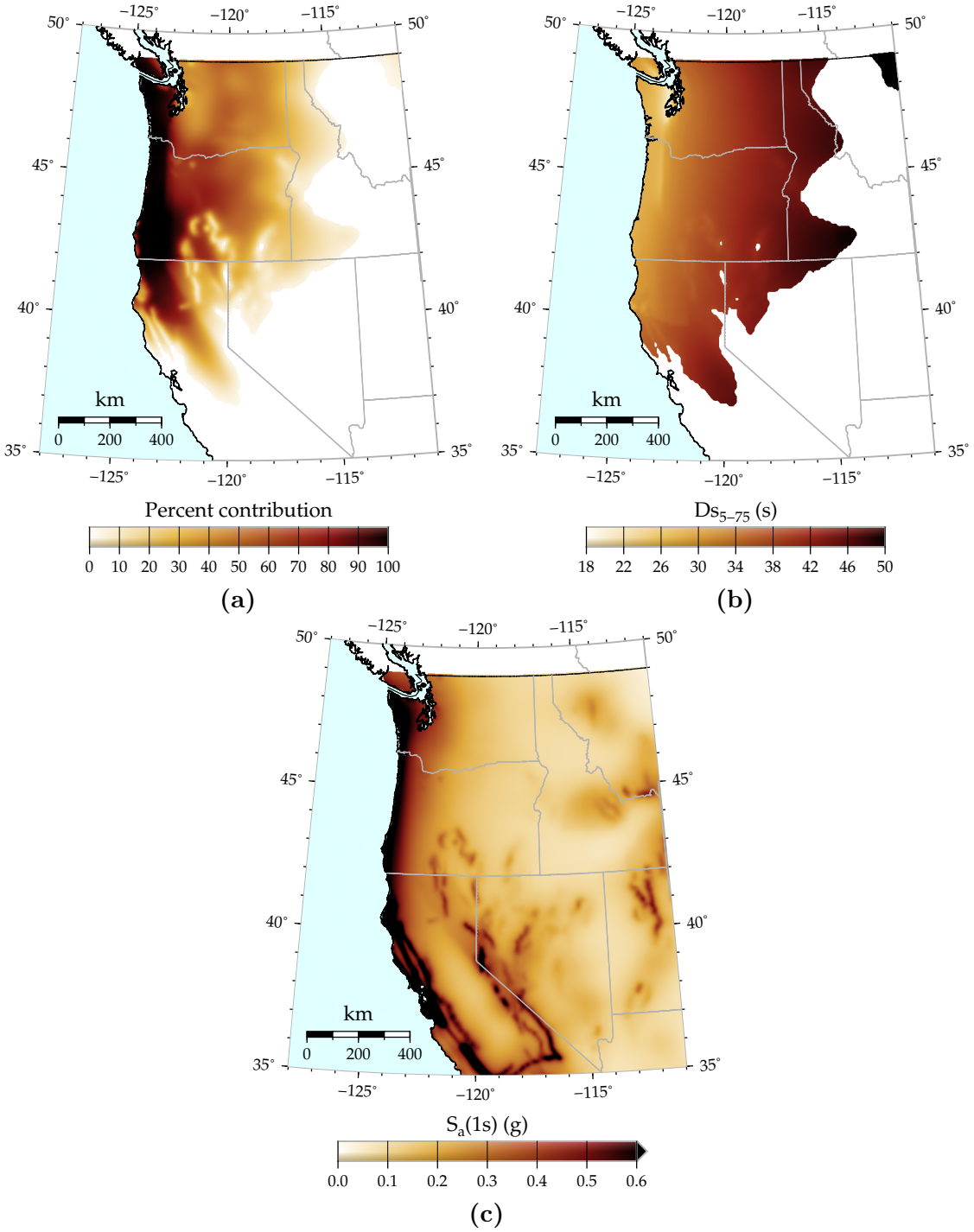

Figure 4.3: (a) Percentage contribution to the total seismic hazard from interface earthquakes, and (b) conditional median target Ds_{5-75} of ground motions produced by interface earthquakes (only plotted for sites with non-zero contributions to their seismic hazard from interface earthquakes), conditional on the exceedance of the $S_a(1\,\mathrm{s})$ values shown in (c), which are exceeded with a probability of 2 % in 50 years.

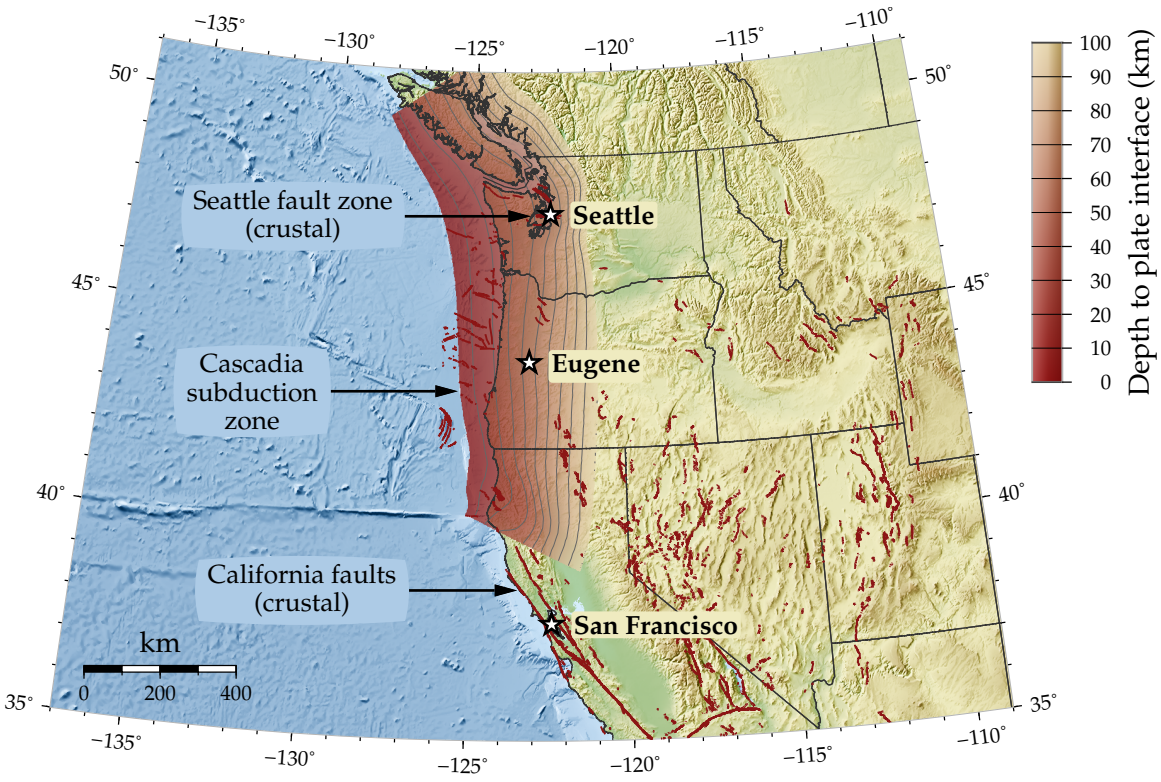

Figure 4.4: Sites chosen for sample calculations of target distributions of duration, and the seismic sources that significantly contribute to their seismic hazard.

probability of $S_a(1\,\text{s})$, for all three sites, are shown in Figure 4.5. The contributions from each type of seismic source are easily distinguishable since they have distinct magnitude and source-to-site distance ranges. The computed source-specific conditional median target Ds_{5-75} values, and the corresponding percentage contributions to the total seismic hazard from each type of seismic source, conditional on the 2 % in 50 year exceedance probability of $S_a(1\,\text{s})$, are summarized in Table 4.1. The source-specific conditional distributions of Ds_{5-75}, and the source-specific conditional spectra, which are computed in an analogous manner, are plotted in Figure 4.6. Note that the conditional standard deviations of the conditional spectra are omitted for readability, and the percentage contributions of each type of source to the total seismic hazard are noted in the legends. The Abrahamson et al. (2016) prediction equation was used to compute the conditional spectra for the interface and in-slab earthquakes, and the Campbell and Bozorgnia (2014) prediction equation was used for the crustal earthquakes. The correlation coefficients between the ε-values of response spectral ordinates at different periods from Baker and Jayaram (2008) were used for crustal and in-slab earthquakes, and those from Al Atik (2011) were used for interface earthquakes. The difference in the expected frequency content of ground motions produced by earthquakes from different types of seismic sources, is evident from Figure 4.6. As seen from the plotted conditional mean spectra, ground motions from interface earthquakes are expected to have less high-frequency content, whereas those from in-slab earthquakes are expected to have less low-frequency content, when compared to crustal earthquakes.

4.4.2 Sensitivity of targets to seismic hazard level and conditioning period

The duration targets computed above were conditional on the 2 % in 50 year exceedance probability of $S_a(1\,\text{s})$. Figure 4.7 plots the duration targets in Seattle corresponding to interface earthquakes, for three conditioning periods, and for $S_a(T^*)$ values with varying return periods. Figure 4.7a shows that for shorter conditioning periods, intense ground motions (corresponding to longer return periods) are likely to

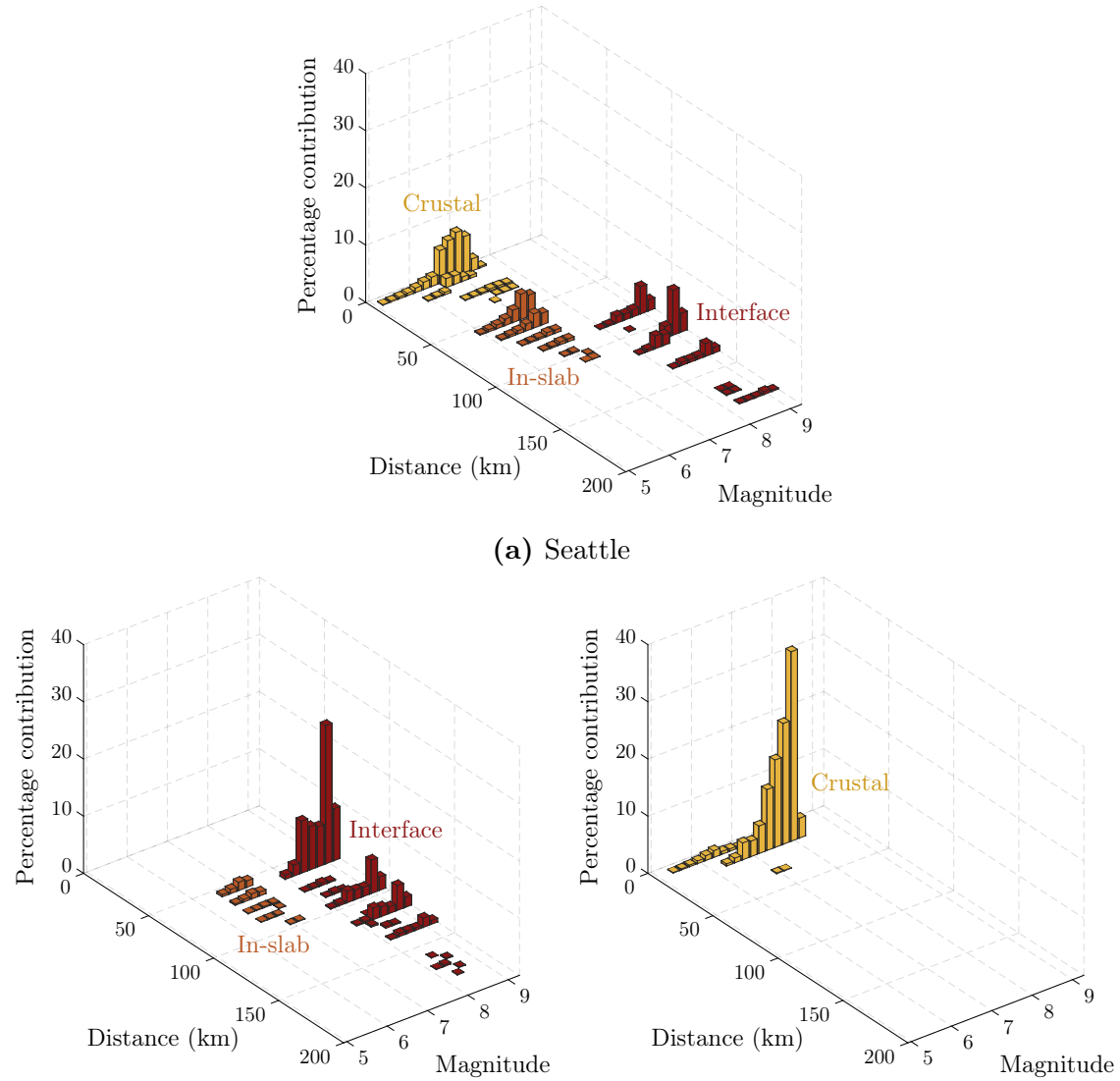

(a) Seattle

(b) Eugene

(c) San Francisco

Figure 4.5: Seismic hazard deaggregation plots for all three considered sites, conditional on the 2 % in 50 year exceedance probability of $S_a(1\,\mathrm{s})$. The types of seismic sources associated with specific magnitude and distance combinations are noted on each plot.

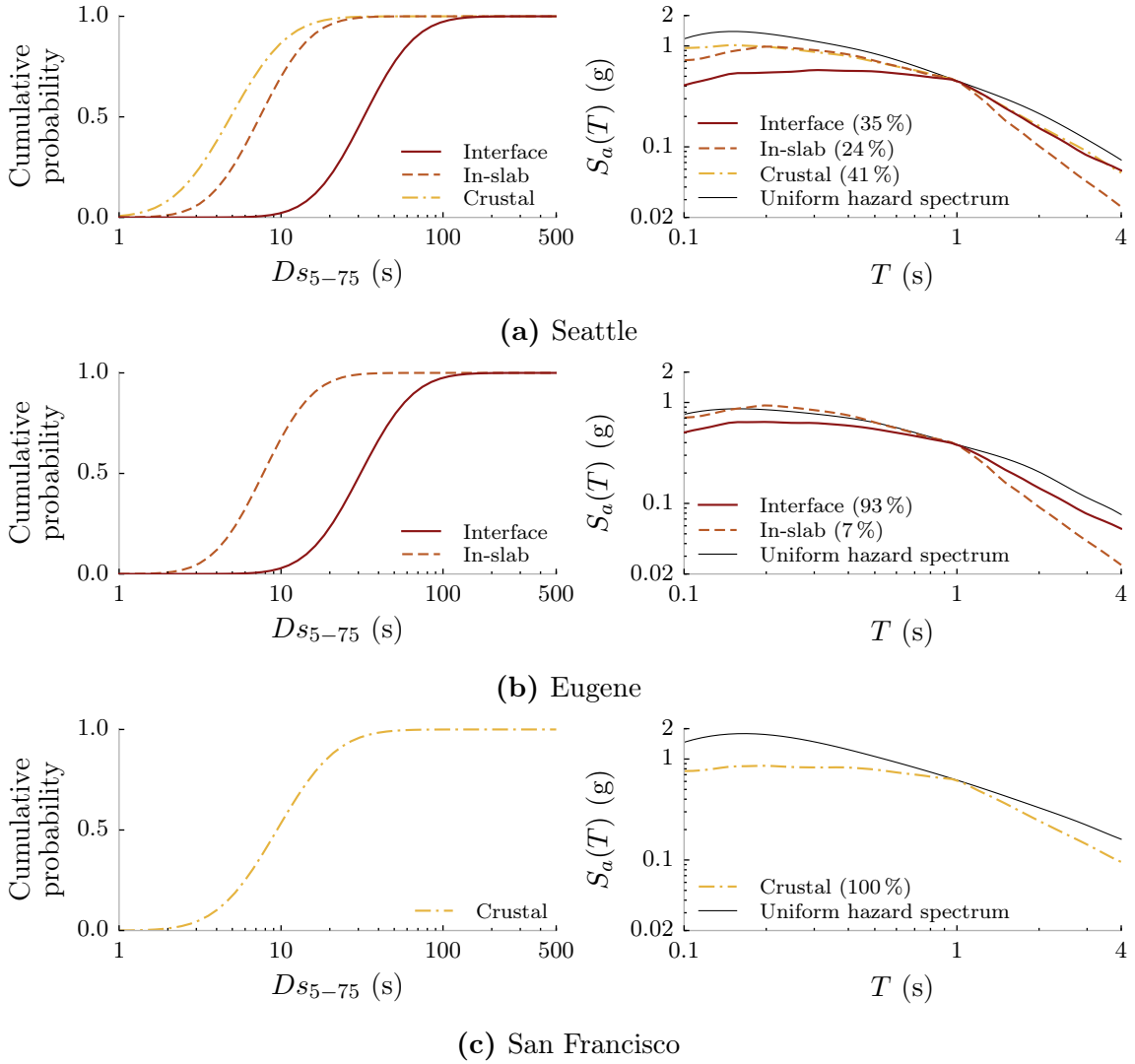

Figure 4.6: (Left) Source-specific conditional distributions of Ds_{5-75}, and (Right) source-specific conditional mean spectra and corresponding uniform hazard spectra for all three considered sites, conditional on the 2 % in 50 year exceedance probability of $S_a(1\,\text{s})$.

Table 4.1: Source-specific conditional median target Ds_{5-75} values, and the corresponding percentage contributions to the total seismic hazard from each type of seismic source (indicated in parentheses), conditional on the 2 % in 50 year exceedance probability of $S_a(1\,\text{s})$, for all three considered sites. Conditional median target Ds_{5-75} values are not indicated for source types that contribute less than 1 % to the site seismic hazard.

Site	Interface earthquakes	In-slab earthquakes	Crustal earthquakes
Seattle	32 s (35 %)	7 s (24 %)	5 s (41 %)
Eugene	30 s (93 %)	8 s (7 %)	–
San Francisco	–	–	9 s (100 %)

have shorter durations. This trend is explained by the larger ε-values associated with rarer ground motions, and the negative correlation between the ε-values of Ds_{5-75} and $S_a(T^*)$ for shorter conditioning periods (Bradley 2011), used in Equation (4.2a). For longer conditioning periods, Bradley (2011) predicts positive correlation coefficients, resulting in rare, intense ground motions being associated with longer durations. The unconditional median target durations were found to stay relatively constant over different hazard levels, and thus, do not contribute significantly to the observed trends.

Figure 4.7b shows that the relative contribution of interface earthquakes to the total seismic hazard is higher at longer return periods, on average. A consequence of this is that when analyzing a structure in Seattle, a larger proportion of long duration ground motions, characteristic of interface earthquakes, would need to be used at higher ground motion intensity levels. It is also observed from Figure 4.7b that interface earthquakes contribute more to the seismic hazard at longer conditioning periods. This is explained by the fact that the prediction equations for interface earthquakes used in the 2008 national seismic hazard model (Petersen et al. 2008) predict ground motions that are rich in low-frequency content. It, therefore, follows that large $S_a(T^*)$ values at long periods are more likely to be caused by interface earthquakes. This pattern is, however, not reflected in the conditional mean spectra for Seattle plotted in Figure 4.6a, where the conditional mean spectrum corresponding to crustal earthquakes has about the same low-frequency content ($S_a(T > 1\,\text{s})$) as the one corresponding to interface earthquakes. This discrepancy is a consequence of using the Abrahamson et al. (2016) prediction equation to compute the conditional

mean spectra in Figure 4.6a, although it is not used in the deaggregation computations in Petersen et al. (2008) used to plot Figure 4.7b. The Abrahamson et al. (2016) model predicts a rapid decay in the low-frequency content of ground motions produced by interface earthquakes with distance, thus resulting in the prediction of less low-frequency content in Seattle, which is about 100 km away from the Cascadia subduction zone (Petersen et al. 2014). Although Petersen et al. (2008) is the most recent hazard model for which national deaggregation data is presently available, the newer Abrahamson et al. (2016) was adopted for the calculations here, since it is more refined and based, in part, on data from recent large magnitude subduction earthquakes. Therefore, deaggregation calculations based on the 2014 national seismic hazard model (Petersen et al. 2014), which incorporates Abrahamson et al. (2016), are likely to predict lesser separation between the curves in Figure 4.7b.

4.4.3 Motivation for computing source-specific targets

To understand the motivation for computing source-specific targets, consider the consequences of computing only one target distribution of Ds_{5-75} and conditional spectrum at the hazard level corresponding to the 2 % in 50 year exceedance probability of $S_a(1\,\mathrm{s})$ in Seattle, without discriminating between contributing earthquake scenarios based on the type of seismic source, as recommended by Lin et al. (2013a). In this case, one conditional median target Ds_{5-75} of 10 s, and one conditional mean spectrum would be computed as the average of the source-specific conditional median targets, weighted by their corresponding $\bar{p}_{(st)}$ values. The standard deviations of these targets would be larger than the standard deviations of the individual source-specific targets, since they would account for the variability (*i*) among the different types of seismic sources, and (*ii*) in the characteristics of the ground motions produced by each type of seismic source. Using these targets could lead to the selection of long duration records with a response spectral shape characteristic of shorter duration crustal records, and vice versa, which would not reflect the known differences in the characteristics of ground motions produced by the three types of seismic sources, as observed in Figure 4.6. Although this is a concern in a site like Seattle, with hazard

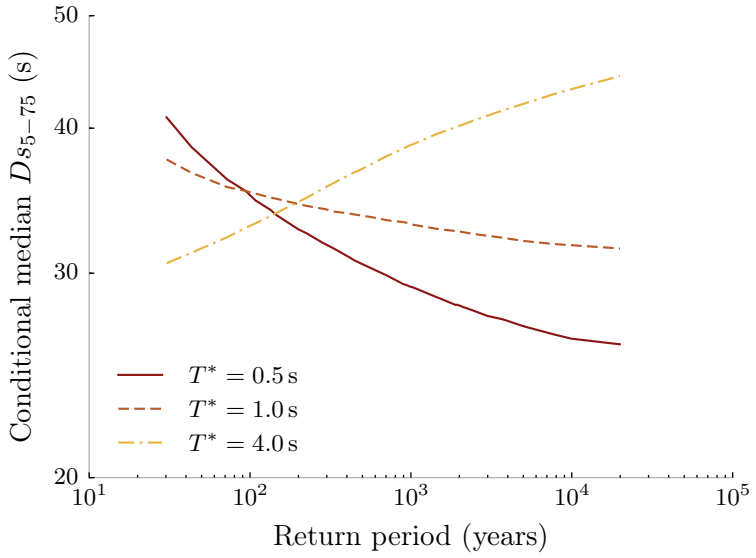

(a)

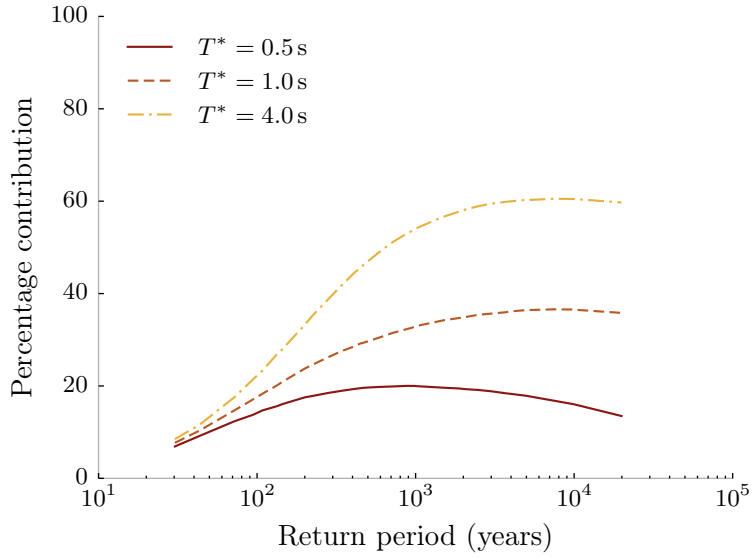

(b)

Figure 4.7: (a) Conditional median target Ds_{5-75} of ground motions in Seattle produced by interface earthquakes, and (b) the percentage contribution to the total seismic hazard of Seattle from interface earthquakes, conditional on different exceedance rates of $S_a(T^*)$, i.e., different seismic hazard levels, for different conditioning periods, T^*.

contributions from multiple types of sources, it is less of a concern in a site like San Francisco, whose seismic hazard is dominated by one type of source.

Goda and Atkinson (2011) address this issue by selecting ground motions to match source-specific conditional mean spectra but they do not consider the spectral standard deviations or ground motion duration. Bradley (2012) addresses this issue by recommending the selection of ground motions with characteristics consistent with deaggregated contributing earthquake scenarios, that are simulated from a probability mass function defined by the seismic hazard deaggregation weights. The use, here, of targets averaged over types of seismic sources, although slightly less rigorous than the Bradley procedure, represents a practical middle ground between the recommendations of Bradley (2012) and Lin et al. (2013a). This approach takes advantage of the similarity in the causal parameters that define the contributing earthquake scenarios from each type of source, as observed in Figure 4.5. Moreover, the adopted procedure allows the explicit quantification and comparison of the expected duration and frequency content of ground motions produced by interface, in-slab, and crustal earthquakes. It also allows the selection of ground motions representing individual source types to be more finely optimized than the Bradley procedure, as illustrated in the following section.

4.5 Collapse risk assessment of a reinforced concrete moment frame building

4.5.1 Structural model

A ductile eight-story reinforced concrete moment frame building, designed to current standards for a site in Seattle, is used to illustrate the proposed method for characterizing ground motion hazard, and to quantify the influence of ground motion duration on structural collapse risk. The height of the first story of the building is 4.6 m, and the height of all subsequent stories is 4.0 m. The width of each bay of the building is 6.1 m. A schematic of the two-dimensional numerical model of the structure, created and analyzed using OpenSees rev. 5184 (McKenna et al. 2006), is shown

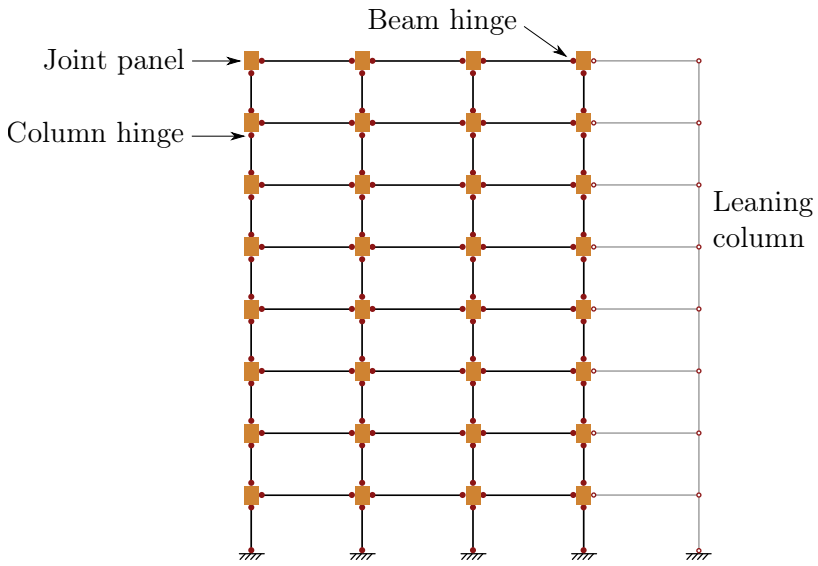

Figure 4.8: Schematic of the eight-story reinforced concrete moment frame model.

in Figure 4.8. This model was developed by Raghunandan et al. (2015) to study the collapse risk of structures in the Pacific Northwest. The beams and columns of the frame were modeled using linear elastic elements, with zero-length plastic hinges located at the ends of each beam and column. The plastic hinges were modeled using the Modified Ibarra-Medina-Krawinkler peak-oriented model (Ibarra et al. 2005) that includes a post-peak negative stiffness branch of the backbone curve to capture in-cycle deterioration, as well as cyclically deteriorating strength and stiffness based on the cumulative hysteretic energy dissipated. Finite beam-column joints were modeled, with elastic shear deformations. The contribution of the adjacent gravity system to the destabilizing $P - \Delta$ effect was modeled using a pin-connected leaning column. Previous studies have demonstrated that structural models need to capture the deterioration in strength and stiffness of structural components at large inelastic deformations, as well as the destabilizing effect of gravity loads, to capture the effect of ground motion duration on structural response (Raghunandan and Liel 2013; Chapter 2/Chandramohan et al. 2016b). Further details about the design and the numerical model are provided in Raghunandan et al. (2015).

4.5.2 Ground motion selection

The multiple stripe analysis technique (Jalayer 2003), which allows the use of a different set of hazard-consistent ground motions at each intensity level, was used to estimate the collapse fragility curve of the structure. Three groups of ground motions were selected to demonstrate the importance of considering ground motion duration when estimating structural collapse risk. Each group consists of sets of 100 ground motions selected at eight ground motion intensity levels. The ground motions were selected to match targets computed for a site in Seattle, using a conditioning period of 1.8 s, the fundamental period of the structure. Seismic hazard deaggregation results for $S_a(1\,\text{s})$ and $S_a(2\,\text{s})$, obtained from USGS (2008), were interpolated to compute the targets conditional on $S_a(1.8\,\text{s})$. The conditional median target Ds_{5-75} values and the percentage contribution of interface, in-slab, and crustal earthquakes to the site seismic hazard, at all eight intensity levels, are summarized in the digital appendix, available at http://purl.stanford.edu/nj619hk1456. An upper limit of 5.0 was imposed on the factor used to scale the selected ground motions.

The ground motions in the first group, called the *CS and duration* group, were selected to match the source-specific target distributions of Ds_{5-75} and response spectra, conditional on exceedance of each ground motion intensity level. Ground motions corresponding to interface earthquakes were selected from a collection of 3955 ground motions recorded from the following interface earthquakes: 1974 Lima (Peru), 1985 Valparaiso (Chile), 1985 Michoacan (Mexico), 2003 Hokkaido (Japan), 2010 Maule (Chile), and 2011 Tohoku (Japan). Of these 3955 ground motions, 2448 are from the 2011 Tohoku earthquake, 1314 are from the 2003 Hokkaido earthquake, and the remaining 193 are from the other earthquakes. Ground motions corresponding to both crustal and in-slab earthquakes were selected from the PEER NGA-West2 database (Ancheta et al. 2013), even though the database contains ground motions only from shallow crustal earthquakes. This was considered reasonable since the magnitudes and target ground motion durations of the contributing in-slab earthquakes were similar to those of the ground motions in the database. Moreover, only a small fraction of ground motions from in-slab earthquakes were required at the high intensity levels,

due to their low percentage contribution to the seismic hazard at these intensity levels.

A slightly modified version of the algorithm proposed by Jayaram et al. (2011b) was used to select ground motions to match a target multivariate normal distribution of logarithms of intensity measures. Ds_{5-75} was added as an additional intensity measure to a vector of response spectral ordinates at different periods. The quality of fit of a set of ground motions to the target multivariate distribution was assessed by first computing the Kolmogorov-Smirnov test (K-S test) statistic for each intensity measure, and then computing a weighted average of the test statistics for all intensity measures, similar to the procedure adopted by Bradley (2012). From preliminary trials, weights of 0.5 for the K-S test statistic of Ds_{5-75} and 0.5 for the mean K-S test statistic of all response spectral ordinates were found to produce ground motion sets that matched the targets reasonably well. The durations and response spectra of the set of ground motions selected at the $S_a(1.8\,\mathrm{s}) = 0.24\,\mathrm{g}$ intensity level (corresponding to the 2 % in 50 year hazard level) are shown in Figure 4.9.

A second group of ground motion sets, called the *CS only* group, was created to control for the effect of response spectral shape. These ground motions were selected to match only the target distributions of response spectral ordinates, without considering ground motion duration. For this group, ground motions corresponding to all three types of seismic sources were chosen from the PEER NGA-West2 database. The objective of selecting this group was to analyze the consequences of selecting ground motions without explicit consideration of their durations. The durations and response spectra of the ground motions selected to match the targets corresponding to interface earthquakes, at the $S_a(1.8\,\mathrm{s}) = 0.24\,\mathrm{g}$ intensity level, are shown in Figure 4.10. As expected, the response spectra of the selected ground motions match the target well, but their durations are shorter than the target. On the other hand, the durations of the ground motions corresponding to crustal and in-slab earthquakes were found to approximately match their targets since the targets are similar to the durations of the ground motions in the PEER NGA-West2 database. These trends were consistent among all eight ground motion sets in the group. A similar ground motion selection exercise by Chapter 2/Chandramohan et al. (2016b) found that no

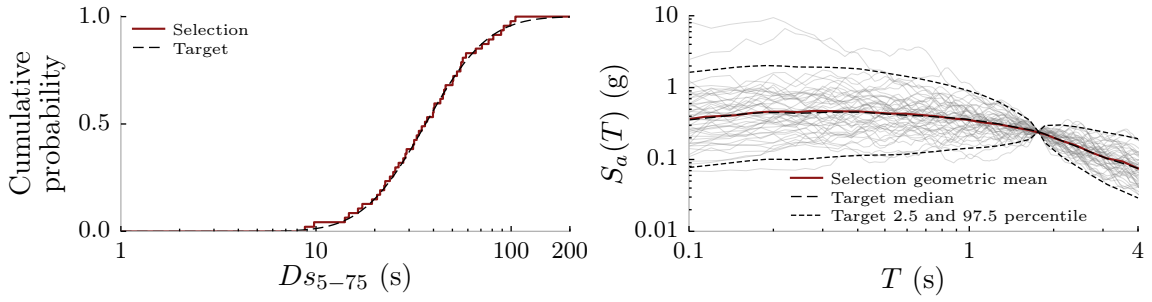

(a) Interface earthquakes: 47 / 100 ground motions

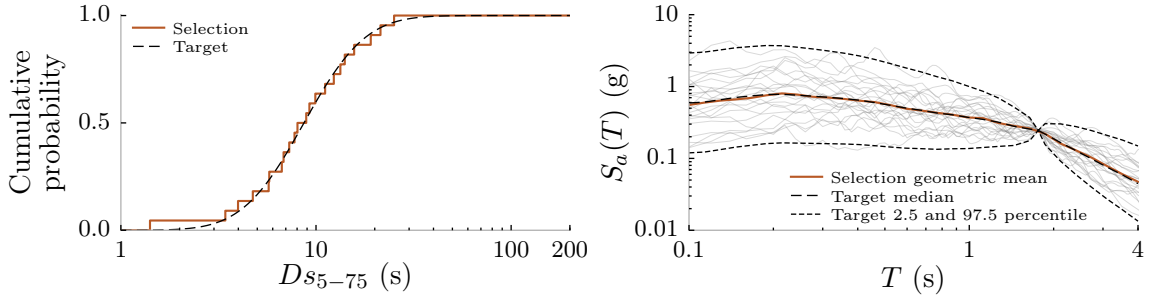

(b) In-slab earthquakes: 22 / 100 ground motions

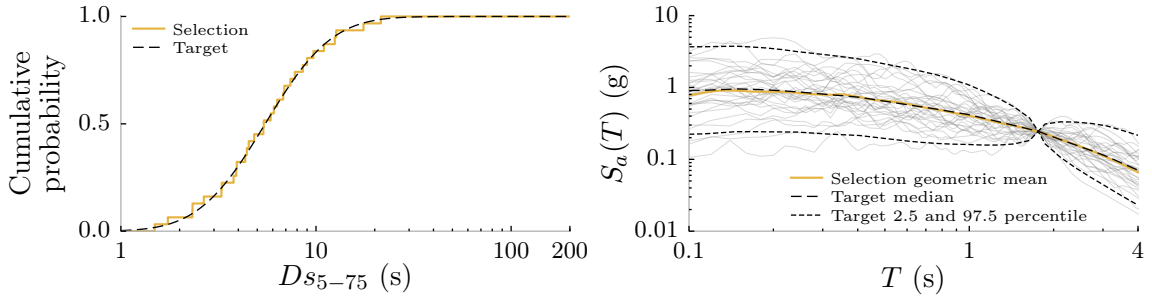

(c) Crustal earthquakes: 31 / 100 ground motions

Figure 4.9: Ground motions selected in the *CS and duration* group at the $S_a(1.8\,\text{s}) = 0.24\,\text{g}$ intensity level (2 % in 50 year hazard level) in Seattle, corresponding to each type of contributing seismic source.

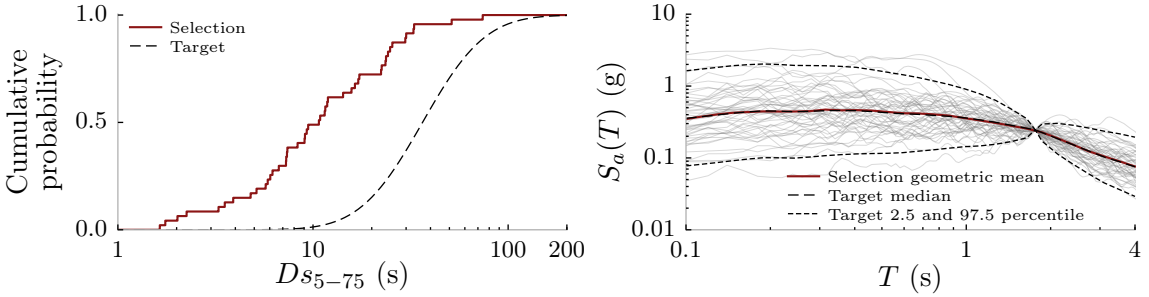

(a) Interface earthquakes: 47 / 100 ground motions

Figure 4.10: Ground motions selected in the *CS only* control group at the $S_a(1.8\,\text{s}) = 0.24\,\text{g}$ intensity level (2 % in 50 year hazard level) in Seattle, corresponding to interface earthquakes.

statistically significant differences are introduced with respect to ground motion characteristics other than response spectra and duration, when comparing the response of a structure to two groups of ground motions recorded from interface and crustal earthquakes respectively. Therefore, any difference observed in the structural collapse risk estimated using the *CS and duration* and *CS only* groups can be attributed to the difference in the durations of their ground motions.

Finally, a third group of ground motion sets, called the *CS and causal parameters* group, was created to evaluate the effectiveness of widely employed ground motion selection procedures that use causal parameters like magnitude, source-to-site distance, and site Vs_{30} to implicitly account for the effects of ground motion characteristics like duration, that are not entirely captured by response spectra. The ground motions in this group were also selected to match the target distributions of response spectral ordinates, similar to the other two groups. In addition, only those ground motions recorded from earthquakes whose magnitudes and source-to-site distances lie within an allowable range around the mean magnitude and source-to-site distance of earthquakes from each type of contributing source, obtained from seismic hazard deaggregation results, were considered. Constraints were also placed on the site Vs_{30} of the ground motions selected from the PEER NGA-West2 database, assuming the structure is located on a rock site with $Vs_{30} = 760\,\text{m/s}$. Since Vs_{30} data was not available for many of the interface earthquake ground motions, the Vs_{30} constraint was not

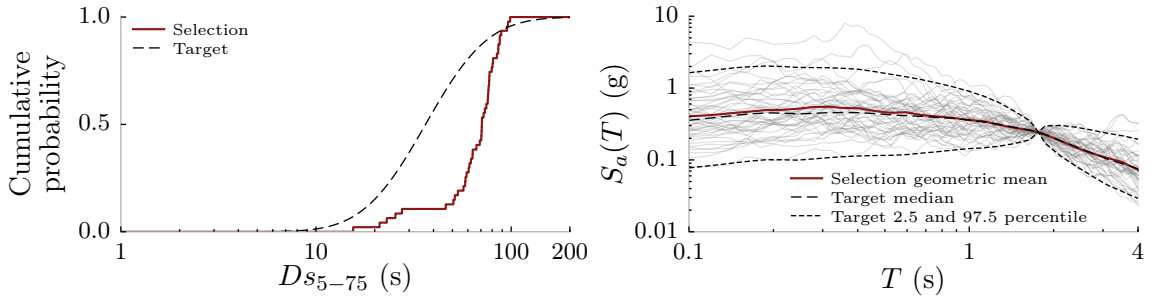

(a) Interface earthquakes: 47 / 100 ground motions

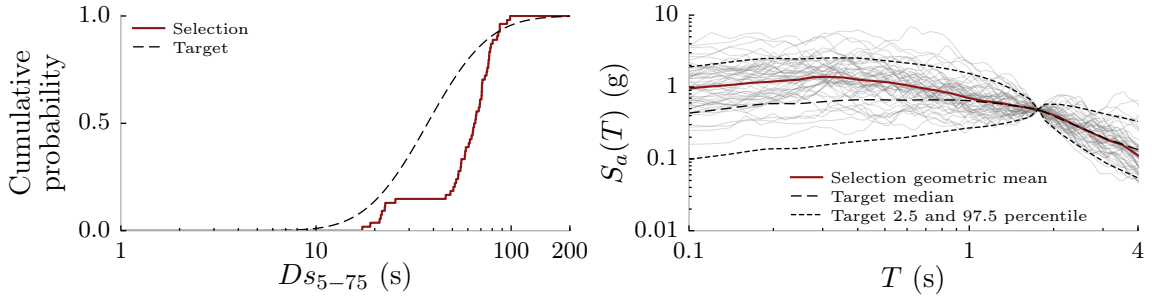

(b) Interface earthquakes: 54 / 100 ground motions

Figure 4.11: Ground motions selected in the *CS and causal parameters* group at the (a) $S_a(1.8\,\text{s}) = 0.24\,\text{g}$ intensity level (2 % in 50 year hazard level), and the (b) $S_a(1.8\,\text{s}) = 0.49\,\text{g}$ intensity level (0.25 % in 50 year hazard level) in Seattle, corresponding to interface earthquakes.

imposed on them. The specific constraints imposed at the $S_a(1.8\,\text{s}) = 0.24\,\text{g}$ intensity level, corresponding to each type of contributing seismic source, are summarized in Table 4.2. The durations and response spectra of the ground motions corresponding to interface earthquakes, selected at the $S_a(1.8\,\text{s}) = 0.24\,\text{g}$ and $0.49\,\text{g}$ intensity levels (corresponding to the 2 % and 0.25 % in 50 year hazard levels respectively), are shown in Figure 4.11.

The response spectra of the interface earthquake ground motions selected at the $S_a(1.8\,\text{s}) = 0.24\,\text{g}$ intensity level are seen to match their targets well, but those selected at the $S_a(1.8\,\text{s}) = 0.49\,\text{g}$ intensity level produce a poorer fit, with larger response spectral ordinates than the targets at periods below the conditioning period. The response spectra of the ground motions corresponding to crustal and in-slab earthquakes also follow similar trends. These poorer fits are a consequence of the limited number of

Table 4.2: Constraints on the magnitude, M, source-to-site distance, R, and site Vs_{30} of the ground motions selected into the *CS and causal parameters* group, relative to the target source-specific mean causal magnitude and source-to-site distance obtained from deaggregation results, at the $S_a(1.8\,\text{s}) = 0.24\,\text{g}$ intensity level (2 % in 50 year hazard level) in Seattle.

Seismic source type	**Target**			**Selection constraints**					**No. of suitable records**	**No. of selected records**
	$\bar{M}$	$\bar{R}$ (km)	$\boldsymbol{Vs_{30}}$ (m/s)	$\boldsymbol{M_{min}}$	$\boldsymbol{M_{max}}$	$\boldsymbol{R_{min}}$ (km)	$\boldsymbol{R_{max}}$ (km)	$\boldsymbol{Vs_{30,min}}$ (m/s)	$\boldsymbol{Vs_{30,max}}$ (m/s)	
Interface	8.9	114	760	8.6	9.2	74	154	–	–	168	47
In-slab	6.9	62	760	6.4	7.4	42	82	360	1160	48	22
Crustal	6.9	7	760	6.4	7.4	2	12	360	1160	82	31

recorded ground motions that satisfy the constraints imposed on the causal parameters, even though the constraints used here are somewhat relaxed compared to those used in conventional ground motion selection practice. This is evident from the last two columns of Table 4.2, which list the number of ground motions available to select from, and the number of selected ground motions, at the $S_a(1.8\,\mathrm{s}) = 0.24\,\mathrm{g}$ intensity level. Although this problem could be slightly alleviated by increasing the maximum permissible ground motion scale factor, the scaling of low amplitude ground motions by large scale factors can produce other inconsistencies, and is not recommended. The number of available ground motions gets even smaller at higher intensity levels, thus leading to even poorer fits. Therefore, while the selection of ground motions based on causal parameters might work well for evaluations conducted at low intensity levels, it is not as reliable when selecting ground motions at higher intensity levels for collapse risk estimation. This suggests that aggressive screening of candidate ground motions with respect to causal parameters can be counter-productive, since it can result in the selection of ground motions with less desirable response spectra and durations: properties known to more directly influence structural response. Causal parameters like magnitude, source-to-site distance, and site Vs_{30}, which only implicitly control time series characteristics, should be a secondary consideration to the time series characteristics themselves.

The durations of the selected ground motions corresponding to interface earthquakes are seen to be longer than their target at both intensity levels. This trend is observed at all eight intensity levels, and is an artifact of the limited number of recorded earthquakes with magnitudes within the range of the imposed constraints: in this case, only the 2010 Maule (Chile) and 2011 Tohoku (Japan) earthquakes. The step in the empirical cumulative distributions of Ds_{5-75} distinguish the relatively shorter duration records from the 2010 Maule earthquake ($Ds_{5-75} \sim 20\,\mathrm{s}$–$30\,\mathrm{s}$) from the relatively longer duration records from the 2011 Tohoku earthquake ($Ds_{5-75} \sim 50\,\mathrm{s}$–$90\,\mathrm{s}$). The durations of the selected ground motions corresponding to crustal and in-slab earthquakes do, however, approximately match their targets at all eight intensity levels for same the reasons described above for the *CS only* control group.

Plots of the durations and response spectra of all the ground motions selected into

the three groups (similar to Figure 4.9), at all eight intensity levels, are available in the digital appendix. Summaries of the constraints imposed on the magnitude, source-to-site distance, and site Vs_{30} of the ground motions selected into the *CS and causal parameters* group (similar to Table 4.2), at each intensity level, are also included.

4.5.3 Collapse risk estimation

The collapse fragility of the reinforced concrete moment frame building was estimated using each of the three groups of ground motions described in § 4.5.2, selected to match the seismic hazard targets computed for Seattle. This entailed analyzing the structure under each ground motion and checking whether it led to structural collapse, which is indicated by the unbounded increase in the drift ratio at a story, above a threshold of 0.10. The adopted collapse story drift ratio threshold of 0.10 was chosen based on studies which indicated that it provides a fairly consistent measure of when the structure collapses by dynamic instability. Numerical time integration was performed using the explicit central difference scheme, since it was found to be more robust and efficient than implicit time integration schemes, which sometimes failed to converge. The fraction of ground motions that caused structural collapse at each intensity level was plotted against $S_a(1.8\,\mathrm{s})$, and a collapse fragility curve was computed by fitting a lognormal cumulative distribution function to the data using maximum likelihood estimation. Note that maximum likelihood estimation requires all ground motions at an intensity level to be independent, but this may not be the case for ground motions recorded from the same earthquake. Nonetheless, this is not expected to significantly influence the obtained results (Baker 2015). The resulting collapse fragility curves estimated using the three groups of ground motions are shown in Figure 4.12, along with the seismic hazard curve for Seattle.

The first observation from Figure 4.12 is that a larger fraction of the ground motions at the four highest intensity levels cause structural collapse in the *CS and duration* group than the *CS only* control group. Since the ground motions in these two groups have equivalent response spectra, the larger fraction of collapses can be

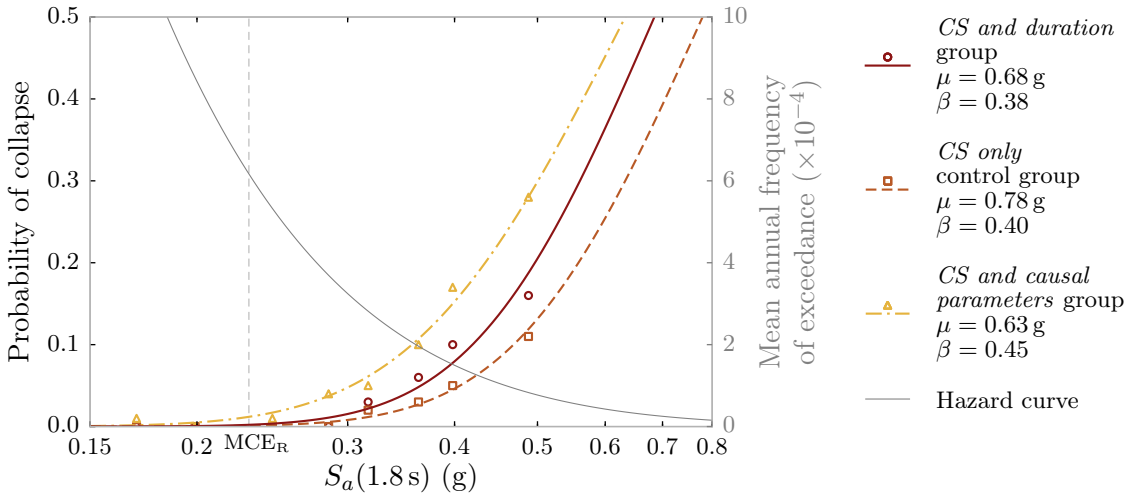

Figure 4.12: Collapse fragility curves of the reinforced concrete moment frame building, estimated using the three groups of selected ground motions (with median, μ, and lognormal standard deviation, β, indicated in the legend), along with the seismic hazard curve and the MCE$_R$ ground motion intensity for Seattle.

attributed to the presence of longer duration ground motions corresponding to interface earthquakes in the *CS and duration* group (compare Figures 4.9a and 4.10). This inference is supported by the fact that at the four highest intensity levels, 3 out of 3, 5 out of 6, 8 out of 10, and 10 out of 16 of the ground motions from the *CS and duration* group that caused structural collapse are from interface earthquakes. These results are consistent with those obtained by Raghunandan et al. (2015), who also concluded that long duration ground motions from interface earthquakes are more likely to cause the collapse of ductile moment frame buildings in Seattle. A more detailed comparison of the results is, however, not possible since Raghunandan et al. (2015) did not employ hazard-consistent ground motions. Although the adopted analysis procedure accounts for the uncertainty in the characteristics of the anticipated ground motions, it ignores the uncertainty in the characteristics of the structural model (FEMA 2009b). This simplification was considered appropriate for this study since it is the relative values of collapse risk estimates that are used to compare ground motion selection procedures; the absolute values are of lesser concern. The mean annual frequency of collapse, $\lambda_{collapse}$, computed by integrating the

product of the collapse fragility curve and the derivative of the seismic hazard curve, is estimated to be 5.4×10^{-5} using the *CS and duration* group, and 3.8×10^{-5} using the *CS only* control group. Therefore, ignoring ground motion duration results in an unconservative underestimation of $\lambda_{collapse}$ by 29 %. Note that if the Kempton and Stewart (2006) prediction equation for Ds_{5-75} were used instead of Abrahamson and Silva (1996), longer duration ground motions would have been selected in the *CS and duration* group (see Figure 4.2), and subsequently, an even larger effect of duration on $\lambda_{collapse}$ would have been observed.

This estimate of the percentage difference in $\lambda_{collapse}$, hereby abbreviated as $\Delta\lambda_{collapse}$, has an associated standard error, which can be estimated by bootstrapping (Efron and Tibshirani 1994). Here, we extend the method proposed by Eads et al. (2013), by enabling the estimation of the standard error in collapse risk estimates obtained using a multiple stripe analysis. Bootstrapping estimates the distribution of a statistic by repeatedly resampling from the observed data with replacement. In this case, a bootstrap estimate of the fraction of ground motions that cause structural collapse at an intensity level was made by sampling 100 ground motions with replacement, from the original 100 ground motions used at that intensity level. A collapse fragility curve was then fit to the resampled fractions of ground motions causing structural collapse at all eight intensity levels, and the corresponding $\lambda_{collapse}$ was computed.

Ten thousand such bootstrap estimates of the collapse fragility curve corresponding to the *CS and duration* group were made, a subset of which are plotted in Figure 4.13a. The standard error of the value of $\lambda_{collapse}$ estimated using the *CS and duration* group was then computed as the sample standard deviation of the ten thousand values of $\lambda_{collapse}$ computed from the bootstrapped collapse fragility curves. The computed standard error was 0.68×10^{-5}, which is 13 % of 5.4×10^{-5}, the estimated value of $\lambda_{collapse}$. It is evident from Figure 4.13a that the collapse fragility curve is well constrained only below the highest intensity level at which analyses were conducted ($S_a(1.8\,\text{s}) = 0.49\,\text{g}$ in this case). Large contributions to the structural collapse risk from higher intensity levels would, therefore, cause the standard error of the estimate of $\lambda_{collapse}$ to increase, thus highlighting the importance of appropriately selecting the ground motion intensity levels at which to analyze the structure. The

standard error of any other parameter, like the median or lognormal standard deviation of the collapse fragility curve, could be estimated in a similar manner. Following the same procedure, ten thousand bootstrap estimates of the collapse fragility curve corresponding to the *CS only* control group were also made, and the corresponding $\lambda_{collapse}$ values were computed. The ten thousand bootstrap estimates from the two groups were then taken in pairs and used to compute ten thousand values of $\Delta\lambda_{collapse}$. The histogram of these $\Delta\lambda_{collapse}$ values, shown in Figure 4.13b, describes the empirical sampling distribution of $\Delta\lambda_{collapse}$, and quantifies the influence of ground motion duration on the collapse risk of the structure located in Seattle. Although the number of bootstrap simulations used is in excess of that required to obtain stable estimates, no effort was made to optimize this number given the ease of producing large numbers of simulations. The standard error of $\Delta\lambda_{collapse}$ was computed to be 16 %. The empirical p-value of a hypothesis test (Rice 2006) with null hypothesis $\Delta\lambda_{collapse} = 0$ was computed as 0.06: the fraction of all simulated $\Delta\lambda_{collapse}$ values that are lesser than zero. This is only slightly above the conventionally accepted threshold of 0.05 and indicates that if the effect of duration is considered to be statistically significant by rejecting the null hypothesis, there is a 6 % probability of doing so erroneously, i.e., encountering a Type-1 error. The standard error of $\Delta\lambda_{collapse}$ can be reduced by analyzing the structure using more ground motions at each intensity level.

It can also be observed from Figure 4.12 that the fraction of ground motions from the *CS and causal parameters* group that cause structural collapse at each intensity level is even larger than the *CS and duration* group. This overestimation of the collapse risk can be attributed to (*i*) the longer durations of the ground motions in the *CS and causal parameters* group selected to match targets corresponding to interface earthquakes (with median Ds_{5-75} almost twice the conditional median targets at all intensity levels), and (*ii*) the larger response spectral ordinates at periods below the conditioning period, of the ground motions selected to match targets corresponding to all types of sources at high intensity levels (e.g., compare Figures 4.9a and 4.11, or refer to similar plots in the digital appendix). Of the two factors, the effect of longer duration ground motions is expected to be more dominant, since the collapse response of the structure is expected to be controlled primarily by spectral ordinates

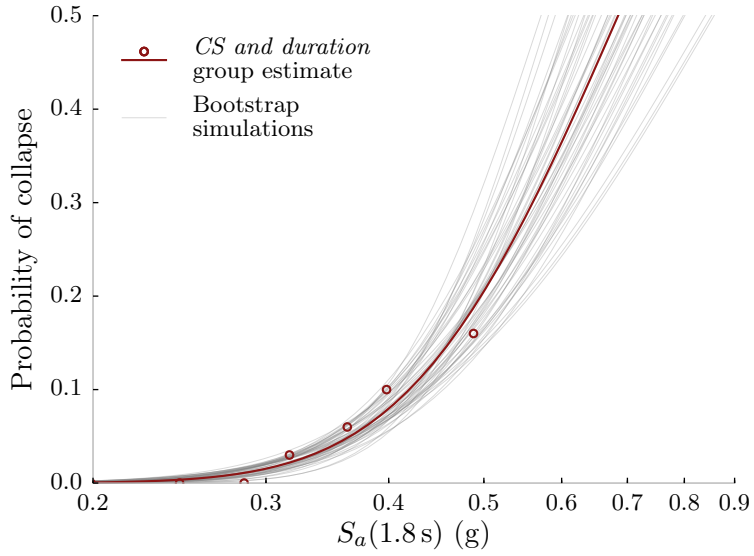

(a)

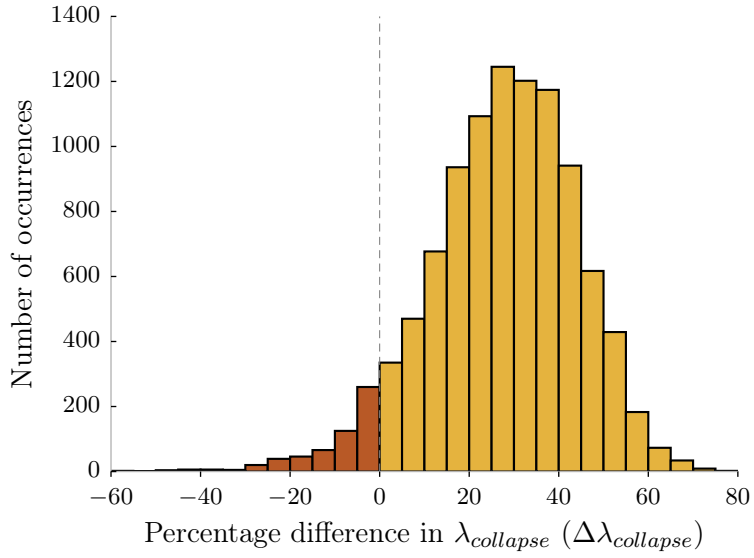

(b)

Figure 4.13: (a) Bootstrap estimates of the collapse fragility curve corresponding to the *CS and duration* group, and (b) the histogram of bootstrap estimates of the percentage difference in $\lambda_{collapse}$ estimated by the *CS and duration* and *CS only* ground motion groups ($\Delta\lambda_{collapse}$).

at periods above the conditioning period. The $\lambda_{collapse}$ estimated by the *CS and causal parameters* group is 53 % larger than the value estimated using the *CS and duration* group. The standard error of this $\Delta\lambda_{collapse}$ value is 25 %, and the empirical p-value is 0.00, which implies that the estimated value of $\Delta\lambda_{collapse}$ is statistically significant. This bias in the estimated collapse risk provides further evidence of the drawbacks of relying too much on earthquake causal parameters to capture effects that are better represented by duration and response spectra.

To contrast the influence of ground motion duration on structural collapse risk for sites in Eugene and San Francisco, the ground motion selection and collapse risk assessment procedure described above, was repeated for these two sites. The durations and response spectra of the ground motions selected into the three groups for Eugene and San Francisco were found to follow identical trends as those selected for Seattle, when compared to their respective targets. The same building was used at all sites, although it was designed for a site in Seattle, to simplify the comparison of different ground motion selection procedures. Plots of the durations and response spectra of all the selected ground motions are available in the digital appendix, along with the collapse fragility curves estimated using them. The $\lambda_{collapse}$ values estimated using the three groups of ground motions selected for Seattle, Eugene, and San Francisco, are summarized in Table 4.3. In Eugene, the $\lambda_{collapse}$ estimated by the *CS only* control group is 59 % lower than that estimated by the *CS and duration* group. This decrease is larger than the 29 % decrease observed in Seattle and can be explained by the larger percentage contribution from interface earthquakes to the seismic hazard at Eugene, hence resulting in a difference in the durations of a larger fraction of ground motions in the two groups, at each intensity level. In San Francisco, the $\lambda_{collapse}$ estimated by the *CS only* control group is only 7 % lower. This small $\Delta\lambda_{collapse}$ value is the consequence of a near 100 % contribution from crustal earthquakes to the seismic hazard at San Francisco, hence resulting in the selection of ground motions of almost similar duration in both groups. The $\lambda_{collapse}$ estimated by the *CS and causal parameters* group is greater than the $\lambda_{collapse}$ estimated by the *CS and duration* and *CS only* groups in both Eugene and San Francisco, following the same trend observed for Seattle. In the case of Eugene, this can be attributed to the longer durations of

Table 4.3: Mean annual frequency of collapse ($\lambda_{collapse}$) of the reinforced concrete moment frame building, as estimated using the three groups of ground motions selected for the three considered sites. The percentage by which the $\lambda_{collapse}$ values estimated using the *CS only* control group and the *CS and causal parameters* group differ from the value estimated using the *CS and duration* group is indicated in parentheses.

Ground motion group	**Seattle**	**Eugene**	**San Francisco**
CS and duration group	5.4×10^{-5}	7.2×10^{-5}	15×10^{-5}
CS only control group	3.8×10^{-5} (−29 %)	2.9×10^{-5} (−59 %)	14×10^{-5} (−7 %)
CS and causal parameters group	8.2×10^{-5} (+53 %)	9.7×10^{-5} (+34 %)	23×10^{-5} (+51 %)

the ground motions selected to match targets corresponding to interface earthquakes, as well as the larger response spectral ordinates at periods below the conditioning period, of all the ground motions selected at high intensity levels, similar to the reasons outlined for Seattle above. In the case of San Francisco, however, this can be attributed only to the larger response spectral ordinates, since the durations of ground motions in the *CS and causal parameters* group are similar to those in the other two groups.

Finally, the lognormal collapse fragility curves estimated using the three groups of ground motions, selected for each of the three sites, were modified to incorporate model uncertainty in an approximate manner, as per the recommendations of FEMA (2009b). They were recomputed using the same median, but by adding a lognormal standard deviation of 0.35, corresponding to modeling uncertainty (as recommended by FEMA 2009b), using the square root of sum of squares method. Although this change increased the computed $\lambda_{collapse}$ values as expected, the relative trends between the different ground motion groups and sites were found to remain the same. These trends are expected to be present even if an explicit simulation-based method were used to account for model uncertainty.

4.6 Conclusion

A procedure to compute source-specific probability distributions of ground motion duration, conditional on the exceedance of a spectral acceleration value, $S_a(T^*)$, was developed. This calculation procedure is based on the generalized conditional intensity measure (GCIM) approach (Bradley 2010). These source-specific conditional distributions of duration, along with conditional spectra, serve as targets for the selection of hazard-consistent ground motions for structural performance assessment. They were used in this study to assess the impact of considering hazard-consistent duration targets when selecting ground motions for structural collapse risk assessment.

The contribution of long duration ground motions produced by large magnitude interface earthquakes in the Cascadia subduction zone, to the seismic hazard in Western USA was studied. Target distributions of duration and response spectra were computed for sites in Seattle, Eugene, and San Francisco, each of which are located in distinct tectonic settings. While interface, in-slab, and crustal earthquakes contribute to the seismic hazard at Seattle, only interface and in-slab earthquakes contribute to the hazard at Eugene, and only crustal earthquakes contribute to the hazard at San Francisco. Considerations for selecting an appropriate mix of hazard-consistent ground motions for a given seismic hazard environment were discussed, using Seattle as an example.

The impact of explicitly considering ground motion duration targets when selecting records for structural collapse risk assessment was demonstrated by analyzing a ductile eight-story reinforced concrete moment frame building, designed for a site in Seattle. The mean annual frequency of collapse, $\lambda_{collapse}$, of the structure was first estimated by conducting a multiple stripe analysis using hazard-consistent ground motions, selected to match both duration and response spectrum targets computed for Seattle. When analyzed using standard duration ground motions from the PEER NGA-West2 database, selected to match only response spectrum targets, $\lambda_{collapse}$ was found to be underestimated by 29 %. This difference was attributed to the difference in the durations of the ground motions in the two groups. Similarly, $\lambda_{collapse}$

was underestimated by 59 % and 7 % when the same structure was analyzed using ground motions selected to match targets computed for Eugene and San Francisco respectively. As expected, ground motion duration was found to be a more important consideration in sites with large contributions to their seismic hazard from large magnitude interface earthquakes. These collapse risk estimates were obtained using the Abrahamson and Silva (1996) prediction equation for Ds_{5-75}. A larger effect of duration would have been observed if the Kempton and Stewart (2006) prediction equation were used instead, since it predicts longer ground motion durations. These results are specific to the eight-story moment frame building studied here, and the effect of duration on structural collapse risk may vary depending on structural characteristics like period, ductility, and rate of strength and stiffness deterioration (Chapter 2/Chandramohan et al. 2016b).

The bootstrap was proposed as a convenient tool to estimate the sampling distribution and standard error of structural collapse risk parameters estimated using multiple stripe analysis. It was used here to estimate the standard error of the difference in the mean annual frequency of collapse computed using two groups of ground motions.

Commonly used ground motion selection procedures that employ earthquake causal parameters like magnitude, source-to-site distance, and site Vs_{30} as surrogates for ground motion characteristics like duration, were found to produce poorer fits to the duration and response spectrum targets due to the limited number of recorded ground motions that satisfy the imposed constraints on the ranges of the causal parameters. As a consequence, ground motions selected using this method to match targets computed for Seattle, were found to overestimate $\lambda_{collapse}$ by 53 %.

The results of this study demonstrate and quantify the potential contribution of ground motion duration to the collapse risk of structures located at sites where large magnitude earthquakes contribute significantly to the seismic hazard. This warrants an explicit consideration of ground motion duration, in addition to response spectra, in the design and assessment of structures located near active subduction zones, which typically produce such large magnitude earthquakes ($M_W \sim 9.0$). It should be noted, however, that although duration can have a significant influence on

structural collapse, its effect on structural response at lower ground motion intensity levels that do not produce deformations large enough to cause significant strength and stiffness deterioration is much less pronounced (Bommer et al. 2015). Therefore, code-based nonlinear structural assessments conducted at or below the MCE_R ground motion intensity level are unlikely to detect the influence of duration (Chapter 2/ Chandramohan et al. 2016b). This suggests that methods to incorporate the effect of ground motion duration in code-based design procedures should be assessed and calibrated using collapse risk analyses, and then factored into design criteria that are typically evaluated at the MCE_R intensity level.

Chapter 5

Hazard-consistent structural collapse risk assessment using incremental dynamic analysis

5.1 Abstract

This study develops a structural reliability framework that can be used to compute a hazard-consistent collapse fragility curve from the results of an incremental dynamic analysis (IDA), conducted using a generic set of ground motions. The inability to produce hazard-consistent collapse risk estimates has long been considered the biggest shortcoming of IDA, and hence, this development brings its capabilities on par with multiple stripe analysis (MSA). The developed reliability framework quantifies ground motion intensity using $S_a(T_1)$, response spectral shape using a scalar, dimensionless parameter called S_aRatio, and duration using significant duration, Ds. A failure surface is estimated by fitting a linear regression model containing S_aRatio and Ds as predictors, to the ground motion collapse intensities computed from an IDA. S_aRatio and Ds were found to be capable of explaining 81 % of the variance in the ground motion collapse intensities computed by analyzing an eight-story reinforced concrete

moment frame building. They were similarly found to produce good fits to the collapse intensities computed by analyzing 50 other reinforced concrete moment frame buildings as well. The target distributions of S_aRatio and Ds anticipated at the site are then integrated over the failure domain to compute a hazard-consistent collapse fragility curve. The computed fragility curve of the analyzed eight-story reinforced concrete frame, was found to agree well with that obtained by conducting MSA using hazard-consistent ground motions, at three different sites with distinct S_aRatio and Ds targets: Seattle (Washington), Eugene (Oregon), and San Francisco (California).

5.2 Introduction

Obtaining an accurate estimate of the seismic collapse risk of a structure requires explicit consideration of the nature and characteristics of the ground motions that can be anticipated at the site where it is located, commonly referred to as site-specific seismic hazard information (Bommer et al. 2000; Katsanos et al. 2010). More specifically, it requires the consideration of those ground motion characteristics that are known to influence structural collapse capacity, e.g., amplitude, frequency content, duration, velocity pulses. Hazard-consistent target distributions of any set of ground motion intensity measures (IMs), conditional on the exceedance of a primary, amplitude-based IM, can be computed using the framework developed by Bradley (2010) and Baker (2011). Incremental dynamic analysis (IDA) (Vamvatsikos and Cornell 2002) is a commonly used method of analysis, wherein a structure is analyzed using ground motions that are incrementally scaled to higher intensity levels, until they cause structural collapse. IDA is frequently conducted using generic ground motion sets like the FEMA P695 far-field set (FEMA 2009b, Appendix A), the Large-Magnitude Small-Distance (LMSR) set (Krawinkler et al. 2003), and the PEER Transportation sets (Baker et al. 2011, Chapter 3), which were developed to be structure and site-independent, and hence, do not represent the seismic hazard at any particular site. Although IDA can be conducted using site-specific ground motions, the additional effort involved in selecting these ground motions makes it an unattractive option. Even if site-specific ground motions are used, using the same set of ground motions scaled to

different intensity levels has been shown to produce inaccurate, hazard-inconsistent structural collapse risk estimates, since ground motions of different intensities are inherently expected to possess different characteristics, like duration and response spectral shape (Bradley 2013; Kwong et al. 2015). A procedure to compute a hazard-consistent median collapse capacity by iteratively conducting a modified version of IDA using ground motions selected to match targets conditional on different successive intensity levels is described in FEMA P-58 (FEMA 2012b, Appendix J), but this method is limited and cumbersome. This paper develops a structural reliability framework (Melchers 1999) incorporating ground motion duration and response spectral shape, that can be used to compute a hazard-consistent collapse fragility curve by post-processing the results of an IDA conducted using a generic record set, thereby eliminating its biggest shortcoming, and making it a competitive alternative to multiple stripe analysis (MSA) (Jalayer 2003, Chapter 4).

MSA is yet another method of analysis, wherein a structure is analyzed using different sets of ground motions, each scaled to a different intensity level. Hazard-consistent collapse risk estimates can be obtained by ensuring the characteristics of the ground motions selected at each intensity level, like duration and response spectral shape, match their corresponding hazard-consistent target distributions, conditional on that intensity level. This advantage of MSA was the reason for its adoption by FEMA P-58 as the recommended procedure to conduct time-based structural performance assessments (FEMA 2012b, Chapter 4). IDA, nevertheless, still remains a popular choice due to its relative simplicity, especially since it can be conducted using readily available generic ground motion sets. The FEMA P695 methodology for quantifying building seismic performance factors, for example, requires conducting a modified version of IDA using a generic prescribed record set, to estimate structural collapse risk (FEMA 2009b, Chapter 6). It attempts to improve the accuracy of the collapse risk estimate by adjusting the computed median collapse capacity using a spectral shape factor, empirically calibrated using ε (Baker and Cornell 2005) as a proxy for response spectral shape (FEMA 2009b, Appendix B). Haselton et al. (2011a) also similarly proposes an adjustment to the median collapse capacity based on ε. In addition to being approximate, this adjustment is shown in this study to be

inadequate at sites susceptible to long duration ground motions from large magnitude earthquakes, where an analogous correction for duration is also required. Most previous attempts to enhance IDA have focussed on improving either its (*i*) *precision*, by developing efficient scalar and vector IMs, usually derived from response spectra, that exhibit a low degree of variability when used to represent the computed collapse fragility curve (e.g., Cordova et al. 2000; Vamvatsikos and Cornell 2005; Bojórquez and Iervolino 2011; Eads et al. 2015; Marafi et al. 2016), or its (*ii*) *computational efficiency* (e.g., Vamvatsikos 2011; Hardyniec and Charney 2015). Some studies like Dolšek (2009) and Vamvatsikos (2014) have attempted to improve its *accuracy* by developing the capability to account for model uncertainty, in addition to record-to-record uncertainty. This study seeks to improve its accuracy, in line with previous attempts like FEMA (2009b) (Appendix B), Haselton et al. (2011a), and FEMA (2012b) (Appendix J), by imparting the ability to compute a site-specific, hazard-consistent collapse fragility curve, using a generic set of ground motions. A simplified procedure is also proposed to efficiently compute the hazard-consistent median collapse capacity of a structure, in case the entire collapse fragility curve is not required.

Ground motion selection guidelines contained in current structural design and performance assessment standards (e.g., PEER TBI 2010, Chapter 5; FEMA 2012b, Chapter 4; ASCE 2016) explicitly ensure that only the response spectra of the selected ground motions match site-specific targets. They relegate other ground motion characteristics to qualitative consideration. The response spectrum of a ground motion, which quantifies its amplitude and frequency content, has been shown by a number of studies to be well correlated to the peak deformations and collapse capacity of a structure (e.g., Shome et al. 1998; Baker and Cornell 2006b), thus justifying its prominent use as a vector ground motion intensity measure. Recent studies have, however, also demonstrated the influence of ground motion duration on structural collapse risk (Raghunandan and Liel 2013; Chapter 4/Chandramohan et al. 2016a), warranting its explicit consideration in structural performance assessment and design, in addition to response spectra. This paper corroborates the findings of these studies by demonstrating that a ground motion's response spectral shape and duration are both efficient predictors of its collapse intensity. The collapse intensity of a ground

motion, which is a commonly used metric to quantify its damage potential, refers to the lowest intensity it needs to be scaled to, to cause structural collapse. Ground motion intensity is quantified by the spectral acceleration at the fundamental modal period of the structure, $S_a(T_1)$, in line with current structural design practice. Response spectral shape is quantified using a scalar parameter called S_aRatio (Eads et al. 2016), and duration using significant duration, Ds (Trifunac and Brady 1975).

The computation of hazard-consistent target distributions of S_aRatio and Ds, which constitute the site-specific *loads* within the structural reliability framework, is first described. The computation of the structure-specific *failure surface* using the results of an IDA is demonstrated using a ductile eight-story reinforced concrete moment frame building located in Seattle. The procedure to compute a hazard-consistent collapse fragility curve by evaluating the *reliability integral* is then described, and the results are shown to compare well with those obtained by conducting MSA using hazard-consistent ground motions. In fact, hazard-consistent MSA is demonstrated to represent an alternative simulation-based approach to solve the same structural reliability problem, which the proposed framework solves analytically. Although $S_a(T_1)$ is used as the primary IM, and S_aRatio and Ds as the secondary IMs in this study, the proposed reliability framework is general in nature, and can accommodate any alternate set of IMs as well. Factors governing the choice of IMs to be used in the reliability framework are discussed and used to demonstrate the effectiveness of the chosen set of IMs. The reliability framework is then applied to a total of 51 reinforced concrete moment frame buildings, to evaluate and compare the predictive power of a number of duration metrics proposed in the literature (Bommer and Martinez-Pereira 1999), including different percentage ranges used to compute Ds. The efficiency of different period ranges used to compute S_aRatio is also examined. Finally, a broad set of guidelines for ground motion selection to obtain accurate collapse risk estimates using the reliability framework, are proposed.

5.3 Computation of S_aRatio and Ds of a ground motion

The parameter S_aRatio was proposed by Eads et al. (2016) as a scalar, dimensionless measure of a ground motion's response spectral shape. It is computed according to Equation (5.1a), as the ratio of the spectral acceleration at a specific period, $S_a(T)$, and the geometric mean of the portion of the response spectrum that lies between the periods T_{start} (usually $< T$) and T_{end} (usually $> T$), denoted by $S_{a,avg}(T_{start}, T_{end})$. Note that 5 % damped pseudo acceleration response spectra are used throughout this paper. $S_{a,avg}(T_{start}, T_{end})$ is computed according to Equation (5.1b), as the sample geometric mean of response spectral ordinates, discretely sampled at n linearly spaced periods from T_{start} to T_{end}: τ_1, τ_2, ..., τ_n, such that $\tau_1 = T_{start}$ and $\tau_n = T_{end}$ (Baker and Cornell 2006a; Eads et al. 2015):

$$S_aRatio(T, T_{start}, T_{end}) = \frac{S_a(T)}{S_{a,avg}(T_{start}, T_{end})} \tag{5.1a}$$

$$S_{a,avg}(T_{start}, T_{end}) = \left(\prod_{j=1}^{n} S_a(\tau_j) \right)^{1/n} \tag{5.1b}$$

A more general method to compute $S_{a,avg}$, as the geometric mean of the function $S_a(T)$, is described in Appendix B. This method offers the advantage of not requiring the re-sampling of the response spectrum at a set of specific linearly spaced periods, and avoids any loss in accuracy in the computation of $S_{a,avg}$ due to widely spaced periods.

The response spectra of two ground motions with low and high $S_aRatio(1.0\,\text{s}, 0.2\,\text{s}, 3.0\,\text{s})$ values, normalized to have $S_a(1.0\,\text{s}) = 1\,\text{g}$, are plotted in Figure 5.1. Since S_aRatio is a dimensionless metric, its value remains unchanged as the ground motions are linearly scaled. The ground motion with a low S_aRatio value has a low response spectral ordinate at 1.0 s and relatively high response spectral ordinates at all other periods between 0.2 s and 3.0 s. The opposite is true for the ground motion with a high S_aRatio value. Since the two ground motions are scaled to the same $S_a(1.0\,\text{s})$ value,

assuming they also have similar durations, the ground motion with a low S_aRatio value is expected to be more damaging, because it possesses more energy at periods above and below 1.0 s. Eads et al. (2015) recommended using the period range $0.2T$ to $3.0T$ to compute S_aRatio at the period T, since it was found to be most efficient in predicting the collapse intensity of a ground motion used to analyze a structure with fundamental elastic modal period T. This recommendation was based on observations from conducting collapse analyses on a number of reinforced concrete moment frame and shear wall buildings. Although the optimal period range to compute S_aRatio is expected to be a function of structural characteristics like material, structural system, fundamental elastic modal period, ductility, etc., the range $0.2T$ to $3.0T$ was found to perform close to optimal for all the structures considered in this study as well.

The parameter $\varepsilon\big[S_a(T)\big]$, defined as the number of standard deviations the natural logarithm of $S_a(T)$ of a ground motion is above or below the natural logarithm of the median $S_a(T)$ value predicted by a prediction equation, has been previously used as an implicit measure of a ground motion's response spectral shape in standards like FEMA P695 (FEMA 2009b, Appendix B; Haselton et al. 2011a). The parameter S_aRatio is, however, preferred over $\varepsilon\big[S_a(T)\big]$ in this study, because it offers the advantage of being computable directly from a ground motion time series, without any knowledge of its causal parameters, like magnitude, source-to-site distance, and site Vs_{30} (the time-averaged shear wave velocity of the top 30 m of the soil profile). Eads et al. (2016) also demonstrated that S_aRatio is a better predictor of a ground motion's collapse intensity, than $\varepsilon\big[S_a(T)\big]$.

The significant duration of a ground motion is defined as the time interval over which a specific percentage range of the integral $\int_0^{t_{max}} a^2(t)dt$ is accumulated, where $a(t)$ represents the ground acceleration at time t, and t_{max} represents the length of the accelerogram. The computation of 5–75 % significant duration, Ds_{5-75}, of an accelerogram is illustrated in Figure 5.2. Significant duration is used here since it was identified to be the duration metric best suited for ground motion selection for collapse risk assessment in Chapter 2/Chandramohan et al. (2016b).

Although S_aRatio and Ds are used in conjunction with $S_a(T_1)$ in the calculations presented below, the reliability framework proposed in this paper is general in nature,

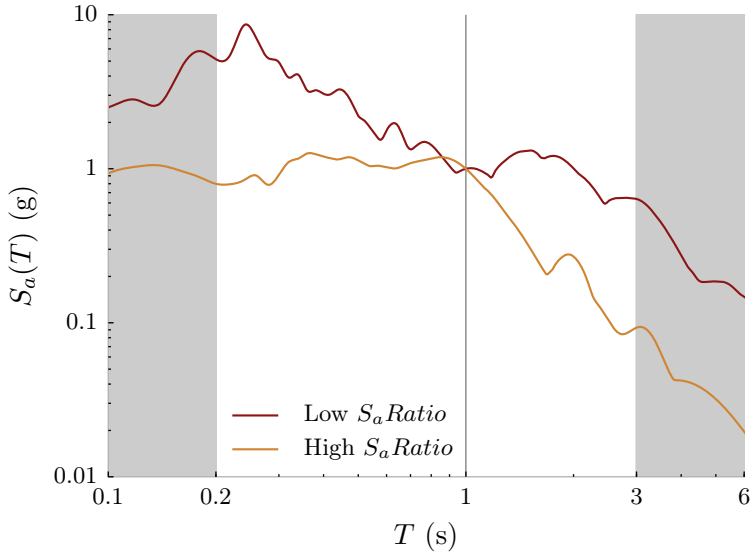

Figure 5.1: Response spectra of two ground motions with low and high $S_aRatio(1.0\,\text{s}, 0.2\,\text{s}, 3.0\,\text{s})$ values, normalized to have $S_a(1.0\,\text{s}) = 1\,\text{g}$. The vertical line at 1.0 s corresponds to the period at which S_a in the numerator of Equation (5.1a) is computed, and the unshaded period range from 0.2 s to 3.0 s corresponds to the domain over which $S_{a,avg}$ in the denominator of Equation (5.1a) is computed. The ground motion with a low $S_aRatio(1.0\,\text{s}, 0.2\,\text{s}, 3.0\,\text{s})$ value of 0.88 was recorded from the 1979 Imperial Valley earthquake, at the El Centro Array #11 station; and the one with a high $S_aRatio(1.0\,\text{s}, 0.2\,\text{s}, 3.0\,\text{s})$ value of 2.95 was recorded from the 1999 Duzce, Turkey earthquake, at the Bolu station. Both ground motions are taken from the FEMA P695 far-field set.

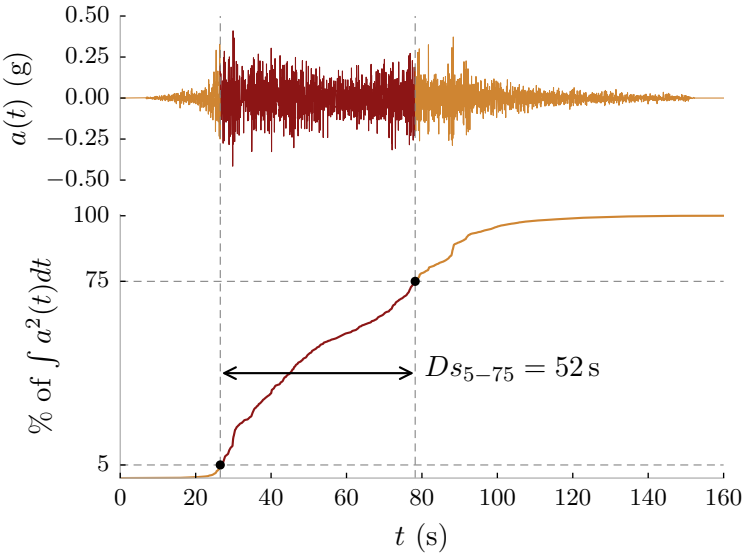

Figure 5.2: (Top) East-West component of the accelerogram recorded from the 2010 Maule (Chile) earthquake at the Talca station; and (Bottom) the normalized, cumulative integral of $a^2(t)$—known as a Husid plot (Husid 1969)—illustrating the computation of 5–75 % significant duration of the accelerogram.

and can be used with any set of IMs that possess the characteristics described in § 5.6. $S_a(T_1)$, S_aRatio, and Ds are, however, shown to possess a number of characteristics that make them well suited for use in the reliability framework.

5.4 Computation of hazard-consistent target distributions of S_aRatio and Ds

The procedure to compute hazard-consistent target probability distributions of S_aRatio and Ds is an extension of previously developed methods to compute a conditional spectrum (Abrahamson and Al Atik 2010; Jayaram et al. 2011b) and generalized conditional intensity measure (GCIM) (Bradley 2010). These distributions are computed conditional on the exceedance of a primary, amplitude-based, scalar ground motion intensity measure, which is quantified by traditional probabilistic seismic hazard analysis (PSHA) (McGuire 2004). This method sidesteps the complications associated

with vector PSHA (Bazzurro 1998; Baker and Cornell 2005; Kohrangi et al. 2016), while retaining all the benefits of using a vector IM over a scalar IM, as demonstrated in § 5.5.3. The spectral acceleration at the fundamental modal period of the structure under consideration, $S_a(T_1)$, is used as the conditioning intensity measure in this study, in line with current structural evaluation practice.

Let $\mathbf{\ln IM}$ represent the vector containing the natural logarithms of $S_a(\tau_j)$: the response spectral ordinates at the same linearly spaced periods used to compute $S_{a,avg}$ according to Equation (5.1b), and Ds:

$$\mathbf{\ln IM} = \begin{Bmatrix} \ln S_a(\tau_1) \\ \ln S_a(\tau_2) \\ \vdots \\ \ln S_a(\tau_n) \\ \ln Ds \end{Bmatrix} = \begin{Bmatrix} \ln IM_1 \\ \ln IM_2 \\ \vdots \\ \ln IM_n \\ \ln IM_{n+1} \end{Bmatrix} \tag{5.2}$$

Since values of $S_a(\tau_j)$ and Ds for a given earthquake scenario, are usually modeled as lognormal random variables, $\mathbf{\ln IM}$ for a given earthquake scenario, has a multivariate normal distribution (Abrahamson and Silva 1996; Jayaram and Baker 2008). Computing the mean and covariance of $\mathbf{\ln IM}$ conditional on the exceedance of a certain $S_a(T_1)$ value: $\boldsymbol{\mu}_{\mathbf{\ln IM} \mid \ln S_a(T_1)}$ and $\boldsymbol{\Sigma}_{\mathbf{\ln IM} \mid \ln S_a(T_1)}$ respectively, requires knowledge of the seismic hazard deaggregation, i.e., the earthquake scenarios that are most likely to cause the exceedance of that $S_a(T_1)$ value at the site. Let the i^{th} of m earthquake scenarios be defined by (i) magnitude, M_i; (ii) source-to-site distance, R_i; (iii) other characteristics (e.g., Vs_{30}, faulting mechanism), $\boldsymbol{\Theta}_i$; (iv) total residual or ε-value for $S_a(T_1)$, $\varepsilon_i\big[S_a(T_1)\big]$; and (v) relative contribution p_i.

The marginal mean and standard deviation of $\ln IM_k$: the k^{th} element of $\mathbf{\ln IM}$, for the i^{th} earthquake scenario, is then computed using a prediction equation for IM_k:

$$\mu_{\ln IM_k(i)} = g_{IM_k}(M_i, R_i, \boldsymbol{\Theta}_i) \tag{5.3a}$$

$$\sigma_{\ln IM_k(i)} = h_{IM_k}(M_i, R_i, \boldsymbol{\Theta}_i) \tag{5.3b}$$

where g_{IM_k} and h_{IM_k} represent functions defined by the prediction equation for IM_k. For a site like Seattle, which receives seismic hazard contributions from multiple types of seismic sources (interface and in-slab earthquakes from the Cascadia subduction zone, and crustal earthquakes from the Seattle fault zone), appropriate models specific to each type of source should be used in the computations. This study uses Campbell and Bozorgnia (2014) to predict response spectral ordinates for crustal earthquakes and Abrahamson et al. (2016) for interface and in-slab earthquakes. Abrahamson and Silva (1996) is used to predict significant duration for all types of seismic sources. It is worth noting that empirical prediction equations are currently limited in their ability to capture the anticipated amplification in response spectral ordinates and durations of ground motions at sites atop sedimentary basins, e.g., Seattle, Los Angeles, and Mexico City, although some attempt to do so via a basin-depth term (Marafi et al. 2017). Physics-based ground motion simulations, on the other hand, show tremendous promise in quantifying the seismic hazard at such sites (Chávez-García and Bard 1994; Frankel 2000; Pitarka 2004; Frankel et al. 2007; Olsen et al. 2008).

The covariance matrix of $\mathbf{ln}\,\boldsymbol{IM}$ for the i^{th} earthquake scenario is given by

$$\boldsymbol{\Sigma}_{\mathbf{ln}\,\boldsymbol{IM}(i)} = \boldsymbol{\sigma}_{\mathbf{ln}\,\boldsymbol{IM}(i)}\ \boldsymbol{\rho}_{\boldsymbol{IM}}\ \boldsymbol{\sigma}_{\mathbf{ln}\,\boldsymbol{IM}(i)} \tag{5.4a}$$

$$\boldsymbol{\sigma}_{\mathbf{ln}\,\boldsymbol{IM}(i)} = \begin{bmatrix} \sigma_{\ln IM_1(i)} & & & \\ & \sigma_{\ln IM_2(i)} & & \\ & & \ddots & \\ & & & \sigma_{\ln IM_{n+1}(i)} \end{bmatrix} \tag{5.4b}$$

$$\boldsymbol{\rho}_{\boldsymbol{IM}} = \begin{bmatrix} 1 & \rho\big[IM_1, IM_2\big] & \dots & \rho\big[IM_1, IM_{n+1}\big] \\ \rho\big[IM_2, IM_1\big] & 1 & \dots & \rho\big[IM_2, IM_{n+1}\big] \\ \vdots & \vdots & \ddots & \vdots \\ \rho\big[IM_{n+1}, IM_1\big] & \rho\big[IM_{n+1}, IM_2\big] & \dots & 1 \end{bmatrix} \tag{5.4c}$$

where $\sigma_{\ln IM_k(i)}$ is computed using Equation (5.3b) and $\rho\big[IM_k, IM_l\big]$ represents the correlation between the ε-values of IM_k and IM_l. In this study, the Baker and Jayaram (2008) model for the correlation between the ε-values of response spectral ordinates is used for crustal and in-slab earthquakes, while the Al Atik (2011) model is

used for interface earthquakes. The Bradley (2011) model for the correlation between the ε-values of significant duration and response spectral ordinates is used for all types of seismic sources. Note that the Abrahamson and Silva (1996) and Bradley (2011) models for significant duration are used for all types of seismic sources although they were developed only for crustal sources, since similar models for interface and in-slab earthquakes have not yet been developed. Although these models are believed to be reasonable for the calculations performed here, additional studies are necessary to verify the validity of their use in this context.

The conditional mean of $\mathbf{\ln} \boldsymbol{IM}$ for the i^{th} earthquake scenario is then computed as

$$\boldsymbol{\mu}_{\mathbf{\ln} \boldsymbol{IM}(i) \,|\, \ln S_a(T_1)} = \begin{Bmatrix} \mu_{\ln IM_1(i)} + \rho\big[IM_1, S_a(T_1)\big]\ \varepsilon_i\big[S_a(T_1)\big]\ \sigma_{\ln IM_1(i)} \\ \mu_{\ln IM_2(i)} + \rho\big[IM_2, S_a(T_1)\big]\ \varepsilon_i\big[S_a(T_1)\big]\ \sigma_{\ln IM_2(i)} \\ \vdots \\ \mu_{\ln IM_{n+1}(i)} + \rho\big[IM_{n+1}, S_a(T_1)\big]\ \varepsilon_i\big[S_a(T_1)\big]\ \sigma_{\ln IM_{n+1}(i)} \end{Bmatrix} \tag{5.5}$$

where $\mu_{\ln IM_k(i)}$ and $\sigma_{\ln IM_k(i)}$ are computed using Equations (5.3a) and (5.3b) respectively. The conditional covariance of $\mathbf{\ln} \boldsymbol{IM}$ for the i^{th} earthquake scenario is computed as

$$\boldsymbol{\Sigma}_{\mathbf{\ln} \boldsymbol{IM}(i) \,|\, \ln S_a(T_1)} = \boldsymbol{\Sigma}_{\mathbf{\ln} \boldsymbol{IM}(i)} - \boldsymbol{a}_i\, \boldsymbol{a}_i^T \tag{5.6a}$$

$$\boldsymbol{a}_i = \begin{Bmatrix} \rho\big[IM_1, S_a(T_1)\big]\ \sigma_{\ln IM_1(i)} \\ \rho\big[IM_2, S_a(T_1)\big]\ \sigma_{\ln IM_2(i)} \\ \vdots \\ \rho\big[IM_{n+1}, S_a(T_1)\big]\ \sigma_{\ln IM_{n+1}(i)} \end{Bmatrix} \tag{5.6b}$$

where $\boldsymbol{\Sigma}_{\mathbf{\ln} \boldsymbol{IM}(i)}$ is computed using Equation (5.4a). Note that the computations described in Equations (5.4a) to (5.6b) are similar to those described in Equations (6) to (9) from Jayaram et al. (2011b). The equations in Jayaram et al. (2011b), however, describe the computation of a conditional spectrum only, and are extended here by appending $\ln Ds$ to the vector of logarithms of response spectral ordinates, consistent

with the GCIM approach. Equations (3) to (7) proposed by Bradley (2012) also provide similar information, although they individually compute conditional standard deviations and correlations, which can be combined in a manner similar to Equation (5.4a), to compute a conditional covariance matrix. Finally, the weighted average conditional mean and covariance of $\mathbf{ln}\,\boldsymbol{IM}$, over all m deaggregated earthquake scenarios, can be computed using

$$\boldsymbol{\mu}_{\mathbf{ln}\,\boldsymbol{IM}\,|\,\ln S_a(T_1)} = \sum_{i=1}^{m} p_i\,\boldsymbol{\mu}_{\mathbf{ln}\,\boldsymbol{IM}(i)\,|\,\ln S_a(T_1)} \tag{5.7a}$$

$$\boldsymbol{\Sigma}_{\mathbf{ln}\,\boldsymbol{IM}\,|\,\ln S_a(T_1)} = \sum_{i=1}^{m} p_i \left[\boldsymbol{\Sigma}_{\mathbf{ln}\,\boldsymbol{IM}(i)\,|\,\ln S_a(T_1)} + \boldsymbol{\Delta\mu}_{\mathbf{ln}\,\boldsymbol{IM}(i)\,|\,\ln S_a(T_1)}\,\boldsymbol{\Delta\mu}_{\mathbf{ln}\,\boldsymbol{IM}(i)\,|\,\ln S_a(T_1)}^{T}\right] \tag{5.7b}$$

$$\boldsymbol{\Delta\mu}_{\mathbf{ln}\,\boldsymbol{IM}(i)\,|\,\ln S_a(T_1)} = \boldsymbol{\mu}_{\mathbf{ln}\,\boldsymbol{IM}(i)\,|\,\ln S_a(T_1)} - \boldsymbol{\mu}_{\mathbf{ln}\,\boldsymbol{IM}\,|\,\ln S_a(T_1)} \tag{5.7c}$$

where $\boldsymbol{\mu}_{\mathbf{ln}\,\boldsymbol{IM}(i)\,|\,\ln S_a(T_1)}$ and $\boldsymbol{\Sigma}_{\mathbf{ln}\,\boldsymbol{IM}(i)\,|\,\ln S_a(T_1)}$ are computed using Equations (5.5) and (5.6a) respectively. Equations (5.7a) to (5.7c) are similar to the equations proposed by Lin et al. (2013a), but extend them by computing not just the conditional standard deviations of the elements of $\mathbf{ln}\,\boldsymbol{IM}$, but their entire conditional covariance matrix.

The conditional distribution of $\ln S_a Ratio$ is also normal since it can be shown to be an affine function of other normal random variables. Taking the natural logarithm of Equations (5.1a) and (5.1b), we get

$$\ln S_a Ratio = \ln S_a(T_1) - \frac{1}{n}\sum_{j=1}^{n} \ln S_a(\tau_j) \tag{5.8}$$

It is important to note that $\ln S_a(T_1)$ in Equation (5.8) is not random since it is the conditioning intensity measure. Let $\mathbf{ln}\,\widetilde{\boldsymbol{IM}}$ represent the vector containing the natural logarithms of $S_a Ratio$ and Ds:

$$\mathbf{ln}\,\widetilde{\boldsymbol{IM}} = \begin{Bmatrix} \ln S_a Ratio \\ \ln Ds \end{Bmatrix} \tag{5.9}$$

Using Equations (5.2), (5.8) and (5.9), $\ln \widetilde{\boldsymbol{IM}} \mid \ln S_a(T_1)$ can be written as an affine transformation of $\ln \boldsymbol{IM} \mid \ln S_a(T_1)$ using the following matrix equations:

$$\ln \widetilde{\boldsymbol{IM}} \mid \ln S_a(T_1) = \boldsymbol{A}\ \ln \boldsymbol{IM} \mid \ln S_a(T_1) + \boldsymbol{b} \tag{5.10a}$$

$$\boldsymbol{A} = \begin{bmatrix} -1/n & -1/n & \dots & -1/n & 0 \\ 0 & 0 & \dots & 0 & 1 \end{bmatrix} \tag{5.10b}$$

$$\boldsymbol{b} = \begin{Bmatrix} \ln S_a(T_1) \\ 0 \end{Bmatrix} \tag{5.10c}$$

The conditional mean and covariance of $\ln \widetilde{\boldsymbol{IM}}$ are now given by

$$\boldsymbol{\mu}_{\ln \widetilde{\boldsymbol{IM}} \mid \ln S_a(T_1)} = \boldsymbol{A}\ \boldsymbol{\mu}_{\ln \boldsymbol{IM} \mid \ln S_a(T_1)} + \boldsymbol{b} \tag{5.11a}$$

$$\boldsymbol{\Sigma}_{\ln \widetilde{\boldsymbol{IM}} \mid \ln S_a(T_1)} = \boldsymbol{A}\ \boldsymbol{\Sigma}_{\ln \boldsymbol{IM} \mid \ln S_a(T_1)}\ \boldsymbol{A}^T \tag{5.11b}$$

where $\boldsymbol{\mu}_{\ln \boldsymbol{IM} \mid \ln S_a(T_1)}$ and $\boldsymbol{\Sigma}_{\ln \boldsymbol{IM} \mid \ln S_a(T_1)}$ are computed using Equations (5.7a) and (5.7b) respectively. $\boldsymbol{\mu}_{\ln \widetilde{\boldsymbol{IM}} \mid \ln S_a(T_1)}$ and $\boldsymbol{\Sigma}_{\ln \widetilde{\boldsymbol{IM}} \mid \ln S_a(T_1)}$ computed using Equations (5.11a) and (5.11b) respectively, fully define the hazard-consistent joint target distribution of S_aRatio and Ds, conditional on the exceedance of any $S_a(T_1)$ value. Note that computing the marginal conditional median target S_aRatio using Equation (5.11a) is equivalent to computing the S_aRatio value directly from the conditional mean spectrum (CMS) (Baker 2011) using Equations (5.1a) and (5.1b).

The median $S_aRatio(1.76\,\text{s}, 0.35\,\text{s}, 5.00\,\text{s})$ and Ds_{5-75} targets, conditional on the exceedance of a range of $S_a(1.76\,\text{s})$ values at three sites in Western USA: Seattle (Washington), Eugene (Oregon), and San Francisco (California) are plotted in Figure 5.3. The period 1.76 s corresponds to the fundamental modal period of the eight-story reinforced concrete moment frame building used in the demonstration of the reliability framework. S_aRatio was computed only until 5.00 s instead of $3.0T_1 = 5.28\,\text{s}$ since the Al Atik (2011) model does not provide correlation coefficients for response spectral ordinates at periods above 5.00 s. This is, however, not expected to alter the obtained results noticeably. Targets were computed at discrete $S_a(1.76\,\text{s})$ levels

at which deaggregation information was available from USGS (2008), and were interpolated and linearly extrapolated to higher $S_a(1.76\,\text{s})$ levels using smoothing splines (James et al. 2013, p. 277). The amount of extrapolation required in the computations described below was small, and judged to be reasonable considering the trends in the targets at large $S_a(1.76\,\text{s})$ levels are almost linear. The increasing trends in the S_aRatio and Ds targets indicate that intense ground motions tend to have more peaked response spectral shapes, i.e., low response spectral ordinates at periods above and below T_1, compared to T_1 itself (as indicated by the peaked shape of the CMS), and longer durations. The target durations at Eugene are long because large magnitude interface earthquakes from the Cascadia subduction zone, that produce long duration ground motions, are the major contributors to its seismic hazard. On the other hand, target durations at San Francisco are short because its seismic hazard is dominated by lower magnitude crustal sources, which produce shorter duration ground motions. Seattle receives comparable contributions to its seismic hazard from interface, in-slab, and crustal earthquakes, and therefore, its target durations lie between San Francisco and Eugene.

5.5 Collapse risk assessment using the structural reliability framework

A ductile eight-story reinforced concrete moment frame building, designed for a site in Seattle, is used to demonstrate the application of the proposed structural reliability framework for collapse risk estimation. This frame was chosen because it had been previously analyzed by the authors in a related study (Chapter 4/ Chandramohan et al. 2016a), and hazard-consistent collapse risk estimates obtained by conducting MSA were readily available for comparison. The two-dimensional, centerline model of the structure, which was created and analyzed in OpenSees rev. 5184 (McKenna et al. 2006), is illustrated in Figure 5.4. The model was originally developed by Raghunandan et al. (2015) to study the collapse risk of reinforced concrete structures in the US Pacific Northwest. The first story of the frame is 4.57 m tall and each

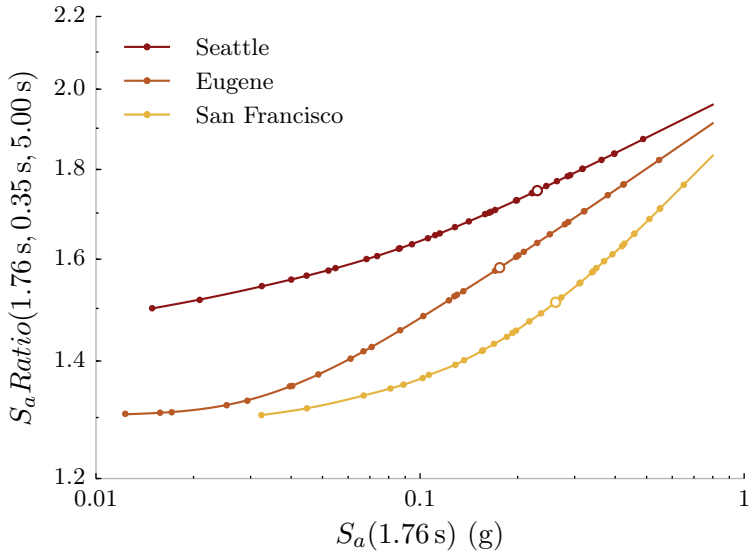

(a)

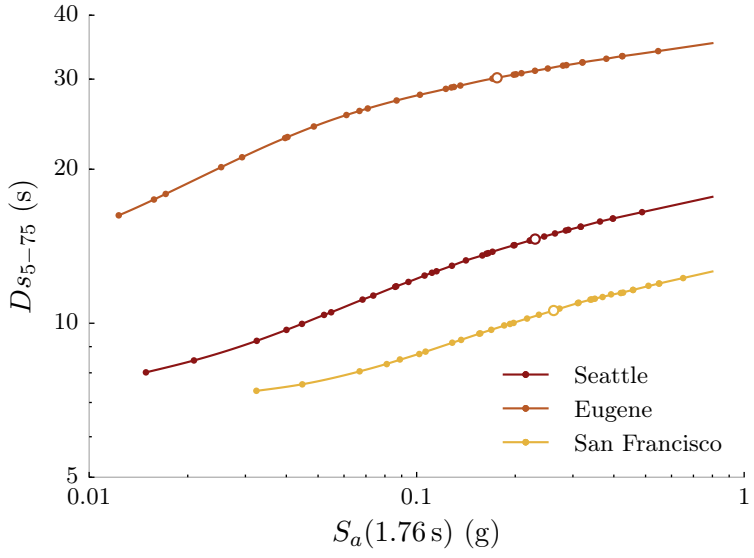

(b)

Figure 5.3: Median (a) $S_a Ratio(1.76\,\mathrm{s}, 0.35\,\mathrm{s}, 5.00\,\mathrm{s})$ and (b) Ds_{5-75} targets, conditional on the exceedance of different $S_a(1.76\,\mathrm{s})$ values at Seattle, Eugene, and San Francisco. The solid circles represent computed median targets conditional on $S_a(1.76\,\mathrm{s})$ levels at which deaggregation information was available, and the curve is a smoothing spline used to interpolate and linearly extrapolate the targets to higher $S_a(1.76\,\mathrm{s})$ levels. Targets at the risk-targeted maximum considered earthquake ($\mathrm{MCE_R}$) intensity level (ASCE 2016) at each site are represented by hollow circles.

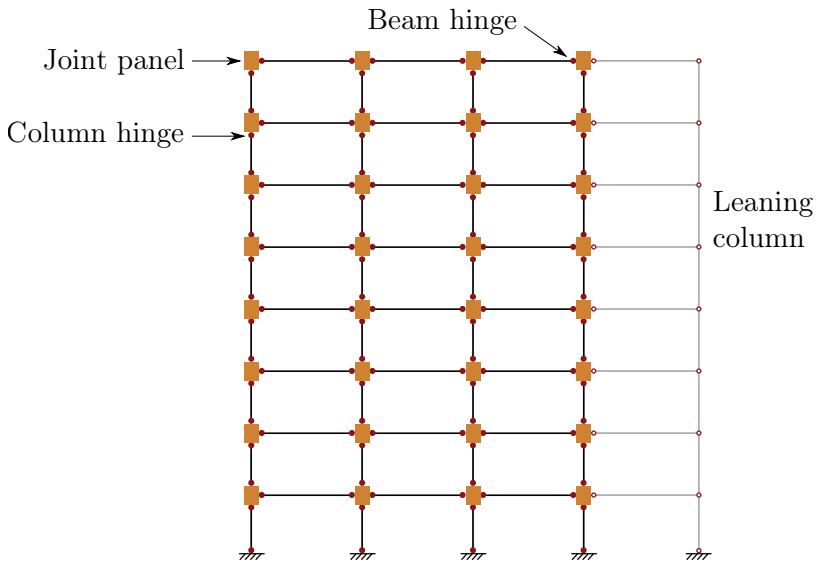

Figure 5.4: Schematic of the eight-story reinforced concrete moment frame model.

remaining story is 3.96 m tall; each bay is 6.10 m wide. The beams and columns of the frame were modeled using linear elastic elements, with zero-length plastic hinges located at either end. The hysteretic behavior of the plastic hinges was modeled using the peak-oriented Ibarra-Medina-Krawinkler model (Ibarra et al. 2005), modified as per the recommendations of Lignos and Krawinkler (2012) (p. 26). This model includes a post-peak negative stiffness branch of the backbone curve to capture in-cycle deterioration, as well as cyclically deteriorating strength and stiffness based on the cumulative hysteretic energy dissipated. Finite beam-column joints were modeled, with elastic shear deformations. The destabilizing $P - \Delta$ effect of the gravity loads tributary to other parts of the structure was captured using a pin-connected leaning column. Previous studies have demonstrated the need to model deterioration in strength and stiffness of structural components at large inelastic deformations, as well as the destabilizing effect of gravity loads, in order to capture the effect of ground motion duration on structural response (Raghunandan and Liel 2013; Chapter 2/Chandramohan et al. 2016b). The structure is assumed to be located on a site with $Vs_{30} = 760\,\text{m/s}$. Further details about the design and the numerical model are provided in Raghunandan et al. (2015).

A generic set of 88 recorded ground motions was selected to analyze the structure, in a manner not meant to represent the hazard at any specific site. 44 of these ground motions were taken from the FEMA P695 far-field set, which contains relatively short duration ground motions (with $Ds_{5-75} < 25\,\text{s}$), recorded from shallow crustal earthquakes. These ground motions have a wide range of $S_aRatio(1.76\,\text{s}, 0.35\,\text{s}, 5.00\,\text{s})$ values, which is shown to help improve the accuracy of the obtained collapse risk estimates, as described in § 5.7. The remaining 44 were selected from long duration ground motions (with $Ds_{5-75} > 25\,\text{s}$) recorded from both large magnitude interface earthquakes like the 2011 Tohoku (Japan), 2010 Maule (Chile), and 1985 Michoacan (Mexico) earthquakes, and large magnitude crustal earthquakes like the 2008 Wenchaun (China) and 2002 Denali (USA) earthquakes. This was done so that the 88 selected records have a wide range of Ds_{5-75} values as well, covering the broad range of ground motion durations anticipated at Seattle. In addition, each of the 44 long duration ground motions was selected to have a similar response spectrum to one of the short duration ground motions, using the same procedure outlined in Chapter 2/Chandramohan et al. (2016b). The objective of doing so was to introduce *orthogonality* in the selection procedure, i.e., to select records with the same $S_aRatio(1.76\,\text{s}, 0.35\,\text{s}, 5.00\,\text{s})$ value, but different Ds_{5-75} values, the benefits of which are described in § 5.7. Detailed information regarding the selected records, including response spectra and time series plots, is provided in Appendix A. Although just one record set is used in the sample computations performed below, the proposed framework is general in nature, and similar results can be expected using any set of records, as long as a few record selection guidelines described in § 5.7 are adhered to. The selected ground motions were used to conduct IDA on the structural model. Each ground motion was scaled to incrementally higher intensity levels until structural collapse, indicated by the exceedance of a peak story drift ratio (SDR) of 0.10, was observed. The collapse intensity of each ground motion, computed as its $S_a(T_1)$ value when scaled to the lowest intensity level required to cause structural collapse, was recorded. The explicit central difference numerical time integration scheme was used to conduct all analyses, since it was found to be more robust and efficient than implicit time integration schemes, which sometimes failed to converge (Chapter 7).

5.5.1 Computation of the failure surface

The following multiple linear regression equation is fit to the recorded ground motion collapse intensities, using the least-squares method:

$$\ln S_a(T_1) \text{ at collapse} = c_0 + c_{ss} \ln S_aRatio + c_{dur} \ln Ds + \epsilon \tag{5.12}$$

where ϵ represents the error term that implicitly accounts for all other ground motion characteristics that influence collapse intensity, but were not explicitly considered in the regression model. This error term is assumed to be independent of the other random variables and normally distributed with zero mean and standard deviation σ, which can be estimated as

$$\hat{\sigma} = \sqrt{\frac{RSS}{n_{gm} - 3}} \tag{5.13}$$

where RSS represents the sum of the squares of the residuals, n_{gm} is the number of ground motions used in the analysis ($n_{gm} = 88$ in this case), and the number 3 in the denominator refers to the number of degrees of freedom, or the number of unknown coefficients in the regression equation. The expected collapse intensity of a ground motion with a certain S_aRatio and Ds value is now given by

$$E\big[\ln S_a(T_1) \text{ at collapse} \,|\, \ln S_aRatio, \ln Ds\big] = c_0 + c_{ss} \ln S_aRatio + c_{dur} \ln Ds \tag{5.14}$$

This equation represents a plane in three dimensional space, and is plotted in Figure 5.5. It can be observed from Figure 5.5b that ground motions with longer durations and lower S_aRatio values (high response spectral ordinates at periods above and below T_1, relative to $S_a(T_1)$) generally cause structural collapse when scaled to lower intensities, i.e., they are inherently more damaging. Specifically, the coefficients c_{ss} and c_{dur} quantify the influence of ground motion response spectral shape and duration respectively, on collapse intensity, while holding the other parameter constant. For instance, the coefficient c_{dur}, which is estimated to be -0.21, can be interpreted to imply that a 0.21 % decrease in collapse intensity is expected for every 1 % increase in Ds, while holding S_aRatio constant.

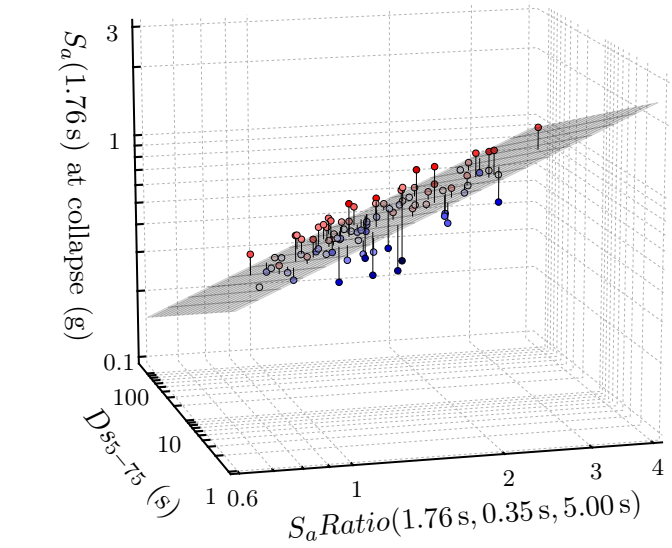

(a)

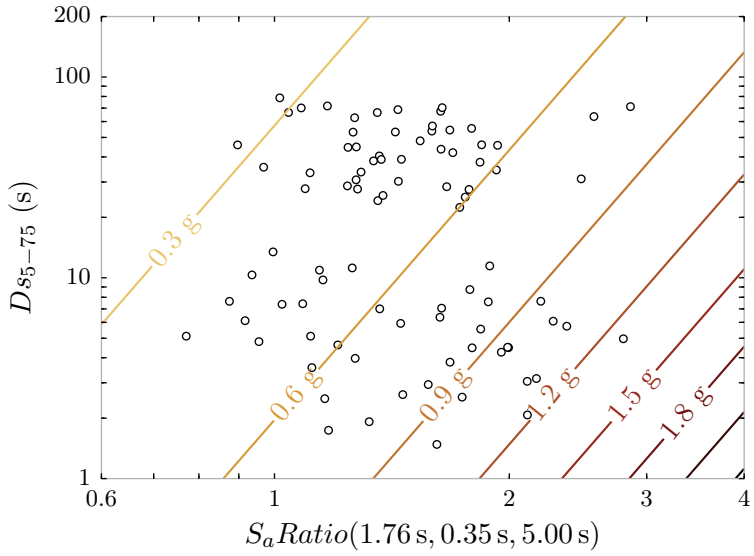

(b)

Figure 5.5: (a) Surface and (b) contour plots of Equation (5.14): the expected collapse intensity of a ground motion used to analyze the eight-story reinforced concrete moment frame building, modeled as a linear function of its $S_aRatio(1.76\,\text{s}, 0.35\,\text{s}, 5.00\,\text{s})$ and Ds_{5-75}. Individual data points used to fit the multiple linear regression model are shown as circles in both plots. In (a), circles lying above the regression plane are shaded red, and those lying below are shaded blue; the vertical lines represent the residuals. In (b), the contours represent the expected $S_a(1.76\,\text{s})$ value at collapse.

The coefficient of determination, R^2, from the regression analysis is 0.81, which implies that response spectral shape and duration, together explain 81 % of the variance in the ground motion collapse intensities. The introduction of higher order or interaction terms into the regression equation was not found to produce any significant improvements in the R^2; hence the simple linear model was retained. The R^2 was computed to be 0.45 for a model containing only S_aRatio (i.e., the model in Equation (5.12) with $c_{dur} = 0$), and 0.40 for one containing only Ds, indicating that they each contribute almost equal predictive power to the regression model involving them both. The fact that the R^2 obtained using Equation (5.12) (0.81) is nearly equal to the sum of the R^2 values obtained using S_aRatio and Ds individually (0.45 and 0.40 respectively), also implies that response spectral shape and duration provide mostly non-redundant information in predicting a ground motion's collapse intensity. It is worth noting here that the R^2 obtained by fitting a linear regression model containing only S_aRatio to the collapse intensities of the 44 short duration ground motions from the FEMA P695 far-field set only, is 0.79, which is significantly larger than 0.45, the R^2 obtained using all 88 ground motions. This observation provides the following explanation for why a number of previous studies like Shome et al. (1998), Bianchini et al. (2009), Mehanny (2009), Bojórquez and Iervolino (2011), Eads et al. (2015), and Kazantzi and Vamvatsikos (2015) found IMs based on response spectra alone to be good predictors of structural response: they used predominantly short duration ground motions from shallow crustal earthquakes. These results justify the use of both S_aRatio and Ds as secondary IMs in the proposed reliability framework. They also possess a number of the other characteristics of IMs well suited for use in the reliability framework, described in § 5.6.

Equation (5.12) can now be cast in the following form, to represent a failure surface (Melchers 1999, Chapter 1), q:

$$q = \left(c_0 + c_{ss} \ln S_aRatio + c_{dur} \ln Ds + \epsilon\right) - \ln S_a(T_1) = 0 \tag{5.15}$$

which is a function of the following four random variables: S_aRatio, Ds, $S_a(T_1)$, and ϵ. This failure surface can be viewed as a *response surface* (Melchers 1999, § 5.5),

i.e., a simplified model of the collapse response of the structure. By virtue of being a failure surface, the domain $q \leq 0$ contains all possible combinations of S_aRatio, Ds, $S_a(T_1)$, and ϵ that lead to structural collapse. The probability that a ground motion with a certain S_aRatio and Ds, when scaled to a certain $S_a(T_1)$ value, will cause structural collapse, can now be computed without conducting any additional structural analyses, by just integrating the probability density function of ϵ over the domain $q \leq 0$. From Equation (5.15), this is equivalent to integrating the probability density function of ϵ over the domain $\epsilon \leq \ln S_a(T_1) - \big(c_0 + c_{ss} \ln S_aRatio + c_{dur} \ln Ds\big)$:

$$P\big[\text{collapse} \,|\, \ln S_aRatio,\, \ln Ds,\, \ln S_a(T_1)\big] = \Phi\left[\frac{\ln S_a(T_1) - \big(c_0 + c_{ss} \ln S_aRatio + c_{dur} \ln Ds\big)}{\hat{\sigma}}\right] \quad (5.16)$$

where Φ represents the standard normal cumulative distribution function and $\hat{\sigma}$ is computed using Equation (5.12). The probability of causing collapse is, therefore, equal to 0.5 when the ground motion is scaled such that its $S_a(T_1)$ is equal to $\exp\big(c_0 + c_{ss} \ln S_aRatio + c_{dur} \ln Ds\big)$. This probability approaches 0 at lower $S_a(T_1)$ values, and 1 at higher $S_a(T_1)$ values. It is worth noting that this simplified representation of the collapse response of a structure does not consider the possibility of structural *resurrection* (Vamvatsikos and Cornell 2002), wherein the structure does not collapse under a ground motion scaled to certain $S_a(T_1)$ values above its collapse intensity. The small likelihood of encountering structural resurrection, however, justifies ignoring this phenomenon.

5.5.2 Computation of the hazard-consistent collapse fragility curve

A collapse fragility curve describes the probability of collapse as a function of the ground motion intensity level. The probability of collapse at any $S_a(T_1)$ level can be

computed by numerically evaluating the following reliability integral:

$$P\left[\text{collapse} \mid \ln S_a(T_1)\right] = \iint P\left[\text{collapse} \mid \ln S_aRatio,\, \ln Ds,\, \ln S_a(T_1)\right] f\left[\ln S_aRatio,\, \ln Ds \mid \ln S_a(T_1)\right]\, d\left(\ln S_aRatio\right)\, d\left(\ln Ds\right) \tag{5.17}$$

The two terms in the integrand of the reliability integral, conditional on two different $S_a(T_1)$ levels in Seattle, are illustrated in Figure 5.6. The term $P\left[\text{collapse} \mid \ln S_aRatio,\, \ln Ds,\, \ln S_a(T_1)\right]$ is computed using Equation (5.16). It represents the probability of observing structural collapse as a function of the ground motion characteristics and is depicted by the linear contours in Figure 5.6. This term depends only on the structure under consideration and is site-independent. It is worth noting that the linear contour corresponding to a probability of 0.5 represents the intersection of the regression plane defined by Equation (5.14) and a horizontal plane drawn through the considered $S_a(T_1)$ level. The term $f\left[\ln S_aRatio,\, \ln Ds \mid \ln S_a(T_1)\right]$ is computed as the probability density function of a bivariate normal distribution whose mean, $\boldsymbol{\mu}_{\ln \widetilde{\boldsymbol{IM}} \mid \ln S_a(T_1)}$, and covariance, $\boldsymbol{\Sigma}_{\ln \widetilde{\boldsymbol{IM}} \mid \ln S_a(T_1)}$, are given by Equations (5.11a) and (5.11b) respectively. It represents the distribution of the characteristics of the anticipated ground motions and is depicted by the elliptical contours in Figure 5.6. This term depends only on the site-specific seismic hazard and is structure-independent. The larger degree of overlap between the two sets of contours at the higher $S_a(T_1)$ value indicates a larger likelihood of observing structural collapse at this $S_a(T_1)$ value, as intuitively expected. Although Equation (5.17) is similar to Equations (20) and (21) in Baker (2007), this study extends upon it in a number of ways, most importantly, by identifying S_aRatio and Ds as efficient predictors of a ground motion's collapse intensity.

A collapse fragility curve is computed by evaluating Equation (5.17) at multiple $S_a(T_1)$ levels. The computed curve is plotted in Figure 5.7a with the label "*IDA: Using $S_a(T_1)$, S_aRatio, and Ds*". The collapse fragility curve computed in this manner is non-parametric in nature and does not require the assumption of any parametric functional form; a lognormal cumulative distribution function is otherwise commonly assumed. The median collapse capacity, μ, defined as the $S_a(T_1)$ level corresponding to a 50 % probability of collapse, is computed to be 0.70 g, and the mean annual

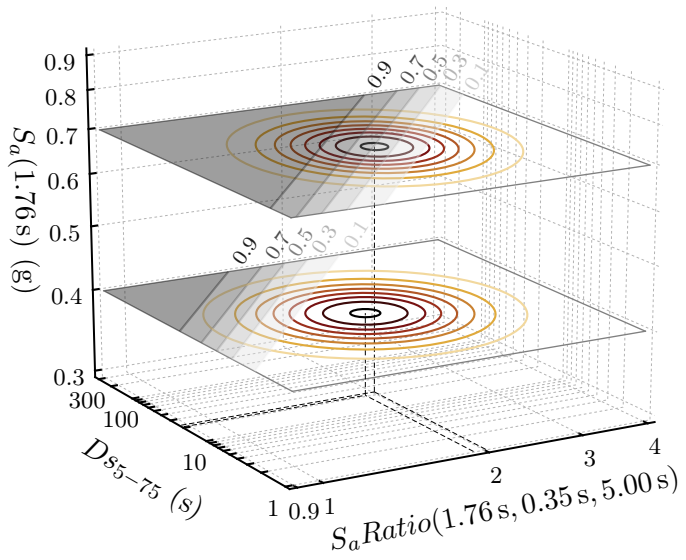

Figure 5.6: A schematic illustrating the two terms in the integrand of the reliability integral in Equation (5.17), conditional on two $S_a(1.76\,\mathrm{s})$ levels in Seattle: $0.4\,\mathrm{g}$ and $0.7\,\mathrm{g}$

frequency of collapse, $\lambda_{collapse}$, computed by integrating the product of the collapse fragility curve and the derivative of the seismic hazard curve, is determined to be 5.6×10^{-5}. These collapse risk metrics are summarized in Table 5.1. The proposed procedure to compute the hazard-consistent collapse fragility curve of a structure using the results of an IDA, as per the developed structural reliability framework, is summarized in Procedure 5.1.

5.5.3 Comparison to other collapse risk estimation methods

To evaluate the accuracy of the collapse risk estimates obtained using the proposed reliability framework, they were compared to those obtained by conducting MSA using 8 sets of 100 hazard-consistent ground motions, selected to match source-specific target distributions of response spectra and Ds_{5-75} conditional on different $S_a(T_1)$ levels, as per the procedure outlined in Chapter 4/Chandramohan et

Procedure 5.1: Compute the hazard-consistent collapse fragility curve of a structure using the results of an IDA.

1. Develop a numerical model of the structure that incorporates the in-cycle and cyclic deterioration of strength and stiffness of the structural components, and the destabilizing $P-\Delta$ effect.
2. Define the set of $S_a(T_1)$ levels at which the probability of collapse is to be computed.
3. Compute the site-specific, hazard-consistent joint probability distributions of S_aRatio and Ds conditional on each of these $S_a(T_1)$ levels, using Equations (5.11a) and (5.11b).
4. Either select a generic set of records as per the recommendations outlined in § 5.7, or use the same set of 88 records used in this study.
5. Conduct IDA to compute the collapse intensity of each ground motion, i.e., the lowest $S_a(T_1)$ value it needs to be scaled to, to cause structural collapse.
6. Fit the linear regression model in Equation (5.12) to the computed ground motion collapse intensities, and compute $\hat{\sigma}$ using Equation (5.13).
7. Evaluate the reliability integral in Equation (5.17) to compute the probability of collapse at each $S_a(T_1)$ level.

al. (2016a). The fragility curve computed using hazard-consistent MSA is plotted in Figure 5.7a with the label "*MSA: Using response spectra and Ds*". This curve is parametric in nature and is described by a lognormal cumulative distribution function. The collapse risk metrics obtained using MSA ($\mu = 0.68\,\mathrm{g}$ and $\lambda_{collapse} = 5.4 \times 10^{-5}$) are found to be in good agreement with the metrics computed using the proposed reliability framework. This equivalence of the two approaches can be explained by viewing MSA as just a simulation-based approach to evaluate the reliability integral in Equation (5.17). Selecting hazard-consistent ground motions at an $S_a(T_1)$ level is equivalent to simulating S_aRatio and Ds values from the distribution $f\big[\ln S_aRatio, \ln Ds \,\big|\, \ln S_a(T_1)\big]$. Computing the probability of collapse as the fraction of these ground motions that cause structural collapse is equivalent to integrating it with $P\big[\text{collapse} \,\big|\, \ln S_aRatio, \ln Ds, \ln S_a(T_1)\big]$ over all S_aRatio and Ds values. The reliability framework proposed here, on the other hand, employs an analytical approach to evaluate the same reliability integral, by explicitly determining the failure surface. A minor difference between the two approaches is that a vector of

response spectral ordinates at different periods is usually considered when selecting hazard-consistent ground motions to conduct MSA, while only $S_a(T_1)$ and S_aRatio are used to quantify ground motion intensity and response spectral shape respectively, in the proposed reliability framework. The agreement between the results obtained using the two methods, however, suggests that a vector containing just $S_a(T_1)$ and S_aRatio exhibits a nearly similar degree of statistically sufficiency (Rice 2006, p. 305) for the estimated structural collapse risk, as the entire response spectrum.

The hazard-consistency of the collapse risk estimates obtained by conducting MSA is contingent on the relevant IMs of the selected ground motions providing a close match to their respective target distributions, which is often hard to achieve when selecting small sets of ground motions at each $S_a(T_1)$ level. In addition, although some of proposed ground motion selection algorithms like Jayaram et al. (2011b), Wang (2011), and Bradley (2012) account for the correlation between the considered IMs, neither of them explicitly ensure that the correlation structure of the IMs in the final selected record set matches the target. The proposed reliability framework, however, does not suffer from these drawbacks since it treats the target distributions of the IMs analytically. It also explicitly accounts for the correlation between S_aRatio and Ds when evaluating the reliability integral, and the correlation structure among the response spectral ordinates themselves—within the period range T_{start} to T_{end}—when computing the marginal distribution of S_aRatio.

The conventional practice of computing a collapse fragility curve from the results of an IDA involves using only $S_a(T_1)$, a scalar IM, while ignoring both response spectral shape and duration. To evaluate the effectiveness of this method, another collapse fragility curve was computed by fitting the moments of a lognormal distribution to the sample moments of the ground motion collapse intensities using the maximum likelihood approach. The computed fragility curve is plotted in Figure 5.7a with the label "*IDA: Using* $S_a(T_1)$ *only*", and is found to significantly over-estimate the collapse risk ($\mu = 0.56\,\text{g}$ and $\lambda_{collapse} = 10 \times 10^{-5}$). The inaccuracy of this method stems from the fact that it does not incorporate any site-specific seismic hazard information. Hence, the same fragility curve would be computed irrespective of where the structure was located. The fragility curve obtained by adjusting the median collapse capacity

estimated using only the 44 ground motions from the FEMA P695 far-field set, by a spectral shape factor, as per the recommendations of FEMA (2009b) (Appendix B), on the other hand, is found to significantly under-estimate the collapse risk ($\mu = 1.13\,\mathrm{g}$ and $\lambda_{collapse} = 1.0 \times 10^{-5}$). This fragility curve is also plotted in Figure 5.7a with the label "*IDA: Using $S_a(T_1)$ and FEMA P695 spectral shape adjustment*". The error in this method is not just a consequence of the approximate nature of the spectral shape adjustment based on ε, recommended by FEMA P695, but also of ignoring duration. Further adjustment of the median collapse capacity by a duration factor, analogous to the spectral shape factor, could presumably improve the accuracy of this method.

To demonstrate the consistency of the trends in the fragility curves obtained using the different methods described above, the structure was re-analyzed, assuming it to be located first in Eugene, and then in San Francisco. As described in § 5.4 above, the nature of the seismic hazard at these two sites is completely different from the seismic hazard at Seattle. The computed fragility curves are plotted in Figure 5.7b and Figure 5.7c respectively. At both these sites, the collapse risk estimates obtained using the reliability framework are found to agree well with those obtained by conducting hazard-consistent MSA, thus reaffirming their equivalence. For the same reasons described previously, the fragility curve computed by considering only $S_a(T_1)$ is the same at all three sites, and the one incorporating the spectral shape adjustment as per the recommendations of FEMA P695, significantly under-estimates the collapse risk. It is worth noting that the median collapse capacity of the structure is lowest in Eugene ($\mu = 0.58\,\mathrm{g}$) since it experiences the longest duration ground motions, with moderately low S_aRatio values (refer to Figure 5.3). The median collapse capacities at both Seattle and San Francisco are nearly identical ($\mu = 0.70\,\mathrm{g}$ in both cases), however, since although San Francisco experiences ground motions of shorter duration, its effect is counteracted by their lower S_aRatio values. The collapse risk metrics computed using each method of analysis, at all the three sites, is summarized in Table 5.1.

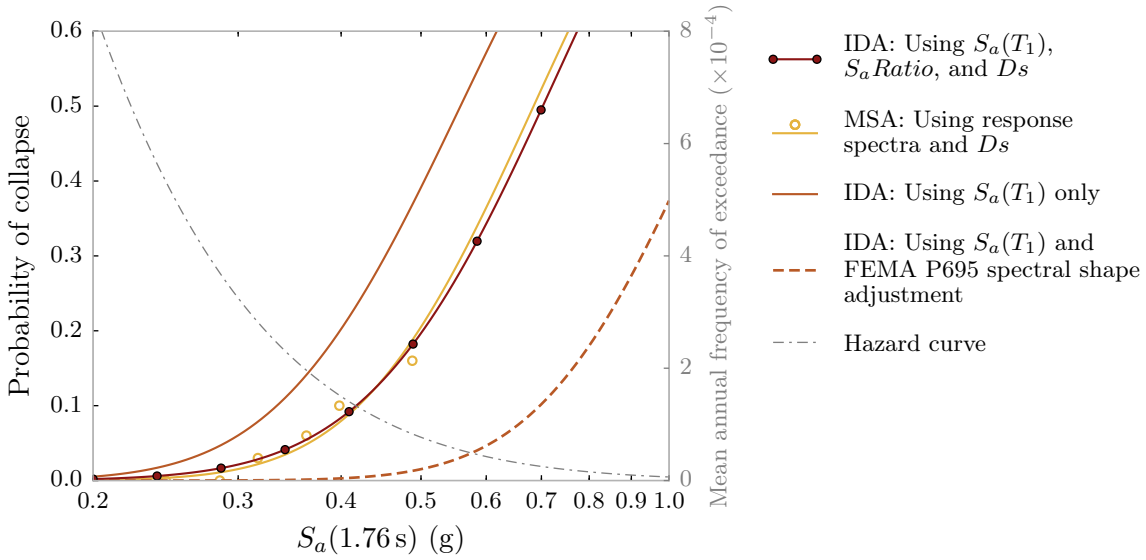

(a) Seattle

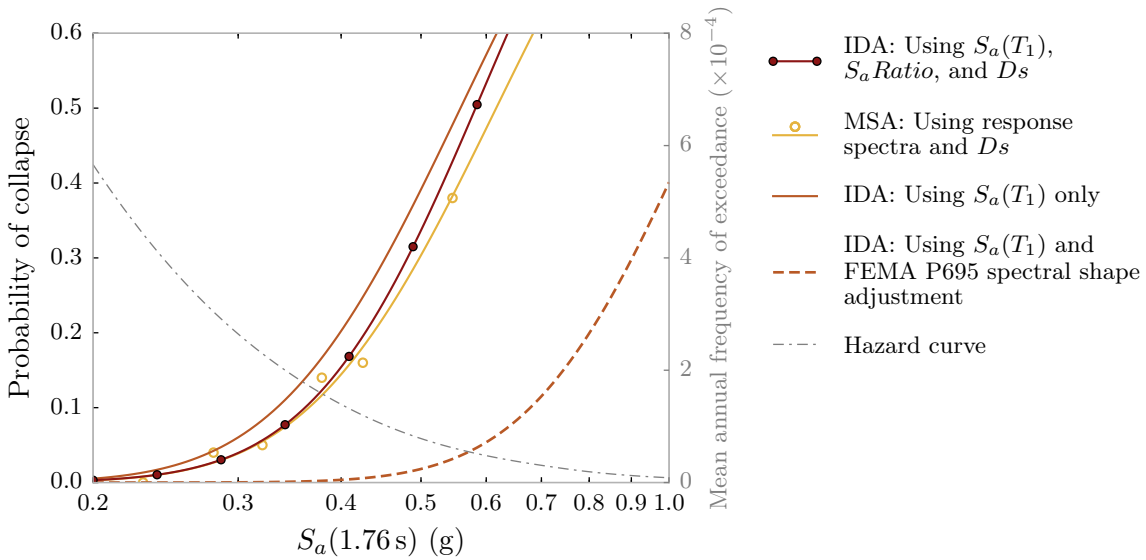

(b) Eugene

Table 5.1: Median collapse capacities, μ, and mean annual frequencies of collapse, $\lambda_{collapse}$, of the eight-story reinforced concrete moment frame estimated using different methods of analysis, at the three considered sites.

Method of analysis	**Seattle**		**Eugene**		**San Francisco**	
	μ (g)	$\lambda_{collapse}$ ($\times 10^{-5}$)	μ (g)	$\lambda_{collapse}$ ($\times 10^{-5}$)	μ (g)	$\lambda_{collapse}$ ($\times 10^{-5}$)
IDA: Using $S_a(T_1)$, S_aRatio, and Ds	0.70	5.6	0.58	7.9	0.70	16
MSA: Using response spectra and Ds	0.68	5.4	0.62	7.2	0.72	16
IDA: Using $S_a(T_1)$ only	0.56	10	0.56	9.1	0.56	31
IDA: Using $S_a(T_1)$ and FEMA P695 spectral shape adjustment	1.13	1.0	1.10	1.3	1.14	2.6

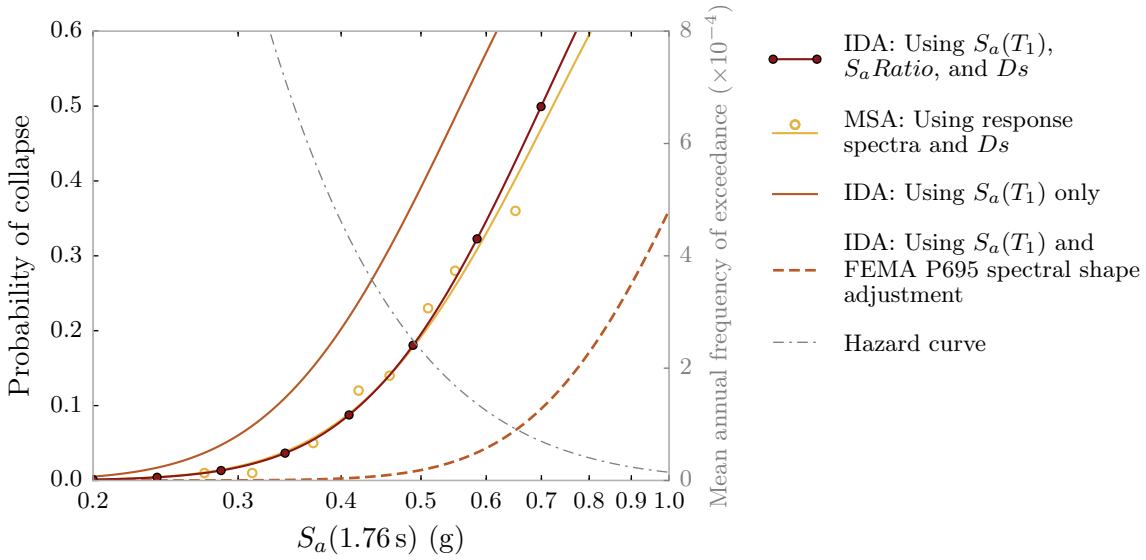

(c) San Francisco

Figure 5.7: Comparison of the collapse fragility curves of the eight-story reinforced concrete frame estimated using different methods of analysis, at the three considered sites.

5.5.4 Simplified estimation of median collapse capacity

In a number of situations, the objective of the analysis is to compute only the median collapse capacity, and not the entire collapse fragility curve. For instance, the analyst may choose to construct a lognormal collapse fragility curve using the computed median, but with a lognormal standard deviation that is inflated to account for the uncertainty in structural model characteristics, in addition to the uncertainty in ground motion characteristics, as per the recommendations of FEMA (2009b) (Chapter 7) or FEMA (2012b) (Chapter 5). In this scenario, the use of the following simplified method that does not require the explicit evaluation of the reliability integral, is recommended.

The simplified method proposed here requires an initial estimate of the median collapse capacity, μ_0. For new structural designs, $\mu_0 = 2.2 \times \mathrm{MCE_R}$ is considered a reasonable first guess, where $\mathrm{MCE_R}$ corresponds to the risk-targeted maximum considered earthquake ground motion intensity level (ASCE 2016, § 11.4.3). The factor 2.2 is obtained by assuming the structure has a lognormal collapse fragility curve

with a 10 % probability of collapse at the MCE_R intensity level, and a lognormal standard deviation of 0.6 (ASCE 2016). Median target S_aRatio and Ds values conditional on the ground motion intensity level $S_a(T_1) = \mu_0$, are then computed using Equation (5.11a). Let these median target values be called S_aRatio_0 and Ds_0 respectively. These median targets are then substituted into Equation (5.14) to compute the expected collapse intensity, μ_1. Equation (5.16) indicates that if a ground motion with $S_aRatio = S_aRatio_0$ and $Ds = Ds_0$, were to be scaled to have $S_a(T_1) = \mu_1$, it would have a 50 % probability of causing structural collapse, implying that μ_1 is a good estimate of the hazard-consistent median collapse capacity of the structure.

There is, however, a small discrepancy in that the median targets, S_aRatio_0 and Ds_0, were computed conditional on the $S_a(T_1) = \mu_0$ intensity level. This implies that only ground motions with $S_a(T_1) = \mu_0$ are expected to have $S_aRatio = S_aRatio_0$ and $Ds = Ds_0$ on average, not ground motions with $S_a(T_1) = \mu_1$. So if the computed $\mu_1 \neq \mu_0$, the estimate of the median collapse capacity can be improved by computing median targets S_aRatio_1 and Ds_1 conditional on the ground motion intensity level $S_a(T_1) = \mu_1$, and iteratively computing μ_2, μ_3, ..., until the median collapse capacity estimates over successive iterations are almost equal. This final value of μ that the iterations converge to, represents the hazard-consistent median collapse capacity of the structure, and it is the same value that would have been computed using the detailed method outlined in § 5.5.2. This method is conceptually similar to the procedure outlined in FEMA (2012b) (Appendix J), which requires iteratively conducting a modified version of IDA using ground motions selected to match targets conditional on different successive $S_a(T_1)$ levels. The proposed method, however requires conducting IDA just once to fit the regression model described by Equation (5.12), and the median collapse capacity is estimated at each subsequent iteration by just evaluating Equation (5.14).

This proposed procedure was found to be robust with respect to the initial choice of μ_0, and to converge rapidly to the final solution. For the three considered sites, using $\mu_0 = 2.2 \times \text{MCE}_\text{R}$, the median collapse capacity of the eight-story reinforced concrete frame was estimated to an accuracy of 2 % after just one iteration. Using a poorer initial estimate of $\mu_0 = \text{MCE}_\text{R}$, the median collapse capacity was estimated

to an accuracy of 2 % after just two iterations. The proposed simplified procedure to compute the hazard-consistent median collapse capacity of a structure using the results of an IDA, as per the developed structural reliability framework, is summarized in Procedure 5.2.

Procedure 5.2: Compute the hazard-consistent median collapse capacity of a structure using the results of an IDA.

1 Develop a numerical model of the structure that incorporates the in-cycle and cyclic deterioration of strength and stiffness of the structural components, and the destabilizing $P-\Delta$ effect.

2 Either select a generic set of records as per the recommendations outlined in § 5.7, or use the same set of 88 records used in this study.

3 Conduct IDA to compute the collapse intensity of each ground motion, i.e., the lowest $S_a(T_1)$ value it needs to be scaled to, to cause structural collapse.

4 Fit the linear regression model in Equation (5.12) to the computed ground motion collapse intensities.

5 Obtain an initial estimate of the median collapse capacity, μ_0. For new structures, $\mu_0 = 2.2 \times \text{MCE}_\text{R}$ serves as a good initial estimate.

6 Set $\mu_{-1} \leftarrow 0$

7 Set $i \leftarrow 0$

8 **while** $\frac{|\mu_i - \mu_{i-1}|}{\mu_{i-1}} > tolerance$ **do**

9 Compute the site-specific median target S_aRatio and Ds values conditional on μ_i, using Equation (5.11a). Let these median target values be called S_aRatio_i and Ds_i respectively.

10 Substitute S_aRatio_i and Ds_i in Equation (5.14) to compute μ_{i+1}.

11 Set $i \leftarrow i + 1$

12 **end**

13 μ_i is the final estimate of the hazard-consistent median collapse capacity.

5.6 Characteristics of intensity measures well suited for use in the reliability framework

The calculations presented above use $S_a(T_1)$ as the primary amplitude-based IM, and S_aRatio and Ds as the secondary IMs that quantify the relative frequency content and duration of a ground motion respectively. The proposed reliability framework, however, is general in nature, and can be used in conjunction with any set of IMs to compute a hazard-consistent collapse fragility curve from the results of an IDA, subject to the guidelines described here. The primary IM should be

(i) *amplitude-based*, since it is used to represent the collapse intensity of a ground motion used to conduct IDA, e.g., $S_a(T)$, peak ground acceleration (PGA), and peak ground velocity (PGV);

(ii) *efficient* (Luco and Cornell 2007), i.e., the ground motion collapse intensities represented by it, should have low variability; and

(iii) *hazard-computable*, i.e., quantified using PSHA and predictable to a reasonable precision as a function of earthquake causal parameters like magnitude, M, source-to-site distance, R, and site Vs_{30}.

Each secondary IM used in conjunction with the primary IM should be

(i) *amplitude-invariant*, as also recommended by Vamvatsikos and Cornell (2005), because first, it needs to provide information not already quantified by the primary amplitude-based IM, and second, if its value changes as a record is scaled, its definition at the collapse intensity is ambiguous, as discussed in Chapter 2/Chandramohan et al. (2016b);

(ii) *efficient*, i.e., it should be able to reduce the uncertainty in the collapse intensities; or in other words, it should have a relatively high R^2 value when individually regressed against ground motion collapse intensity;

(iii) *uncorrelated* to the other secondary IMs used, i.e., it should provide non-redundant information not already quantified by the other secondary IMs, that

is helpful in predicting ground motion collapse intensity; or in other words, its removal from the regression model should result in a significant reduction in the model's R^2 value; and

(*iv*) *hazard-computable*, i.e., predictable to a reasonable precision as a function of earthquake causal parameters, with defined correlations between the ε-values of the secondary and primary IMs.

In addition, the entire vector IM consisting of the primary IM and all secondary IMs should be sufficient (Rice 2006, p. 305; Luco and Cornell 2007), i.e., the ground motion collapse intensities represented by the primary IM, conditioned on the set of secondary IMs, should be independent of all other IMs not included in the vector. This can be assessed by regressing the residuals from the regression model defined by Equation (5.12) against other IMs that could potentially influence structural collapse capacity, and evaluating the statistical significance and magnitude of any observed trends. Using an insufficient vector IM could produce biased collapse risk estimates. It is important to note that the record set used in the analysis can significantly influence the inferred efficiency and sufficiency of a chosen vector IM. For example, as noted previously in § 5.5.1, studies that used only short duration ground motions found IMs based on response spectra alone to be both efficient and sufficient.

If the set of chosen IMs is inefficient, i.e., the regression model defined by Equation (5.12) has a small R^2 value, it results in the spreading of the linear contours in Figure 5.6, corresponding to the term $P\big[\text{collapse} \,|\, \ln S_a Ratio, \ln Ds, \ln S_a(T_1)\big]$. Similarly, if any of the chosen IMs are only predictable with a large uncertainty, it results in the spreading of the elliptical contours in Figure 5.6, corresponding to the term $f\big[\ln S_a Ratio, \ln Ds \,|\, \ln S_a(T_1)\big]$. Both these consequences are undesirable since they result in an increase in the dispersion of the computed collapse fragility curve.

Although the efficiency of a chosen set of IMs, as defined above, can be increased by just including a large number of secondary IMs, this could lead to overfitting, and a consequent loss in predictive power. In addition, it would lead to a decrease in computational efficiency since Equation (5.17) involves integration over as many dimensions as there are secondary IMs. This was the motivation behind using a scalar

IM, S_aRatio, instead of a vector of response spectral ordinates at periods above and below T_1, normalized by $S_a(T_1)$, to quantify response spectral shape. When investigating the feasibility of using a vector of linearly spaced, normalized response spectral ordinates in place of S_aRatio, the predictive power of the regression model was found to decrease if either too few or too many normalized response spectral ordinates were used due to bias-variance trade-off (James et al. 2013, p. 33). The ideal number of required normalized response spectral ordinates was found to depend on the number of ground motions used in the analysis, and the predictive power when using this ideal number of predictors was found to be only marginally better than the model using S_aRatio, hence not justifying the increased model complexity. This option could, however, be considered if the analyst has reason to believe that the degree of statistical sufficiency of S_aRatio for the estimated structural collapse risk, is significantly lower than the entire normalized response spectrum. A number of other scalar and vector IMs based on the response spectrum have been proposed in the literature (e.g., Cordova et al. 2000; Vamvatsikos and Cornell 2005; Tothong and Luco 2007; Baker and Cornell 2008; Mehanny 2009; Bojórquez and Iervolino 2011), but S_aRatio was preferred over them due to its simplicity, efficiency, and hazard-computability. Marafi et al. (2016) proposed a scalar IM that incorporates the effects of ground motion intensity, response spectral shape, and duration. Similarly, Eads et al. (2015) recommends using $S_{a,avg}$, which incorporates the effects of both ground motion intensity and response spectral shape. The treatment of each ground motion characteristic as an individual component of a vector IM was, however, considered appropriate for the reliability formulation proposed in this paper. This approach also allows the analyst to obtain a deeper understanding of the individual contributions of each of these ground motion characteristics to the total potential of a ground motion to cause structural collapse, as quantified by the coefficients c_{ss} and c_{dur} from Equation (5.12).

The IMs used in this study: $S_a(T_1)$, S_aRatio, and Ds, possess a number of the desirable characteristics described above, some of which, like efficiency and low correlation, have been demonstrated in the context of the analyzed eight-story reinforced concrete moment frame building in § 5.5.1. To demonstrate these qualities of the

chosen set of IMs on a broader range of structural models, the regression model in Equation (5.12) was fit to 20 of the other ductile reinforced concrete moment frame buildings designed by Raghunandan et al. (2015), and 30 ductile reinforced concrete moment frames designed by Haselton and Deierlein (2008) (Chapter 6), ranging in height from 1 to 20 stories. While the ground motion Ds_{5-75} values are not structure-dependent, different ground motion $S_a(T_1)$ and $S_aRatio(T_1, 0.2T_1, 3.0T_1)$ values were used for each frame, depending on its fundamental elastic modal period, T_1. The range of R^2 values obtained from these fits is plotted under the label "S_aRatio *and* Ds" in Figure 5.8, and the high median R^2 of 0.83 reaffirms the efficiency of the chosen set of IMs. The ranges of R^2 values obtained by fitting linear models containing only S_aRatio and only Ds are also shown in Figure 5.8, and their medians are 0.53 and 0.37 respectively. As demonstrated earlier for the eight-story reinforced concrete moment frame in § 5.5.1, the fact that the sum of these median R^2 values is nearly equal to the median R^2 value of the model containing them both, indicates that S_aRatio and Ds contribute mostly non-redundant information in predicting ground motion collapse intensity. Although non-ductile structures were not explicitly examined as part of this study, they are expected to experience relatively smaller effects of both response spectral shape and duration compared to the ductile structures (Haselton et al. 2011a; Liel et al. 2011; Raghunandan and Liel 2013; Chapter 2/Chandramohan et al. 2016b).

Eads et al. (2015) has demonstrated the sufficiency of $S_{a,avg}$ using short duration ground motions, which corresponds directly to the sufficiency of S_aRatio, when used in conjunction with $S_a(T_1)$. The inclusion of Ds in the vector IM is only expected to improve its sufficiency when considering both short and long duration ground motions. The sufficiency of the chosen vector IM is the characteristic that ensures that nearly the same coefficients of the regression model in Equation (5.12) are estimated, irrespective of which set of records is used to estimate them, as long as the records are selected following the guidelines outlined in § 5.7. It was verified that nearly similar regression coefficients were estimated for the eight-story reinforced concrete moment frame using a different set of 292 records (consisting of 146 long duration records and 146 spectrally equivalent short duration records) selected as part of a different study

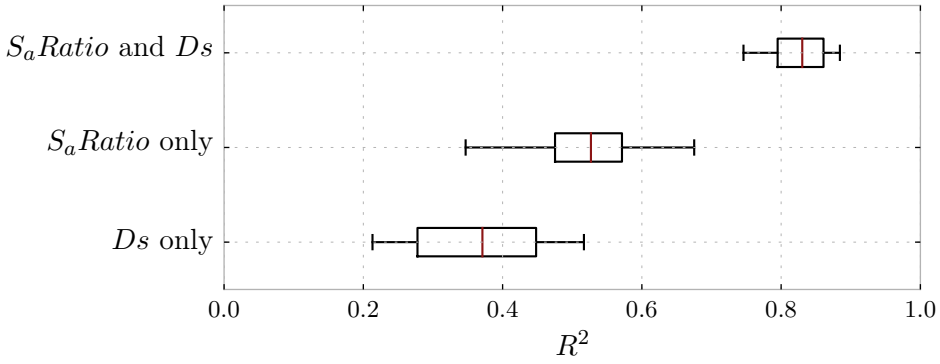

Figure 5.8: Distribution of R^2 values obtained by fitting linear regression models to predict ground motion collapse intensity using different sets of ground motion intensity measures, for all 51 ductile reinforced concrete moment frames considered in this study. The whiskers of each boxplot extend from the 5^{th} to the 95^{th} percentile R^2 values.

by the authors (Chapter 2/Chandramohan et al. 2016b).

5.6.1 Efficiency of *Ds* and other duration metrics

Although 5–75 % significant duration, Ds_{5-75}, was used in all the calculations presented above, other percentage ranges are also commonly used to compute Ds, e.g., 5–95 %, 2.5–97.5 %, and 20–80 % (Boore and Thompson 2014; Afshari and Stewart 2016). The efficiency of a specific percentage range used to compute Ds is quantified by the R^2 value obtained by fitting the regression model in Equation (5.12) to the ground motion collapse intensities computed for the eight-story reinforced concrete moment frame, using that definition of Ds and $S_aRatio(1.76\,\text{s}, 0.35\,\text{s}, 5.00\,\text{s})$. The retention of S_aRatio in the regression model facilitates the comparison of the information provided by different duration metrics to predict a ground motion's collapse intensity, in addition to the information already provided by response spectral shape. This aids the selection of a duration metric to be included in a vector IM that already contains $S_a(T_1)$ and S_aRatio. Since the regression model containing only S_aRatio produces an R^2 of 0.45, considering any definition of Ds, in addition to S_aRatio, is expected to produce an R^2 larger than 0.45. R^2 values computed for different combinations of start and end percentages used to define Ds are plotted in Figure 5.9.

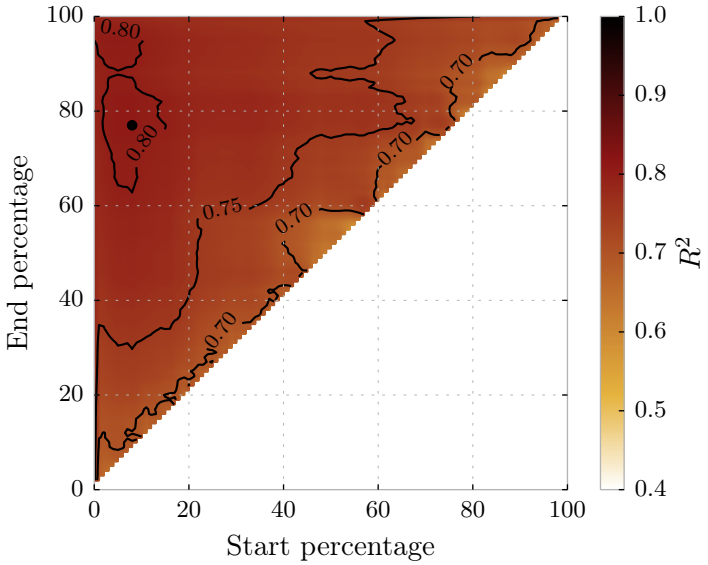

Figure 5.9: Comparison of the R^2 values obtained by fitting the regression model in Equation (5.12) to the ground motion collapse intensities computed for the eight-story reinforced concrete moment frame, using significant duration, Ds, defined by different percentage ranges, and $S_aRatio(1.76\,\text{s}, 0.35\,\text{s}, 5.00\,\text{s})$. The percentage range that produces the largest R^2 value is plotted as a black circle.

It can be observed from the plot that the optimal percentage range for the analyzed moment frame is 8–77 %, which produces an R^2 of 0.81. This is, however, almost exactly equal to the R^2 produced by both 5–75 % and 5–95 % significant duration as well. The obtained R^2 value is, in fact, not observed to be significantly affected by the exact start and end percentages used to define Ds, as long as the chosen start percentage is lesser than 20 % and the chosen end percentage is greater than 60 %. Similar conclusions could also be drawn for the other 50 reinforced concrete moment frames analyzed in this study, further corroborating this inference. Note that $S_a(T_1)$ and $S_aRatio(T_1, 0.2T_1, 3.0T_1)$ were used to fit the regression model for each frame, using its corresponding T_1.

The efficiencies of 5–75 % and 5–95 % significant duration, the two most commonly used percentage ranges, are compared to a number of other amplitude-invariant duration metrics proposed in the literature (Bommer and Martinez-Pereira 1999). The distribution of R^2 values obtained for all 51 reinforced concrete frames, using each

of the considered duration metrics along with $S_a(T_1)$ and $S_aRatio(T_1, 0.2T_1, 3.0T_1)$ in Equation (5.12), is plotted in Figure 5.10. $\overline{Db}_x$ represents normalized bracketed duration, which is defined as the time elapsed between the first and last excursions of the accelerogram above a threshold equal to x% of the PGA (Kawashima and Aizawa 1989). $\overline{Du}_x$ represents normalized uniform duration, which is defined as the sum of all time intervals over which the accelerogram exceeds a threshold equal to x% of the PGA (Bolt 1973). $I_D = \frac{\int_0^{t_{max}} a^2(t)dt}{PGA \times PGV}$ is a dimensionless duration metric proposed by Cosenza and Manfredi (1997). $N_{eq} = \sum_{i=1}^{2n} \left(\frac{a_i}{a_{max}}\right)^2$ represents the equivalent number of cycles of the accelerogram (Bommer et al. 2006), where n is the total number of cycles calculated using the rainflow counting method (ASTM 2011), a_i is the amplitude of the i^{th} half-cycle, and a_{max} is the amplitude of the largest half-cycle. *Velocity* Ds_{5-75} and *Velocity* Ds_{5-95} represent significant duration computed from the velocity time history instead of the acceleration time history. *Spectral* $Ds_{5-95}(T_1, 5\,\%)$ and *Spectral* $N_{eq}(T_1, 5\,\%)$ represent significant duration and the number of equivalent cycles computed from the relative displacement response history of an elastic single degree of freedom oscillator of period T_1 and damping equal to 5 % of the critical value. Finally, the boxplot labeled "*No duration metric*" represents the distribution of R^2 values obtained using only S_aRatio in the regression model. The first observation from Figure 5.10 is that the consideration of any of the duration metrics, in addition to S_aRatio, produces a significant improvement in the efficiency of the vector IM. Among the significant durations, the efficiencies of Ds_{5-75} and Ds_{5-95} are found to be almost identical. $\overline{Db}_{10}$ and $\overline{Du}_{10}$ are found to outperform their counterparts corresponding to thresholds of 20 % and 30 % of PGA. I_D and N_{eq} are found to perform relatively poorly in comparison. The metrics computed from the velocity time history and the relative displacement response history of a single degree of freedom oscillator do not produce any significant improvements over common acceleration time history based metrics, hence not justifying their use, given the additional complexity involved in their calculation. Finally, the availability of a number of prediction equations for Ds (e.g., Abrahamson and Silva 1996; Kempton and Stewart 2006; Bommer et al. 2009; Afshari and Stewart 2016) make it a more appealing option than $\overline{Db}$ and $\overline{Du}$, for use within the proposed reliability framework.

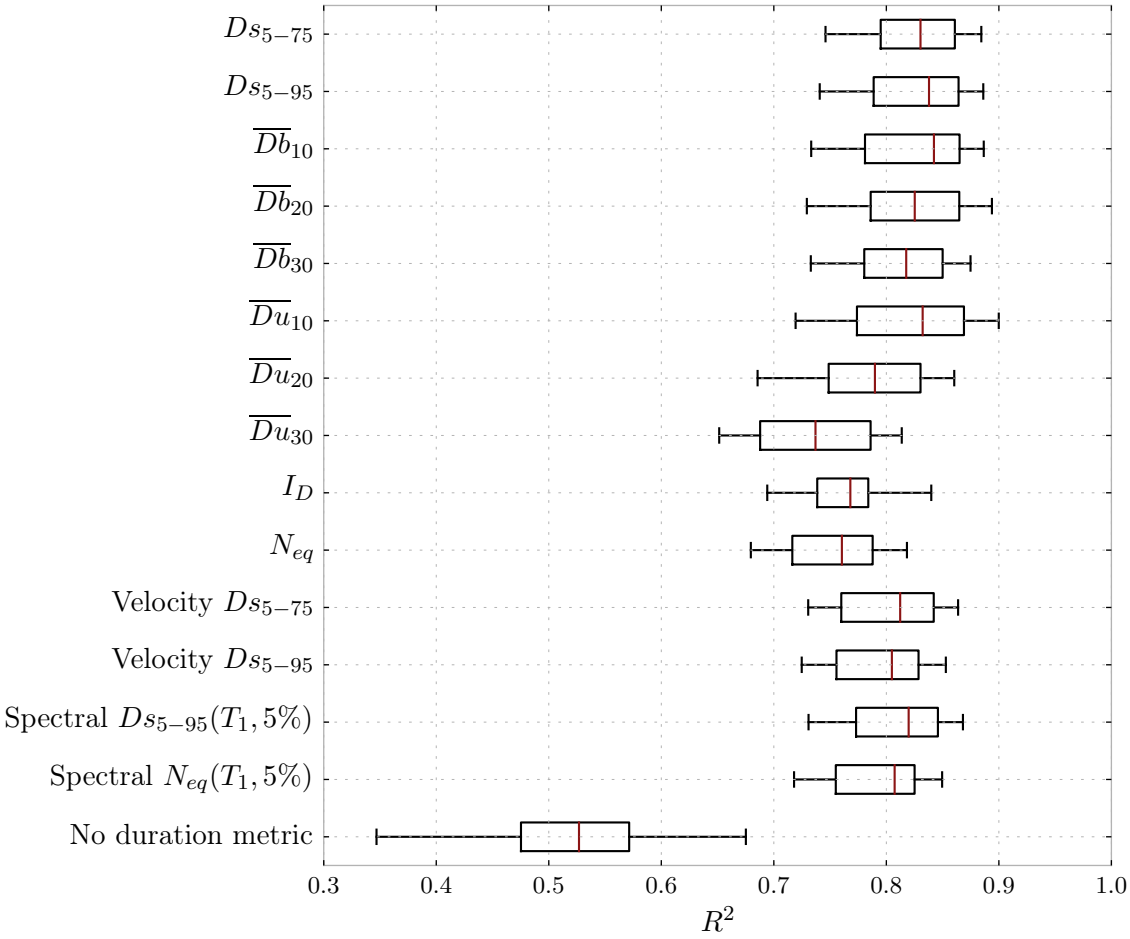

Figure 5.10: Distribution of the R^2 values obtained for all 51 reinforced concrete moment frames, by fitting the regression model in Equation (5.12) using a number of different amplitude-invariant duration metrics in place of Ds, and $S_aRatio(T_1, 0.2T_1, 3.0T_1)$. The whiskers of each boxplot extend from the 5$^{\text{th}}$ to the 95$^{\text{th}}$ percentile R^2 values for the corresponding duration metric.

5.6.2 Efficiency of S_aRatio

The start and end periods used to compute S_aRatio for optimal efficiency are functions of structural characteristics, in much the same way the optimal period at which to compute S_a is also a function of structural characteristics (Vamvatsikos and Cornell 2005). The variation of the optimal start and end periods with structural parameters like number of stories, period, ductility, etc., has been previously examined by Bianchini (2008) and Eads (2013). Since these studies used only short duration ground motions, the fact that they ignored the contribution of duration in their comparisons probably did not significantly influence their results. In all the calculations presented above, the period range $0.2T_1$ to $3.0T_1$ was used to compute S_aRatio, as recommended by Eads et al. (2015). Nevertheless, the efficiencies of other period ranges were also examined by comparing the R^2 values obtained by fitting the regression model in Equation (5.12) to the ground motion collapse intensities computed for the eight-story reinforced concrete moment frame, using S_aRatio computed over different period ranges, and Ds_{5-75}. As discussed in § 5.6.1 above, the retention of Ds in the regression model helps account for the contribution of duration in predicting ground motion collapse intensity. Since the regression model containing only Ds_{5-75} has an R^2 of 0.40, the inclusion of S_aRatio computed over any period range, in addition to Ds_{5-75}, is expected to produce an R^2 of at least 0.40. The R^2 values obtained by computing S_aRatio over different period ranges are plotted in Figure 5.11. It can be observed from the plot that the optimal period range for the analyzed moment frame is $0.1T_1$ to $2.6T_1$, which produces an R^2 of 0.82. This is, however, only marginally better than the R^2 of 0.81 computed using the period range $0.2T_1$ to $3.0T_1$, thereby justifying the general recommendation by Eads et al. (2015) to use the period range $0.2T_1$ to $3.0T_1$ to compute S_aRatio. Comparing Figures 5.9 and 5.11, it can be observed that the choice of the period range over which to compute S_aRatio has a larger impact on the results of the reliability framework than the choice of the percentage range used to compute Ds. Similar inferences could be drawn by examining plots corresponding to the other 50 reinforced concrete frames as well.

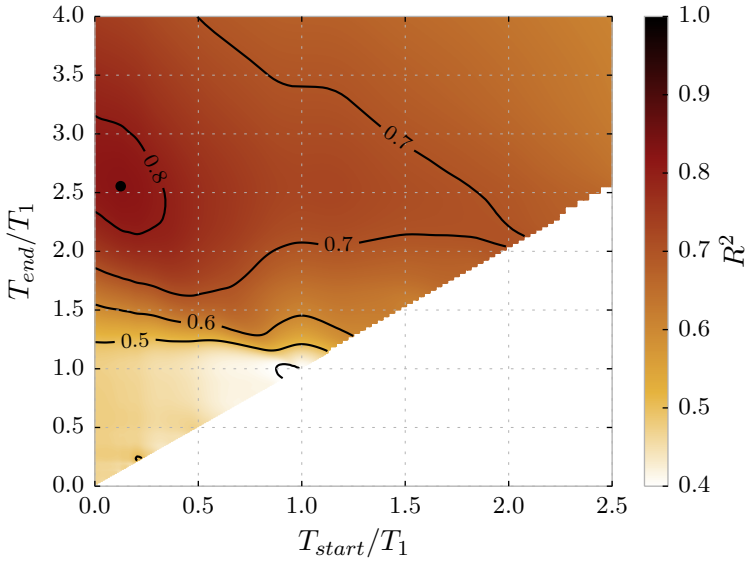

Figure 5.11: Comparison of the R^2 values obtained by fitting the regression model in Equation (5.12) to the ground motion collapse intensities computed for the eight-story reinforced concrete moment frame, using S_aRatio defined by different period ranges, and Ds_{5-75}. The period range that produces the largest R^2 value is plotted as a black circle.

5.7 Guidelines for ground motion selection

As highlighted previously, the ability to use a generic record set, that is not specific to any structure or site, is considered to be the one of the most attractive features of IDA. A drawback of using a generic record set is, however, the inability to produce hazard-consistent collapse risk estimates by failing to capture (*i*) site-specific variations in the characteristics of anticipated ground motions; and (*ii*) the variation in the expected characteristics of ground motions of different intensities, by scaling the same set of ground motions to different intensity levels. The reliability framework proposed in this paper imparts IDA the ability to compute hazard-consistent collapse risk estimates, although it does come at the expense of the requirement to adhere to a few broad guidelines when selecting ground motions. It is worth noting though, that these guidelines are by no means as stringent as the requirements to select hazard-consistent ground motions to conduct MSA, and could be used to select a broad generic set of ground motions which can be employed to analyze different types of structures

at different types of sites, as per the analyst's requirements. The set of 88 ground motions used in this study was originally assembled as part of the procedure developed in § 6.6 to incorporate the effect of duration in the FEMA P695 methodology, and not to specifically adhere to the guidelines described in this section. Nevertheless, they were found to satisfy a number of the selection criteria outlined below, and therefore, either the entire set or a subset could be used to analyze a broad range of structures at a number of different sites.

The objective of the ground motion selection strategy used in conjunction with the reliability framework is to minimize the uncertainty in predicting ground motion collapse intensity, within the range of S_aRatio and Ds values of the ground motions anticipated at the site. Thus, the selection of ground motions can be viewed as an experimental design problem (Kutner et al. 2005, Chapter 15). The contours in Figure 5.12 represent the standard error in predicting the mean of the logarithm of the collapse intensity. Their elliptical shape is a consequence of using a linear regression model to predict collapse intensity. The standard error is observed to be the least at the sample geometric mean S_aRatio and Ds of all the ground motions, which lies at the geometric center of all the contours, and to increase radially outwards. Therefore, the geometric mean S_aRatio and Ds values of the selected ground motions should ideally be close the corresponding median targets conditional on the $S_a(T_1)$ level that contributes most to the collapse risk of the structure. This $S_a(T_1)$ level corresponds to the peak of the collapse risk deaggregation curve, which is computed as the product of the collapse fragility curve and the slope of the hazard curve (Eads et al. 2013). Unfortunately, this value is not known before actually conducting the analysis, but $2.0\times\text{MCE}_\text{R}$ serves as an approximate initial estimate for new structures. Nevertheless, this condition needs to be evaluated after conducting the analysis. The median targets at the three considered sites, conditional on this $S_a(T_1)$ level, are plotted using hollow colored circles. The median targets at all three sites can be seen to lie reasonably close to the geometric mean S_aRatio and Ds values of the ground motions.

In addition, it is important to ensure that the marginal variances of the S_aRatio and Ds values of the selected ground motions are large relative to the marginal variances of the corresponding targets. The observation that the S_aRatio and Ds

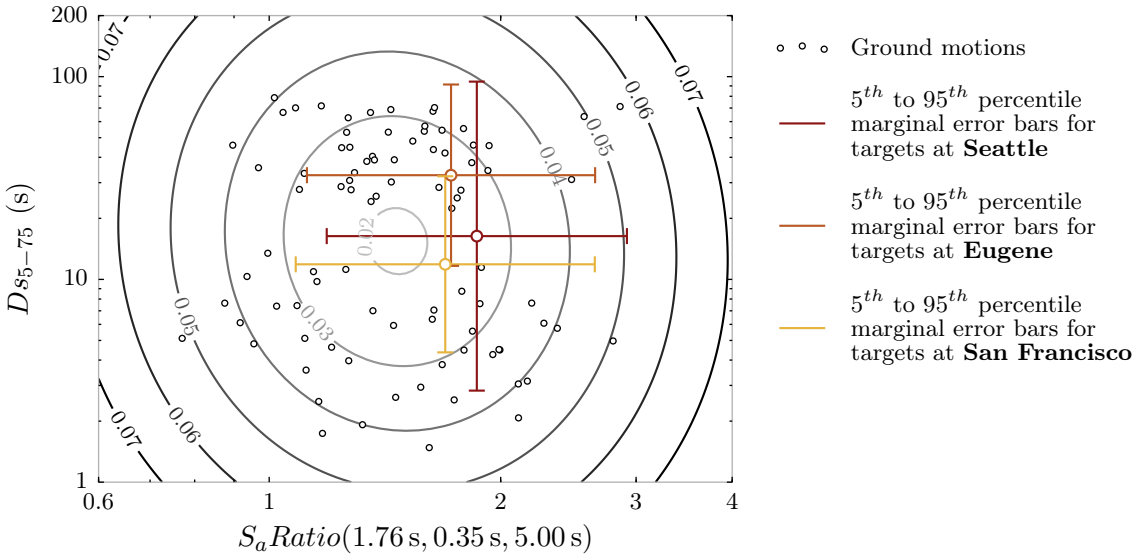

Figure 5.12: Contours depicting the standard error in predicting the mean of the logarithm of the $S_a(1.76\,\mathrm{s})$ value at collapse. The $S_aRatio(1.76\,\mathrm{s}, 0.35\,\mathrm{s}, 5.00\,\mathrm{s})$ and Ds_{5-75} values of the selected ground motions are plotted as hollow black circles, and the median targets at the three considered sites, conditional on a ground motion intensity level corresponding to $2.0 \times \mathrm{MCE_R}$, are plotted using hollow colored circles, along with 5^{th} to 95^{th} percentile marginal error bars.

values of the selected ground motions are well spread out over the area defined by the 5^{th} to 95^{th} percentile marginal error bars of the targets at the three sites, plotted in Figure 5.12, confirms the satisfaction of this requirement. *Orthogonality* can be introduced into the ground motion selection procedure by selecting pairs of records with similar S_aRatio values but different Ds values or vice versa, thus further lowering prediction standard errors. The selection of long duration records that are spectrally equivalent to the short duration records approximately satisfies this requirement. Finally, using more ground motions will produce more precise predictions.

A closer examination of the target distributions of S_aRatio and Ds plotted in Figure 5.12 reveals that although the marginal variance of the S_aRatio targets at all three sites are almost equal, the marginal variance of the Ds targets are not. The large variance of the Ds target at Seattle is a consequence of both short duration ground motions from crustal earthquakes and long duration ground motions from interface earthquakes contributing to its seismic hazard. Hence, the use of all 88 short and long duration ground motions is considered necessary for Seattle. On the other hand, reasonable collapse risk estimates could possibly have been obtained for Eugene using just the 44 long duration records, if supplemented with a few more records with $10\,\text{s} < Ds_{5-75} < 20\,\text{s}$. Interestingly, the median Ds target at San Francisco is observed to be longer than the Ds values of most of the 44 short duration ground motions from the FEMA P695 far-field set, although the set consists of ground motions recorded from shallow crustal earthquakes of magnitude as large as 7.6. This is a consequence of earthquakes of magnitude 8.0 and above on the San Andreas fault contributing to its seismic hazard, thereby requiring the use of relatively long duration ground motions, with Ds_{5-75} as long as 30 s, to obtain accurate collapse risk estimates. The FEMA P695 far-field set is, however, expected to be adequate for other sites in coastal California, like Los Angeles and Berkeley, whose median Ds targets are expected to be much shorter.

For sites like Eugene and San Francisco, whose Ds targets have low marginal variances, reasonably accurate collapse risk estimates could presumably be obtained by ignoring Ds from the reliability integral in Equation (5.17), if (i) the variation in the Ds targets conditional on different $S_a(T_1)$ levels that contribute significantly to

the collapse risk, is small; (*ii*) the Ds values of the selected ground motions match the target Ds distribution conditional on the $S_a(T_1)$ level that contributes most to the collapse risk; and (*iii*) the anticipated variation in structural collapse capacity, as quantified by the regression model described by Equation (5.12), over the range of Ds values anticipated at the site, is small. Although the second requirement is equivalent to selecting site-specific ground motions, the selected records could be used in a wide range of sites located in similar tectonic settings. It is also worth noting here, that the target S_aRatio and Ds values at the three sites are expected to vary significantly with the chosen conditioning period and site Vs_{30}. This variation needs to be considered to ensure the applicability of a generic set of ground motions selected based on these guidelines, to a wide range of sites and structures.

5.8 Conclusion

A structural reliability framework was developed to post-process the results of an incremental dynamic analysis (IDA) conducted using a generic ground motion set and compute a hazard-consistent collapse fragility curve. This resolves the largest drawback of the traditional IDA procedure: its inability to produce hazard-consistent collapse risk estimates, thus making it a competitive alternative to multiple stripe analysis (MSA). The proposed procedure employs a scalar parameter, S_aRatio, that quantify response spectral shape, and significant duration, Ds, as secondary intensity measures. These two parameters are shown to be good predictors of the potential of a ground motion to cause damage, quantified here as its collapse intensity, or the lowest $S_a(T_1)$ value it needs to be scaled to, to cause structural collapse. They are demonstrated to be capable of explaining 81 % of the variance in the collapse intensities of a set of short and long duration ground motions used to analyze a ductile eight-story reinforced concrete moment frame building, designed for a site in Seattle. Using S_aRatio alone explains only 45 % of the variance, and using Ds alone explains only 40 % of the variance of the collapse intensities, thus highlighting the importance of considering both ground motion response spectral shape and duration in structural collapse risk assessment.

S_aRatio and Ds are used in conjunction with $S_a(T_1)$ to define a linear failure surface using the results of an IDA. Hazard-consistent target distributions of S_aRatio and Ds, conditional on the exceedance of a specific $S_a(T_1)$ level, are integrated over the failure domain to estimate the probability of observing structural collapse at that $S_a(T_1)$ level. Evaluating this reliability integral at many different $S_a(T_1)$ levels allows computing a non-parametric, hazard-consistent collapse fragility curve, which, for the case of the reinforced concrete moment frame analyzed in this study, was found to agree well with the fragility curve computed by conducting MSA using hazard-consistent ground motions. In addition, the computed regression coefficients corresponding to S_aRatio and Ds provide deeper insight into the influence of response spectral shape and duration on the collapse response of the structure. The conventional practice of computing a fragility curve using only $S_a(T_1)$, a scalar IM, and ignoring both S_aRatio and Ds, was found to significantly over-estimate the collapse risk. The inaccuracy of this method stems from ignoring all site-specific seismic hazard information when computing a collapse fragility curve. Adjusting the median collapse capacity using an approximate, empirically calibrated spectral shape factor, as recommended by FEMA P695, was, on the other hand, found to significantly under-estimate the collapse risk. The accuracy of this method could potentially be improved by further adjusting the median collapse capacity by an analogous duration factor. These trends were found to hold even when the same structure was analyzed at Eugene and San Francisco: sites with different S_aRatio and Ds targets compared to Seattle. A simplified method that does not require the evaluation of the reliability integral, was also proposed to estimate just the hazard-consistent median collapse capacity instead of the entire collapse fragility curve.

Finally, the proposed structural reliability framework and hazard-consistent MSA were shown to represent two different approaches to solving the same structural reliability problem. The proposed structural reliability framework represents an analytical approach, while hazard-consistent MSA represents a simulation-based approach. Since both methods have been demonstrated to produce similar results, the choice between the two now hinges on the relative ease of the ground motion selection requirements of each method and their computational efficiencies, which remains to be

assessed.

Chapter 6

Strategies to consider ground motion duration in addition to response spectra in standards for structural performance assessment and design

6.1 Abstract

Strategies are proposed to explicitly account for the effect of duration on structural response, in addition to the effect of response spectra, in the analysis procedures contained in the following standards for structural performance assessment and design: (*i*) the FEMA P-58 seismic performance assessment methodology; (*ii*) the FEMA P695 methodology to quantify seismic performance factors; and (*iii*) the ASCE 7-16 seismic design provisions. The effect of duration is considered in multiple stripe analysis by selecting records to match site-specific target distributions of duration, computed using the generalized conditional intensity measure (GCIM) framework, in addition to target conditional spectra. It is considered in incremental dynamic

analysis by fitting a multiple linear regression model to the computed ground motion collapse intensities using a scalar, dimensionless measure of response spectral shape called S_aRatio and significant duration, Ds, as predictors. The hazard-consistent median collapse capacity is then computed by iteratively evaluating the regression surface using site-specific median S_aRatio and Ds targets computed conditional on different intensity levels. The effects of response spectral shape and duration are incorporated in ASCE 7-16's equivalent lateral force procedure by developing site and structural system-specific adjustment factors for the design base shear based on the conditional median S_aRatio and Ds targets at the site. Sample calculations indicate, for example, that a 1 s reinforced concrete moment frame building at San Francisco would need to be designed to a base shear that is 43 % higher than the value used in current practice; a similar structure in Eugene would need to be designed to a base shear that is 67 % higher. The acceptance criteria used in conjunction with ASCE 7-16's nonlinear response history analysis procedure are unlikely to reliably capture the effect of duration; hence, it is recommended that the selected records be scaled to an MCE_R level modified by a duration adjustment factor, analogous to the one developed for the equivalent lateral load procedure. The consequence of ignoring the effect of duration in each case is demonstrated by analyzing an eight-story reinforced concrete moment frame building.

6.2 Introduction

Current standards for structural performance assessment and design quantify seismic hazard primarily in terms of the response spectra of the ground motions anticipated at a site, while relegating other ground motion characteristics to qualitative consideration (NIST 2011, Chapter 3). The response spectrum of a ground motion, which quantifies its amplitude and frequency content, has been shown by a number of previous studies to be well correlated to important structural demands like peak deformations and collapse capacity (Shome et al. 1998; Baker and Cornell 2006b), thereby justifying its prominent use in structural performance assessment. Recent studies by the authors and others (e.g., Chapter 5; Raghunandan and Liel 2013;

Chapter 4/Chandramohan et al. 2016a) have demonstrated the additional influence of ground motion duration on structural collapse risk. In these studies, long duration ground motions produced by large magnitude earthquakes were shown to be more likely to cause structural collapse when compared to short duration ground motions with similar response spectra. This finding warrants the explicit consideration of ground motion duration in structural performance assessment and design, in conjunction with response spectra, to ensure that structures possess equivalent margins of safety against collapse irrespective of the response spectral shapes and durations of the ground motions they are likely to experience. This study proposes strategies to incorporate the effect of duration into the FEMA P-58 seismic performance assessment methodology (FEMA 2012b), the FEMA P695 methodology to quantify seismic performance factors (FEMA 2009b), and the ASCE 7-16 seismic design provisions (ASCE 2016). Although these standards do already contain provisions to account for the effect of response spectral shape, recommendations are made to improve the manner in which response spectral shape is handled in some of these provisions using a scalar, dimensionless metric called $S_a Ratio$, proposed by Eads et al. (2016).

Although the structural engineering community largely acknowledges that ground motion duration is likely to influence structural response, there is still considerable debate regarding the nature and magnitude of its influence, and the manner in which it is to be addressed in design and assessment. As a consequence, ground motion duration is presently not explicitly considered in structural design and assessment practice. The lack of consensus regarding the consideration of duration stems from (*i*) the broad conclusion of previous research on the topic, that ground motion duration mainly influences cumulative damage metrics, and has little measurable effect on peak structural deformations (e.g., Cornell 1997; Bommer et al. 2004; Hancock and Bommer 2006; Iervolino et al. 2006; Hancock and Bommer 2007; Oyarzo-Vera and Chouw 2008; Barbosa et al. 2014; Hou and Qu 2015); and (*ii*) the prevalent use of peak structural deformations in acceptance criteria for structural design (PEER TBI 2010; LATBSDC 2014; ASCE 2016) and performance assessment (FEMA 2012b). The inability of previous studies to capture the effect of duration on peak structural deformations can be attributed to one or more of the following factors: (*i*) the

prevalent use of non-deteriorating structural models; (*ii*) the scarcity of long duration ground motion records before the 2010 Maule (Chile) and 2011 Tohoku (Japan) earthquakes; (*iii*) the lack of consensus on an effective metric to quantify ground motion duration (Chapter 2/Chandramohan et al. 2016b); and (*iv*) the lack of adequate controls for the effect of response spectral shape. Only recently, have studies employing realistic structural models that simulate the in-cycle and cyclic deterioration of structural strength and stiffness, and the destabilizing $P-\Delta$ effect of gravity loads, been able to capture and quantify the effect of duration on peak structural deformations and collapse capacity (Raghunandan and Liel 2013; Chapter 2/Chandramohan et al. 2016b; Marafi et al. 2016). Since structural collapse capacity is an important metric used in the calibration of seismic design codes, and an integral component of seismic loss assessment studies, these findings motivate the need to explicitly consider ground motion duration in structural design and assessment practice. Ground motion response spectral shape and duration were demonstrated to together be capable of explaining around 80 % to 85 % of the variance in the collapse intensities of ground motions used to analyze 51 reinforced concrete moment frame buildings in Chapter 5. This suggests that response spectra and duration are sufficient considerations in the design and assessment of structures, and the consideration of additional ground motion characteristics is expected to produce diminishing returns.

Different methods are proposed to incorporate the effect of duration—and response spectral shape where necessary—in each of the considered standards, tailored to their own individual objectives. While most of the recommendations just require a few additional considerations in the existing procedures, some involve deeper revisions of the current procedures. Where possible, options have been provided between accurate but computationally intensive options and approximate but computationally efficient procedures. Significant duration (Trifunac and Brady 1975), Ds, is used to quantify ground motion duration in all the proposed strategies. Recommended modifications to the FEMA P-58 methodology involve the selection of records for response history analysis to match target distributions of both duration and response spectra. The shortcomings of the existing method to account for the effect of response spectral shape in the FEMA P695 methodology, using a spectral shape factor developed based

on ε (Baker and Cornell 2005), are highlighted. The consideration of site-specific seismic hazard information in terms of conditional median S_aRatio and Ds targets, is proposed as a more accurate alternative. Methods are then proposed to adjust the median collapse capacities of the structural archetypes, computed by conducting nonlinear dynamic analysis using a generic record set, to reflect these site-specific S_aRatio and Ds targets. The influence of response spectral shape and duration is incorporated in ASCE 7-16's equivalent lateral force (ELF) procedure by developing site and structural system-specific factors to adjust the design base shear. Finally, the ability of acceptance criteria employed by ASCE 7-16's nonlinear response history analysis (NLRHA) procedure to capture the effect of duration is evaluated, and strategies are proposed to address the shortcomings. The benefits of the improvements proposed to each procedure are demonstrated by analyzing an eight-story reinforced concrete moment frame building.

6.3 Computation of S_aRatio and Ds of a ground motion

The parameter S_aRatio is a scalar, dimensionless measure of a ground motion's response spectral shape, proposed by Eads et al. (2016). It is computed according to Equation (6.1a), as the ratio of the pseudo spectral acceleration at a specific period, $S_a(T)$, and the geometric mean of the portion of the response spectrum that lies between the periods T_{start} (usually $< T$) and T_{end} (usually $> T$), denoted by $S_{a,avg}(T_{start}, T_{end})$. $S_{a,avg}(T_{start}, T_{end})$ is computed according to Equation (6.1b), as the sample geometric mean of response spectral ordinates, discretely sampled at n linearly spaced periods from T_{start} to T_{end}: τ_1, τ_2, ..., τ_n, such that $\tau_1 = T_{start}$ and

$\tau_n = T_{end}$ (Baker and Cornell 2006a; Eads et al. 2015):

$$S_aRatio(T, T_{start}, T_{end}) = \frac{S_a(T)}{S_{a,avg}(T_{start}, T_{end})} \tag{6.1a}$$

$$S_{a,avg}(T_{start}, T_{end}) = \left(\prod_{j=1}^{n} S_a(\tau_j) \right)^{1/n} \tag{6.1b}$$

A more general method to compute $S_{a,avg}$, as the geometric mean of the function $S_a(T)$, is described in Appendix B. This alternative method offers the advantage of not requiring the re-sampling of the response spectrum at a set of specific linearly spaced periods, and thus avoids any loss in accuracy in the computation of $S_{a,avg}$ due to widely spaced periods.

The response spectra of two ground motions with low and high $S_aRatio(1.0\,\text{s}, 0.2\,\text{s}, 3.0\,\text{s})$ values, normalized to have $S_a(1.0\,\text{s}) = 1\,\text{g}$, are plotted in Figure 6.1. Since S_aRatio is a dimensionless metric, its value remains unchanged as the ground motions are linearly scaled. The ground motion with a low S_aRatio value has relatively high response spectral ordinates at periods between 0.2 s and 3.0 s compared to the response spectral ordinate at 1.0 s. The opposite is true for the ground motion with a high S_aRatio value. Since the two ground motions are scaled to the same $S_a(1.0\,\text{s})$ value, the ground motion with a low S_aRatio value is generally expected to be more damaging, because it possesses more energy at periods above and below 1.0 s compared to the ground motion with a high S_aRatio value. Eads et al. (2015) recommended using the period range $0.2T$ to $3.0T$ to compute S_aRatio at the period T, since it was found to be most efficient in predicting the collapse intensity of a ground motion used to analyze a structure with fundamental elastic modal period T. This recommendation was based on observations from collapse analyses on a number of reinforced concrete moment frame and shear wall buildings conducted by Eads et al. (2015), and is supported by results from the analysis of 51 reinforced concrete moment frame buildings in Chapter 5. Hence, this period range is adopted to compute S_aRatio throughout this paper, unless explicitly noted otherwise. A number of other metrics of response spectral shape have been proposed in the literature (e.g., Cordova et al. 2000; Vamvatsikos and Cornell 2005; Tothong and Luco 2007; Baker and Cornell 2008; Mehanny

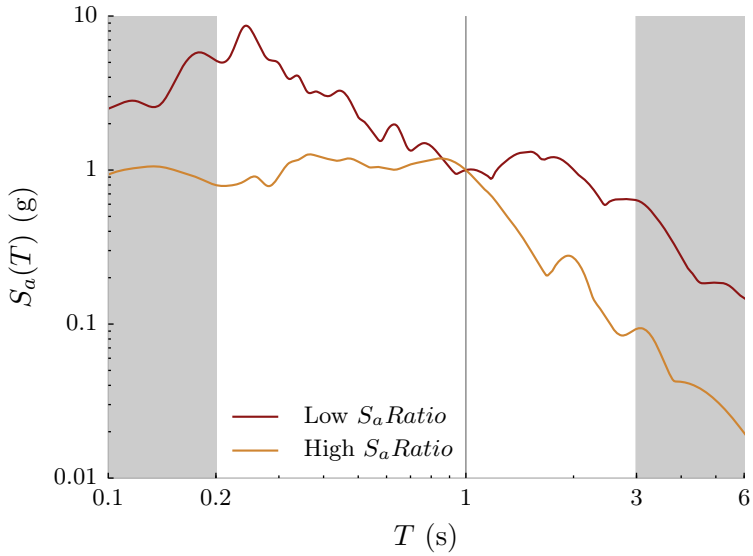

Figure 6.1: Response spectra of two ground motions with low and high $S_aRatio(1.0\,\text{s}, 0.2\,\text{s}, 3.0\,\text{s})$ values, normalized to have $S_a(1.0\,\text{s}) = 1\,\text{g}$. The vertical line at 1.0 s corresponds to the period at which S_a in the numerator of Equation (6.1a) is computed, and the unshaded period range from 0.2 s to 3.0 s corresponds to the domain over which $S_{a,avg}$ in the denominator of Equation (6.1a) is computed. The ground motion with a low $S_aRatio(1.0\,\text{s}, 0.2\,\text{s}, 3.0\,\text{s})$ value of 0.88 was recorded from the 1979 Imperial Valley earthquake, at the El Centro Array #11 station; and the one with a high $S_aRatio(1.0\,\text{s}, 0.2\,\text{s}, 3.0\,\text{s})$ value of 2.95 was recorded from the 1999 Duzce, Turkey earthquake, at the Bolu station. Both ground motions are taken from the FEMA P695 far-field set.

2009; Bojórquez and Iervolino 2011), but S_aRatio was preferred over them due to its simplicity, efficiency, and hazard-computability.

Significant duration, Ds, is used to quantify ground motion duration since previous studies by the authors (e.g., Chapter 5; Chapter 2/Chandramohan et al. 2016b) have shown it to possess a number of desirable characteristics, including strong correlation to structural collapse capacity. A comparative assessment also demonstrated it to be better suited than other duration metrics to guide the selection of ground motions for structural performance assessment. The significant duration of a ground motion is defined as the time interval over which a specific percentage range of the integral $\int_0^{t_{max}} a^2(t)dt$ is accumulated, where $a(t)$ represents the ground acceleration at time t, and t_{max} represents the length of the accelerogram. Common ranges used

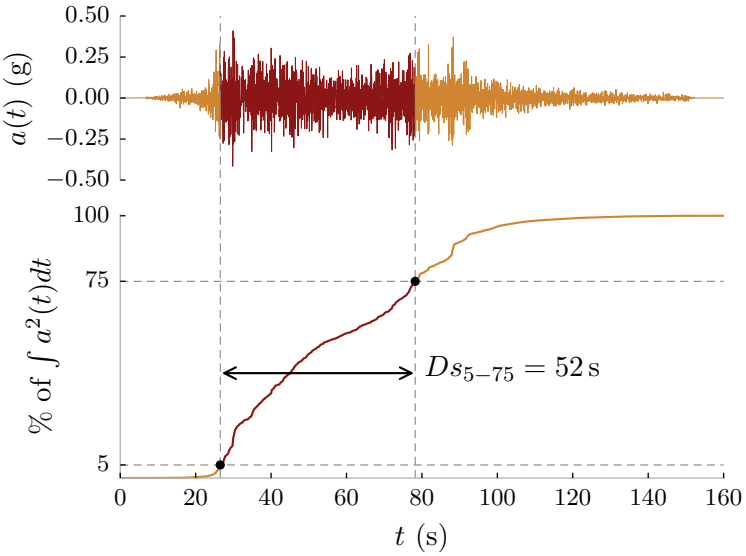

Figure 6.2: (Top) East-West component of the accelerogram recorded from the 2010 Maule (Chile) earthquake at the Talca station; and (Bottom) the normalized, cumulative integral of $a^2(t)$—known as a Husid plot (Husid 1969)—illustrating the computation of 5–75 % significant duration of the accelerogram.

to compute Ds include 5–75 %, 5–95 %, 2.5–97.5 %, and 20–80 % (Boore and Thompson 2014; Afshari and Stewart 2016). Although 5–75 % significant duration is used throughout this paper, previous studies by the authors have shown that 5–95 % significant duration also produces good results (Chapter 5; Chapter 2/Chandramohan et al. 2016b). The computation of 5–75 % significant duration, Ds_{5-75}, of an accelerogram is illustrated in Figure 6.2.

6.4 Reinforced concrete moment frame model

A ductile eight-story reinforced concrete moment frame building, designed for a site in Seattle (Washington), is used to demonstrate the benefits of the improvements proposed to each procedure. This frame was designed and modeled by Raghunandan et al. (2015) as part of a larger study on the collapse safety of reinforced concrete frames in the US Pacific Northwest, and it was previously analyzed in related studies

by the authors (e.g., Chapter 5; Chapter 4/Chandramohan et al. 2016a). The two-dimensional, centerline model of the structure, which was created and analyzed in OpenSees rev. 5184 (McKenna et al. 2006), is illustrated in Figure 6.3. The first story of the frame is 4.57 m tall and each remaining story is 3.96 m tall; each bay is 6.10 m wide. The beams and columns of the frame were modeled using linear elastic elements, with zero-length plastic hinges located at either end. The hysteretic behavior of the plastic hinges was modeled using the peak-oriented Ibarra-Medina-Krawinkler model (Ibarra et al. 2005), modified as per the recommendations of Lignos and Krawinkler (2012) (p. 26). This model includes a post-peak negative stiffness branch of the backbone curve to capture in-cycle deterioration, as well as cyclically deteriorating strength and stiffness based on the cumulative hysteretic energy dissipated. Finite beam-column joints were modeled with elastic shear deformations. The destabilizing $P-\Delta$ effect of the gravity loads tributary to other parts of the structure was captured using a pin-connected leaning column. The fundamental elastic modal period of the structure 1.76 s. All response history analyses of the structure were carried out using the explicit central difference time integration scheme, since it was found to be more robust and efficient than implicit time integration schemes, which sometimes failed to converge (Chapter 7).

6.5 The FEMA P-58 methodology

The FEMA P-58 seismic performance assessment methodology (FEMA 2012b) is used to assess the performance of individual buildings under earthquakes loads, in terms of the anticipated human losses (injuries and fatalities), direct economic losses (repair and replacement costs), and indirect losses (downtime and unsafe placarding). Two essential components of the methodology that involve structural analysis include (*i*) estimating the collapse capacity; and (*ii*) estimating structural demands given collapse has not occurred. The collapse capacity is estimated either by (*i*) conducting multiple stripe analysis (MSA) (Jalayer 2003, Chapter 4) using ground motions selected to match a target response spectrum; or by (*ii*) iteratively conducting a modified version of incremental dynamic analysis (IDA) (Vamvatsikos and Cornell 2002)

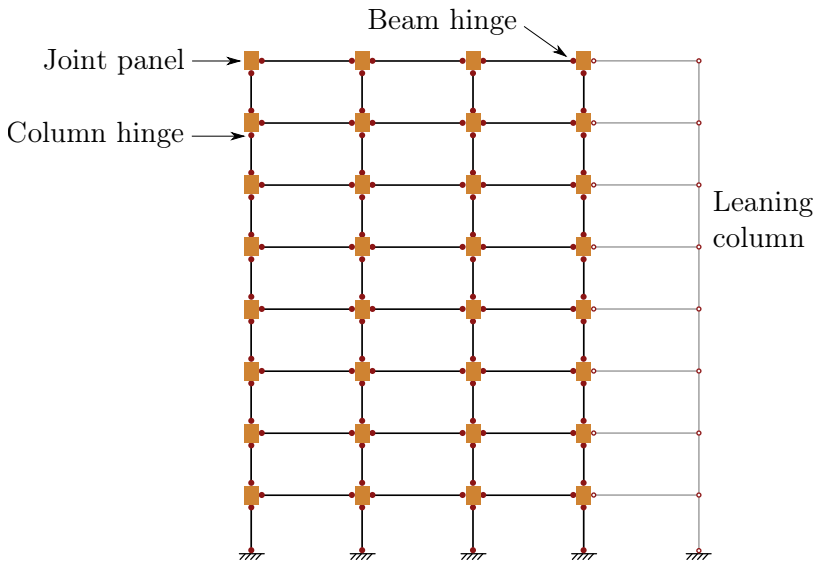

Figure 6.3: Schematic of the eight-story reinforced concrete moment frame model.

using ground motions selected to match target response spectra computed at different intensity levels. Procedures are outlined to conduct three types of assessments, viz., scenario-based, intensity-based, and time-based assessments, to estimate structural demands given collapse has not occurred. Guidelines to conduct all three types of assessments, similar to those proposed to compute the collapse capacity, recommend the selection of ground motions to explicitly match only a target response spectrum. Provided options for target response spectra include (*i*) the uniform hazard spectrum (UHS) (McGuire 2004); (*ii*) the conditional mean spectrum (CMS) (Baker 2011); and (*iii*) the conditional spectrum (CS) (Abrahamson and Al Atik 2010; Jayaram et al. 2011b). The features of these target response spectra, including reasons why the CS is considered to be a more accurate representation of the site hazard than the other target spectra, are summarized in NIST (2011) (Chapter 5). Other ground motion characteristics, like duration and the presence of velocity pulses, are implicitly accounted for by the selection of records whose causal parameters, like magnitude, source-to-site distance, and site Vs_{30} (the time-averaged shear wave velocity of the top 30 m of the soil profile), match corresponding target values that control the seismic hazard at the site. These target causal parameter values can be obtained using seismic

hazard deaggregation computations (McGuire 1995). Recent studies (e.g., Chapter 4/ Chandramohan et al. 2016a; Tarbali and Bradley 2016) have, however, highlighted the drawbacks and limitations of relying on causal parameters to capture the effects of these other ground motion characteristics. Strategies are proposed to explicitly account for the effect of duration when estimating structural collapse capacity using both MSA and IDA, as well as when conducting scenario-based, intensity-based, and time-based assessments to estimate structural demands given collapse has not occurred.

6.5.1 Estimating structural collapse capacity

Structural collapse capacity is a measure of the ability of a structure to resist collapse under earthquake ground motion. It is defined by a collapse fragility curve, which is a monotonically increasing function that relates the intensity of ground motion to the probability of observing structural collapse. Intensity is, however, not the only characteristic of a ground motion that determines its influence on structural response; other characteristics like response spectral shape and duration also play a role. Hence, the collapse capacity of a structure also depends on the response spectral shapes and durations of the ground motions anticipated at the site where it is located. A collapse fragility curve estimated by taking these other characteristics into account, is termed *hazard-consistent*.

The structural modeling guidelines provided in FEMA (2012b) (§ 5.2.1) recommend incorporating the anticipated in-cycle and cyclic deterioration of the strength and stiffness of the structural components, and the destabilizing $P-\Delta$ effect of gravity loads in the numerical model of the structure. Both these measures are necessary to adequately capture the effect of duration on structural collapse capacity. Failure to incorporate these key elements in the structural model is likely to produce unconservative collapse capacity estimates at sites susceptible to long duration ground motions, for reasons outlined in Chapter 3/Chandramohan et al. (2017).

Multiple stripe analysis (MSA)

Multiple stripe analysis (MSA) is a method of analysis, wherein the structure is analyzed using multiple sets of ground motions, each scaled to different ground motion intensity levels. As defined in FEMA (2012b) (p. 4-7), ground motion intensity is quantified using the 5 % damped pseudo spectral acceleration at a period $\bar{T}$, $S_a(\bar{T})$; where $\bar{T}$ is usually taken to be equal to the fundamental elastic modal period of the structure. As per the procedure outlined in FEMA (2012b) (§ 4.4) to conduct MSA, each set of ground motions scaled to a particular intensity level is selected to match a target response spectrum computed at that intensity level. Among the provided target response spectrum options, use of the CS is recommended, since it provides the most realistic representation of the range of response spectral shapes of the ground motions anticipated at the site. The CS at an intensity level is computed as the probability distribution of a vector of S_a values at periods above and below $\bar{T}$, conditional on the exceedance of the $S_a(\bar{T})$ value corresponding to that intensity level. An extension of the CS, known as the generalized conditional intensity measure (GCIM) (Bradley 2010), can be used to compute the probability distribution of Ds, conditional on the exceedance of the same $S_a(\bar{T})$ value, using the following inputs:

(i) seismic hazard deaggregation information (McGuire 1995), which is also required to compute a CS;

(ii) an equation to predict Ds as a function of causal parameters like magnitude and source-to-site distance (e.g., Abrahamson and Silva 1996; Kempton and Stewart 2006; Bommer et al. 2009; Afshari and Stewart 2016); and

(iii) a model for the correlation coefficient between the total prediction residuals, or ε-values, of Ds and $S_a(\bar{T})$ (e.g., Bradley 2011).

A detailed description of the procedure to compute conditional distributions of Ds using the GCIM framework, along with sample calculations, is provided in Chapter 4/Chandramohan et al. (2016a) and Chapter 5. As an additional refinement, for sites like Seattle that receive seismic hazard contributions from different types of seismic sources (e.g., interface, in-slab, and crustal earthquakes), a procedure is

outlined to compute source-specific conditional spectra and conditional distributions of Ds, corresponding to each type of contributing seismic source. This helps distinguish the unique characteristics of the ground motions produced by different types of seismic sources, e.g., large magnitude interface earthquakes are known to produce ground motions of much longer duration than shallow crustal earthquakes. Finally, the selection of a set of ground motions to match the target source-specific CS and conditional distribution of Ds at each ground motion intensity level, in appropriate proportions as defined by the relative contribution of each source to the total seismic hazard at the site, is described.

The selection of ground motions to match target distributions of Ds, in addition to a target CS, is the only modification proposed to the procedure outlined in FEMA (2012b) (§ 6.2.4). Once the hazard-consistent sets of ground motions are selected, they are used to analyze the structural model, and the probability of collapse at each ground motion intensity level is computed as the fraction of the ground motions at that intensity level that cause structural collapse. A lognormal collapse fragility curve is then fit through these data points, and the hazard-consistent median collapse capacity is estimated as the ground motion intensity level corresponding to a collapse probability of 0.5. The associated lognormal standard deviation, β, of the estimated fragility curve accounts only for the record-to-record uncertainty. The effect of model uncertainty can be incorporated either by increasing this value of β by an amount corresponding to model uncertainty taken from FEMA (2012b) (§ 5.2.5), using the square root of sum of squares method; or by simply assuming a total β of 0.6, as recommended by FEMA (2012b) (§ J.5).

Selecting ground motions to explicitly match only target conditional spectra as per the original FEMA P-58 methodology, without consideration of duration, was shown by Chapter 4/Chandramohan et al. (2016a) to often result in biased collapse risk estimates. The magnitude of the bias was shown to depend both on the seismic hazard at the site, and the characteristic durations of the ground motions in the database used for record selection. For example, when the reinforced concrete moment frame described in § 6.4 was analyzed using records selected from the PEER NGA-West2 database (Ancheta et al. 2014), to match only target conditional spectra, a median

collapse capacity of 0.78 g was computed. When records were selected from a larger database consisting of records from large magnitude interface earthquakes as well, but under constraints imposed on their causal parameters, a value of 0.63 g was obtained. Both these estimates are removed from 0.68 g, the hazard-consistent value obtained using records selected to match both target conditional spectra and distributions of Ds. If the structure is assumed to be located in Eugene (Oregon) instead of Seattle, and a similar set of analyses are conducted as before, median collapse capacities of 0.92 g and 0.55 g are computed for the first two cases, which are more further removed from the hazard-consistent value of 0.62 g. The larger bias in this case is because the seismic hazard at Eugene is dominated by long duration ground motions produced by $M_W \sim 9.0$ interface earthquakes, whereas Seattle additionally receives hazard contributions from lower magnitude crustal earthquakes as well. These results are described in further detail in Chapter 4/Chandramohan et al. (2016a).

Incremental dynamic analysis (IDA)

The objective of the iterative modified IDA procedure described in FEMA (2012b) (Appendix J), is to obtain a hazard-consistent estimate of the collapse capacity. The *full* IDA procedure proposed by Vamvatsikos and Cornell (2002) involves incrementally scaling each ground motion from a set to higher intensity levels until it causes structural collapse at an intensity level known as its collapse intensity. The collapse fragility curve of the structure is then computed by fitting a lognormal cumulative distribution function to the collapse intensities estimated using all the ground motions in the set. There are two reasons for modifying this full IDA procedure for use with the FEMA P-58 methodology:

(i) Only the median collapse capacity, i.e., the ground motion intensity corresponding to a collapse probability of 0.5, needs to be computed; not the entire collapse fragility curve. Hence, a modified version of IDA is adopted, which allows computing just the median by expending fewer computational resources.

(ii) The response spectral shapes and durations of ground motions of different intensities anticipated at a site, are expected to be different. Hence, the collapse

capacity computed by scaling the same set of ground motions to different intensity levels is not likely to be hazard-consistent (Bradley 2013; Kwong et al. 2015). This was the motivation behind adopting an iterative version of the IDA.

The iterative modified IDA procedure outlined in FEMA (2012b) (Appendix J) requires an initial estimate of the median collapse capacity, μ_0. For newly designed structures, $\mu_0 = 2.2 \times \text{MCE}_\text{R}$ serves as a good initial estimate, where MCE_R corresponds to the risk-targeted maximum considered earthquake ground motion intensity level (ASCE 2016, § 11.4.3). The factor 2.2 is obtained by assuming the structure has a lognormal collapse fragility curve with a 10 % probability of collapse at the MCE_R intensity level, and a lognormal standard deviation of 0.6 (ASCE 2016). A set of ground motions is then selected to match either a UHS or CMS computed at the intensity level μ_0, of which, the CMS is recommended as the more realistic option. This set of ground motions is used to conduct modified IDA, wherein the records are all scaled to the same intensity level, and the fraction of them that cause structural collapse is computed. Depending on the computed fraction, they are together scaled to either higher or lower intensities until at one point, exactly half of them cause structural collapse. The intensity level at which this occurs is an improved estimate of the median collapse capacity, μ_1. The CS is not one of the provided target response spectrum options since the computation of the median collapse capacity requires knowledge of only the median target response spectral shape, i.e., the CMS; hence, the variability in the target need not be considered.

There is, however, a potential inconsistency in the adopted approach that the records selected to match a target response spectrum computed at the intensity level μ_0 were used to estimate the median collapse capacity μ_1. Therefore, if μ_1 is significantly different from μ_0, the modified IDA procedure should be re-conducted using records selected to match a target response spectrum computed at μ_1, to compute a further improved estimate, μ_2, and so on, until the difference in the estimates obtained over successive iterations is small. The final value that the iterations converge to, is the hazard-consistent estimate of the median collapse capacity. The hazard-consistent collapse capacity curve is then constructed using the estimated median and a lognormal standard deviation that accounts for both record-to-record and model

uncertainties, as per the recommendations of FEMA (2012b) (§ J.5).

One straightforward method to incorporate the effect of duration in this iterative modified IDA procedure is to select ground motions to match not just a target CMS at each iteration, but also a conditional median Ds target, the computation of which is described in Chapter 4/Chandramohan et al. (2016a). A different procedure, which was previously described in § 5.5.4 and summarized in Procedure 5.2, is however proposed as a simpler and more efficient alternative to the iterative IDA procedure originally recommended by the FEMA P-58 methodology. This procedure requires just a generic set of records, that need not be chosen to match any target response spectrum or distribution of durations, as long as they adhere to a set of broad guidelines outlined in § 5.7. This represents a significant computational savings over the original FEMA P-58 procedure, which requires the selection of a hazard-consistent set of ground motions at each new iteration. These ground motions are used to conduct full IDA, wherein each ground motion is incrementally scaled to higher intensity levels until it causes structural collapse. Although there is a larger computational effort involved in conducting a full IDA when compared to the modified version proposed by FEMA P-58, this analysis needs to be conducted only once. The original FEMA P-58 procedure, on the other hand, requires a modified IDA to be conducted at each iteration. The computed collapse intensities of the generic set of records are then used to fit the following multiple linear regression model, which describes a ground motion's collapse intensity as a function of its S_aRatio and Ds values, using the least-squares method:

$$\ln S_a(\bar{T}) \text{ at collapse} = c_0 + c_{ss} \ln S_aRatio + c_{dur} \ln Ds + \epsilon \tag{6.2}$$

where ϵ represents the zero-mean error term. Coefficient of determination (R^2) values of around 0.80 to 0.85 were obtained when this model was fit to the analysis results of 51 reinforced concrete moment frame buildings in Chapter 5. These large R^2 values imply that the S_aRatio and Ds values of a ground motion are good predictors of its collapse intensity. The expected collapse intensity of any arbitrary ground motion with a given S_aRatio and Ds value can now be estimated without conducting any

additional structural analyses, as

$$E\big[\ln S_a(\bar{T}) \text{ at collapse} \,\big|\, \ln S_aRatio,\, \ln Ds\big] = c_0 + c_{ss} \ln S_aRatio + c_{dur} \ln Ds \quad (6.3)$$

This simplified alternative procedure is also iterative in nature and requires an initial estimate of the median collapse capacity, μ_0. As mentioned previously, $\mu_0 = 2.2 \times \text{MCE}_\text{R}$ serves as a good initial estimate for newly designed structures. The site-specific median S_aRatio target conditional on the intensity level μ_0 is computed as the S_aRatio value of the CMS at this intensity level, using Equations (6.1a) and (6.1b). The conditional median Ds target is computed analogously using the GCIM framework, as per the procedure outlined in Chapter 4/Chandramohan et al. (2016a) and Chapter 5. Let these conditional median target values be called S_aRatio_0 and Ds_0 respectively. An improved estimate of the hazard-consistent median collapse capacity, μ_1 can now be obtained by substituting S_aRatio_0 and Ds_0 into Equation (6.3). This step provides an alternative to conducting a modified IDA using records selected to match a target CMS and median Ds value, conditional on the intensity level μ_0. The implicit assumption that the scalar parameter S_aRatio exhibits a certain degree of statistically sufficiency (Rice 2006, p. 305) for the entire vector CMS, has been previously validated in Chapter 5. Similar to the original FEMA P-58 procedure, if μ_1 is significantly different from μ_0, conditional median targets S_aRatio_1 and Ds_1 can be computed conditional on the intensity level μ_1, and Equation (6.3) can be iteratively evaluated until the difference in the median collapse capacities estimated over successive iterations is small. The final value that the iterations converge to is the hazard-consistent median collapse capacity, which can then be used in conjunction with a lognormal standard deviation computed as per the recommendations of FEMA (2012b) (§ J.5), to construct the hazard-consistent collapse fragility curve.

When this method was applied to the eight-story reinforced concrete moment frame, a hazard-consistent median collapse capacity of $S_a(1.76\,\text{s}) = 0.70\,\text{g}$ was obtained, which is in good agreement with the value $0.68\,\text{g}$ computed by conducting MSA using hazard-consistent ground motions. These computations are described in further detail in Chapter 5, along with similar comparisons assuming the structure is

located at sites other than Seattle, in different tectonic regimes.

6.5.2 Estimating structural demands given collapse has not occurred

FEMA P-58 provides guidelines to conduct three types of assessments to estimate structural demands given collapse has not occurred, viz., scenario-based, intensity-based, and time-based assessments. The objective of a *scenario-based* assessment is to estimate the range of structural demands under a prescribed earthquake scenario, defined by parameters like magnitude, hypocenter location, rupture mechanism, source-to-site distance, site Vs_{30}, etc. Ground motions are selected to match a target median response spectrum constructed using the median response spectral ordinates predicted by an appropriate ground motion prediction equation (GMPE) (e.g., Abrahamson et al. 2014; Boore et al. 2014; Chiou and Youngs 2014; Abrahamson et al. 2016) for the considered scenario. The effect of ground motion duration can be considered in this procedure by selecting records to additionally match a target median Ds value computed using an appropriate prediction equation for Ds (e.g., Abrahamson and Silva 1996; Kempton and Stewart 2006; Bommer et al. 2009; Afshari and Stewart 2016). An *intensity-based* assessment is conducted to evaluate structural demands conditional on the event of observing ground motion at a site whose intensity exceeds a certain specified value. Conducting a *time-based* assessment is equivalent to conducting a series of intensity-based assessments at different intensity levels. Ground motions to conduct intensity-based and time-based assessments are selected to match either a target UHS, CMS, or CS at each intensity level, of which, the CS is recommended as the preferred option. The effect of duration can be incorporated into these procedures by selecting ground motions to match a target conditional distribution of Ds, the computation of which is described in Chapter 4/Chandramohan et al. (2016a) and Chapter 5, in addition to the CS, at each ground motion intensity level.

Peak story drift ratio, peak floor acceleration, and peak ground velocity are the primary demand parameters used to define the component damage fragility functions in the FEMA P-58 methodology. Although ground motion duration is expected to

influence peak story drift ratios at intensity levels large enough to produce significant inelastic structural deformations and consequent strength and stiffness degradation (Chapter 2/Chandramohan et al. 2016b), it is not expected to significantly affect peak floor accelerations and peak floor velocities. These demand parameters, however, all quantify the peak value of a response parameter over the entire response history. Cumulative damage metrics like equivalent number of cycles, total hysteretic energy dissipated, accumulated plastic strain, and the Park & Ang index (Park and Ang 1985) are expected to be more strongly influenced by ground motion duration than peak responses. Although studies such as Krawinkler and Zohrei (1983), Lee and Goel (1987), and Mander et al. (1994) have shown cumulative metrics to be well correlated to the damage observed in structural steel components and reinforcing bars due to local buckling and fracture initiated by low-cycle fatigue, these metrics are currently not used to define any of the fragility functions in the FEMA P-58 methodology. FEMA P-58 also uses residual drift ratio as an input to the performance assessment methodology. It recommends the estimation of residual drift ratios using predictive equations based on peak story drift ratios; not from the conducted structural analyses (FEMA 2012b, Appendix C). Although the influence of duration on residual drift ratio was not explicitly quantified in this study, the gradual unidirectional ratcheting of drifts observed under long duration ground motions in Chapter 3 suggests that duration could influence residual drifts. Any observed effect of duration on residual drifts could be incorporated in the FEMA P-58 methodology by revising the predictive equations in FEMA (2012b) (§ 5.4).

6.6 The FEMA P695 methodology

Current building design standards that employ a force-based seismic design philosophy (e.g., ASCE 2016) use seismic performance factors—response modification coefficient (R-factor), system overstrength factor (Ω_0), and deflection amplification factor (C_d)—to estimate the demands imposed on structures responding in the nonlinear range, using equivalent linear analysis procedures. The FEMA P695 methodology (FEMA 2009b) provides an objective basis for quantifying these seismic performance

factors either for a new structural system that is proposed for inclusion in the design code, or for existing structural systems already contained in the design code. The methodology involves

(*i*) the development of a set of archetypical structural designs, which cover the permissible range of structural configurations and design parameters for the structural system under consideration;

(*ii*) the creation of nonlinear models to simulate the dynamic response of the developed structural archetypes under earthquake ground motions, until the onset of structural collapse;

(*iii*) the estimation of the collapse fragility curves of the structural archetypes using nonlinear dynamic analysis; and

(*iv*) the evaluation of structural performance based on the inferred margins of safety against collapse.

The recommendations provided in FEMA (2009b) (Chapter 5), to guide the creation of nonlinear models, are intended to be sufficient to adequately capture the effect of duration on the collapse response of the structural archetypes. Among the list of recommendations, incorporating the in-cycle and cyclic deterioration of the strength and stiffness of structural components, and the destabilizing $P-\Delta$ effect of gravity loads, is critical to capture the effect of duration (Chapter 3/Chandramohan et al. 2017).

The strategies presented in this section, to incorporate the effect of duration in the FEMA P695 methodology, propose modifications to the existing procedure to estimate the collapse capacity of each structural archetype. The existing procedure to estimate structural collapse capacity requires conducting a modified version of IDA using a prescribed set of 22 pairs of horizontal ground motions recorded from large magnitude crustal earthquakes. This prescribed record set is known as the far-field set since it consists entirely of ground motions recorded at distances greater than 10 km from the seismic source (FEMA 2009b, Appendix A). The modified IDA procedure involves analyzing the structure using all the records in the set, normalized by their

respective peak ground velocities, and then linearly scaled by the same scalar factor. This procedure is repeated by appropriately adjusting the scale factor until exactly half the records cause structural collapse. The median $S_a(T_1)$ value of the ground motions, where T_1 corresponds to the fundamental elastic modal period of the structure, scaled such that exactly half of them cause structural collapse, is the estimated median collapse capacity of the structure. A lognormal collapse fragility curve is then constructed using the estimated median collapse capacity and a lognormal standard deviation chosen based on the guidelines provided in FEMA (2009b) (§ 7.3).

It was recognized that the collapse capacity estimated in this manner is generally biased, because the records in the far-field set do not possess response spectral shapes that are representative of intense ground motions typically observed in high seismic regions in the US. This discrepancy necessitated the development of a spectral shape factor to correct the bias in the estimated median collapse capacity (FEMA 2009b, Appendix B). Response spectral shape was quantified using ε, which is defined as the number of standard deviations the natural logarithm of $S_a(T)$ of a ground motion is above or below the natural logarithm of the median $S_a(T)$ value predicted by a GMPE. The development of the spectral shape factor was a two-stage process that involved (*i*) computing target ε-values that are representative of actual sites located in high seismic regions in the US; and (*ii*) characterizing the magnitude of the influence of ε on structural collapse capacity, as a function of structural characteristics. Owing to the number of simplifying assumptions that were made in the process of developing the spectral shape factor, several shortcomings and inconsistencies were identified with potential for improvement:

(*i*) ε is an implicit measure of response spectral shape and has been shown to be less efficient compared to explicit metrics of response spectral shape, like $S_a Ratio$, in predicting structural collapse capacity (Eads et al. 2016).

(*ii*) The structural archetypes are designed based only on generic MCE_R spectral ordinates corresponding to the limits of the seismic design category (SDC) definitions (ASCE 2016, § 11.6). This required the computation of SDC-specific target ε-values by averaging ε targets over all sites in the US that fall within

an SDC, thereby resulting in a considerable loss of granularity.

(*iii*) $\varepsilon(1\,\text{s})$ targets were used to compute the spectral shape factor applied to structural archetypes of all periods.

(*iv*) ε targets computed for sites with $Vs_{30} = 760\,\text{m/s}$, corresponding to the boundary between soil site classes B and C (ASCE 2016, Chapter 20), were used to compute the spectral shape factor applied to structural archetypes, which are all designed for site class D.

(*v*) Using the average ε-value of all the far-field ground motions at each period to compute the spectral shape factor, instead of the individual ε-value of each ground motion, is associated with a loss of precision. Simplifying the actual average ε vs. period relation by a piecewise linear curve results in a further loss of precision.

(*vi*) There is large degree of uncertainty associated with using a simplified relation to predict the influence of ε on structural collapse capacity using the ductility of the structural archetype, as inferred from a nonlinear static pushover analysis.

(*vii*) Studies on ductile and non-ductile reinforced concrete moment frame buildings and wood frame buildings were used to characterize the relation between ε and structural collapse capacity, which were then generalized for application to all structural systems.

The importance of ground motion duration in assessing structural collapse capacity using deteriorating structural models is acknowledged (FEMA 2009b, p. 6-5) and cited as the reason for selecting ground motions recorded from large magnitude earthquakes in the far-field set (FEMA 2009b, § A.7). The durations of the selected records are, however, significantly shorter than those likely to be produced by $M_W \sim 9.0$ subduction earthquakes in the US Pacific Northwest (Figure 1.1; Raghunandan et al. 2015) and even $M_W \sim 8.0$ crustal earthquakes on the San Andreas fault. Regardless, no adjustment for the effect of duration, analogous to the spectral shape factor, is prescribed. Recommendations were developed as part of this study,

to incorporate such an adjustment for the effect of duration, and to simultaneously refine the original method of accounting for the effect of response spectral shape using a correction based on ε, in an effort to address the drawbacks listed above. The nature of these recommendations, in some situations, require minor modifications to the procedure used to design the structural archetypes, related to the consideration of site-specific seismic hazard information. Ground motion response spectral shape is quantified using S_aRatio and duration using Ds. The proposed procedures fall into two broad categories: (*i*) to define site-specific S_aRatio and Ds targets for each structural archetype; and (*ii*) to adjust the estimated median collapse capacity based on these computed site-specific targets.

6.6.1 Defining site-specific S_aRatio and Ds targets

The original FEMA P695 methodology requires all structural archetypes to be designed using the ELF procedure (ASCE 2016, § 12.8), unless it is not permitted for a specific structural configuration. Since site-specific seismic hazard information is quantified only in terms of the MCE_R response spectrum in the ELF procedure, the structural archetype designs are based just on the MCE_R response spectral ordinates corresponding to SDC boundaries, without any translation of the designs to actual physical sites (FEMA 2009b, § 5.2.2). While this lends a certain degree of simplicity to the process of defining performance groups, which are used to classify structural archetypes that share a set of common design parameters, e.g., fundamental period and SDC (FEMA 2009b, § 4.3), it necessitates the definition of a single ε target that is representative of all sites that fall within an SDC, to define the SDC-specific spectral shape factor. The FEMA P695 methodology computes average ε targets over all sites within an SDC, which results in the loss of critical information regarding the variation of ε targets over different geographical regions in the US. For example, target $\varepsilon(1\,\text{s})$-values in the range of 1.25 to 1.75 are expected in most of California at the 2 % in 50 year hazard level, whereas values below 0.75 are typical in the New Madrid fault zone (FEMA 2009b, § B.3.2). Two methods by which the original procedure could be improved, to more rationally account for the geographic variation in seismic

hazard, are proposed.

Method 1: Design structural archetypes to be located at sites with high population density

The primary application of the FEMA P695 methodology is to benchmark the collapse performance of structural systems proposed for inclusion into building design codes. Hence, a logical approach is to design the structural archetypes to be located at actual sites where the structural system is most likely to be implemented in large numbers: sites with a high population density within cities. This approach can be easily incorporated into the FEMA P695 methodology by binning structural archetypes into performance groups not based on the SDC they were designed for, but based on the city they were designed to be located in. The analogue of the original recommendation to create performance groups corresponding to SDC D_{max} and D_{min}, is to choose an appropriate mix of cities located in high and low seismic environments, as quantified by the mapped MCE_R spectral ordinates in Figures 6.4 and 6.5. For example, San Francisco (California), Los Angeles (California), Seattle (Washington), and Salt Lake City (Utah) can be seen to have high levels of seismicity, while Portland (Oregon), Eugene (Oregon), Memphis (Tennessee), and Chareston (South Carolina) have moderately high levels of seismicity; these can be considered in lieu of SDC D_{max} sites. Care must, however, be taken not to select near-fault sites within cities like San Francisco and Los Angeles, whose seismic hazard is controlled by the deterministic cap on the MCE_R response spectral ordinates (ASCE 2016, § 21.2.2), since structures at these sites are expected to have a higher collapse risk than the stated performance objective of ASCE (2016) (FEMA 2009b, § 5.2.2). Although the SDC D_{min} intensity level is not expected to control the performance evaluation for most structural systems, cities with a relatively low level of seismicity, like Las Vegas (Nevada), Albuquerque (New Mexico), Nashville (Tennessee), St. Louis (Missouri), and Little Rock (Arkansas), could be chosen for this level of evaluation.

An advantage of choosing real locations to design the structural archetypes is it readily allows the computation of site-specific S_aRatio and Ds targets for each structural archetype. The site-specific conditional median S_aRatio target is computed as

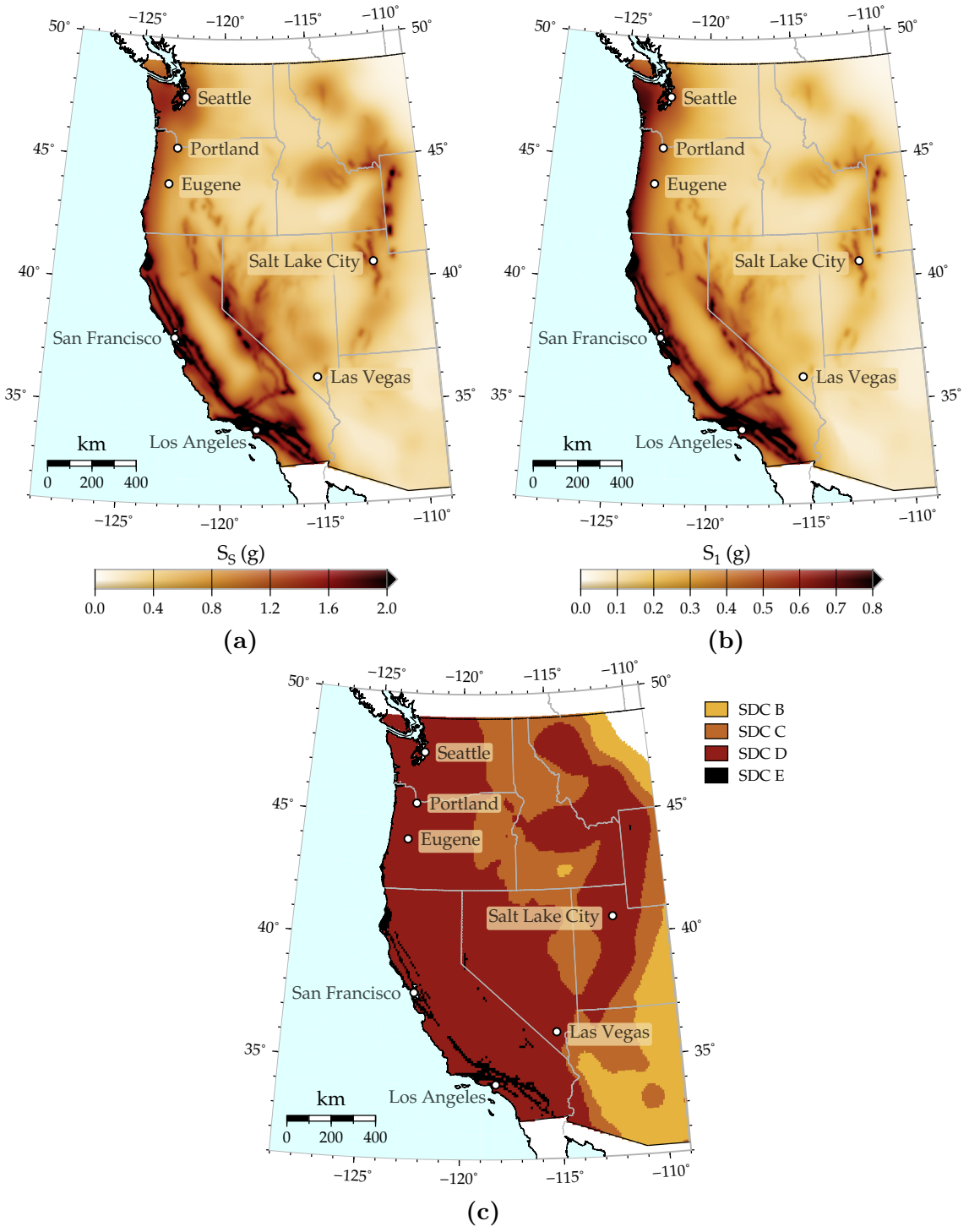

Figure 6.4: MCE_R response spectral ordinates at (a) 0.2 s and (b) 1 s in Western USA, computed as per ASCE (2010). The seismic design category (SDC) classification in (c) assumes the soil conditions at all sites correspond to site class D.

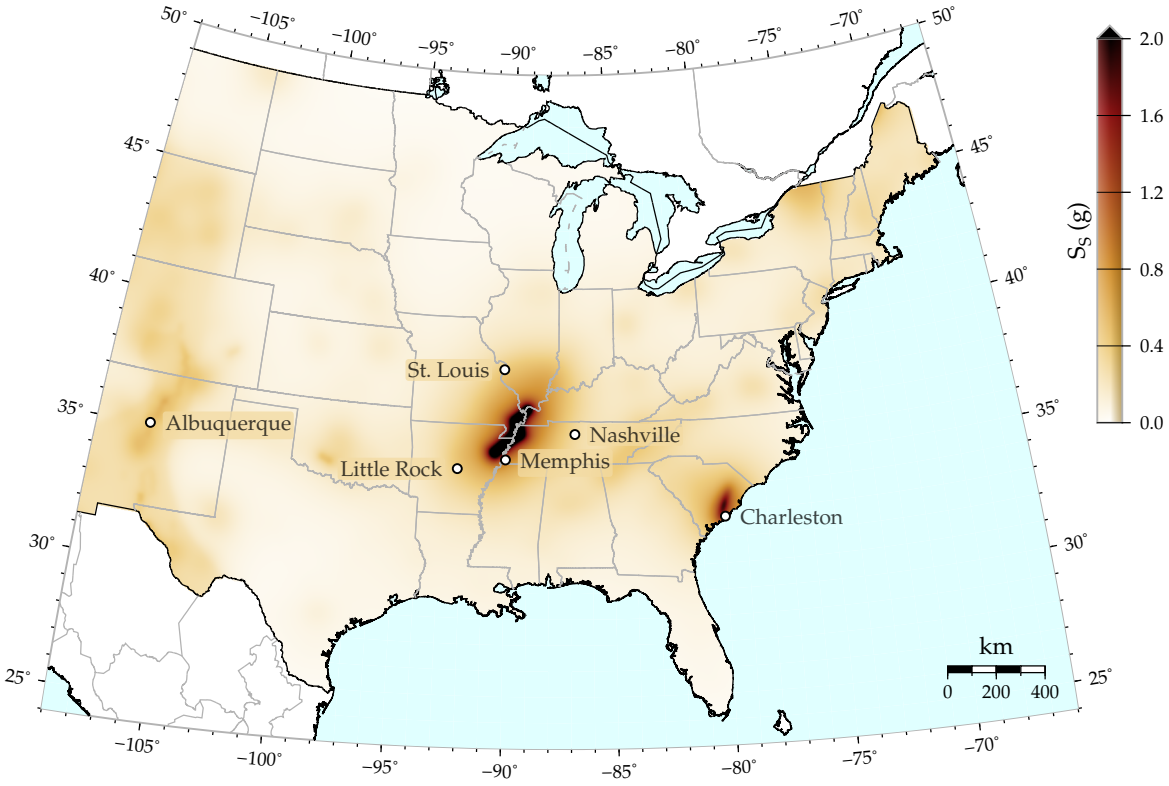
St. Louis
Albuquerque
Nashville
Little Rock
Memphis
Charleston
km
0 200 400
S_S (g)
2.0
1.6
1.2
0.8
0.4
0.0

(a)

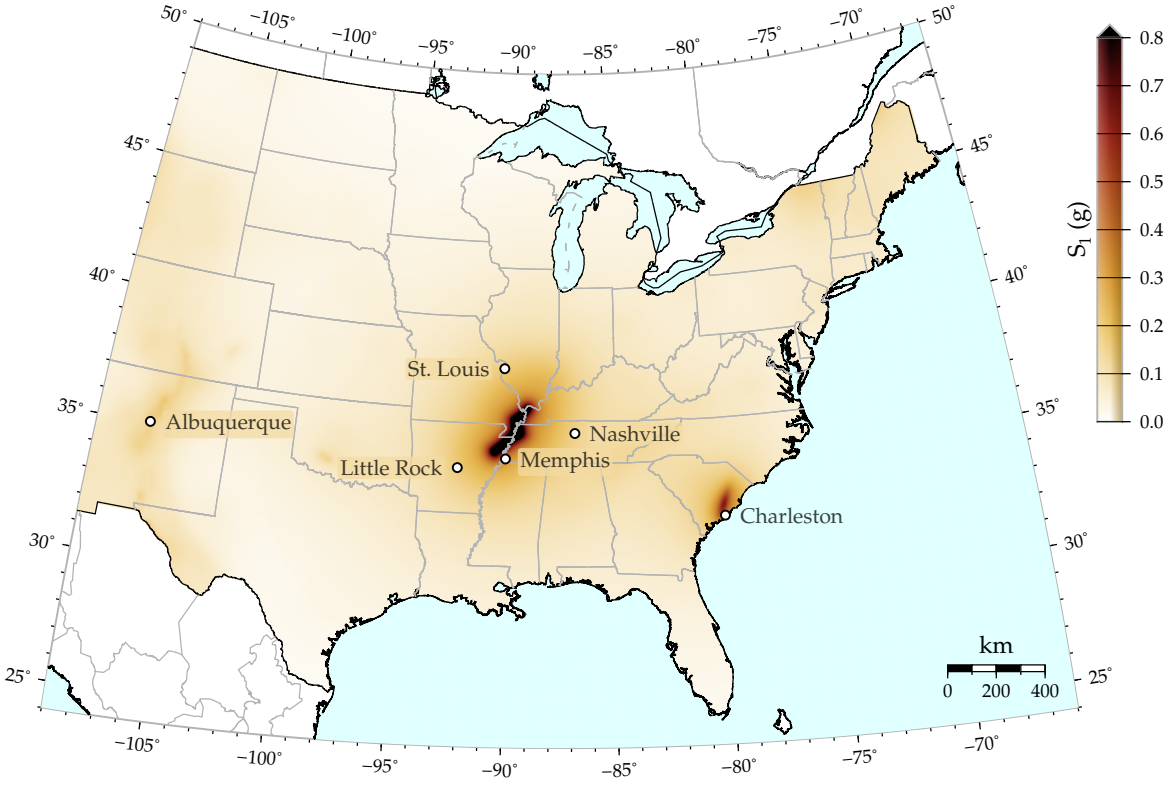
St. Louis
Albuquerque
Nashville
Little Rock
Memphis
Charleston
km
0 200 400
S_1 (g)
0.8
0.7
0.6
0.5
0.4
0.3
0.2
0.1
0.0

(b)

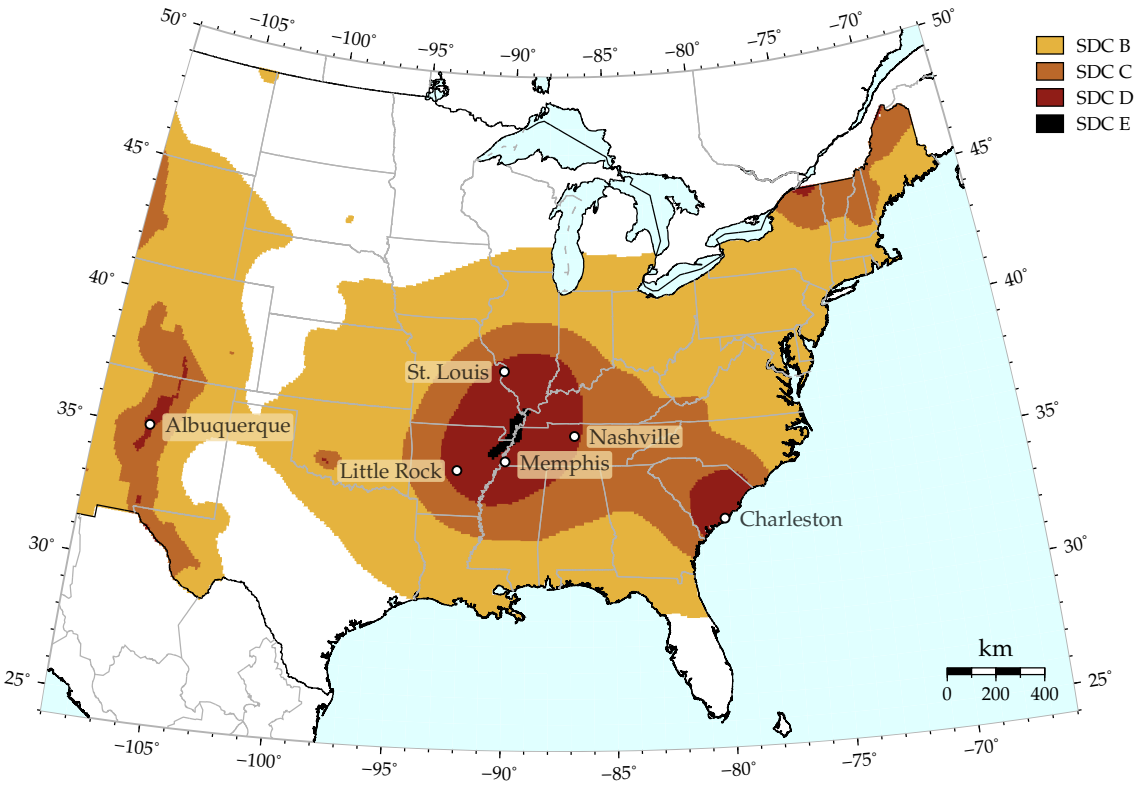

(c)

Figure 6.5: MCE_R response spectral ordinates at (a) 0.2 s and (b) 1 s in Central and Eastern USA, computed as per ASCE (2010). The seismic design category (SDC) classification in (c) assumes the soil conditions at all sites correspond to site class D.

the S_aRatio value of the CMS, using Equations (6.1a) and (6.1b), and the conditional median Ds target is computed analogously using the GCIM framework, as per the procedure outlined in Chapter 4/Chandramohan et al. (2016a). Median S_aRatio and Ds targets in Western USA, conditional on the 0.5 % in 50 year exceedance probability of $S_a(1.0\,\text{s})$, are plotted in Figure 6.6. These targets can be used as a guide to ensure the selection of cities with low S_aRatio and/or long Ds targets, in addition to a high level of seismicity, since structural archetypes designed at such sites are expected to possess relatively low margins of safety against collapse, and thereby control the performance evaluation. The S_aRatio targets plotted in Figure 6.6a were computed using the Campbell and Bozorgnia (2014) and Abrahamson et al. (2016) GMPEs to predict response spectra from crustal and interface earthquakes respectively, and the Baker and Jayaram (2008) model for the correlation between the ε-values of $S_a(T)$ at different periods for all types of earthquakes. The Al Atik (2011) correlation model for the ε-values of $S_a(T)$ for interface earthquakes was not used because its predictions were limited to a period of 5.0 s. Although the Baker and Jayaram (2008) model was developed for crustal earthquakes, its applicability to interface earthquakes has been verified by Jayaram et al. (2011a). Since in-slab earthquakes could not be distinguished from crustal earthquakes in the deaggregation results provided by USGS (2008), they were treated in a manner similar to crustal earthquakes in the computations. This approximation is not expected to significantly influence the computed targets since their relative contribution to the seismic hazard at long return periods is small compared to interface and crustal earthquakes. There is also a small discrepancy in using the more recent and refined Abrahamson et al. (2016) model to compute S_aRatio targets, although it is not one of the GMPEs for interface earthquakes used in the deaggregation computations conducted as per Petersen et al. (2008), the latest national seismic hazard model for which deaggregation results are currently available. Abrahamson et al. (2016) predicts relatively lower response spectral ordinates at periods longer than 1.0 s, when compared to Zhao et al. (2006), the GMPE assigned the largest weight in Petersen et al. (2008) (Petersen et al. 2014, Figure 112). This results in the computation of larger ε-values at periods above around 0.6 s, and consequently

higher S_aRatio targets at sites in the Pacific Northwest region, compared to the targets computed using Zhao et al. (2006), plotted in Figure 6.6b. There is, however, almost no difference seen in the S_aRatio targets conditional on the period 0.2 s (Figure C.1) since the predictions of the two GMPEs are similar at periods shorter than 0.6 s. This issue can be resolved using the method proposed by Lin et al. (2013a), to compute a CMS proportionally aggregated over all GMPEs used in the logic tree for seismic hazard analysis, in conjunction with deaggregation results from the Petersen et al. (2014) national seismic hazard model, when they are made available. The Ds targets plotted in Figure 6.6c were computed using the Abrahamson and Silva (1996) prediction equation and the Bradley (2011) model for the correlation between the ε-values of Ds and $S_a(T)$ for all types of earthquakes, although they were both developed for crustal earthquakes, since analogous models for interface and in-slab earthquakes have not yet been developed. The Abrahamson and Silva (1996) prediction equation for Ds was chosen over others like Kempton and Stewart (2006) and Afshari and Stewart (2016) since it predicts the shortest ground motion durations when extrapolated to large magnitudes, thereby allowing the effect of duration to be demonstrated using the most conservative model (Chapter 4/Chandramohan et al. 2016a). Hence, caution must be exercised in interpreting the plotted S_aRatio and Ds targets. Although targets in Central and Eastern USA could be computed analogously using the NGA-East GMPEs (PEER 2015) and the Lee and Green (2014) duration prediction model for stable continental regions, they were considered to be out of the scope of the present study. The targets plotted in Figure 6.6 assume site soil conditions characterized by $Vs_{30} = 270$ m/s, which corresponds to site class D, in line with the recommendations of the FEMA P695 methodology (FEMA 2009b, § 5.2.2). The targets are computed conditional on the ground motion intensity corresponding to the 0.5 % in 50 year hazard level, since it is shown in FEMA (2009b) (§ B.3.2) to approximately correspond to the median collapse capacity of new structural designs, although $2.2 \times \text{MCE}_\text{R}$ is expected to be a better estimate. Although the targets vary considerably depending on the conditioning period, some common trends are observed at all periods, e.g.,

(*i*) Ds targets are longer at sites in the US Pacific Northwest due to the high likelihood of experiencing ground motions from $M_W \sim 9.0$ interface earthquakes; and

(*ii*) S_aRatio targets are lower at sites located along active crustal faults since the return period of the 0.5 % in 50 year ground motion at these sites is longer than the return period of the earthquake that causes that ground motion by a smaller amount compared to the surrounding areas.

This can be verified from the plots of targets computed conditional on the periods 0.2 s and 4.0 s in Appendix C. Targets corresponding to $Vs_{30} = 760$ m/s at the 0.5 % in 50 year and 2 % in 50 year hazard levels are also included.

The hazard-consistent median collapse capacity of the eight-story reinforced concrete moment frame was estimated using Method 1 from the three methods proposed in § 6.6.2 below, to adjust the estimated median collapse capacity based on the site-specific conditional median S_aRatio and Ds targets. The structure was assumed to be located on a site with $Vs_{30} = 760$ m/s for the purpose of these calculations. The median collapse capacity was estimated to be $S_a(1.76\,\text{s}) = 0.70\,\text{g}$, and the median $S_aRatio(1.76\,\text{s}, 0.35\,\text{s}, 5.00\,\text{s})$ and Ds_{5-75} targets conditional on this intensity level were computed to be 1.94 and 17.3 s respectively. Although the structure was designed to be located in Seattle, its median collapse capacity was re-estimated using targets computed at three other sites located in high seismic regions of Western USA: Eugene, San Francisco, and Los Angeles, to evaluate the impact of explicitly considering S_aRatio and Ds targets at different sites. The median collapse capacities computed at all the sites are summarized in Table 6.1, along with the median S_aRatio and Ds targets at these sites, conditional on the median collapse intensity level. The procedure followed to compute these S_aRatio and Ds targets was similar to that used to compute the targets plotted in Figure 6.6, except the Al Atik (2011) correlation model for the ε-values of $S_a(T)$ was used for interface earthquakes, and the contribution of in-slab earthquakes was explicitly considered using the Abrahamson et al. (2016) GMPE, in computing the S_aRatio targets. The use of the Al Atik (2011) model limited the upper end of the period range used to compute S_aRatio to 5.00 s,

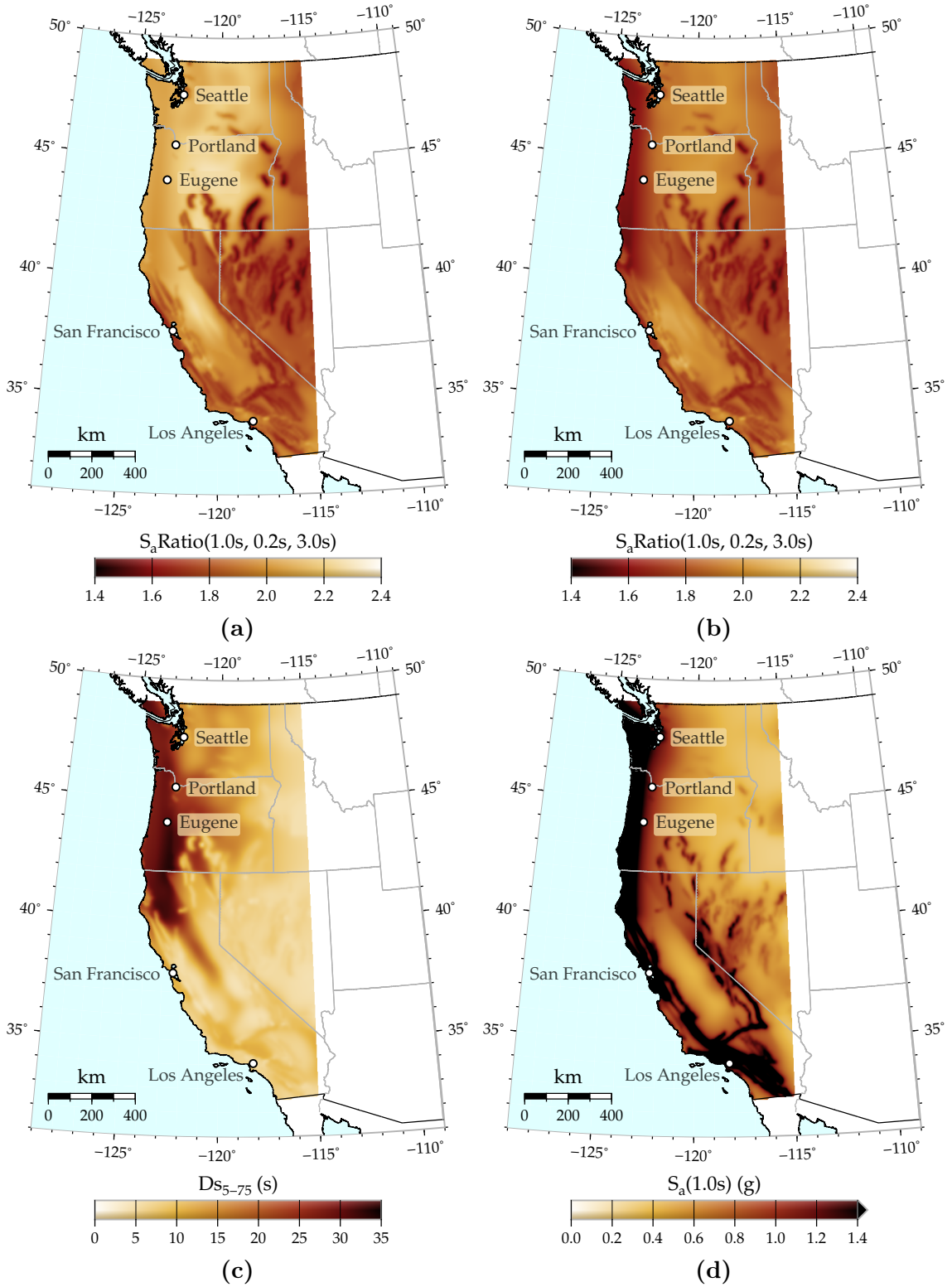

Figure 6.6: Median (a), (b) $S_aRatio(1.0\,\text{s}, 0.2\,\text{s}, 3.0\,\text{s})$ and (c) Ds_{5-75} targets in Western USA, conditional on the exceedance of the $S_a(1.0\,\text{s})$ values in (c). The S_aRatio targets in (a) are computed using the Abrahamson et al. (2016) GMPE for interface earthquakes, and those in (b) are computed using Zhao et al. (2006). The $S_a(1.0\,\text{s})$ values in (c) are exceeded with a probability of 0.5 % in 50 years. $Vs_{30} = 270\,\text{m/s}$ is assumed at all sites.

Table 6.1: Summary of the hazard-consistent median collapse capacities of the eight-story reinforced concrete moment frame building, with ground motion intensity characterized using $S_a(1.76\,\text{s})$, evaluated at different sites located in high seismic regions of Western USA. Median S_aRatio and Ds targets are computed conditional on the estimated median collapse intensity level.

Site	**Median collapse capacity** (g)	**Median target** $\boldsymbol{S_aRatio(1.76\,\text{s}, 0.35\,\text{s}, 5.00\,\text{s})}$	**Median target** $\boldsymbol{Ds_{5-75}}$ (s)
Seattle	0.70	1.94	17.3
Eugene	0.58	1.84	34.2
San Francisco	0.70	1.79	12.4
Los Angeles	0.98	2.13	5.2

instead of $3.0T_1 = 5.29\,\text{s}$; however, this is not expected to significantly influence the obtained results. The lowest median collapse capacity is observed at Eugene due to its long Ds target coupled with a relatively low S_aRatio target. The highest median collapse capacity is observed at Los Angeles due to its short Ds and high S_aRatio target. The median collapse capacity at San Francisco is higher than Eugene since the effect of having a much shorter Ds target outweighs the effect of having a slightly lower S_aRatio target. On the other hand, the median collapse capacities at San Francisco and Seattle are similar since the effect of the difference in their S_aRatio targets is exactly counteracted by the difference in their Ds targets. These observations demonstrate the need to consider the effect of duration, in addition response spectral shape, in structural collapse risk estimation. It is worth noting the range in the S_aRatio and Ds targets computed at the considered sites, all of which could be considered representative of SDC D_{max} sites. This extent of variation in the targets produces median collapse capacities that range from 0.58 g at Eugene to 0.98 g at Los Angeles, which corresponds to a 69 % increase. The median collapse capacity at Los Angeles is also 40 % larger than that at San Francisco, although the two sites are often considered to be located in similar tectonic regimes. These differences cannot be adequately captured by using one common adjustment factor applied to all structural archetypes designed for a specific SDC. This highlights the need to consider site-specific S_aRatio and Ds targets in the performance evaluation process.

Evaluating the performance of structural systems at actual cities they are likely

to be implemented in, also provides the option of developing geographical region-specific seismic performance factors. For example, consider sites in the US Pacific Northwest that can be observed from Figure 6.6c to have relatively long Ds targets. Rapidly deteriorating structural systems that are highly sensitive to the influence of ground motion duration (Raghunandan and Liel 2013; Chapter 2/Chandramohan et al. 2016b) could, therefore, be designed with lower R-factors at these sites. Similarly, sites along active crustal faults can be observed from Figures 6.6a and 6.6b to have relatively low S_aRatio targets. Therefore, structures expected to be sensitive to the effect of response spectral shape, e.g., ductile structures that are likely to experience significant period elongation as they respond in the nonlinear range, and tall structures whose dynamic response is controlled by higher modes corresponding to periods lower than the fundamental period (Haselton et al. 2011a), could be designed using lower R-factors at these sites. This would ensure a more uniform distribution of structural collapse risk over different geographical regions, in line with the objective of developing risk-targeted seismic design maps (Luco et al. 2007). This proposition is similar to other recommendations made in FEMA (2009b) (§ 11.2.1), like developing period and SDC-specific seismic performance factors.

Method 2: Design structural archetypes based on SDC boundaries using extreme S_aRatio and Ds targets

An alternative approach that represents a middle ground between the original FEMA P695 methodology and Method 1, is to design the structural archetypes using MCE_R response spectral ordinates corresponding to SDC limits, but to use the lowest S_aRatio and longest Ds targets observed at sites lying near the geographical SDC boundary (Figure 6.4c) to evaluate their collapse performance. This is in contrast to the procedure employed in the original methodology, wherein average ε targets are computed over all such sites, but consistent with the conservative nature of other elements of the methodology, including (*i*) designing the archetypes to the highest practical MCE_R response spectral ordinates corresponding to the SDC D_max boundary; and (*ii*) assuming all archetypes are located on sites with soft soil corresponding to site class D. To keep the procedure tied to reality, only those sites with a high population

density within cities could be considered for the purpose of choosing targets. For example, targets corresponding to the SDC D_{max} boundary could be chosen from among S_aRatio and Ds target pairs computed at sites in San Francisco, Los Angeles, Seattle, Portland, and Eugene. If a single site does not possess the most extreme S_aRatio and Ds targets compared to all others, it may be necessary to evaluate the structure using two pairs of targets corresponding to different sites, with each pair containing either an extreme S_aRatio or Ds target. The relative sensitivity of the structure to the effects of response spectral shape and duration will decide which of the two pairs controls the evaluation. For example, among the sites in Table 6.1, Eugene has the longest Ds target and San Francisco has the lowest S_aRatio target; however, the median collapse capacity at Eugene is lower since the effect of duration dominates the effect of response spectral shape. It may also be necessary to additionally consider sites that possess relatively low S_aRatio and long Ds targets, but possibly not the most extreme S_aRatio or Ds targets compared to the other sites. Sites and targets to be used to evaluate all structural archetypes are not prescribed here because of the variation in the targets with conditioning period, and the approximations employed in computing them. Additional studies could, however, be undertaken to recommend sites and targets to be used to evaluate structures within specified period ranges.

6.6.2 Adjusting the median collapse capacity based on site-specific S_aRatio and Ds targets

The FEMA P695 methodology requires the evaluation of the median collapse capacity of each structural archetype by conducting modified IDA using a prescribed far-field record set, consisting of 22 pairs of horizontal ground motions recorded from shallow crustal earthquakes. Since the response spectral shapes and durations of the records in this far-field set are not representative of the ground motions likely to be observed at any particular site, the estimated median collapse capacity is not hazard-consistent. Three methods are proposed in this section to adjust the estimated median collapse capacity based on site-specific S_aRatio and Ds targets computed as per the recommendations in § 6.6.1, to obtain the hazard-consistent value. Among the three

proposed methods, Method 1 is considered to be the most refined and accurate, and Method 3 the least. On the other hand, Method 1 is also the most computationally intensive, while Method 3 is the least.

The far-field set contains relatively short duration records (with $Ds_{5-75} < 25\,\text{s}$) that are not representative of the type of ground motions likely to be produced by earthquakes of $M_W \sim 8.0$ and above on the San Andreas fault and those of $M_W \sim 9.0$ in the Cascadia subduction zone. Therefore, Methods 1 and 2 use an additional set of 44 long duration records (with $Ds_{5-75} > 25\,\text{s}$), selected from both large magnitude interface earthquakes like the 2011 Tohoku (Japan), 2010 Maule (Chile), and 1985 Michoacan (Mexico) earthquakes, and large magnitude crustal earthquakes like the 2008 Wenchaun (China) and 2002 Denali (USA) earthquakes. Each of these 44 long duration ground motions was selected to have a similar response spectrum to one of the short duration ground motions, using the procedure outlined in Chapter 2/Chandramohan et al. (2016b). The advantage of selecting the long duration records to be spectrally equivalent to the short duration records is discussed individually in Methods 1 and 2. Henceforth, the far-field set shall be referred to as the short duration set, and the 44 long duration records shall be collectively referred to as the long duration set. The durations of the ground motions in the two sets are compared in Figure 6.7. The geometric mean Ds_{5-75} value of the records in the short and long duration sets are 5.4 s and 44.3 s respectively. Detailed information regarding the short and long duration record sets, including response spectra and time series plots, is provided in Appendix A.

Method 1: Conduct full IDA using the short and long duration record sets

This method is the most refined and accurate of the three methods, but also the most computationally expensive. It is similar to the method proposed in § 6.5.1 above, to account for site-specific $S_a Ratio$ and Ds targets when estimating structural collapse capacity using IDA. It has also been previously described in § 5.5.4 and summarized in Procedure 5.2. It requires conducting full IDA using the 88 records from short and long duration sets, i.e., each ground motion should be incrementally scaled to higher intensity levels until it causes structural collapse. The regression model in

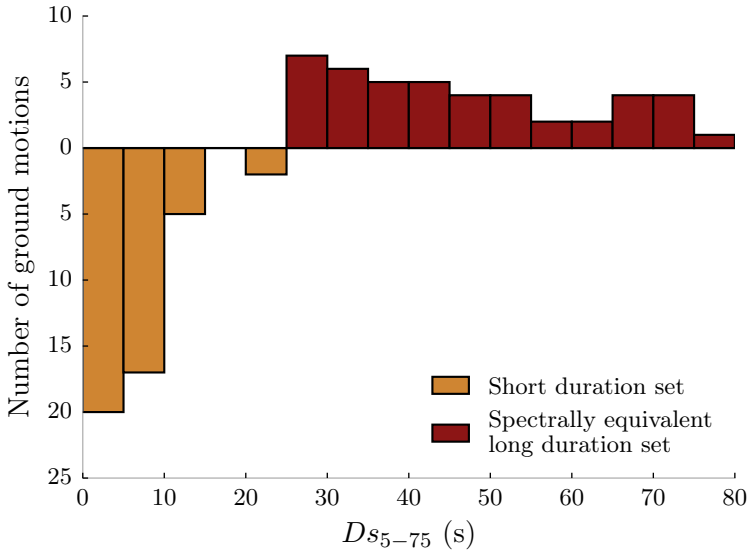

Figure 6.7: Histograms of the 5–75 % significant durations (Ds_{5-75}) of the ground motions in the spectrally equivalent long and short duration record sets.

Equation (6.2) is then fit to the computed ground motion collapse intensities to estimate the coefficients c_0, c_{ss}, and c_{dur}. Selecting the long duration set to be spectrally equivalent to the short duration set is equivalent to using pairs of records with similar S_aRatio values but different Ds values to estimate the regression coefficients. This attributes a property known as *orthogonality* to the predictors, which is one of many factors that ensures the estimated coefficients have low variance. Other factors that control the variance of the estimated coefficients are discussed in § 5.7. Note that an alternative record set, selected to adhere to the guidelines proposed in § 5.7, could also be used in lieu of these 88 records. The coefficients c_{ss} and c_{dur} quantify the sensitivity of structural collapse capacity to ground motion response spectral shape and duration respectively. More specifically, the coefficient c_{dur} represents the expected percent change in structural collapse capacity for every 1 % change in Ds, while holding S_aRatio constant. The coefficient c_{ss} can be interpreted along similar lines.

Median targets S_aRatio_0 and Ds_0 are then computed conditional on a ground motion intensity level corresponding to an initial estimate of the hazard-consistent

median collapse capacity, μ_0. S_aRatio_0 and Ds_0 are then substituted into Equation (6.3) to compute an improved estimate of the hazard-consistent median collapse capacity, μ_1. If μ_1 is significantly different from μ_0, this process is repeated iteratively by computing median targets S_aRatio_1 and Ds_1 conditional on the intensity level μ_1, and so on, until the difference in the estimated median collapse capacity over successive iterations is small. The final value that the iterations converge to is the hazard-consistent median collapse capacity. The reader is referred to the *IDA* section of § 6.5.1, and § 5.5.4 for further details regarding the theory behind the method.

The hazard-consistent median collapse capacity of the eight-story reinforced concrete frame is computed to be 0.70 g using this method. Since this is considered to be the most accurate of the three proposed methods, the accuracy of Methods 2 and 3 will be evaluated by comparing the median collapse capacity of the same structure estimated using each of them, to this value. The good agreement of the estimate 0.70 g with the value 0.68 g obtained by conducting MSA using hazard-consistent ground motions in Chapter 4/Chandramohan et al. (2016a), confirms the accuracy of this method. The estimate obtained following the procedure outline in the original FEMA P695 methodology, however, is 1.13 g, whose inaccuracy stems both from the approximate nature of the spectral shape adjustment based on ε and the lack of an analogous adjustment for the effect of duration.

Method 2: Conduct modified IDA using the short and long duration record sets

This method is ranked in between the other two methods in terms of accuracy and computational cost. It requires conducting modified IDA, as described in the original FEMA P695 methodology, first using the short duration set, and then using the long duration set, to compute two separate estimates of the unadjusted median collapse capacity: μ^{short} and μ^{long} respectively (with μ^{short} typically greater than μ^{long}). It is, however, recommended that the records be scaled based on their individual $S_a(T_1)$ values instead of the median $S_a(T_1)$ value of all the records in each set, as proposed in FEMA (2009b) (§ 6.2.3 and § A.8), since the long duration records have not been normalized based on their peak ground velocities. Like Method 1, an initial estimate

of the hazard-consistent median collapse capacity, μ_0, is required. $2.2\times MCE_{\mathrm{R}}$ usually serves as a good initial estimate; however, the computed values μ^{short} and μ^{long} could also serve as a guide to estimate μ_0. μ^{short} and μ^{long} are then adjusted for the effect of response spectral shape by multiplying each of them by a spectral shape adjustment factor, k_{ss}, computed individually for each set as follows:

$$k_{ss} = \left(\frac{S_a Ratio^{target}}{S_a Ratio^{records}} \right)^{c_{ss}} \tag{6.4}$$

where $S_a Ratio_0^{target}$ represents the site-specific median $S_a Ratio$ target, conditional on the ground motion intensity level $S_a(T_1) = \mu_0$; $S_a Ratio^{records}$ represents the geometric mean $S_a Ratio$ value of all the records in the set; and c_{ss} is a typically positive coefficient that quantifies the magnitude of the influence of response spectral shape on the collapse capacity of the structure. The functional form of this relation is derived from Equation (6.3). The value of c_{ss} can be predicted as a function of structural characteristics as described in the *Predicting c_{ss} and c_{dur}* section below. The accuracy of this method largely hinges on the accuracy with which c_{ss} can be predicted. The k_{ss} values computed for the two sets, k_{ss}^{short} and k_{ss}^{long}, are expected to be nearly equal since the sets are spectrally equivalent. Alternatively, the spectral shape factor defined in FEMA (2009b) (§ 7.2.2) could also be used to adjust μ^{short} and μ^{long}. This factor is applicable to the long duration set, even though it was developed for the short duration set, since the two sets are spectrally equivalent. The adjustment based on $S_a Ratio$ described above is, however, expected to be more accurate. Like the original spectral shape factor, the value of k_{ss} is expected to be greater than 1, since the response spectral shapes of intense ground motions expected at sites are typically more benign, compared to the records in the two sets.

Ds_0^{target} is computed analogous to $S_a Ratio_0^{target}$, as the site-specific median Ds target, conditional on the $S_a(T_1) = \mu_0$ intensity level. An improved estimate of the hazard-consistent median collapse capacity, μ_1, is now computed corresponding to Ds_0^{target} by linear interpolation between $k_{ss}^{short}\mu^{short}$ and $k_{ss}^{long}\mu^{long}$ (or in some rare cases, extrapolation) in log space. This computation is equivalent to multiplying

$k_{ss}^{short}\mu^{short}$ by a duration adjustment factor, k_{dur}, computed as follows:

$$k_{dur} = \left(\frac{Ds^{target}}{Ds^{short}}\right)^{c_{dur}} \tag{6.5a}$$

$$c_{dur} = \frac{\ln\left(k_{ss}^{long}\mu^{long}/k_{ss}^{short}\mu^{short}\right)}{\ln\left(Ds^{long}/Ds^{short}\right)} \tag{6.5b}$$

where Ds^{short} and Ds^{long} refer to the geometric mean Ds values of the short and long duration records respectively. The functional form of Equation (6.5a) is similar to Equation (6.4), and is also derived from Equation (6.3). c_{dur}, analogous to c_{ss}, quantifies the magnitude of the influence of ground motion duration on the collapse capacity of the structure, and is typically a negative coefficient since longer duration ground motions produce lower collapse capacities. Consequently, the value of k_{dur} will be lesser than 1 when the ground motions anticipated at the site are longer than those contained in the short duration set, and greater than 1 otherwise. If $\mu_1 = k_{dur}k_{ss}^{short}\mu^{short}$ is significantly different from μ_0, this procedure should be repeated by computing $S_aRatio_1^{target}$ and Ds_1^{target} conditional on the $S_a(T_1) = \mu_1$ intensity level, and so on. The final value that the iterations converge to is the hazard-consistent median collapse capacity. This method is summarized in Procedure 6.1.

Upon analyzing the eight-story reinforced concrete frame using modified IDA, μ^{short} is computed to be $S_a(1.76\,\text{s}) = 0.71\,\text{g}$, and μ^{long} as $0.44\,\text{g}$. Since the frame is a modern structure, designed as per the 2012 IBC (ICC 2012), μ_0 is computed as $2.2\times MCE_\text{R} = 0.99\,\text{g}$. To apply the spectral shape adjustments, $S_aRatio(1.76\,\text{s}, 0.35\,\text{s}, 5.00\,\text{s})_0^{target}$ at Seattle, conditional on μ_0, is computed as 2.00; and $S_aRatio(1.76\,\text{s}, 0.35\,\text{s}, 5.00\,\text{s})^{records}$ is computed as 1.47 for both the short and long duration sets. c_{ss} is estimated as 0.92 corresponding to a period of 1.76 s, using the predictive relation Equation (6.6), the development of which is described in the *Predicting c_{ss} and c_{dur}* section below. It is worth noting that Equation (6.6) is strictly valid only when the period range $0.2T_1$ to $3.0T_1$ is used to compute S_aRatio. Using this equation when S_aRatio is computed over a slightly different period range, however, is not expected to produce a significantly different c_{ss} estimate. Substituting these values into Equation (6.4), k_{ss}^{short} and k_{ss}^{long} are both computed to be 1.33. The median collapse capacities adjusted for the effect

Procedure 6.1: Compute the hazard-consistent median collapse capacity of a structure using results from modified IDAs conducted using the short and long duration record sets.

1. Develop a numerical model of the structure that incorporates the in-cycle and cyclic deterioration of strength and stiffness of the structural components, and the destabilizing $P-\Delta$ effect, as described in FEMA (2009b) (Chapter 5).
2. Conduct modified IDA individually using the short and long duration record sets to compute the unadjusted median collapse capacity estimates, μ^{short} and μ^{long} respectively. Simplified IDA is conducted as per the original FEMA P695 methodology, with the exception that records are scaled based on their individual $S_a(T_1)$ values.
3. Obtain an initial estimate of the median collapse capacity, μ_0. For new structures, $\mu_0 = 2.2 \times \text{MCE}_\text{R}$ serves as a good initial estimate. The values μ^{short} and μ^{long} could also be used to guide the selection of μ_0.
4. Compute $S_aRatio^{records(short)}$ and $S_aRatio^{records(long)}$ as the geometric mean S_aRatio values of the records in the short and long duration sets respectively.
5. Compute Ds^{short} and Ds^{long} as the geometric mean Ds values of the records in the short and long duration sets respectively.
6. Estimate c_{ss} as a function of structural characteristics as per the procedure described in the *Predicting c_{ss} and c_{dur}* section of § 6.6.2.
7. Set $\mu_{-1} \leftarrow 0$
8. Set $i \leftarrow 0$
9. **while** $\frac{|\mu_i - \mu_{i-1}|}{\mu_{i-1}} > tolerance$ **do**
10. Compute the site-specific median target S_aRatio and Ds values conditional on μ_i, using Equation (5.11a). Let these median target values be called $S_aRatio_i^{target}$ and Ds_i^{target} respectively.
11. Compute $k_{ss(i)}^{short}$ and $k_{ss(i)}^{long}$ by substituting $S_aRatio^{records(short)}$ and $S_aRatio^{records(long)}$ respectively in Equation (6.4) along with $S_aRatio_i^{target}$.
12. Compute $c_{dur(i)}$ by substituting $k_{ss(i)}^{short}$ and $k_{ss(i)}^{long}$ in Equation (6.5b).
13. Compute $k_{dur(i)}$ by substituting Ds_i^{target} and $c_{dur(i)}$ in Equation (6.5a).
14. Compute $\mu_{i+1} = k_{dur(i)} k_{ss(i)}^{short} \mu^{short}$.
15. Set $i \leftarrow i + 1$
16. **end**
17. μ_i is the final estimate of the hazard-consistent median collapse capacity.

of response spectral shape are now $k_{ss}^{short}\mu^{short} = 0.94\,\text{g}$ and $k_{ss}^{long}\mu^{long} = 0.58\,\text{g}$. To apply the duration adjustment, $Ds_{5-75(0)}^{target}$ at Seattle, conditional on μ_0, is computed as 18.2 s. Substituting these values along with $Ds_{5-75}^{short} = 5.4\,\text{s}$ and $Ds_{5-75}^{long} = 44.3\,\text{s}$ into Equations (6.5a) and (6.5b), c_{dur} is computed as −0.23 and k_{dur} as 0.76. The improved estimate of the hazard-consistent median collapse capacity, μ_1, is now computed as $k_{dur}k_{ss}^{short}\mu^{short} = 0.71\,\text{g}$ Since $\mu_1 = 0.71\,\text{g}$ is not very close to the initial estimate $\mu_0 = 0.99\,\text{g}$, a second iteration is conducted following the same procedure, to produce $\mu_2 = 0.70\,\text{g}$. Since μ_2 is close to μ_1, further iterations are not necessary. The final estimate 0.70 g is equal to the value computed using Method 1 to two significant digits. It is also very close to $\mu^{short} = 0.71\,\text{g}$ computed from the modified IDA using the short duration set, implying that the adjustment for response spectral shape is almost exactly counteracted by the adjustment for duration. This could not have been achieved using the original FEMA P695 methodology, which prescribes an adjustment only for the effect of response spectral shape.

Method 3: Conduct modified IDA using just the short duration record set

This method is the least refined and accurate of the three methods, but also the least computationally expensive. It requires conducting modified IDA using the short duration set only, as per the original recommendations of the FEMA P695 methodology, to compute the unadjusted median collapse capacity, μ. Records could be scaled either based on their individual $S_a(T_1)$ values, or using the median $S_a(T_1)$ value of all the records in the set, as originally proposed in FEMA (2009b) (§ 6.2.3 and § A.8). Again, an initial estimate of the hazard-consistent median collapse capacity, μ_0, is required. $2.2 \times MCE_{\text{R}}$ usually serves as a good initial estimate, although the computed value of μ can be used to guide the selection of this μ_0. Site-specific median S_aRatio and Ds targets, $S_aRatio_0^{target}$ and Ds_0^{target} respectively, are computed conditional on the intensity level μ_0. In a manner similar to Method 2, μ is adjusted for the effect of response spectral shape by multiplying either with k_{ss} computed using Equation (6.4), or the spectral shape factor defined in FEMA (2009b) (§ 7.2.2), although the former is expected to be more accurate. The value of c_{ss} to be used in Equation (6.4) can be predicted as a function of structural characteristics using

the procedure outlined in the *Predicting c_{ss} and c_{dur}* section below. An additional adjustment for the effect of duration is now made by multiplying with k_{dur}, which is computed using Equation (6.5a). Equation (6.5b) can unfortunately not be used to compute c_{dur} in this case since μ^{long} and Ds^{long} are undefined. Therefore, c_{dur} needs to be predicted as a function of structural characteristics as well, as described in the *Predicting c_{ss} and c_{dur}* section below. The accuracy of this method, therefore, depends on the quality of the predictions of c_{dur} and c_{ss}, in contrast to Method 2, which only required the value of c_{ss} to be predicted. $\mu_1 = k_{dur}k_{ss}\mu$ now represents an improved estimate of the hazard-consistent median collapse capacity. Finally, if μ_1 is significantly different from μ_0, the procedure is repeated by computing $S_aRatio_1^{target}$ and Ds_1^{target} conditional on μ_1, and so on. The final value that the iterations converge to is the hazard-consistent median collapse capacity. This method is summarized in Procedure 6.2.

The application of this procedure to the eight-story reinforced concrete frame requires repeating a number of the steps previously conducted for Method 2. For example, μ is computed to be $S_a(1.76\,\text{s}) = 0.71\,\text{g}$ by conducting modified IDA using the short duration set. Defining μ_0 as $2.2\times MCE_{\text{R}} = 0.99\,\text{g}$, $S_aRatio(1.76\,\text{s}, 0.35\,\text{s}, 5.00\,\text{s})_0^{target}$ is computed as 2.00 and $Ds_{5-75(0)}^{target}$ as 18.2 s. Substituting $S_aRatio(1.76\,\text{s}, 0.35\,\text{s}, 5.00\,\text{s})^{records} = 1.47$ and $c_{ss} = 0.92$ into Equation (6.4), k_{ss} is computed to be 1.33. Now departing from the procedure followed in Method 2, c_{dur} is estimated as -0.18 corresponding to a period of 1.76 s, from the predictive relation in Equation (6.7), whose development is outlined in the *Predicting c_{ss} and c_{dur}* section below. Substituting this value of c_{dur} and $Ds_{5-75}^{short} = 5.4\,\text{s}$ into Equation (6.5a), k_{dur} is computed as 0.80. μ_1 is now computed as $k_{dur}k_{ss}\mu = 0.76\,\text{g}$, which is not very close to the initial estimate $\mu_0 = 0.66\,\text{g}$. Hence, a second iteration of the procedure is conducted, to produce $\mu_2 = 0.74\,\text{g}$, which is now close to μ_1. Hence, 0.74 g is the estimate of the hazard-consistent median collapse capacity obtained using this method, which can be considered reasonably close to the value 0.70 g obtained using Methods 1 and 2.

Procedure 6.2: Compute the hazard-consistent median collapse capacity of a structure using results from a modified IDA conducted using just the short duration record set.

1. Develop a numerical model of the structure that incorporates the in-cycle and cyclic deterioration of strength and stiffness of the structural components, and the destabilizing $P-\Delta$ effect, as described in FEMA (2009b) (Chapter 5).
2. Conduct modified IDA as per the original FEMA P695 methodology using the short duration record set, to compute the unadjusted median collapse capacity, μ. Records could be scaled either based on their individual $S_a(T_1)$ values or the median $S_a(T_1)$ value of all the records in the set.
3. Obtain an initial estimate of the median collapse capacity, μ_0. For new structures, $\mu_0 = 2.2 \times \text{MCE}_\text{R}$ serves as a good initial estimate. The value μ could also be used to guide the selection of μ_0.
4. Compute $S_aRatio^{records}$ as the geometric mean S_aRatio value of the records in the short duration set.
5. Compute Ds^{short} as the geometric mean Ds value of the records in the short duration set.
6. Estimate c_{ss} and c_{dur} as functions of structural characteristics as per the procedure described in the *Predicting c_{ss} and c_{dur}* section of § 6.6.2.
7. Set $\mu_{-1} \leftarrow 0$
8. Set $i \leftarrow 0$
9. **while** $\frac{|\mu_i - \mu_{i-1}|}{\mu_{i-1}} > tolerance$ **do**
10. Compute the site-specific median target S_aRatio and Ds values conditional on μ_i, using Equation (5.11a). Let these median target values be called $S_aRatio_i^{target}$ and Ds_i^{target} respectively.
11. Compute $k_{ss(i)}$ by substituting $S_aRatio_i^{target}$ in Equation (6.4).
12. Compute $k_{dur(i)}$ by substituting Ds_i^{target} in Equation (6.5a).
13. Compute $\mu_{i+1} = k_{dur(i)} k_{ss(i)} \mu$.
14. Set $i \leftarrow i + 1$
15. **end**
16. μ_i is the final estimate of the hazard-consistent median collapse capacity.

Predicting c_{ss} and c_{dur}

The coefficients c_{ss} and c_{dur} quantify the magnitude of the effects of response spectral shape and duration respectively, on structural collapse capacity. They are used to compute factors to adjust the median collapse capacity estimated using a generic record set based on site-specific conditional median S_aRatio and Ds targets. Method 2 requires the prediction of c_{ss} alone, while Method 3 requires the prediction of both c_{ss} and c_{dur}, as functions of structural characteristics. Haselton et al. (2011a) develops a relation to compute a parameter analogous to c_{ss} using the number of stories and RDR_{ult}: the roof drift ratio at the point of 20 % base shear strength loss from a nonlinear static pushover analysis, as predictors. On similar lines, FEMA (2009b) (§ B.3.3) proposes a relation to predict the effect of response spectral shape on structural collapse capacity based on μ_T: the period-based ductility of the structure. μ_T is computed as the ratio of RDR_{ult} and the roof drift ratio corresponding to the yield point of the pushover curve. The motivation behind modeling the effect of response spectral shape using the ductility of a structure is that ductile structures are expected to undergo more significant inelastic period elongation, and thereby be more influenced by response spectral ordinates at periods longer than T_1. Attempts were made to develop similar relations for c_{ss} and c_{dur} by analyzing

(*i*) 51 reinforced concrete (RC) ductile moment frames (MFs) ranging in height from 1 to 20 stories, 21 of which were designed for sites in Seattle, Portland, and Los Angeles by Raghunandan et al. (2015) and 30 by Haselton and Deierlein (2008) (Chapter 6);

(*ii*) 3 steel ductile MFs, of which the 3 and 9-story variants were designed for a site in Seattle as part of the SAC Steel Project (FEMA 2000), and the 5-story structure represents an actual building located in San Francisco, previously analyzed in Chapter 2/Chandramohan et al. (2016b), Chapter 3/Chandramohan et al. (2017), and FEMA (2014); and

(*iii*) 3 steel buckling-restrained braced frames (BRBFs) and 3 steel special concentrically braced frames (SCBFs), each category containing 3, 6, and 12-story

structures, designed as part of NIST (2010) (Chapter 5 and Appendix C).

All 60 structures were analyzed using Method 1 to compute their c_{ss} and c_{dur} values. The computed c_{ss} and c_{dur} values are plotted against the fundamental elastic modal period (T_1), number of stories, RDR_{ult}, and ductility of the structures in Figures 6.8 and 6.9 respectively. Note that $-c_{dur}$ is plotted instead of c_{dur} in all the plots of Figure 6.9 since the coefficient is generally negative. The plotted values of ductility do not exactly correspond to μ_T as described in FEMA (2009b) (§ B.3.3), since the yield roof drift ratios used to compute them were computed directly from the pushover curves, instead of employing a period-based computation. The 6 and 12-story SCBFs were excluded from the plots of RDR_{ult} and ductility (Figures 6.8c, 6.8d, 6.9c and 6.9d) since they could not be successfully analyzed using a nonlinear static pushover analysis. Least-squares regression lines fit only to the RC ductile MFs, using the logarithm of each parameter, are superimposed on all the plots.

The observation of clear trends of c_{ss} with respect to all four parameters in Figure 6.8 can be explained by the inherent correlation between the parameters. Tall structures with long periods tend to exhibit low ductility and RDR_{ult} values due to the localization of inelastic behavior over only a few stories along the height of the building (Haselton et al. 2011b). This is verified by correlation coefficients of 0.94, -0.92, and -0.87 computed between T_1 and the number of stories, RDR_{ult}, and ductility respectively, for the RC ductile MFs. Hence, the use of just one of these parameters to predict c_{ss} values for RC ductile MFs is considered sufficient, in contrast to Haselton et al. (2011a), which uses both the number of stories and RDR_{ult}. T_1 is chosen as the preferred predictor of c_{ss} since it exhibits lower scatter than the number of stories, and unlike RDR_{ult} and ductility, it can be computed without conducting a pushover analysis. Hence, the following predictive equation for c_{ss} is proposed, which is expected to be valid for structures that fall within the range $0.4\,\text{s} \leq T_1 \leq 2.6\,\text{s}$:

$$c_{ss} = 0.99 - 0.13 \ln T_1 \tag{6.6}$$

Trends of $-c_{dur}$ with respect to the four parameters plotted in Figure 6.9 involve a lot more scatter than observed for c_{ss} in Figure 6.8. There is, however, a discernible

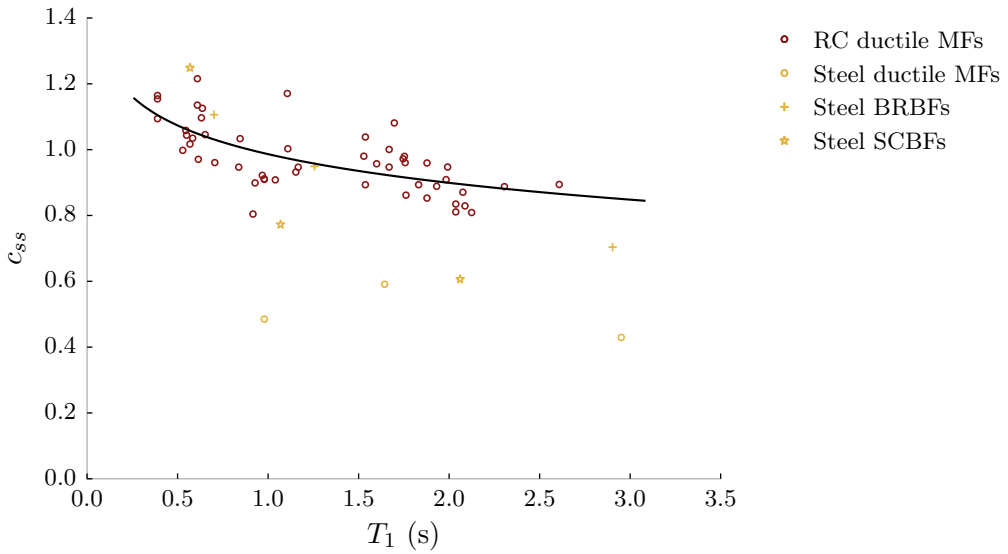
1.4
1.2
1.0
0.8
0.6
0.4
0.2
0.0
c_{ss}
0.0
0.5
1.0
1.5
2.0
2.5
3.0
3.5
T_1 (s)
RC ductile MFs
Steel ductile MFs
Steel BRBFs
Steel SCBFs

(a)

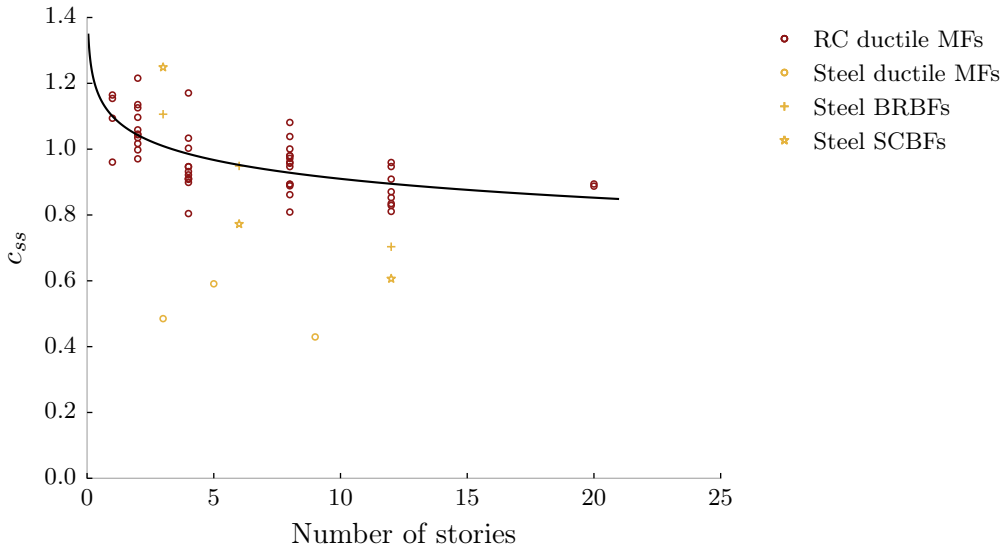
1.4
1.2
1.0
0.8
0.6
0.4
0.2
0.0
c_{ss}
0
5
10
15
20
25
Number of stories
RC ductile MFs
Steel ductile MFs
Steel BRBFs
Steel SCBFs

(b)

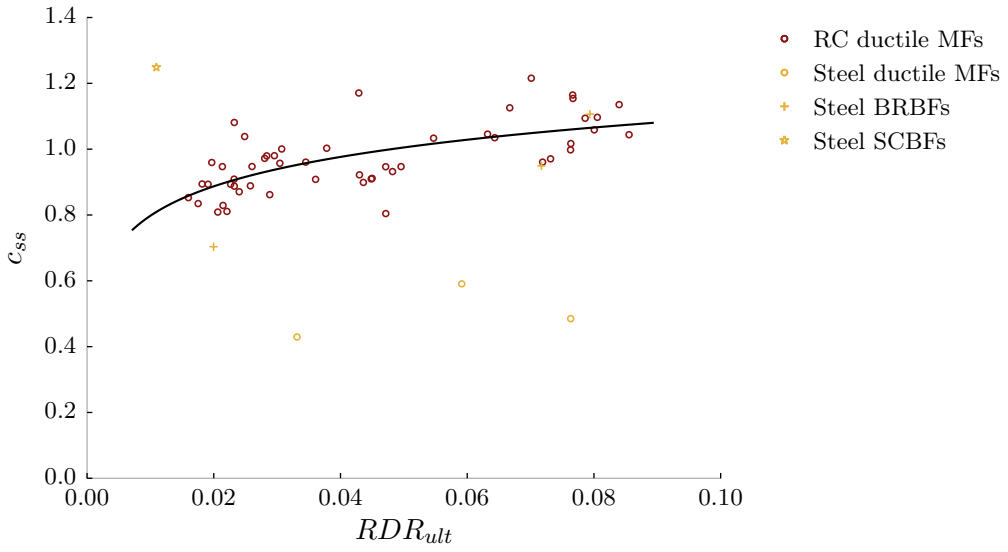

(c)

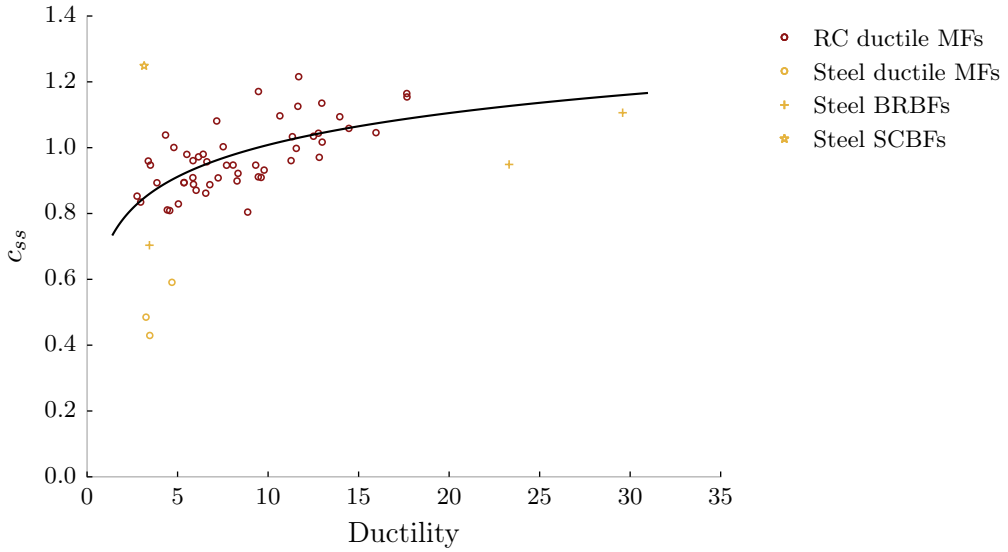

(d)

Figure 6.8: c_{ss} values for all the analyzed structures plotted against their (a) fundamental elastic modal period, (b) ductility, (c) number of stories, and (d) ultimate roof drift ratio. The trend lines are fit only to the reinforced concrete ductile moment frames.

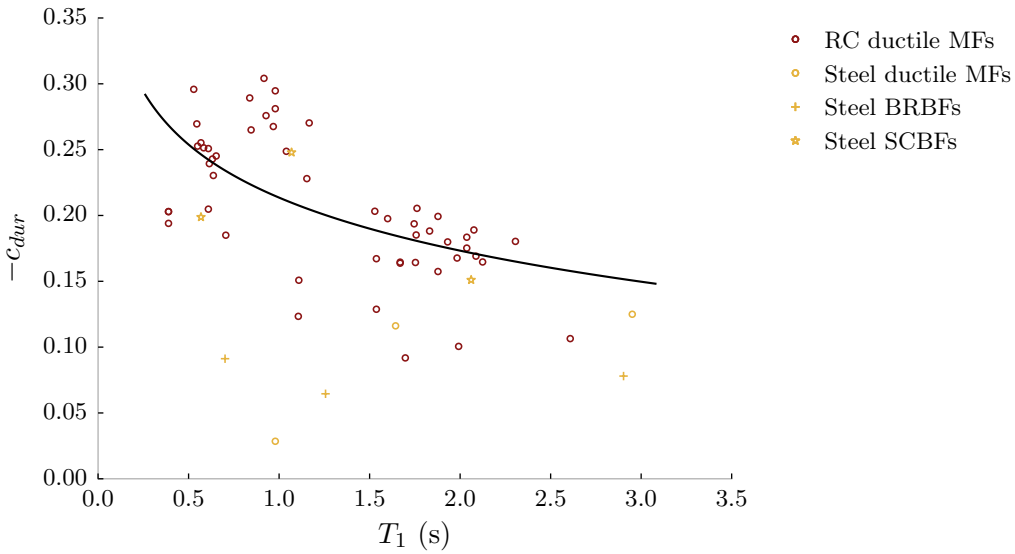
0.35
0.30
0.25
0.20
0.15
0.10
0.05
0.00
$-c_{dur}$
0.0
0.5
1.0
1.5
2.0
2.5
3.0
3.5
T_1 (s)
RC ductile MFs
Steel ductile MFs
Steel BRBFs
Steel SCBFs

(a)

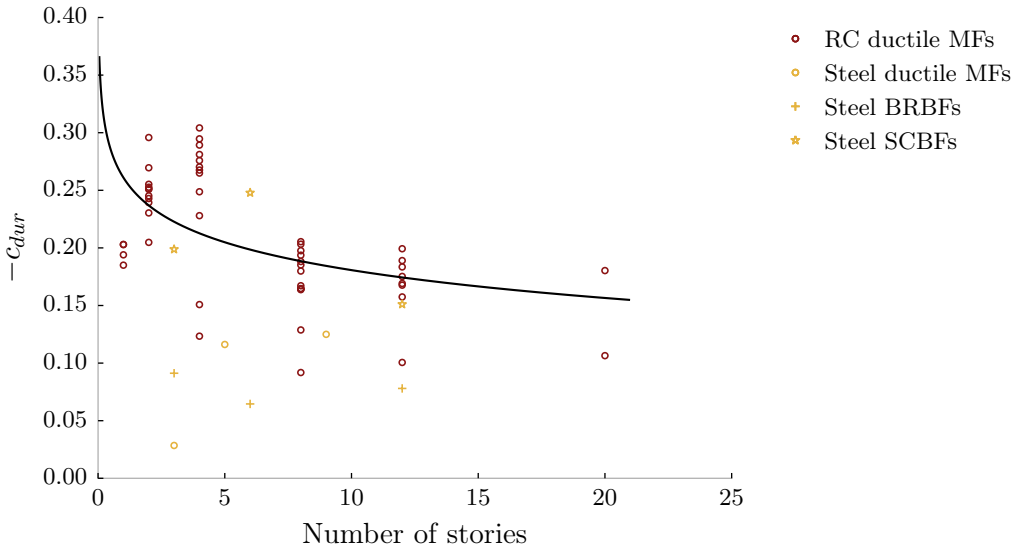
0.40
0.35
0.30
0.25
0.20
0.15
0.10
0.05
0.00
$-c_{dur}$
0
5
10
15
20
25
Number of stories
RC ductile MFs
Steel ductile MFs
Steel BRBFs
Steel SCBFs

(b)

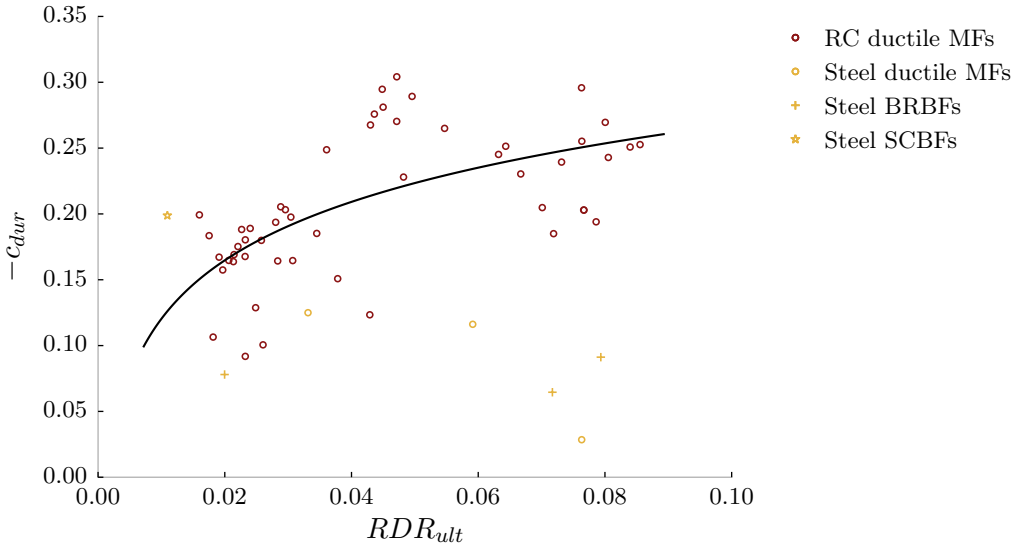

(c)

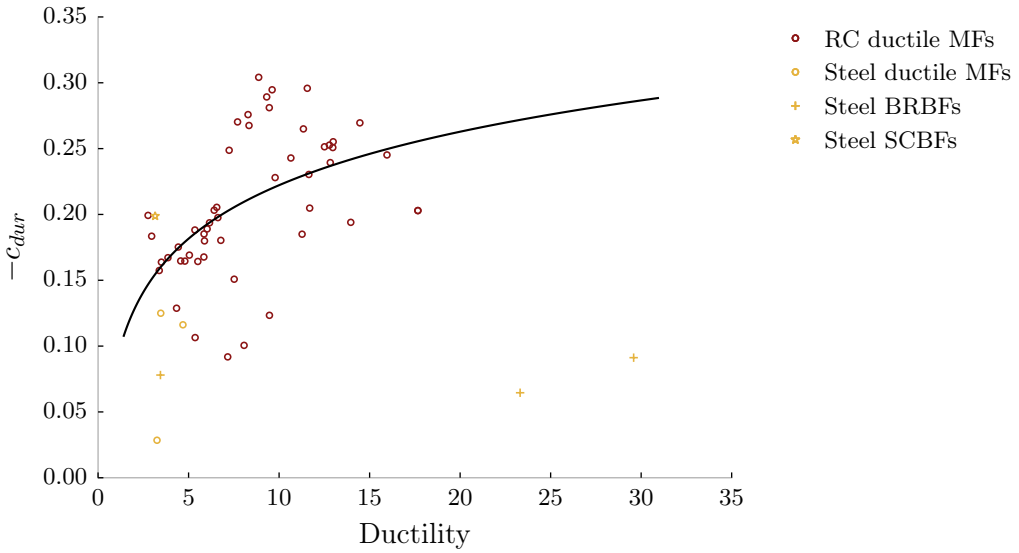

(d)

Figure 6.9: $-c_{dur}$ values for all the analyzed structures plotted against their (a) fundamental elastic modal period, (b) ductility, (c) number of stories, and (d) ultimate roof drift ratio. $-c_{dur}$ is plotted instead of c_{dur} since the coefficient is generally negative. The trend lines are fit only to the reinforced concrete ductile moment frames.

increasing trend of $-c_{dur}$ with respect to RDR_{ult} and ductility, which could be attributed to previous observations by Chapter 2/Chandramohan et al. (2016b) and Raghunandan and Liel (2013) that a larger effect of ground motion duration is observed in ductile structures. A more plausible explanation for this trend, however, is the negative correlation of RDR_{ult} and ductility with T_1, and long period structures undergoing fewer inelastic excursions under long duration ground motions, thereby dissipating lesser hysteretic energy compared to shorter period structures. Since the cyclic deterioration of structural strength and stiffness is commonly modeled as a function of the cumulative hysteretic energy dissipated (Ibarra et al. 2005), long period structures are less influenced by ground motion duration, as evidenced by their smaller $-c_{dur}$ values. Hence, T_1 is chosen as the preferred predictor for the c_{dur} values of RC ductile MFs as well, and the following predictive equation is proposed for structures that fall within the range $0.4\,\text{s} \leq T_1 \leq 2.6\,\text{s}$:

$$c_{dur} = -0.21 + 0.058 \ln T_1 \tag{6.7}$$

The rate of cyclic deterioration of structural strength and stiffness is expected to be a good predictor of c_{dur} (Bommer et al. 2004; Raghunandan and Liel 2013; Chapter 2/ Chandramohan et al. 2016b; Marafi et al. 2016); however, quantifying this characteristic for a multiple degree of freedom structure is not straightforward. This feature could potentially be quantified by conducting a cyclic pushover analysis, but difficulties related to the folding-over of stories due to the concentration of inelastic deformations were experienced by conducting a load-controlled pushover analysis. Conducting a displacement-controlled cyclic pushover analysis was considered as a potential solution to this problem, but was found to be infeasible due to the manner in which kinematic constraints were employed in creating the structural models. Hence, this option was not explored further in this study, but could be developed in the future, as a means to predict c_{dur} in conjunction with T_1. For RC ductile MFs, considering the larger scatter in the predictive equation of c_{dur} compared to c_{ss}, the use of Method 2 is likely to produce significantly more accurate results compared to Method 3, as observed for the eight-story RC MF example.

Another important observation from the plots in Figures 6.8 and 6.9 is that the steel structures generally do not follow the trends fit to the data from the RC ductile MFs. The steel BRBFs, for instance, can be seen in Figure 6.9 to have comparatively low $-c_{dur}$ values, indicating that their collapse response is influenced by ground motion duration to a lesser extent than the RC ductile MFs. This result is expected since the strength and stiffness of buckling-restrained braces do not degrade significantly under cyclic loading (Black et al. 2004). The steel SCBFs, on the other hand, are influenced by ground motion duration to a greater extent than the steel BRBFs since regular braces are prone to buckling and eventual fracture under cyclic loading (Uriz and Mahin 2008). In general, structures of different materials and lateral force-resisting systems, with components that exhibit different hysteretic behaviors, can be expected to be influenced to different extents by ground motion response spectral shape and duration. This indicates that equations developed to predict c_{ss} and c_{dur} by analyzing structures of a specific material and lateral force-resisting system, will generally be applicable only to that specific class of structures. Therefore, the relations developed by FEMA (2009b) (§ B.3.3) and Haselton et al. (2011a) for example, which are based largely on the results of collapse analyses conducted on ductile and non-ductile RC MFs, are expected to be applicable only to RC MFs. The relation from FEMA (2009b) (§ B.3.3) though, could also potentially be applied to wood frame buildings, since they were also used in its development. This, however, poses a problem since Methods 2 and 3 are often employed to analyze archetypes of a new structural system being proposed for inclusion in the building design code, for which predictive equations for c_{ss} and c_{dur} have not yet been developed. Once the process of calibrating c_{ss} and c_{dur} values for RC ductile MFs conducted in this study is repeated for other materials and structural systems, however, the relations corresponding to the structural system whose dynamic response is expected to most closely resemble that of the structural system under consideration, could be used. If reliable predictive equations for c_{ss} and c_{dur} are not available, use of Method 1 should be favored over Methods 2 and 3.

6.7 The ASCE 7-16 seismic design provisions

ASCE 7-16 (ASCE 2016) defines analysis procedures and acceptance criteria to be employed in the design of buildings to resist seismic loads. Buildings designed to satisfy the prescribed acceptance criteria when analyzed using the defined procedures, are expected to meet certain implicit minimum performance targets under seismic loading. This implicit performance goal is quantified in terms of the maximum probability of observing total or partial structural collapse when subjected to an earthquake ground motion of intensity corresponding to the risk-targeted maximum considered earthquake (MCE_R) at the site. For structures classified under Risk Categories I and II, the probability of collapse under the MCE_R level ground motion is limited to 10 % (FEMA 2015, § 1.1.1; ASCE 2016, Table C1.3.1b). The interaction of ground motion response spectral shape and duration with this implicit performance target is investigated using the eight-story reinforced concrete moment frame building as an example. Since the structure was designed as per the 2012 IBC (ICC 2012), which in turn references ASCE 7-10 (ASCE 2010), it is expected to possess the level of seismic performance guaranteed by ASCE 7-10. The performance targets stated in ASCE 7-10 are similar to those of ASCE 7-16, described above.

The structure was first analyzed by conducting full IDA using the records from the short duration FEMA P695 far-field set and the spectrally equivalent long duration set, described previously in § 6.6.2. The near-zero ε-values of the records in the short duration set at periods longer than about 1.5 s (FEMA 2009b, § B.3.1) indicate that their response spectra resemble the UHS at these periods. The lognormal collapse fragility curves fit to the collapse intensities of the records in the two sets are plotted in Figure 6.10 using dashed lines. The lognormal standard deviations of these fragility curves account only for the uncertainty in the ground motion characteristics, also known as record-to-record (RTR) uncertainty. Fragility curves that account for the uncertainty in the model characteristics, in addition to RTR uncertainty, are estimated using the same medians as the original fragility curves, μ^{short} and μ^{long}, in conjunction with an inflated lognormal standard deviation, β, of 0.6 (FEMA 2015,

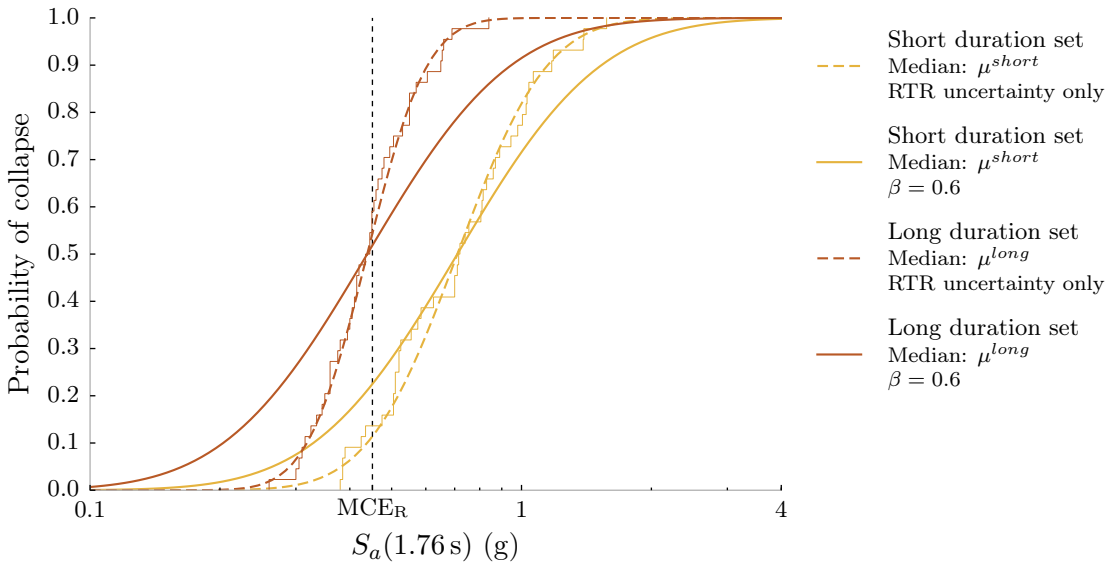

Figure 6.10: Collapse fragility curves of the eight-story reinforced concrete moment frame building estimated by conducting IDA using the short and long duration record sets described in § 6.6.2. The dashed fragility curves are estimated directly from the IDA results and incorporate RTR uncertainty only. The solid fragility curves are computed using the estimated medians and a lognormal standard deviation, β, of 0.6; they incorporate RTR and model uncertainties.

§ C16.4.1.1; ASCE 2016, § 21.2.1.2). These fragility curves are also plotted in Figure 6.10 using solid lines. Probabilities of collapse of 22 % and 52 % are inferred from the short and long duration fragility curves respectively, at $S_a(1.76\,\text{s}) = 0.45\,\text{g}$: the MCE$_R$ ground motion intensity at the site in Seattle the structure was designed for. Since the records in the two sets have equivalent response spectra, the 2.4 times larger probability of observing structural collapse under long duration ground motions at the MCE$_R$ level, when compare to the short duration ground motions, can be attributed to the difference in their durations. These values cannot, however, be directly compared to the implicit performance target of ASCE 7-16 since the response spectral shapes and durations of the ground motions used to analyze the structure do not correspond to those of the ground motions anticipated at the site in Seattle the structure was designed to be located in.

To demonstrate the influence of response spectral shape on the collapse probability

at the MCE_R level, these collapse probabilities are compared to those computed using two new short and long duration record sets, selected to match the CMS as per the recommendations of ASCE (2016) (§ 16.2.1.2). 44 records were selected in each of these record sets, to match the CMS conditional on the MCE_R intensity level, computed using a conditioning period of 1.76 s: the fundamental elastic modal period of the structure. The ground motions in the short duration set were selected from the subset of records in the PEER NGA-West2 database with $Ds_{5-75} < 25$ s. The ground motions in the long duration set were selected from among records in the PEER NGA-West2 database and others recorded from large magnitude earthquakes like the 2010 Maule (Chile) and 2011 Tohoku (Japan) earthquakes, with $Ds_{5-75} > 25$ s. $Ds_{5-75} = 25$ s was previously shown to represent an appropriate threshold to distinguish long from short duration records by Chapter 2/Chandramohan et al. (2016b). An upper limit of 5.0 was imposed on the factor used to scale individual records during the selection process. The response spectra of the records in the two sets are plotted in Figure 6.11, and the distribution of their durations are compared in Figure 6.12. The geometric mean Ds_{5-75} values of the records in the short and long duration sets are 8.1 s and 46.9 s respectively, which are close to 5.4 s and 44.3 s: the geometric mean Ds_{5-75} values of the short and long duration record sets from § 6.6.2.

The collapse fragility curves estimated by conducting full IDA on the reinforced concrete frame model using each of the two record sets are plotted in Figure 6.13. As before, the fragility curves in Figure 6.13a are fit directly to the ground motion collapse intensities and incorporate RTR uncertainty only. Although the records in the two sets were selected to match the site-specific CMS, accurate estimation of the hazard-consistent median collapse capacity requires the CMS to have been computed conditional on the median collapse intensity level. Since the CMS was computed conditional on the MCE_R level instead, this necessitated small adjustments to the median collapse capacities, μ^{short} and μ^{long}, using factors $k_{ss}^{short} = 1.04$ and $k_{ss}^{long} = 1.06$, computed using Equation (6.4). Fragility curves constructed using the adjusted medians, $k_{ss}^{short}\mu^{short}$ and $k_{ss}^{long}\mu^{long}$, along with a β of 0.6 to approximately account for both RTR and model uncertainties, are plotted using yellow and orange lines respectively in Figure 6.13b. The probability of collapse at the MCE_R level inferred

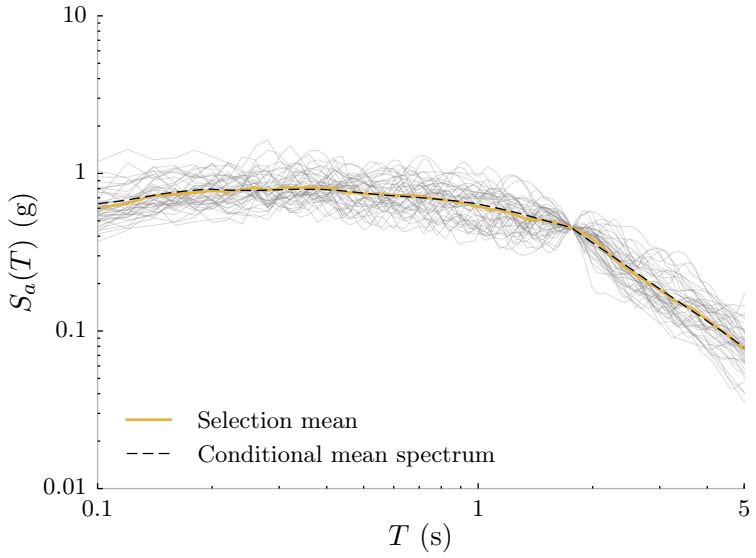

(a)

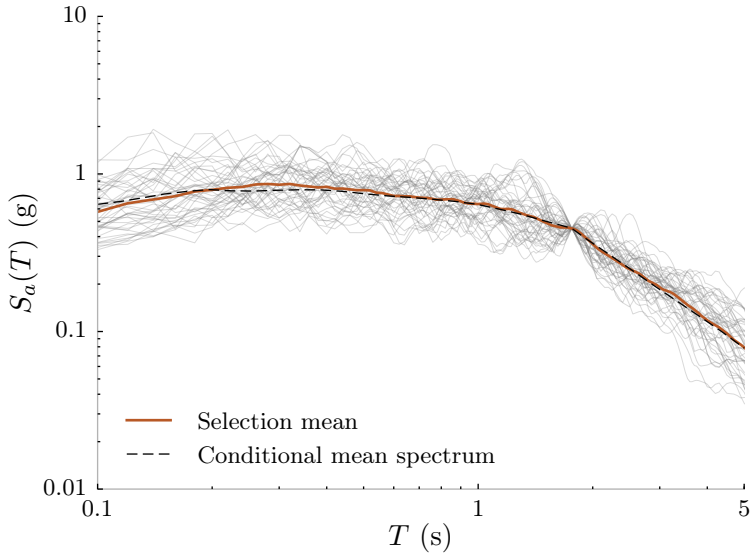

(b)

Figure 6.11: Response spectra of the 44 ground motions in the (a) short and (b) long duration record sets, selected to match the CMS conditional on the MCE_R ground motion intensity level at Seattle.

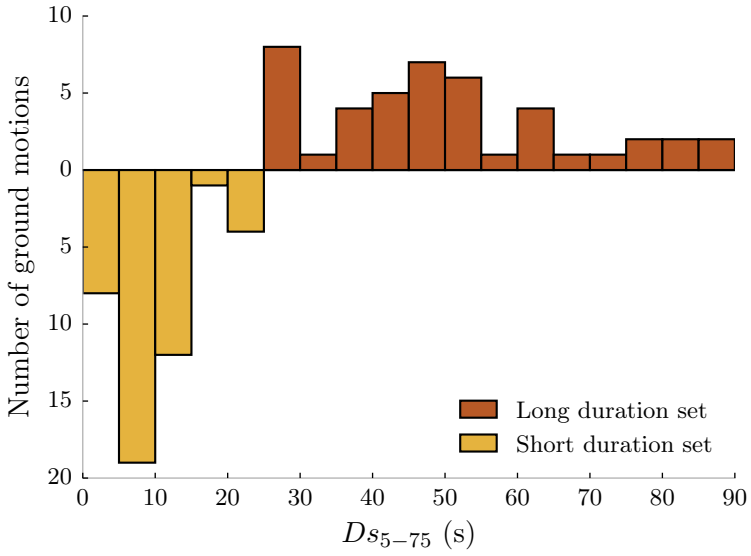

Figure 6.12: Histograms of the Ds_{5-75} values of the ground motions in the short and long duration record sets selected to match the CMS conditional on the MCE_R ground motion intensity level at Seattle.

from these short and long duration fragility curves are 10 % and 31 % respectively, which are significantly lower than the 22 % and 52 % values previously computed using the short and long duration record sets from § 6.6.2. Since the geometric mean durations of the two short duration record sets and the two long duration record sets are close to each other, this reduction in the collapse probabilities can be attributed primarily to the difference in their response spectral shapes. The lower collapse probabilities under records with response spectral shapes that resemble the CMS, compared to those that resemble the UHS, highlight the conservative nature of the UHS, as previously indicated by studies like Reiter (1990), Naeim and Lew (1995), and Bommer et al. (2000). This effect of response spectral shape on the probability of collapse at the MCE_R level highlights the need to explicitly consider it in structural design.

The hazard-consistent median collapse capacity, further adjusted for the effect of duration, was computed by linear interpolation between $k_{ss}^{short}\mu^{short}$ and $k_{ss}^{long}\mu^{long}$, based on the conditional median Ds_{5-75} target at the site: 17.3 s, and the geometric mean Ds_{5-75} values of the records in the short and long duration sets: 8.1 s and 46.9 s

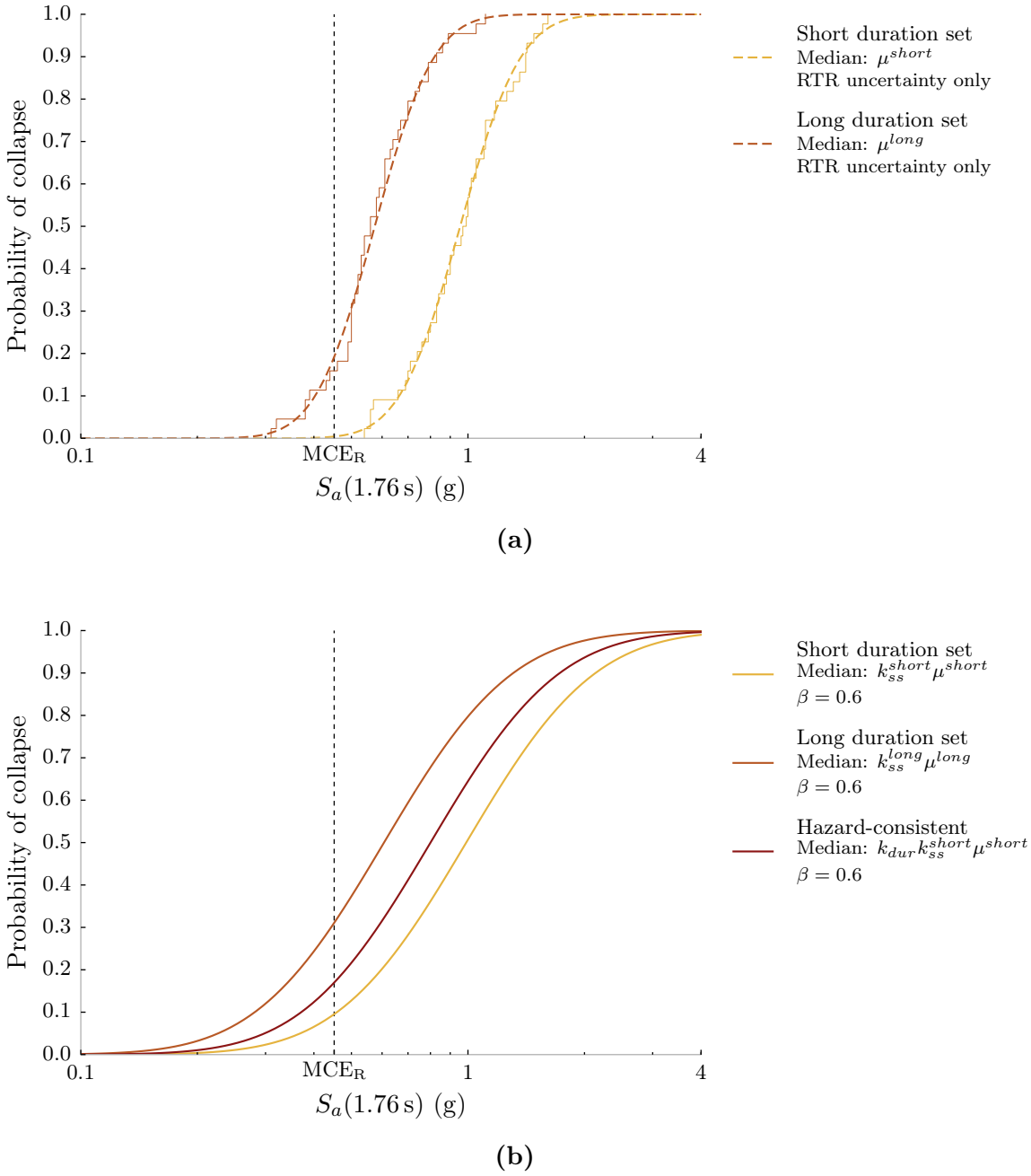

Figure 6.13: Collapse fragility curves of the eight-story reinforced concrete moment frame building estimated by conducting IDA using the short and long duration record sets selected to match the CMS. The fragility curves in (a) are estimated directly from the IDA results and incorporate RTR uncertainty only. The yellow and orange fragility curves in (b) are constructed using median values adjusted slightly for the effect of response spectral shape, and a lognormal standard deviation, β, of 0.6; they incorporate RTR and model uncertainties. The red hazard-consistent fragility curve in (b) is constructed using the median value adjusted for the effect of duration as well, and a β of 0.6.

respectively. The hazard-consistent collapse fragility curve computed using this median value and a β of 0.6, is plotted in Figure 6.13b using a red line. This fragility curve indicates a hazard-consistent collapse probability of 17 % at the MCE_R level, which lies in between the 10 % and 31 % values indicated by the short and long duration fragility curves respectively. Therefore, if the structure were to experience only short duration ground motions of $Ds_{5-75} \sim 8.1\,\text{s}$, it would portend a 10 % probability of collapse at the MCE_R level, which exactly corresponds to ASCE 7-16's implicit performance target. On the other hand, if it were to experience only long duration ground motions of $Ds_{5-75} \sim 46.9\,\text{s}$, the expected probability of collapse would be as high as 31 %, which is more than three times ASCE 7-16's performance goal, and about 1.6 times the maximum limit of 20 % prescribed by FEMA (2009b) (§ 7.1.2). This latter scenario could be considered representative of structures designed at sites with relatively long Ds targets, like Seattle, Portland, and Eugene. Structures at these sites are expected to possess larger collapse probabilities at the MCE_R level, on average, than intended by ASCE 7-16. The magnitude of its observed influence on the collapse probability at the MCE_R level, therefore, highlights the need to explicitly consider ground motion duration, in addition to response spectral shape, in code-based structural design guidelines.

6.7.1 The equivalent lateral force procedure

The equivalent lateral force (ELF) procedure (ASCE 2016, § 12.8) is more frequently employed in structural design practice than any of the other available options, like response spectrum analysis and response history analysis, due to its relative simplicity. It first requires the computation of the site-specific design response spectral ordinate at the fundamental elastic modal period of the structure, as two-thirds the MCE_R ordinate ASCE (2016) (§ 11.4). The seismic response coefficient, C_s, is computed by dividing the design response spectral ordinate by a structural system-specific response modification factor, or R-factor (ASCE 2016, Table 12.2-1), assuming an importance factor of 1. The design base shear is computed as C_s times the effective seismic weight of the structure, and is distributed over the height of the structure as per

ASCE (2016) (§ 12.8.3). The deformation demands computed from a linear static analysis are then used to evaluate the acceptance criteria in ASCE (2016) (§ 12.12). In the entire procedure, site-specific seismic hazard is quantified only in terms of the MCE_R response spectral ordinate, which is a measure of the intensity of ground motion anticipated at the site. Hence, neither the response spectral shapes nor the durations of the anticipated ground motions are accounted for.

ASCE 7-16's implicit performance objective, as stated in FEMA (2015) (§ 1.1.1) and ASCE (2016) (Table C1.3.1b), is to limit the probability of collapse under the MCE_R level ground motion to 10 % for Risk Category I and II structures. Since this exact value is less important for our current purposes, let us assume that ASCE 7-16's objective is to achieve an x % collapse probability at the MCE_R level. As demonstrated previously using the eight-story reinforced concrete frame as an example, however, a ground motion's intensity is not its only characteristic that determines its collapse potential. Its collapse potential is also influenced by its response spectral shape and duration. Among records scaled to the same intensity level, as usually quantified by $S_a(T_1)$, the ones with lower S_aRatio values and longer Ds values are more likely to cause structural collapse (Chapter 5). This suggests that the statement of ASCE 7-16's performance objective is incomplete. It requires the additional definition of the response spectral shape and duration of the ground motion, which when scaled to the MCE_R intensity level, will possess an x % probability of causing structural collapse. Let this reference response spectral shape and duration be denoted by S_aRatio^{ref} and Ds^{ref} respectively. In this study, S_aRatio^{ref} and Ds^{ref} are taken to be the median S_aRatio and Ds targets at Los Angeles, conditional on the exceedance of the ground motion intensity corresponding to the $2.2 \times \text{MCE}_\text{R}$. The choice of Los Angeles as the reference site was motivated by the historical emphasis on sites in coastal California with high population densities when calibrating building design codes, which suggests that ASCE 7-16's implicit performance objective is potentially likely to be valid here. The impact of choosing San Francisco as the reference site instead of Los Angeles is also evaluated. As noted previously, the reason for choosing the $2.2 \times \text{MCE}_\text{R}$ intensity level to compute the targets is that it approximately corresponds to the median collapse capacity of new structural designs, assuming $x = 10$

and $\beta = 0.6$. This factor of 2.2 can be appropriately modified for use with other values of x or β.

Now consider a hypothetical site—say site X—with the same MCE_R response spectral ordinates as Los Angeles, but a lower conditional median $S_a Ratio$ target and/or a longer conditional median Ds target. As per the current design provisions, the same structural design would be permissible at both Los Angeles and site X, on account of their similar MCE_R ordinates. As observed in the case of the eight-story reinforced concrete frame example, however, the structure located at site X is expected to have a probability of collapse greater than $x\,\%$ at the MCE_R level because it is likely to experience ground motions with more damaging response spectral shapes and/or longer durations. This calls for designing the structure at site X to a larger base shear, to ensure it also has a $x\,\%$ probability of collapse at the MCE_R level. Now consider two structures with similar fundamental periods, but different structural systems—say structures A and B—located adjacent to each other at site X. Let us assume structure A is influenced by response spectral shape and duration to a larger extent than structure B, because it is more ductile and it deteriorates more rapidly under cyclic loading (Haselton et al. 2011a; Raghunandan and Liel 2013; Chapter 2/ Chandramohan et al. 2016b). Although both structures are likely to experience similar ground motions, structure A is expected to have a larger probability of collapse at the MCE_R level. This calls for designing structure A to a larger base shear than structure B, to ensure they both have similar collapse probabilities. Hence, to maintain a more uniform risk of structural collapse over different geographical locations and across different structural systems, a site and structural system-specific adjustment to the design base shear is proposed. The objective of this adjustment is in line with the objective of developing risk-targeted seismic design maps (Luco et al. 2007).

It is proposed that the computation of the design base shear, V, using ASCE (2016) (Equation (12.8-1)), be modified to include adjustment factors for the effects

of response spectral shape and duration: k'_{ss} and k'_{dur}, as follows:

$$V = k'_{ss} k'_{dur} C_s W \tag{6.8a}$$

$$k'_{ss} = \left(\frac{S_a Ratio^{ref}}{S_a Ratio^{target}} \right)^{c_{ss}} \tag{6.8b}$$

$$k'_{dur} = \left(\frac{Ds^{ref}}{Ds^{target}} \right)^{c_{dur}} \tag{6.8c}$$

In these equations, W denotes the effective seismic weight of the structure. $S_a Ratio^{target}$ and Ds^{target} are site-specific parameters that represent the median $S_a Ratio$ and Ds targets, conditional on the exceedance of the ground motion intensity corresponding to $2.2 \times \text{MCE}_\text{R}$. c_{ss} and c_{dur} are structural system-specific coefficients that quantify the sensitivity of a structure to the effects of response spectral shape and duration respectively, as described previously in § 6.6.2.

The following is the basis for developing these equations. Consider a generic newly designed structure located at a generic site. As per the modified performance objective of ASCE 7-16, the structure is expected to possess an $x\,\%$ probability of collapse at the site-specific MCE_R level, under ground motions that possess the reference response spectral shape and duration: $S_a Ratio^{ref}$ and Ds^{ref} respectively. Let μ^{ref} represent the median collapse capacity of the structure under these reference ground motions. μ^{ref} is linearly proportional to MCE_R for a given value of x and β, e.g., if $x = 10$ and $\beta = 0.6$, $\mu^{ref} = 2.2 \times \text{MCE}_\text{R}$. Now, since the response spectral shapes and durations of the ground motions anticipated at the site: $S_a Ratio^{target}$ and Ds^{target}, are likely different from $S_a Ratio^{ref}$ and Ds^{ref}, the median collapse capacity is expected to shift to $(1/k'_{ss})\,(1/k'_{dur})\,\mu^{ref}$ (compare Equations (6.8b) and (6.8c) to Equations (6.4) and (6.5a)). Assuming the β of the collapse fragility curve remains unchanged as its median shifts, the ground motion intensity level corresponding to an $x\,\%$ probability of collapse also shifts to $(1/k'_{ss})\,(1/k'_{dur})\,\text{MCE}_\text{R}$. It is, however, desirable to design the structure so as to have a median collapse capacity μ^{ref} and a $x\,\%$ probability of collapse at the MCE_R level, despite the deviation in the site-specific response spectral shape and duration targets from the reference values. This can be achieved by designing the structure to a base shear modified by the factor $k'_{ss} k'_{dur}$, which is equivalent

to designing the structure to the following modified MCE_R value: $k'_{ss}k'_{dur}\text{MCE}_\text{R}$. The derivation of the adjustment factors implicitly assumes that the acceptance criteria enforced on analyses conducted using lateral loads corresponding to a certain MCE_R level are calibrated such that structures designed to satisfy them will possess an $x\,\%$ probability of collapse at that MCE_R level on average, under ground motions with certain reference response spectral shapes and durations. This assumption is based on the fact that the peak story drift ratios, on which the acceptance criteria are based, are proportional to the applied lateral loads, which are in turn proportional to the MCE_R level. This assumption is also considered to be valid in an average sense since it can be directly inferred from ASCE 7-16's implicit performance objective.

Median S_aRatio and Ds targets computed at different sites in Western USA, conditional on the $2.2 \times \text{MCE}_\text{R}$ ground motion intensity level at different periods, are tabulated in Table 6.2. The targets were computed using the procedure described in § 6.6.1, except the contribution of in-slab earthquakes was explicitly considered using the Abrahamson et al. (2016) GMPE, in computing the S_aRatio targets. $Vs_{30} = 760\,\text{m/s}$ was assumed at all sites. Corresponding response spectral shape and duration adjustment factors: k'_{ss} and k'_{dur}, for RC ductile MFs, using Los Angeles as the reference site, are also included in Table 6.2. The c_{ss} and c_{dur} coefficients used to calculate the adjustment factors were computed using Equations (6.6) and (6.7) respectively. Extrapolation of these equations beyond their limits of validity was necessary for conditioning periods of 0.2 s and 4.0 s. Maps of k'_{ss} and k'_{dur} values computed at different sites in Western USA using Los Angeles as the reference site, for conditioning periods 0.2 s and 1.0 s, are plotted in Figure 6.14. These values were computed based on targets conditional on the exceedance of the 0.5 % in 50 year ground motion, and the contribution of in-slab earthquakes was not considered in the computation of the S_aRatio targets. Hence, they may differ slightly from the values tabulated in Table 6.2.

Eugene is seen to have consistently high k'_{dur} values at all conditioning periods due to a relatively large contribution to its seismic hazard from $M_W \sim 9.0$ interface earthquakes in the Cascadia subduction zone. Other sites along the US Pacific Northwest coast are similarly observed to have high k'_{dur} values. k'_{ss} values, on the other

Table 6.2: Median S_aRatio and Ds targets conditional on the exceedance of the $2.2 \times \text{MCE}_\text{R}$ ground motion intensity level at different periods, assuming $Vs_{30} = 760\,\text{m/s}$; and corresponding k'_{ss} and k'_{dur} adjustment factors for RC ductile MFs computed at different sites in Western USA using Los Angeles as the reference site. S_aRatio targets at all conditioning periods are computed using the period range $0.2T$ to $3.0T$, except for the conditioning period of 4.0 s, in which case the period range 0.8 s to 10.0 s is used.

(a) Eugene

Conditioning period (s)	**Median target** $\boldsymbol{S_aRatio}$	$\boldsymbol{k'_{ss}}$	**Median target** $\boldsymbol{Ds_{5-75}}$ (s)	$\boldsymbol{k'_{dur}}$	$\boldsymbol{k'_{ss}k'_{dur}}$
0.2	1.66	1.13	21.5	1.91	2.16
0.5	1.97	1.04	23.4	1.65	1.72
1.0	2.16	1.11	29.4	1.50	1.67
2.0	2.12	1.10	34.7	1.37	1.50
4.0	1.91	0.97	40.5	1.24	1.19

(b) Seattle

Conditioning period (s)	**Median target** $\boldsymbol{S_aRatio}$	$\boldsymbol{k'_{ss}}$	**Median target** $\boldsymbol{Ds_{5-75}}$ (s)	$\boldsymbol{k'_{dur}}$	$\boldsymbol{k'_{ss}k'_{dur}}$
0.2	1.71	1.09	3.6	1.10	1.20
0.5	1.89	1.09	4.6	1.10	1.20
1.0	2.20	1.09	9.6	1.18	1.29
2.0	2.25	1.04	19.5	1.24	1.29
4.0	1.90	0.97	21.3	1.14	1.10

(c) Portland

Conditioning period (s)	**Median target** $\boldsymbol{S_aRatio}$	$\boldsymbol{k'_{ss}}$	**Median target** $\boldsymbol{Ds_{5-75}}$ (s)	$\boldsymbol{k'_{dur}}$	$\boldsymbol{k'_{ss}k'_{dur}}$
0.2	1.61	1.17	4.8	1.20	1.40
0.5	1.80	1.15	5.3	1.14	1.31
1.0	2.16	1.11	11.2	1.23	1.36
2.0	2.20	1.06	21.9	1.27	1.35
4.0	1.92	0.96	28.9	1.18	1.14

(d) San Francisco

Conditioning period (s)	**Median target** S_aRatio	k'_{ss}	**Median target** Ds_{5-75} (s)	k'_{dur}	$k'_{ss}k'_{dur}$
0.2	1.80	1.02	4.4	1.16	1.19
0.5	2.05	1.00	6.7	1.20	1.21
1.0	2.02	1.19	10.2	1.20	1.43
2.0	1.91	1.20	13.0	1.16	1.40
4.0	1.66	1.08	15.5	1.09	1.18

(e) Berkeley

Conditioning period (s)	**Median target** S_aRatio	k'_{ss}	**Median target** Ds_{5-75} (s)	k'_{dur}	$k'_{ss}k'_{dur}$
0.2	1.77	1.05	3.0	1.03	1.08
0.5	2.02	1.02	3.5	1.03	1.05
1.0	2.38	1.01	4.9	1.03	1.04
2.0	2.34	1.00	6.1	1.02	1.02
4.0	1.82	1.00	8.3	1.00	1.01

(f) Los Angeles

Conditioning period (s)	**Median target** S_aRatio	k'_{ss}	**Median target** Ds_{5-75} (s)	k'_{dur}	$k'_{ss}k'_{dur}$
0.2	1.84	1.00	2.7	1.00	1.00
0.5	2.06	1.00	3.2	1.00	1.00
1.0	2.40	1.00	4.3	1.00	1.00
2.0	2.34	1.00	5.4	1.00	1.00
4.0	1.83	1.00	8.0	1.00	1.00

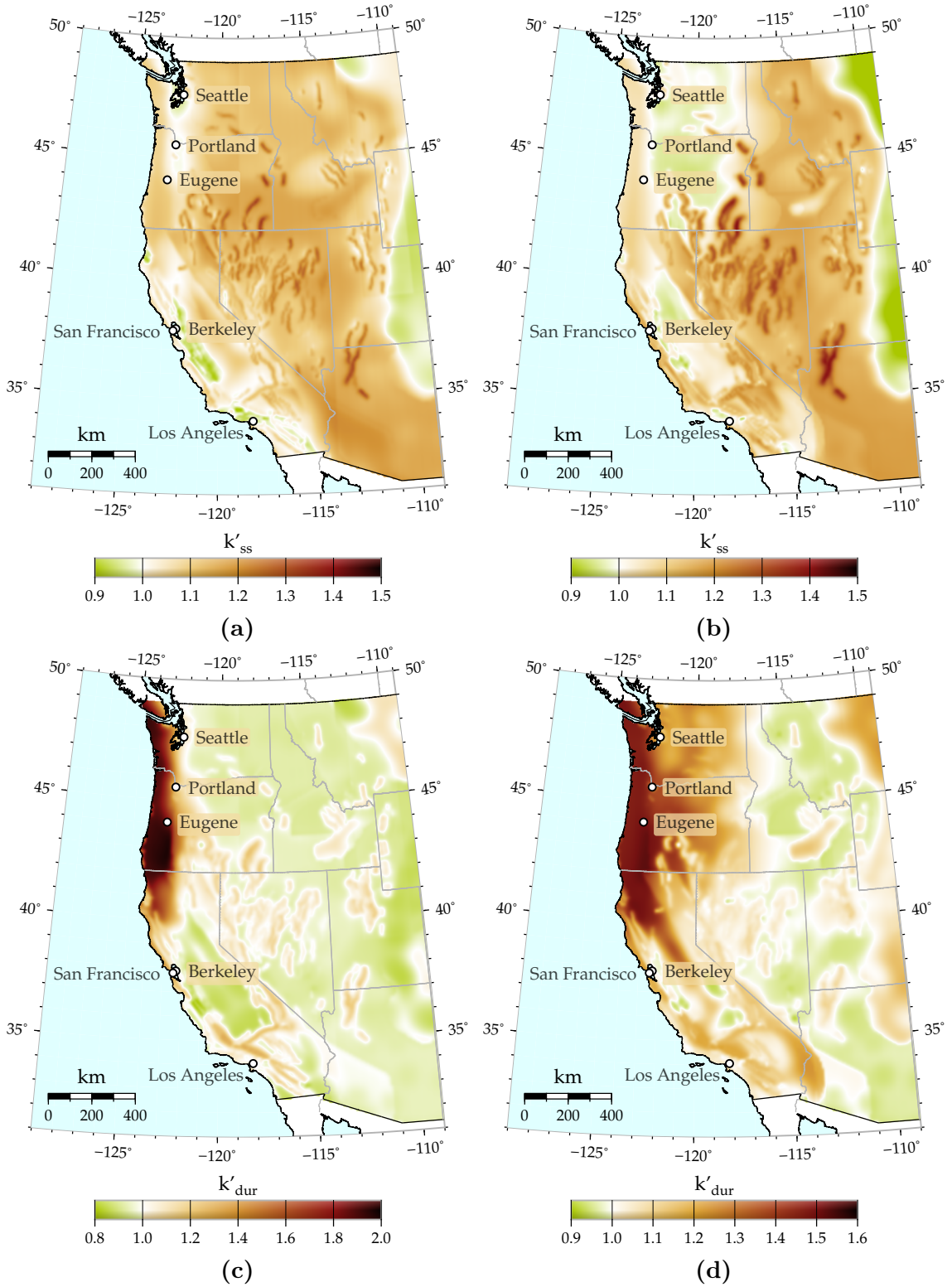

Figure 6.14: k'_{ss} values at periods (a) 0.2 s and (b) 1.0 s, and k'_{dur} values at periods (c) 0.2 s and (d) 1.0 s for RC ductile MFs based on Los Angeles as the reference site, computed using S_aRatio and Ds targets conditional on the exceedance of the 0.5 % in 50 year ground motion intensity level, assuming $Vs_{30} = 760$ m/s.

hand, are seen to be high along active crustal faults for reasons described previously in § 6.6.1. k'_{dur} values at San Francisco are comparable to both Seattle and Portland, since although San Francisco receives almost no contribution to its seismic hazard from $M_W \sim 9.0$ interface earthquakes, it is susceptible to earthquakes of $M_W \sim 8.0$ and above on the San Andreas fault. Seattle and Portland, on the other hand, have lower k'_{dur} values than Eugene, since lower magnitude earthquakes on nearby crustal faults contribute to their seismic hazard in addition to large magnitude interface earthquakes. Their k'_{dur} values are especially small at short conditioning periods since the contribution of crustal earthquakes dominates at these periods. k'_{ss} and k'_{dur} values at Berkeley are small at all conditioning periods since its S_aRatio and Ds targets are almost similar to the targets at Los Angeles, the reference site, on account of the similarity in their tectonic settings.

As an example, to ensure that a 1 s structure in Eugene has a probability of collapse close to x % at the MCE_R level, considering both the response spectral shapes and durations of the ground motions anticipated at the site, it will need to be designed to a base shear 67 % higher than the value computed using ASCE (2016) (Equation (12.8-1)). A 0.2 s structure in Eugene, on the other hand, will need to be designed to a base shear more than twice as large as the value computed using ASCE (2016) (Equation (12.8-1)). At both periods, the effect of duration dominates the effect of response spectral shape, as indicated by the relative magnitudes of k'_{ss} and k'_{dur}. Similarly, a 1 s structure in San Francisco needs to be designed to a base shear that is 43 % higher. The effects of response spectral shape and duration are approximately similar in this case. As previously mentioned in § 6.6.1, however, it is important to consider the possible effect of using the Abrahamson et al. (2016) model to predict response spectra for interface earthquakes although it is not used in the deaggregation calculations, and the conservative nature of the Abrahamson and Silva (1996) model used to predict duration from all earthquakes, when interpreting the presented results.

The computed k'_{ss} and k'_{dur} factors are significantly influenced by the chosen S_aRatio^{ref} and Ds^{ref} values, or alternatively, the site whose conditional median response spectral shape and duration targets are used to represent these values. To

demonstrate the potential impact of the choice of reference site, k'_{ss} and k'_{dur} computed using San Francisco as the reference site instead of Los Angeles are summarized in Table 6.3 and Figure 6.15. The relatively lower conditional median S_aRatio targets and longer Ds targets at San Francisco result in significantly smaller k'_{ss} and k'_{dur} factors at all sites and conditioning periods, when compared to those summarized in Table 6.2 and Figure 6.14. Although the sheer length of the duration targets at Eugene ensure structures located there still need to be designed to increased base shears, the $k'_{ss}k'_{dur}$ factors are seen to be lesser than 1 for a number of other sites, indicating that structures at these sites can be designed to lower base shears. A 1 s structure in Berkeley, for instance, could be designed to a base shear that is 27 % lower than the value computed using ASCE (2016) (Equation (12.8-1)). It is worth noting that the median Ds_{5-75} targets at Los Angeles are close to the geometric mean Ds_{5-75} values of the records in benchmark sets like the FEMA P695 far-field set: 5.4 s, and PEER Transportation set 2 (Baker et al. 2011): 5.6 s. It was observed in Chapter 4/Chandramohan et al. (2016a), however, that the Ds_{5-75} values of intense records in the PEER NGA-West2 database closely match the conditional median Ds_{5-75} targets at San Francisco. Hence, the choice of a reference site is not immediately apparent and additional studies are required to determine the S_aRatio^{ref} and Ds^{ref} values that best reflect ASCE 7-16's implicit performance objective. While various combinations of S_aRatio^{ref} and Ds^{ref} are likely to be able to produce an x % probability of collapse at the MCE_R level on average, careful judgment needs to be exercised in choosing an appropriate combination to compute the k'_{ss} and k'_{dur} factors.

One possible simplification of the proposed procedure is to consider only the geographical variation in the S_aRatio and Ds targets, and to use average c_{ss} and c_{dur} factors that are considered representative of most commonly used structural systems. In this case, the k'_{ss} and k'_{dur} factors could be incorporated directly into the computation of the MCE_R value at a site, allowing the continued use of ASCE (2016) (Equation (12.8-1)), with the k'_{ss} and k'_{dur} factors being implicitly accounted for in the computation of C_s using the modified MCE_R values. The proposal to account for the effect of duration by modifying the design ground motion intensity concurs with recommendations made previously by Raghunandan (2013) (p. 133) and Liel

Table 6.3: Median S_aRatio and Ds targets conditional on the exceedance of the $2.2 \times \text{MCE}_\text{R}$ ground motion intensity level at different periods, assuming $Vs_{30} = 760\,\text{m/s}$; and corresponding k'_{ss} and k'_{dur} adjustment factors for RC ductile MFs computed at different sites in Western USA using San Francisco as the reference site. S_aRatio targets at all conditioning periods are computed using the period range $0.2T$ to $3.0T$, except for the conditioning period of 4.0 s, in which case the period range 0.8 s to 10.0 s is used.

(a) Eugene

Conditioning period (s)	**Median target** $\boldsymbol{S_aRatio}$	$\boldsymbol{k'_{ss}}$	**Median target** $\boldsymbol{Ds_{5-75}}$ (s)	$\boldsymbol{k'_{dur}}$	$\boldsymbol{k'_{ss}k'_{dur}}$
0.2	1.66	1.11	21.5	1.64	1.81
0.5	1.97	1.04	23.4	1.37	1.43
1.0	2.16	0.94	29.4	1.25	1.17
2.0	2.12	0.91	34.7	1.18	1.08
4.0	1.91	0.89	40.5	1.13	1.01

(b) Seattle

Conditioning period (s)	**Median target** $\boldsymbol{S_aRatio}$	$\boldsymbol{k'_{ss}}$	**Median target** $\boldsymbol{Ds_{5-75}}$ (s)	$\boldsymbol{k'_{dur}}$	$\boldsymbol{k'_{ss}k'_{dur}}$
0.2	1.71	1.07	3.6	0.94	1.01
0.5	1.89	1.09	4.6	0.91	0.99
1.0	2.20	0.92	9.6	0.99	0.91
2.0	2.25	0.86	19.5	1.07	0.92
4.0	1.90	0.90	21.3	1.04	0.94

(c) Portland

Conditioning period (s)	**Median target** $\boldsymbol{S_aRatio}$	$\boldsymbol{k'_{ss}}$	**Median target** $\boldsymbol{Ds_{5-75}}$ (s)	$\boldsymbol{k'_{dur}}$	$\boldsymbol{k'_{ss}k'_{dur}}$
0.2	1.61	1.15	4.8	1.03	1.18
0.5	1.80	1.15	5.3	0.94	1.08
1.0	2.16	0.93	11.2	1.02	0.95
2.0	2.20	0.88	21.9	1.09	0.96
4.0	1.92	0.89	28.9	1.08	0.96

(d) San Francisco

Conditioning period (s)	**Median target** S_aRatio	k'_{ss}	**Median target** Ds_{5-75} (s)	k'_{dur}	$k'_{ss}k'_{dur}$
0.2	1.80	1.00	4.4	1.00	1.00
0.5	2.05	1.00	6.7	1.00	1.00
1.0	2.02	1.00	10.2	1.00	1.00
2.0	1.91	1.00	13.0	1.00	1.00
4.0	1.66	1.00	15.5	1.00	1.00

(e) Berkeley

Conditioning period (s)	**Median target** S_aRatio	k'_{ss}	**Median target** Ds_{5-75} (s)	k'_{dur}	$k'_{ss}k'_{dur}$
0.2	1.77	1.02	3.0	0.89	0.91
0.5	2.02	1.02	3.5	0.85	0.87
1.0	2.38	0.85	4.9	0.86	0.73
2.0	2.34	0.83	6.1	0.88	0.73
4.0	1.82	0.93	8.3	0.92	0.86

(f) Los Angeles

Conditioning period (s)	**Median target** S_aRatio	k'_{ss}	**Median target** Ds_{5-75} (s)	k'_{dur}	$k'_{ss}k'_{dur}$
0.2	1.84	0.98	2.7	0.86	0.84
0.5	2.06	1.00	3.2	0.83	0.83
1.0	2.40	0.84	4.3	0.83	0.70
2.0	2.34	0.83	5.4	0.86	0.72
4.0	1.83	0.93	8.0	0.92	0.85

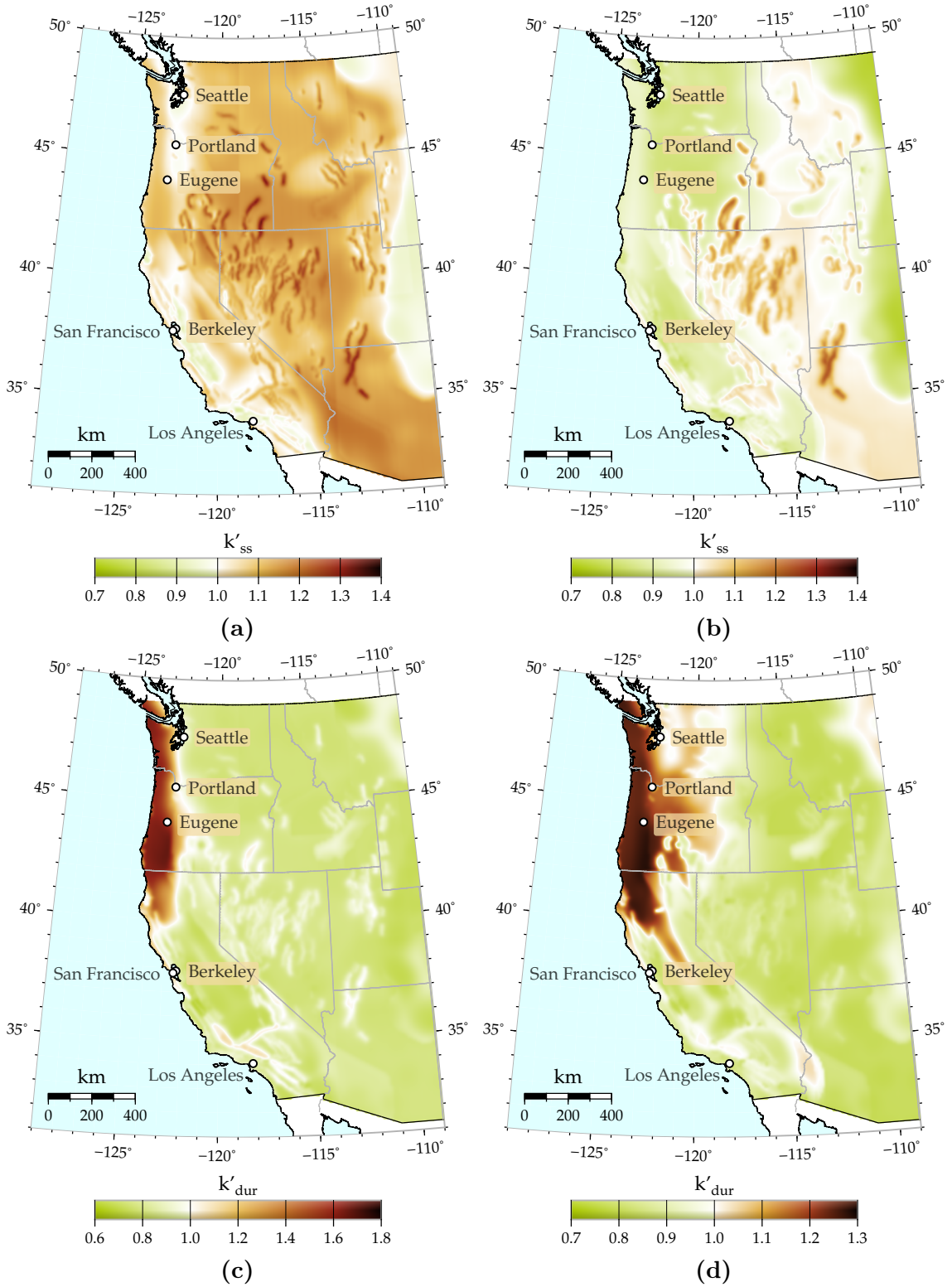

Figure 6.15: k'_{ss} values at periods (a) 0.2 s and (b) 1.0 s, and k'_{dur} values at periods (c) 0.2 s and (d) 1.0 s for RC ductile MFs based on San Francisco as the reference site, computed using S_aRatio and Ds targets conditional on the exceedance of the 0.5 % in 50 year ground motion intensity level, assuming $Vs_{30} = 760$ m/s.

et al. (2015). Liel et al. (2015) proposed a method to incorporate the effect of ground motion duration in the computation of risk-targeted MCE_R values by deaggregating the seismic hazard contributions from crustal and subduction earthquakes, and using different fragility curves for each type of earthquake. The median collapse capacity under subduction earthquakes was computed by increasing the median under crustal earthquakes by constant factor. The procedure proposed in this paper, however, develops a more rational and comprehensive basis for quantifying the effect of ground motion duration on structural collapse capacity by (*i*) using prediction models to quantify the durations of ground motions anticipated at a site; and (*ii*) adequately controlling for the effect of response spectral shape.

An alternative approach to incorporate the effects of response spectral shape and duration in the ELF procedure is to use the FEMA P695 methodology, incorporating the modifications proposed in § 6.6, to re-evaluate design guidelines and seismic performance factors—R, Ω_0, and C_d—for all structural systems. Studies that have applied the original FEMA P695 methodology to existing structural systems (e.g., FEMA 2009b, Chapter 9; NIST 2010; Zareian et al. 2010; Hsiao et al. 2013) did account for the effect of response spectral shape, albeit in an approximate manner using ε. Additional studies are required to verify the adequacy of currently used design guidelines and seismic performance factors upon accounting for the effect of ground motion duration as well. Following this approach is likely result in the tuning of design guidelines and seismic performance factors to provide adequate collapse resistance at sites susceptible to ground motions with both damaging response spectral shapes and long durations. This would potentially entail the revision of detailing requirements, acceptance criteria, etc. to provide the cyclic fatigue resistance necessary to withstand long duration ground motions. It is, however, open to debate whether all structures, including those located at sites unlikely to experience long duration ground motions should be subjected to such strict design requirements. If considered feasible, one possible solution is to develop geographical region-specific design guidelines and seismic performance factors, as proposed previously in § 6.6.1.

6.7.2 The nonlinear response history analysis procedure

The nonlinear response history analysis (NLRHA) procedure (ASCE 2016, Chapter 16) is frequently employed in the design of tall or important structures. It requires the selection of at least 11 ground motions to match a target response spectrum, which can be either the MCE_R spectrum: an idealized response spectrum constructed using spectral ordinates at 0.2 s and 1.0 s (ASCE 2016, § 11.4), or a CMS. The selected ground motions are then used to numerically simulate the dynamic response of a nonlinear model of the structure, and the inferred force and deformation demands are used to evaluate the acceptance criteria in ASCE (2016) (§ 16.4). It is, however, not possible to reliably ascertain the probability of collapse at the MCE_R level by analyzing the structure using just 11 ground motions, especially since model uncertainty is not explicitly accounted for in the analysis. The procedure, therefore, relies on acceptance criteria imposed on force and deformation demands inferred from the analyses, to enforce the implicit performance target of 10 % probability of collapse at the MCE_R level.

The NLRHA procedure attempts to explicitly account for the response spectral shapes of the ground motions anticipated at the site by recommending the selection of ground motions to match the CMS, computed conditional on the MCE_R ground motion intensity level. If records are, instead, selected to match the MCE_R spectrum, whose shape resembles the uniform hazard spectrum (UHS) (FEMA 2015, § C16.2.2), the assessment is expected to be more conservative (Reiter 1990; Naeim and Lew 1995; Bommer et al. 2000), thereby producing a stronger structural design. There are currently no explicit requirements to select the ground motions to match a target duration analogous to a target response spectrum. The use of ground motions recorded from earthquakes with mechanisms and magnitudes similar to those that control the target response spectrum at the site is recommended instead, in an attempt to implicitly enforce the selection records of appropriate durations (ASCE 2016, § C16.2.2). Although these ground motion selection requirements are motivated by the demonstrated influence of response spectral shape and duration on the probability of collapse at the MCE_R level, their utility eventually hinges on the ability

of the employed acceptance criteria to reflect the implicit performance target. It is worth noting that previous studies undertaken to verify the satisfaction of the implicit performance objective using the FEMA P695 methodology have primarily focused on just the ELF and response spectrum analysis procedures (e.g., FEMA 2009b, Chapter 9; NIST 2010; Zareian et al. 2010; Hsiao et al. 2013). The ability of the acceptance criteria to capture the effect of duration on the probability of collapse at the MCE_R level was investigated using the eight-story reinforced concrete frame.

Let us first consider the hypothetical scenario where the structure is likely to experience only short duration ground motions of $Ds_{5-75} \sim 8.1\,\text{s}$. The short duration collapse fragility curve in Figure 6.13a indicates a near-zero probability of collapse at the MCE_R level. This is well within the upper limit of 1 collapse (or *unacceptable response* as per ASCE (2016) (§ 16.4.1.1)) out of 11 permitted by the NLRHA procedure, which corresponds to a 9 % probability of collapse. It is fitting that the acceptance criterion imposed on the number of collapses is satisfied using short duration records, since the short duration fragility curve in Figure 6.13b indicates a 10 % collapse probability at the MCE_R level, which is exactly equal to the implicit performance target. Let us now assume the structure is likely to experience only long duration ground motions of $Ds_{5-75} \sim 46.9\,\text{s}$. The collapse probability indicated by the long duration fragility curve in Figure 6.13a is 20 %, which is significantly larger than the near-zero probability obtained using the short duration set. Since it is also above the permissible limit of 9 %, it indicates a failure to satisfy the acceptance criterion imposed on the number of unacceptable responses. This again seems fitting, considering the collapse probability of 31 % at the MCE_R level indicated by the long duration fragility curve in Figure 6.13b is much larger than the implicit performance target of 10 %. Failure to satisfy this acceptance criterion is likely to result in the strengthening of the structural design to reduce the collapse probability at the MCE_R level. This indicates that the acceptance criterion imposed on the number of unacceptable responses, in conjunction with the requirement to use numerical models that incorporate the deterioration in strength and stiffness of structural components and destabilizing $P-\Delta$ effects (ASCE 2016, § 16.3), is able to capture the effect of duration on structural collapse capacity. ASCE (2016) (§ C16.4.1.1), however, states

that "*... unacceptable response acceptance criteria are not the primary acceptance criteria that ensure collapse safety of the building; the primary acceptance criteria are the story drift criteria .... The unacceptable response acceptance criteria were developed to be a secondary protection to supplement the primary criteria. ... there is high variability in unacceptable responses ... the other primary acceptance criteria are much more stable and reliable ....*" This prompted an investigation of the influence of ground motion duration on peak story drift ratios.

Figure 6.16 plots the arithmetic mean peak story drift ratio (SDR) over all ground motions in each set, at different ground motion intensity values. The mean peak SDR is computed directly at the ground motion intensity levels where none of the 44 ground motions in each set cause structural collapse. The point at which the first collapse is observed is indicated by a small circle in Figure 6.16. At ground motion intensity levels where 1 to 4 out of 44 ground motions cause structural collapse, the mean peak SDR is estimated as the maximum of 1.2 times the median, and the mean of the values obtained from records that have not yet caused structural collapse, as recommended in ASCE (2016) (§ 16.4). The limit of 4 collapses out of 44 ground motions corresponds to the allowable limit of 1 collapse out of 11 ground motions prescribed in ASCE (2016) (§ 16.4.1.1). At the intensity level where the fourth collapse occurs, the solid line becomes flat, indicating that the acceptance criterion related to the number of unacceptable responses is not satisfied above this intensity level. The mean peak SDR value that would be estimated at higher intensity levels if this acceptance criterion were ignored, is plotted using a dashed line. This dashed line extends until the median collapse intensity, above which, the median peak SDR for a given intensity level is undefined. The manner in which the two curves trace each other until about $S_a(1.76\,\mathrm{s}) = 0.4\,\mathrm{g}$ supports the conclusion of Chapter 2/Chandramohan et al. (2016b) that the influence of ground motion duration on peak deformations is expected to be observed only at intensities high enough to produce significant inelastic deformations and subsequent strength and stiffness deterioration. If the acceptance criterion related to the number of unacceptable responses is ignored, the long duration set produces a slightly larger mean peak SDR of 0.028 at the $\mathrm{MCE_R}$ level, compared to a mean peak SDR of 0.022 produced by the short duration set. Both mean peak SDR

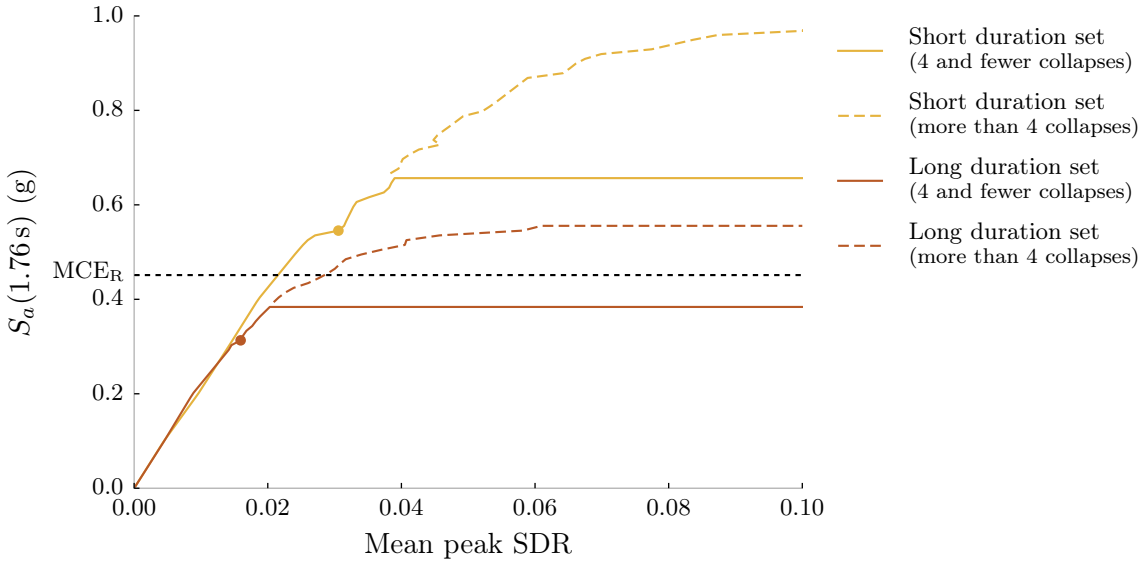

Figure 6.16: Mean peak SDR of the eight-story reinforced concrete moment frame computed using the short and long duration record sets, when scaled to different $S_a(1.76\,\mathrm{s})$ values. The mean peak SDR at the intensity level where the first collapse occurs is indicated by a circle. Mean peak SDR is estimated above this intensity level as the maximum of 1.2 times the median and the mean of the values obtained from records that have not yet caused structural collapse. The solid line becomes flat at the intensity level where 4 out of the 44 ground motions cause structural collapse. The dashed line continues until the median collapse intensity, beyond which the median peak SDR is not computable.

values are, however, well within the upper limit of 0.04 prescribed by ASCE (2016) (§ 16.4.1.2). The primary acceptance criterion based on the peak SDR, therefore, fails to recognize that the collapse probability of 31 % at the MCE$_R$ level under the long duration ground motions significantly exceeds the 10 % implicit performance target. These results indicate that the primary acceptance criterion based on peak SDR may not be able to reliably capture the effect of ground motion duration on the probability of collapse at the MCE$_R$ level. Although the secondary acceptance criterion based on the number of unacceptable responses might potentially be able to do so, this criterion is associated with a high degree of variability as indicated in ASCE (2016) (§ C16.4.1.1) and cannot be relied upon. This inference is supported by similar analyses conducted on the remaining 50 RC ductile MFs analyzed as part of this study as well.

The results of the analysis, therefore, suggest that just ensuring the selection of records to explicitly match a site-specific median target duration is unlikely to adequately account for the effect of duration in the NLRHA procedure. An alternative solution is to conduct the nonlinear response history analyses at an MCE_R level adjusted by the k'_{dur} factor computed using Equation (6.8c), and described in § 6.7.1. This recommendation again assumes that the acceptance criteria enforced on response history analyses conducted at the MCE_R level are calibrated such that structures designed to satisfy them will possess an $x\,\%$ probability of collapse at that MCE_R level on average, under ground motions with a certain reference duration. The basis for this assumption is the near-linear trend in mean peak SDR with ground motion intensity observed in Figure 6.16, about until the MCE_R intensity level, above which the collapse cases significantly influence the computation of mean peak SDR. This linear trend in mean peak SDR with ground motion intensity, even when the structure responds in the inelastic range, is commonly referred to as the *Newmark rule* or the *equal displacement rule* (Veletsos and Newmark 1960). If the durations of the anticipated ground motions are longer than the reference duration, k'_{dur} would be greater than 1, which implies that the analyses would need to be conducted at a proportionately higher intensity level, which would in turn produce proportionately higher mean peak SDR values. Hence, this would enable the effect of duration to be enforced using the primary acceptance criterion based on peak SDR, without relying on the secondary acceptance criterion based on the number of unacceptable responses. As mentioned previously, this assumption also follows directly from the statement of ASCE 7-16's implicit performance objective. The small effect of duration on the mean peak SDR at the MCE_R level observed in Figure 6.16 indicates that this procedure is unlikely to result in double counting the effect of duration when the analyses are additionally conducted using hazard-consistent ground motions. Nevertheless, the selection of ground motions with durations comparable to the reference duration under which ASCE 7-16's implicit performance objective is considered to be valid, is recommended when conducting the analyses at an intensity level corresponding to $k'_{dur} \times \text{MCE}_\text{R}$. Another relevant question at this juncture is whether the selection of records to explicitly match a CMS is sufficient to adequately account for the effect

of response spectral shape in the NLRHA procedure, or whether the MCE_R level would need to be additionally adjusted by the k_{ss} factor. Answering this question, however, would require an analogous assessment of structural response using two sets of records with similar durations, but low and high S_aRatio values. This assessment was deemed to be beyond the scope of the present study.

Alternatively, the effect of duration could be accounted for by analyzing the structure using more than just 11 ground motions, to enable the reliable estimation of the probability of collapse at the MCE_R level, as noted in ASCE (2016) (§ C16.4.1.1). These ground motions would need to be selected to explicitly match a site-specific target distribution of durations since recent studies like Chapter 4/Chandramohan et al. (2016a) and Tarbali and Bradley (2016) have highlighted the drawbacks of using causal parameters like earthquake magnitude and source-to-site distance to implicitly quantify ground motion duration. Explicitly estimating the probability of collapse in this manner is guaranteed to adequately account for the effect of response spectral shape as well, if the records are selected to match the conditional spectrum (CS). It is not sufficient to select records to match just the median targets since the objective of the analysis not to estimate the median collapse capacity; the uncertainty in the targets, therefore, needs to be explicitly considered. The acceptance criterion related to the number of unacceptable responses described in ASCE (2016) (§ 16.4.1.1), would also need to be modified to account for the actual number of ground motions used in the analysis.

6.8 Conclusion

Strategies were proposed to incorporate the effect of ground motion duration into the FEMA P-58 seismic performance assessment methodology, the FEMA P695 methodology to quantify seismic performance factors, and the ASCE 7-16 seismic design provisions. All the procedures contained in these standards that require the simulation of structural response using nonlinear dynamic analysis, recommend modeling the cyclic deterioration in strength and stiffness of the structural components and the destabilizing $P-\Delta$ effect of gravity loads. The incorporation of these features in the

structural model is essential to capture the effect of ground motion duration (Chapter 3/ Chandramohan et al. 2017). Ground motion duration was quantified using significant duration, Ds, in all the proposed strategies. Recommendations were also made to improve the effectiveness of some of the existing provisions in these standards by accounting for the effect of response spectral shape using a scalar, dimensionless metric called S_aRatio.

The FEMA P-58 methodology outlines procedures to estimate both the hazard-consistent collapse capacity of a structure and structural demands when collapse has not occurred. It describes the use of multiple stripe analysis (MSA) and an iterative modified version of incremental dynamic analysis (IDA) to estimate structural collapse capacity. The effect of duration is incorporated in MSA by selecting records at each intensity level to match not just a target conditional spectrum, but also target source-specific conditional distributions of Ds. A simpler alternative to the iterative modified IDA procedure is proposed, that requires full IDA to be conducted just once. The hazard-consistent median collapse capacity is then estimated by iteratively evaluating a regression surface fit to the collapse intensities, using site-specific median S_aRatio and Ds targets conditional on different intensity levels. Duration is considered in time, intensity, and scenario-based assessments to estimate structural demands in a manner similar to how it is considered when conducting MSA.

Modifications are proposed to the FEMA P695 methodology, to consider site-specific seismic hazard information in the design of the structural archetypes. Three methods are then proposed to adjust the median collapse capacities of the structural archetypes estimated by conducting IDA using a generic record set, based on the site-specific median S_aRatio and Ds targets. The first and most accurate method is analogous to the alternative IDA method proposed for incorporation in the FEMA P-58 methodology, and requires full IDA to be conducted using short and long duration record sets. The second method requires modified IDA to be conducted using both short and long duration record sets. The third and least accurate method requires modified IDA to be conducted using only the short duration set, similar to the original methodology. The hazard-consistent median collapse capacity of an eight-story reinforced concrete moment frame building designed for a site in Seattle is estimated

to be 0.70 g, 0.70 g, and 0.74 g using Methods 1, 2, and 3 respectively, which agree well with the value 0.68 g obtained by conducting MSA using hazard-consistent ground motions. The value 1.13 g obtained using the original FEMA P695 procedure, however, is inaccurate due to both the approximate nature of the spectral shape factor based on ε, and the absence of any correction for the effect of duration. The demonstrated accuracy of these methods when compared to the originally proposed spectral shape factor, largely offsets the additional effort involved in their use. The second and third methods require the prediction of c_{ss} and c_{dur} coefficients, which quantify the magnitude of the effects of response spectral shape and duration respectively, on structural collapse capacity. Relations have been developed to predict these coefficients for reinforced concrete ductile moment frames based on their fundamental modal periods, but similar relations could also be developed for other structural systems.

The proposed strategy to incorporate the effects of response spectral shape and duration in the ASCE 7-16 equivalent lateral force procedure involves adjusting the design base shear by k'_{ss} and k'_{dur} factors respectively. These adjustment factors are computed using site-specific conditional median $S_a Ratio$ and Ds targets and structural system-specific c_{ss} and c_{dur} coefficients. They attempt to ensure a uniform distribution of structural collapse risk over different geographical regions and across different structural systems. They do so by increasing the design base shear at sites likely to experience ground motions with damaging response spectral shapes and/or long durations, based on the amount by which the structure is expected to be influenced by the two ground motion characteristics. For example, a 1 s reinforced concrete frame in Eugene (Oregon) needs to be designed to a base shear 67 % higher than the value computed using ASCE (2016) (Equation (12.8-1)) to ensure it satisfies ASCE 7-16's implicit performance objective of a 10 % collapse probability at the MCE_R level. Similarly, a 1 s reinforced concrete frame in San Francisco (California) needs to be designed to base shear that is 43 % higher. The nonlinear response history analysis procedure attempts to account for the effect of response spectral shape by recommending the selection of records to match the conditional mean spectrum. The effect of duration, however, is unlikely to be reliably captured by just selecting

records to match hazard-consistent target distributions of duration, since the acceptance criteria enforced on analyses conducted at the MCE_R level are not very sensitive to ground motion duration. It is, therefore, recommended that the effect of duration be incorporated in this procedure by conducting the analyses at an intensity level corresponding to the MCE_R level adjusted by the k'_{dur} factor.

All of the procedures described above require the computation of site-specific target distributions of ground motion duration, using equations to predict duration as a function of causal parameters like earthquake magnitude, source-to-site distance, and site Vs_{30}. Existing models to predict duration (e.g., Abrahamson and Silva 1996; Kempton and Stewart 2006; Bommer et al. 2009; Afshari and Stewart 2016) and models for the correlation between the ε-values of duration and $S_a(T)$ (e.g., Bradley 2011) are valid only for crustal earthquakes. The effect of duration is, however, most pronounced in sites located near active subduction zones, that are likely to experience long duration ground motions from large magnitude interface earthquakes. Ground motion duration was predicted at these sites by extrapolating Abrahamson and Silva (1996): the most conservative of the prediction models for duration, to higher magnitudes that are typical of interface earthquakes. This simplification must be borne in mind when interpreting the presented results. The magnitude of the observed influence of ground motion duration on structural collapse capacity at these sites signals the urgent need to develop such models for interface and in-slab earthquakes.

Chapter 7

Robust and efficient estimation of structural collapse capacity

7.1 Abstract

The explicit central difference time integration scheme is proposed as a robust and efficient alternative to commonly used implicit schemes, like the Newmark average acceleration scheme. Numerical non-convergence is frequently encountered when the average acceleration scheme is used to simulate the nonlinear dynamic response of structures under earthquake ground motions. Persistent numerical non-convergence that cannot be resolved by strategies like using alternative solution algorithms, lowering the analysis time step, and trying alternative time integration schemes, is often incorrectly interpreted as an indicator of structural collapse. This practice is shown to result in the underestimation of the median collapse capacity of a nine-story steel moment frame building by 10 %. The robustness of the central difference scheme is a consequence of its non-iterative nature, which makes it immune to numerical non-convergence. The efficiency of the average acceleration scheme is hampered by the computationally intensive strategies employed to overcome the frequent occurrences of numerical non-convergence when estimating structural collapse capacity. Although

the conditionally stable nature of the central difference scheme requires the use of relatively smaller time steps, the computational cost of executing each time step is small, which results in overall efficient runtimes. The efficiency of the central difference scheme can be further improved by using a constant damping matrix, which permits the dynamic tangent matrix to be factorized only once over the entire analysis. For example, the time taken to conduct IDA on the steel moment frame in parallel on 160 processors using the average acceleration scheme was 118 min, while the runtime using the central difference scheme was just 32 min. Efficient parallel algorithms were developed to conduct multiple stripe analysis (MSA) and incremental dynamic analysis (IDA) on multi-core computers and distributed parallel clusters, to facilitate the adoption of these computationally intensive analysis procedures in traditional design and assessment practice. The algorithms employ dynamic load balancing schemes using a master-slave approach, which is demonstrated to significantly outperform their corresponding naïve parallel analogues that do not employ any load balancing, when using more than around 5 processors. They are implementable using just the basic MPI message-passing features currently available in OpenSees.

7.2 Introduction

With the advancement in computational capabilities over the last few decades, numerical simulation has evolved into a practical and useful tool for structural engineers to study and understand the dynamic behavior of structures under earthquake ground motions. Numerical simulations have been widely used to augment observational and experimental studies, because of the advantages they offer in terms of economy and efficiency. Most current structural design and assessment standards (e.g., ASCE 2013; ASCE 2016), including the modern performance-based earthquake engineering (PBEE) paradigm (Moehle and Deierlein 2004), implicitly assume the capability to accurately simulate the dynamic response of structures under earthquake loads. Simulating dynamic structural response involves numerically integrating the equation of motion over the entire extent of the structure, and over the duration of transient loading. The finite element method is widely used to integrate the equation over space,

while several numerical time integration schemes have been developed to perform the integration over time (Hughes 2000). Implicit time integration schemes, like the Newmark average acceleration scheme (Newmark 1959), which are used almost exclusively in current practice, are often observed to be unable to converge to a solution when simulating the nonlinear response of structures under intense ground motions. Persistent numerical non-convergence is commonly interpreted to represent structural collapse—often incorrectly, as demonstrated in this study and others like Araki and Hjelmstad (2000) and Haselton et al. (2009)—thereby introducing a conservative bias in the estimated structural collapse capacity. Nevertheless, numerical issues like non-convergence typically receive little attention compared to structural modeling and ground motion selection considerations. This study proposes the use of the explicit central difference time integration scheme as a robust and efficient alternative to commonly used implicit schemes. In a bid to facilitate the adoption of computationally intensive analysis procedures like multiple stripe analysis (MSA) (Jalayer 2003, Chapter 4) and incremental dynamic analysis (IDA) (Vamvatsikos and Cornell 2002) in design and assessment practice, algorithms are developed to efficiently conduct them in parallel.

The estimation of structural collapse capacity forms an integral component of modern performance-based design and assessment methodologies (e.g., FEMA 2012b). The calibration of modern building design codes, whose primary objective is to ensure safety against collapse, also involves evaluating the collapse capacities of representative structural archetypes (FEMA 2009b). Prior research to improve the accuracy of structural collapse simulations has, however, focussed primarily on (*i*) developing numerical models that more faithfully simulate the inelastic response of structures under intense ground motions (Deierlein et al. 2010); and (*ii*) selecting ground motions that better represent the seismic hazard at the site (NIST 2011). Although most studies that use implicit schemes to conduct nonlinear dynamic analyses encounter numerical non-convergence issues, research into the consequences and measures to mitigate these issues has been limited. Studies like Vamvatsikos and Cornell (2004), Haselton et al. (2009), Mandal et al. (2012), Eads (2013) (§ 3.4.6), Kolozvari et al. (2015) (Appendix B), Guo et al. (2015), and Hardyniec and Charney (2015) have

employed workarounds that involve decreasing the analysis time step, trying different solution algorithms, increasing the convergence tolerance, etc. in an attempt to overcome non-convergence. This approach is, however, not always successful, and is akin to addressing the *symptoms* of a problem rather than the underlying *causes*.

Non-convergence issues are more likely to be encountered when using large, complex structural models, and long duration ground motions. The gradual advancement in computational capabilities over time is likely to prompt a shift towards bigger and more complex structural models, and analyses involving larger numbers of ground motions in the near future. This warrants the use of robust and efficient numerical time integration schemes (FEMA 2009b, § 6.1.1) and analysis procedures, that lend themselves to execution on parallel computers. The robust nature of the explicit central difference time integration scheme makes it the preferred choice when conducting blast and crash simulations that involve large nonlinear deformations (e.g., Lawver et al. 2003; Dundulis et al. 2007; Danielson et al. 2008). Structural collapse simulations, which also typically involve large nonlinear deformations, are therefore also expected to benefit from the use of the central difference scheme, despite the longer duration of earthquake loads compared to impulse loads like blast and crash loads. The preference of explicit over implicit schemes when simulating structural collapse is even highlighted by FEMA P-58 (FEMA 2012b, § 6.2.1). The biggest drawback that has limited the use of the explicit schemes in practice is their conditionally stable nature, which imposes restrictions on (*i*) the analysis time step; and (*ii*) prevalent modeling practices like the assignment of zero mass to certain degrees of freedom and the use of stiff members and penalty constraints. The performance of the explicit central difference and implicit average acceleration schemes are compared in this study, in terms of their robustness and efficiency, with special emphasis on conducting collapse analyses in parallel. Comparative collapse analyses of a nine-story steel moment frame building are used to demonstrate their advantages and disadvantages, and to quantify the bias in the estimated collapse capacity introduced by numerical non-convergence.

The wide proliferation of parallel computers and easy access to high-performance computing resources like NHERI DesignSafe-CI (NHERI 2016) and Amazon EC2

(Amazon 2016) provide tremendous opportunity to improve the efficiency of a number of common structural analysis procedures by effectively harnessing their computational capabilities. Improvement in efficiency is a necessary first step before computationally intensive simulations can be adopted in mainstream structural design and assessment practice. To this end, algorithms to efficiently estimate structural collapse capacity by conducting MSA and IDA in parallel are developed and implemented in OpenSees (McKenna et al. 2006). These parallel algorithms build on previous algorithms proposed by Vamvatsikos (2011) and Hardyniec and Charney (2015).

7.3 Comparison of the average acceleration and central difference schemes

Both schemes provide a means to numerically integrate the following equation of motion over time, in order to obtain a solution in terms of the displacements $\boldsymbol{u}$, velocities $\dot{\boldsymbol{u}}$, and accelerations $\ddot{\boldsymbol{u}}$ at all degrees of freedom, and the internal forces in all elements, at each discrete time step of the analysis:

$$\boldsymbol{M}\ddot{\boldsymbol{u}} + \boldsymbol{C}\dot{\boldsymbol{u}} + \boldsymbol{f} = -\boldsymbol{M}\boldsymbol{\iota}\ddot{\boldsymbol{u}}_g \tag{7.1}$$

where $\boldsymbol{M}$ represents the mass matrix, $\boldsymbol{C}$ the viscous damping matrix, $\boldsymbol{f}$ the vector of forces resisted by the structure, $\boldsymbol{\iota}$ the influence matrix, and $\boldsymbol{u}_g$ the imposed ground acceleration (Chopra 2012, Chapter 16). Both time integration schemes are members of the Newmark family of schemes, parameterized by the coefficients γ and β (Newmark 1959). The average acceleration scheme is obtained using the parameter combination $\gamma = 1/2$, $\beta = 1/4$, and the central difference scheme using $\gamma = 1/2$, $\beta = 0$ (Hughes 2000, § 9.1). This seemingly small difference in the β parameter of the two schemes results in vast differences in their properties and characteristics described below.

7.3.1 Average acceleration scheme

The average acceleration scheme is considered an *implicit* scheme since it requires $\boldsymbol{u}_{i+1}$ (the displacements at time t_{i+1}, corresponding to the end of the current time step) to be computed by enforcing equilibrium via Equation (7.1) at time t_{i+1}. This entails solving the following nonlinear matrix equation at the i^{th} time step (Chopra 2012, § 16.3.3):

$$\left(\frac{4}{\Delta t^2}\boldsymbol{M} + \frac{2}{\Delta t}\boldsymbol{C}\right)\boldsymbol{u}_{i+1} = \boldsymbol{p}\left[\boldsymbol{M}, \boldsymbol{C}, \Delta t, \boldsymbol{u}_i, \dot{\boldsymbol{u}}_i, \ddot{\boldsymbol{u}}_i, (\ddot{\boldsymbol{u}}_g)_i\right] - \boldsymbol{f}_{i+1} \tag{7.2}$$

where Δt represents the size of the analysis time step and $\boldsymbol{p}$ represents a vector function of the parameters indicated in parentheses. The nonlinear nature of Equation (7.2) is a consequence of the nonlinear relation between $\boldsymbol{f}_{i+1}$ and $\boldsymbol{u}_{i+1}$, the two unknowns in the equation. The Newton-Raphson algorithm (Chopra 2012, § 16.3.2) is by far the most commonly employed algorithm to linearize and iteratively solve Equation (7.2). The algorithm attempts to iteratively refine an initial estimate of the solution using a tangent matrix evaluated at each iteration. Figure 7.1a demonstrates the application of the algorithm to solve a generic scalar nonlinear equation $f(x) = 0$, which is easily extended to a system of nonlinear equations like Equation (7.2). There exist a number of situations where the algorithm could fail to converge to the intended solution, as illustrated in Figures 7.1b to 7.1d. Alternative strategies like line-search, arc-length, and quasi-Newton methods (Crisfield 1991, Chapter 9) have been developed to help circumvent these pitfalls of the Newton-Raphson algorithm. Nevertheless, the possibility of non-convergence or convergence to an unintended solution always exists. The likelihood of encountering these problems increases with the size and complexity of the model, which determines the number and degree of nonlinearity of the equations that need to be simultaneously solved at each time step; and the length of the ground motion, which determines the total number of times a system of nonlinear equations needs to be solved. Poor conditioning of the system of equations as the structure approaches dynamic instability and eventual collapse could also lead to difficulties in achieving numerical convergence, although it is often

difficult to distinguish this case from those illustrated in Figures 7.1b and 7.1c. It is, therefore, incorrect to consider numerical non-convergence to be an indicator of structural collapse.

Upon encountering numerical non-convergence, a series of strategies are commonly employed to overcome it (Vamvatsikos and Cornell 2004; Haselton et al. 2009; Mandal et al. 2012; Eads 2013, § 3.4.6; Kolozvari et al. 2015, Appendix B; Guo et al. 2015; Hardyniec and Charney 2015). These strategies often include

(*i*) decreasing the analysis time step Δt, which aids convergence by increasing the relative contribution of the mass matrix to the dynamic tangent matrix (Bathe 1996, § 9.5.2);

(*ii*) using other solution algorithms like modified Newton-Raphson, Newton-Raphson with initial stiffness, and the BFGS (Broyden-Fletcher-Goldfarb-Shanno) algorithm (Dennis 1976);

(*iii*) re-running the analysis with a slightly perturbed ground motion scale factor;

(*iv*) executing a few time steps without conducting any iterations, before switching back to an iterative solution algorithm; and

(*v*) increasing the convergence tolerance.

These strategies are not always successful, but are computationally intensive, and can significantly hamper the efficiency of the analysis if invoked too frequently. Dynamically varying the analysis time step also makes the duration of a simulation hard to predict beforehand. This poses problems when simultaneously analyzing the structure under different ground motions on multiple processors, using static parallel load balancing techniques, wherein tasks are pre-assigned to processors before job initiation (Xu and Lau 1997, § 1.2). It is common practice to declare structural collapse if all these attempts fail, even if other non-simulated collapse indicators have not been triggered, which can lead to conservative collapse capacity estimates for reasons described above.

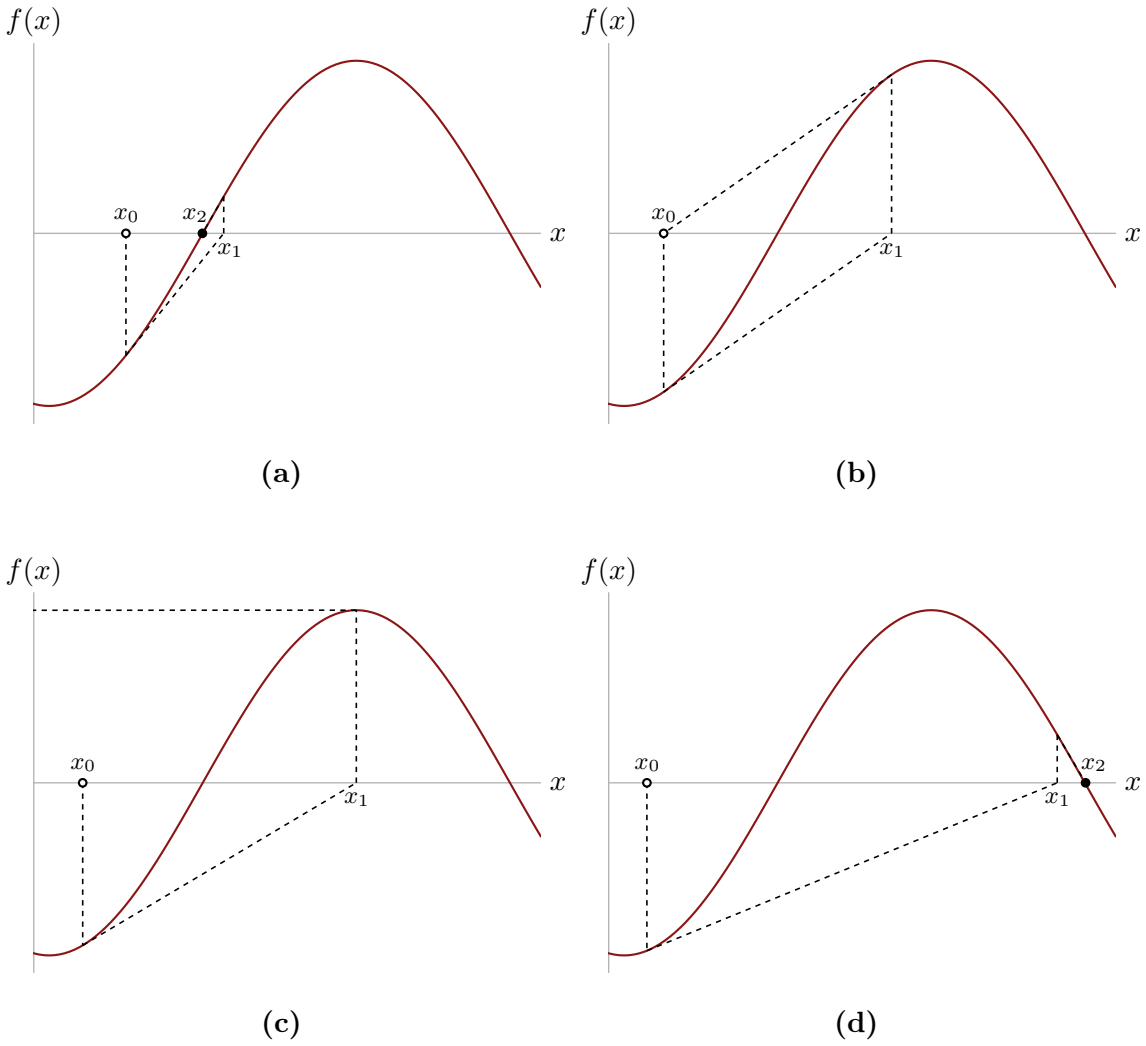

Figure 7.1: Application of the Newton-Raphson algorithm to iteratively solve a generic scalar nonlinear equation $f(x) = 0$. x_i refers to the estimate of the solution at the end of the i^{th} iteration. Depending on the initial estimate, x_0, the algorithm could either (a) successfully converge to the intended solution; (b) get stuck in an infinite loop; (c) diverge; or (d) converge to an unintended solution.

Despite their shortcomings with respect to numerical non-convergence, implicit schemes like the average acceleration scheme remain popular because of their unconditionally stable nature, i.e., the analysis time step is limited only by accuracy considerations, not by stability considerations. Therefore, they can be used in conjunction with relatively large time steps (typically $\sim 10^{-3}\,\mathrm{s}$ to $10^{-2}\,\mathrm{s}$ depending on the complexity of the model), with the following caveats:

(i) the time step is usually reduced upon encountering non-convergence; and

(ii) multiple systems of equations are typically solved at each time step.

Although the average acceleration scheme does not incorporate any algorithmic damping, other implicit schemes like (i) Newmark schemes with $\gamma > 1/2$ (Hughes 2000, § 9.1); (ii) the HHT-α (Hilber-Hughes-Tayler) scheme (Hilber et al. 1977); (iii) the generalized-α scheme (Chung and Hulbert 1993); (iv) the Wilson-θ scheme (Wilson 1968); (v) the Houbolt scheme (Houbolt 1950); and (vi) Park's scheme (Park 1975) incorporate some level of algorithmic damping (Hughes 2000, § 9.3.3). Algorithmic damping has been demonstrated to aid convergence by damping out spurious high-frequency modes, but it still does not entirely eliminate the likelihood of encountering non-convergence.

7.3.2 Central difference scheme

The central difference scheme is considered an *explicit* scheme since it computes $\boldsymbol{u}_{i+1}$ by enforcing equilibrium at time t_i (corresponding to the beginning of the current time step). This entails solving the following linear matrix equation at the i^{th} time step (Chopra 2012, § 16.3.1):

$$\left(\frac{1}{\Delta t^2}\boldsymbol{M} + \frac{1}{2\Delta t}\boldsymbol{C}\right)\boldsymbol{u}_{i+1} = \boldsymbol{p}\left[\boldsymbol{M}, \boldsymbol{C}, \Delta t, \boldsymbol{u}_i, \boldsymbol{u}_{i-1}, (\ddot{\boldsymbol{u}}_g)_i\right] - \boldsymbol{f}_i \tag{7.3}$$

The linear nature of Equation (7.3) follows from the fact that $\boldsymbol{u}_{i+1}$ is the only unknown in it. Hence, it does not require iterative solution, thereby effectively side-stepping the issue of numerical non-convergence. This feature makes it an attractive option for

simulations that involve large nonlinear deformations, like structural collapse, crash, and blast simulations, which would otherwise be significantly impeded by numerical non-convergence issues using implicit schemes. It is also a popular choice in real-time hybrid simulations since the time to execute each time step remains fairly uniform throughout the simulation due to its non-iterative nature, thereby aiding the synchronization of the analytical and physical substructures. Additionally, unlike most implicit schemes, it does not require the tangent stiffness as input, which is difficult to measure during a hybrid test (Mahin and Shing 1985; Takanashi and Nakashima 1987; Bonnet et al. 2008). Since the time taken to conduct a simulation is almost directly proportional to the length of the ground motion, the central difference scheme is amenable to the simultaneous analysis of structures under different ground motions using static parallel load balancing techniques. Explicit schemes based on finite difference formulations are also generally preferred over implicit schemes in computational fluid dynamics simulations.

The biggest disadvantage of the central difference scheme is its conditionally stable nature, which effectively limits the size of the time step it can be used with, to $\Delta t_{max} = {}^{T_{min}}/_{\pi}$, where T_{min} refers to the shortest modal period of the structural model. The value of Δt_{max} is not influenced by the level of viscous damping present in the structural model, unlike a number of other schemes in the Newmark family (Bathe 1996, p. 809). This limitation precludes the presence of massless degrees of freedom, and infinitely stiff elements and penalty constraints in the structural model, since they would cause $T_{min} \to 0$, rendering Δt_{max} too small and impractical. Hence, use of the central difference scheme requires the explicit assignment of at least small values of mass to all translational degrees of freedom, and moment of inertia to all rotational degrees of freedom, when using a lumped mass matrix formulation as per conventional practice. Although this entails some additional effort during model creation, it allows reaping the benefits of the central difference scheme, and has even been linked to improved convergence performance when using implicit schemes (Bathe 1996, § 9.5.2; Haselton et al. 2009). This is, however, less of a concern when using a consistent mass matrix formulation (Hughes 2000, § 7.3.2). Even the recommendation to avoid the use of infinitely stiff elements and penalty constraints is not unique to

the central difference scheme, since their presence increases the condition number of the stiffness matrix (McGuire et al. 2000, § 11.6), thereby adversely affecting the convergence of implicit schemes as well. T_{min}, and consequently Δt_{max}, is generally controlled by the lightest and/or stiffest elements in the structural model. For the type of structural models generally used for collapse capacity estimation, $\Delta t_{max} \sim 10^{-4}\,\text{s}$. It is worth noting that the value of T_{min} could change during the course of a nonlinear analysis. Since most civil engineering structures soften in the inelastic range, however, T_{min} could only increase during the course of the analysis. Therefore, ensuring the satisfaction of the stability criterion based on the initial elastic T_{min} is often sufficient. Structures with stiffening elements like cables, on the other hand, require checks to guard against the possibility of transient violations of the stability criterion (Bathe 1996, § 9.5.1).

A closer examination of Equation (7.3) reveals a number of opportunities to optimize the efficiency of the central difference scheme. The dynamic tangent matrix that needs to be factorized at each time step is a linear combination of $\boldsymbol{M}$ and $\boldsymbol{C}$, of which, $\boldsymbol{M}$ is usually constant and diagonal when a lumped mass matrix formulation is used. If $\boldsymbol{C}$ is also constant, the resulting constant dynamic tangent matrix needs to be factorized only at the first time step, and the computed factors can be used to solve different dynamic load vectors at all subsequent time steps, resulting in large computational savings. Unfortunately, the prevalent practice of using a Rayleigh damping matrix, computed as $\boldsymbol{C} = a_M \boldsymbol{M} + a_K \boldsymbol{K}_{current}$, renders $\boldsymbol{C}$ non-constant. Using a constant Rayleigh damping matrix, computed as $\boldsymbol{C} = a_M \boldsymbol{M} + a_K \boldsymbol{K}_{initial}$, is generally discouraged since it has been reported to produce spurious damping forces (Charney 2008). In the author's opinion, however, our current level of understanding of the origin and nature of damping forces does not justify the need for a non-constant damping matrix. Hence, the use of alternative constant damping matrix formulations like the modal damping matrix (Chopra and McKenna 2016) is recommended. If $\boldsymbol{C}$ does not depend on $\boldsymbol{K}_{current}$, Equation (7.3) does not require the tangent stiffness matrix to even be assembled, which results in additional computational savings. Alternatively, the use of a diagonal $\boldsymbol{C}$ produces a diagonal dynamic tangent stiffness matrix, whose factorization is trivial. Finally, a substantial speedup can be obtained when solving

Equation (7.3) in parallel using multiple processors, by a process called *domain decomposition* that allows each individual processor to analyze a substructure of the larger model. The use of a constant dynamic tangent matrix, therefore, significantly minimizes the communication overhead between the processors, resulting in improved parallel efficiency (Noor and Lambiotte 1979; Hajjar and Abel 1989; Chiang and Fulton 1990; Sotelino 2003; Chopra 2012, § 16.3.1). This discussion demonstrates that although the use of a shorter Δt compared to the average acceleration scheme requires the solution of Equation (7.3) a larger number of times for a given length of ground motion, Equation (7.3) can be solved much more efficiently than Equation (7.2).

Hybrids of implicit and explicit schemes could also be used to exploit each of their advantages and overcome their individual drawbacks. Spatial hybrids, popularly known as implicit-explicit schemes, partition the model into implicit, explicit, and interface substructures. Locally refined sections of the model are analyzed using an implicit scheme, while the rest of the model is analyzed using an explicit scheme (Hughes and Liu 1978; Hughes et al. 1979; Chung and Hulbert 1994) This ensures that the time-step restriction when using the explicit scheme is not too severe. A temporal hybrid could also be conceived, wherein an implicit scheme is used until non-convergence is encountered, and an explicit scheme is used to tide over the portion of the ground motion that causes non-convergence (Liang et al. 2016). These hybrid schemes are, however, not considered in this study due to issues experienced while attempting to implement them in OpenSees rev. 5184.

7.3.3 Steel moment frame model

A nine-story steel moment frame building, designed for a site in Seattle as part of the SAC Steel Project (FEMA 2000), was analyzed using the average acceleration and central difference schemes to compare their performance. A two-dimensional centerline model of the structure was created and analyzed using OpenSees rev. 5184. A schematic of this model is illustrated in Figure 7.2. The beams and columns were modeled using linear elastic elements, with all the inelastic deformation concentrated in zero-length plastic hinges located at the RBS hinges on each beam, and at the

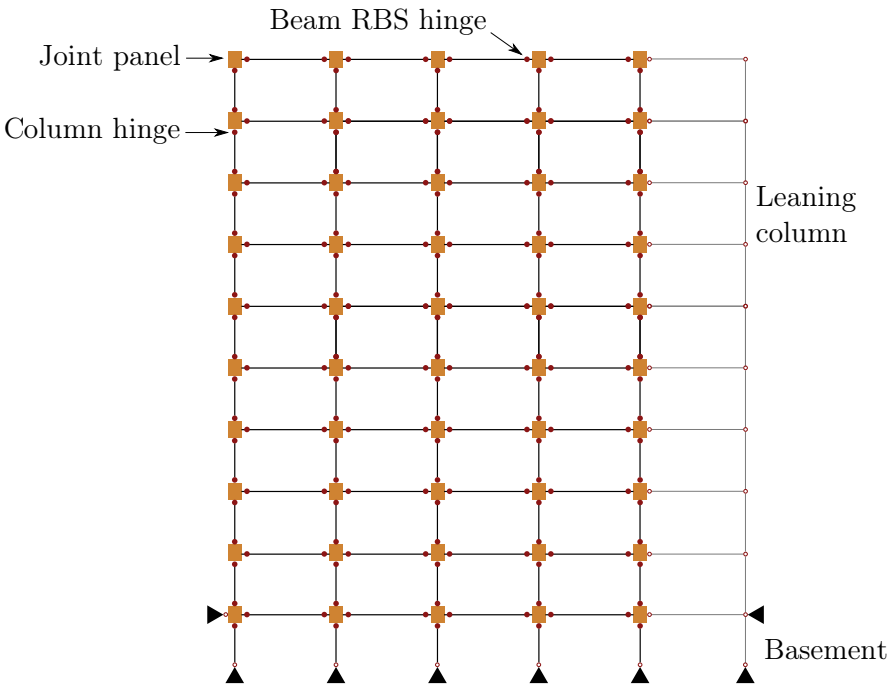

Figure 7.2: Schematic of the nine-story steel moment frame model.

ends of each column. The hysteretic behavior of the plastic hinges was modeled using the bilinear Ibarra-Medina-Krawinkler hysteretic model (Ibarra et al. 2005). This model incorporates (*i*) a post-capping negative stiffness branch of the backbone curve to capture in-cycle deterioration; and (*ii*) an algorithm to cyclically deteriorate both strength and stiffness based on the cumulative hysteretic energy dissipated. The hysteretic shear behavior of the finite panel zones was modeled using a trilinear backbone curve. The contribution of the adjacent gravity frame to the destabilizing $P-\Delta$ effect was captured using a pin-connected leaning column. The fundamental elastic modal period of the structure is 2.95 s.

Analyzing the model using the central difference scheme required at least a small mass to be assigned to each translational degree of freedom, and moment of inertia to each rotational degree of freedom. The seismic mass at each story level was proportionally distributed to the beam-column joints and the leaning column based on their respective tributary areas. The moment of inertia at a beam-column joint was approximately estimated based on the uniform load tributary to the frame, over a

length computed as the sum of the depth of the column and the depths of the beams framing into the joint. The exact value of this moment of inertia is, however, not of concern, since it is usually too small to have any significant influence on the overall dynamic behavior of the structure. Since it is often these small moments of inertia that control the shortest modal period of the structure, they can even be adjusted to obtain a required Δt_{max}, as long as they remain small enough to not significantly influence global structural behavior. In cases where multiple nodes were present at a beam-column joint, the mass and moment of inertia assigned to the joint was equally distributed among the nodes. The shortest elastic modal period was computed to be 5.5×10^{-4} s, which permitted a Δt_{max} of 1.7×10^{-4} s. Hence, analyses using the central difference scheme were conducted using a Δt of 1.5×10^{-4} s. The Tcl scripts used to create the model have been made available along with other software developed as part of this study at the git repository linked to in § 7.6.

7.3.4 Influence of numerical non-convergence on estimated collapse capacity

The collapse capacity of the steel moment frame building was estimated using both time integration schemes by conducting incremental dynamic analysis (IDA) (Vamvatsikos and Cornell 2002) using 44 ground motions from the FEMA P695 (FEMA 2009b) far-field record set. Each ground motion was incrementally scaled to higher intensity levels until it caused structural collapse, indicated by the exceedance of a peak story drift ratio (SDR) of 0.10. Ground motion intensity was quantified by the 5 % damped pseudo spectral acceleration, S_a, at the fundamental elastic modal period of the structure, $T_1 = 2.95$ s. When using the average acceleration scheme in conjunction with the Newton-Raphson solution algorithm, the following sequence of attempts were made to overcome numerical non-convergence, if it was encountered during a simulation with peak transient deformations still below the collapse threshold. Alternative solution algorithms including (*i*) Newton-Raphson with the initial elastic stiffness matrix; (*ii*) modified Newton-Raphson; (*iii*) Krylov subspace accelerated version of modified Newton-Raphson; (*iv*) Newton-Raphson with line-search;

(*v*) Broyden; and (*vi*) BFGS (Broyden–Fletcher–Goldfarb–Shanno) were first tried. The initial analysis Δt of 5×10^{-3} s was then decreased by a factor of 5, followed by a factor of 10, and finally by a factor of 50. The previously listed solution algorithms were then re-tried at $1/10^{th}$ the initial Δt. Finally, the following alternative implicit time integration schemes were used, again at $1/10^{th}$ the initial Δt: (*i*) HHT-α (Hilber-Hughes-Taylor) with $\alpha = -0.2$ and then $\alpha = -0.3$, to assess the benefits of algorithmic damping; and (*ii*) TRBDF2 (Bank et al. 1985; Bathe 2007). If all these attempts failed, structural collapse was assumed to have occurred at the point of non-convergence as per conventional practice.

The collapse intensities of the ground motions, defined as the lowest $S_a(2.95\,\text{s})$ values they need to be scaled to, to cause structural collapse, were noted. The collapse intensities computed using the average acceleration scheme were found to be lesser than the corresponding values computed using the central difference scheme by more than 10 %, for 12 out of the 44 ground motions used in the analysis. IDA curves that trace the peak SDR values produced by a ground motion as it is incrementally scaled are plotted for 4 of these ground motions in Figure 7.3. The IDA curves computed using the two schemes are seen to be almost exactly identical until they separate at a certain intensity level. This corresponds to the intensity level at which persistent numerical non-convergence is encountered using the average acceleration scheme, prompting the premature declaration of structural collapse. The observation that analyses conducted using the central difference scheme at and above this intensity level do not indicate the occurrence of structural collapse, clearly highlights the error in interpreting persistent numerical non-convergence as an indicator of structural collapse. Representative time histories comparing the drift ratio at the controlling story computed using the two schemes, at one such point of separation of the IDA curves, are plotted in Figure 7.4a. As depicted in this plot, the time histories computed using the two schemes are generally almost identical until the point of non-convergence, if any. In some instances, small differences are observed at large story drift ratios, as illustrated in the section of the time histories beyond 26 s, plotted in Figure 7.4b. One of the two schemes cannot be deemed more accurate than the other from such comparisons, since assumptions are involved in both their formulations.

It is a common misconception that implicit schemes are more accurate than explicit schemes since they enforce equilibrium at the end of each time step by iteratively minimizing the out-of-balance forces. It is worth recollecting that the enforcement of equilibrium using the average acceleration scheme, for example, is still subject to the assumption of a constant acceleration over the time step (Chopra 2012, § 5.4). Although explicit schemes do not require iterative solution, they produce comparable results in terms of accuracy, as a consequence of the small time steps they are usually conducted with. Nevertheless, the differences introduced by these small deviations between the collapse capacities estimated using the two schemes, are insignificant compared to those introduced due to numerical non-convergence.

An analysis of the series of strategies employed to overcome non-convergence when using the average acceleration scheme revealed the use of alternative solution algorithms and the reduction of the analysis Δt to be the most successful strategies. Alternative implicit time integration schemes, even those that employed algorithmic damping, were unable to overcome any instance of numerical non-convergence. A more detailed analysis of the efficacy of each employed strategy is, however, not possible since they were employed in a sequential fashion, with one strategy being used only if all the strategies employed before it failed.

The collapse intensities computed using the average acceleration scheme were found to differ from the corresponding values computed using the central difference scheme by less than 1 %, for 29 out of the 44 ground motions. IDA curves computed from 4 of these ground motions are plotted in Figure 7.5. These plots indicate that similar collapse intensities are generally computed using the two schemes as long as the average acceleration scheme does not encounter persistent non-convergence below the collapse intensity level.

The empirical distribution of the ground motion collapse intensities computed using each scheme and the collapse fragility curves obtained by fitting lognormal distributions to them are plotted in Figure 7.6. The conservative bias in the fragility curve computed using the average acceleration scheme, as a consequence of incorrectly interpreting persistent numerical non-convergence as an indicator of structural collapse, is evident from the plot. The median collapse capacity estimated using the

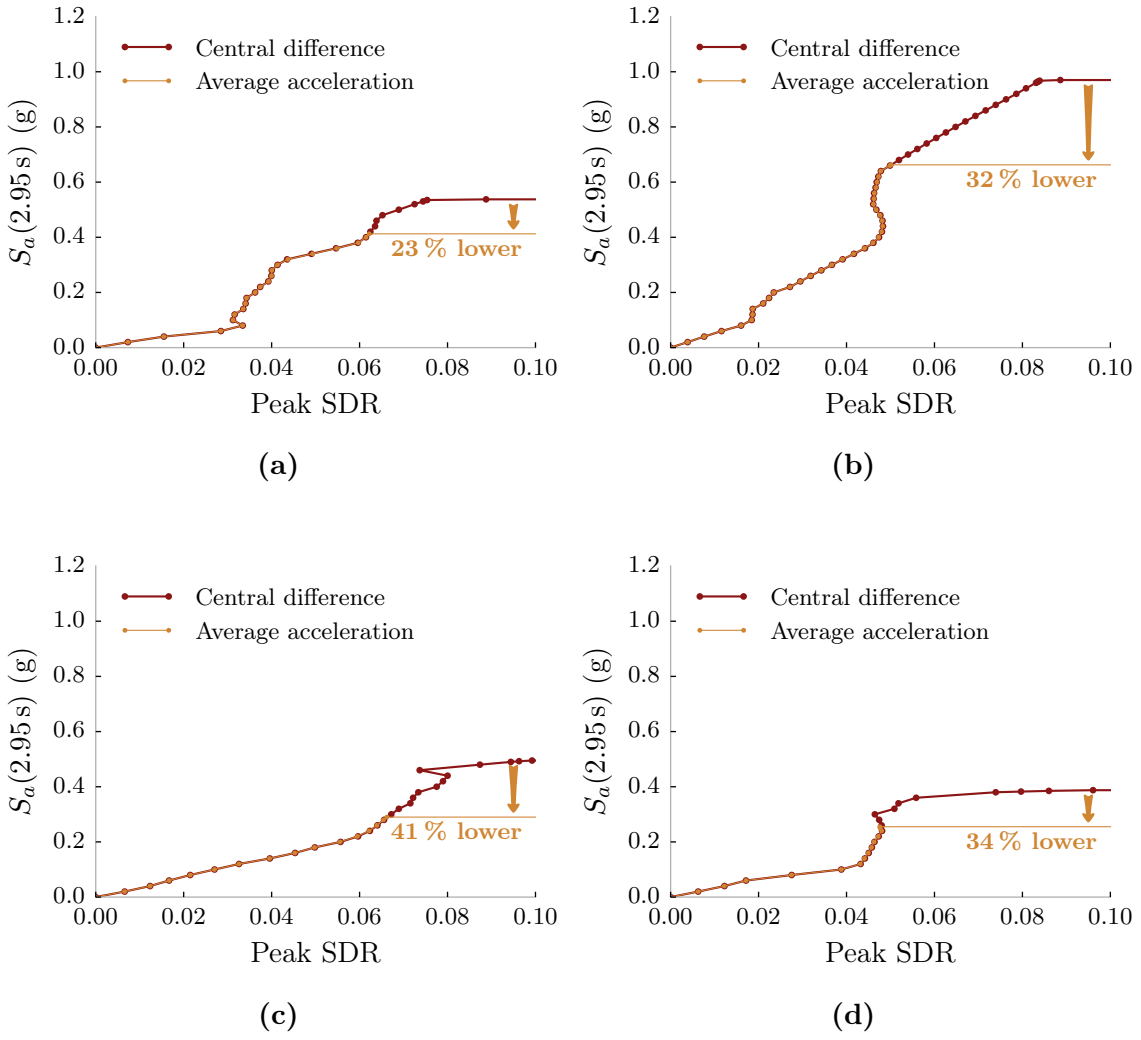

Figure 7.3: IDA curves computed using the two schemes for 4 of the 12 ground motions whose collapse intensity estimated using the average acceleration scheme is lesser than the corresponding value computed using the central difference scheme by more than 10 %.

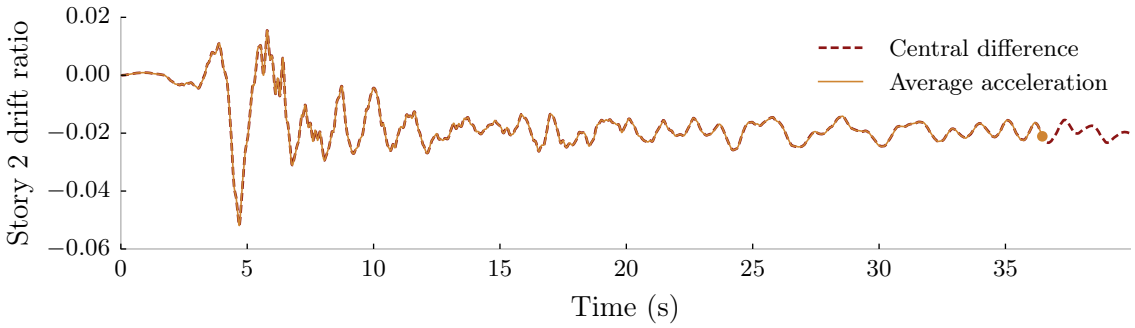

(a)

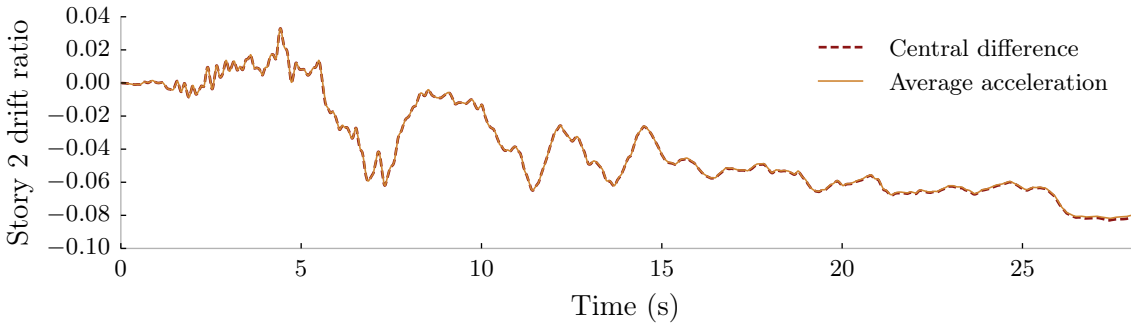

(b)

Figure 7.4: Time histories of the drift ratio at the second story computed using both schemes under (a) the 90° component of the ground motion from the 1989 Loma Prieta earthquake recorded at the Gilroy Array #3 station, scaled to $S_a(2.95\,\mathrm{s}) = 0.680\,\mathrm{g}$ (the solid circle indicates the point of persistent non-convergence using the average acceleration scheme); and (b) the 180° component of the ground motion from the 1971 San Fernando earthquake recorded at the Hollywood Storage Grounds, Los Angeles station, scaled to $S_a(2.95\,\mathrm{s}) = 0.564\,\mathrm{g}$.

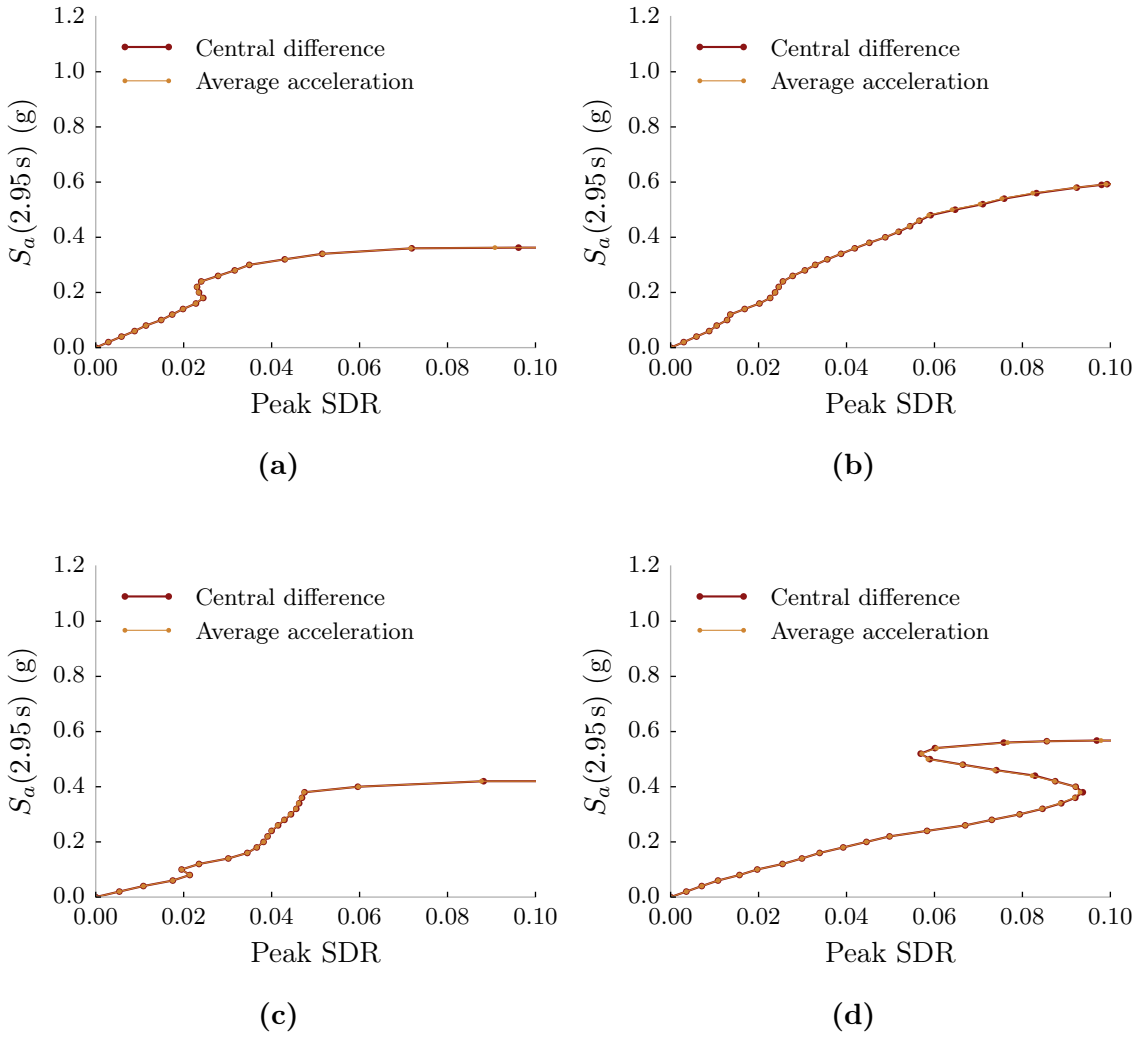

Figure 7.5: IDA curves computed using the two schemes for 4 of the 27 ground motions whose collapse intensity estimated using the average acceleration scheme is different from the corresponding value computed using the central difference scheme by less than 1 %.

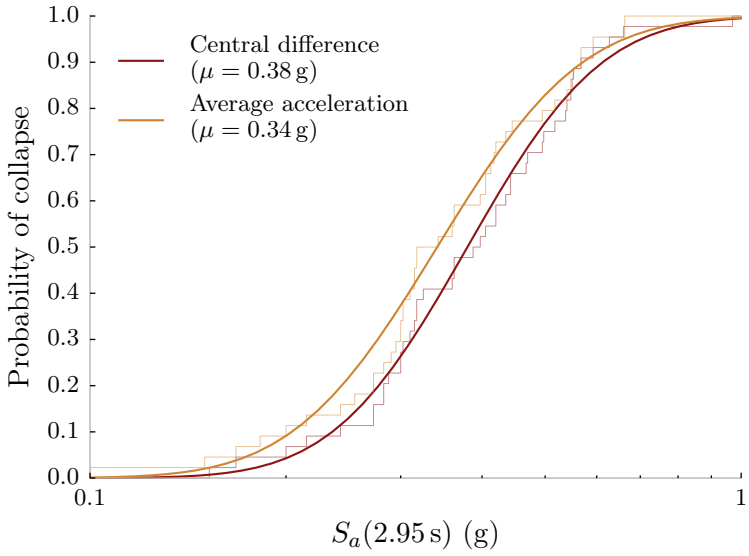

Figure 7.6: Collapse fragility curves of the nine-story steel moment frame building estimated by conducting IDA using the average acceleration and central different time integration schemes.

average acceleration scheme is 10 % lower than that estimated using the central difference scheme. These results demonstrate the superiority of the central difference scheme with respect to accuracy in structural collapse simulation, which can be attributed to its immunity against numerical non-convergence. The use of elements like force-based fiber elements (Spacone et al. 1996), whose internal force recovery schemes require iterative solution, however, can detract from the benefits of the central difference scheme. Nevertheless, the use of small analysis time steps is expected to aid in the convergence of their internal force recovery schemes.

7.3.5 Comparison of efficiency

The efficiencies of the two schemes were compared by conducting timed simulations of the response of the steel moment frame building under the longitudinal component of the ground motion recorded from the 1992 Landers earthquake, at the Coolwater station. A slightly modified version of the structural model described in § 7.3.3 was used in these analyses, since the shear formulation of the *Joint2D* element used to model

Table 7.1: Summary of the time taken to simulate the response of the steel moment frame building under the longitudinal component of the ground motion recorded from the 1992 Landers earthquake, at the Coolwater station, using the two schemes and different permutations of Rayleigh damping matrix formulations and types of solvers.

Time integration scheme	**Rayleigh damping matrix**	**Type of solver**	Δt (10^{-4} s)	**Runtime** (min)
Average acceleration *low scale factor* *w/o convergence attempts*	$a_M \boldsymbol{M} + a_K \boldsymbol{K}_{current}$ *non-constant*	Sparse	50	1.0
Average acceleration *high scale factor* *w/ convergence attempts*	$a_M \boldsymbol{M} + a_K \boldsymbol{K}_{current}$ *non-constant*	Sparse	≤ 50	20.9
Central difference	$a_M \boldsymbol{M} + a_K \boldsymbol{K}_{current}$ *non-constant*	Sparse	1.5	15.9
Central difference	$a_M \boldsymbol{M} + a_K \boldsymbol{K}_{initial}$ *constant*	Sparse *factor once*	1.5	3.3
Central difference	$a_M \boldsymbol{M}$ *constant and diagonal*	Diagonal *factor once*	1.5	2.9

the panel zones was discovered to result in an unconventional, non-constant element mass matrix.* Since this did not permit factorizing the dynamic tangent matrix only once when using the central difference scheme as described in § 7.3.2, the shear deformation of the panel zones was disabled for these analyses. This modification did not significantly influence the T_{min} value of the model, thereby permitting analysis using the central difference scheme with the same Δt as before: 1.5×10^{-4} s. It is also not expected to affect the conclusions of this section in any way, since the same modified model is analyzed using both time integration schemes. The time taken to conduct the analysis using the two schemes and different permutations of Rayleigh damping matrix formulations and types of solvers, on an Intel Xeon E5-2640 v3 processor, is summarized in Table 7.1.

Using the average acceleration scheme in conjunction with a typical Δt of 5×10^{-3} s, the analysis completes in 1.0 min as long as numerical non-convergence issues are not

*Thanks to Frank McKenna for helping trace the source of the discrepancies observed when factorizing the dynamic tangent matrix only once, to the *Joint2D* element.

encountered. When the analysis is repeated by scaling the ground motion to a higher intensity level, closer to its collapse intensity, the runtime increases to 20.9 min since encountering numerical non-convergence compels the use of computationally intensive strategies to overcome it. For example, the Newton-Raphson with initial elastic stiffness and modified Newton-Raphson solution algorithms require many more iterations to converge to a solution at each time step compared to the full Newton-Raphson algorithm. The reduction of the analysis Δt also has a detrimental effect on the efficiency of the analysis. The time taken to conduct the analysis using the central difference scheme using a Δt of 1.5×10^{-4} s, and a Rayleigh damping matrix computed as $a_M \boldsymbol{M} + a_K \boldsymbol{K}_{current}$, is 15.9 min. This non-constant damping matrix, however, for reasons described in § 7.3.2, does not permit the desirable features of the central difference scheme to be fully exploited. By using a constant damping matrix computed as $a_M \boldsymbol{M} + a_K \boldsymbol{K}_{initial}$, the dynamic tangent matrix needs to be factorized only once, and the analysis runtime drops to 3.3 min. The runtime using any other constant damping matrix formulation, e.g., a modal damping matrix, is expected to be close to 3.3 min as well. If a purely mass-proportional constant diagonal damping matrix is used instead, the runtime drops slightly to 2.9 min since it permits the use of a more efficient diagonal solver. Although purely mass-proportional damping is seldom used in practice, this result equivalently applies to any other means of obtaining a diagonal damping matrix.

In summary, the average acceleration scheme is more efficient than the central difference scheme, as long as numerical non-convergence is not encountered. If multiple processors are used to conduct the simulation in parallel, however, the larger speedup obtained using the central difference scheme could make it more competitive. If non-convergence is encountered, the efficiency of the average acceleration scheme decreases by a degree dependent on the length of the ground motion that remains to be analyzed using relatively inefficient solution algorithms and a decreased Δt. In this case, non-convergence is found to render the average acceleration scheme less efficient than the central difference scheme. The estimation of structural collapse capacity using IDA or MSA generally requires the simulation of structural response under a number of intense (and potentially long duration) ground motions, that are typically

associated with a larger likelihood of causing numerical non-convergence. Hence, the efficiency of the average acceleration scheme in conducting an entire IDA or MSA depends on the number of the conducted simulations that encounter non-convergence.

The time taken to conduct an entire IDA using the two schemes is summarized in Table 7.2. The IDAs were conducted using the 44 ground motions from the FEMA P695 far-field record set, on a parallel cluster containing 160 Intel Xeon E5-2640 v3 processors. Although each simulation was run using a single processor, as many as 160 simulations were conducted simultaneously with dynamic load balancing. The reason for conducting the IDAs on a relatively large distributed parallel cluster, rather than a smaller multi-core computer or serially using a single processor, was to compare the efficiency of the two schemes in conducting large-scale simulations. Simulations of this magnitude are conducted relatively frequently in current research practice, and are likely to become the norm in design and assessment practice as well, in the near future. The algorithm used to conduct IDA in parallel is described in § 7.4.2, and requires a number of analyses to be conducted near, and even above the collapse intensity of a ground motion. Hence, out of the 632 total simulations conducted using the average acceleration scheme, only 1 successfully completed using the full Newton-Raphson algorithm and a Δt of 5×10^{-3} s without encountering numerical non-convergence. 567 of the remaining simulations successfully completed using alternative solution algorithms like Newton-Raphson with initial elastic stiffness, Newton-Raphson with line search, etc. 23 simulations successfully completed upon lowering the Δt by factors of 5, 10, and 50. This indicates that the initially chosen Δt was probably high for this particular model, although 5×10^{-3} s is considered to be on the lower side of Δt values typically used in practice with the average acceleration scheme, for a relatively long period structural model. It also demonstrates the potential to experience numerical non-convergence when structural response simulations are conducted under ground motions scaled to both low and high intensities. The net effect of the use of these computationally intensive efforts to enforce convergence in most of the conducted simulations, however, was a relatively long IDA runtime of 118 min using the average acceleration scheme. Although certain aspects of the parallel algorithm used to conduct the IDA are tuned for efficiency using the central

difference scheme, the impact on the runtime using the average acceleration scheme is not expected to be significant. Using the central difference scheme in conjunction with a non-constant damping matrix, the IDA runtime was 154 min. This runtime was, however, reduced to 32 min using a constant damping matrix, and slightly further down to 27 min using a constant diagonal damping matrix. Hence, even if a non-constant damping matrix is used, the runtime using the central difference scheme is only 31 % longer than the average acceleration scheme, which is considered a small price to pay for the improved robustness against numerical non-convergence. When a constant damping matrix is used, however, the runtime using the central difference scheme is observed to be 73 % shorter than the average acceleration scheme in this particular case, as a consequence of factorizing the dynamic tangent matrix just once over the entire analysis. In general, the relative efficiencies of the two schemes are expected to depend on (*i*) the structural model characteristics; (*ii*) the ground motions characteristics; (*iii*) the analysis parameters; and (*iv*) the parallel algorithm employed to conduct IDA. The central difference scheme is, however, observed to be a competitive alternative to the average acceleration scheme in structural collapse simulation, not just in terms of robustness, but also in terms of efficiency. These findings are in general agreement with other previous studies like McNamara (1974), Mikkola et al. (1981), and Xie (1996), that analyze and compare numerical time integration schemes.

7.4 Parallel algorithms to conduct MSA and IDA

Most modern computers are parallel computers, i.e., they contain multiple processors that are capable of executing more than one thread of computation simultaneously. Effectively utilizing the capabilities of parallel computers requires the use of parallel algorithms that efficiently divide the computation to be conducted into smaller tasks that can be executed simultaneously, and optimally schedule the execution of these tasks. Parallel algorithms to conduct multiple stripe analysis (MSA) and incremental dynamic analysis (IDA), two commonly used methods to estimate structural collapse capacity recommended by standards like FEMA P-58 (FEMA 2012b) and FEMA

Table 7.2: Summary of the time taken to conduct IDA on the steel moment frame building using the two schemes and different permutations of Rayleigh damping matrix formulations and types of solvers. The IDAs were conducted on a parallel cluster with 160 processors using the 44 ground motions from the FEMA P695 far-field record set.

Time integration scheme	**Rayleigh damping matrix**	**Type of solver**	$\boldsymbol{\Delta t}$ (10^{-4} s)	**Runtime** (min)
Average acceleration	$a_M\boldsymbol{M} + a_K\boldsymbol{K}_{current}$ *non-constant*	Sparse	≤ 50	118
Central difference	$a_M\boldsymbol{M} + a_K\boldsymbol{K}_{current}$ *non-constant*	Sparse	1.5	154
Central difference	$a_M\boldsymbol{M} + a_K\boldsymbol{K}_{initial}$ *constant*	Sparse *factor once*	1.5	32
Central difference	$a_M\boldsymbol{M}$ *constant and diagonal*	Diagonal *factor once*	1.5	27

P695 (FEMA 2009b), are proposed in this section. FEMA P-58 recommends conducting either MSA or IDA to assess the seismic performance of individual buildings, while FEMA P695 recommends performing IDA on a set of structural archetypes to quantify seismic performance factors used in building design codes. These standards, however, recommend conducting a modified version of IDA, for which specialized parallel algorithms have been developed by Hardyniec and Charney (2015); the algorithm presented here is to conduct *full* IDA, as originally proposed by Vamvatsikos and Cornell (2002). The results of both MSA and *full* IDA can be used to compute a hazard-consistent collapse fragility curve, as described in Chapter 4/Chandramohan et al. (2016a) and Chapter 5 respectively. Conducting MSA and IDA typically involves the simulation of structural response under a large number of ground motions scaled to different intensity levels, which can often take days or even weeks to run sequentially, making them suitable candidates for parallelization. Analyses of this magnitude, typically used to accurately characterize the uncertainty in structural response stemming from uncertainty in the characteristics of (*i*) the anticipated ground motions and (*ii*) the structural model, are presently confined to research practice. It is hoped that the development of algorithms to conduct them more efficiently, in conjunction with the advancement in available computational resources and easy access

to high-performance computing resources like NHERI DesignSafe-CI (NHERI 2016), enables their adoption in structural design and assessment practice as well in the near future. In line with this objective, Tcl scripts implementing the proposed algorithms in OpenSees have been made available with an open-source license at the git repository linked to in § 7.6. These scripts can be run using OpenSeesMP, a version of OpenSees that implements the message passing interface (MPI) (Gropp et al. 2014), thereby enabling structural response simulations to be conducted in parallel.

Vamvatsikos (2011) proposes a number of algorithms to conduct IDA in parallel, some of which are tailored for use on multi-core computers and others on distributed parallel clusters. This distinction is often necessary since the two types of parallel computers impose unique constraints on computations conducted on them. Multi-core computers, for example, typically contain only around 4–12 processors, but are generally privately owned, and hence, do not impose any restrictions on the durations of the analyses. Since the primary bottleneck on multi-core computers is the number of available processors, the main objective of a parallel algorithm is to ensure that all available processors are optimally used at all times. Distributed parallel clusters like those provided by NSF XSEDE (Towns et al. 2014), on the other hand, can contain thousands to hundreds of thousands of processors. Since these computers are commonly shared with other users though, they generally use job scheduling policies that limit the durations of jobs that can be run on them to around 24 h–48 h. Hence, the primary objective of a parallel algorithm used on large clusters is often to complete the analysis in the shortest amount of time, using as many processors as available. An ideal parallel algorithm, however, should be scalable, i.e., it should be efficient irrespective of the number of processors it is used with (Pacheco 2011, § 2.6). Additionally, a simple algorithm is to be preferred over a complex one, as long as their performances are comparable. The objective of this study, therefore, was to develop a single, simple MPI algorithm for each type of analysis, that provides comparable speedup when run on both multi-core computers and distributed parallel clusters, to cater to the diverse needs of structural engineering researchers and practitioners.

7.4.1 Algorithm to conduct MSA in parallel

Multiple stripe analysis (MSA) is conducted by analyzing the structure under multiple sets of hazard-consistent ground motions, each reflecting the site-specific seismic hazard at a different ground motion intensity level, typically represented by $S_a(T_1)$. Algorithms to conduct MSA in parallel can exploit the fact that the complete list of simulations to be run is known beforehand, and the results from one simulation (analysis of the structure under one ground motion) do not have any bearing on the other simulations, i.e., there are no dependencies among the simulations. This renders conducting MSA an *embarrassingly parallel* problem.

The described algorithm assumes that each simulation is conducted on one processor, although it is easily extended to the case where a single simulation is run on more than one processor by domain decomposition. Domain decomposition is not recommended unless the number of available processors, n, exceeds the total number of simulations to be run, m. It may, however, be necessary when the longest simulation cannot be successfully completed on just one processor within the job duration limit prescribed by the scheduling policy implemented on parallel clusters. Load balancing: the process of distributing jobs equivalently to all available processors so as to optimize resource usage and minimize runtime, is not required when $n \geq m$. If $n < m$, however, some form of load balancing is recommended for optimal efficiency. The proposed algorithm employs a dynamic load balancing scheme, wherein processors are assigned tasks to execute in real-time as they complete executing other tasks. Dynamic load balancing is achieved using a master-slave design, wherein the master process maintains a stack of the ground motions the structure needs to be analyzed under. When requested for a ground motion by an idle slave process, it *pops* one from this job stack. Each slave process repeatedly requests a ground motion from the master, simulates the response of the structure under it, and writes a binary flag indicating whether collapse occurred to a text file. If additional structural response information like peak story drift ratio (SDR) is required, this information could also be written to disk. These text files are later accessed in the post-processing stage for collapse fragility computation using, for example, the methods described in Baker

(2015). The efficiency of each structural response simulation is improved by checking if the structure has collapsed at regular intervals, for instance, after simulating response under every 1 s ground motion interval, and immediately halting execution if it has. This helps avoid simulating structural response beyond the point of collapse, which can be particularly wasteful when collapse occurs during the early stages of a long duration ground motion.

It is trivial to incorporate checkpoint/restart functionality in the algorithm, to enable an analysis aborted at a certain point to resume execution from the same point when restarted. This is accomplished by ensuring that the analysis results corresponding to a ground motion have not been written to disk before adding the ground motion to the master job stack at the start of the analysis. Simulations that did not complete execution at the time the job was aborted though, will have to begin from scratch. The need to analyze more than one structural model back-to-back is encountered at times, e.g., when explicitly accounting for model uncertainty (e.g., Gokkaya et al. 2016) or performing community-level performance assessment studies (e.g., Burton 2014, Chapter 8). Nevertheless, the ability to analyze more than one structure is also easily incorporated in the proposed algorithm by adding jobs defined not just by a ground motion name, but also a structural model name, to the master job stack and dynamically allocating these jobs to slave processes. The proposed algorithm to analyze one structural model is summarized in Algorithm 7.1.

The efficiency of the algorithm was quantified by analyzing the steel moment frame building described in § 7.3.3 under eight sets of 40 ground motions each (320 ground motions in total), selected to represent the seismic hazard at San Francisco, following the procedure described in Chapter 4/Chandramohan et al. (2016a). All simulations were conducted using the central difference time integration scheme and a constant damping matrix. The analysis was repeated using different numbers of Intel Xeon E5-2640 v3 processors, n, and the runtimes, $T(n)$, are plotted in Figure 7.7a. Each value of $T(n)$ was computed as the average over three analyses conducted using n processors to account for the variability in the runtimes of repeated analyses. As expected, the runtimes decrease as more processors are used to conduct the analysis. The curve labelled "*w/o Oversubscription*" corresponds to the case where n MPI

Algorithm 7.1: Conduct multiple stripe analysis (MSA) on one structural model using m ground motions in parallel.

MASTER

```
Initialize num_completed to the number of ground motions that have been previously run
Initialize a stack called runlist with the ground motions that have not been previously run
Initialize a stack called free_procs with the ids of all slave processes
while num_completed < m do
    while runlist is not empty and free_procs is not empty do
        Pop a ground motion from runlist
        Pop a slave process from free_procs
        Send the ground motion to the slave process
    end
    Receive a COMPLETE message from a slave process
    Set num_completed ← num_completed + 1
    Add the slave process to free_procs
end
Send a TERMINATE message to all slave processes
```

SLAVE

```
Receive a message from the master process
while the received message is not TERMINATE do
    Analyze the structure under the ground motion named in the message
    Write the binary collapse indicator to file
    Send a COMPLETE message to the master process
    Receive a message from the master process
end
```

processes are spawned, so that one can be bound to each of the n available processors. Although this allows each process to run uninterrupted on its own processor, it requires dedicating a processor to run the master process, whose functions require meager computational resources in comparison to the slaves. Hence, only $n-1$ simulations can be conducted simultaneously. Alternatively, the number of available processors could be oversubscribed by one process[†], i.e., $n+1$ MPI processes could be spawned to run on the n available processors. While oversubscription permits n simulations to be conducted simultaneously, it requires one or more of the slaves to share CPU time with the master, which results in slightly reduced performance. The influence of oversubscription on performance can be mitigated by ensuring that the master process does not occupy a processor for inordinate amounts of time while polling for messages from slaves. Modern MPI libraries do provide fine-grained controls to instruct idle processes to yield the processor to other processes. Else, this behavior can be explicitly programmed using non-blocking communication between the master and slave processes, although OpenSees does not currently implement this feature. Modern MPI libraries and operating systems will also generally ensure that the processors spend the bulk of their time running the computationally intensive slave processes. Nevertheless, to avoid any ambiguity in how the processes are executed on the available processors, each slave process could be explicitly bound to a unique processor, while leaving the master process unbound. The computed runtimes when the processors are oversubscribed by one process are plotted in Figure 7.7a with the label "*w/ Oversubscription*". The loss in efficiency using each approach can be quantified by comparing the respective curves with the "*Benchmark*" curve obtained by shifting the "*w/o Oversubscription*" curve to the left by 1 processor. Hence, the benchmark case represents the scenario where n slaves are run on n processors using dynamic load balnacing, without any additional overheads due to the dedication of one processor to run the master or due to context switching. The proposed algorithm is then compared to a commonly employed, naïve approach to parallelizing MSA, wherein ground motions are statically distributed to processors based on their serial number within a set, without using any static or dynamic load balancing techniques.

[†]Thanks again to Frank McKenna for this idea.

Runtimes using this naïve approach are plotted with the label "*No load balancing*".

The parallel efficiency of the algorithm, $E(n)$, was computed using

$$E(n) = \frac{T(1)}{nT(n)} \tag{7.4}$$

for different values of n and all the four cases discussed above. $T(1)$ in Equation (7.4) refers to the runtime using the most efficient sequential implementation of the algorithm. In this case, $T(1)$ is taken as ordinate of the "*Benchmark*" curve from Figure 7.7a corresponding to $n = 1$. The computed values of $E(n)$ are plotted in Figure 7.7b. The inverted U-shape of the "*w/ Oversubscription*" and "*w/o Oversubscription*" curves indicates that the parallel algorithm most efficiently utilizes all the available processors when used with around 4 to 40 processors. The decrease in efficiency indicated by both curves as n is lowered below 4 is caused by the overhead induced by the master process, as discussed previously. The benchmark curve indicates that the efficiency of the proposed algorithm is near-optimal for n lesser than about 20 in the absence of this overhead. Although 1.0 represents a theoretical upper limit for $E(n)$, the values of $E(n)$ slightly greater than 1.0 plotted in Figure 7.7b are caused by the variability in the runtimes of repeated analyses. The impact of the overhead, indicated by the vertical separation of the two curves from the benchmark curve, is seen to be relatively small when using around 4 to 20 processors, and negligible when using more than 20 processors. This indicates that the overhead induced by the additional master process is not a significant concern when using around 4 or more processors, which represents the most likely scenario when modern parallel computers are employed to conduct structural analyses. Oversubscribing the number of available processors by one process is observed to exhibit significantly improved performance with respect to the case without oversubscription only when n is small (lesser than about 4 in this case). This indicates that the dedication of one processor to run the master process is, again, less of a concern when 4 or more processors are used, which covers most practically encountered scenarios. The efficiency of 0.5 corresponding to the "*w/ Oversubscription*" curve at $n = 1$ indicates that the implementation of the proposed algorithm is not ideal, since it allows a master and slave

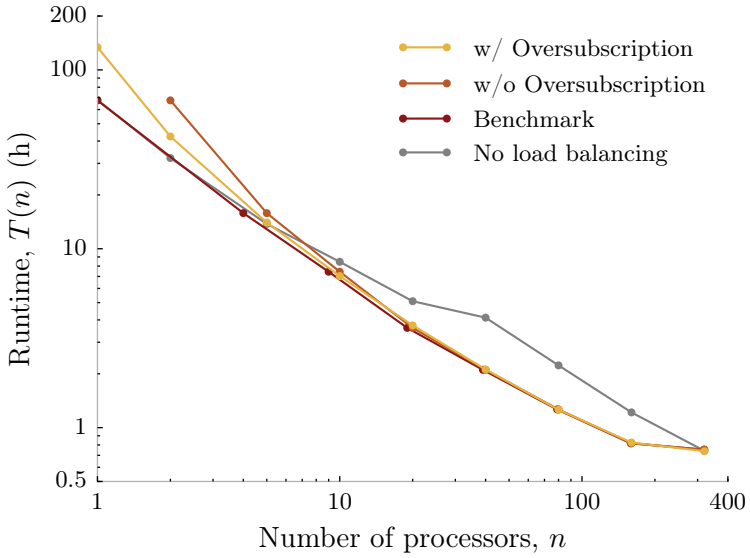

(a)

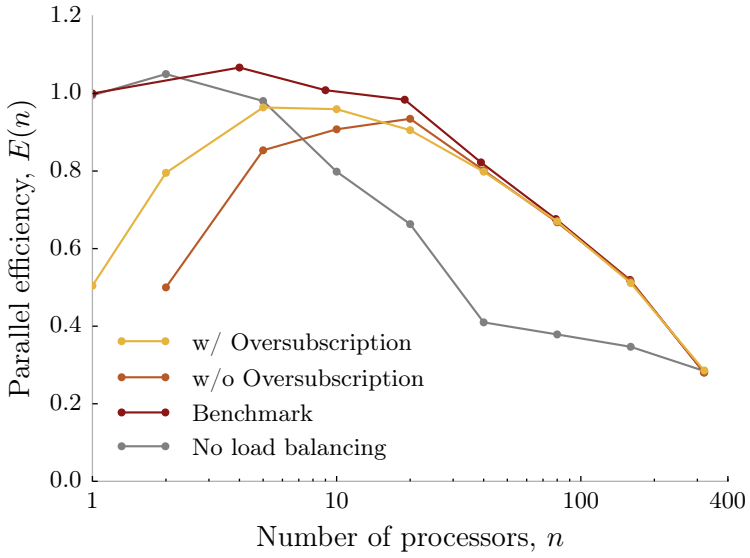

(b)

Figure 7.7: (a) Runtime and (b) efficiency of the proposed algorithm to conduct multiple stripe analysis (MSA) in parallel on different numbers of processors. The yellow and orange curves quantify the performance of the algorithm with and without the oversubscription of the number of available processors by one process, respectively. The red benchmark curve indicates the performance of the proposed algorithm without any overheads induced by the master process. The gray curve quantifies the efficiency of an alternative naïve parallel algorithm that does not employ any static or dynamic load balancing.

process that are bound to the same processor, to share it equally. The efficiency of the algorithm at small n could potentially be improved by ensuring that the master process does not inordinately occupy a processor while waiting for messages from the slaves.

The decrease in efficiency as n is increased above 40, however, is a consequence of the reduction in the effectiveness of the employed dynamic load balancing scheme. Once the master job stack is empty, i.e., all jobs have been allotted to slaves and are awaiting completion, the duration that each processor remains idle from the time it completes its final simulation until the last processor completes its final simulation, represents unused processor time that impacts parallel efficiency. This total unused processor time generally increases as the m/n ratio, which represents the average number of simulations per processor, decreases, or equivalently, when n increases for a given m. As a limiting case, when n is increased above m, the runtime remains constant, which translates to a decrease in efficiency as $1/n$. If more processors are available than ground motions, the use of multiple processors to conduct each simulation by domain decomposition could be considered for improved efficiency. The peak of the efficiency curve is found to occur at approximately $n = 10$ to 20, where the total impact of the additional master process (which decreases with n) and the dynamic load balancing scheme (which increases with n) is the least.

The efficiency of the naïve approach to parallelizing MSA without any load balancing is found to be close to optimal for n lesser than about 5, where load balancing is not as critical. As n is increased above 5, however, the efficiency drops significantly below that of the proposed algorithm due to the absence of effective load balancing. As an example of the potential benefits of load balancing, the runtime using 40 processors with load balancing is 2.1 h, which is nearly half the runtime without load balancing: 4.1 h. As n approaches m, however, the impact of load balancing diminishes again until the point where $n = m$ and one ground motion is run per processor, which requires no load balancing.

Since the problem being solved is embarrassingly parallel, keeping the number of processors per simulation fixed, the only means to improve the efficiency of the algorithm is by smarter load balancing. If the central difference time integration

scheme is used to conduct the analyses, the duration of each simulation is known to be directly proportional to the length of the ground motion, which makes it easy to implement static load balancing techniques (Xu and Lau 1997). Although dynamic load balancing techniques can be slightly less efficient compared to static load balancing techniques in certain situations, especially when n is large, they are preferred here because of their relative simplicity. Dynamic load balancing, however, is likely to be the more efficient option when implicit schemes are used, since they render the duration of a simulation difficult to predict for reasons described in § 7.3.1.

Another method to achieve dynamic load balancing, that does not require a master-slave hierarchical structure, involves using a text file as a job stack. In this method, the list of ground motions to be run is initially written to a text file. Each process reads a row from the file containing the name of a ground motion and deletes the row to prevent another process from picking up the same ground motion. It then simulates the response of the structure under the ground motion and writes the analysis results to a text file. Since this method does not suffer from any of the overheads of the master-slave configuration that result in decreased performance when n is very small, it is capable of achieving the level of efficiency indicated by the "*Benchmark*" curves in Figure 7.7. This option was, however, not adopted since it is presently not possible to atomically read from and write to a text file using OpenSeesMP, which could potentially lead to race conditions. In other words, it is not possible for one process to read from and write to a text file without other processes simultaneously reading from and writing to it, which could produce unintended consequences like multiple processes running the same ground motion, and/or a ground motion not being run at all. Additionally, it is difficult to ensure robustness against external modifications to the text file maintaining the job stack when using this method. In a computer with shared memory, the job stack could be maintained in the shared memory instead of the disk, although OpenSees does not currently implement this feature. Shared memory architectures are, however, not as scalable as distributed memory architectures.

7.4.2 Algorithm to conduct IDA in parallel

The parallel algorithm to conduct IDA proposed in this study builds on algorithms previously developed by Vamvatsikos (2011), with major differences and improvements highlighted in the ensuing description. The most important difference with respect to Vamvatsikos (2011) is that a single, efficient algorithm is developed, that can be implemented on both multi-core computers and large parallel clusters using just the basic MPI message-passing capabilities currently available in OpenSees. Conducting IDA involves simulating the response of a structure under each ground motion from a set, scaled to incrementally higher intensity levels, until it causes structural collapse. Hence, unlike MSA, the list of simulations to be run is not known beforehand, but is determined dynamically based on the results of completed simulations. This feature makes conducting IDA amenable to parallelization by dynamic load balancing using a master-slave approach, similar to the one adopted previously to parallelize MSA. Although simulations under different ground motions are independent from each other, dependencies exist between simulations involving the same ground motion scaled to different intensity levels. Conducting IDA, therefore, unlike MSA, is not an embarrassingly parallel problem.

Estimating the collapse intensity of a ground motion falls in the class of nonlinear scalar root-finding problems, for which, a number of numerical algorithms have been developed (Press et al. 2007, Chapter 9). The strategy adopted here follows the hunt and bracket approach described previously in Vamvatsikos and Cornell (2002) and Vamvatsikos and Cornell (2004), with a few modifications. In the initial *hunting* stage, the structure is analyzed under the ground motion scaled to linearly increasing intensities, spaced by a constant $\Delta S_a(T_1)$ value, until structural collapse is observed. Linearly increasing intensities are favored over quadratically increasing intensities, as proposed by Vamvatsikos and Cornell (2002), Vamvatsikos and Cornell (2004), and Vamvatsikos (2011), since the use of just one parameter to control the scaling of ground motion intensities makes the algorithm simpler, while maintaining a comparable efficiency. The recommendation to use quadratically increasing intensities is one of many made by Vamvatsikos and Cornell (2002), Vamvatsikos and Cornell

(2004), and Vamvatsikos (2011) to mitigate the effects of numerical non-convergence. These measures are obviated by the use of the central difference scheme for reasons described in § 7.3.2. Once structural collapse is observed in one of the hunt stage simulations, the *bracketing* stage initiates, wherein the bisection algorithm is employed to estimate the collapse intensity to a finer precision. At the start of the bracketing stage, $S_a(T_1)^{collapse}$ is assigned the lowest hunt stage intensity at which collapse is observed, and $S_a(T_1)^{no-collapse}$ is initialized to $S_a(T_1)^{collapse} - \Delta S_a(T_1)$. The first level of bisection is conducted at the intensity level halfway in between $S_a(T_1)^{no-collapse}$ and $S_a(T_1)^{collapse}$. If structural collapse is observed at this intensity level, the value of $S_a(T_1)^{collapse}$ is updated to this intensity, else the value of $S_a(T_1)^{no-collapse}$ is. k such levels of bisection are conducted, after which, the ground motion collapse intensity is conservatively estimated as the final value of $S_a(T_1)^{no-collapse}$. A $1/3 - 2/3$ rule was proposed by Vamvatsikos (2011) as an alternative to the bisection algorithm, also in an effort to mitigate the consequences of numerical non-convergence. The bisection algorithm is, however, more efficient in the absence of numerical non-convergence using the central difference scheme. No *filling* stage, as described in Vamvatsikos and Cornell (2002), is necessary, since the objective here is only to estimate the ground motion collapse intensity, not to trace the entire IDA curve to a fine precision. The proposed algorithm can, however, be easily be extended to incorporate such a filling stage. The chosen values of $\Delta S_a(T_1)$ and k determine the precision of the estimated ground motion collapse intensities. The benefits of using quadratically increasing ground motion intensities can be closely replicated using a relatively large $\Delta S_a(T_1)$ value. As noted in Vamvatsikos and Cornell (2004), however, coupled with the absence of a filling stage, using $\Delta S_a(T_1)$ values that are too large could increase the likelihood of skipping an instance of structural *resurrection*, thereby overestimating the ground motion collapse intensity. Structural resurrection refers to the phenomenon where the structure does not collapse when analyzed under a ground motion scaled to certain intensities above its collapse intensity.

The sequential implementation of the hunt and bracket approach to estimate the collapse intensities of a set of m ground motions is relatively straightforward. The efficiency of a parallel implementation, however, is largely determined by the ability

to meet two conflicting goals:

(i) to keep all available processors occupied; and

(ii) to minimize the execution of superfluous simulations.

The proposed algorithm employs a master process to maintain a job queue, which allows more fine-grained control over the scheduling of jobs compared to the stack structure that was used in § 7.4.1. Each job is completely defined by a ground motion name and the intensity it is to be scaled to, typically represented by an $S_a(T_1)$ value. When requested for a job by an idle slave process, the master dequeues one from the head of this queue. Each slave process repeatedly requests a job from the master, simulates the response of the structure under the specified ground motion scaled to the specified intensity, and communicates the occurrence or non-occurrence of structural collapse back to the master. If additional structural response information like peak SDR is required, this information could also be sent back to the master. Based on the received value, the master decides whether jobs corresponding to that ground motion need to be added to or removed from the queue. The two-level master-slave structure of the proposed algorithm is depicted in Figure 7.8, and is relatively simpler than the three-level hierarchical structure proposed by Vamvatsikos (2011). It is again assumed that each simulation is conducted on a single processor, although the reasons discussed in § 7.4.1 why individual simulations may need to be conducted on multiple processors apply here as well.

When the master creates the job queue at the start of the hunt stage, it begins by enqueueing m jobs corresponding to all the ground motions scaled to the intensity $\Delta S_a(T_1)$. It then enqueues m more jobs corresponding to all the ground motions taken in the same sequence, scaled to $2 \times \Delta S_a(T_1)$, and so on, until jobs corresponding to intensities high enough to safely exceed the largest anticipated ground motion collapse intensity are enqueued. Enqueueing jobs in an interwoven manner as described here, ensures maximum possible separation between jobs requiring analysis under the same ground motion scaled to different intensities, in the queue. This separation helps minimize the likelihood of the simultaneous execution of such jobs, and thereby decreases the likelihood of running superfluous simulations above the ground motion

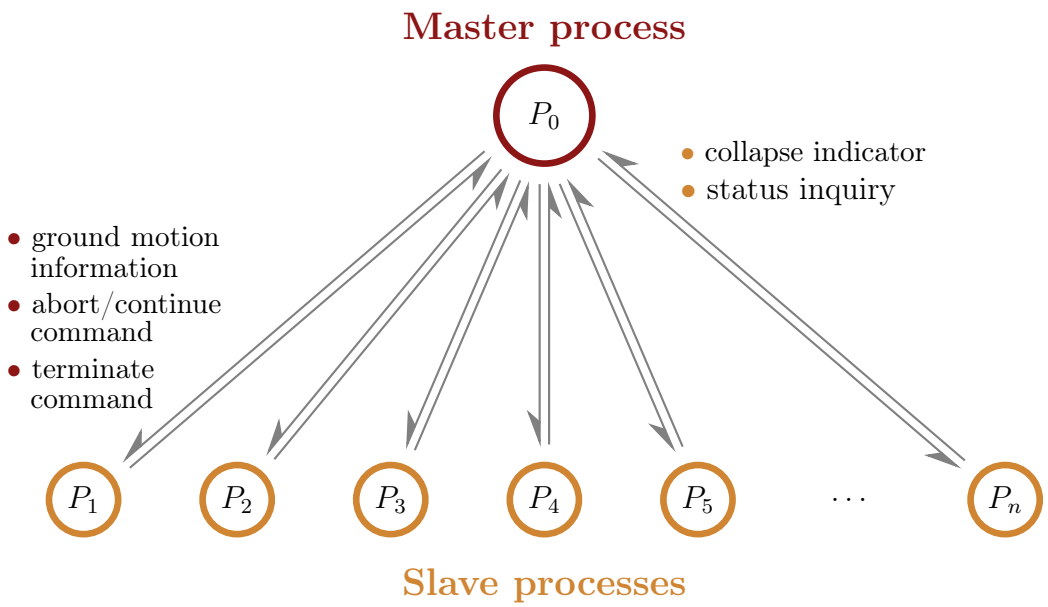

Figure 7.8: Schematic of the two-level master-slave hierarchical structure of the proposed algorithm to conduct incremental dynamic analysis (IDA) in parallel.

collapse intensities. Since jobs are dequeued from the head of the queue, hunt stage jobs corresponding to low ground motion intensities are executed first before moving on to higher intensity levels.

At the start of the hunt stage, the $S_a(T_1)^{no-collapse}$ values of all ground motions are set to 0, and their $S_a(T_1)^{collapse}$ values to ∞. When a slave reports to the master that a ground motion scaled to a certain intensity has caused structural collapse, the master (i) updates the $S_a(T_1)^{collapse}$ value of the ground motion to that intensity if it is lower than the current value of $S_a(T_1)^{collapse}$ and (ii) removes jobs in the queue corresponding to higher intensities of that ground motion. If, additionally, all other simulations corresponding to that ground motion at lower intensities have also completed and did not cause collapse, the bracketing stage of that ground motion is begun by setting $S_a(T_1)^{no-collapse}$ to $S_a(T_1)^{collapse} - \Delta S_a(T_1)$. It is important to wait until all the lower intensities have not caused collapse, and not just the intensity immediately below it, to ensure that structural resurrection has not occurred.

Bracketing stage jobs are identified by the scalar δ, which represents a ground motion intensity computed using the expression $S_a(T_1)_0^{no-collapse} + \delta\Delta S_a(T_1)$, where

$S_a(T_1)_0^{no-collapse}$ refers to the $S_a(T_1)^{no-collapse}$ value at the start of the bracketing stage. The $\delta = 1/2$ job corresponding to the first bisection level is enqueued at the head of the queue. All potential jobs corresponding to subsequent bisection levels, e.g., $\delta = 1/4, 3/4$ corresponding to the second bisection level, $\delta = 1/8, 3/8, 5/8, 7/8$ corresponding to the third bisection level, and so on until the k^{th} bisection level, are enqueued at the tail of the queue. The slave that completed the last hunt stage job is likely to begin executing the $\delta = 1/2$ job immediately. Hence, the bracketing stage begins at the first bisection level. Enqueueing later bisection level jobs at the tail of the queue ensures maximum separation from the first bisection level job, thereby giving the first bisection level job the largest possible amount of time to complete before potentially superfluous jobs belonging to later bisection levels begin. When a slave completes execution of a bisection stage job, the master updates the $S_a(T_1)^{collapse}$ value of the ground motion to the intensity of the completed simulation if collapse occurred and the intensity is lower than the current value of $S_a(T_1)^{collapse}$. If collapse has not occurred and the intensity is higher than the current value of $S_a(T_1)^{no-collapse}$, the $S_a(T_1)^{no-collapse}$ value is updated instead. The master then removes jobs in the queue corresponding to that ground motion at intensities higher than $S_a(T_1)^{collapse}$ and lower than $S_a(T_1)^{no-collapse}$. The completion of the current bisection level is indicated by the absence of any intensities associated with that bisection level (e.g., intensities identified by $\delta = 1/4, 3/4$ associated with the second bisection level) in the interval $\left(S_a(T_1)^{no-collapse}, S_a(T_1)^{collapse}\right)$, which excludes the end points. If the completion of a bracketing stage job signals the end of the current bisection level, the only remaining job from the next bisection level, if present in the queue, is moved to the head, and jobs from later bisection levels, also if present in the queue, are moved to the tail, for reasons described previously. Once the final bisection level is complete, the $S_a(T_1)^{no-collapse}$ value represents the estimated ground motion collapse intensity. A collapse fragility curve can then be fit to the estimated collapse intensities of all the ground motions using one of the methods described in Baker (2015).

To further improve the efficiency of the proposed algorithm, a strategy was devised to abort currently running jobs that have either already simulated collapse, or have been rendered redundant by the completion of another job. As part of this strategy,

each slave simulates the response of the structure under a ground motion scaled to a particular intensity, in batches of time steps, for instance, corresponding to 1 s ground motion intervals. Upon the execution of each batch of time steps, it (*i*) checks if collapse has already occurred and aborts the simulation if it has; and (*ii*) sends a message to the master requesting a status update. The master, in turn, checks whether recent developments have pushed either the ground motion's $S_a(T_1)^{collapse}$ value below the intensity of the simulation, or its $S_a(T_1)^{no-collapse}$ value above the intensity, thereby rendering the simulation redundant. If the simulation is deemed to have become redundant, the master sends a message back instructing the slave to abort the simulation and start a new job, else it instructs the slave to continue running the next batch of time steps. These regular intermediate checks are extremely quick and do not significantly affect the efficiency of jobs that do not have to be aborted.

The following details of each job are written to disk by the master immediately upon completion, to implement checkpoint/restart functionality: (*i*) ground motion, (*ii*) intensity, (*iii*) collapse indicator, (*iv*) $S_a(T_1)^{no-collapse}$, (*v*) $S_a(T_1)^{collapse}$, and (*vi*) bisection level (if applicable). The master could then check for the existence of previous, incomplete analysis results, and take them into account when creating the initial job queue. This algorithm is also easily extended to the case where IDA needs to be conducted on multiple structures, by slightly modifying the way the job queue is initially populated with the hunt stage jobs. It is recommended to first enqueue the lowest intensity jobs corresponding all structures, followed by the second lowest intensity jobs with the structures taken in the same sequence, and so on, to again ensure maximum separation between simulations analyzing the same structure under the same ground motion scaled to different intensities. All other tasks remain the same, except for additional accounting requirements for the master to keep track of which structure each job belongs to. The proposed algorithm to analyze one structural model is summarized in Algorithm 7.2.

Algorithm 7.2: Conduct incremental dynamic analysis (IDA) on one structural model using m ground motions in parallel.

MASTER

Data: $\Delta S_a(T_1)$, k, max_jobs

for $i \leftarrow 1$ **to** max_jobs **do**
  for $j \leftarrow 1$ **to** m **do**
    Enqueue job with ground motion j scaled to intensity $i \times \Delta S_a(T_1)$ to the *runlist* queue
  end
end
for $j \leftarrow 1$ **to** m **do**
  Set $S_a(T_1)^{no-collapse}[j] \leftarrow 0$
  Set $S_a(T_1)^{collapse}[j] \leftarrow \infty$
end
Enqueue/dequeue jobs to/from *runlist*, infer analysis stage, and modify $S_a(T_1)^{no-collapse}$ and $S_a(T_1)^{collapse}$ values based on previously conducted incomplete analyses if they exist
Initialize $num\_completed$ to the number of ground motions that have previously completed execution
Initialize a stack called $free\_procs$ with the ids of all slave processes
while $num\_completed < m$ **or** *runlist* is not empty **or** length($free\_procs$) $< n$ **do**
  while *runlist* is not empty **and** $free\_procs$ is not empty **do**
    Dequeue a ground motion and intensity from the head of *runlist*
    Pop a slave process from $free\_procs$
    Send the ground motion and intensity to the slave process
  end
  Set $status\_check\_flag \leftarrow$ True
  while $status\_check\_flag$ is True **do**
    Receive a message from a slave process along with the ground motion number j and intensity $S_a(T_1)$ it has been running

```
        if the received message is STATUS then
            if S_a(T_1) > S_a(T_1)^collapse[j] or S_a(T_1) < S_a(T_1)^no−collapse[j] then
                Send an ABORT message back to the slave process
            else
                Send a CONTINUE message back to the slave process
            end
        else
            Add the slave process to free_procs
            Set status_check_flag ← False
        end
    end
    if simulation was not aborted then
        if collapse occurred then
            Set S_a(T_1)^collapse[j] ← min[S_a(T_1)^collapse[j], S_a(T_1)]
            Dequeue all jobs from runlist corresonding to ground motion j at
            intensities greater than S_a(T_1)^collapse[j]
        end
        if the simulation signals the end of ground motion j's hunt stage then
            Set S_a(T_1)^no−collapse[j] ← S_a(T_1)^collapse[j] − ΔS_a(T_1)
            Enqueue the first bisection level job at the head of runlist
            for i ← 2 to k do
                Enqueue the i^th bisection level jobs at the tail of runlist
            end
        end
        if simulation was from bracketing stage and collapse did not occur then
            Set S_a(T_1)^no−collapse[j] ← max[S_a(T_1)^no−collapse[j], S_a(T_1)]
            Dequeue all jobs from runlist corresonding to ground motion j at
            intensities lower than S_a(T_1)^no−collapse[j]
        end
    end
```

```
50      if simulation was from the bracketing stage and it signals the completion of a
        bisection level of ground motion j then
51          Move the job in runlist corresponding to ground motion j's next bisection
            level to the head if present
52          Move jobs in runlist corresponding to ground motion j's later bisection
            levels to the tail if present
53      end
54      if simulation was not aborted then
55          Write the intensity, collapse indicator, S_a(T_1)^{no-collapse}[j], S_a(T_1)^{collapse}[j],
            and analysis stage to a text file corresponding to ground motion j
56      end
57      Set num_completed to the number of ground motions whose hunt and bracket
        stages have been completed
58  end
59  Send a TERMINATE message to all slave processes
```

```
SLAVE
Data: batch_size
Receive a message from the master process
while the received message is not TERMINATE do
    Scale the specified ground motion to the specified intensity and split it into
    num_batches batches of size batch_size
    for i ← 1 to num_batches do
        Analyze the structure under batch i of the ground motion
        Send a STATUS message to the master process
        Receive a message from the master process
        if the received message is ABORT then
            break
        end
    end
    if the simulation was aborted then
        Send an ABORTED message to the master process
    else
        Send a binary collapse indicator to the master process
    end
    Receive a message from the master process
end
```

The efficiency of the proposed algorithm was again quantified by analyzing the steel moment frame building using the 44 ground motions from the FEMA P695 far-field records set. All simulations were conducted using the central difference time integration scheme and a constant damping matrix. The runtimes using different numbers of processors are plotted in Figure 7.9a, and the parallel efficiencies computed using Equation (7.4) are plotted in Figure 7.9b. Cases with and without the oversubscription of the number of available processors by one process are considered separately as before. These are compared to the benchmark, which quantifies the performance of the underlying algorithm when not affected by the overheads induced

by the additional master process. The benchmark runtime corresponding to $n = 1$ was used as the reference sequential runtime, $T(1)$, to compute all parallel efficiencies since the parallel algorithm conducted using one slave processor exactly reproduces the sequential version of the algorithm by not permitting any superfluous analyses. As observed previously for the MSA algorithm, a comparison to the benchmark case indicates that the overheads are insignificant when n is greater than about 4. Over-subscribing the number of available processors by one process is again observed to produce a significant improvement in efficiency only at small values of n (lesser than about 4). The inverted U-shape of the efficiency plot is similar to that obtained for the MSA algorithm, although the increase in the likelihood of encountering aborted and superfluous simulations with n, contributes to the decreased efficiency at large values of n. The performance of the proposed algorithm is again compared to a commonly employed, naïve approach to parallelizing IDA, wherein ground motions are statically distributed to processors based on their serial numbers within a set, without any static or dynamic load balancing. The processors then execute sequential versions of the hunt and bracket procedure for each ground motion they are assigned. Although this approach performs well for small values of n, its performance quickly deteriorates as n is increased above 5, in spite of conducting no superfluous analyses, due to the lack of effective load balancing. This approach limits the maximum number of processors that can be used to m, which is 44 in this case. No noticeable improvement in efficiency is observed when using 11, 22, or 44 processors instead of 10, 20, or 40 processors respectively, such that all processors execute equal numbers of ground motions. The observation that the runtime using 40 processors with load balancing: 1.3 h, is nearly half the runtime without load balancing: 2.4 h, provides a measure of the importance of effective load balancing.

Using a disk-based text file to implement a dynamic load balancing scheme is again a feasible alternative to the master-slave hierarchical structure, that eliminates all overheads and is capable of attaining the efficiency described by the "*Benchmark*" curve in Figure 7.9. This method would require each slave to assume all the responsibilities of the master described above. They would have to update the text files used to implement the job queue, and the current status of each ground motion, including

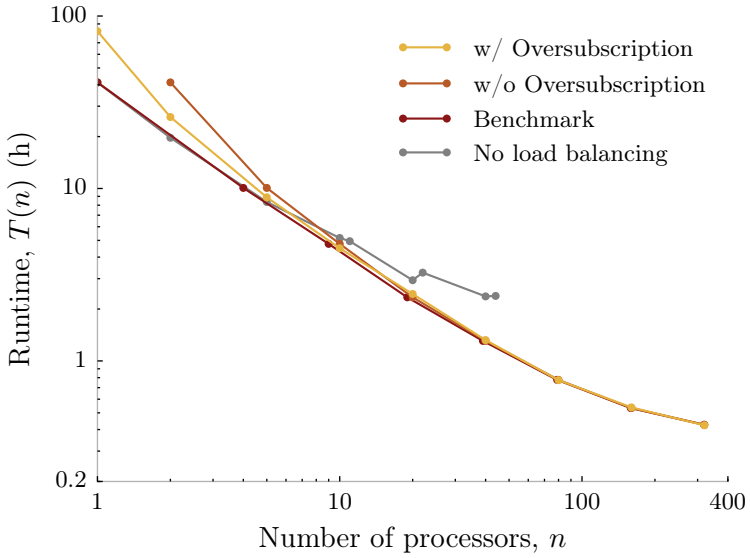

(a)

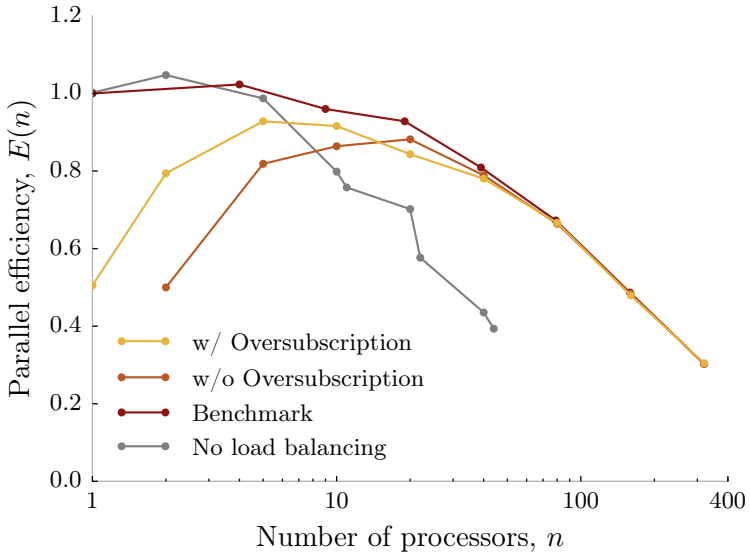

(b)

Figure 7.9: (a) Runtime and (b) efficiency of the proposed algorithm to conduct incremental dynamic analysis (IDA) in parallel on different numbers of processors. The yellow and orange curves quantify the performance of the algorithm with and without the oversubscription of the number of available processors by one process. The red benchmark curve indicates the performance without any overheads induced by the master process. The gray curve quantifies the efficiency of an alternative naïve parallel algorithm that does not employ any static or dynamic load balancing.

its $S_a(T_1)^{no-collapse}$ and $S_a(T_1)^{collapse}$ values, upon the termination of each simulation. Upon executing each batch of time steps, they could infer from the contents of these text files, whether or not they need to abort their current simulation and proceed to the next job. This option was, however, not chosen due to the current inability to implement atomic file input/output operations in OpenSeesMP, as described previously in § 7.4.1.

7.5 Conclusion

The explicit central difference time integration scheme was demonstrated to be a robust and efficient alternative to commonly used implicit schemes like the Newmark average acceleration scheme, when numerically simulating the nonlinear dynamic response of structures. Its robustness is attributed to its non-iterative nature, which makes it immune to numerical non-convergence issues that implicit schemes frequently suffer from. The issue of numerical non-convergence when using implicit schemes is widely acknowledged and even finds mention in modern structural design standards like ASCE (2016) (Chapter 16) in the form of *unacceptable responses*. As per conventional practice, persistent numerical non-convergence that cannot be resolved using strategies like (*i*) trying alternative solution algorithms; (*ii*) reducing the analysis time step; and (*iii*) trying alternative time integration schemes that possess algorithmic damping properties, is commonly interpreted as an indicator of structural collapse. The consequence of this practice was quantified by conducting incremental dynamic analysis (IDA) on a nine-story steel moment frame building using the central difference and average acceleration schemes. The median collapse capacity estimated using the average acceleration scheme was found to be 10 % lower than the value computed using the central difference scheme. This conservative underestimation of the collapse capacity using the average acceleration scheme was attributed to the incorrect interpretation of persistent numerical non-convergence encountered at intensities below the respective collapse intensities of a subset of the ground motions, to represent structural collapse.

The conditionally stable nature of the central difference scheme generally requires

analyses to be conducted using relatively small time steps. Analysis of the steel moment frame building used in this study, for instance, required a time step of 1.5×10^{-4} s, which is about an order of magnitude smaller than the time step of 5×10^{-3} s used with the average acceleration scheme. The relatively small computational cost of executing each time step, however, results in overall efficient runtimes. The efficiency of the scheme can be significantly improved by using a constant damping matrix, in which case, the dynamic tangent matrix needs to be factorized only once over the entire analysis. This feature also makes the central difference scheme very amenable to parallelization by domain decomposition. The average acceleration scheme, on the other hand, is often much faster since its unconditionally stable nature permits its use with relatively large time steps. The computationally intensive efforts made to overcome numerical non-convergence when it is encountered, however, significantly hamper its efficiency. Since non-convergence is encountered relatively frequently when conducting structural response simulations that produce significant inelastic response, the average acceleration scheme took 118 min to conduct IDA on the steel moment frame building, while the central difference scheme using a constant damping matrix took only 32 min. Use of the central difference scheme, however, does not permit the presence of massless degrees of freedom and infinitely stiff elements or penalty constraints in the structural model, which entails some additional effort during model creation.

Efficient algorithms were developed to estimate structural collapse capacity by conducting multiple stripe analysis (MSA) and incremental dynamic analysis (IDA) in parallel, both on multi-core computers and distributed parallel clusters. While conducting MSA in parallel is an embarrassingly parallel problem, conducting IDA in parallel requires addressing dependencies between simulations involving the same ground motion scaled to different intensities. Both algorithms employ dynamic load balancing schemes using a master-slave approach and incorporate checkpoint/restart functionality. The IDA algorithm is tuned to minimize the execution of superfluous simulations and incorporates the ability to immediately abort simulations that have been rendered redundant by the completion of other simulations. The parallel efficiency of these algorithms is shown to be optimal when used with a number of

processors, n, that is neither too small nor too large. For values of n less than around 4, the overheads induced by the additional master process result in slightly reduced performance. This is, however, of little concern since most practical applications of these algorithms are likely to use 4 or more processors. The reduction in efficiency for large values of n can be countered by using more processors to conduct individual simulations by domain decomposition. Each algorithm was shown to outperform its corresponding naïve parallel implementation that does not use any form of static or dynamic load balancing, at values of n larger than about 5. The proposed algorithms are implementable using just the basic MPI message-passing features currently available in OpenSees.

The recommendations of this study are broadly geared towards improving the reliability and efficiency of structural response simulations. Numerical simulations form the basis of current structural design and assessment practice, and the foundation of the modern performance-based earthquake engineering (PBEE) paradigm. The anticipated advancement in available computational capabilities over time is likely to fuel a shift towards large, complex structural models and rigorous probabilistic analysis procedures involving large numbers of ground motions and structural model realizations. It is, therefore, imperative that computational tools used by structural engineers keep pace with these technological advancements, to enable researchers and practitioners to effectively harness the computational resources at their disposal.

7.6 Software

Tcl scripts developed as part of this study to (*i*) create the numerical model of the nine-story steel moment frame building; and (*ii*) implement the algorithms developed to conduct MSA and IDA in parallel using OpenSeesMP, have been made freely available with an open-source license at the following git repository: `https://bitbucket.org/reaganc/msa_ida_parallel`. Readers are encouraged to use these scripts and report any encountered bugs.

Chapter 8

Conclusion

8.1 Summary

The broad objective of this study was to evaluate the influence of ground motion duration on structural collapse risk, and if found to be significant, to propose methods to consider it in structural performance assessment and design. To this end, the influence of ground motion duration on structural collapse capacity was first assessed by comparing the collapse response of structures under short and long duration ground motions. Care was taken in these comparisons (*i*) to use structural models that captured dominant modes of deterioration; and (*ii*) to control for the effect of response spectral shape. Upon observing a significant influence of duration on structural collapse capacity, the effect of duration on structural collapse risk was then investigated by additionally considering the durations of ground motions likely to be observed at sites with seismic hazard contributions from different types of sources. These investigations revealed the potential to obtain biased collapse risk estimates either when duration is ignored during record selection, or when it is implicitly accounted for using causal parameters like earthquake magnitude and source-to-site distance. The magnitude of this bias was found to be largest at sites likely to experience long duration ground motions from large magnitude ($M_W \sim 9.0$) interface earthquakes produced in active subduction zones. These findings prompted the development of strategies to

explicitly consider the effect of duration, in addition to response spectral shape, in common nonlinear dynamic analysis procedures like multiple stripe analysis (MSA) (Jalayer 2003, Chapter 4) and incremental dynamic analysis (IDA) (Vamvatsikos and Cornell 2002). These strategies were then simplified and individually tailored for incorporation in the following standards for structural performance assessment and design: FEMA P-58 (FEMA 2012b), FEMA P695 (FEMA 2009b), and ASCE 7-16 (ASCE 2016).

8.1.1 Influence of duration on structural collapse capacity

Previous research into the influence of duration on structural response has largely concluded that ground motion duration primarily influences cumulative damage metrics, with comparatively little effect on peak structural deformations (e.g., Cornell 1997; Bommer et al. 2004; Hancock and Bommer 2006; Iervolino et al. 2006; Hancock and Bommer 2007; Oyarzo-Vera and Chouw 2008; Barbosa et al. 2014; Hou and Qu 2015). A series of measures were adopted in this study to capture the effect of duration on peak structural deformations at ground motion intensity levels high enough to produce significant inelastic deformation and subsequent strength and stiffness deterioration. This consequently allowed demonstrating and quantifying the influence of duration on structural collapse capacity. Structural collapse capacity refers to the capacity of a structure to resist collapse under earthquake ground motions, and is described by a collapse fragility curve, which is a monotonically increasing function that relates ground motion intensity (typically quantified by $S_a(T_1)$) to a probability of collapse. The measures adopted in this study that enabled accomplishing this objective are outlined below. The reason why a number of previous studies were unable to capture this effect of duration can be attributed to their omission of one or more of these factors.

(i) *Employed realistic, deteriorating structural models.*
The structural models employed in this study incorporated the in-cycle and cyclic deterioration in strength and stiffness of the structural components, and the destabilizing $P-\Delta$ effect of gravity loads. Both model characteristics were

shown to be necessary to capture the effect of duration on structural collapse capacity. Most previous studies qualitatively attribute the effect of duration on structural response to the cyclic deterioration of strength and stiffness (e.g., Bommer et al. 2004; Beyer and Bommer 2007; Chapter 2/Chandramohan et al. 2016b; Marafi et al. 2016). A careful analysis of story drift ratio time histories under short and long duration ground motions using a newly developed response parameter called the *ratcheting inteval*, however, revealed that the gradual, unidirectional ratcheting of drifts, driven by the $P-\Delta$ effect, is an equally important mechanism by which duration influences structural collapse capacity. A parametric study conducted on a simple reinforced concrete bridge pier model, wherein individual model parameters were varied while holding others constant, helped establish that structures with rapid rates of strength and stiffness deterioration and those with larger deformation capacities are most strongly influenced by duration. A study of ductile reinforced concrete moment frame buildings also indicated a decreasing influence of duration with increasing fundamental elastic modal period, which can be explained by the fewer inelastic excursions experienced by longer period structures, which leads to a slower rate of strength and stiffness deterioration.

(*ii*) *Used long duration ground motions.*

Long duration ground motions recorded from recent large magnitude interface earthquakes like 2010 Maule (Chile, M_W 8.8), and 2011 Tohoku (Japan, M_W 9.0) were used in this study. Only a limited number of long duration ground motions recorded from earthquakes of such large magnitude were available before 2010. Hence, earlier studies on the effects of duration relied either on ground motions of relatively shorter duration recorded from lower magnitude earthquakes (refer to Figure 1.1), or on simulated ground motions, whose applicability in structural response history analysis is yet to be conclusively validated (Galasso et al. 2013; Burks and Baker 2014; Rezaeian et al. 2015).

(*iii*) *Controlled for the effect of response spectral shape.*

Two methods were used to quantify the effect of duration while controlling for

the effect of response spectral shape. The first method, used in Chapter 2, involves comparing the collapse capacities computed by conducting incremental dynamic analysis (IDA) using spectrally equivalent long and short duration record sets. These record sets were created by first assembling a set of 146 intense, long duration ground motions, with duration quantified using significant duration (Trifunac and Brady 1975), Ds, and then selecting a short duration ground motion with a response spectrum similar to each long duration ground motion. The second method, used in Chapter 5, involves fitting a linear regression model to the collapse intensities computed by conducting IDA using a generic record set, using S_aRatio (a scalar metric used to quantify response spectral shape, proposed by Eads et al. 2016) and Ds as predictors. The coefficient corresponding to Ds was then used to quantify the expected change in collapse capacity for a unit change in Ds, while holding S_aRatio constant.

(*iv*) *Used effective and efficient duration metrics.*
A number of commonly used duration metrics (described in Bommer and Martinez-Pereira 1999) were evaluated against criteria used to identify metrics that are ideally suited for use in structural performance assessment and design. Of these, significant duration, Ds, was identified as the most optimally suited duration metric from a qualitative and quantitative comparison. It was demonstrated to possess a number of useful characteristics, including (a) efficiency in predicting structural collapse capacity; (b) low correlation with response spectral shape; (c) invariance under intensity scaling of ground motions; and (d) predictability as a function of causal parameters like earthquake magnitude and source-to-site distance, using a number of readily available prediction equations, e.g., Abrahamson and Silva (1996), Kempton and Stewart (2006), Bommer et al. (2009), and Afshari and Stewart (2016). Although 5–75 % significant duration, Ds_{5-75}, was extensively used in this study, Ds_{5-95} was also found to be equally effective and efficient. Some issues are, however, anticipated if Ds_{5-95} is used in conjunction with simulated ground motions, since the late arrival of reflected seismic waves, commonly observed in simulated records, is likely to influence

Ds_{5-95} values. Ds_{5-75} is expected to be more robust against such artifacts.

(*v*) *Used the robust central difference time integration scheme.*
The explicit central difference numerical time integration scheme was preferred over more commonly used implicit schemes, like the Newmark average acceleration scheme, to conduct all nonlinear dynamic analyses, since it was shown to be robust against numerical non-convergence issues, which implicit schemes frequently suffer from. Persistent numerical non-convergence is often incorrectly interpreted to represent structural collapse when analyses are conducted using implicit schemes. Since the likelihood of encountering numerical non-convergence is larger when analyzing structures under long duration ground motions, the effect of duration on structural collapse capacity could potentially be overestimated if implicit schemes are used to conduct the simulations. Further details are provided in § 8.1.4.

When the spectrally equivalent long and short duration record sets were used to conduct IDA on a five-story steel moment frame building, the median collapse capacity estimated using the long duration set was computed to be 29 % lower. When considered along with the geometric mean Ds_{5-75} values of the records in the long and short duration sets: 42 s and 6 s respectively, this provides a measure of the influence of duration on structural collapse capacity while controlling for the effect of response spectral shape. When a linear regression model was used to fit the logarithms of the ground motion collapse intensities obtained by conducting IDA on an eight-story reinforced concrete moment frame building, using logarithms of S_aRatio and Ds as predictors, the coefficient corresponding to $\ln Ds$, c_{dur}, was computed to be -0.21. This implies that a 0.21 % decrease in collapse capacity is expected for every 1 % increase in Ds while holding S_aRatio constant. Hence, this method provides an alternate approach to quantifying the effect of duration while controlling for the effect of response spectral shape. To enable a comparison of the relative influence of duration on the two structures, the median collapse capacity of the reinforced concrete frame estimated using the long duration set was 38 % lower, and the value of c_{dur} computed for the steel moment frame was -0.12.

8.1.2 Influence of duration on structural collapse risk

The procedure to quantify the probability distribution of the durations of ground motions anticipated at a site, conditional on the exceedance of a certain ground motion intensity level, was described. These target distributions of Ds are computed using the generalized conditional intensity measure (GCIM) framework (Bradley 2010), in a manner analogous to the computation of a conditional spectrum (Abrahamson and Al Atik 2010; Jayaram et al. 2011b). The computation of different targets corresponding to each type of contributing seismic source (e.g., interface, in-slab, and crustal earthquakes) is recommended, to distinguish the unique characteristics—like frequency content and duration—of the ground motions produced by each type of source. The influence of duration can be explicitly accounted for in structural collapse risk estimation using multiple stripe analysis (MSA), by selecting ground motions to match source-specific target distributions of Ds, in addition to target conditional spectra at each intensity level.

The consequences of failing to explicitly match target distributions of Ds when selecting records for collapse risk estimation were demonstrated using an eight-story reinforced concrete moment frame building designed for a site in Seattle (Washington). Seattle is expected to experience long duration ground motions from large magnitude ($M_W \sim 9.0$) interface earthquakes in the Cascadia subduction zone, in addition to short duration ground motions from lower magnitude earthquakes on nearby crustal faults. Therefore, the selection of ground motions from the PEER NGA-West2 database (Ancheta et al. 2014)—which contains predominantly short duration ground motions—to explicitly match only target conditional spectra, was shown to underestimate the mean annual frequency of collapse, $\lambda_{collapse}$, of the structure by 29 %. Upon repeating the same analysis assuming the structure is located at a site in Eugene (Oregon), its $\lambda_{collapse}$ was found to be underestimated by 59 % when using only short duration ground motions. A larger bias was observed in the estimated collapse risk at Eugene, since unlike Seattle, its seismic hazard is almost completely dominated by long duration ground motions from interface earthquakes. On the other hand, if the structure is assumed to be located at a site in San Francisco (California), the

bias in the estimated $\lambda_{collapse}$ is only 7 %, since the durations of the ground motions anticipated at San Francisco are closer to those of the records in the PEER NGA-West2 database. The conventional practice of implicitly accounting for duration by selecting records to match target ranges of causal parameters, like earthquake magnitude, source-to-site distance, and site Vs_{30} (the time-averaged shear wave velocity of the top 30 m of the soil profile), in addition to target conditional spectra, was also shown to produce biased collapse risk estimates at all three considered sites. The inaccuracy of this method was identified to stem from (*i*) a mismatch in the durations of the selected records and the Ds targets due to limitations of the ground motion databases used for record selection; and (*ii*) the poorer fits of the selected records to the target conditional spectra, since fewer records are available for selection once screened based on causal parameters and a maximum scale factor. Similar findings by Tarbali and Bradley (2016) confirm the drawbacks of relying on causal parameters to select ground motions of appropriate duration.

A structural reliability framework was developed to enable the effect of duration to be accounted for in structural collapse risk estimation using IDA. It involves first fitting a linear regression model to the ground motion collapse intensities obtained by conducting IDA, using S_aRatio and Ds as predictors, to define a failure surface. Site-specific target distributions S_aRatio and Ds, conditional on a certain intensity level, are then integrated over the failure domain to compute the probability of collapse at that intensity level. Repeating this procedure at different intensity levels allows computing a non-parametric, hazard-consistent collapse fragility curve. The collapse fragility curve of the eight-story reinforced concrete moment frame computed using this method was found to agree well with the fragility curve computed by conducting MSA using hazard-consistent ground motions at Seattle, Eugene, and San Francisco. The ability to obtain hazard-consistent collapse risk estimates by post-processing the results of IDA conducted using a generic record set, resolves IDA's largest drawback, and makes it a competitive alternative to MSA. MSA can, in fact, be shown to represent an alternative simulation-based approach to solve the same structural reliability problem, that the proposed framework solves analytically. A simplified version of the procedure that does not require any numerical integration,

is proposed to compute just a hazard-consistent median collapse capacity instead of the entire collapse fragility curve. This simplified method is useful when a lognormal collapse fragility curve is to be computed using a hazard-consistent median and an aggregate lognormal standard deviation that accounts for model uncertainty in addition to record-to-record uncertainty (e.g., FEMA 2009b, § 7.3; FEMA 2012b, § 5.2.5).

The Abrahamson and Silva (1996) prediction equation for Ds, which was used to compute target conditional distributions of Ds in this study, predicts the lowest Ds values for large magnitude earthquakes among other alternatives like Kempton and Stewart (2006), Bommer et al. (2009), and Afshari and Stewart (2016). Hence, the influence of duration on structural collapse risk was demonstrated in this study using the most conservative prediction equation for Ds. A larger effect of duration is likely to be observed if either one of the other models is used, or the predictions of all available models are aggregated using a logic tree (Kulkarni et al. 1984; Bommer 2005).

8.1.3 Incorporating duration in standards for structural performance assessment and design

Strategies were proposed to explicitly account for the demonstrated effect of duration on structural collapse risk in the following standards for structural performance assessment and design, alongside response spectral shape:

(i) the FEMA P-58 seismic performance assessment methodology;

(ii) the FEMA P695 methodology to quantify seismic performance factors; and

(iii) the ASCE 7-16 seismic design provisions.

Two essential components of the FEMA P-58 methodology that involve structural analysis include (i) estimating structural collapse capacity and (ii) estimating structural demands given collapse has not occurred. The hazard-consistent median collapse capacity can be estimated either by conducting MSA or a modified iterative version of IDA. The effect of duration can be considered in MSA just by selecting records

at each intensity level to match site-specific target conditional distributions of Ds in addition to conditional spectra. The simplified version of the structural reliability framework described in § 5.5.4, is proposed as a simpler and more efficient alternative to the modified iterative IDA procedure. This method involves fitting a linear regression model to the ground motion collapse intensities estimated by conducting full IDA, using S_aRatio and Ds as predictors. Beginning with an initial estimate of the hazard-consistent median collapse capacity, the expected median collapse intensity is iteratively evaluated by substituting the conditional median site-specific S_aRatio and Ds targets in the fitted regression model . When estimating structural demands given collapse has not occurred, duration is expected to influence peak story drift ratios at intensity levels large enough to produce significant inelastic deformations and consequent strength and stiffness degradation. It is, however, not expected to significantly influence other structural demands like peak floor acceleration and peak floor velocity, which are commonly used to define fragility functions for non-structural components.

The modifications proposed to the FEMA P695 methodology require structural archetypes to be designed based on the seismic hazard at actual cities located in high seismic regions. This represents a refinement of the approach adopted in the current methodology, wherein structural archetypes are designed based just on generic risk-targeted maximum considered earthquake (MCE_R) (ASCE 2016, § 11.4.3) ordinates corresponding to seismic design category (SDC) boundaries (ASCE 2016, § 11.6) The objective of the proposed method is to obtain a more realistic estimate of the collapse risk of structures employing a specific structural system, at actual sites they are most likely to be deployed in. An additional advantage of this method is that it allows the computation of site-specific median S_aRatio and Ds targets. These targets can be used to compute more accurate estimates of the hazard-consistent median collapse capacities of the structural archetypes, than those obtained using SDC-specific spectral shape factors developed based on ε targets averaged over all sites that classify under an SDC. Three methods were proposed by which the hazard-consistent median collapse capacity of a structure can be computed by post-processing the results of IDA conducted using a generic record set, using site-specific median

S_aRatio and Ds targets:

(*i*) *Method 1*, which is the most accurate but also the most computationally intensive, requires full IDA to be conducted using short and long duration record sets. The short duration set contains the 44 records from the FEMA P695 far-field set, and the long duration set contains 44 records with $Ds_{5-75} > 25\,\mathrm{s}$ selected to be spectrally equivalent to the short duration set. The simplified version of the structural reliability framework, described previously as part of the recommendations to incorporate duration in FEMA P-58's IDA procedure, is then employed to compute the hazard-consistent median collapse capacity.

(*ii*) *Method 2* ranks intermediate in accuracy and computational requirements, and involves conducting modified IDA using the short and long duration record sets. Conducting modified IDA entails scaling the entire record set to different intensity levels until exactly half the records cause structural collapse. The median collapse capacities obtained using the two sets are individually corrected for the effect of spectral shape based on the site-specific median S_aRatio target and the geometric mean S_aRatio value of the records in each set. Although the existing spectral shape factor based on ε could be used here instead, it is expected to be less accurate. The hazard-consistent median collapse capacity is then computed by linear interpolation based on the site-specific median Ds target and the geometric mean Ds values of the records in each set.

(*iii*) *Method 3* is the least accurate and also the least computationally intensive. It involves conducting modified IDA using just the short duration set, as per the current FEMA P695 recommendations. The hazard consistent median collapse capacity is then adjusted based on the site-specific median S_aRatio and Ds targets, and the geometric mean S_aRatio and Ds values of the records in the set, in a manner similar to Method 2. Again, the existing spectral shape factor could be used to perform the spectral shape component of the adjustment instead of S_aRatio, but it is expected to be less accurate.

Methods 2 and 3 require one or both of the coefficients c_{ss} and c_{dur}, which quantify the magnitudes of the respective influences of response spectral shape and duration on a

structure's collapse capacity, to be predicted as functions of structural characteristics. Relations were developed to predict c_{ss} and c_{dur} for reinforced concrete ductile moment frames based on the fundamental elastic modal period of the structure, and guidelines are provided to develop similar relations for other structural systems. Upon analyzing the eight-story reinforced concrete moment frame building located in Seattle using the three proposed methods, hazard-consistent median collapse capacities of 0.70 g, 0.70 g, and 0.74 g were respectively computed, which are all close to the estimate 0.68 g computed by conducting MSA using hazard-consistent ground motions. All three estimates represent significant improvements over the value 1.13 g obtained using the current FEMA P695 methodology.

Proposals were made to incorporate the effects of response spectral shape and duration in ASCE 7-16's equivalent lateral force (ELF) procedure (ASCE 2016, § 12.8) by modifying the design base shear using site and structural system-specific adjustment factors. These adjustment factors counter the anticipated shift in the structure's median collapse capacity due to the effects of response spectral shape and duration. The adjustment factors are estimated as functions of:

(*i*) The contrast between the median S_aRatio and Ds targets at the site where the structure is to be located, and the corresponding targets at a reference site where ASCE 7-16's implicit performance target of 10 % probability of collapse at the MCE_R level is most likely to be valid.

(*ii*) The magnitudes of the respective effects of response spectral shape and duration on structural collapse capacity, as quantified by the c_{ss} and c_{dur} coefficients.

The definition of a reference site, or alternatively, reference targets, is a critical component of this calculation. The historical emphasis on coastal California during the development of seismic design provisions suggests that ASCE 7-16's performance objective is more likely to be valid at a site located in this region. Sample calculations using Los Angeles as the reference site indicate, for example, that a reinforced concrete moment frame building with a 1 s period, located at a site in downtown San Francisco, needs to be designed to a base shear that is 43 % higher than the value computed using ASCE (2016) (Equation (12.8-1)). A similar structure in Eugene

would have to be designed to a base shear that is 67 % higher. Adjustment factors computed using San Francisco as a reference site are less conservative on account of the smaller S_aRatio and longer Ds targets at San Francisco, compared to Los Angeles. The use of structural system-specific adjustment factors is recommended because different classes of structures are expected to be influenced by response spectral shape and duration, to different extents. For instance, the effect of duration, as quantified by the c_{dur} coefficient, was found to be much more pronounced in steel special concentrically braced frames (SCBFs) than steel buckling-restrained braced frames (BRBFs). The difference in their sensitivities to duration is explained by the fact that regular braces employed in SCBFs are prone to buckling and eventual fracture under cyclic loading, whereas buckling-restrained braces used in BRBFs exhibit full hysteresis loops with insignificant cyclic deterioration of strength and stiffness.

An examination of ASCE 7-16's nonlinear response history analysis (NLRHA) procedure (ASCE 2016, Chapter 16) revealed that the effect of duration on structural collapse capacity may not be adequately captured by just selecting records to match a site-specific Ds target. It was demonstrated using the example of the eight-story reinforced concrete moment frame building, that the acceptance criteria imposed on structural demands inferred from analyses conducted at the MCE_R ground motion intensity level do not reliably capture the effect of duration on the probability of collapse at the MCE_R level. The effect of duration could be captured using the secondary acceptance criterion imposed on the number of unacceptable responses out of 11 structural response simulations, but this acceptance criterion is associated with a large degree of uncertainty. The effect of duration is unlikely to be captured using the primary acceptance criterion imposed on the peak story drift ratio. Hence, it is recommended that response history analyses be conducted by scaling records to an MCE_R intensity level that is modified by the duration adjustment factor developed as part of the recommendations to incorporate the effect of duration in the ELF procedure. Additional studies are required to evaluate whether an analogous spectral shape adjustment to the MCE_R intensity level is necessary.

8.1.4 Robust and efficient estimation of structural collapse capacity

The central difference numerical time integration scheme is proposed as a more robust and efficient alternative to commonly used implicit schemes, like the Newmark average acceleration scheme, for conducting nonlinear response history analyses. Its robustness is attributed to its non-iterative nature, which makes it immune to numerical non-convergence issues that implicit schemes frequently suffer from. The conventional practice of interpreting persistent numerical non-convergence as an indicator of structural collapse was shown to result in the conservative underestimation of the median collapse capacity of a nine-story steel moment frame building by 10 %.

Although the conditionally stable nature of the central difference scheme requires analyses to be conducted using significantly smaller time steps, the relatively small computational cost of executing each time step results in overall efficient runtimes. When a constant damping matrix is used, the dynamic tangent matrix needs to be factorized just once over the entire analysis, resulting in further improvements in efficiency. The unconditionally stable nature of the average acceleration scheme permits the use of large time steps, resulting in generally faster runtimes as long as numerical non-convergence is not encountered. The computationally intensive strategies typically employed to overcome non-convergence when it is encountered, however, significantly hamper its efficiency. The larger likelihood of encountering numerical non-convergence when estimating structural collapse capacity using analysis techniques like IDA, therefore, result in significantly longer runtimes using the average acceleration scheme. For example, conducting IDA on the nine-story steel moment frame building in parallel using 160 processors required only 32 min using the central difference scheme, but took 118 min using the average acceleration scheme. Using the central difference scheme, however, entails some additional efforts during model creation to ensure that all degrees of freedom are assigned non-zero mass or moment of inertia, and extremely stiff elements or penalty constraints are not used.

Efficient parallel algorithms were developed to conduct MSA and IDA both on

multi-core computers and distributed parallel clusters. Both algorithms employ dynamic load balancing schemes using a master-slave approach and incorporate checkpoint/restart functionality. They are shown to significantly outperform their corresponding naïve parallel analogues that do not employ any load balancing, when using more than around 5 processors The algorithm to conduct IDA is tuned to minimize the execution of superfluous analyses and incorporates the ability to immediately abort simulations that have been rendered redundant by the completion of other simulations. Both algorithms are implementable using just the basic MPI message-passing capabilities currently available in OpenSees.

8.2 Conclusion

The duration of earthquake ground motion was shown to significantly influence structural collapse risk, thereby warranting its explicit consideration in structural performance assessment and design, in addition to response spectra. Ignoring ground motion duration and selecting short duration records—which currently dominate popular ground motion databases like the PEER NGA-West2 database—was shown to result in the unconservative underestimation of the collapse risk of structures at sites susceptible to long duration ground motions from large magnitude ($M_W \sim 9.0$) interface earthquakes. For example, the $\lambda_{collapse}$ of an eight-story reinforced concrete moment frame building located in Seattle (Washington), was shown to be underestimated by 29 % if short duration ground motions with hazard-consistent response spectra are used, instead of ground motions with both hazard-consistent durations and response spectra. This bias in the estimated collapse risk was shown to be larger at sites like Eugene (Oregon), whose seismic hazard is dominated by large magnitude interface earthquakes in the Cascadia subduction zone. This is in contrast to sites like Seattle, whose seismic hazard is additionally influenced by lower magnitude earthquakes from nearby crustal faults. For example, if the same structure were located in Eugene, its $\lambda_{collapse}$ was found to be underestimated by 59 % when analyzed using short duration ground motions. If the structure were located in San Francisco (California), on the other hand, $\lambda_{collapse}$ is underestimated by only 7 % since the durations of the ground

motions anticipated at San Francisco are closer to those of the records in the PEER NGA-West2 database. The prevalent practice of implicitly accounting for duration using causal parameters like rupture mechanism, earthquake magnitude, source-to-site distance, and site Vs_{30} was shown to result in the selection of records that poorly fit both duration and response spectrum targets. This result is a consequence of the limitations of ground motion databases commonly used for record selection. The demonstrated influence of duration on structural response, therefore, warrants its explicit consideration in structural design and assessment practice, following a similar line of reasoning by which ground motion response spectra are explicitly considered in design and assessment, instead of doing so implicitly via causal parameters.

Significant duration (Trifunac and Brady 1975), Ds, was shown to be better suited than other duration metrics for application in structural performance assessment and design, since it is (*i*) amenable to incorporation in a vector intensity measure consisting of response spectral shape and duration; and (*ii*) an efficient predictor of a ground motion's potential to cause structural collapse, quantified by its collapse intensity. 5–75 % significant duration, Ds_{5-75}, was used extensively in this study since it was judged to be slightly more robust and effective than Ds_{5-95}, which is more likely to be influenced by artifacts present in the record like late arrivals. Site-specific target conditional distributions of Ds can be computed in a manner analogous to the computation of a conditional spectrum, using the generalized conditional intensity measure (GCIM) framework (Bradley 2010). The effect of duration can be explicitly accounted for in structural collapse risk assessment either by (*i*) conducting multiple stripe analysis (MSA) using records selected to match site-specific target conditional distributions of Ds, in addition to target conditional spectra; or by (*ii*) employing the structural reliability framework developed in Chapter 5 in conjunction with incremental dynamic analysis (IDA). The structural reliability framework involves conducting IDA using a generic record set and fitting a linear regression model to the estimated collapse intensities using S_aRatio and Ds as predictors, to define a failure surface. The hazard-consistent collapse fragility curve is then computed by integrating the target distributions of S_aRatio and Ds, conditional on different intensity levels, over the failure domain. S_aRatio and Ds were together demonstrated to be capable of

explaining around 80 % to 85 % of the variance in the collapse intensities of ground motions used to analyze 51 reinforced concrete moment frame buildings, as indicated by the R^2 metric from the regression analyses. Excluding either S_aRatio or Ds from the regression model was found to significantly diminish its predictive power. This suggests that both response spectral shape and duration are important considerations in structural design and assessment, and that the consideration of additional ground motion characteristics is likely to produce diminishing returns.

Incorporating the cyclic deterioration in the strength and stiffness of structural components and the destabilizing $P-\Delta$ effect of gravity loads in the nonlinear structural model was shown to be critical to adequately capture the effect of duration on structural response. Structures that deteriorate rapidly under cyclic loading and ductile structures are expected to be most strongly influenced by duration. For instance, the effect of duration was found to be more pronounced in steel special concentrically braced frames (SCBFs) than steel buckling-restrained braced frames (BRBFs), since regular braces deteriorate much more rapidly under cyclic loading than buckling-restrained braces. Most previous studies have distinguished the effect of duration on cumulative damage metrics and peak structural deformations. They have largely found duration to strongly influence cumulative damage metrics, but not peak structural deformations (e.g., Cornell 1997; Bommer et al. 2004; Hancock and Bommer 2006; Iervolino et al. 2006; Hancock and Bommer 2007; Oyarzo-Vera and Chouw 2008; Barbosa et al. 2014; Hou and Qu 2015). The hysteretic models used to simulate the behavior of the structures analyzed in this study algorithmically deteriorate strength and stiffness based on the cumulative hysteretic energy dissipated, which allows translating the cumulative damage experienced under cyclic loading to amplified deformations (Ibarra et al. 2005). The use of these models, therefore, allowed quantifying the effect of duration on peak structural deformations, and consequently, on structural collapse capacity. In addition to cyclic deterioration, the gradual unidirectional ratcheting of drifts aided by the $P-\Delta$ effect was also demonstrated to drive the observed effect of duration on structural collapse capacity.

Strategies were developed to incorporate the effect of duration on structural collapse capacity, in standards for structural performance assessment and design. The

FEMA P-58 seismic performance assessment methodology describes procedures to estimate the collapse fragility curve of a structure by conducting either MSA or an iterative modified version of IDA. The effect of duration can be incorporated in MSA by just selecting ground motions at each intensity level to match target conditional distributions of duration, in addition to target conditional spectra. A simpler and more efficient alternative to the iterative modified IDA procedure, that employs a simplified version of the structural reliability framework developed in § 5.5.4, is proposed to consider the effects of duration and response spectral shape. The proposed procedure involves fitting a linear regression model to the ground motion collapse intensities computed by conducting IDA, using S_aRatio and Ds as predictors. The regression surface is then used to iteratively estimate the median collapse capacity using site-specific median S_aRatio and Ds targets computed conditional on different intensity levels. Refinements to the FEMA P695 methodology for quantifying seismic performance factors were proposed, to consider the effect of duration alongside the effect of response spectral shape. Guidelines were developed to design structural archetypes based on the seismic hazard at actual physical locations instead of generic MCE_R ground motion intensities corresponding to SDC boundaries. Three methods of varying levels of complexity, based on the structural reliability framework, were then proposed to modify the median collapse capacities estimated by conducting IDA using a generic record set, to reflect the site-specific conditional median S_aRatio and Ds targets. All three methods were demonstrated to perform better than the originally proposed spectral shape factor based on ε (Baker and Cornell 2005).

A method was proposed to incorporate the effects of response spectral shape and duration in ASCE 7-16's ELF procedure by modifying the design base shear using site and structural system-specific adjustment factors computed based on (i) the conditional median S_aRatio and Ds targets at the site; and (ii) coefficients which quantify the magnitude of the anticipated effects of response spectral shape and duration on the collapse capacity of the structure. The acceptance criteria used in conjunction with ASCE 7-16's NLRHA procedure was shown to be unable to reliably detect the effect of duration. Hence, the effect of duration cannot be adequately accounted for just by selecting records of appropriate durations. It is, therefore, recommended

that the selected ground motions be scaled to an MCE_R level modified by the duration adjustment factor described previously as part of proposed modifications to the ELF procedure. Additional research is required to determine whether an analogous adjustment to the MCE_R level for the effect of response spectral shape is necessary.

The explicit central difference numerical time integration scheme is proposed as a robust and efficient alternative to implicit schemes like the Newmark average acceleration scheme, when conducting nonlinear dynamic analyses to estimate structural collapse capacity. Its robustness is a consequence of its non-iterative nature, which makes it immune to numerical non-convergence issues that most implicit schemes suffer from, especially when large, complex structural models are analyzed under long duration ground motions. The common practice of interpreting persistent numerical non-convergence encountered when using implicit schemes, as an indicator of structural collapse, was shown to result in the conservative underestimation of the median collapse capacity of a nine-story steel moment frame building by 10 %. The central difference scheme was also shown to be more efficient than the average acceleration scheme despite the requirement to conduct analyses using smaller time steps, in order to satisfy its stability criterion. IDA was conducted on the nine-story steel moment frame using 160 processors in just 32 min using the central difference scheme, while analysis using the average acceleration scheme took 118 min. The longer runtime using the average acceleration scheme is attributed to the computationally intensive strategies employed to overcome numerical non-convergence when it is encountered. Finally, efficient algorithms that implement dynamic load balancing techniques using a master-slave approach, were developed to conduct MSA and IDA in parallel on both multi-core computers and distributed parallel clusters. These algorithms are implementable using just the basic MPI message-passing features currently available in OpenSees.

8.3 Limitations and future work

The effect of duration on structural collapse capacity can be readily captured using structural models that employ non-simulated failure modes, typically consisting of

a cycle counting scheme in conjunction with a variant of Miner's rule (Miner 1945). Such an approach is employed in this study to model the fracture of the braces in the steel SCBF models. Quantifying the influence of duration using models that attempt to explicitly simulate structural collapse response, however, requires the use of sophisticated structural models that incorporate the anticipated strength and stiffness deterioration of structural components under cyclic loading. The modified Ibarra-Medina-Krawinkler (IMK) hysteretic model (Ibarra et al. 2005) used in this study to model the hysteretic behavior of the zero-length plastic hinges located at beam-column joints in the analyzed frame structures, is an example of such a model. The IMK model is a phenomenological model that incorporates a post-capping negative stiffness branch of the backbone curve to capture in-cycle deterioration, as well as an algorithm to cyclically degrade strength and stiffness based on the cumulative hysteretic energy dissipated. Equations developed by Haselton et al. (2008) and Lignos and Krawinkler (2011) were used to predict median values of the model parameters for reinforced concrete and steel components respectively, as functions of member and cross-section properties. These predictive equations were developed based on data recorded from cyclic tests on beam-column joints, conducted primarily using loading protocols developed to simulate short duration ground motions from relatively small magnitude ($M_W < 8.0$) crustal earthquakes (e.g., ATC 1992, Chapters 4 and C.4; SAC 1997, Appendix E; Krawinkler et al. 2001). Structural components are, however, expected to exhibit different hysteretic behavior under different loading protocols, specifically under those developed to simulate long duration ground motions (Takemura and Kawashima 1997; FEMA 2009a; Krawinkler 2009; Bazaez and Dusicka 2016). Although the IMK deterioration algorithm was designed to dynamically adjust the backbone curve based on the loading history to capture these anticipated differences in the hysteretic behavior, its ability to accurately reproduce structural response under long duration ground motions has not yet been verified. This observation is expected to hold for most other commonly used phenomenological deterioration algorithms as well. Hence, the applicability of commonly used phenomenological deterioration algorithms and procedures proposed to predict their parameters using currently available cyclic test data, in simulating structural response

under long duration ground motions, requires further investigation. Recent findings from experimental tests conducted by Galanis et al. (2016), which suggest that the IMK model calibrated using equations proposed by Haselton et al. (2008) might overestimate the rate of cyclic deterioration in reinforced concrete structures under long duration ground motions, highlight the need for such investigations.

These investigations would first require the development and validation of long duration cyclic loading protocols, like the one recently proposed by Bazaez and Dusicka (2016). Data from cyclic tests conducted on structural components using these long duration loading protocols could then be used to assess the applicability of common phenomenological deterioration algorithms and equations used to predict their parameters, when simulating structural response under long duration ground motions. If found to be inadequate, either new prediction equations could be developed, or the functional forms of the deterioration algorithms could be revised as necessary. These improved hysteretic models could then be used to re-evaluate the influence of ground motion duration on structural collapse risk using the framework developed in this study. The perceived importance of accurately modeling strength and stiffness deterioration also motivates the development and use of more realistic physics-based models that explicitly capture dominant deterioration modes, including local buckling and crack initiation and propagation until fracture (Krawinkler and Zohrei 1983; Deierlein et al. 2010), instead of phenomenological models that do so implicitly. The use of long duration loading protocols could, additionally, be mandated by standards like AISC (2010) and ACI (2014) to qualify structural components to be used in structures that are likely to experience long duration ground motions. Just as the acknowledgement of the distinctive nature of the demands imposed by near-fault ground motions has prompted the development and use of near-fault loading protocols, the unique nature of the demands imposed by long duration ground motions also warrants similar consideration.

Quantifying the influence of duration on structural collapse risk required the probabilistic characterization of the durations of ground motions anticipated at various sites. The computation of site-specific target distributions of duration using the GCIM framework involves the use of equations to predict duration as a function of

causal parameters like rupture mechanism, earthquake magnitude, and source-to-site distance (e.g., Abrahamson and Silva 1996; Kempton and Stewart 2006; Bommer et al. 2009; Afshari and Stewart 2016); and models for the correlation between the ε-values of duration and $S_a(T)$ (e.g., Bradley 2011). Models are currently available only to characterize the durations of ground motions produced by shallow crustal earthquakes; such models have not yet been developed for interface and in-slab earthquakes. Therefore, the models developed for crustal earthquakes were used in this study to characterize the durations of ground motions produced by large magnitude ($M_W \sim 9.0$) interface earthquakes as well. Specifically, the Abrahamson and Silva (1996) prediction equation was used in conjunction with the Bradley (2011) model for the correlation between the ε-values of duration and $S_a(T)$. The Abrahamson and Silva (1996) equation was chosen since it was found to predict the shortest durations among the available alternatives for large magnitude earthquakes, which allowed the influence of duration on structural collapse risk to be demonstrated using the most conservative prediction model. Durations predicted by the recently developed Afshari and Stewart (2016) prediction equation, for instance, are much longer. Hence, a larger effect of duration is likely to be observed if either the Afshari and Stewart (2016) model is used, or the predictions of all available models are aggregated using a logic tree (Kulkarni et al. 1984; Bommer 2005), to compute target distributions of duration. The demonstrated increase in structural collapse risk at sites likely to experience long duration ground motions from large magnitude interface earthquakes, using the most conservative prediction equation for duration, therefore, highlights the need to develop such models for interface earthquakes as well. Recently developed capabilities to simulate ground motions from interface earthquakes using physics-based ground motion simulation tools (e.g., Frankel et al. 2007; Olsen et al. 2008; Skarlatoudis et al. 2015) also demonstrate potential for future use in characterizing seismic hazard at sites located near active subduction zones. It is worth noting that empirical ground motion prediction equations are currently limited in their ability to capture the amplification in the duration and response spectral ordinates of ground motions at sites atop sedimentary basins, e.g., Seattle, Los Angeles, and Mexico City, although some attempt to do so via a basin-depth term (Marafi et al. 2017). Physics-based

ground motion simulations, on the other hand, show tremendous promise in quantifying the seismic hazard at such sites, accounting for these basin effects (Chávez-García and Bard 1994; Frankel 2000; Pitarka 2004; Frankel et al. 2007; Olsen et al. 2008).

The proposed recommendations to incorporate the effect of duration in the FEMA P-58 methodology were limited to the consideration of peak story drift ratios and structural collapse only. These recommendations could be extended to account for residual drifts and non-structural components as well. In the strategies proposed to incorporate the effects of response spectral shape and duration in ASCE 7-16's ELF procedure, k'_{ss} and k'_{dur} adjustment factors for the design base shear were computed only for ductile reinforced concrete moment frame buildings. The number of steel moment frames and braced frames analyzed were insufficient to characterize the c_{ss} and c_{dur} coefficients used to compute these adjustment factors. Future studies could be undertaken to characterize these coefficients for different materials and structural systems as functions of structural characteristics, following the procedure outlined in the *Predicting c_{ss} and c_{dur}* section of § 6.6.2. These coefficients could then be used to compute design base shear adjustment factors for response spectral shape and duration, to design these structures using the modified ELF procedure. Such studies could also help identify materials and structural systems that are better suited than others to resist the demands imposed by long duration ground motions. The adjustment factors computed for reinforced concrete moment frames, however, help provide a sense of the magnitude of the required adjustments to the design base shear to adequately account for the effects of response spectral shape and duration. For reasons described previously, larger adjustment factors for duration are likely to be computed at sites in the US Pacific Northwest using prediction models other than Abrahamson and Silva (1996), thereby requiring structures at these sites to be designed to even larger base shears.

8.4 Concluding remarks

Previous research has demonstrated a significant influence of ground motion duration on cumulative damage metrics, but found a comparatively smaller effect on peak

structural deformations. Hence, current standards for structural performance assessment and design, which are based primarily on peak deformation demands, do not require explicit consideration of ground motion duration. This study, however, demonstrates the influence of duration on peak structural deformations and collapse risk, and develops a framework to explicitly account for its effect in structural design and assessment. The findings of this study, therefore, make a strong case for the explicit consideration of ground motion duration in structural design and assessment, instead of doing so implicitly via causal parameters like earthquake magnitude, source-to-site distance, and site Vs_{30}. This recommendation follows a similar line of reasoning behind the explicit, rather than implicit, consideration of ground motion response spectra in current design and assessment practice, on account of their demonstrated influence on structural response (e.g., Shome et al. 1998; Baker and Cornell 2006b). The primary reason for the continued emphasis on causal parameters in current design and assessment standards is to capture the cumulative damage potential of ground motions by exploiting the implicit correlation of magnitude with ground motion duration (Bommer and Acevedo 2004). The explicit consideration of both response spectra and duration will, however, permit the relaxation of guidelines related to the consideration of causal parameters. Explicitly accounting for the effect of duration using the proposed framework will ensure that structures designed at sites likely to experience long duration ground motions have equivalent margins of safety against collapse as structures designed at other sites likely to experience only short duration ground motions.

Appendix A

Spectrally equivalent short and long duration record sets

This appendix contains detailed information about the spectrally equivalent short and long duration record sets used in Chapters 3, 5 and 6. The short duration set consists of the 22 horizontal record pairs (44 individual records) from the FEMA P695 (FEMA 2009b) far-field record set. The ground motions in this set were recorded from moderately large magnitude shallow crustal earthquakes and have 5–75 % significant durations (Ds_{5-75}) lesser than 25 s. For each individual record in the short duration set, there exists a companion long duration record, with a closely matching response spectral shape and Ds_{5-75} greater than 25 s, in the spectrally equivalent long duration set. These long duration records were recorded from large magnitude interface and crustal earthquakes. A detailed description of the procedure employed to select the spectrally equivalent record pairs is provided in Chapter 2/Chandramohan et al. (2016b).

All records obtained from sources other than the PEER NGA-West2 database Ancheta et al. 2013 were baseline corrected and filtered using the recommendations of Boore and Bommer 2005. First, the mean of the pre-event portion of the accelerogram was subtracted from the whole accelerogram to remove any offset in the baseline. If no pre-event portion was detected, the mean of the entire accelerogram was subtracted.

The accelerogram was then tapered using a Tukey window of taper ratio 0.05, zero-padded as per the recommendations of Boore 2005, and filtered using an acausal, 4th order, band-pass Butterworth filter. The high-cut frequency was chosen to be slightly smaller than the Nyquist frequency, while the low-cut frequency was chosen by visual inspection of the Fourier amplitude spectra of the accelerograms and the filtered velocity and displacement time histories. A low-cut frequency of 0.10 Hz was found to be adequate for processing all records, except those from the 1985 Michoacan and 2011 Tohoku earthquakes, for which a low-cut frequency of 0.12 Hz was used.

§§ A.1 and A.2 list the records in the short and long duration sets respectively, and provide relevant metadata. The sources of the records in the long duration set are indicated in footnotes at the end of the table. § A.3 plots the geometric mean response spectra of all the records in the two sets. The closely overlapping curves confirm the spectral equivalence of the two record sets. § A.4 plots the response spectra and time histories of each of the 44 spectrally equivalent record pairs. Short duration records are plotted in orange and long duration records in red.

A.1 Records in the FEMA P695 far-field (short duration) set

Record #	Earthquake	Station name	Filename	Ds_{5-75} (s)
1	1990 Manjil, Iran	Abbar	ABBARL.AT2	7.4
2			ABBART.AT2	11.5
3	1999 Kocaeli, Turkey	Arcelik	ARCELIK000.AT2	7.6
4			ARCELIK090.AT2	5.1
5	1999 Duzce, Turkey	Bolu	BOLU000.AT2	2.6
6			BOLU090.AT2	1.5
7	1989 Loma Prieta, USA	Capitola Fire Station	CAPITOLA000.AT2	5.7
8			CAPITOLA090.AT2	5.6
9	1999 Chi-Chi, Taiwan	CHY101	CHY101E.AT2	13.5
10			CHY101N.AT2	10.3
11	1992 Landers, USA	Coolwater	COOLWATERLN.AT2	5.9
12			COOLWATERTR.AT2	3.8
13	1979 Imperial Valley, USA	Delta	DELTA262.AT2	24.2
14			DELTA352.AT2	22.4
15	1999 Kocaeli, Turkey	Duzce	DUZCE180.AT2	6.1
16			DUZCE270.AT2	2.1

Record #	Earthquake	Station name	Filename	Ds_{5-75} (s)
17	1979 Imperial Valley, USA	El Centro Array #11	ELCENTRO140.AT2	4.5
18			ELCENTRO230.AT2	4.6
19	1989 Loma Prieta, USA	Gilroy Array #3	GILROY000.AT2	1.7
20			GILROY090.AT2	3.1
21	1999 Hector Mine, USA	Hector	HECTOR000.AT2	6.4
22			HECTOR090.AT2	7.6
23	1971 San Fernando, USA	Los Angeles - Hollwood Storage Grounds	HOLLYWOOD090.AT2	5.1
24			HOLLYWOOD180.AT2	4.8
25	1987 Superstition Hills, USA	El Centro Imperial County Center Grounds	ICC000.AT2	7.0
26			ICC090.AT2	7.6
27	1994 Northridge, USA	Canyon Country - 16628 W. Lost Canyon Road	LOSTCANYON000.AT2	3.1
28			LOSTCANYON270.AT2	2.9
29	1994 Northridge, USA	Beverly Hills - 14145 Mulholland Drive	MULHOLLAND009.AT2	6.1
30			MULHOLLAND279.AT2	5.0
31	1995 Kobe, Japan	Nishi-Akashi	NISHI000.AT2	4.0
32			NISHI090.AT2	4.5
33	1987 Superstition Hills, USA	Poe Road (temp)	POE270.AT2	9.8
34			POE360.AT2	11.2

Record #	**Earthquake**	**Station name**	**Filename**	$\boldsymbol{D_{s_{5-75}}}$ (s)
35	1992 Cape Mendocino, USA	Rio Dell Overpass	RIODELL270.AT2	4.3
36			RIODELL360.AT2	1.9
37	1995 Kobe, Japan	Shin-Osaka	SHIN000.AT2	3.6
38			SHIN090.AT2	4.5
39	1999 Chi-Chi, Taiwan	TCU045	TCU045E.AT2	7.4
40			TCU045N.AT2	8.7
41	1976 Friuli, Italy	Tolmezzo	TOLMEZZO000.AT2	2.5
42			TOLMEZZO270.AT2	2.5
43	1992 Landers, USA	Yermo Fire Station	YERMO270.AT2	7.1
44			YERMO360.AT2	10.9

A.2 Records in the spectrally equivalent, long duration set

Record #	Earthquake	Station name	Filename	Scale factor	Ds_{5-75} (s)
1	2011 Tohoku, Japan*	Ogano	SITH081103111446_H2.th	5.00	37.6
2	2011 Tohoku, Japan*	Yamagata	YMT0101103111446_H1.th	5.00	70.2
3	2011 Tohoku, Japan*	Edosaki	IBR0171103111446_H1.th	0.41	27.8
4	1999 Chi-Chi, Taiwan - 4†	CHY116	CHICHI.04/CHY116W.AT2	4.43	35.5
5	2011 Tohoku, Japan*	Takahagi	IBR0021103111446_H2.th	1.30	38.9
6	1985 Michoacan, Mexico‡	Villita Corona Centro	VILC8509191_H2.th	1.16	33.6
7	2011 Tohoku, Japan*	Hachiohji	TKYH121103111446_H2.th	3.84	46.0
8	2011 Tohoku, Japan*	Sendai	MYG0131103111446_H1.th	0.58	55.5
9	2010 El Mayor-Cucapah, USA†	Ejido Saltillo	SIERRA.MEX/SAL090.AT2	1.85	33.3
10	1999 Chi-Chi, Taiwan†	CHY058	CHICHI/CHY058-N.AT2	5.00	30.8

Record #	**Earthquake**	**Station name**	**Filename**	**Scale factor**	$\boldsymbol{Ds_{5-75}}$ (s)
11	2011 Tohoku, Japan*	Aizutakada	FKSH041103111446_H2.th	1.53	66.6
12	2008 Wenchuan, China†	Hanyuanjiuxiang	WENCHUAN/UA0965.AT2	4.37	38.2
13	2011 Tohoku, Japan*	Takasato	FKSH031103111446_H2.th	1.78	66.5
14	2011 Tohoku, Japan*	Tomioka	GNMH111103111446_H1.th	4.16	44.6
15	2011 Tohoku, Japan*	Yamagata	YMTH021103111446_H1.th	1.79	78.8
16	2011 Tohoku, Japan*	Namie	FKSH201103111446_H2.th	0.97	63.6
17	2011 Tohoku, Japan*	Kakunodate	AKT0141103111446_H1.th	5.00	53.8
18	2011 Tohoku, Japan*	Nagawa	AOMH171103111446_H2.th	2.76	53.2
19	2010 Maule, Chile§	Angol	ANGOLEW.th	0.77	30.2
20	2011 Tohoku, Japan*	Tendou	YMTH011103111446_H1.th	2.07	71.2
21	2011 Tohoku, Japan*	Kawaguchi	SIT0111103111446_H2.th	1.08	45.7
22	2011 Tohoku, Japan*	Hachieda	TKY0181103111446_H1.th	1.14	40.5
23	2007 Chuetsu-oki, Japan†	NIG011	CHUETSU/NIG011EW.AT2	4.04	25.7

Record #	Earthquake	Station name	Filename	Scale factor	Ds_{5-75} (s)
24	2011 Tohoku, Japan*	Hannoh	SIT0121103111446_H2.th	3.53	45.9
25	2011 Tohoku, Japan*	Kumagaya	SIT0021103111446_H1.th	2.23	43.7
26	2003 Hokkaido, Japan*	Date	HKD1330309260450_H1.th	4.14	28.4
27	2011 Tohoku, Japan*	Shuzenji	SZOH421103111446_H2.th	5.00	57.0
28	2011 Tohoku, Japan*	Hijiori	YMT0051103111446_H2.th	4.73	68.8
29	2011 Tohoku, Japan*	Yokoami	TKY0221103111446_H2.th	1.88	42.0
30	2011 Tohoku, Japan*	Shiroishi	MYGH091103111446_H2.th	1.60	70.4
31	2011 Tohoku, Japan*	Atsugi	KNG0091103111446_H2.th	3.02	48.1
32	2002 Denali, USA†	Fairbanks - Geophysical Observatory, CIGO	DENALI/FAIGO360.AT2	5.00	27.7
33	2011 Tohoku, Japan*	Kuji	IWT0021103111446_H1.th	2.25	53.1
34	2011 Tohoku, Japan*	Ashiro	IWT0221103111446_H2.th	2.29	54.4
35	1985 Valparaiso, Chile§	Valparaiso El Almendral	VALPARAISOELALMENDRAL50.th	1.11	31.1

Record #	Earthquake	Station name	Filename	Scale factor	Ds_{5-75} (s)
36	1985 Valparaiso, Chile[§]	Caquenes	CAUQUENESL.th	5.00	25.2
37	2011 Tohoku, Japan[*]	Nishikawa-E	YMTH151103111446_H2.th	2.43	71.7
38	2011 Tohoku, Japan[*]	Hasaki2	IBRH201103111446_H2.th	1.13	28.7
39	2008 Wenchuan, China[†]	Hongyatai	WENCHUAN/UA1040.AT2	2.95	38.8
40	1985 Valparaiso, Chile[§]	Llolleo	LLOLLEO10.th	0.61	27.5
41	2011 Tohoku, Japan[*]	Kohriyama	FKS0181103111446_H2.th	0.48	67.5
42	2011 Tohoku, Japan[*]	Nakaminato	IBR0071103111446_H1.th	0.59	34.4
43	2011 Tohoku, Japan[*]	Hachinohe	AOMH131103111446_H2.th	1.51	62.7
44	2011 Tohoku, Japan[*]	Ukita	TKY0261103111446_H1.th	0.94	44.8

[*]Source: National Research Institute for Earth Science and Disaster Prevention (NIED), Japan (http://www.kyoshin.bosai.go.jp/)

[†]Source: PEER NGA-West2 database (Ancheta et al. 2014) (http://peer.berkeley.edu/ngawest2/databases/)

[‡]Source: Comite de la Base Nacional de Datos de Sismos Fuertes, Mexico

[§]Source: Departamento de Geofisica, Universidad de Chile, via the Center for Engineering Strong Motion Data (http://www.strongmotioncenter.org/)

A.3 Geometric mean response spectra of the records in the two sets

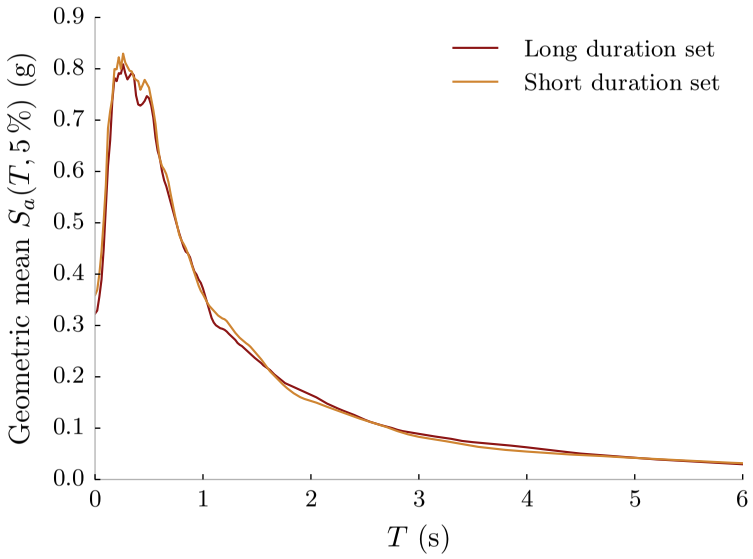

A.4 Response spectra and time history plots of all spectrally equivalent record pairs

Spectrally equivalent record pair #1

Earthquake	Station name	Filename	Scale factor	Ds_{5-75} (s)
1990 Manjil, Iran	Abbar	ABBARL.AT2	–	7.4
2011 Tohoku, Japan	Ogano	SITH081103111446_H2.th	5.00	37.6

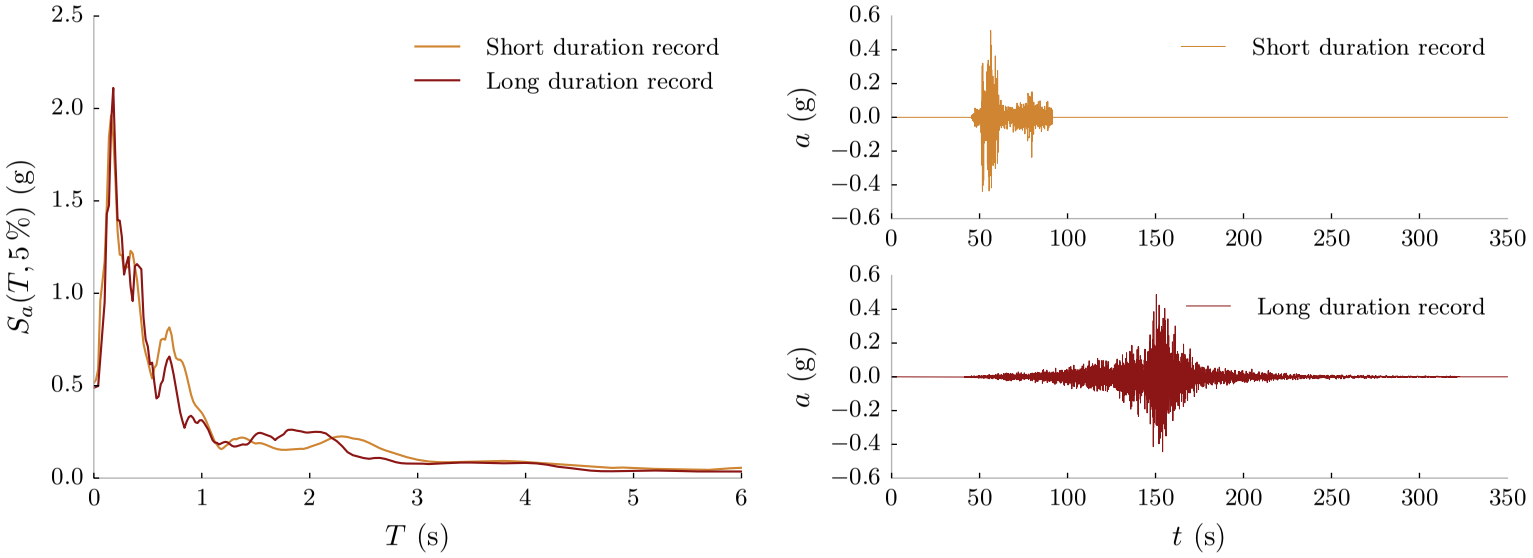

Spectrally equivalent record pair #2

Earthquake	Station name	Filename	Scale factor	$D_{s_{5-75}}$ (s)
1990 Manjil, Iran	Abbar	ABBART.AT2	–	11.5
2011 Tohoku, Japan	Yamagata	YMT01011103111446_H1.th	5.00	70.2

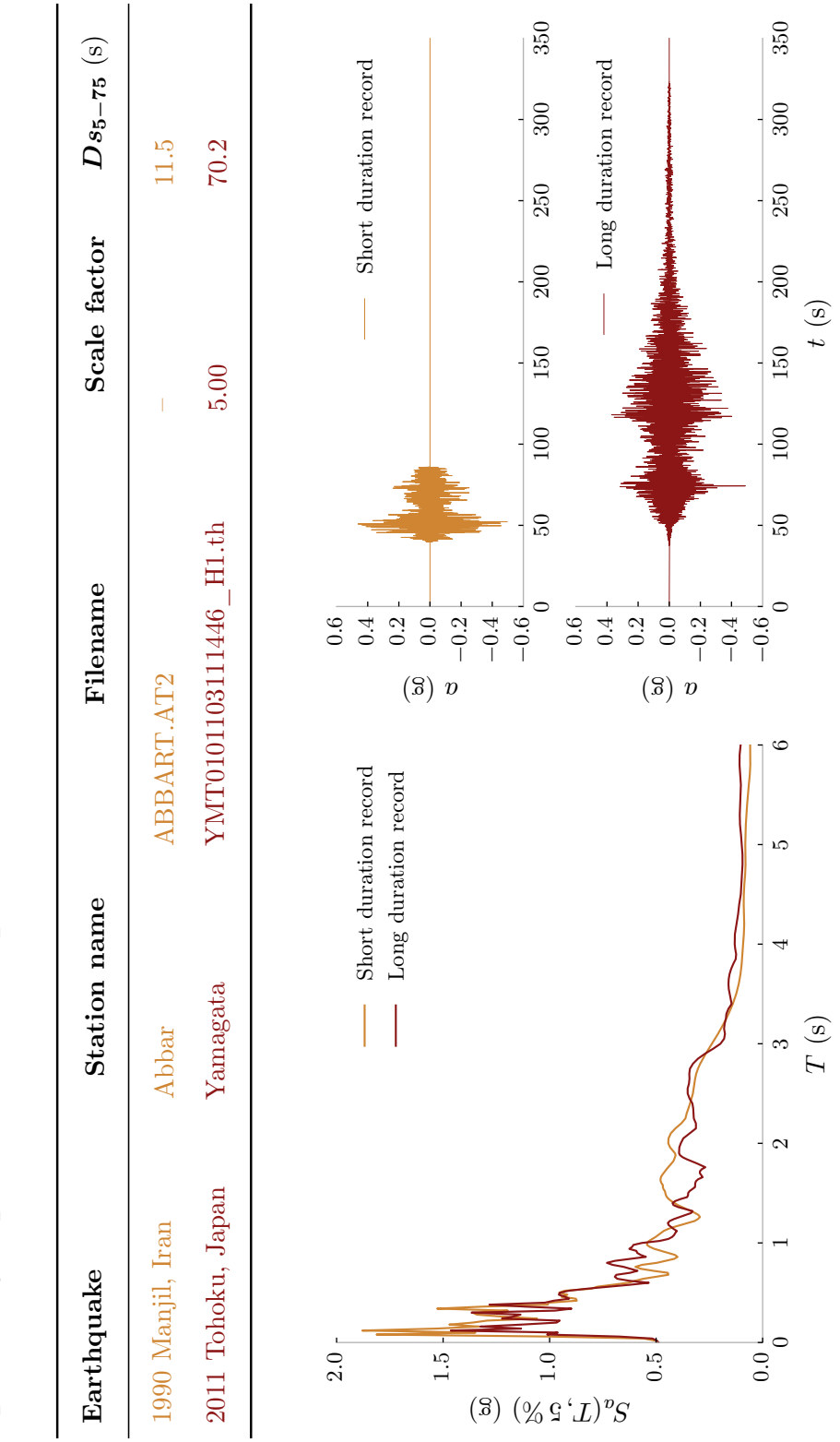

Spectrally equivalent record pair #3

Earthquake	Station name	Filename	Scale factor	Ds_{5-75} (s)
1999 Kocaeli, Turkey	Arcelik	ARCELIK000.AT2	–	7.6
2011 Tohoku, Japan	Edosaki	IBR0171103111446_H1.th	0.41	27.8

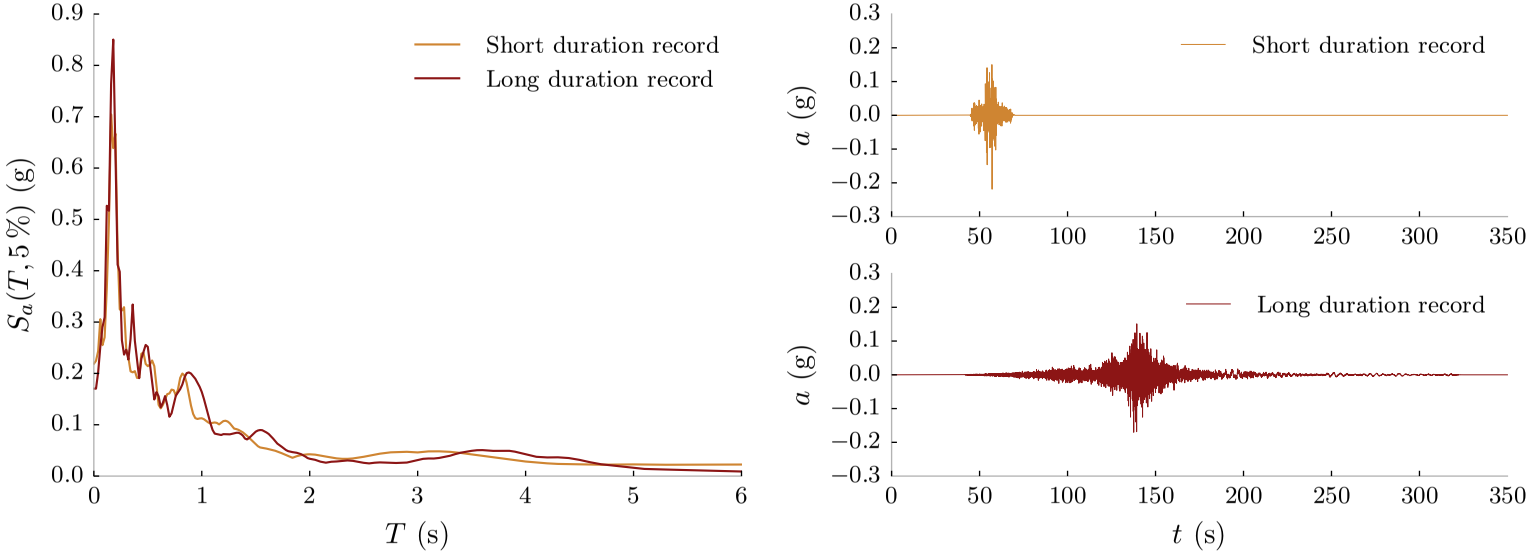

Spectrally equivalent record pair #4

Earthquake	Station name	Filename	Scale factor	Ds_{5-75} (s)
1999 Kocaeli, Turkey	Arcelik	ARCELIK090.AT2	–	5.1
1999 Chi-Chi, Taiwan - 4	CHY116	CHICHI.04/CHY116W.AT2	4.43	35.5

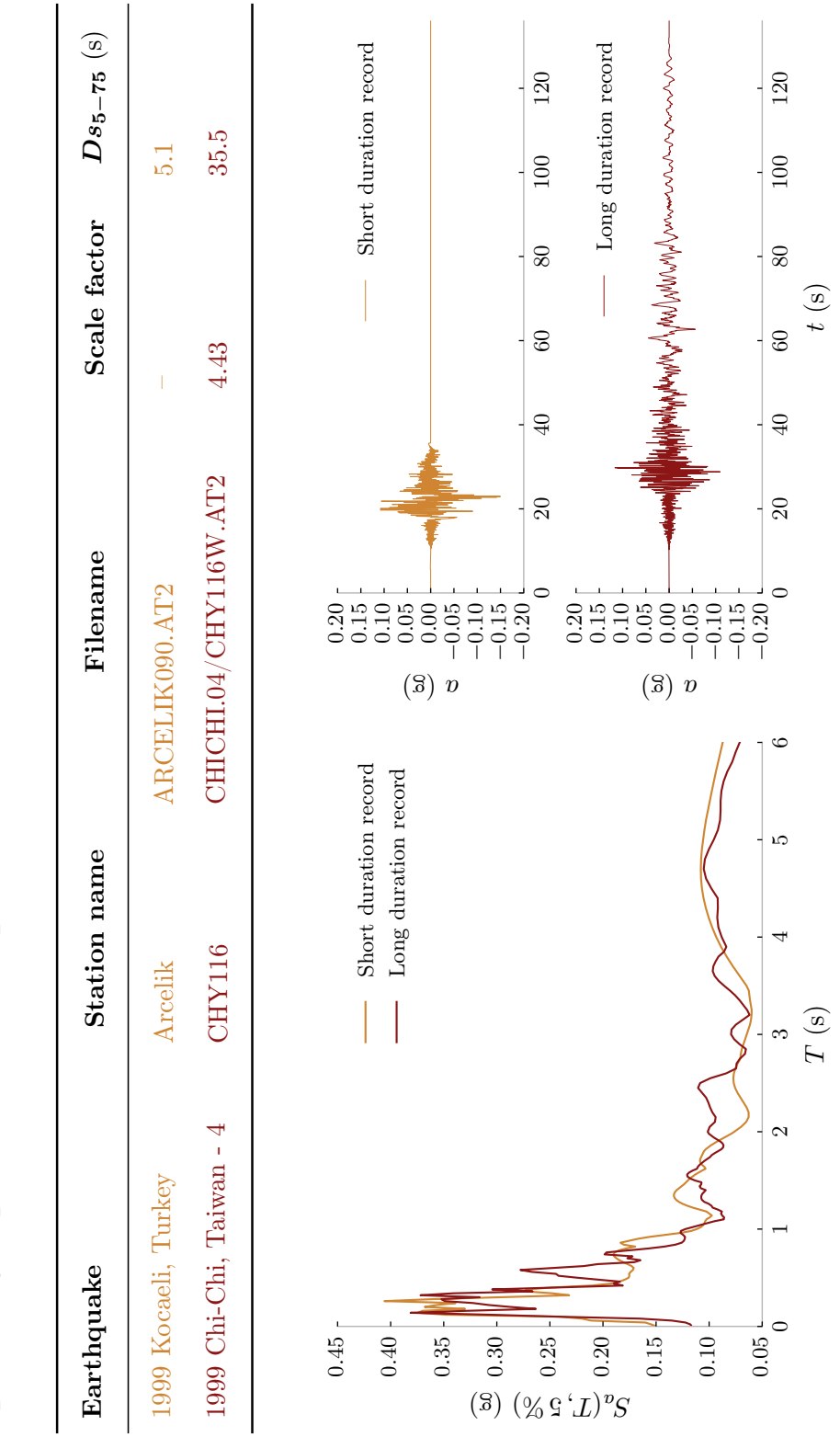

Spectrally equivalent record pair #5

Earthquake	Station name	Filename	Scale factor	Ds_{5-75} (s)
1999 Duzce, Turkey	Bolu	BOLU000.AT2	–	2.6
2011 Tohoku, Japan	Takahagi	IBR002110311144 46_H2.th	1.30	38.9

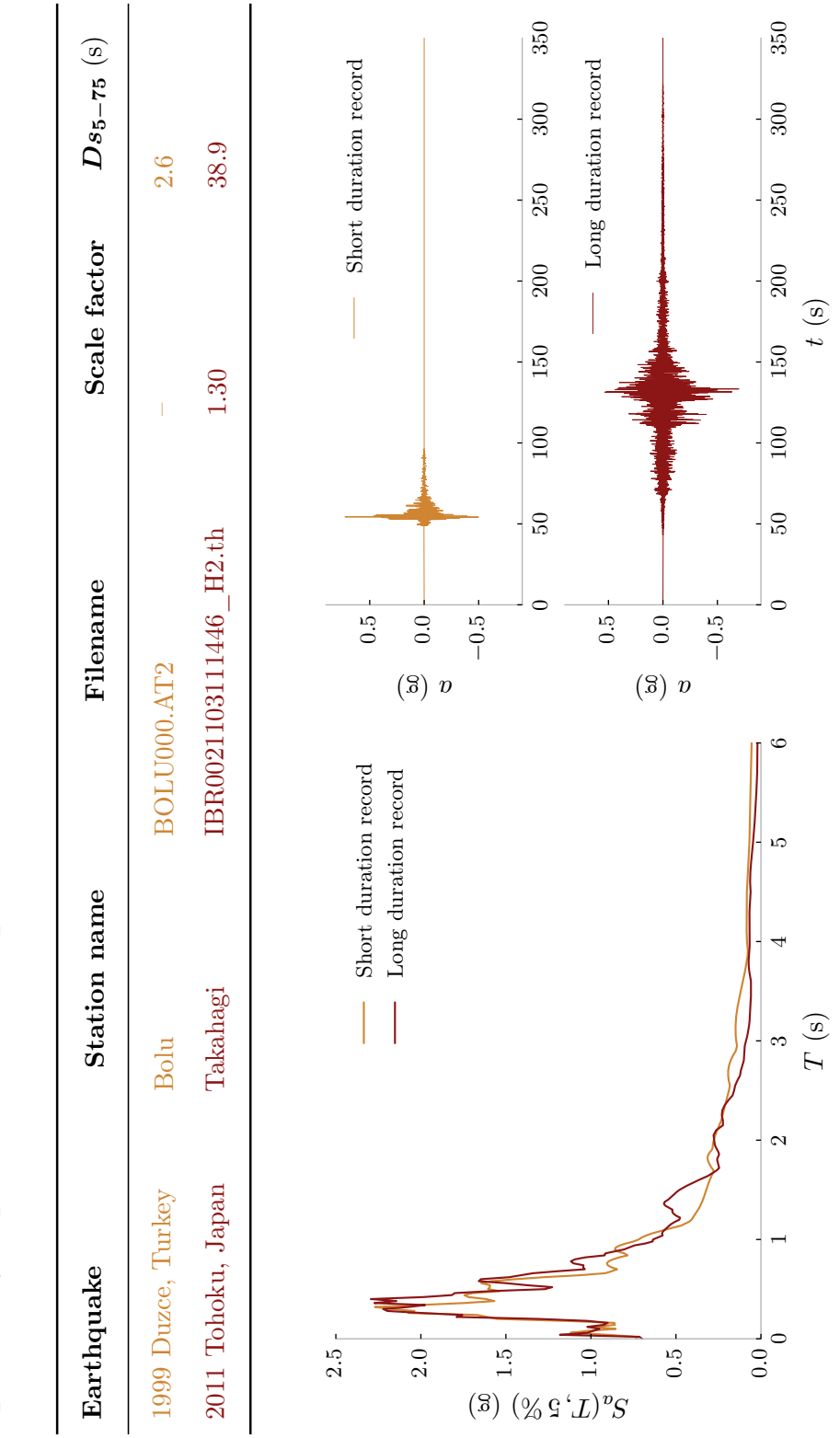

Spectrally equivalent record pair #6

Earthquake	Station name	Filename	Scale factor	D_{s5-75} (s)
1999 Duzce, Turkey	Bolu	BOLU090.AT2	–	1.5
1985 Michoacan, Mexico	Villita Corona Centro	VILC8509191_H2.th	1.16	33.6

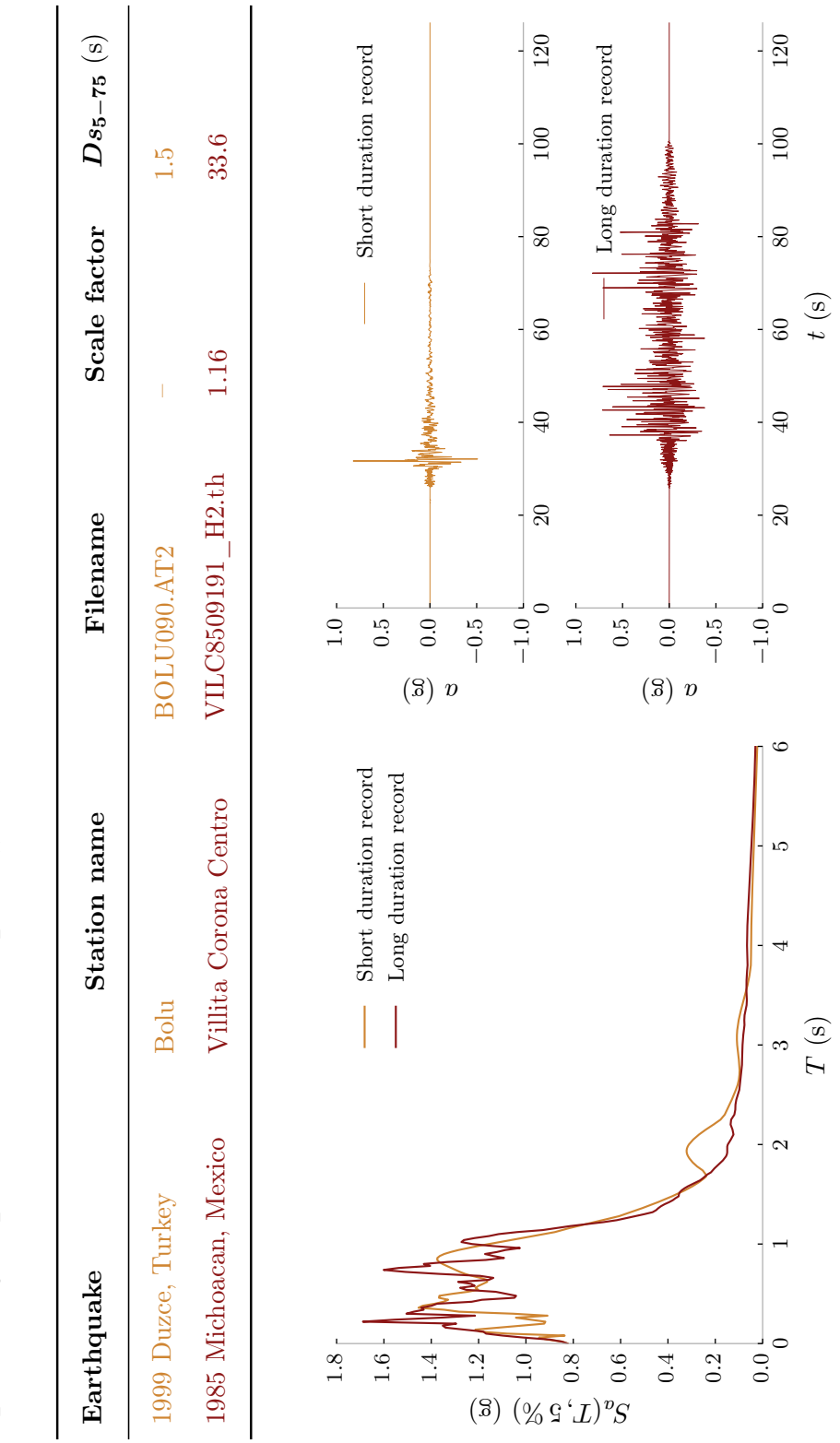

Spectrally equivalent record pair #7

Earthquake	Station name	Filename	Scale factor	Ds_{5-75} (s)
1989 Loma Prieta, USA	Capitola Fire Station	CAPITOLA000.AT2	–	5.7
2011 Tohoku, Japan	Hachiohji	TKYH121103111446_H2.th	3.84	46.0

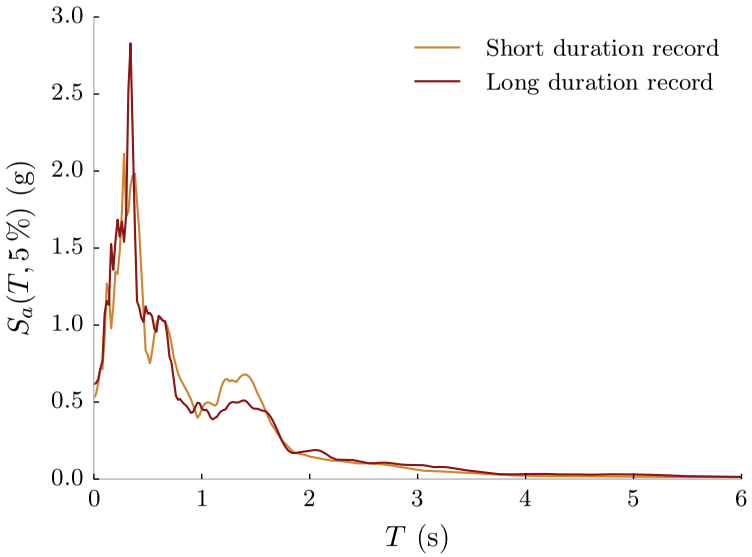

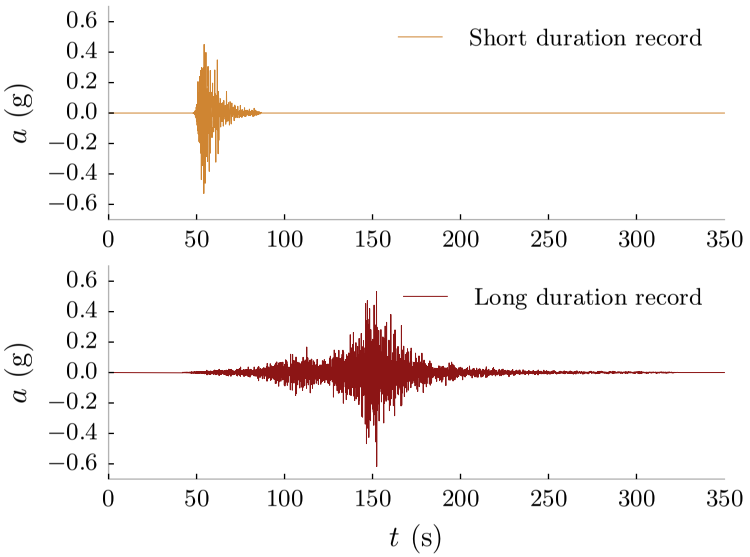

Spectrally equivalent record pair #8

Earthquake	Station name	Filename	Scale factor	Ds_{5-75} (s)
1989 Loma Prieta, USA	Capitola Fire Station	CAPITOLA090.AT2	–	5.6
2011 Tohoku, Japan	Sendai	MYG013110311144 6_H1.th	0.58	55.5

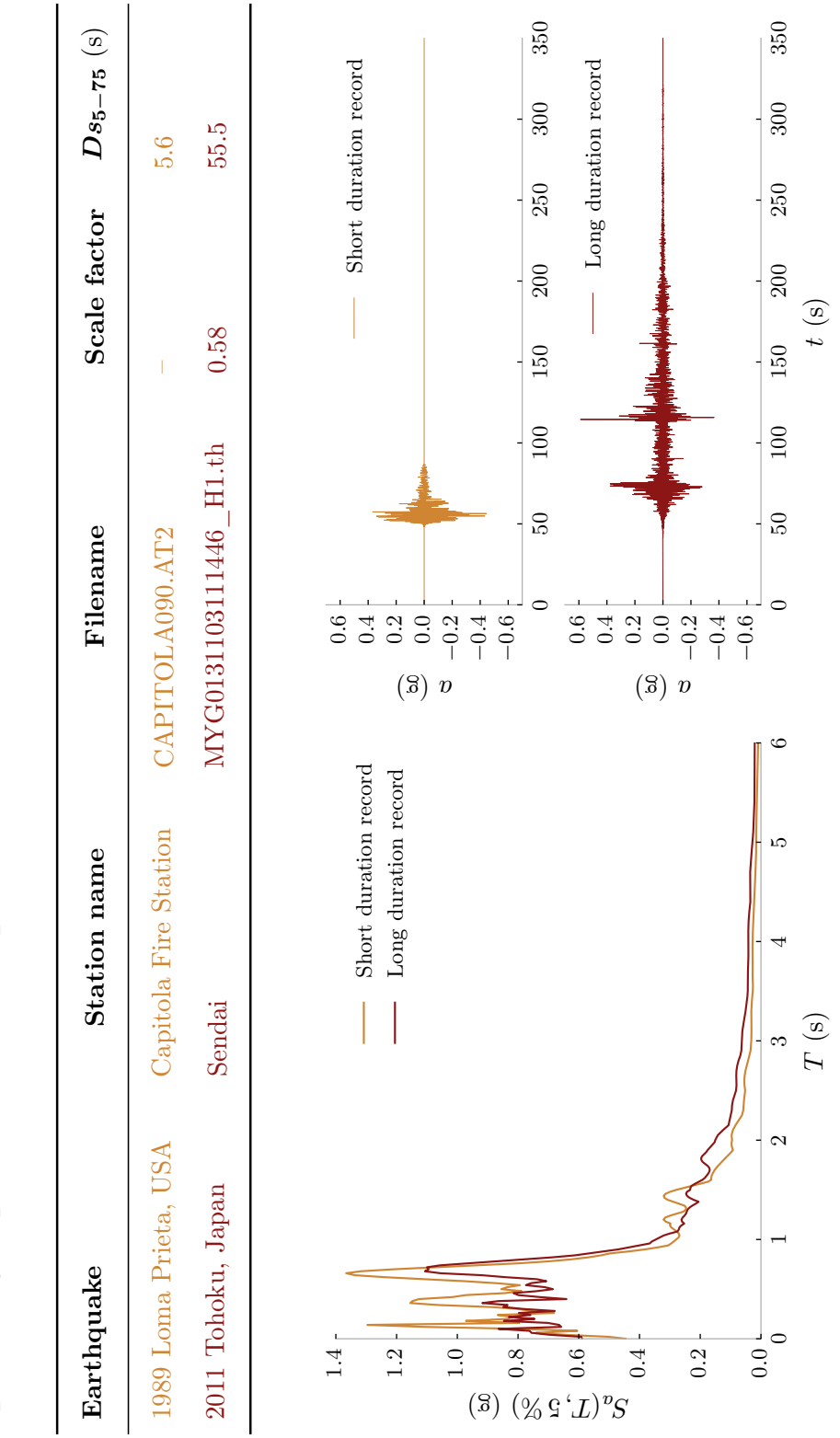

Spectrally equivalent record pair #9

Earthquake	Station name	Filename	Scale factor	Ds_{5-75} (s)
1999 Chi-Chi, Taiwan	CHY101	CHY101E.AT2	–	13.5
2010 El Mayor-Cucapah, USA	Ejido Saltillo	SIERRA.MEX/SAL090.AT2	1.85	33.3

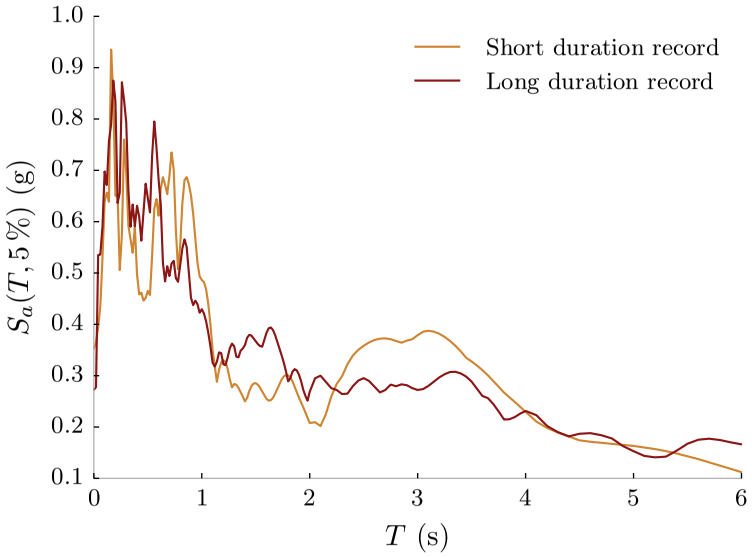

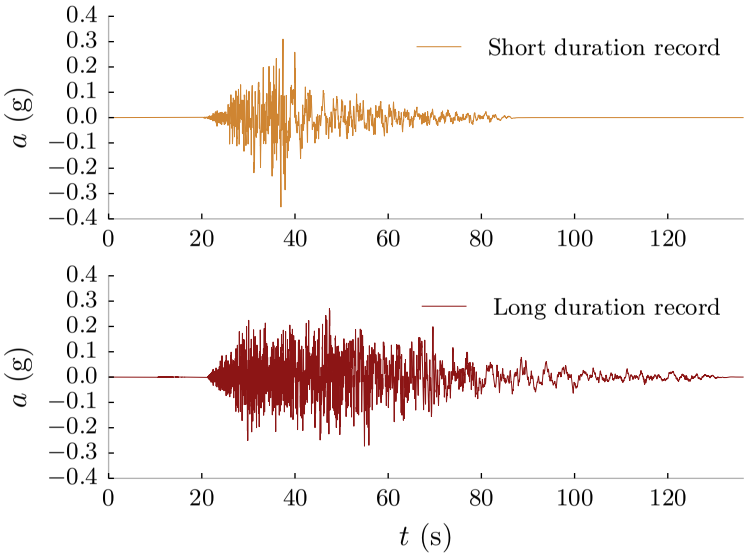

Spectrally equivalent record pair #10

Earthquake	Station name	Filename	Scale factor	Ds_{5-75} (s)
1999 Chi-Chi, Taiwan	CHY101	CHY101N.AT2	–	10.3
1999 Chi-Chi, Taiwan	CHY058	CHICHI/CHY058-N.AT2	5.00	30.8

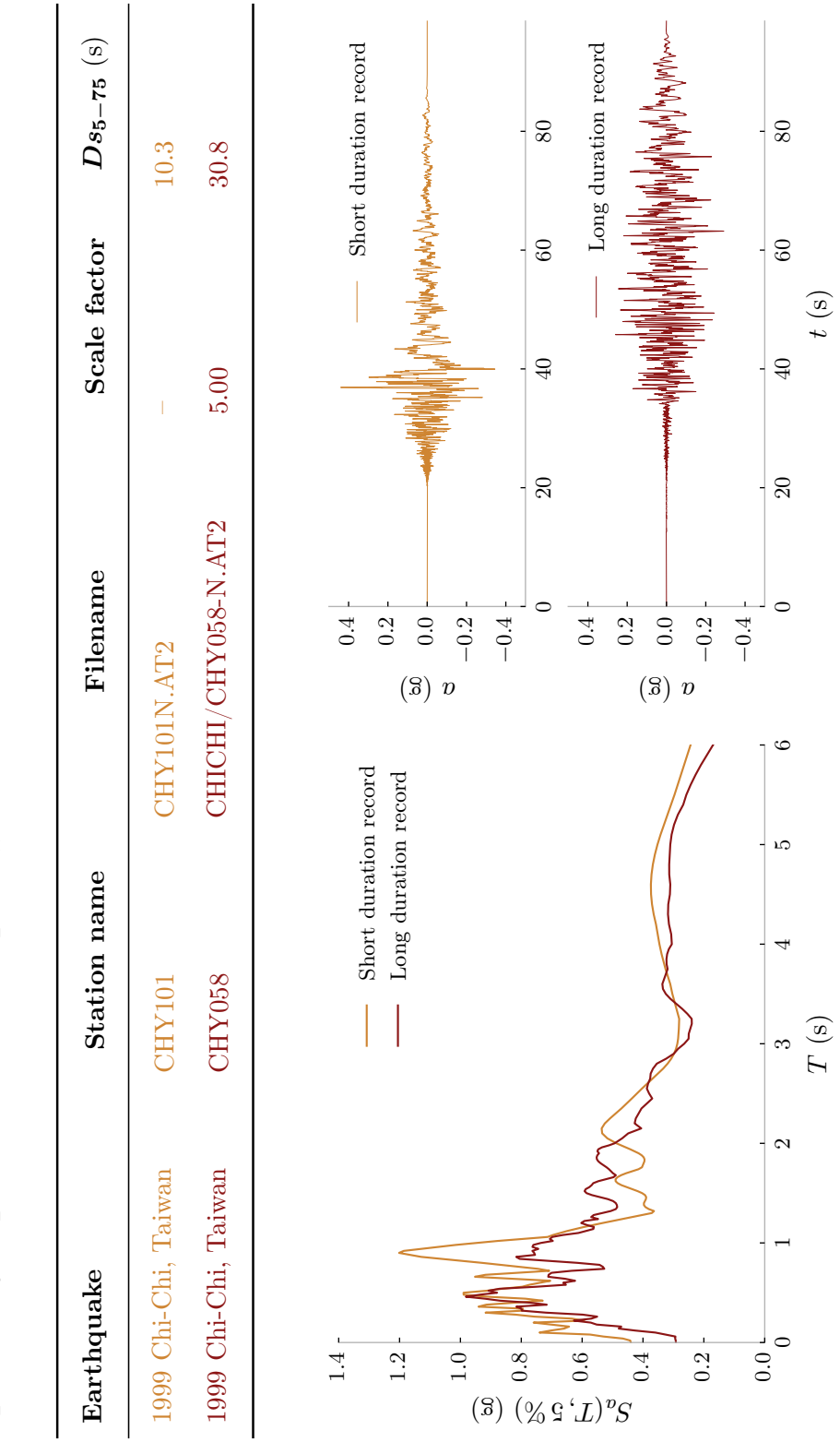

Spectrally equivalent record pair #11

Earthquake	Station name	Filename	Scale factor	Ds_{5-75} (s)
1992 Landers, USA	Coolwater	COOLWATERLN.AT2	–	5.9
2011 Tohoku, Japan	Aizutakada	FKSH041103111446_H2.th	1.53	66.6

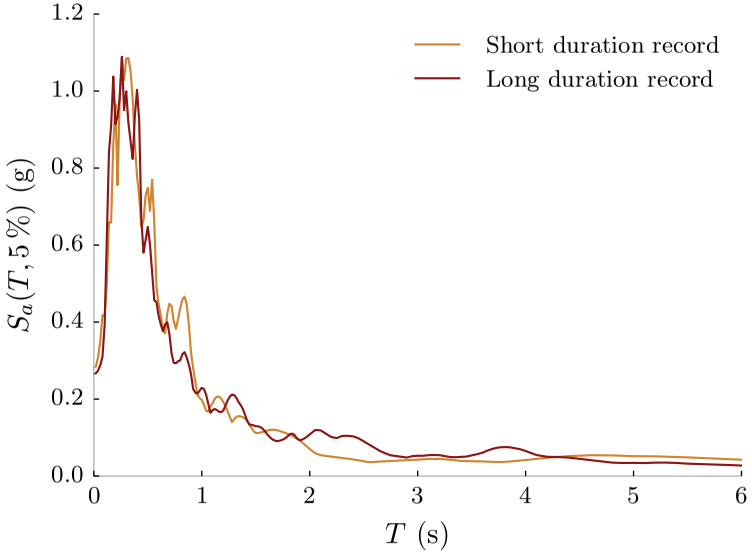

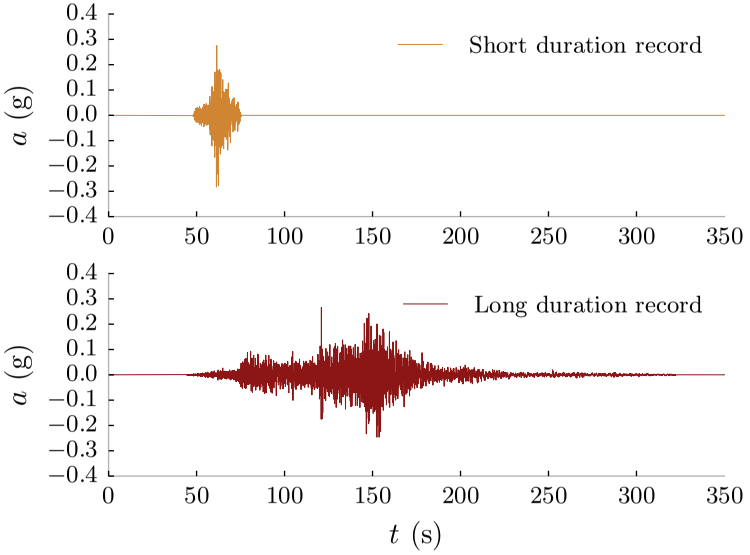

Spectrally equivalent record pair #12

Earthquake	Station name	Filename	Scale factor	Ds_{5-75} (s)
1992 Landers, USA	Coolwater	COOLWATERTR.AT2	–	3.8
2008 Wenchuan, China	Hanyuanjiuxiang	WENCHUAN/UA0965.AT2	4.37	38.2

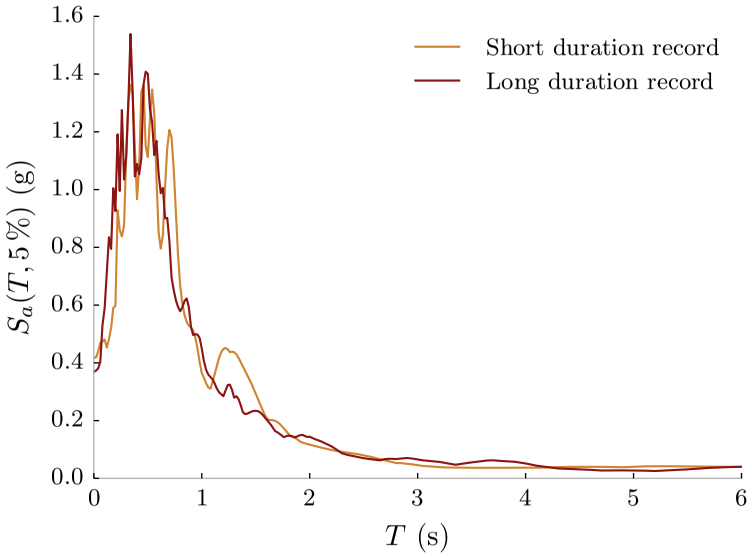

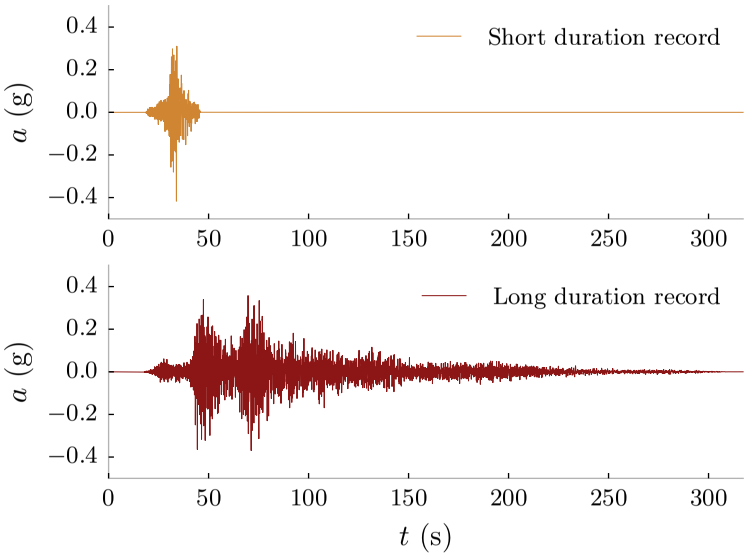

Spectrally equivalent record pair #13

Earthquake	Station name	Filename	Scale factor	Ds_{5-75} (s)
1979 Imperial Valley, USA	Delta	DELTA262.AT2	–	24.2
2011 Tohoku, Japan	Takasato	FKSH031103111446_H2.th	1.78	66.5

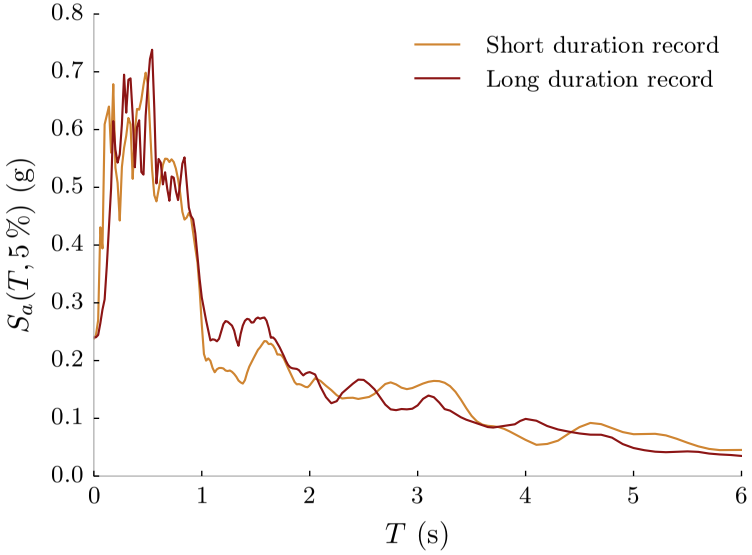

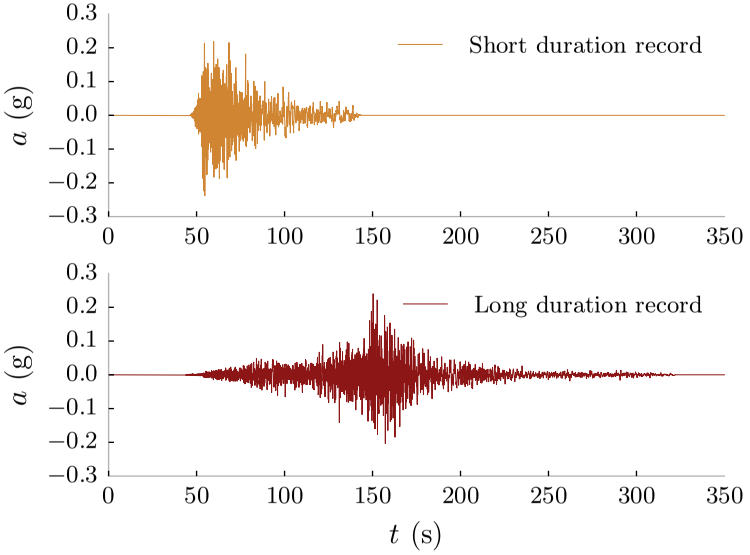

Spectrally equivalent record pair #14

Earthquake	Station name	Filename	Scale factor	Ds_{5-75} (s)
1979 Imperial Valley, USA	Delta	DELTA352.AT2	–	22.4
2011 Tohoku, Japan	Tomioka	GNMH111103111446_H1.th	4.16	44.6

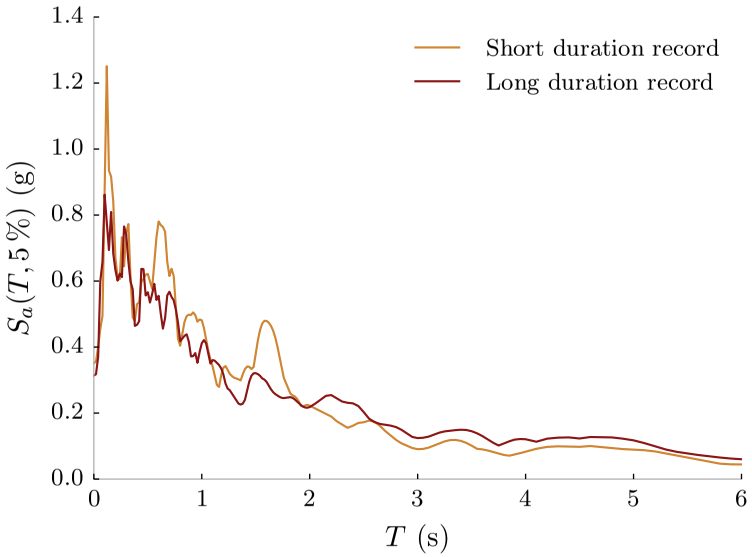

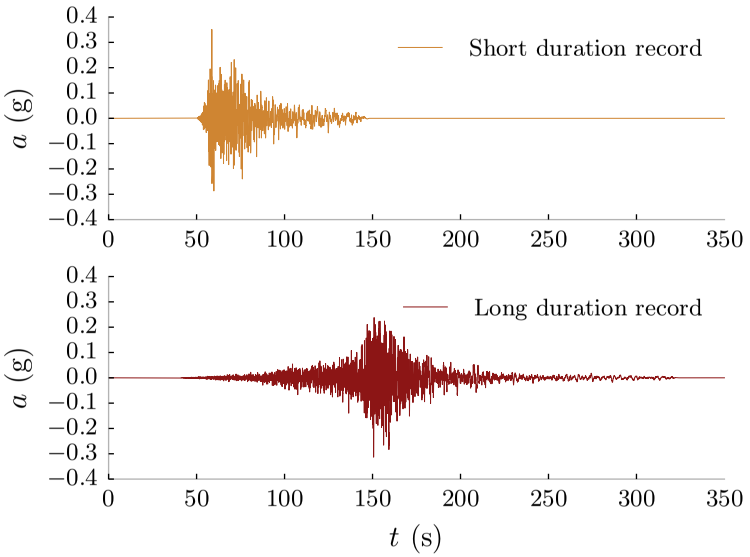

Spectrally equivalent record pair #15

Earthquake	Station name	Filename	Scale factor	Ds_{5-75} (s)
1999 Kocaeli, Turkey	Duzce	DUZCE180.AT2	–	6.1
2011 Tohoku, Japan	Yamagata	YMTH021103111446_H1.th	1.79	78.8

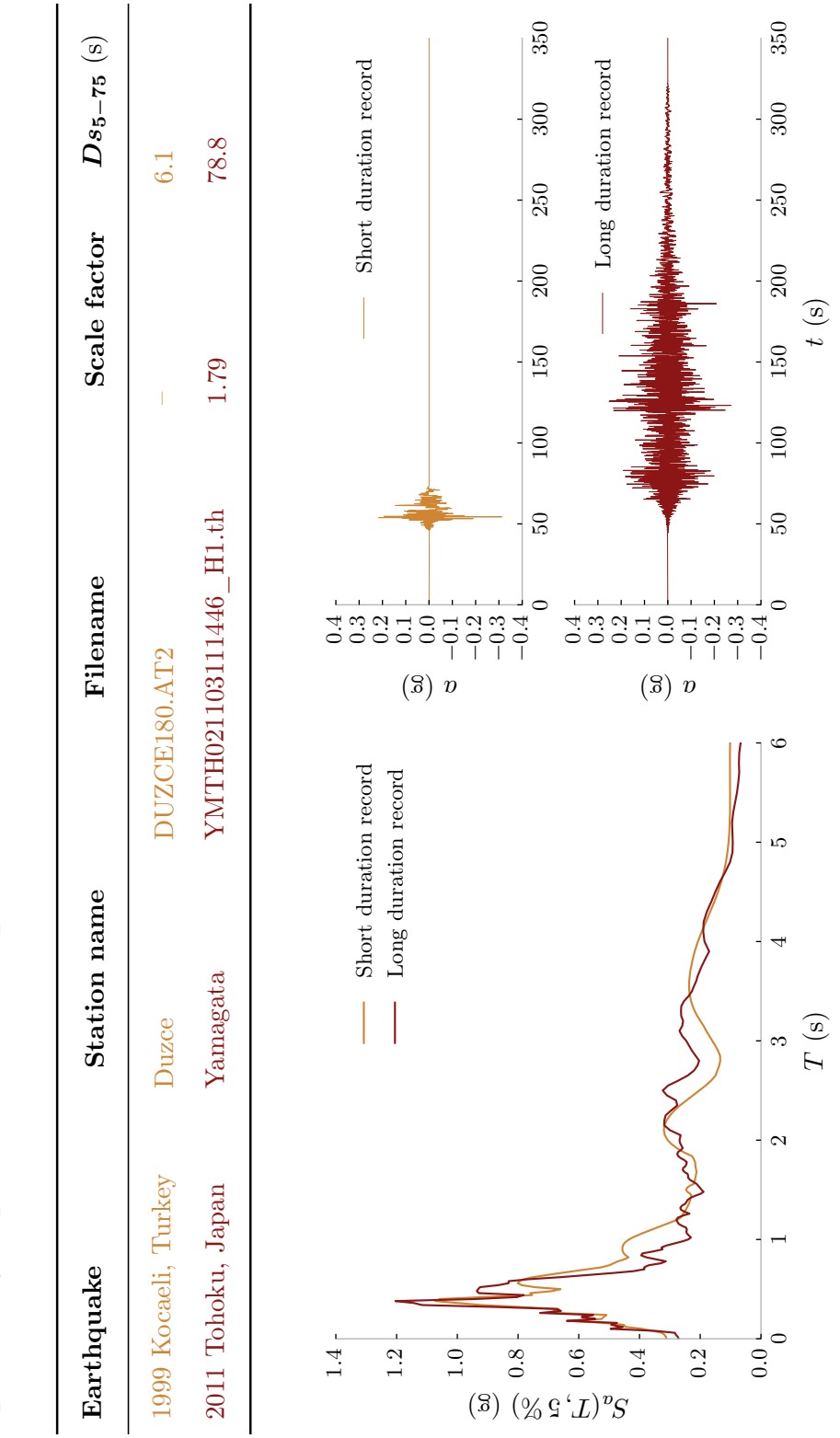

Spectrally equivalent record pair #16

Earthquake	Station name	Filename	Scale factor	Ds_{5-75} (s)
1999 Kocaeli, Turkey	Duzce	DUZCE270.AT2	–	2.1
2011 Tohoku, Japan	Namie	FKSH20110311111446_H2.th	0.97	63.6

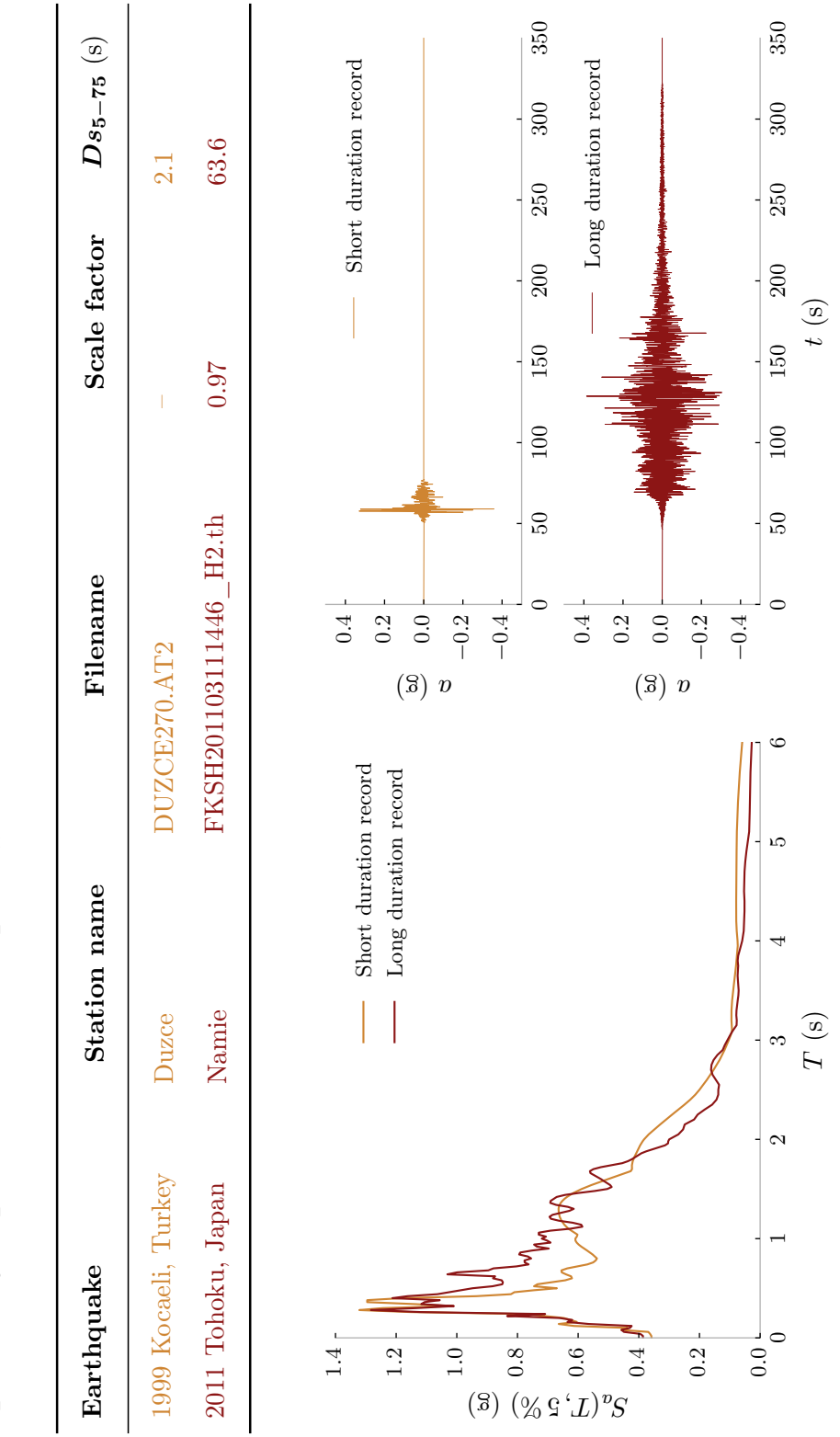

Spectrally equivalent record pair #17

Earthquake	Station name	Filename	Scale factor	Ds_{5-75} (s)
1979 Imperial Valley, USA	El Centro Array #11	ELCENTRO140.AT2	–	4.5
2011 Tohoku, Japan	Kakunodate	AKT0141103111446_H1.th	5.00	53.8

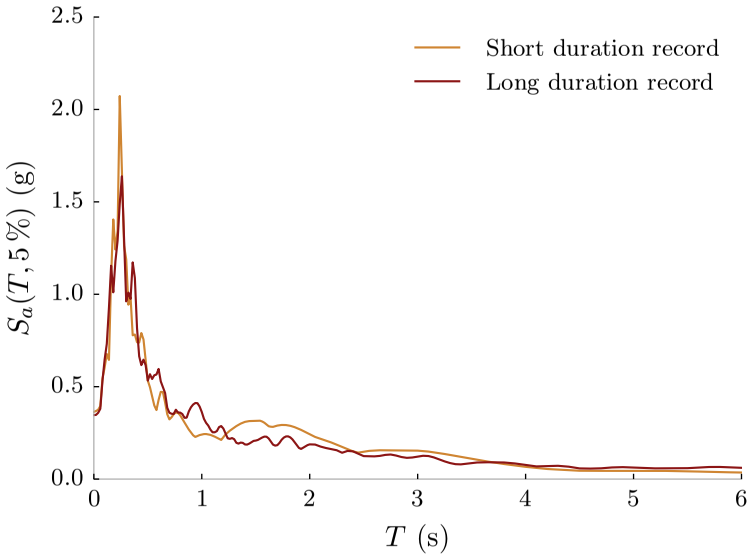

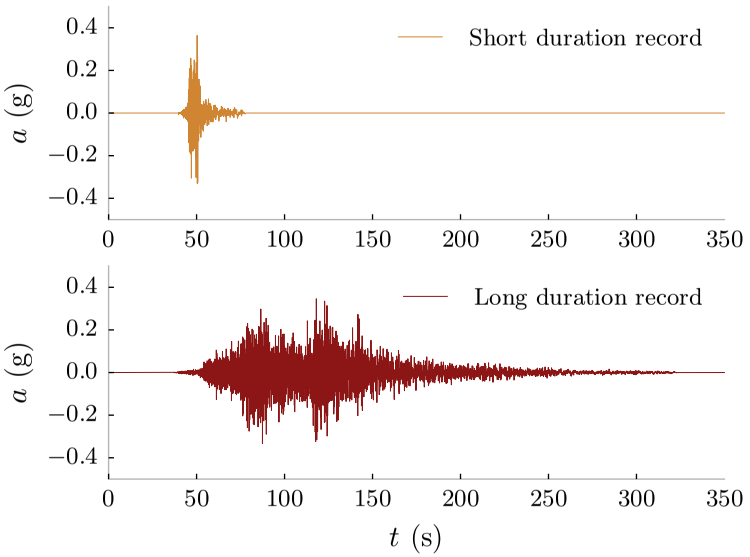

Spectrally equivalent record pair #18

Earthquake	Station name	Filename	Scale factor	Ds_{5-75} (s)
1979 Imperial Valley, USA	El Centro Array #11	ELCENTRO230.AT2	–	4.6
2011 Tohoku, Japan	Nagawa	AOMH171103111446_H2.th	2.76	53.2

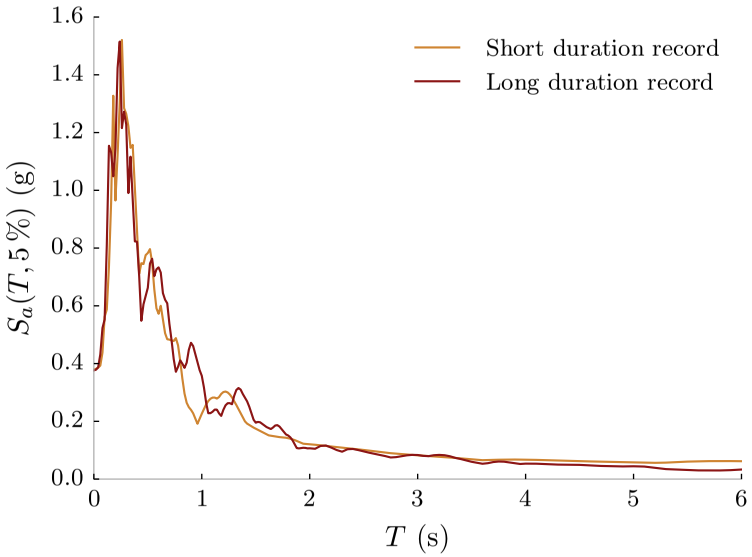

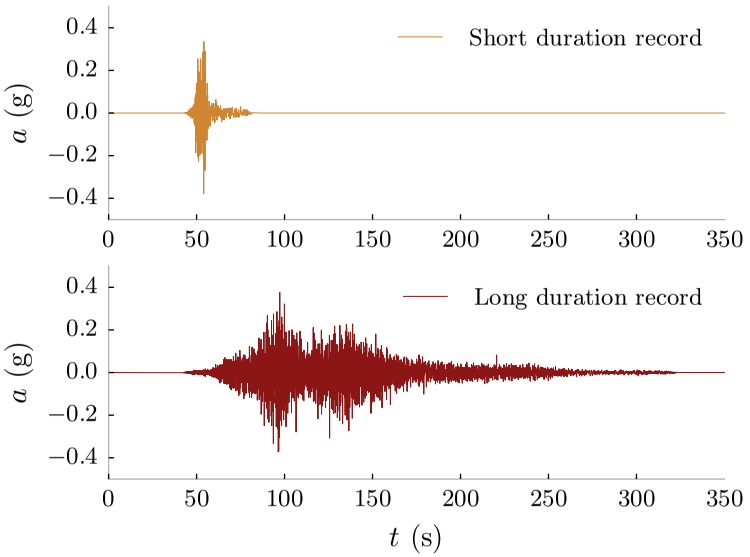

Spectrally equivalent record pair #19

Earthquake	Station name	Filename	Scale factor	Ds_{5-75} (s)
1989 Loma Prieta, USA	Gilroy Array #3	GILROY000.AT2	–	1.7
2010 Maule, Chile	Angol	ANGOLEW.th	0.77	30.2

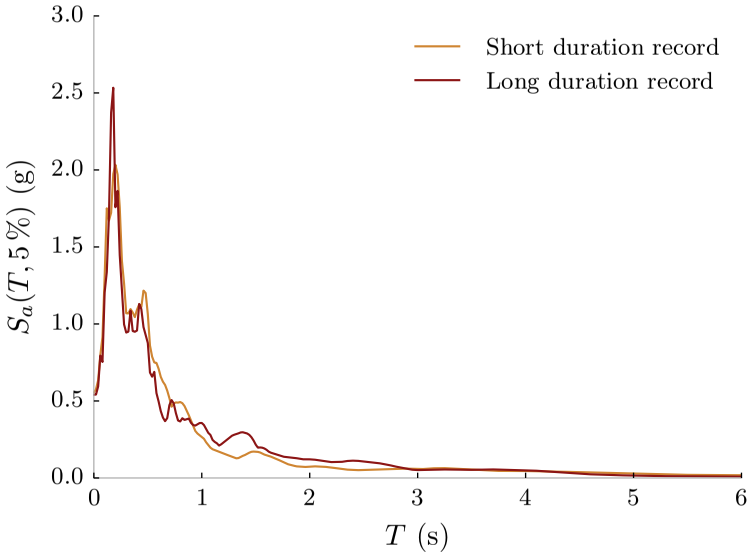

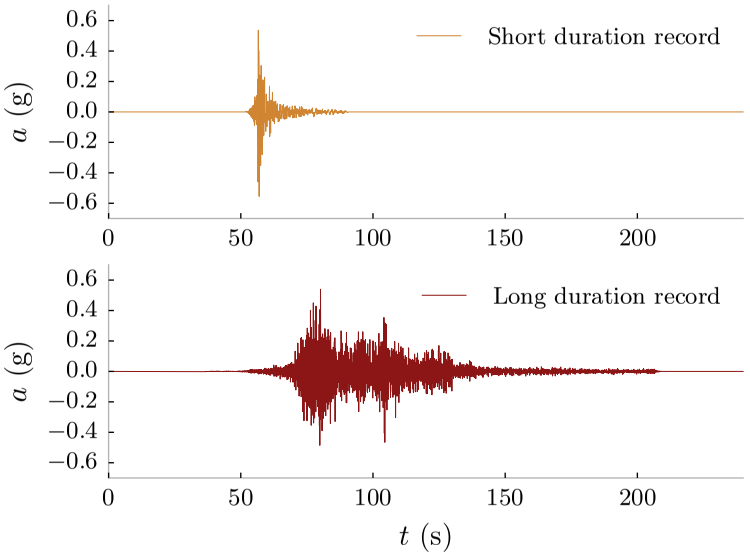

Spectrally equivalent record pair #20

Earthquake	Station name	Filename	Scale factor	Ds_{5-75} (s)
1989 Loma Prieta, USA	Gilroy Array #3	GILROY090.AT2	–	3.1
2011 Tohoku, Japan	Tendou	YMTH011103111446_H1.th	2.07	71.2

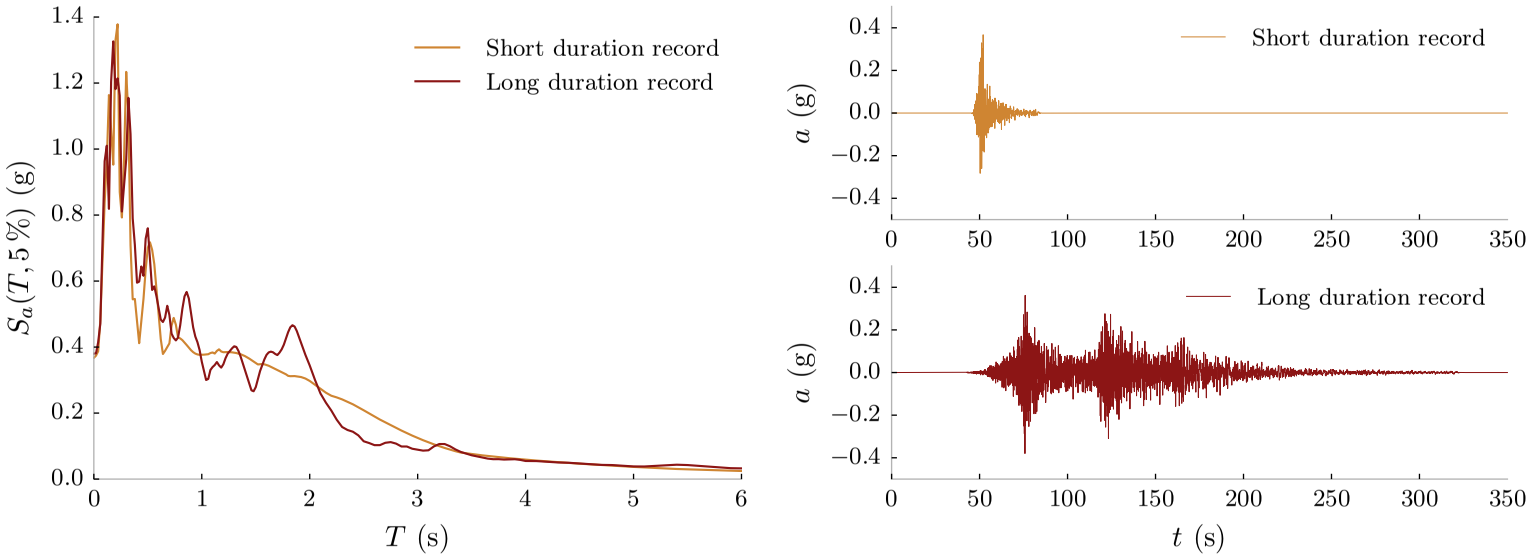

Spectrally equivalent record pair #21

Earthquake	Station name	Filename	Scale factor	Ds_{5-75} (s)
1999 Hector Mine, USA	Hector	HECTOR000.AT2	–	6.4
2011 Tohoku, Japan	Kawaguchi	SIT0111103111446_H2.th	1.08	45.7

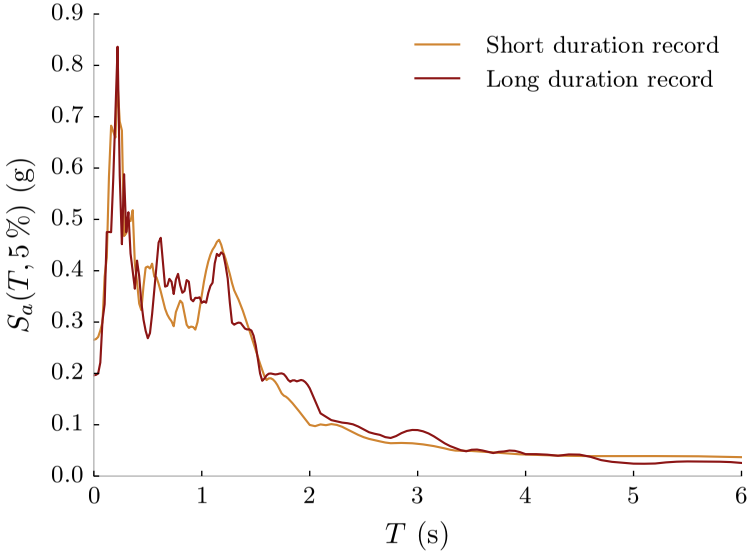

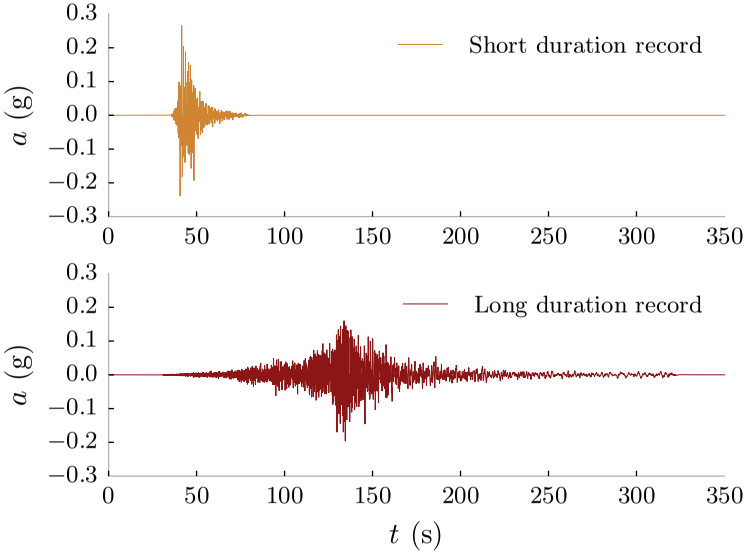

Spectrally equivalent record pair #22

Earthquake	Station name	Filename	Scale factor	Ds_{5-75} (s)
1999 Hector Mine, USA	Hector	HECTOR090.AT2	–	7.6
2011 Tohoku, Japan	Hachieda	TKY0181103111446_H1.th	1.14	40.5

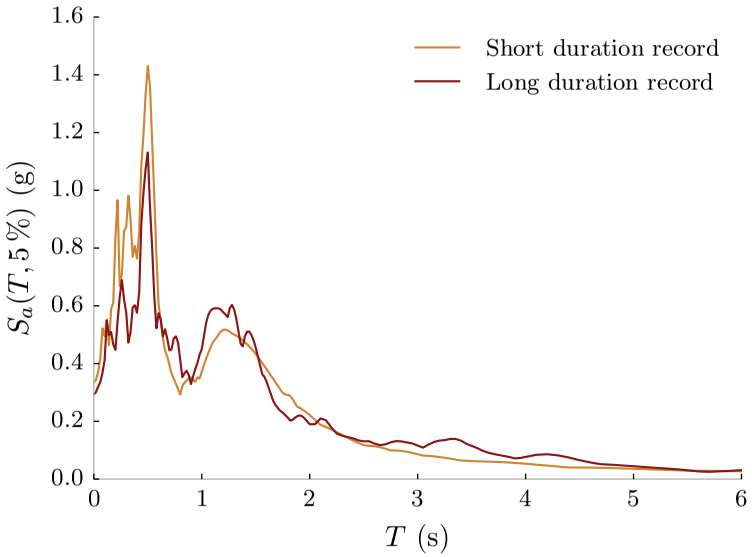

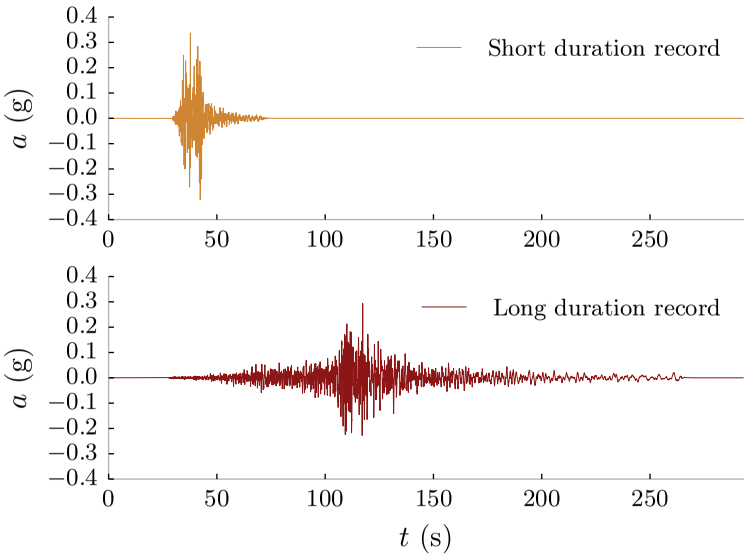

Spectrally equivalent record pair #23

Earthquake	Station name	Filename	Scale factor	D_{s5-75} (s)
1971 San Fernando, USA	Los Angeles - Hollwood Storage Grounds	HOLLYWOOD090.AT2	–	5.1
2007 Chuetsu-oki, Japan	NIG011	CHUETSU/NIG011EW.AT2	4.04	25.7

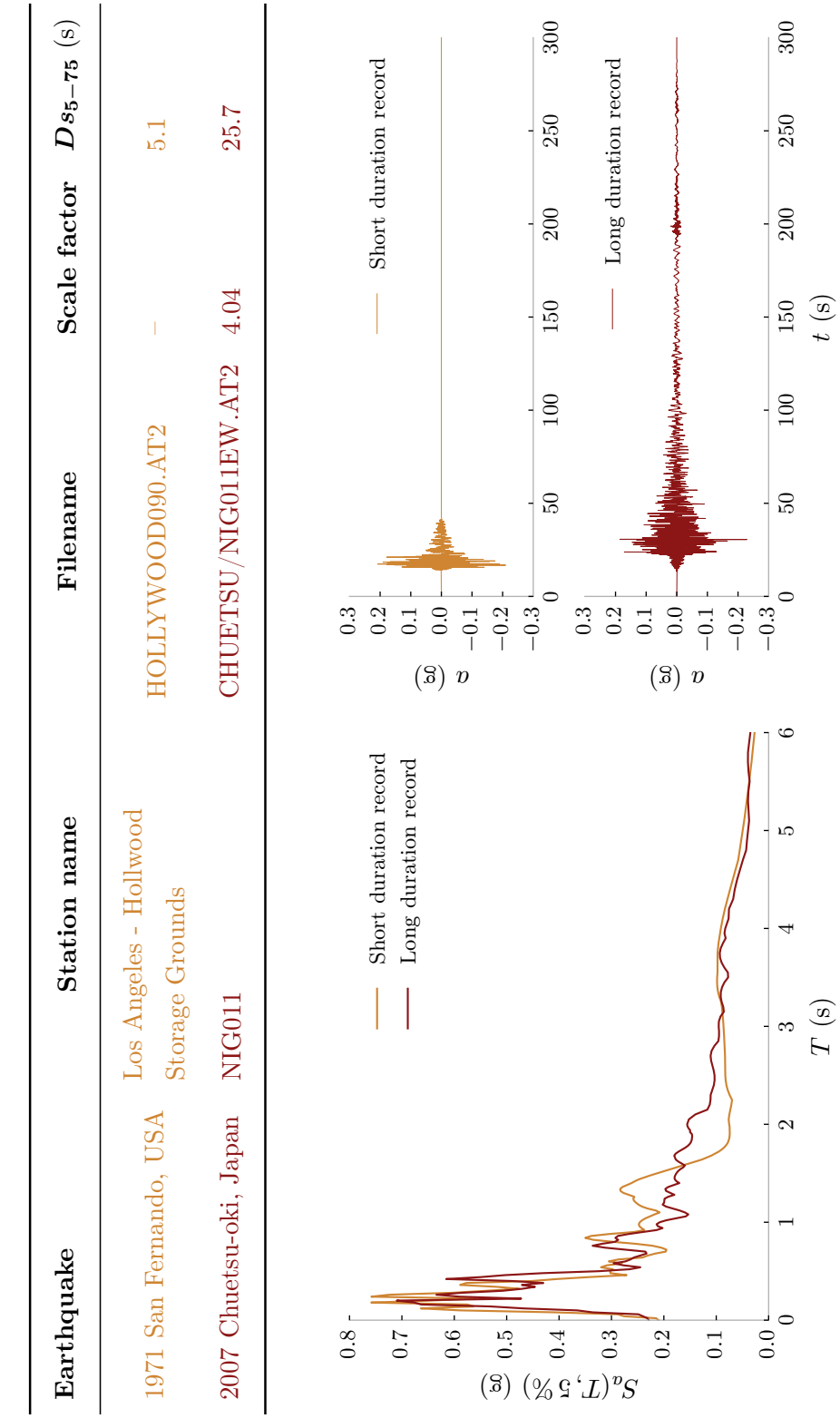

Spectrally equivalent record pair #24

Earthquake	Station name	Filename	Scale factor	D_{s5-75} (s)
1971 San Fernando, USA	Los Angeles - Hollwood Storage Grounds	HOLLYWOOD180.AT2	–	4.8
2011 Tohoku, Japan	Hannoh	SIT01211031111446_H2.th	3.53	45.9

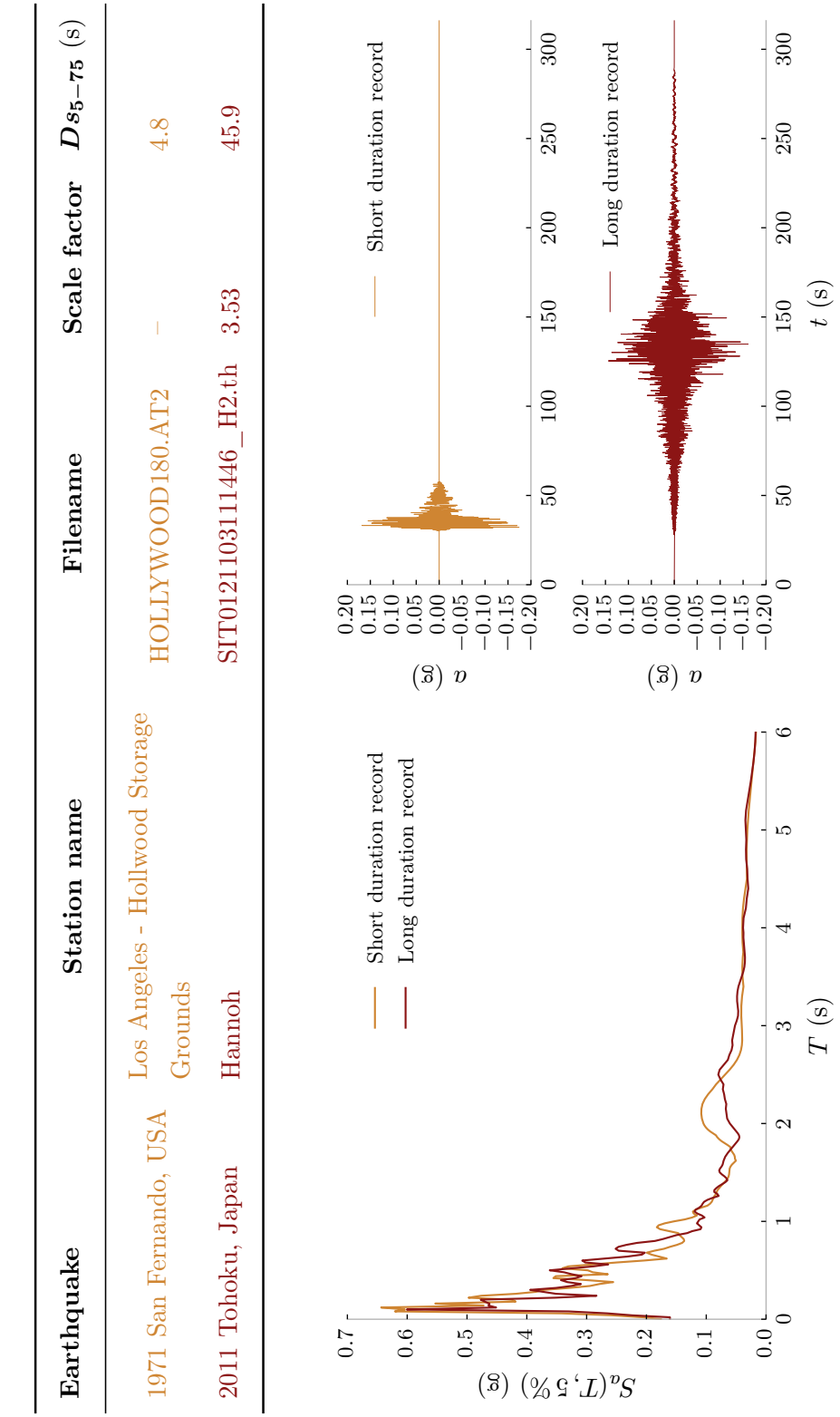

Spectrally equivalent record pair #25

Earthquake	Station name	Filename	Scale factor	Ds_{5-75} (s)
1987 Superstition Hills, USA	El Centro Imperial County Center Grounds	ICC000.AT2	–	7.0
2011 Tohoku, Japan	Kumagaya	SIT0021103111446_H1.th	2.23	43.7

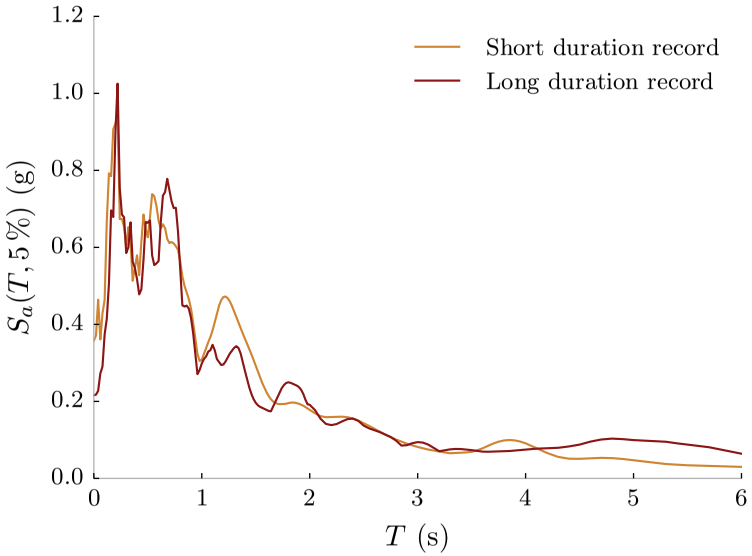

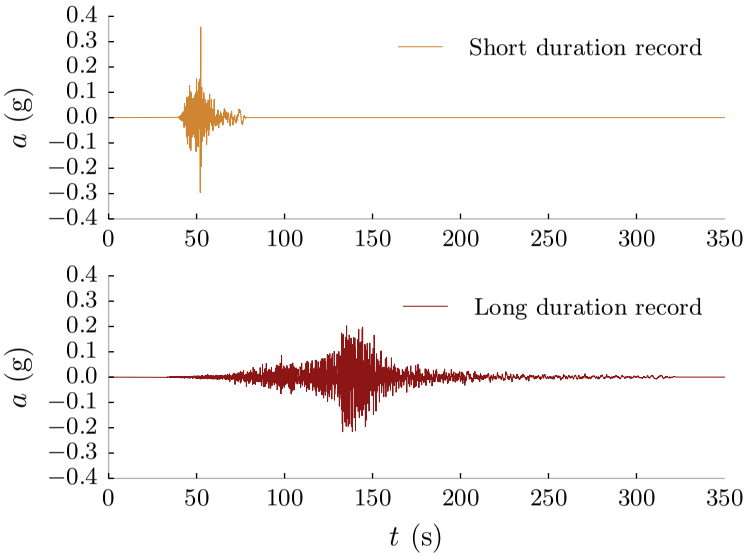

Spectrally equivalent record pair #26

Earthquake	Station name	Filename	Scale factor	Ds_{5-75} (s)
1987 Superstition Hills, USA	El Centro Imperial County Center Grounds	ICC090.AT2	–	7.6
2003 Hokkaido, Japan	Date	HKD1330309260450_H1.th	4.14	28.4

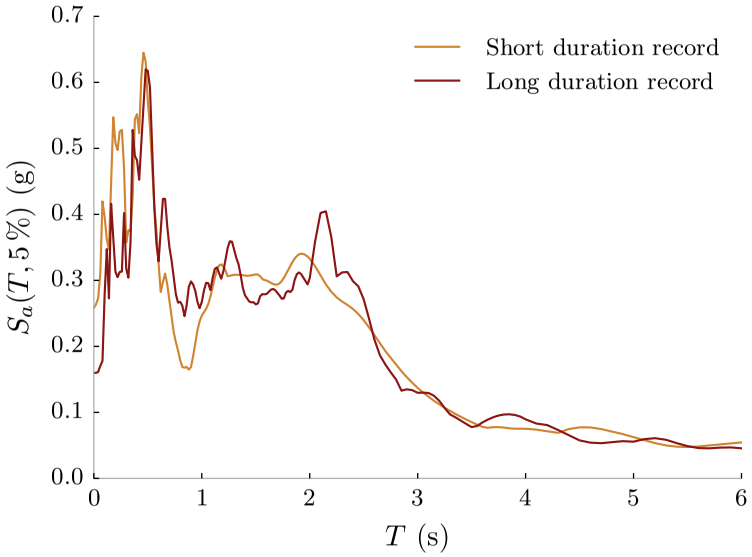

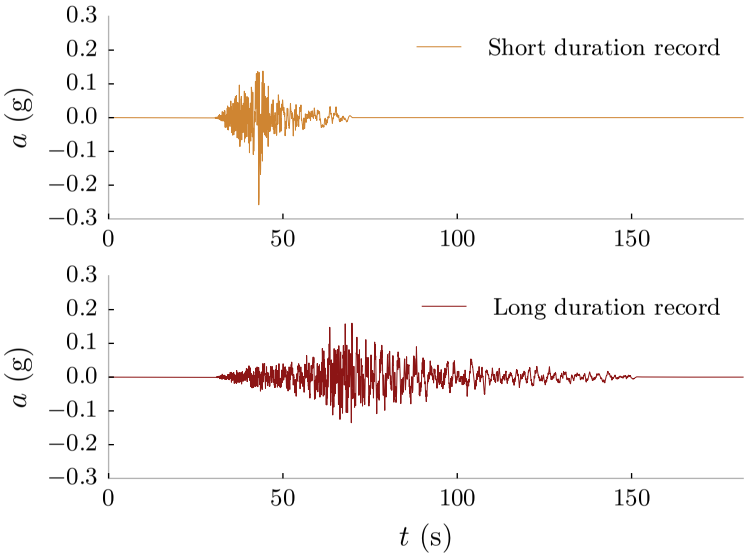

Spectrally equivalent record pair #27

Earthquake	Station name	Filename	Scale factor	Ds_{5-75} (s)
1994 Northridge, USA	Canyon Country - 16628 W. Lost Canyon Road	LOSTCANYON000.AT2	–	3.1
2011 Tohoku, Japan	Shuzenji	SZOH421103111446_H2.th	5.00	57.0

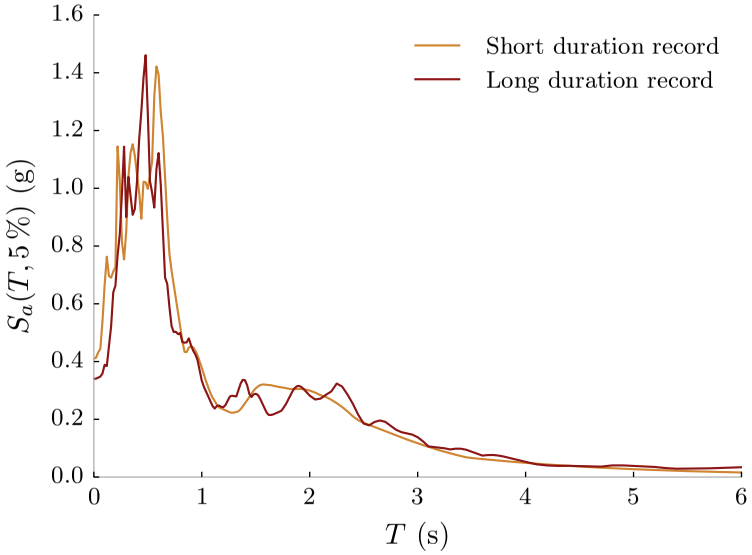

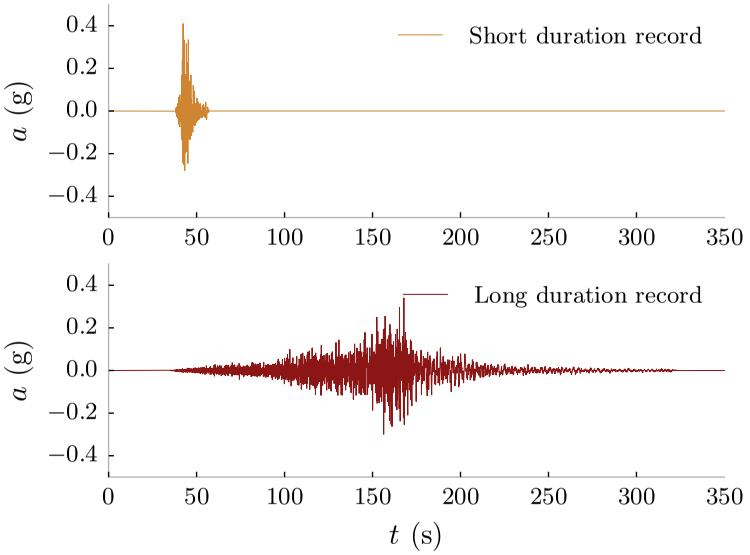

Spectrally equivalent record pair #28

Earthquake	Station name	Filename	Scale factor	D_{s5-75} (s)
1994 Northridge, USA	Canyon Country - 16628 W. Lost Canyon Road	LOSTCANYON270.AT2	–	2.9
2011 Tohoku, Japan	Hijiori	YMT0051103111446_H2.th	4.73	68.8

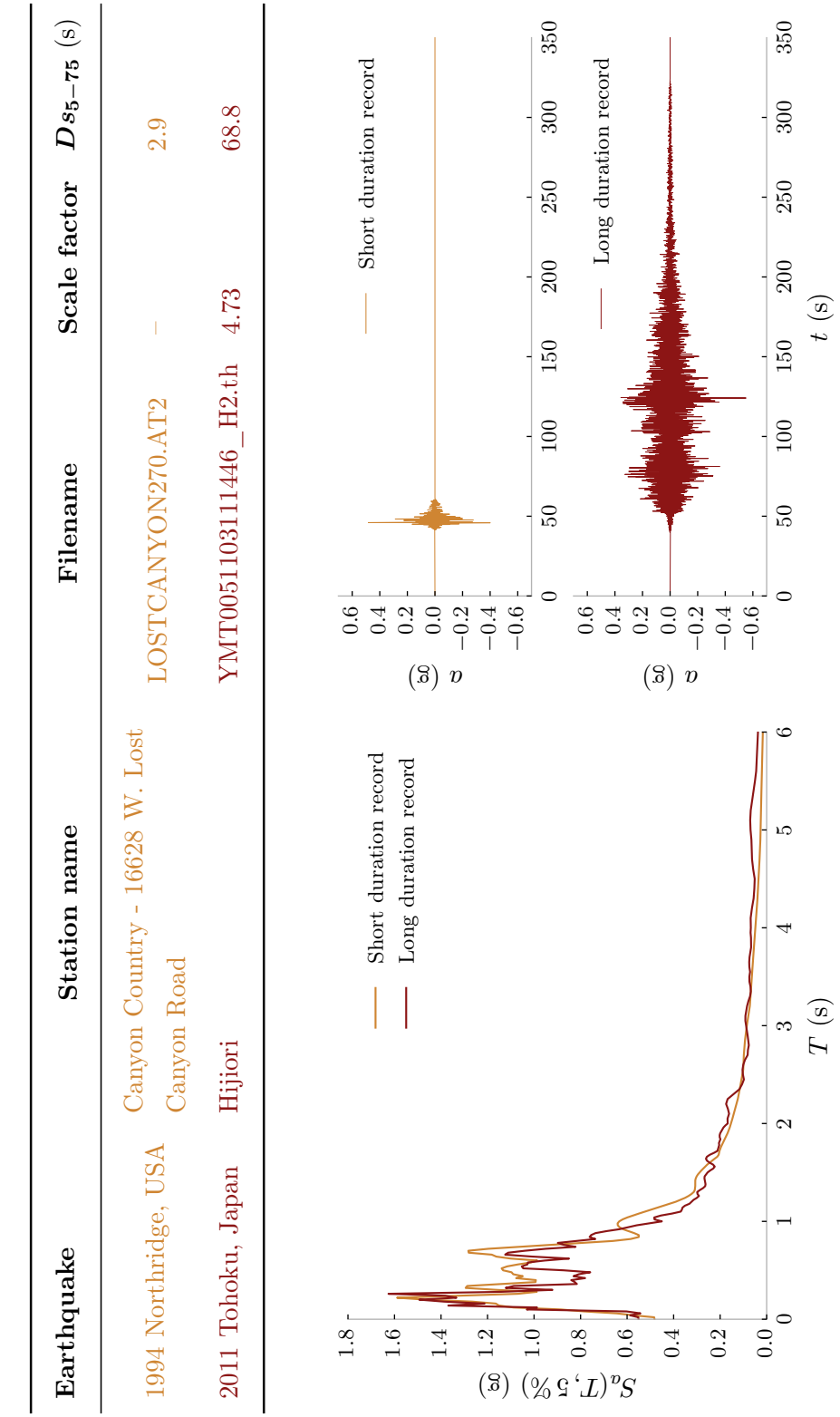

Spectrally equivalent record pair #29

Earthquake	Station name	Filename	Scale factor	Ds_{5-75} (s)
1994 Northridge, USA	Beverly Hills - 14145 Mulholland Drive	MULHOLLAND009.AT2	–	6.1
2011 Tohoku, Japan	Yokoami	TKY0221103111446_H2.th	1.88	42.0

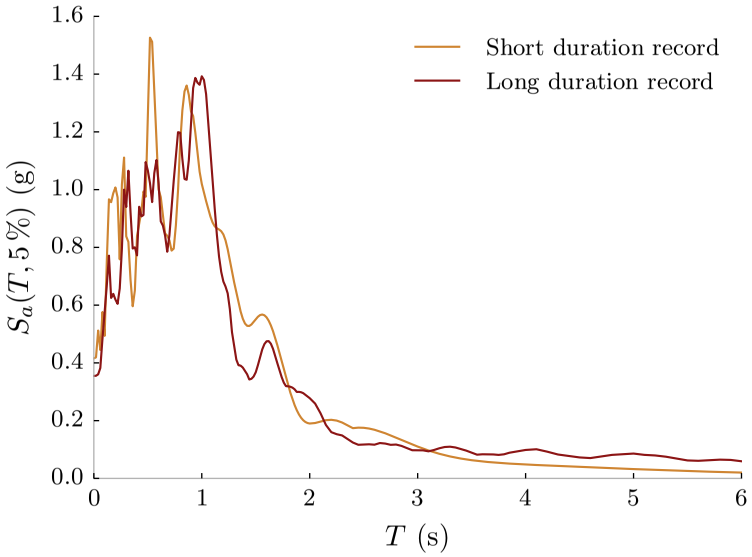

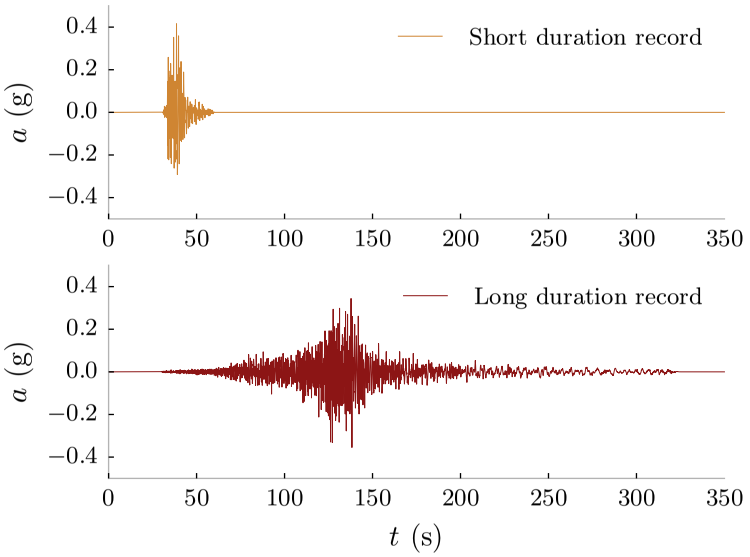

Spectrally equivalent record pair #30

Earthquake	Station name	Filename	Scale factor	D_{s5-75} (s)
1994 Northridge, USA	Beverly Hills - 14145 Mulholland Drive	MULHOLLAND279.AT2	–	5.0
2011 Tohoku, Japan	Shiroishi	MYGH091103111446_H2.th	1.60	70.4

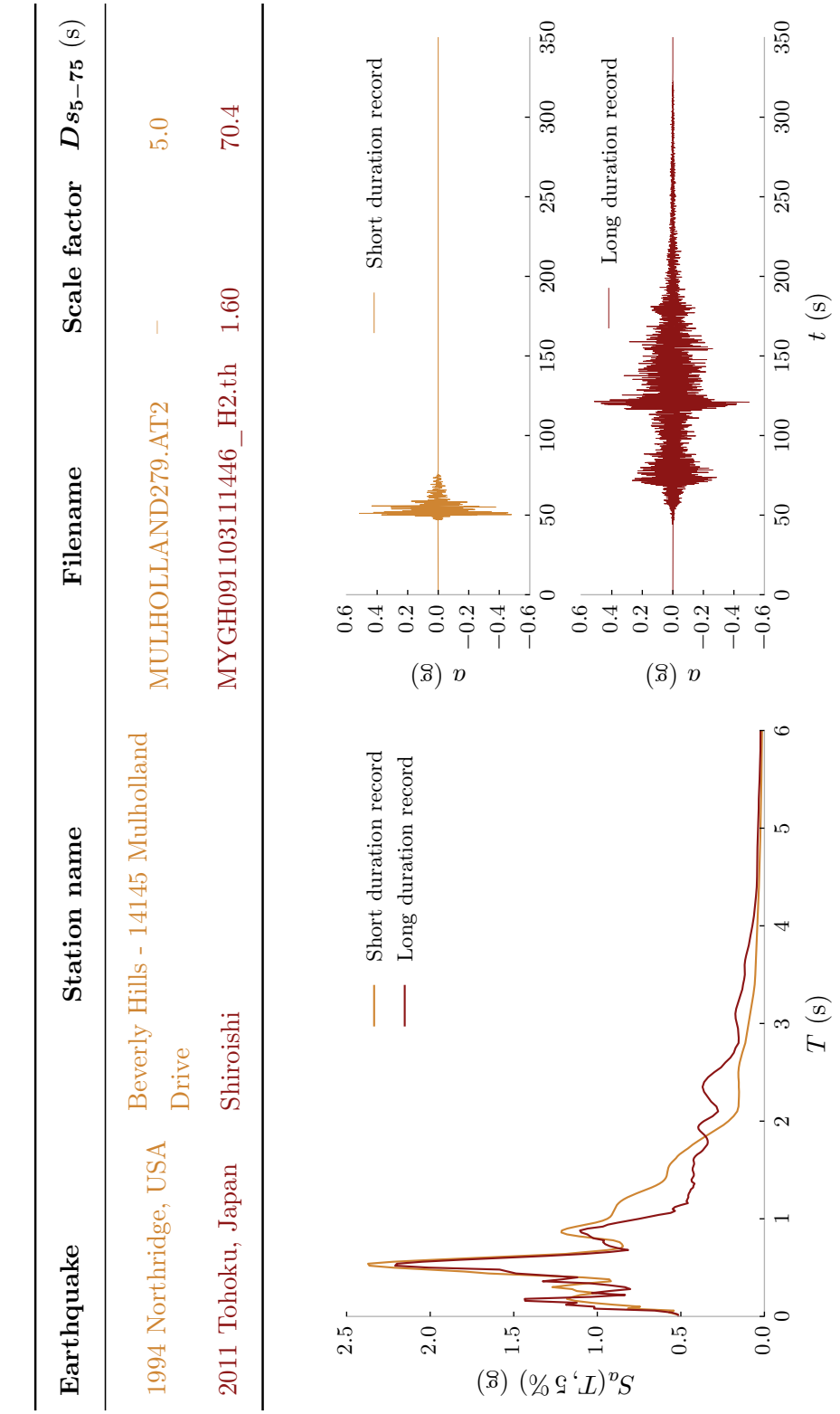

Spectrally equivalent record pair #31

Earthquake	Station name	Filename	Scale factor	Ds_{5-75} (s)
1995 Kobe, Japan	Nishi-Akashi	NISHI000.AT2	–	4.0
2011 Tohoku, Japan	Atsugi	KNG0091103111446_H2.th	3.02	48.1

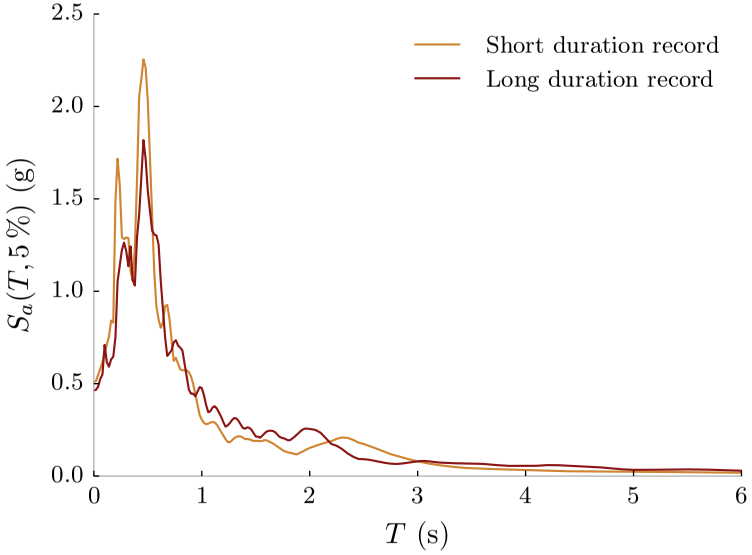

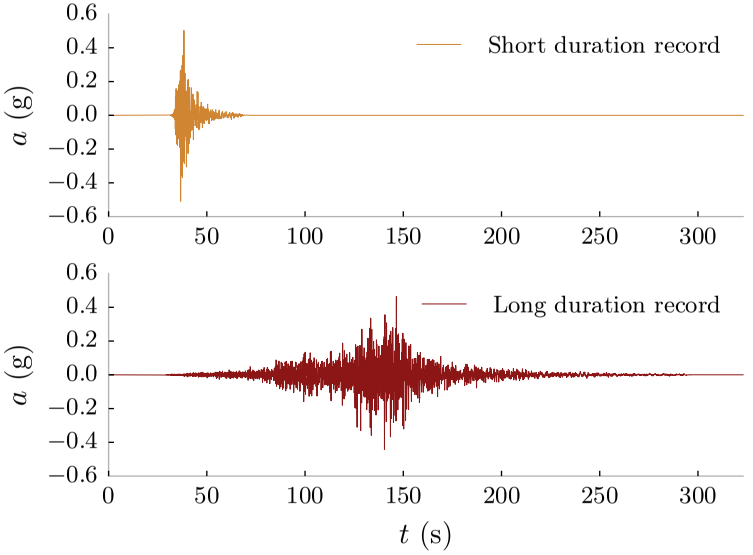

Spectrally equivalent record pair #32

Earthquake	Station name	Filename	Scale factor	Ds_{5-75} (s)
1995 Kobe, Japan	Nishi-Akashi	NISHI090.AT2	–	4.5
2002 Denali, USA	Fairbanks - Geophysical Observatory, CIGO	DENALI/FAIGO360.AT2	5.00	27.7

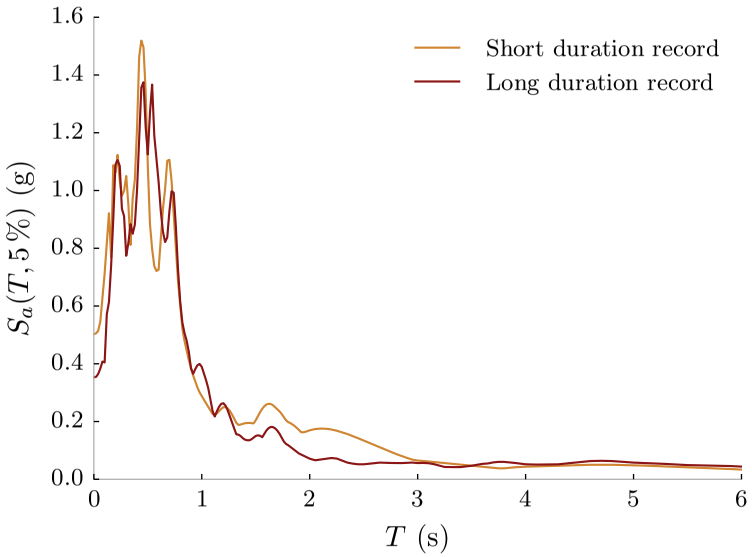

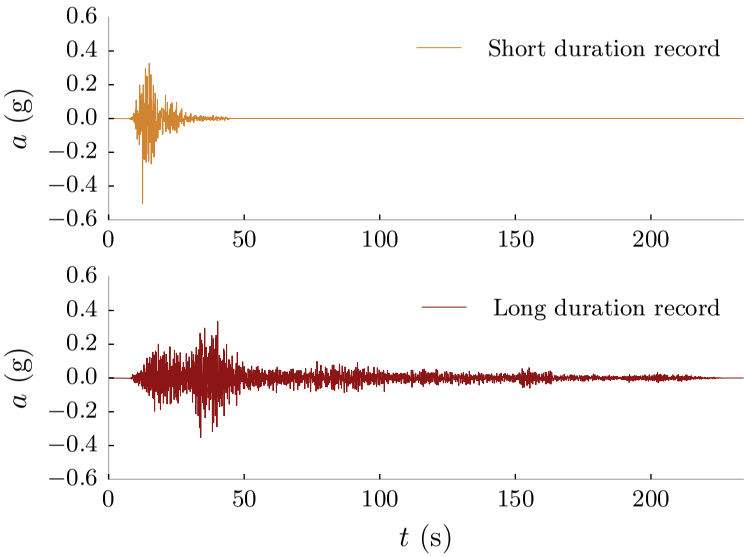

Spectrally equivalent record pair #33

Earthquake	Station name	Filename	Scale factor	Ds_{5-75} (s)
1987 Superstition Hills, USA	Poe Road (temp)	POE270.AT2	–	9.8
2011 Tohoku, Japan	Kuji	IWT0021103111446_H1.th	2.25	53.1

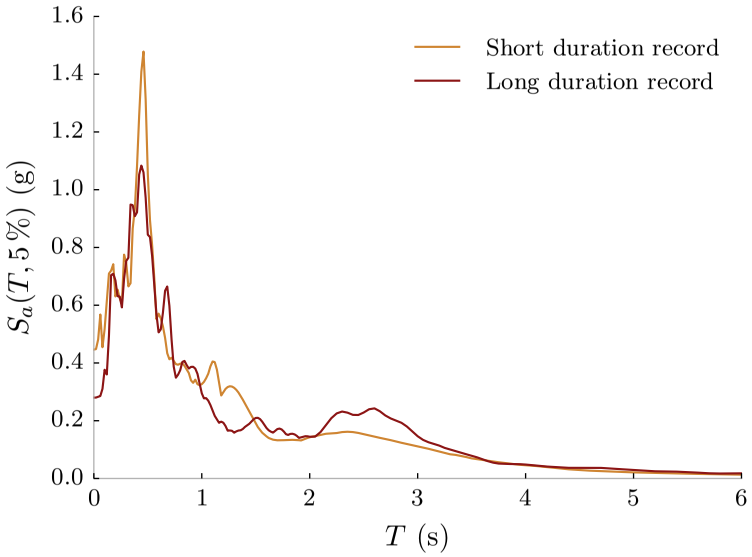

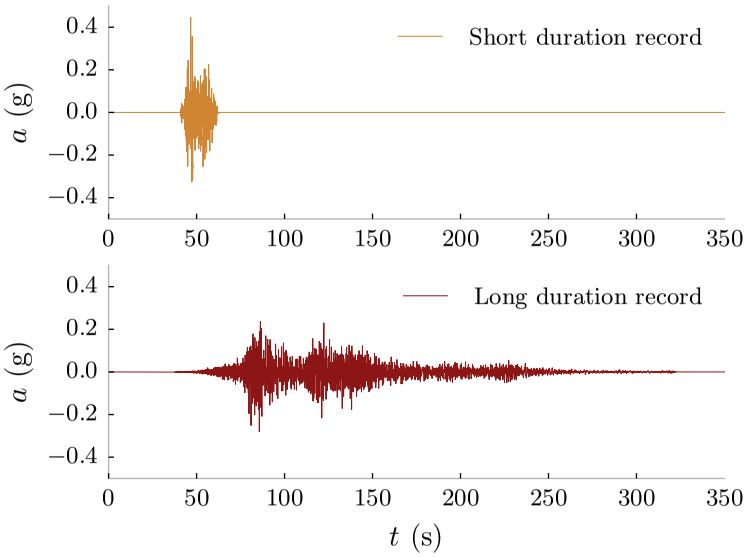

Spectrally equivalent record pair #34

Earthquake	Station name	Filename	Scale factor	Ds_{5-75} (s)
1987 Superstition Hills, USA	Poe Road (temp)	POE360.AT2	–	11.2
2011 Tohoku, Japan	Ashiro	IWT022110311144 6_H2.th	2.29	54.4

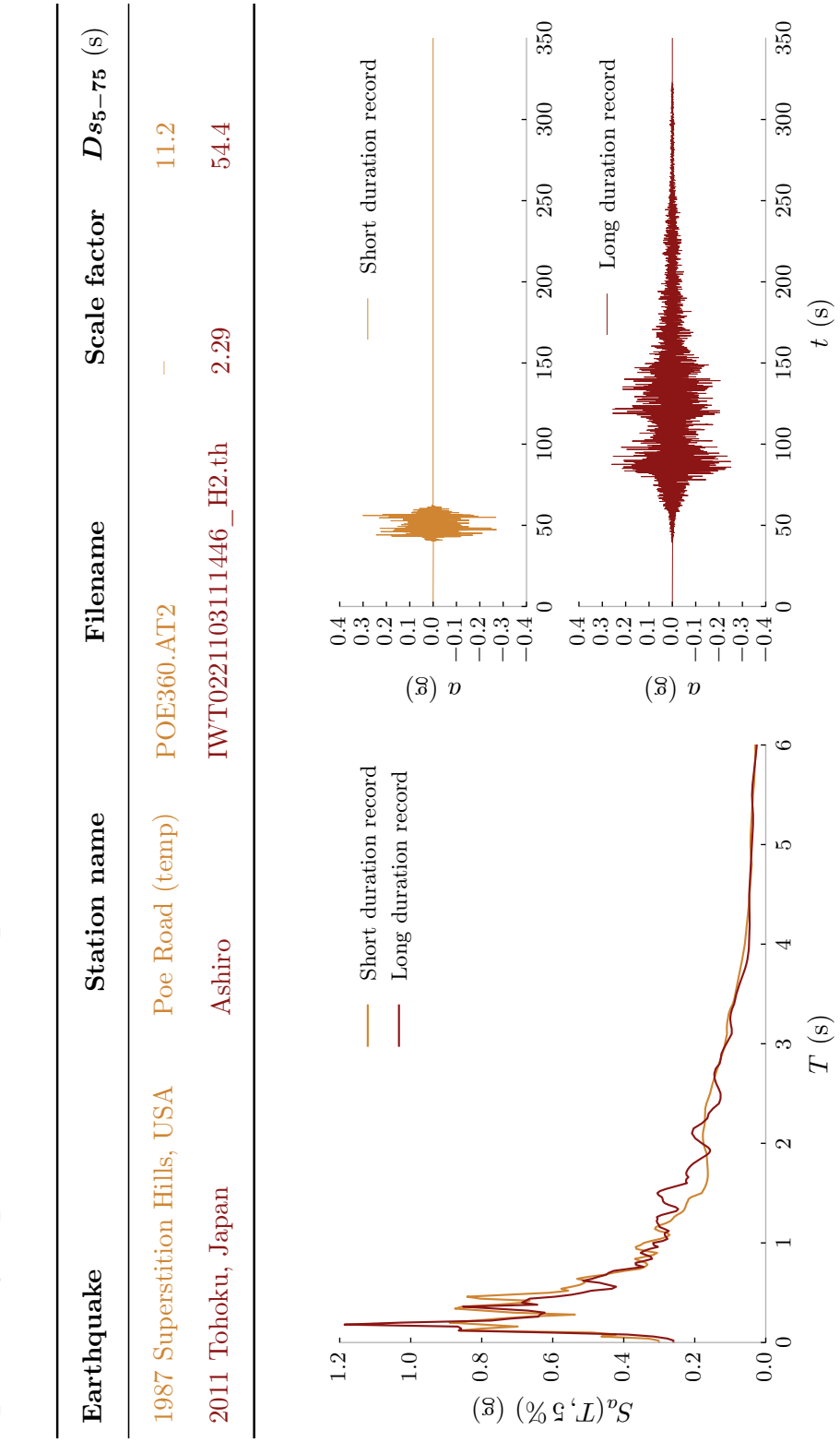

Spectrally equivalent record pair #35

Earthquake	Station name	Filename	Scale factor	Ds_{5-75} (s)
1992 Cape Mendocino, USA	Rio Dell Overpass	RIODELL270.AT2	–	4.3
1985 Valparaiso, Chile	Valparaiso El Almendral	VALPARAISOELALMENDRAL50.th	1.11	31.1

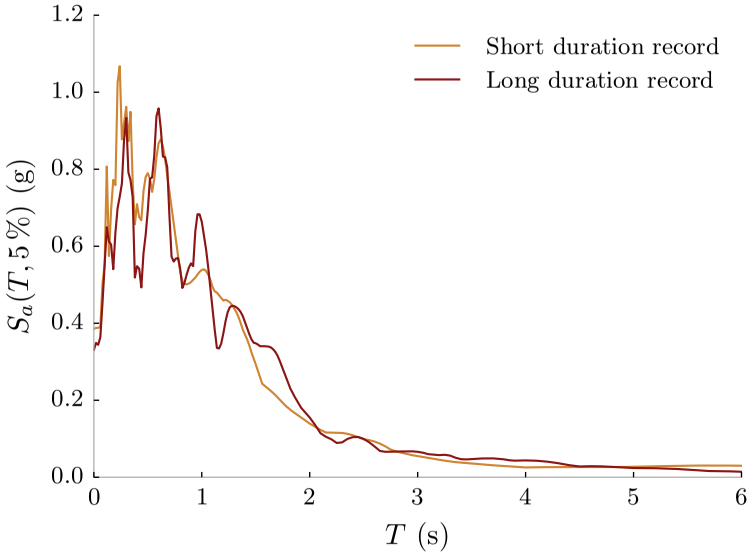

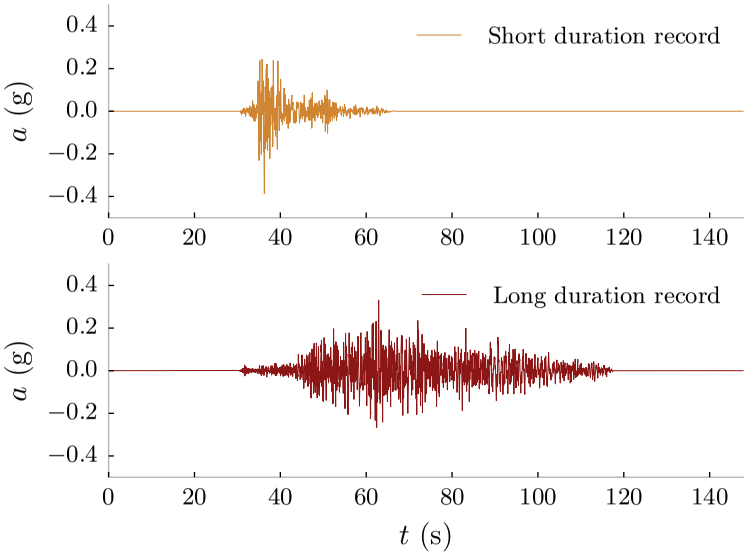

Spectrally equivalent record pair #36

Earthquake	Station name	Filename	Scale factor	Ds_{5-75} (s)
1992 Cape Mendocino, USA	Rio Dell Overpass	RIODELL360.AT2	–	1.9
1985 Valparaiso, Chile	Caquenes	CAUQUENESL.th	5.00	25.2

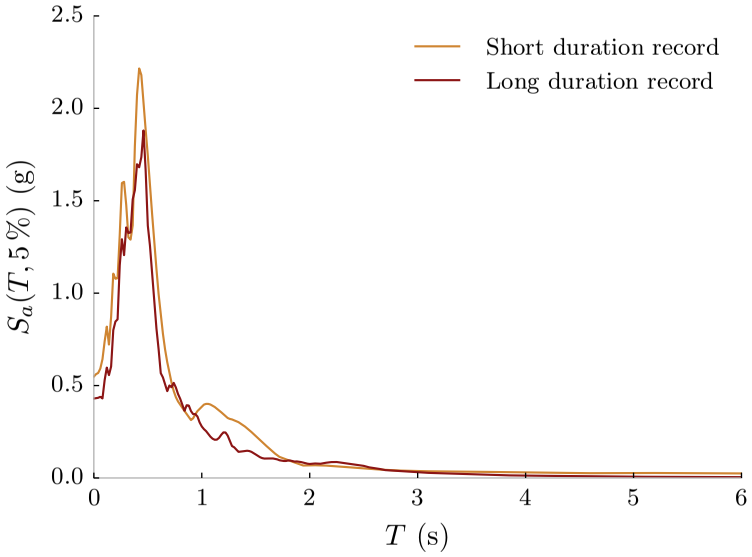

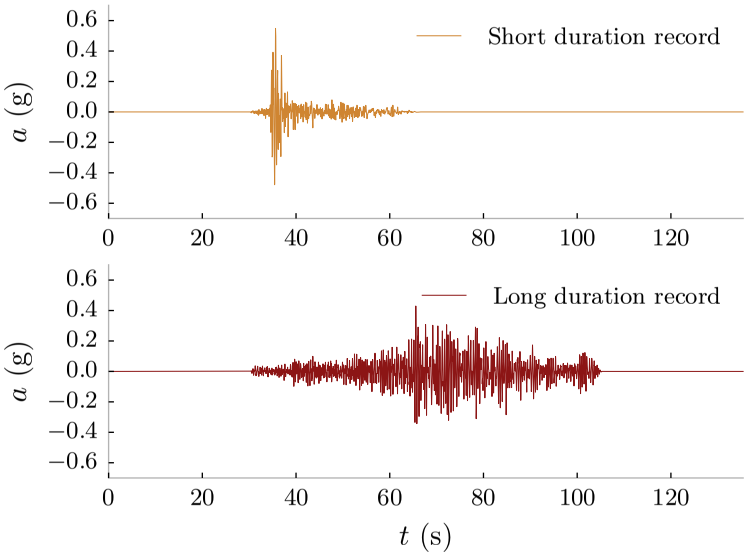

Spectrally equivalent record pair #37

Earthquake	Station name	Filename	Scale factor	Ds_{5-75} (s)
1995 Kobe, Japan	Shin-Osaka	SHIN000.AT2	–	3.6
2011 Tohoku, Japan	Nishikawa-E	YMTH151103111446_H2.th	2.43	71.7

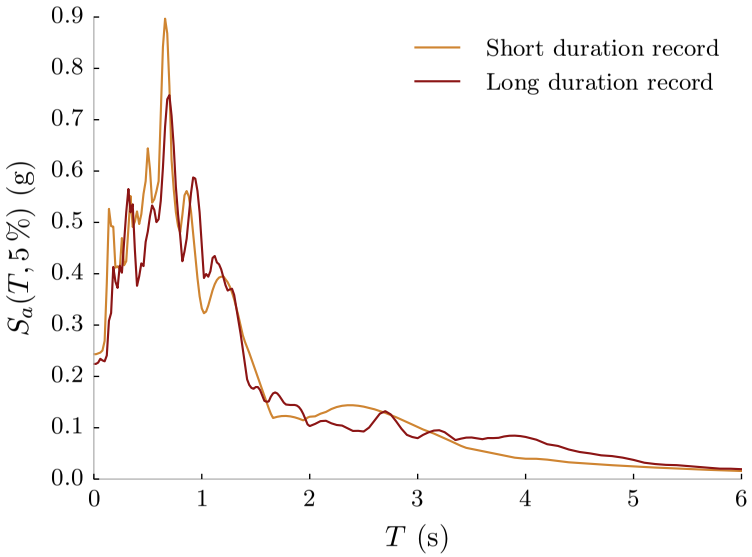

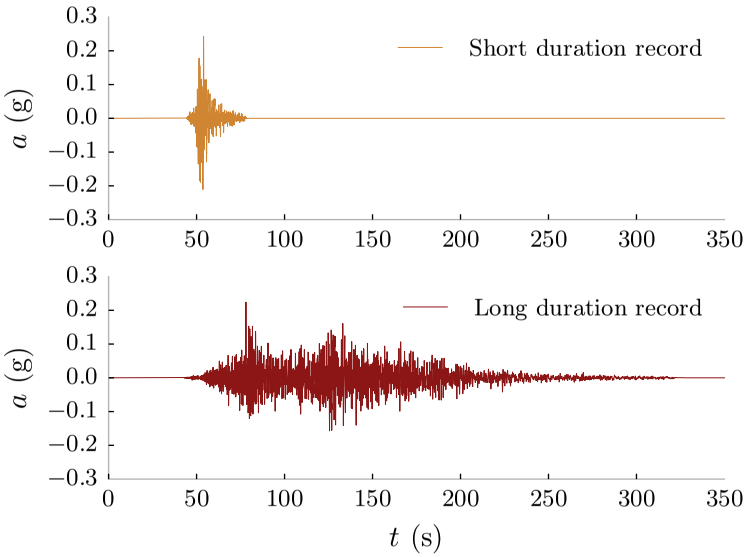

Spectrally equivalent record pair #38

Earthquake	Station name	Filename	Scale factor	D_{s5-75} (s)
1995 Kobe, Japan	Shin-Osaka	SHIN090.AT2	–	4.5
2011 Tohoku, Japan	Hasaki2	IBRH20110311111446_H2.th	1.13	28.7

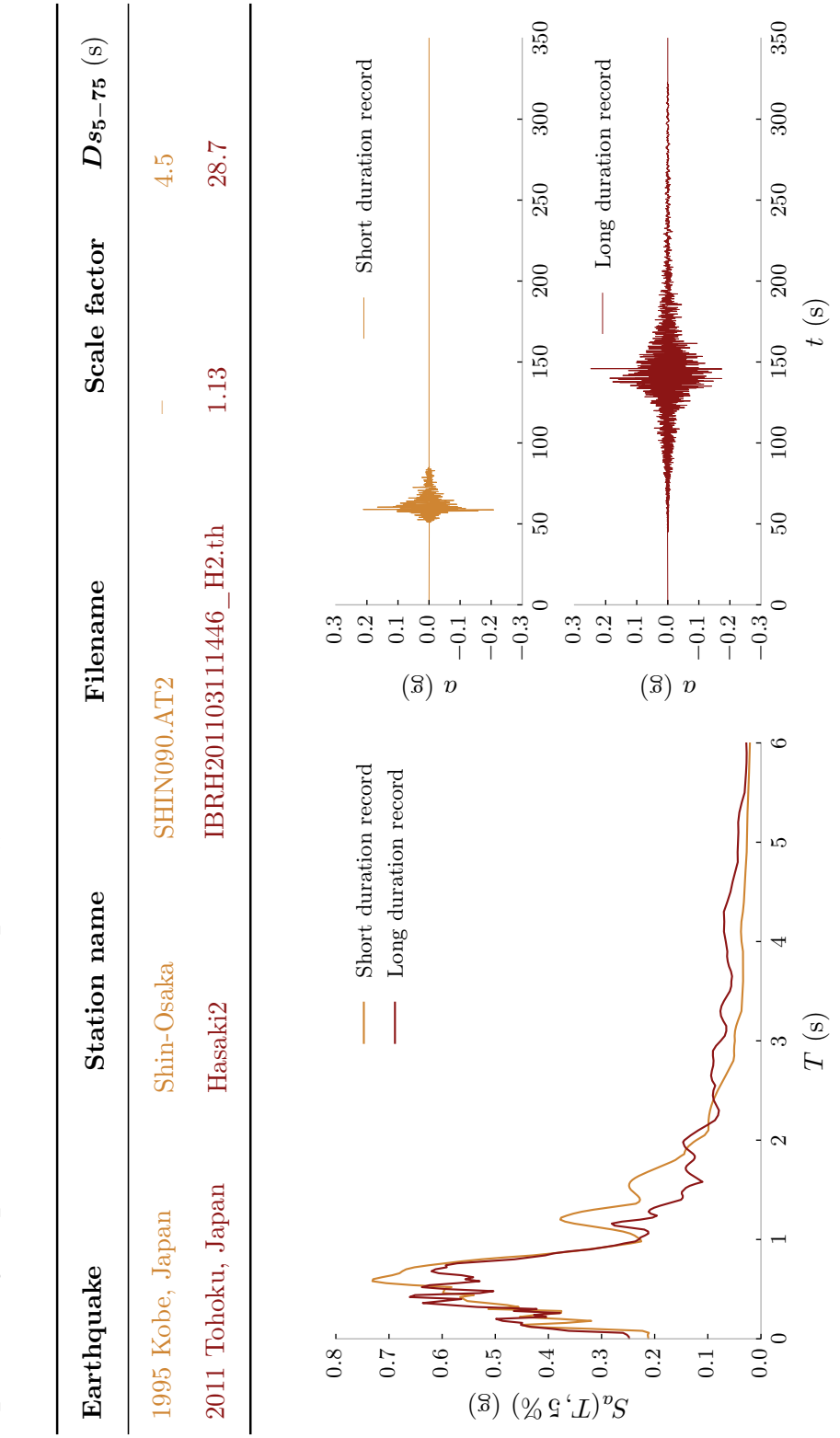

Spectrally equivalent record pair #39

Earthquake	Station name	Filename	Scale factor	Ds_{5-75} (s)
1999 Chi-Chi, Taiwan	TCU045	TCU045E.AT2	–	7.4
2008 Wenchuan, China	Hongyatai	WENCHUAN/UA1040.AT2	2.95	38.8

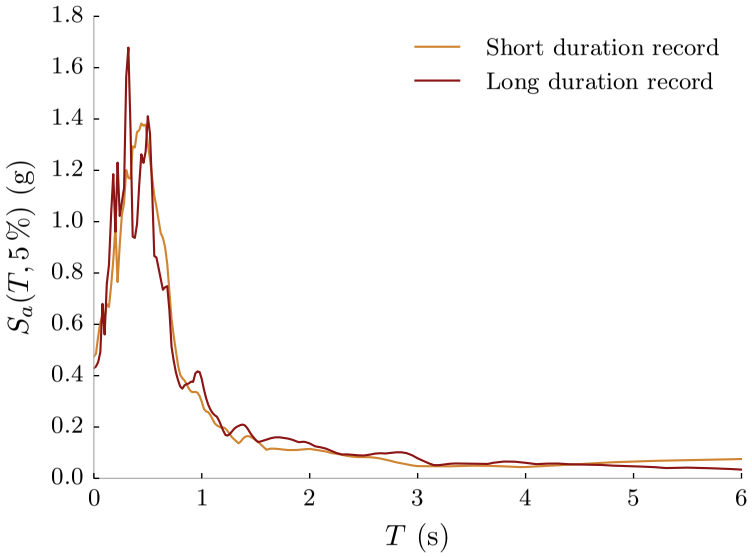

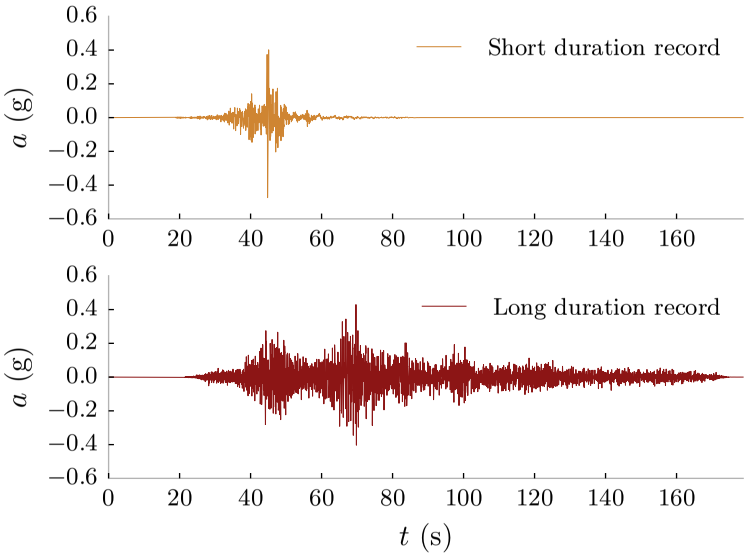

Spectrally equivalent record pair #40

Earthquake	Station name	Filename	Scale factor	Ds_{5-75} (s)
1999 Chi-Chi, Taiwan	TCU045	TCU045N.AT2	–	8.7
1985 Valparaiso, Chile	Llolleo	LLOLLEO10.th	0.61	27.5

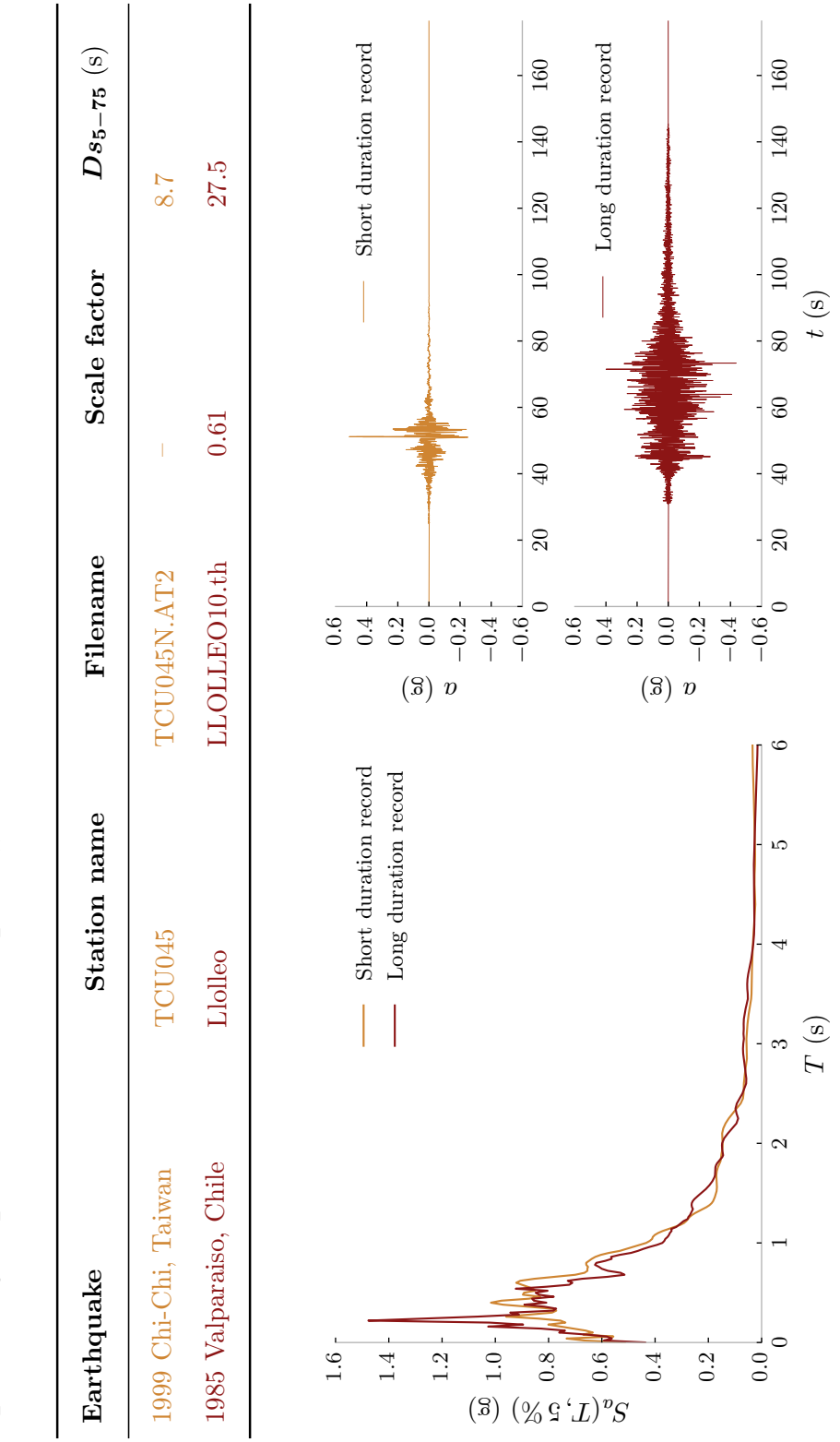

Spectrally equivalent record pair #41

Earthquake	Station name	Filename	Scale factor	D_{s5-75} (s)
1976 Friuli, Italy	Tolmezzo	TOLMEZZO000.AT2	–	2.5
2011 Tohoku, Japan	Kohriyama	FKS018110311144 6_H2.th	0.48	67.5

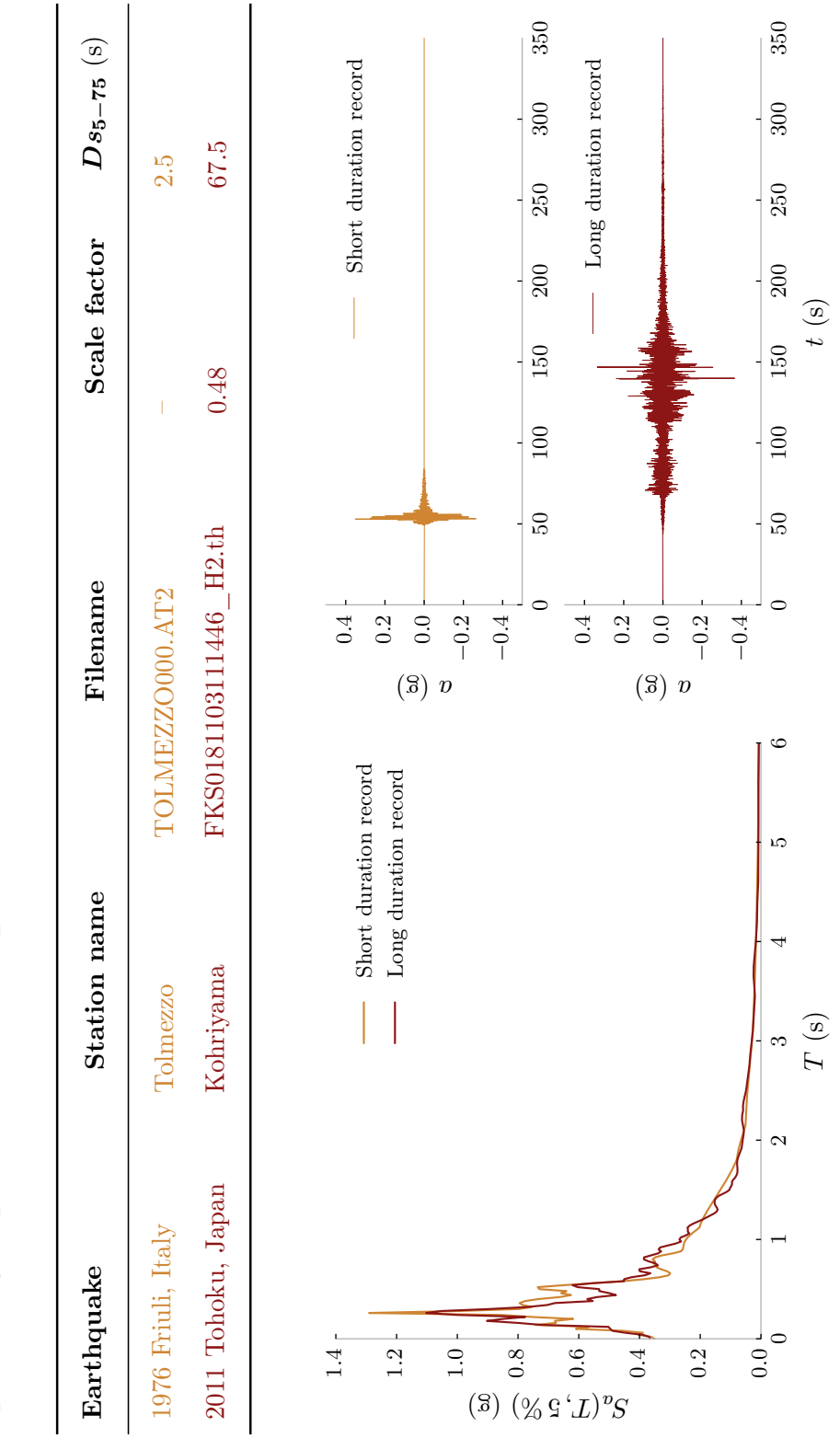

Spectrally equivalent record pair #42

Earthquake	Station name	Filename	Scale factor	Ds_{5-75} (s)
1976 Friuli, Italy	Tolmezzo	TOLMEZZO270.AT2	–	2.5
2011 Tohoku, Japan	Nakaminato	IBR007110311144 46_H1.th	0.59	34.4

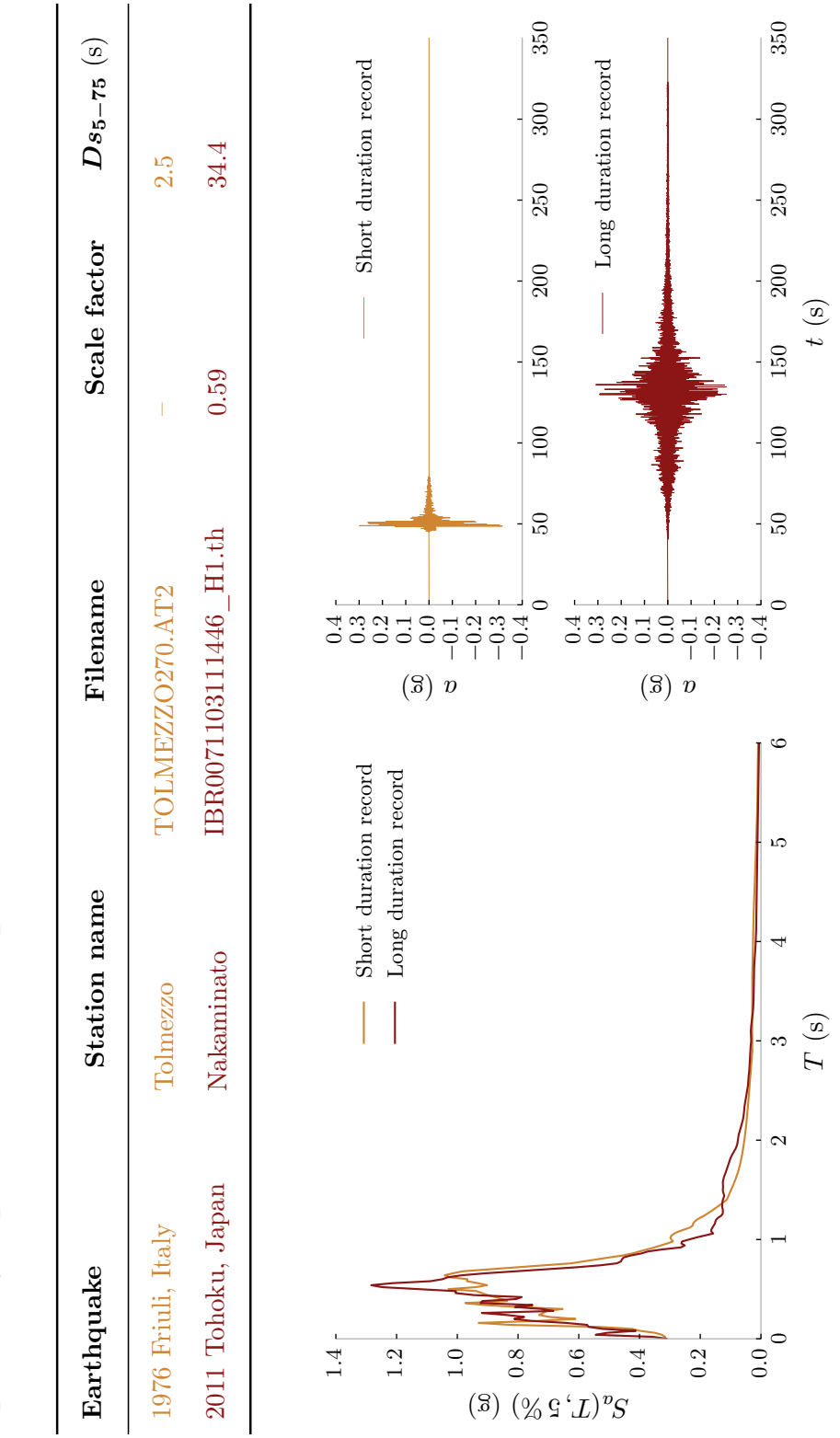

Spectrally equivalent record pair #43

Earthquake	Station name	Filename	Scale factor	Ds_{5-75} (s)
1992 Landers, USA	Yermo Fire Station	YERMO270.AT2	–	7.1
2011 Tohoku, Japan	Hachinohe	AOMH131103111446_H2.th	1.51	62.7

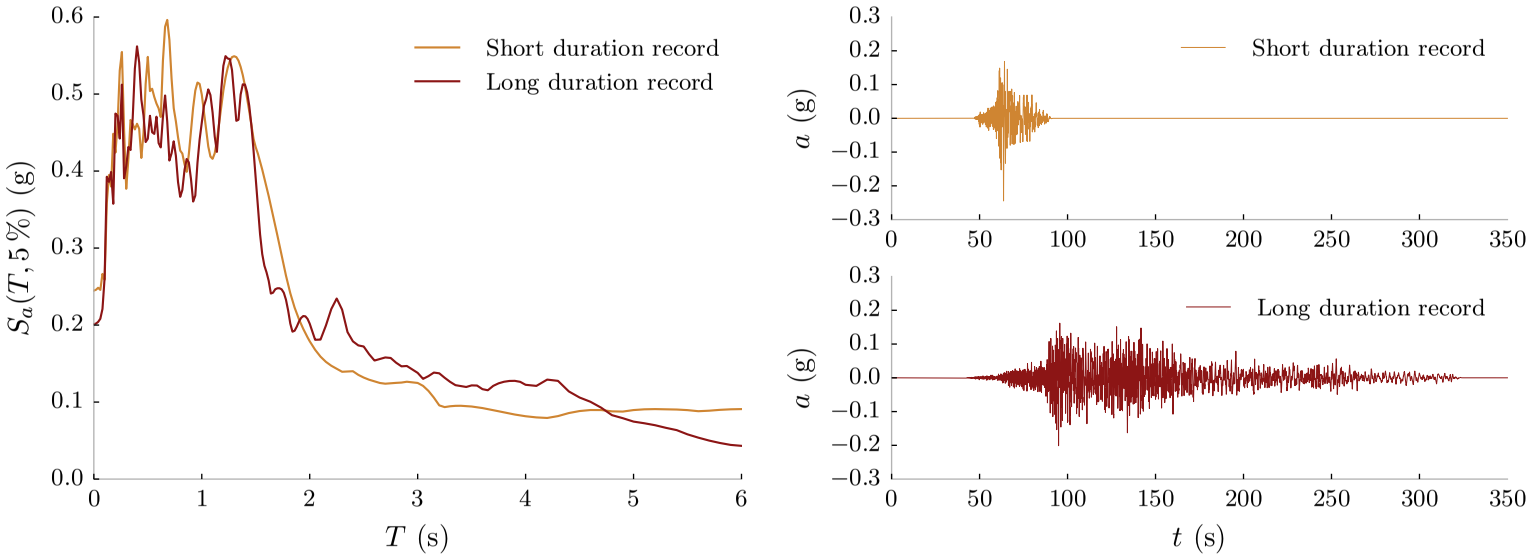

Spectrally equivalent record pair #44

Earthquake	Station name	Filename	Scale factor	D_{s5-75} (s)
1992 Landers, USA	Yermo Fire Station	YERMO360.AT2	–	10.9
2011 Tohoku, Japan	Ukita	TKY026110311144 46_H1.th	0.94	44.8

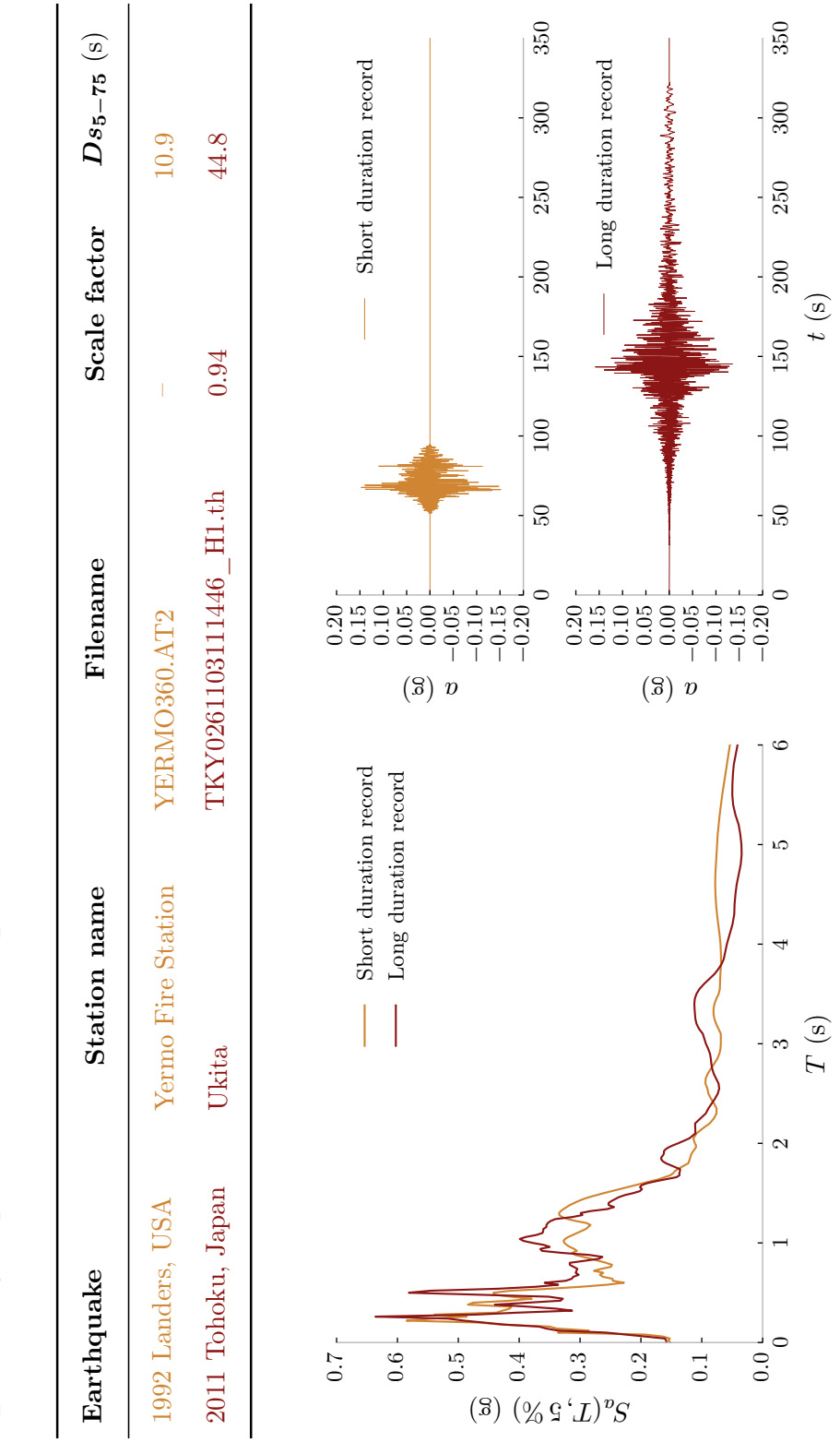

Appendix B

Computation of $S_{a,avg}$ as the geometric mean of the function $S_a(T)$

$S_{a,avg}(T_{start}, T_{end})$ is a ground motion intensity measure that represents the geometric mean of the portion of its response spectrum that lies between the periods T_{start} and T_{end}. Previous studies like Baker and Cornell (2006a), Bianchini et al. (2009), and Eads et al. (2015) have recommended computing $S_{a,avg}(T_{start}, T_{end})$ as the sample geometric mean of response spectral ordinates, sampled at n linearly or logarithmically spaced periods from T_{start} to T_{end}: τ_1, τ_2, ..., τ_n, such that $\tau_1 = T_{start}$ and $\tau_n = T_{end}$:

$$S_{a,avg}(T_{start}, T_{end}) = \left(\prod_{j=1}^{n} S_a(\tau_j) \right)^{1/n} \tag{B.1}$$

This method of computing $S_{a,avg}$, however, usually requires the additional step of re-sampling the response spectrum at a set of n linearly or logarithmically spaced periods between T_{start} and T_{end}, and even deciding what value of n to use, which has been the subject of a number of research efforts (Bianchini 2008; Eads 2013). Using an insufficient number of periods in the calculation could lead to an inaccurate estimate of $S_{a,avg}$.

$S_{a,avg}$ can be computed more generally, as the geometric mean of the function $S_a(T)$:

$$S_{a,avg}(T_{start}, T_{end}) = \exp\left(\frac{\int_{T_{start}}^{T_{end}} \ln S_a(\tau) d\tau}{T_{end} - T_{start}}\right) \tag{B.2}$$

The integral of the natural logarithm of the response spectrum can be computed using any numerical integration scheme, like the trapezoidal rule or Simpson's rule, using the same set of periods the response spectrum was initially computed at. This method requires neither the re-sampling of the response spectrum at any specific set of periods, nor any decision regarding the number of periods to use, as long as the general shape of the response spectrum is accurately represented.

The use of logarithmically spaced periods in Equation (B.1) results in weighting shorter periods more than longer periods in the computation of $S_{a,avg}$. Since response spectral ordinates at periods longer than the fundamental modal period of the structure generally control its collapse response, the use of logarithmically spaced periods, which assigns smaller weights to these longer periods, requires the use of longer T_{end} values when computing $S_{a,avg}$ than when using linearly spaced periods, to be able to efficiently predict structural collapse response (Eads 2013). Depending on the fundamental period of the structure, this often requires the use of response spectral ordinates at periods longer than 10 s, which are often strongly influenced by the low-cut filters usually employed in the baseline-correction and processing of recorded accelerograms (Boore and Bommer 2005). Hence, the use of logarithmically spaced periods to compute $S_{a,avg}$ is discouraged. It is worth noting that Equation (B.2) implicitly uses infinitesimal linearly spaced periods. If the use of infinitesimal logarithmically spaced periods is desired, Equation (B.2) can be slightly modified by computing a weighted geometric mean instead, using $1/\tau$ as the weighting function:

$$S_{a,avg}(T_{start}, T_{end}) = \exp\left(\frac{\int_{T_{start}}^{T_{end}} (1/\tau) \ln S_a(\tau) d\tau}{\int_{T_{start}}^{T_{end}} (1/\tau) d\tau}\right) \tag{B.3}$$

Equation (B.1) is used to compute $S_{a,avg}$, and in turn, S_aRatio, in the structural reliability framework described in Chapter 5. Using Equation (B.2) instead, would

require a few modifications to the procedure described in § 5.4 to compute hazard-consistent target distributions of S_aRatio and Ds. Firstly, the response spectral ordinates constituting the vector $\mathbf{ln}\,\boldsymbol{IM}$, as described by Equation (5.2), could now correspond to any set of arbitrarily spaced periods between T_{start} and T_{end}: $\tau_1, \tau_2, \ldots, \tau_n$; such that $\tau_1 = T_{start}$ and $\tau_n = T_{end}$. Secondly, $\ln S_aRatio$ can now be computed as

$$\ln S_aRatio = \ln S_a(T_1) - \frac{\int_{T_{start}}^{T_{end}} \ln S_a(\tau) d\tau}{T_{end} - T_{start}} \tag{B.4}$$

instead of using Equation (5.8). Using any linear numerical integration scheme, the integral in Equation (B.4) can be written as a linear combination of the logarithms of the individual response spectral ordinates:

$$\int_{T_{start}}^{T_{end}} \ln S_a(\tau) d\tau = \sum_{j=1}^{n} \alpha_j \ln S_a(\tau_j) \tag{B.5}$$

where the α_j depend on the specific numerical integration scheme employed. For example, if the trapezoidal rule is used, $\alpha_1 = {}^{(\tau_2-\tau_1)}/_2$, $\alpha_2 = {}^{(\tau_3-\tau_1)}/_2$, $\alpha_3 = {}^{(\tau_4-\tau_2)}/_2$, $\ldots$, $\alpha_{n-1} = {}^{(\tau_n-\tau_{n-2})}/_2$, and $\alpha_n = {}^{(\tau_n-\tau_{n-1})}/_2$. Consequently, the following definition of the matrix $\boldsymbol{A}$, that describes the affine transformation of $\mathbf{ln}\,\boldsymbol{IM} \mid \ln S_a(T_1)$ to $\mathbf{ln}\,\widetilde{\boldsymbol{IM}} \mid \ln S_a(T_1)$, would need to be used instead of Equation (5.10b):

$$\boldsymbol{A} = \begin{bmatrix} -{}^{\alpha_1}/_{(T_{start}-T_{end})} & -{}^{\alpha_2}/_{(T_{start}-T_{end})} & \ldots & -{}^{\alpha_n}/_{(T_{start}-T_{end})} & 0 \\ 0 & 0 & \ldots & 0 & 1 \end{bmatrix} \tag{B.6}$$

Appendix C

S_aRatio and Ds targets in Western USA

This appendix contains maps of conditional median S_aRatio and significant duration (Ds) targets in Western USA, computed at the 0.5 % and 2 % in 50 year hazard levels; corresponding to site soil profiles characterized by $Vs_{30} = 270\,\text{m/s}$ and 760 m/s; and using conditioning periods of 0.2 s, 1.0 s, and 4.0 s. The different models used to compute these targets are described in § 6.6.1. In line with the discussion in § 6.6.1, S_aRatio targets computed using the Zhao et al. (2006) and Abrahamson et al. (2016) GMPEs for interface earthquakes are juxtaposed for comparison. Since the Zhao et al. (2006) GMPE provides predictions of response spectral ordinates only until a period of 5.0 s, the upper end of the period range used to compute the S_aRatio targets conditional on the period 4.0 s was limited to 5.0 s, instead of $3.0T = 12.0\,\text{s}$. Due to similar constraints, the period range was limited to 10.0 s when Abrahamson et al. (2016) was used. Therefore, S_aRatio targets conditional on the period 4.0 s, computed using the two GMPEs, are not directly comparable. Figure numbers corresponding to each combination of parameters are summarized in Table C.1.

Table C.1: Summary of the parameters used to plot each of the maps of conditional median S_aRatio and Ds targets in Appendix C.

Exceedance probability in 50 years (%)	$\boldsymbol{Vs_{30}}$ (m/s)	**Conditioning period** (s)	**Figure**
0.5	270	0.2	C.1
0.5	270	1.0	C.2
0.5	270	4.0	C.3
0.5	760	0.2	C.4
0.5	760	1.0	C.5
0.5	760	4.0	C.6
2	760	0.2	C.7
2	760	1.0	C.8
2	760	4.0	C.9

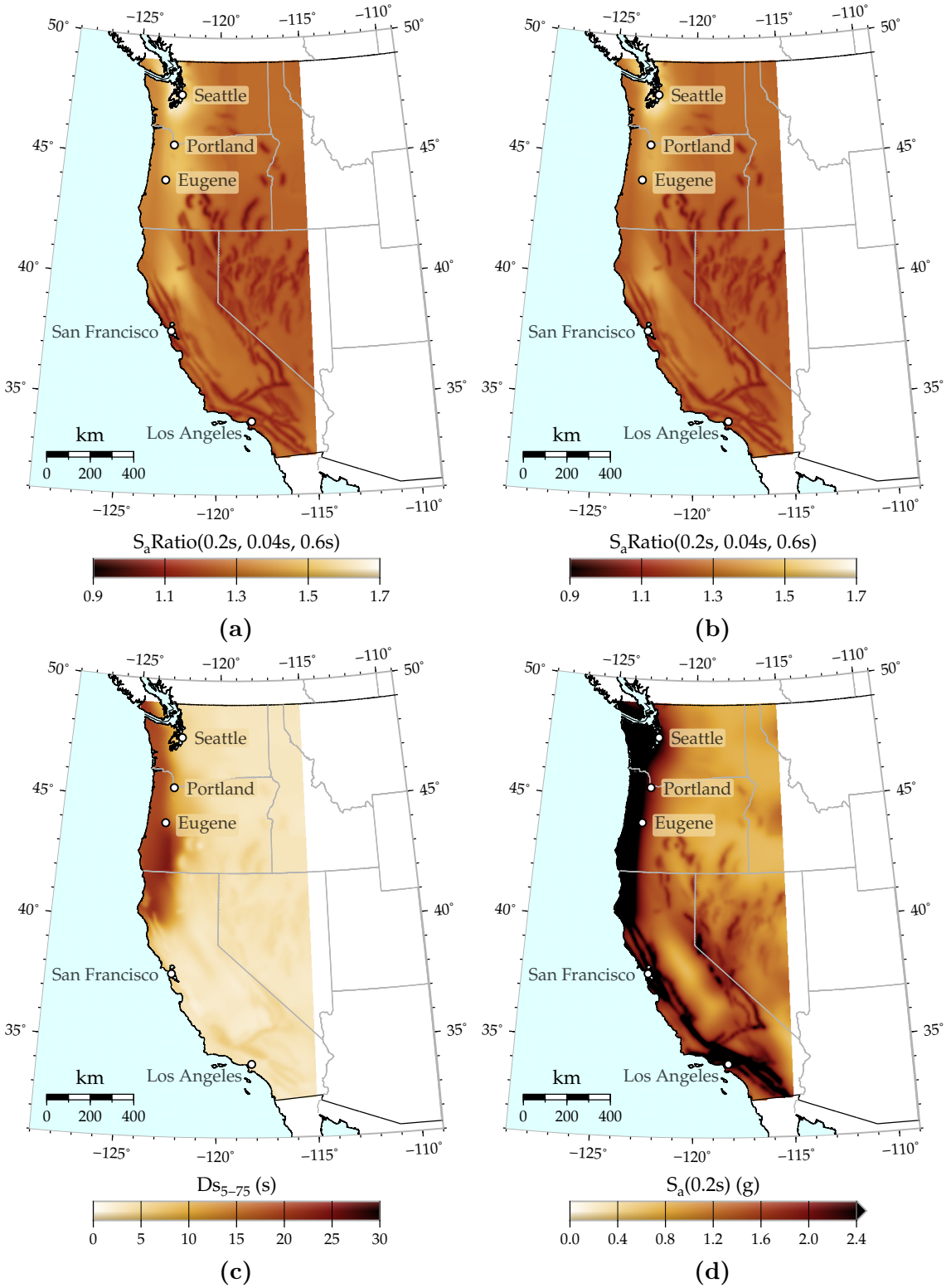

Figure C.1: Median (a), (b) $S_aRatio(0.2\,\text{s}, 0.04\,\text{s}, 0.6\,\text{s})$ and (c) Ds_{5-75} targets in Western USA, conditional on the exceedance of the $S_a(0.2\,\text{s})$ values in (c). The S_aRatio targets in (a) are computed using the Abrahamson et al. (2016) GMPE for interface earthquakes, and those in (b) are computed using Zhao et al. (2006). The $S_a(0.2\,\text{s})$ values in (c) are exceeded with a probability of 0.5 % in 50 years. $Vs_{30} = 270\,\text{m/s}$ is assumed at all sites.

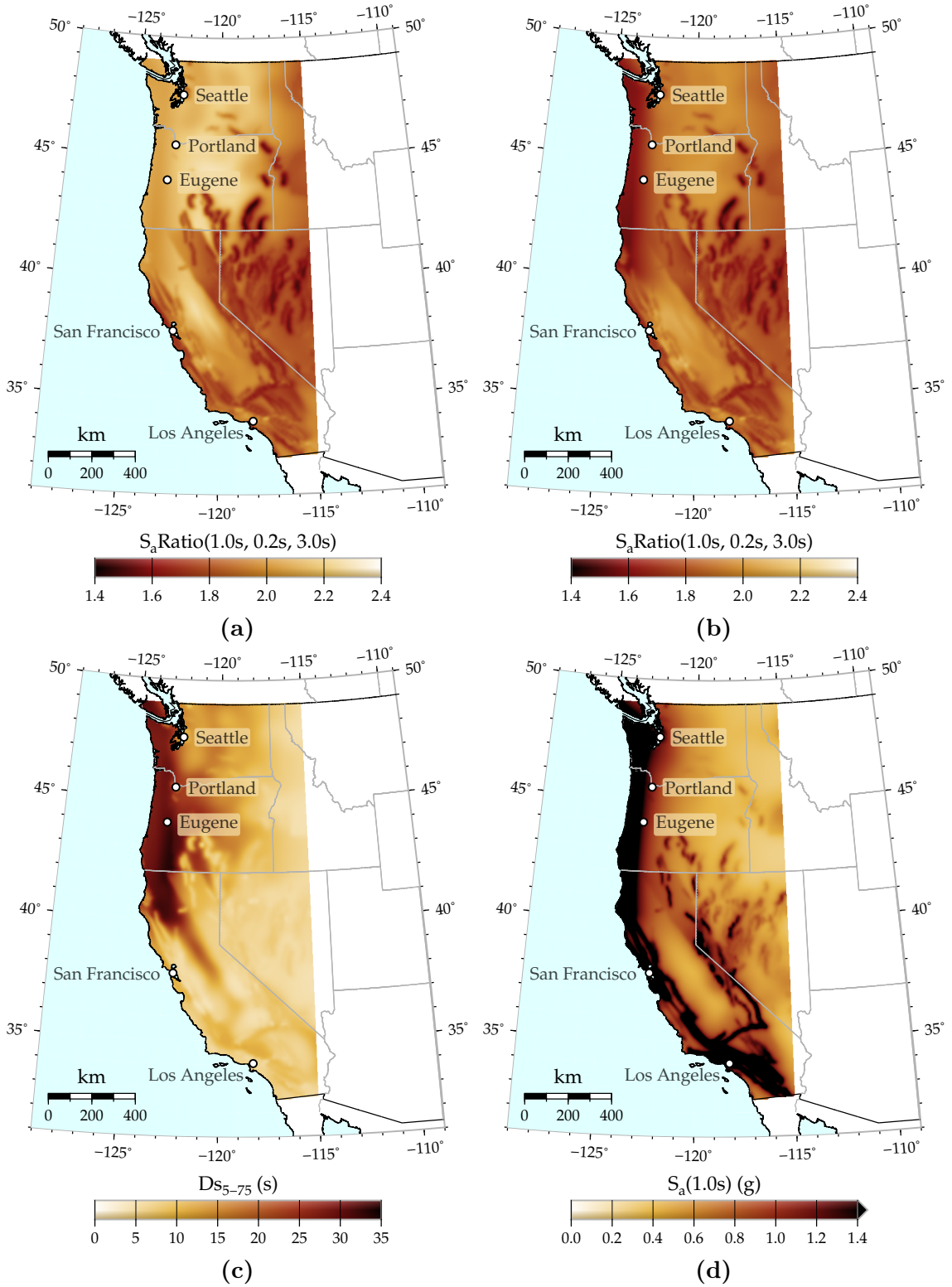

Figure C.2: Median (a), (b) $S_a Ratio(1.0\,\text{s}, 0.2\,\text{s}, 3.0\,\text{s})$ and (c) Ds_{5-75} targets in Western USA, conditional on the exceedance of the $S_a(1.0\,\text{s})$ values in (c). The $S_a Ratio$ targets in (a) are computed using the Abrahamson et al. (2016) GMPE for interface earthquakes, and those in (b) are computed using Zhao et al. (2006). The $S_a(1.0\,\text{s})$ values in (c) are exceeded with a probability of 0.5 % in 50 years. $Vs_{30} = 270\,\text{m/s}$ is assumed at all sites. This is a copy of Figure 6.6.

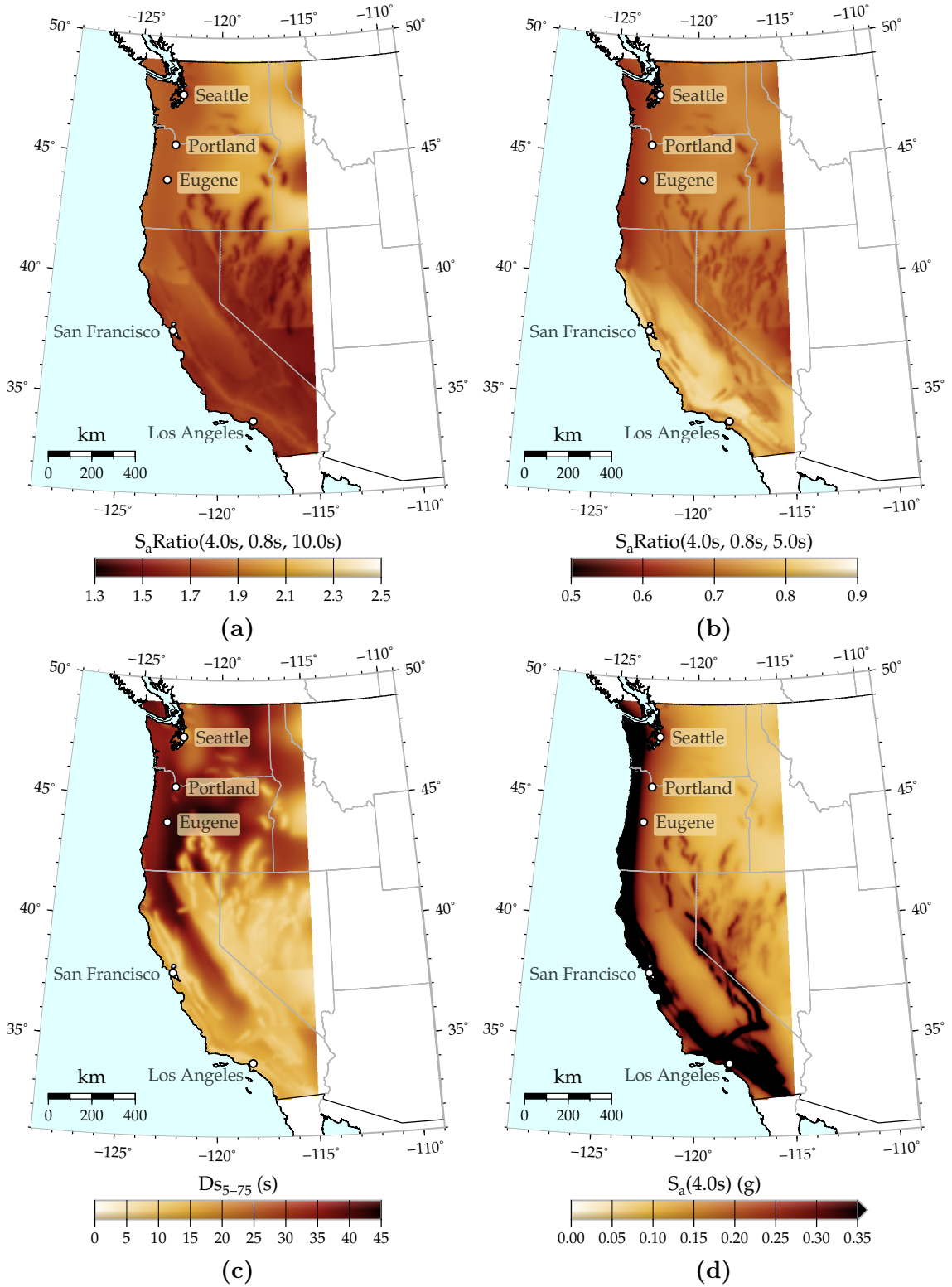

Figure C.3: Median (a) $S_a Ratio(4.0\,\text{s}, 0.8\,\text{s}, 10.0\,\text{s})$, (b) $S_a Ratio(4.0\,\text{s}, 0.8\,\text{s}, 5.0\,\text{s})$, and (c) Ds_{5-75} targets in Western USA, conditional on the exceedance of the $S_a(4.0\,\text{s})$ values in (c). The $S_a Ratio$ targets in (a) are computed using the Abrahamson et al. (2016) GMPE for interface earthquakes, and those in (b) are computed using Zhao et al. (2006). The $S_a(4.0\,\text{s})$ values in (c) are exceeded with a probability of 0.5 % in 50 years. $Vs_{30} = 270\,\text{m/s}$ is assumed at all sites.

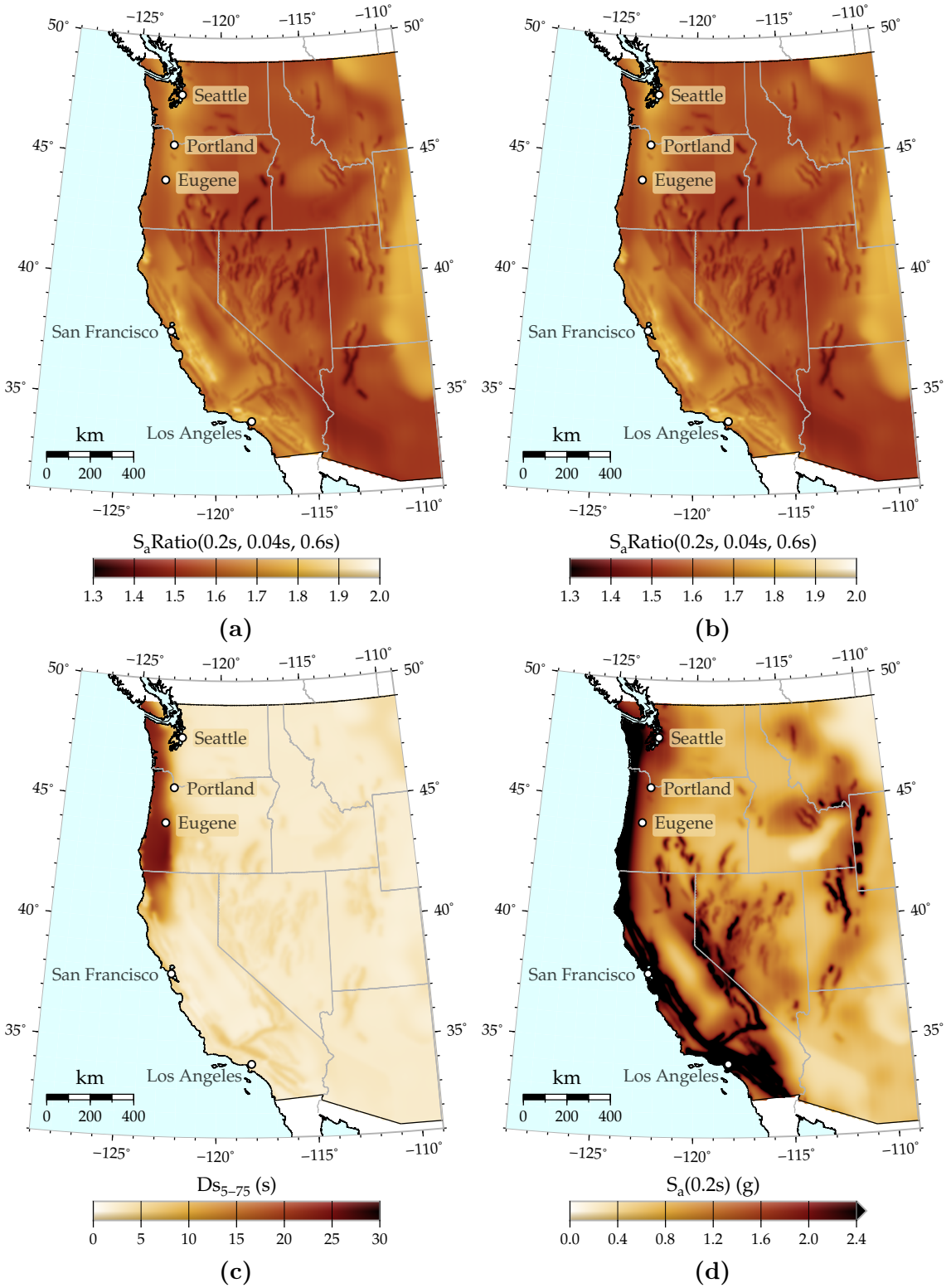

Figure C.4: Median (a), (b) $S_a Ratio(0.2\,\text{s}, 0.04\,\text{s}, 0.6\,\text{s})$ and (c) Ds_{5-75} targets in Western USA, conditional on the exceedance of the $S_a(0.2\,\text{s})$ values in (c). The $S_a Ratio$ targets in (a) are computed using the Abrahamson et al. (2016) GMPE for interface earthquakes, and those in (b) are computed using Zhao et al. (2006). The $S_a(0.2\,\text{s})$ values in (c) are exceeded with a probability of 0.5 % in 50 years. $Vs_{30} = 760\,\text{m/s}$ is assumed at all sites.

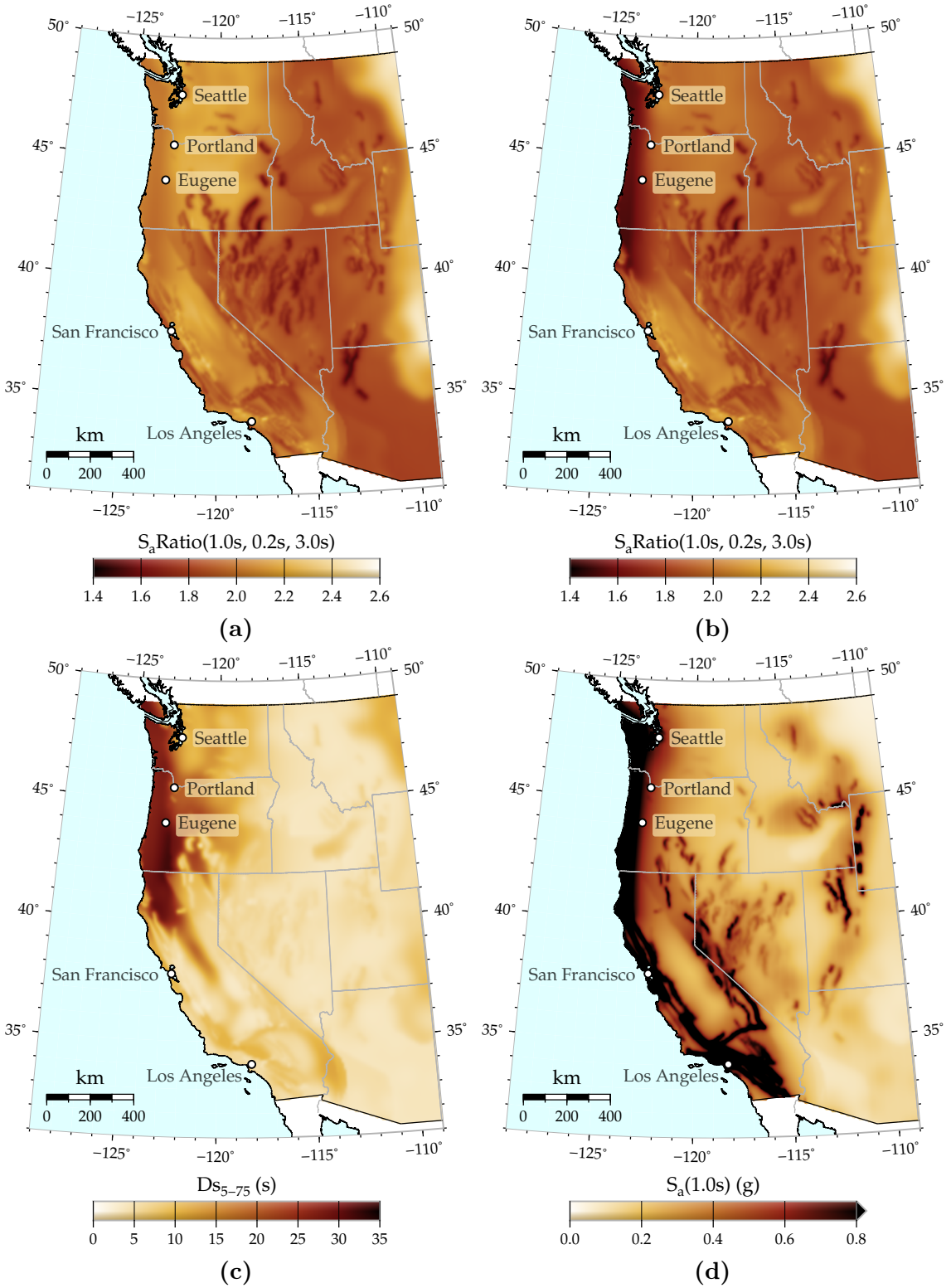

Figure C.5: Median (a), (b) $S_aRatio(1.0\,\text{s}, 0.2\,\text{s}, 3.0\,\text{s})$ and (c) Ds_{5-75} targets in Western USA, conditional on the exceedance of the $S_a(1.0\,\text{s})$ values in (c). The S_aRatio targets in (a) are computed using the Abrahamson et al. (2016) GMPE for interface earthquakes, and those in (b) are computed using Zhao et al. (2006). The $S_a(1.0\,\text{s})$ values in (c) are exceeded with a probability of 0.5 % in 50 years. $Vs_{30} = 760\,\text{m/s}$ is assumed at all sites.

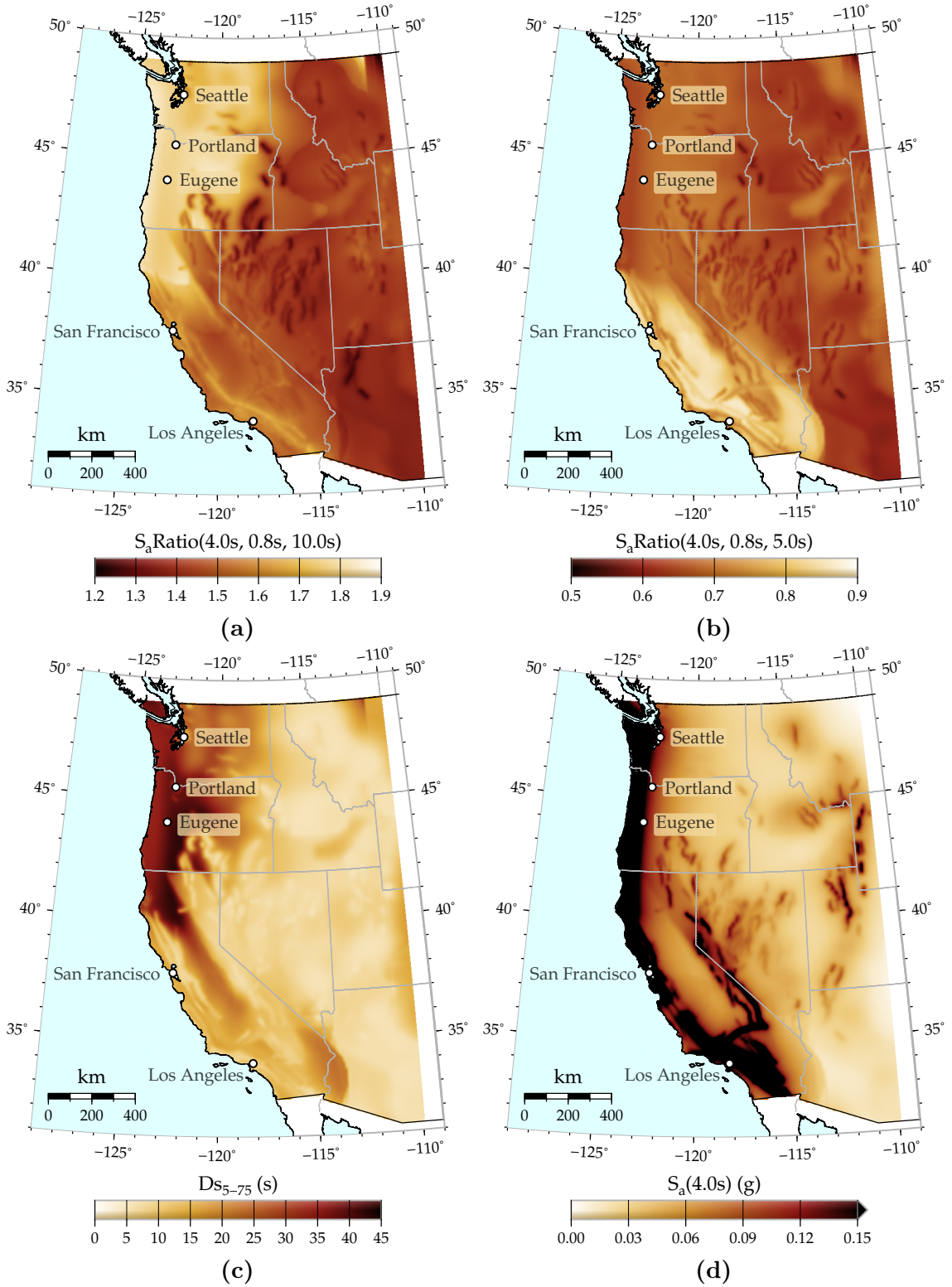

Figure C.6: Median (a) $S_a Ratio(4.0\,\text{s}, 0.8\,\text{s}, 10.0\,\text{s})$, (b) $S_a Ratio(4.0\,\text{s}, 0.8\,\text{s}, 5.0\,\text{s})$, and (c) Ds_{5-75} targets in Western USA, conditional on the exceedance of the $S_a(4.0\,\text{s})$ values in (c). The $S_a Ratio$ targets in (a) are computed using the Abrahamson et al. (2016) GMPE for interface earthquakes, and those in (b) are computed using Zhao et al. (2006). The $S_a(4.0\,\text{s})$ values in (c) are exceeded with a probability of 0.5 % in 50 years. $Vs_{30} = 760\,\text{m/s}$ is assumed at all sites.

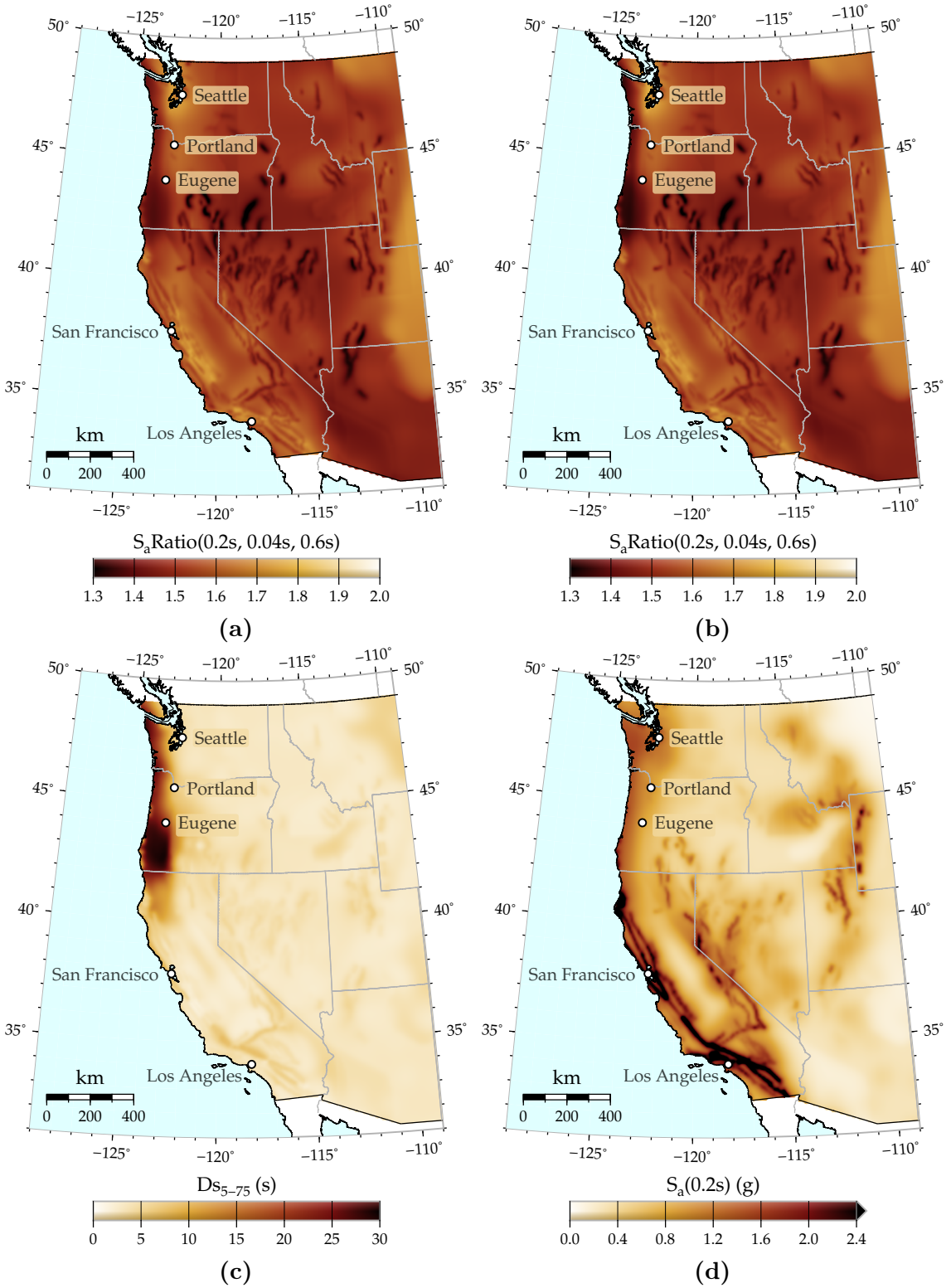

Figure C.7: Median (a), (b) $S_aRatio(0.2\,\text{s}, 0.04\,\text{s}, 0.6\,\text{s})$ and (c) Ds_{5-75} targets in Western USA, conditional on the exceedance of the $S_a(0.2\,\text{s})$ values in (c). The S_aRatio targets in (a) are computed using the Abrahamson et al. (2016) GMPE for interface earthquakes, and those in (b) are computed using Zhao et al. (2006). The $S_a(0.2\,\text{s})$ values in (c) are exceeded with a probability of 2 % in 50 years. $Vs_{30} = 760\,\text{m/s}$ is assumed at all sites.

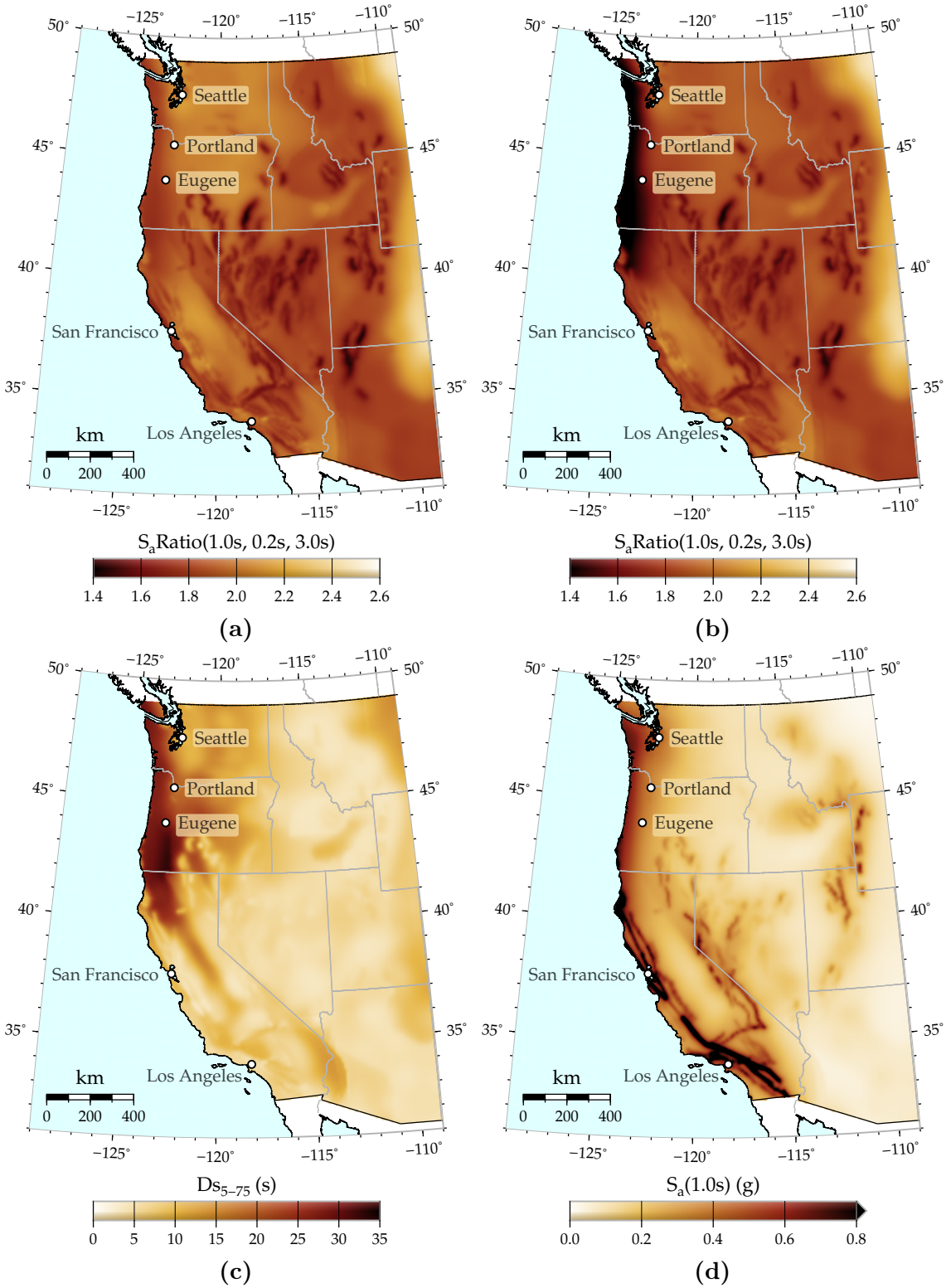

Figure C.8: Median (a), (b) $S_aRatio(1.0\,\text{s}, 0.2\,\text{s}, 3.0\,\text{s})$ and (c) Ds_{5-75} targets in Western USA, conditional on the exceedance of the $S_a(1.0\,\text{s})$ values in (c). The S_aRatio targets in (a) are computed using the Abrahamson et al. (2016) GMPE for interface earthquakes, and those in (b) are computed using Zhao et al. (2006). The $S_a(1.0\,\text{s})$ values in (c) are exceeded with a probability of 2 % in 50 years. $Vs_{30} = 760\,\text{m/s}$ is assumed at all sites.

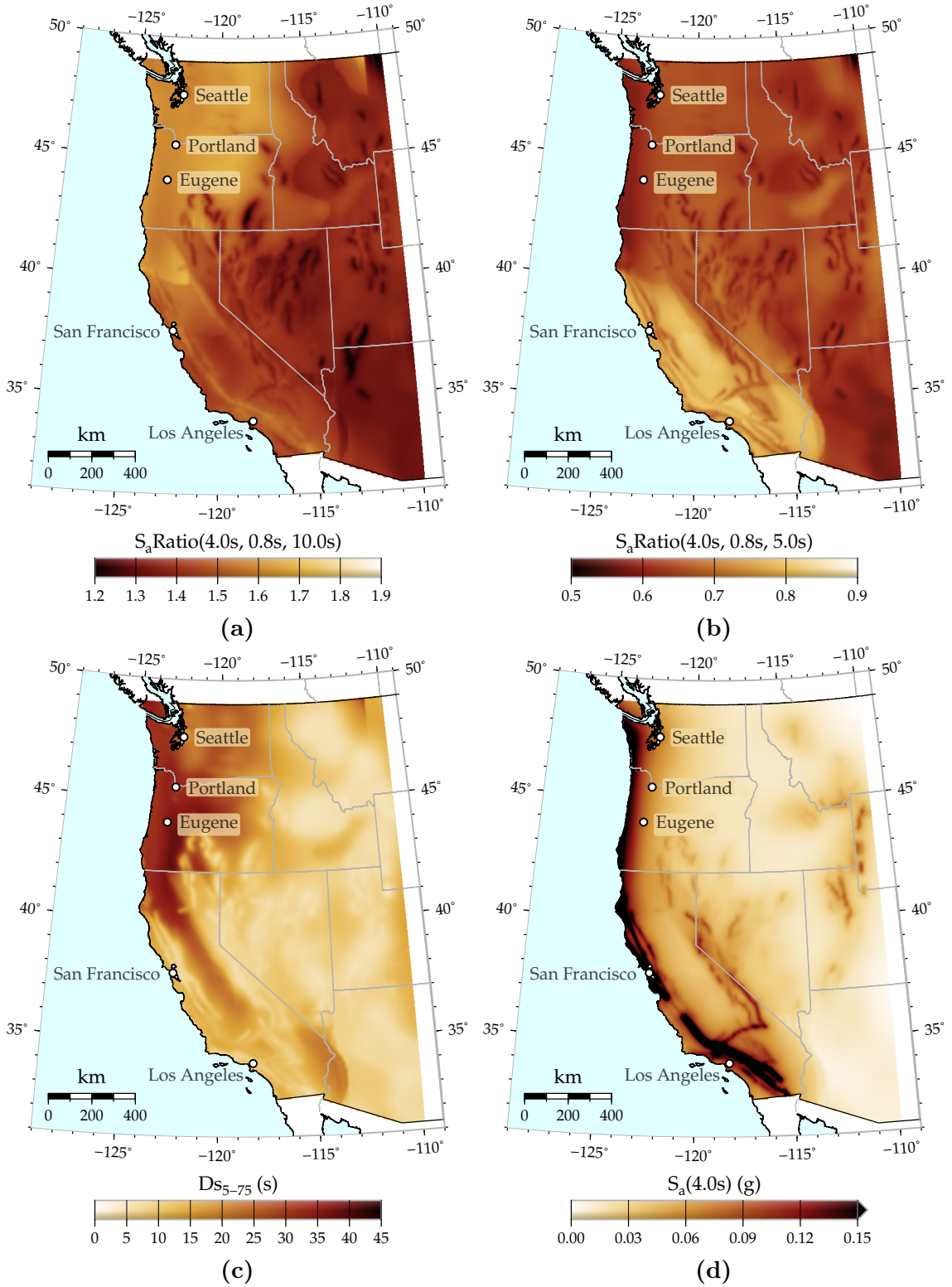

Figure C.9: Median (a) $S_a Ratio(4.0\,\text{s}, 0.8\,\text{s}, 10.0\,\text{s})$, (b) $S_a Ratio(4.0\,\text{s}, 0.8\,\text{s}, 5.0\,\text{s})$, and (c) Ds_{5-75} targets in Western USA, conditional on the exceedance of the $S_a(4.0\,\text{s})$ values in (c). The $S_a Ratio$ targets in (a) are computed using the Abrahamson et al. (2016) GMPE for interface earthquakes, and those in (b) are computed using Zhao et al. (2006). The $S_a(4.0\,\text{s})$ values in (c) are exceeded with a probability of 2 % in 50 years. $Vs_{30} = 760\,\text{m/s}$ is assumed at all sites.

Bibliography

Abrahamson, N. A. and L. Al Atik (2010). "Scenario Spectra for Design Ground Motions and Risk Calculation". *9th US National and 10th Canadian Conference on Earthquake Engineering*. Toronto, Canada.

Abrahamson, N. A., N. Gregor, and K. Addo (2016). "BC Hydro Ground Motion Prediction Equations for Subduction Earthquakes". *Earthquake Spectra* **32** (1), pp. 23–44. DOI: 10.1193/051712EQS188MR.

Abrahamson, N. A. and W. J. Silva (1996). *Empirical Ground Motion Models*. Tech. rep. Upton, NY: Brookhaven National Laboratory.

Abrahamson, N. A., W. J. Silva, and R. Kamai (2014). "Summary of the ASK14 Ground Motion Relation for Active Crustal Regions". *Earthquake Spectra* **30** (3), pp. 1025–1055. DOI: 10.1193/070913EQS198M.

ACI (2014). *Building Code Requirements for Structural Concrete*. Tech. rep. ACI 318-14. Farmington Hills, MI: American Concrete Institute.

Afshari, K. and J. P. Stewart (2016). "Physically Parameterized Prediction Equations for Significant Duration in Active Crustal Regions". *Earthquake Spectra*. DOI: 10.1193/063015EQS106M.

AISC (2010). *Seismic Provisions for Structural Steel Buildings*. Tech. rep. ANSI/AISC 341-10. Chicago, IL: American Institute of Steel Construction.

Al Atik, L. (2011). "Correlation of Spectral Acceleration Values for Subduction and Crustal Models". *COSMOS Technical Session*. Emeryville, CA.

Alıcı, F. S. and H. Sucuoğlu (2016). "Prediction of input energy spectrum: attenuation models and velocity spectrum scaling". *Earthquake Engineering & Structural Dynamics*. DOI: 10.1002/eqe.2749. In press.

Amazon (2016). *Amazon Elastic Compute Cloud*. URL: https://aws.amazon.com/ec2/.

Ambraseys, N. N. and S. K. Sarma (1967). "The Response of Earth Dams to Strong Earthquakes". *Geotechnique* **17** (3), pp. 181–213.

Ancheta, T. D., R. B. Darragh, J. P. Stewart, E. Seyhan, W. J. Silva, B. S. J. Chiou, K. E. Wooddell, R. W. Graves, A. R. Kottke, D. M. Boore, T. Kishida, and J. L. Donahue (2013). *PEER NGA-West2 Database*. Tech. rep. PEER 2013/03. Berkeley, CA: Pacific Earthquake Engineering Research Center.

Ancheta, T. D., R. B. Darragh, J. P. Stewart, E. Seyhan, W. J. Silva, B. S.-J. Chiou, K. E. Wooddell, R. W. Graves, A. R. Kottke, D. M. Boore, T. Kishida, and J. L. Donahue (2014). "NGA-West2 Database". *Earthquake Spectra* **30** (3), pp. 989–1005. DOI: 10.1193/070913EQS197M.

Anderson, J. G., P. Bodin, J. N. Brune, J. Prince, S. K. Singh, R. Quaas, and M. Onate (1986). "Strong ground motion from the Michoacan, Mexico, earthquake." *Science (New York, N.Y.)* **233** (4768), pp. 1043–9.

Araki, Y. and K. D. Hjelmstad (2000). "Criteria for assessing dynamic collapse of elastoplastic structural systems". *Earthquake Engineering & Structural Dynamics* **29** (8), pp. 1177–1198. DOI: 10.1002/1096-9845(200008)29:8<1177::AID-EQE963>3.0.CO;2-E.

Arias, A. (1970). "A measure of earthquake intensity". *Seismic Design for Nuclear Power Plants*. Ed. by R. J. Hansen. Cambridge, MA: The MIT Press, pp. 438–483.

ASCE (2010). *Minimum Design Loads for Buildings and Other Structures*. Tech. rep. ASCE/SEI 7-10. Reston, VA: American Society of Civil Engineers. DOI: 10.1061/9780784412916.

— (2013). *Seismic Evaluation and Retrofit of Existing Buildings*. Tech. rep. ASCE/SEI 41-13. Reston, VA: American Society of Civil Engineers. DOI: 10.1061/9780784412855.

ASCE (2016). *Minimum Design Loads for Buildings and Other Structures*. Tech. rep. ASCE/SEI 7-16. Reston, VA: American Society of Civil Engineers.

ASTM (2011). *Standard Practices for Cycle Counting in Fatigue Analysis*. Tech. rep. ASTM E1049-85. West Conshohocken, PA: American Society for Testing and Materials. DOI: 10.1520/E1049-85R11E01.

ATC (1992). *Guidelines for Cyclic Seismic Testing of Components of Steel Structures*. Tech. rep. ATC-24. Redwood City, CA: Applied Technology Council.

Baker, J. W. (2007). "Probabilistic structural response assessment using vector-valued intensity measures". *Earthquake Engineering & Structural Dynamics* **36** (13), pp. 1861–1883. DOI: 10.1002/eqe.700.

— (2011). "Conditional Mean Spectrum: Tool for Ground-Motion Selection". *Journal of Structural Engineering* **137** (3), pp. 322–331. DOI: 10.1061/(ASCE)ST.1943-541X.0000215.

— (2015). "Efficient Analytical Fragility Function Fitting Using Dynamic Structural Analysis". *Earthquake Spectra* **31** (1), pp. 579–599. DOI: 10.1193/021113EQS025M.

Baker, J. W. and C. A. Cornell (2005). "A vector-valued ground motion intensity measure consisting of spectral acceleration and epsilon". *Earthquake Engineering & Structural Dynamics* **34** (10), pp. 1193–1217. DOI: 10.1002/eqe.474.

— (2006a). "Spectral shape, epsilon and record selection". *Earthquake Engineering & Structural Dynamics* **35** (9), pp. 1077–1095. DOI: 10.1002/eqe.571.

— (2006b). *Vector-Valued Ground Motion Intensity Measures for Probabilistic Seismic Demand Analysis*. Tech. rep. PEER 2006/08. Berkeley, CA: Pacific Earthquake Engineering Research Center.

— (2008). "Vector-valued Intensity Measures Incorporating Spectral Shape For Prediction of Structural Response". *Journal of Earthquake Engineering* **12** (4), pp. 534–554. DOI: 10.1080/13632460701673076.

Baker, J. W. and N. Jayaram (2008). "Correlation of Spectral Acceleration Values from NGA Ground Motion Models". *Earthquake Spectra* **24** (1), pp. 299–317. DOI: 10.1193/1.2857544.

Baker, J. W., T. Lin, S. K. Shahi, and N. Jayaram (2011). *New Ground Motion Selection Procedures and Selected Motions for the PEER Transportation Research*

Program. Tech. rep. PEER 2011/03. Berkeley, CA: Pacific Earthquake Engineering Research Center.

Bank, R., W. Coughran, W. Fichtner, E. Grosse, D. Rose, and R. Smith (1985). "Transient Simulation of Silicon Devices and Circuits". *IEEE Transactions on Computer-Aided Design of Integrated Circuits and Systems* **4** (4), pp. 436–451. DOI: 10.1109/TCAD.1985.1270142.

Barbosa, A. R., H. B. Mason, and K. T. Romney (2012). *SSI-Bridge: Soil-bridge interaction during long-duration earthquake motions*. Tech. rep. 2012-S-OSU-0008. Seattle, WA: Pacific Northwest Transportation Consortium.

Barbosa, A. R., F. L. A. Ribeiro, and L. C. Neves (2014). "Effects of ground-motion duration on the response of a 9-story steel frame building". *10th U.S. National Conference on Earthquake Engineering*. Anchorage, AK.

Bathe, K.-J. (1996). *Finite Element Procedures*. Upper Saddle River, NJ: Prentice Hall.

— (2007). "Conserving energy and momentum in nonlinear dynamics: A simple implicit time integration scheme". *Computers & Structures* **85** (7-8), pp. 437–445. DOI: 10.1016/j.compstruc.2006.09.004.

Bazaez, R. and P. Dusicka (2016). "Cyclic Loading for RC Bridge Columns Considering Subduction Megathrust Earthquakes". *Journal of Bridge Engineering* **21** (5), p. 04016009. DOI: 10.1061/(ASCE)BE.1943-5592.0000891.

Bazzurro, P. (1998). "Probabilistic Seismic Demand Analysis". PhD thesis. Stanford, CA: Stanford University. DOI: 10.16953/deusbed.74839.

Benjamin, J. R. (1988). *A Criterion for Determining Exceedance of the Operating Basis Earthquake*. Tech. rep. EPRI Report NP-5930. Palo Alto, CA: Electric Power Research Institute.

Bernal, D. (1992). "Instability of Buildings Subjected to Earthquakes". *Journal of Structural Engineering* **118** (8), pp. 2239–2260. DOI: 10.1061/(ASCE)0733-9445(1992)118:8(2239).

Beyer, K. and J. J. Bommer (2007). "Selection and Scaling of Real Accelerograms for Bi-Directional Loading: A Review of Current Practice and Code Provisions". *Journal of Earthquake Engineering* **11** (S1), pp. 13–45. DOI: 10.1080/13632460701280013.

Bianchini, M. (2008). *Improved scalar intensity measures in performance-based earthquake engineering*. Tech. rep. 215. Bologna, Italy: Università di Bologna. DOI: 10.6092/unibo/amsacta/2455.

Bianchini, M., P. P. Diotallevi, and J. W. Baker (2009). "Prediction of inelastic structural response using an average of spectral accelerations". *10th International Conference on Structural Safety and Reliability*. Osaka, Japan.

Black, C. J., N. Makris, and I. D. Aiken (2004). "Component Testing, Seismic Evaluation and Characterization of Buckling-Restrained Braces". *Journal of Structural Engineering* **130** (6), pp. 880–894. DOI: 10.1061/(ASCE)0733-9445(2004)130:6(880).

Bojórquez, E. and I. Iervolino (2011). "Spectral shape proxies and nonlinear structural response". *Soil Dynamics and Earthquake Engineering* **31** (7), pp. 996–1008. DOI: 10.1016/j.soildyn.2011.03.006.

Bolt, B. A. (1973). "Duration of strong ground motion". *5th World Conference on Earthquake Engineering*. Vol. 1. Rome, Italy, pp. 1304–1313.

Bommer, J. J. (2005). "On the Use of Logic Trees for Ground-Motion Prediction Equations in Seismic-Hazard Analysis". *Bulletin of the Seismological Society of America* **95** (2), pp. 377–389. DOI: 10.1785/0120040073.

Bommer, J. J. and A. B. Acevedo (2004). "The Use of Real Earthquake Accelerograms as Input to Dynamic Analysis". *Journal of Earthquake Engineering* **8** (1), pp. 43–91. DOI: 10.1142/S1363246904001596.

Bommer, J. J., H. Crowley, and R. Pinho (2015). "A risk-mitigation approach to the management of induced seismicity". *Journal of Seismology* **19** (2), pp. 623–646. DOI: 10.1007/s10950-015-9478-z.

Bommer, J. J., J. Hancock, and J. E. Alarcón (2006). "Correlations between duration and number of effective cycles of earthquake ground motion". *Soil Dynamics and Earthquake Engineering* **26** (1), pp. 1–13. DOI: 10.1016/j.soildyn.2005.10.004.

Bommer, J. J., G. Magenes, J. Hancock, and P. Penazzo (2004). "The Influence of Strong-Motion Duration on the Seismic Response of Masonry Structures". *Bulletin*

of Earthquake Engineering **2** (1), pp. 1–26. DOI: 10.1023/B:BEEE.0000038948.95616.bf.

Bommer, J. J. and A. Martinez-Pereira (1999). "The Effective Duration of Earthquake Strong Motion". *Journal of Earthquake Engineering* **3** (2), pp. 127–172. DOI: 10.1080/13632469909350343.

Bommer, J. J., S. G. Scott, and S. K. Sarma (2000). "Hazard-consistent earthquake scenarios". *Soil Dynamics and Earthquake Engineering* **19** (4), pp. 219–231. DOI: 10.1016/S0267-7261(00)00012-9.

Bommer, J. J., P. J. Stafford, and J. E. Alarcón (2009). "Empirical Equations for the Prediction of the Significant, Bracketed, and Uniform Duration of Earthquake Ground Motion". *Bulletin of the Seismological Society of America* **99** (6), pp. 3217–3233. DOI: 10.1785/0120080298.

Bonnet, P. A., M. S. Williams, and A. Blakeborough (2008). "Evaluation of numerical time-integration schemes for real-time hybrid testing". *Earthquake Engineering & Structural Dynamics* **37** (13), pp. 1467–1490. DOI: 10.1002/eqe.821.

Boore, D. M. (2005). "On Pads and Filters: Processing Strong-Motion Data". *Bulletin of the Seismological Society of America* **95** (2), pp. 745–750. DOI: 10.1785/0120040160.

Boore, D. M. and J. J. Bommer (2005). "Processing of strong-motion accelerograms: needs, options and consequences". *Soil Dynamics and Earthquake Engineering* **25** (2), pp. 93–115. DOI: 10.1016/j.soildyn.2004.10.007.

Boore, D. M., J. P. Stewart, E. Seyhan, and G. M. Atkinson (2014). "NGA-West2 Equations for Predicting PGA, PGV, and 5% Damped PSA for Shallow Crustal Earthquakes". *Earthquake Spectra* **30** (3), pp. 1057–1085. DOI: 10.1193/070113EQS184M.

Boore, D. M. and E. M. Thompson (2014). "Path Durations for Use in the Stochastic-Method Simulation of Ground Motions". *Bulletin of the Seismological Society of America* **104** (5), pp. 2541–2552. DOI: 10.1785/0120140058.

Bora, S. S., F. Scherbaum, N. Kuehn, and P. Stafford (2014). "Fourier spectral- and duration models for the generation of response spectra adjustable to different source-, propagation-, and site conditions". *Bulletin of Earthquake Engineering* **12** (1), pp. 467–493. DOI: 10.1007/s10518-013-9482-z.

Bradley, B. A. (2010). "A generalized conditional intensity measure approach and holistic ground-motion selection". *Earthquake Engineering & Structural Dynamics* **39** (12), pp. 1321–1342. DOI: 10.1002/eqe.995.

— (2011). "Correlation of Significant Duration with Amplitude and Cumulative Intensity Measures and Its Use in Ground Motion Selection". *Journal of Earthquake Engineering* **15** (6), pp. 809–832. DOI: 10.1080/13632469.2011.557140.

— (2012). "A ground motion selection algorithm based on the generalized conditional intensity measure approach". *Soil Dynamics and Earthquake Engineering* **40**, pp. 48–61. DOI: 10.1016/j.soildyn.2012.04.007.

— (2013). "A critical examination of seismic response uncertainty analysis in earthquake engineering". *Earthquake Engineering & Structural Dynamics* **42** (11), pp. 1717–1729. DOI: 10.1002/eqe.2331.

Bray, J. D., E. M. Rathje, A. J. Augello, and S. M. Merry (1998). *Simplified Seismic Design Procedure for Geosynthetic-Lined, Solid-Waste Landfills*. Tech. rep. 1-2. Geosynthetics International, pp. 230–235.

Buratti, N., P. J. Stafford, and J. J. Bommer (2011). "Earthquake Accelerogram Selection and Scaling Procedures for Estimating the Distribution of Drift Response". *Journal of Structural Engineering* **137** (3), pp. 345–357. DOI: 10.1061/(ASCE)ST.1943-541X.0000217.

Burks, L. S. and J. W. Baker (2014). "Validation of Ground-Motion Simulations through Simple Proxies for the Response of Engineered Systems". *Bulletin of the Seismological Society of America* **104** (4), pp. 1930–1946. DOI: 10.1785/0120130276.

Burton, H. (2014). "A Rocking Spine for Enhanced Seismic Performance of Concrete Frames With Infills". PhD thesis. Stanford, CA: Stanford University.

Campbell, K. W. and Y. Bozorgnia (2014). "NGA-West2 Ground Motion Model for the Average Horizontal Components of PGA, PGV, and 5% Damped Linear Acceleration Response Spectra". *Earthquake Spectra* **30** (3), pp. 1087–1115. DOI: 10.1193/062913EQS175M.

Chai, Y. H. (2005). "Incorporating low-cycle fatigue model into duration-dependent inelastic design spectra". *Earthquake Engineering & Structural Dynamics* **34** (1), pp. 83–96. DOI: 10.1002/eqe.422.

Chai, Y. H. and P. Fajfar (2000). "A Procedure for Estimating Input Energy Spectra for Seismic Design". *Journal of Earthquake Engineering* **4** (4), pp. 539–561. DOI: 10.1080/13632460009350382.

Chai, Y. H., P. Fajfar, and K. M. Romstad (1998). "Formulation of Duration-Dependent Inelastic Seismic Design Spectrum". *Journal of Structural Engineering* **124** (8), pp. 913–921. DOI: 10.1061/(ASCE)0733-9445(1998)124:8(913).

Chandramohan, R., J. W. Baker, and G. G. Deierlein (2016a). "Impact of hazard-consistent ground motion duration in structural collapse risk assessment". *Earthquake Engineering & Structural Dynamics* **45** (8), pp. 1357–1379. DOI: 10.1002/eqe.2711.

— (2016b). "Quantifying the Influence of Ground Motion Duration on Structural Collapse Capacity Using Spectrally Equivalent Records". *Earthquake Spectra* **32** (2), pp. 927–950. DOI: 10.1193/122813EQS298MR2.

— (2017). "Physical mechanisms underlying the influence of ground motion duration on structural collapse capacity". *16th World Conference on Earthquake Engineering*. Santiago, Chile.

Charney, F. A. (2008). "Unintended Consequences of Modeling Damping in Structures". *Journal of Structural Engineering* **134** (4), pp. 581–592. DOI: 10.1061/(ASCE)0733-9445(2008)134:4(581).

Chávez-García, F. J. and P.-Y. Bard (1994). "Site effects in Mexico City eight years after the September 1985 Michoacan earthquakes". *Soil Dynamics and Earthquake Engineering* **13** (4), pp. 229–247. DOI: 10.1016/0267-7261(94)90028-0.

Chiang, K. and R. Fulton (1990). "Structural dynamics methods for concurrent processing computers". *Computers & Structures* **36** (6), pp. 1031–1037. DOI: 10.1016/0045-7949(90)90210-S.

Chiou, B. S.-J. and R. R. Youngs (2014). "Update of the Chiou and Youngs NGA Model for the Average Horizontal Component of Peak Ground Motion and Response Spectra". *Earthquake Spectra* **30** (3), pp. 1117–1153. DOI: 10.1193/072813EQS219M.

Chopra, A. K. (2012). *Dynamics of Structures: Theory and Applications to Earthquake Engineering*. 4th ed. Upper Saddle River, NJ: Prentice Hall.

Chopra, A. K. and F. McKenna (2016). "Modeling viscous damping in nonlinear response history analysis of buildings for earthquake excitation". *Earthquake Engineering & Structural Dynamics* **45** (2), pp. 193–211. DOI: 10.1002/eqe.2622.

Chou, C.-C. and C.-M. Uang (2003). "A procedure for evaluating seismic energy demand of framed structures". *Earthquake Engineering & Structural Dynamics* **32** (2), pp. 229–244. DOI: 10.1002/eqe.221.

Chung, J. and G. M. Hulbert (1993). "A Time Integration Algorithm for Structural Dynamics With Improved Numerical Dissipation: The Generalized-α Method". *Journal of Applied Mechanics* **60** (2), p. 371. DOI: 10.1115/1.2900803.

— (1994). "A family of single-step Houbolt time integration algorithms for structural dynamics". *Computer Methods in Applied Mechanics and Engineering* **118** (1-2), pp. 1–11. DOI: 10.1016/0045-7825(94)90103-1.

Cleveland, W. S. (1979). "Robust Locally Weighted Regression and Smoothing Scatterplots". *Journal of the American Statistical Association* **74** (368), pp. 829–836. DOI: 10.1080/01621459.1979.10481038.

Clough, R. W., K. L. Benuska, and E. L. Wilson (1965). "Inelastic Earthquake Response of Tall Buildings". *3rd World Conference on Earthquake Engineering*. Vol. II. Auckland, New Zealand, pp. 68–89.

Coffin Jr., L. F. (1954). "A study of the effects of cyclic thermal stresses in ductile metals". *Transactions of ASME* **76**, pp. 931–950.

Cordova, P. P., G. G. Deierlein, S. S. F. Mehanny, and C. A. Cornell (2000). "Development of a two-parameter seismic intensity measure and probabilistic assessment procedure". *2nd US-Japan Workshop on Performance-based Earthquake Engineering Methodology for Reinforced Concrete Building Structures*. Sapporo, Japan.

Cornell, C. A. (1968). "Engineering seismic risk analysis". *Bulletin of the Seismological Society of America* **58** (5), pp. 1583–1606.

— (1997). "Does Duration Really Matter?" *FHWA/NCEER Workshop on the National Representation of Seismic Ground Motion for New and Existing Highway*

Facilities. Burlingame, CA: National Center for Earthquake Engineering Research, pp. 125–133.

Cosenza, E. and G. Manfredi (1997). "The improvement of the seismic-resistant design for existing and new structures using damage criteria". *Seismic Design Methodologies for the Next Generation of Codes*. Ed. by H. Krawinkler and P. Fajfar. Rotterdam, Netherlands: Balkema, pp. 119–130.

Crisfield, M. A. (1991). *Non-Linear Finite Element Analysis of Solids and Structures, Volume 1: Essentials*. Chichester, England: John Wiley & Sons.

Danielson, K. T., S. A. Akers, J. L. O'Daniel, M. D. Adley, and S. B. Garner (2008). "Large-Scale Parallel Computation Methodologies for Highly Nonlinear Concrete and Soil Applications". *Journal of Computing in Civil Engineering* **22** (2), pp. 140–146. DOI: 10.1061/(ASCE)0887-3801(2008)22:2(140).

Das, S. and V. K. Gupta (2010). "Scaling of response spectrum and duration for aftershocks". *Soil Dynamics and Earthquake Engineering* **30** (8), pp. 724–735. DOI: 10.1016/j.soildyn.2010.03.003.

Deierlein, G. G., A. M. Reinhorn, and M. R. Willford (2010). *Nonlinear structural analysis for seismic design*. Tech. rep. NEHRP Seismic Design Technical Brief No. 4. Gaithersburg, MD: National Institute of Standards and Technology.

Dennis Jr., J. E. (1976). "A Brief Survey of Convergence Results for Quasi-Newton Methods". *SIAM-AMS Proceedings*. Vol. 9, pp. 185–200.

Dobry, R., I. M. Idriss, and E. Ng (1978). "Duration characteristics of horizontal components of strong-motion earthquake records". *Bulletin of the Seismological Society of America* **68** (5), pp. 1487–1520.

Dolšek, M. (2009). "Incremental dynamic analysis with consideration of modeling uncertainties". *Earthquake Engineering & Structural Dynamics* **38** (6), pp. 805–825. DOI: 10.1002/eqe.869.

Dundulis, G., R. F. Kulak, A. Marchertas, and E. Uspuras (2007). "Structural integrity analysis of an Ignalina nuclear power plant building subjected to an airplane crash". *Nuclear Engineering and Design* **237** (14), pp. 1503–1512. DOI: 10.1016/j.nucengdes.2007.01.007.

Eads, L. (2013). "Seismic Collapse Risk Assessment of Buildings: Effects of Intensity Measure Selection and Computational Approach". PhD thesis. Stanford, CA: Stanford University.

Eads, L., E. Miranda, H. Krawinkler, and D. G. Lignos (2013). "An efficient method for estimating the collapse risk of structures in seismic regions". *Earthquake Engineering & Structural Dynamics* **42** (1), pp. 25–41. DOI: 10.1002/eqe.2191.

Eads, L., E. Miranda, and D. Lignos (2016). "Spectral shape metrics and structural collapse potential". *Earthquake Engineering & Structural Dynamics* **45** (10), pp. 1643–1659. DOI: 10.1002/eqe.2739.

Eads, L., E. Miranda, and D. G. Lignos (2015). "Average spectral acceleration as an intensity measure for collapse risk assessment". *Earthquake Engineering & Structural Dynamics* **44** (12), pp. 2057–2073. DOI: 10.1002/eqe.2575.

EERI (2012). *Performance of Engineered Structures in the M9.0 Tohoku, Japan, Earthquake of March 11, 2011*. Tech. rep. EERI Special Earthquake Report. Oakland, CA: Earthquake Engineering Research Institute.

Efron, B. and R. J. Tibshirani (1994). *An Introduction to the Bootstrap*. Boca Raton, FL: CRC Press.

Esteva, L. and E. Rosenblueth (1964). "Espectros de temblores a distancias moderadas y grandes". *Boletin Sociedad Mexicana de Ingenieria Sismica* **2** (1), pp. 1–18.

Eurocode (2004). *Eurocode 8: Design of structures for earthquake resistance - Part 1: General rules, seismic actions and rules for buildings*. Tech. rep. EN 1998-1. Brussels, Belgium: European Committee for Standardization.

Fajfar, P. and T. Vidic (1994). "Consistent inelastic design spectra: Hysteretic and input energy". *Earthquake Engineering & Structural Dynamics* **23** (5), pp. 523–537. DOI: 10.1002/eqe.4290230505.

FEMA (2000). *State of the art report on systems performance of steel moment frames subject to earthquake ground shaking*. Tech. rep. FEMA 335C. Stanford, CA: Federal Emergency Management Agency.

— (2009a). *Effects of Strength and Stiffness Degradation on Seismic Response*. Tech. rep. FEMA P440A. Washington, D.C.: Federal Emergency Management Agency.

FEMA (2009b). *Quantification of Building Seismic Performance Factors*. Tech. rep. FEMA P695. Washington, D.C.: Federal Emergency Management Agency.

— (2012a). *Hazus-MH 2.1: Technical Manual*. Tech. rep. Washington, D.C.: Federal Emergency Management Agency.

— (2012b). *Seismic Performance Assessment of Buildings, Volume 1 - Methodology*. Tech. rep. FEMA P-58-1. Washington, D.C.: Federal Emergency Management Agency.

— (2012c). *Seismic Performance Assessment of Buildings, Volume 2 - Implementation Guide*. Tech. rep. FEMA P-58-2. Washington, D.C.: Federal Emergency Management Agency.

— (2014). *Seismic Performance Assessment of Buildings, Volume 5 - Use of Seismic Performance Assessment Methodologies to Evaluate Code Performance*. Tech. rep. FEMA P-58-5. Washington, D.C.: Federal Emergency Management Agency.

— (2015). *NEHRP Recommended Seismic Provisions for New Buildings and Other Structures, Part 1: Provisions, Part 2: Commentary*. Tech. rep. FEMA P-1050-1. Washington, D.C.: Federal Emergency Management Agency.

Foschaar, J. C., J. W. Baker, and G. G. Deierlein (2011). "Preliminary Assessment of Ground Motion Duration Effects on Structural Collapse". *15th World Conference on Earthquake Engineering*. Lisbon, Portugal.

Frankel, A. D. (2000). "Three-Dimensional Simulations of Ground Motions in the Seattle Region for Earthquakes in the Seattle Fault Zone". *Bulletin of the Seismological Society of America* **90** (5), pp. 1251–1267. DOI: 10.1785/0119990159.

Frankel, A. D., W. J. Stephenson, D. L. Carver, R. A. Williams, J. K. Odum, and S. Rhea (2007). *Seismic Hazard Maps for Seattle, Washington, Incorporating 3D Sedimentary Basin Effects, Nonlinear Site Response, and Rupture Directivity*. Tech. rep. Open-File Report 2007-1175. Reston, VA: United States Geological Survey.

Galanis, P., Y. B. Shin, and J. P. Moehle (2016). "Laboratory and computer simulations of reinforced concrete frames with different ductility". *Earthquake Engineering & Structural Dynamics* **45** (10), pp. 1603–1619. DOI: 10.1002/eqe.2741.

Galasso, C., P. Zhong, F. Zareian, I. Iervolino, and R. W. Graves (2013). "Validation of ground-motion simulations for historical events using MDoF systems". *Earthquake*

Engineering & Structural Dynamics **42** (9), pp. 1395–1412. DOI: 10.1002/eqe.2278.

Goda, K. (2015). "Record selection for aftershock incremental dynamic analysis". *Earthquake Engineering & Structural Dynamics* **44** (7), pp. 1157–1162. DOI: 10.1002/eqe.2513.

Goda, K. and G. M. Atkinson (2011). "Seismic performance of wood-frame houses in south-western British Columbia". *Earthquake Engineering & Structural Dynamics* **40** (8), pp. 903–924. DOI: 10.1002/eqe.1068.

Gokkaya, B. U., J. W. Baker, and G. G. Deierlein (2016). "Quantifying the impacts of modeling uncertainties on the seismic drift demands and collapse risk of buildings with implications on seismic design checks". *Earthquake Engineering & Structural Dynamics* **45** (10), pp. 1661–1683. DOI: 10.1002/eqe.2740.

Gropp, W., E. Lusk, and A. Skjellum (2014). *Using MPI : portable parallel programming with the message-passing interface*. Cambridge, MA: MIT Press.

Guo, T., L.-L. Song, and G.-D. Zhang (2015). "Numerical Simulation and Seismic Fragility Analysis of a Self-Centering Steel MRF with Web Friction Devices". *Journal of Earthquake Engineering* **19** (5), pp. 731–751. DOI: 10.1080/13632469.2014.1003437.

Gupta, A. and H. Krawinkler (2000). "Dynamic P-Delta Effects for Flexible Inelastic Steel Structures". *Journal of Structural Engineering* **126** (1), pp. 145–154. DOI: 10.1061/(ASCE)0733-9445(2000)126:1(145).

Gutenberg, B. and C. F. Richter (1944). "Frequency of earthquakes in California". *Bulletin of the Seismological Society of America* **34**, pp. 185–188.

Hajjar, J. F. and J. F. Abel (1989). "Parallel processing of central difference transient analysis for three-dimensional nonlinear framed structures". *Communications in Applied Numerical Methods* **5** (1), pp. 39–46. DOI: 10.1002/cnm.1630050107.

Hancock, J. and J. J. Bommer (2005). "The effective number of cycles of earthquake ground motion". *Earthquake Engineering & Structural Dynamics* **34** (6), pp. 637–664. DOI: 10.1002/eqe.437.

Hancock, J. and J. J. Bommer (2006). "A State-of-Knowledge Review of the Influence of Strong-Motion Duration on Structural Damage". *Earthquake Spectra* **22** (3), pp. 827–845. DOI: 10.1193/1.2220576.

— (2007). "Using spectral matched records to explore the influence of strong-motion duration on inelastic structural response". *Soil Dynamics and Earthquake Engineering* **27** (4), pp. 291–299. DOI: 10.1016/j.soildyn.2006.09.004.

Hanks, T. C. and R. K. McGuire (1981). "The character of high-frequency strong ground motion". *Bulletin of the Seismological Society of America* **71** (6), pp. 2071–2095.

Hardyniec, A. and F. A. Charney (2015). "A new efficient method for determining the collapse margin ratio using parallel computing". *Computers & Structures* **148**, pp. 14–25. DOI: 10.1016/j.compstruc.2014.11.003.

Haselton, C. B., J. W. Baker, A. B. Liel, and G. G. Deierlein (2011a). "Accounting for Ground-Motion Spectral Shape Characteristics in Structural Collapse Assessment through an Adjustment for Epsilon". *Journal of Structural Engineering* **137** (3), pp. 332–344. DOI: 10.1061/(ASCE)ST.1943-541X.0000103.

Haselton, C. B. and G. G. Deierlein (2008). *Assessing seismic collapse safety of modern reinforced concrete moment frame buildings*. Tech. rep. PEER 2007/08. Berkeley, CA: Pacific Earthquake Engineering Research Center.

Haselton, C. B., A. B. Liel, and G. G. Deierlein (2009). "Simulating structural collapse due to earthquakes: Model idealization, model calibration, and numerical solution algorithms". *ECCOMAS Thematic Conference on Computational Methods in Structural Dynamics and Earthquake Engineering (COMPDYN)*. Rhodes, Greece.

Haselton, C. B., A. B. Liel, G. G. Deierlein, B. S. Dean, and J. H. Chou (2011b). "Seismic Collapse Safety of Reinforced Concrete Buildings. I: Assessment of Ductile Moment Frames". *Journal of Structural Engineering* **137** (4), pp. 481–491. DOI: 10.1061/(ASCE)ST.1943-541X.0000318.

Haselton, C. B., A. B. Liel, S. T. Lange, and G. G. Deierlein (2008). *Beam-column element model calibrated for predicting flexural response leading to global collapse of*

RC frame buildings. Tech. rep. PEER 2007/03. Berkeley, CA: Pacific Earthquake Engineering Research Center.

Hayes, G. P., D. J. Wald, and R. L. Johnson (2012). "Slab1.0: A three-dimensional model of global subduction zone geometries". *Journal of Geophysical Research: Solid Earth* **117** (B1). DOI: 10.1029/2011JB008524.

Hilber, H. M., T. J. R. Hughes, and R. L. Taylor (1977). "Improved numerical dissipation for time integration algorithms in structural dynamics". *Earthquake Engineering & Structural Dynamics* **5** (3), pp. 283–292. DOI: 10.1002/eqe.4290050306.

Hou, H. and B. Qu (2015). "Duration effect of spectrally matched ground motions on seismic demands of elastic perfectly plastic SDOFs". *Engineering Structures* **90**, pp. 48–60. DOI: 10.1016/j.engstruct.2015.02.013.

Houbolt, J. C. (1950). "A Recurrence Matrix Solution for the Dynamic Response of Elastic Aircraft". *Journal of the Aeronautical Sciences* **17** (9), pp. 540–550.

Housner, G. W. (1956). "Limit design of structures to resist earthquakes". *World Conference on Earthquake Engineering*. Berkeley, CA.

— (1965). "Intensity of Earthquake Ground Shaking Near the Causative Fault". *3rd World Conference on Earthquake Engineering*. Auckland, New Zealand, pp. 94–115.

— (1975). "Measures of Severity of Earthquake Ground Shaking". *US National Conference on Earthquake Engineering*. Ann Arbor, MI, pp. 25–33.

Housner, G. W. and P. C. Jennings (1977). *Earthquake design criteria for structures*. Tech. rep. EERL 77-06. Pasadena, CA: California Institute of Technology.

Hsiao, P.-C., D. E. Lehman, and C. W. Roeder (2013). "Evaluation of the response modification coefficient and collapse potential of special concentrically braced frames". *Earthquake Engineering & Structural Dynamics* **42** (10), pp. 1547–1564. DOI: 10.1002/eqe.2286.

Hughes, T. J. R. (2000). *The Finite Element Method: Linear Static and Dynamic Finite Element Analysis*. Mineola, NY: Dover Publications.

Hughes, T. J. R. and W. K. Liu (1978). "Implicit-Explicit Finite Elements in Transient Analysis: Stability Theory". *Journal of Applied Mechanics* **45** (2), p. 371. DOI: 10.1115/1.3424304.

Hughes, T. J. R., K. S. Pister, and R. L. Taylor (1979). "Implicit-explicit finite elements in nonlinear transient analysis". *Computer Methods in Applied Mechanics and Engineering* **17-18**, pp. 159–182. DOI: 10.1016/0045-7825(79)90086-0.

Husid, R. L. (1967). "Gravity Effects on the Earthquake Response of Yielding Structures". PhD thesis. Pasadena, CA: California Institute of Technology.

— (1969). "Características de terremotos. Análisis general". *Revista del IDIEM* **8** (1), pp. 21–42.

Ibarra, L. F. and H. Krawinkler (2005). *Global Collapse of Frame Structures under Seismic Excitations*. Tech. rep. PEER 2005/06. Berkeley, CA: Pacific Earthquake Engineering Research Center.

Ibarra, L. F., R. A. Medina, and H. Krawinkler (2005). "Hysteretic models that incorporate strength and stiffness deterioration". *Earthquake Engineering & Structural Dynamics* **34** (12), pp. 1489–1511. DOI: 10.1002/eqe.495.

ICC (2012). *International Building Code*. Tech. rep. Washington, D.C.: International Code Council.

Iervolino, I., M. Giorgio, and E. Chioccarelli (2014). "Closed-form aftershock reliability of damage-cumulating elastic-perfectly-plastic systems". *Earthquake Engineering & Structural Dynamics* **43** (4), pp. 613–625. DOI: 10.1002/eqe.2363.

— (2016). "Markovian modeling of seismic damage accumulation". *Earthquake Engineering & Structural Dynamics* **45** (3), pp. 441–461. DOI: 10.1002/eqe.2668.

Iervolino, I., M. Giorgio, C. Galasso, and G. Manfredi (2010). "Conditional Hazard Maps for Secondary Intensity Measures". *Bulletin of the Seismological Society of America* **100** (6), pp. 3312–3319. DOI: 10.1785/0120090383.

Iervolino, I., G. Manfredi, and E. Cosenza (2006). "Ground motion duration effects on nonlinear seismic response". *Earthquake Engineering & Structural Dynamics* **35** (1), pp. 21–38. DOI: 10.1002/eqe.529.

Jalayer, F. (2003). "Direct probabilistic seismic analysis: Implementing non-linear dynamic assessments". PhD thesis. Stanford, CA: Stanford University.

Jalayer, F. and H. Ebrahimian (2016). "Seismic risk assessment considering cumulative damage due to aftershocks". *Earthquake Engineering & Structural Dynamics*. DOI: 10.1002/eqe.2792. In press.

James, G., D. Witten, T. Hastie, and R. J. Tibshirani (2013). *An Introduction to Statistical Learning: with Applications in R*. Vol. 103. Springer Texts in Statistics. New York, NY: Springer. DOI: 10.1007/978-1-4614-7138-7.

Jayaram, N. and J. W. Baker (2008). "Statistical Tests of the Joint Distribution of Spectral Acceleration Values". *Bulletin of the Seismological Society of America* **98** (5), pp. 2231–2243. DOI: 10.1785/0120070208.

Jayaram, N., J. W. Baker, H. Okano, H. Ishida, M. W. McCann Jr., and Y. Mihara (2011a). "Correlation of response spectral values in Japanese ground motions". *Earthquakes and Structures* **2** (4), pp. 357–376. DOI: 10.12989/eas.2011.2.4.357.

Jayaram, N., T. Lin, and J. W. Baker (2011b). "A Computationally efficient ground-motion selection algorithm for matching a target response spectrum mean and variance". *Earthquake Spectra* **27** (3), pp. 797–815. DOI: 10.1193/1.3608002.

Jennings, P. C., G. W. Housner, D. E. Hudson, M. D. Trifunac, G. A. Frazier, J. H. Wood, R. F. Scott, W. D. Iwan, and A. G. Brady (1971). *Engineering features of the San Fernando earthquake of February 9, 1971*. Tech. rep. EERL 71-02. Pasadena, CA: California Institute of Technology.

Jennings, P. C., G. W. Housner, and N. C. Tsai (1968). *Simulated earthquake motions*. Tech. rep. Pasadena, CA: California Institute of Technology.

Jeon, J.-S., R. DesRoches, L. N. Lowes, and I. Brilakis (2015). "Framework of aftershock fragility assessment-case studies: older California reinforced concrete building frames". *Earthquake Engineering & Structural Dynamics* **44** (15), pp. 2617–2636. DOI: 10.1002/eqe.2599.

Jeong, G. D. and W. D. Iwan (1988). "The effect of earthquake duration on the damage of structures". *Earthquake Engineering & Structural Dynamics* **16** (8), pp. 1201–1211. DOI: 10.1002/eqe.4290160808.

Katsanos, E. I., A. G. Sextos, and G. D. Manolis (2010). "Selection of earthquake ground motion records: A state-of-the-art review from a structural engineering perspective". *Soil Dynamics and Earthquake Engineering* **30** (4), pp. 157–169. DOI: 10.1016/j.soildyn.2009.10.005.

Kawase, H. and K. Aki (1989). "A study on the response of a soft basin for incident S, P, and Rayleigh waves with special reference to the long duration observed in Mexico City". *Bulletin of the Seismological Society of America* **79** (5), pp. 1361–1382.

Kawashima, K. and K. Aizawa (1986). "Earthquake response spectra taking account of number of response cycles". *Earthquake Engineering & Structural Dynamics* **14** (2), pp. 185–197. DOI: 10.1002/eqe.4290140203.

— (1989). "Bracketed and normalized durations of earthquake ground acceleration". *Earthquake Engineering & Structural Dynamics* **18** (7), pp. 1041–1051. DOI: 10.1002/eqe.4290180709.

Kayen, R. E. and J. K. Mitchell (1997). "Assessment of Liquefaction Potential during Earthquakes by Arias Intensity". *Journal of Geotechnical and Geoenvironmental Engineering* **123** (12), pp. 1162–1174. DOI: 10.1061/(ASCE)1090-0241(1997)123:12(1162).

Kazantzi, A. K. and D. Vamvatsikos (2015). "Intensity measure selection for vulnerability studies of building classes". *Earthquake Engineering and Structural Dynamics* **44** (15), pp. 2677–2694. DOI: 10.1002/eqe.2603.

Kempton, J. J. and J. P. Stewart (2006). "Prediction Equations for Significant Duration of Earthquake Ground Motions Considering Site and Near-Source Effects". *Earthquake Spectra* **22** (4), pp. 985–1013. DOI: 10.1193/1.2358175.

Kennedy, R. P., S. A. Short, K. L. Merz, F. J. Tokarz, I. M. Idriss, M. S. Power, and K. Sadigh (1984). *Engineering Characterization of Ground Motions, Task 1: Effects of Characteristics of Free-Field Motion on Structural Response*. Tech. rep. NUREG/CR-3805. Washington, D.C.: US Nuclear Regulatory Commission. DOI: 10.2172/6848574.

Kohrangi, M., P. Bazzurro, and D. Vamvatsikos (2016). "Vector and Scalar IMs in Structural Response Estimation, Part I: Hazard Analysis". *Earthquake Spectra* **32** (3), pp. 1507–1524. DOI: 10.1193/053115EQS080M.

Kolozvari, K., K. Orakcal, and J. Wallace (2015). *Shear-Flexure Interaction Modeling for Reinforced Concrete Structural Walls and Columns under Reversed Cyclic*

Loading. Tech. rep. PEER 2015/12. Berkeley, CA: Pacific Earthquake Engineering Research Center.

Kramer, S. L. (1996). *Geotechnical earthquake engineering*. Prentice-Hall Series in Civil Engineering and Engineering Mechanics. Upper Saddle River, NJ: Prentice Hall.

Kramer, S. L. and R. A. Mitchell (2006). "Ground Motion Intensity Measures for Liquefaction Hazard Evaluation". *Earthquake Spectra* **22** (2), pp. 413–438. DOI: 10.1193/1.2194970.

Krawinkler, H. (1997). "Impact of duration/energy in design". *FHWA/NCEER Workshop on the National Representation of Seismic Ground Motion for New and Existing Highway Facilities*. Burlingame, CA: National Center for Earthquake Engineering Research, pp. 115–123.

— (2009). "Loading Histories for Cyclic Tests in Support of Performance Assessment of Structural Components". *3rd International Conference on Advances in Experimental Structural Engineering*. San Francisco, CA.

Krawinkler, H., R. A. Medina, and B. Alavi (2003). "Seismic drift and ductility demands and their dependence on ground motions". *Engineering Structures* **25** (5), pp. 637–653. DOI: 10.1016/S0141-0296(02)00174-8.

Krawinkler, H., F. Parisi, L. F. Ibarra, A. Ayoub, and R. Medina (2001). *Development of a testing protocol for woodframe structures*. Tech. rep. CUREE Publication No. W-02. Richmond, CA: Consortium of Universities for Research in Earthquake Engineering.

Krawinkler, H. and M. Zohrei (1983). "Cumulative damage in steel structures subjected to earthquake ground motions". *Computers & Structures* **16** (1-4), pp. 531–541. DOI: 10.1016/0045-7949(83)90193-1.

Kulkarni, R. B., R. R. Youngs, and K. J. Coppersmith (1984). "Assessment of confidence intervals for results of seismic hazard analysis". *8th World Conference on Earthquake Engineering*. Vol. 1. San Francisco, CA, pp. 263–270.

Kunnath, S. K. and Y. H. Chai (2004). "Cumulative damage-based inelastic cyclic demand spectrum". *Earthquake Engineering & Structural Dynamics* **33** (4), pp. 499–520. DOI: 10.1002/eqe.363.

Kutner, M. H., C. J. Nachtsheim, J. Neter, and W. Li (2005). *Applied Linear Statistical Models*. 5th ed. New York, NY: McGraw-Hill/Irwin.

Kwong, N. S., A. K. Chopra, and R. K. McGuire (2015). "Evaluation of ground motion selection and modification procedures using synthetic ground motions". *Earthquake Engineering & Structural Dynamics* **44** (11), pp. 1841–1861. DOI: 10.1002/eqe.2558.

LATBSDC (2014). *An Alternative Procedure for Seismic Analysis and Design of Tall Buildings Located in the Los Angeles Region*. Tech. rep. Los Angeles, CA: Los Angeles Tall Buildings Structural Design Council.

Lawver, D., R. Daddazio, D. Vaughan, M. Stanley, and H. Levine (2003). "Response of AISC Steel Column Sections to Blast Loading". *ASME Pressure Vessels and Piping Conference*. Cleveland, OH: American Society of Mechanical Engineers, pp. 139–148. DOI: 10.1115/PVP2003-1827.

Lee, J. and R. A. Green (2014). "An empirical significant duration relationship for stable continental regions". *Bulletin of Earthquake Engineering* **12** (1), pp. 217–235. DOI: 10.1007/s10518-013-9570-0.

Lee, S. and S. C. Goel (1987). *Seismic behaviour of hollow and concrete-filled square tubular bracing members*. Tech. rep. UMCE 87-11. Ann Arbor, MI: University of Michigan.

Liang, X., K. M. Mosalam, and S. Günay (2016). "Direct Integration Algorithms for Efficient Nonlinear Seismic Response of Reinforced Concrete Highway Bridges". *Journal of Bridge Engineering* **21** (7), p. 04016041. DOI: 10.1061/(ASCE)BE.1943-5592.0000895.

Liel, A. B., C. B. Haselton, and G. G. Deierlein (2011). "Seismic Collapse Safety of Reinforced Concrete Buildings. II: Comparative Assessment of Nonductile and Ductile Moment Frames". *Journal of Structural Engineering* **137** (4), pp. 492–502. DOI: 10.1061/(ASCE)ST.1943-541X.0000275.

Liel, A. B., N. Luco, M. Raghunandan, and C. P. Champion (2015). "Modifications to Risk-Targeted Seismic Design Maps for Subduction and Near-Fault Hazards". *12th International Conference on Applications of Statistics and Probability in Civil Engineering*. Vancouver, Canada.

Lignos, D. G., Y. Chung, T. Nagae, and M. Nakashima (2011). "Numerical and experimental evaluation of seismic capacity of high-rise steel buildings subjected to long duration earthquakes". *Computers & Structures* **89** (11-12), pp. 959–967. DOI: 10.1016/j.compstruc.2011.01.017.

Lignos, D. G. and H. Krawinkler (2011). "Deterioration Modeling of Steel Components in Support of Collapse Prediction of Steel Moment Frames under Earthquake Loading". *Journal of Structural Engineering* **137** (11), pp. 1291–1302. DOI: 10.1061/(ASCE)ST.1943-541X.0000376.

— (2012). *Sidesway collapse of deteriorating structural systems under seismic excitations*. Tech. rep. 177. Stanford, CA: John A. Blume Earthquake Engineering Research Center, Stanford University.

Lin, L., N. Naumoski, M. Saatcioglu, and S. Foo (2010). "Effects of Strong-Motion Duration on the Response of Reinforced Concrete Frame Buildings". *9th US National and 10th Canadian Conference on Earthquake Engineering*. Toronto, Canada.

Lin, T., S. C. Harmsen, J. W. Baker, and N. Luco (2013a). "Conditional Spectrum Computation Incorporating Multiple Causal Earthquakes and Ground-Motion Prediction Models". *Bulletin of the Seismological Society of America* **103** (2A), pp. 1103–1116. DOI: 10.1785/0120110293.

Lin, T., C. B. Haselton, and J. W. Baker (2013b). "Conditional spectrum-based ground motion selection. Part I: Hazard consistency for risk-based assessments". *Earthquake Engineering & Structural Dynamics* **42** (12), pp. 1847–1865. DOI: 10.1002/eqe.2301.

Lindt, J. W. van de and G.-H. Goh (2004). "Effect of earthquake duration on structural reliability". *Engineering Structures* **26** (11), pp. 1585–1597. DOI: 10.1016/j.engstruct.2004.05.017.

Luco, N. and C. A. Cornell (2007). "Structure-Specific Scalar Intensity Measures for Near-Source and Ordinary Earthquake Ground Motions". *Earthquake Spectra* **23** (2), pp. 357–392. DOI: 10.1193/1.2723158.

Luco, N., B. R. Ellingwood, R. O. Hamburger, J. D. Hooper, J. K. Kimball, and C. A. Kircher (2007). "Risk-Targeted versus Current Seismic Design Maps for the

Conterminous United States". *Structural Engineering Association of California 2007 Convention Proceedings*. Squaw Creek, California.

Mahin, S. A. (1980). "Effects of duration and aftershocks on inelastic design earthquakes". *7th World Conference on Earthquake Engineering*. Istanbul, Turkey, pp. 677–680.

Mahin, S. A. and P.-S. B. Shing (1985). "Pseudodynamic Method for Seismic Testing". *Journal of Structural Engineering* **111** (7), pp. 1482–1503. DOI: 10.1061/(ASCE)0733-9445(1985)111:7(1482).

Malhotra, P. K. (2002). "Cyclic-demand spectrum". *Earthquake Engineering & Structural Dynamics* **31** (7), pp. 1441–1457. DOI: 10.1002/eqe.171.

Mandal, T. K., S. Ghosh, and A. S. Pisharady (2012). "Seismic Fragility Analysis of a Primary Containment Structure Using IDA". *International Symposium on Engineering under Uncertainty: Safety Assessment and Management (ISEUSAM)*. Ed. by S. Chakraborty and G. Bhattacharya. Vol. 1. Kolkata, India: Springer India, pp. 371–383. DOI: 10.1007/978-81-322-0757-3_21.

Mander, J. B., F. D. Panthaki, and A. Kasalanati (1994). "Low-Cycle Fatigue Behavior of Reinforcing Steel". *Journal of Materials in Civil Engineering* **6** (4), pp. 453–468. DOI: 10.1061/(ASCE)0899-1561(1994)6:4(453).

Manfredi, G. (2001). "Evaluation of seismic energy demand". *Earthquake Engineering & Structural Dynamics* **30** (4), pp. 485–499. DOI: 10.1002/eqe.17.

Manson, S. S. (1953). *Behavior of materials under conditions of thermal stress*. Tech. rep. NACA TN 2933. Washington, D.C.: National Advisory Committee for Aeronautics.

Mantawy, A. and J. Anderson (2015). "Assessment of Low-Cycle Fatigue Damage in R.C. Frame Buildings Under Long-Duration Earthquakes". *SECED 2015 Conference: Earthquake Risk and Engineering towards a Resilient World*. Cambridge, UK.

Marafi, N. A., J. W. Berman, and M. O. Eberhard (2016). "Ductility-dependent intensity measure that accounts for ground-motion spectral shape and duration". *Earthquake Engineering & Structural Dynamics* **45** (4), pp. 653–672. DOI: 10.1002/eqe.2678.

Marafi, N. A., M. O. Eberhard, and J. W. Berman (2017). "Effects of the Yufutsu basin on structural response during subduction earthquakes". *16th World Conference on Earthquake Engineering*. Santiago, Chile.

McCann Jr., M. W. and H. C. Shah (1979). "Determining strong-motion duration of earthquakes". *Bulletin of the Seismological Society of America* **69** (4), pp. 1253–1265.

McGuire, R. K. (1995). "Probabilistic seismic hazard analysis and design earthquakes: Closing the loop". *Bulletin of the Seismological Society of America* **85** (5), pp. 1275–1284.

— (2004). *Seismic hazard and risk analysis*. Oakland, CA: Earthquake Engineering Research Institute.

McGuire, R. K. and T. P. Barnhard (1979). "The usefulness of ground motion duration in prediction of severity of seismic shaking". *2nd US National Conference on Earthquake Engineering*. Stanford, CA.

McGuire, W., R. H. Gallagher, and R. D. Ziemian (2000). *Matrix Structural Analysis*. 2nd ed. New York, NY: John Wiley & Sons.

McKenna, F., G. L. Fenves, and M. H. Scott (2006). *OpenSees: Open system for earthquake engineering simulation*. Berkeley, CA. URL: http://opensees.berkeley.edu (visited on 2016-07-26).

McNamara, J. F. (1974). "Solution Schemes for Problems of Nonlinear Structural Dynamics". *Journal of Pressure Vessel Technology* **96** (2), p. 96. DOI: 10.1115/1.3454158.

Mehanny, S. S. F. (2009). "A broad-range power-law form scalar-based seismic intensity measure". *Engineering Structures* **31** (7), pp. 1354–1368. DOI: 10.1016/j.engstruct.2009.02.003.

Melchers, R. E. (1999). *Structural reliability analysis and prediction*. 2nd ed. Chichester, England: John Wiley & Sons.

Mikkola, M. J., M. Tuomala, and H. Sinisalo (1981). "Comparison of numerical integration methods in the analysis of impulsively loaded elasto-plastic and viscoplastic structures". *Computers & Structures* **14** (5-6), pp. 469–478. DOI: 10.1016/0045-7949(81)90067-5.

Miner, M. A. (1945). "Cumulative damage in fatigue". *Journal of applied mechanics* **12** (3), pp. 159–164.

Moehle, J. P. and G. G. Deierlein (2004). "A Framework Methodology for Performance-Based Earthquake Engineering". *13th World Conference on Earthquake Engineering*. Vancouver, Canada.

Mohammed, M. S., D. Sanders, and I. Buckle (2015). "Shake Table Tests of Reinforced Concrete Bridge Columns Under Long Duration Ground Motions". *6th International Conference on Advances in Experimental Structural Engineering and 11th International Workshop on Advanced Smart Materials and Smart Structures Technology*. Urbana-Champaign, IL.

Montejo, L. A. and M. J. Kowalsky (2008). "Estimation of Frequency-Dependent Strong Motion Duration Via Wavelets and Its Influence on Nonlinear Seismic Response". *Computer-Aided Civil and Infrastructure Engineering* **23** (4), pp. 253–264. DOI: 10.1111/j.1467-8667.2007.00534.x.

Naeim, F. and M. Lew (1995). "On the Use of Design Spectrum Compatible Time Histories". *Earthquake Spectra* **11** (1), pp. 111–127. DOI: 10.1193/1.1585805.

Newmark, N. M. (1959). "A Method of Computation for Structural Dynamics". *Journal of the Engineering Mechanics Division, Proceedings of the American Society of Civil Engineers* **85** (EM3), pp. 67–94.

NHERI (2016). *Natural Hazards Engineering Research Infrastructure: DesignSafe-CI*. URL: https://www.designsafe-ci.org/ (visited on 2016-07-26).

Nicknam, A., A. Yazdani, and K. Saeedi (2010). "Earthquake duration effect on the nonlinear response of MDOF system using a new version of Incremental Dynamic Analysis (IDA)". *5th National Congress on Civil Engineering*. Mashhad, Iran.

NIST (2010). *Evaluation of the FEMA P-695 Methodology for Quantification of Building Seismic Performance Factors*. Tech. rep. NIST GCR 10-917-8. Gaithersburg, MD: National Institute of Standards and Technology.

— (2011). *Selecting and Scaling Earthquake Ground Motions for Performing Response-History Analyses*. Tech. rep. NIST GCR 11-917-15. Gaithersburg, MD: National Institute of Standards and Technology.

Noor, A. K. and J. J. Lambiotte (1979). "Finite element dynamic analysis on CDC STAR-100 computer". *Computers & Structures* **10** (1-2), pp. 7–19. DOI: 10.1016/0045-7949(79)90068-3.

Novikova, E. I. and M. D. Trifunac (1994). "Duration of strong ground motion in terms of earthquake magnitude, epicentral distance, site conditions and site geometry". *Earthquake Engineering & Structural Dynamics* **23** (9), pp. 1023–1043. DOI: 10.1002/eqe.4290230907.

Olsen, K. B., W. J. Stephenson, and A. Geisselmeyer (2008). "3D crustal structure and long-period ground motions from a M9.0 megathrust earthquake in the Pacific Northwest region". *Journal of Seismology* **12** (2), pp. 145–159. DOI: 10.1007/s10950-007-9082-y.

Ou, Y.-C., J. Song, P.-H. Wang, L. Adidharma, K.-C. Chang, and G. C. Lee (2014). "Ground Motion Duration Effects on Hysteretic Behavior of Reinforced Concrete Bridge Columns". *Journal of Structural Engineering* **140** (3), p. 04013065. DOI: 10.1061/(ASCE)ST.1943-541X.0000856.

Oyarzo-Vera, C. and N. Chouw (2008). "Effect of earthquake duration and sequences of ground motions on structural responses". *10th International Symposium on Structural Engineering for Young Experts*. Changsha, China.

Pacheco, P. (2011). *An Introduction to Parallel Programming*. Burlington, MA: Morgan Kaufmann.

Page, R. A., D. M. Boore, W. B. Joyner, and H. W. Coulter (1972). *Ground Motion Values for Use in the Seismic Design of the Trans-Alaska Pipeline System*. Tech. rep. 672. Washington, D.C.: United States Geological Survey.

Park, K. C. (1975). *Evaluating time integration methods for nonlinear dynamics analysis*. Ed. by T. Belytschko, J. R. Osias, and P. V. Marcal. New York, NY: ASME Applied Mechanics Symposia Series (AMD-14), pp. 35–58.

Park, Y. and A. H. S. Ang (1985). "Mechanistic Seismic Damage Model for Reinforced Concrete". *Journal of Structural Engineering* **111** (4), pp. 722–739. DOI: 10.1061/(ASCE)0733-9445(1985)111:4(722).

PEER (2010a). *Concrete Column Blind Prediction Contest*. Berkeley, CA. URL: http://nisee2.berkeley.edu/peer/prediction_contest/ (visited on 2016-02-04).

PEER (2010b). *Modeling and acceptance criteria for seismic design and analysis of tall buildings*. Tech. rep. PEER/ATC-72-1. Berkeley, CA: Pacific Earthquake Engineering Research Center.

— (2015). *NGA-East: Median Ground-Motion Models for the Central and Eastern North America Region*. Tech. rep. PEER 2015/04. Berkeley, CA: Pacific Earthquake Engineering Research Center.

PEER TBI (2010). *Guidelines for Performance-Based Seismic Design of Tall Buildings*. Tech. rep. PEER 2010/05. Berkeley, CA: Pacific Earthquake Engineering Research Center.

Peng, M.-H., F. E. Elghadamsi, and B. Mohraz (1989). "A simplified procedure for constructing probabilistic response spectra". *Earthquake Spectra* **5** (2), pp. 393–408.

Petersen, M. D., A. D. Frankel, S. C. Harmsen, C. S. Mueller, K. M. Haller, R. L. Wheeler, R. L. Wesson, Y. Zeng, O. S. Boyd, D. M. Perkins, N. Luco, E. H. Field, C. J. WIlls, and K. S. Rukstales (2008). *Documentation for the 2008 Update of the United States National Seismic Hazard Maps*. Tech. rep. Open-File Report 2008-1128. Reston, VA: United States Geological Survey.

Petersen, M. D., M. P. Moschetti, P. M. Powers, C. S. Mueller, K. M. Haller, A. D. Frankel, Y. Zeng, S. Rezaeian, S. C. Harmsen, O. S. Boyd, N. Field, R. Chen, K. S. Rukstales, N. Luco, R. L. Wheeler, R. A. Williams, and A. H. Olsen (2014). *Documentation for the 2014 Update of the United States National Seismic Hazard Maps*. Tech. rep. Open-File Report 2014-1091. Reston, VA: United States Geological Survey. DOI: 10.3133/ofr20141091.

Pitarka, A. (2004). "Validation of a 3D Velocity Model of the Puget Sound Region Based on Modeling Ground Motion from the 28 February 2001 Nisqually Earthquake". *Bulletin of the Seismological Society of America* **94** (5), pp. 1670–1689. DOI: 10.1785/012003177.

Press, W. H., S. A. Teukolsky, W. T. Vetterling, and B. P. Flannery (2007). *Numerical Recipes: The Art of Scientific Computing*. 3rd ed. Cambridge, UK: Cambridge University Press.

Raghunandan, M. (2013). "Influence of long duration ground shaking on collapse of reinforced concrete structures". PhD thesis. Boulder, CO: University of Colorado.

Raghunandan, M. and A. B. Liel (2013). "Effect of ground motion duration on earthquake-induced structural collapse". *Structural Safety* **41**, pp. 119–133. DOI: 10.1016/j.strusafe.2012.12.002.

Raghunandan, M., A. B. Liel, and N. Luco (2014). "Aftershock collapse vulnerability assessment of reinforced concrete frame structures". *Earthquake Engineering & Structural Dynamics* **44** (3), pp. 419–439. DOI: 10.1002/eqe.2478.

— (2015). "Collapse Risk of Buildings in the Pacific Northwest Region due to Subduction Earthquakes". *Earthquake Spectra* **31** (4), pp. 2087–2115. DOI: 10.1193/012114EQS011M.

Rahnama, M. and L. Manuel (1996). "The effect of strong motion duration on seismic demands". *11th World Conference on Earthquake Engineering*. Acapulco, Mexico.

Rauch, A. F. and J. R. Martin II (2000). "EPOLLS Model for Predicting Average Displacements on Lateral Spreads". *Journal of Geotechnical and Geoenvironmental Engineering* **126** (4), pp. 360–371. DOI: 10.1061/(ASCE)1090-0241(2000)126:4(360).

Reinoso, E. and M. Ordaz (2001). "Duration of strong ground motion during Mexican earthquakes in terms of magnitude, distance to the rupture area and dominant site period". *Earthquake Engineering & Structural Dynamics* **30** (5), pp. 653–673. DOI: 10.1002/eqe.28.

Reinoso, E., M. Ordaz, and R. Guerrero (2000). "Influence of strong ground-motion duration in seismic design of structures". *12th World Conference on Earthquake Engineering*. Auckland, New Zealand.

Reiter, L. (1990). *Earthquake Hazard Analysis: Issues and Insights*. New York, NY: Columbia University Press.

Rezaeian, S., P. Zhong, S. Hartzell, and F. Zareian (2015). "Validation of Simulated Earthquake Ground Motions Based on Evolution of Intensity and Frequency Content". *Bulletin of the Seismological Society of America* **105** (6), pp. 3036–3049. DOI: 10.1785/0120140210.

Rice, J. A. (2006). *Mathematical Statistics and Data Analysis*. Boston, MA: Cengage Learning.

Romney, K. T., A. R. Barbosa, and H. B. Mason (2014). "Developing a Soil Bridge-Interaction Model for Studying the Effects of Long-Duration Earthquake Motions". *10th U.S. National Conference on Earthquake Engineering*. Anchorage, AK.

Ruiz-García, J. and E. Miranda (2005). *Performance-Based Assessment of Existing Structures Accounting for Residual Displacements*. Tech. rep. 153. Stanford, CA: John A. Blume Earthquake Engineering Research Center.

SAC (1997). *Protocol for Fabrication, Inspection, Testing, and Documentation of Beam-Column Connection Tests and Other Experimental Specimens*. Tech. rep. SAC/BD-97/02. Sacramento, CA: SAC Joint Venture.

Sánchez-Carratalá, C. R. and I. Ferrer (2004). "Equivalent earthquake duration from amplitude modulation functions". *13th World Conference on Earthquake Engineering*. Vancouver, Canada.

Saragoni, G. R. (1977). "The $\alpha\beta\gamma$ Method for the Characterization of Earthquake Accelerograms". *6th World Conference on Earthquake Engineering*. New Delhi, India, pp. 357–364.

Sarieddine, M. and L. Lin (2013). "Investigation Correlations between Strong-motion Duration and Structural Damage". *Structures Congress 2013*. Reston, VA: American Society of Civil Engineers, pp. 2926–2936. DOI: 10.1061/9780784412848.255.

Satake, K., K. Wang, and B. F. Atwater (2003). "Fault slip and seismic moment of the 1700 Cascadia earthquake inferred from Japanese tsunami descriptions". *Journal of Geophysical Research* **108** (B11), p. 2535. DOI: 10.1029/2003JB002521.

Seed, H. B. and I. M. Idriss (1982). *Ground motions and soil liquefaction during earthquakes*. Berkeley, CA: Earthquake Engineering Research Institute.

Sewell, R. T. (1992). "Effects of duration on structural response factors and on ground-motion damageability". *SMIP92 Seminar on Seismological and Engineering Implications of Recent Strong-Motion Data*. Sacramento, CA, pp. 7.1–7.15.

Sewell, R. T., G. R. Toro, and R. K. McGuire (1996). *Impact of Ground Motion Characterization on Conservatism and Variability in Seismic Risk Estimates*. Tech. rep.

No. NUREG/CR–6467. Washington, D.C.: US Nuclear Regulatory Commission. DOI: 10.2172/285473.

Shome, N., C. A. Cornell, P. Bazzurro, and J. E. Carballo (1998). "Earthquakes, Records, and Nonlinear Responses". *Earthquake Spectra* **14** (3), pp. 469–500. DOI: 10.1193/1.1586011.

Sideras, S. S. and S. L. Kramer (2012). "Potential Implications of Long Duration Ground Motions on the Response of Liquefiable Soil Deposits". *9th International Conference on Urban Earthquake Engineering / 4th Asia Conference on Earthquake Engineering*. Tokyo, Japan.

Singh, S. K., M. Ordaz, J. F. Pacheco, R. Quaas, L. Alcantara, S. Alcocer, C. Gutierrez, R. Meli, and E. Ovando (1999). "A Preliminary Report on the Tehuacan, Mexico Earthquake of June 15, 1999 (Mw = 7.0)". *Seismological Research Letters* **70** (5), pp. 489–504. DOI: 10.1785/gssrl.70.5.489.

Skarlatoudis, A. A., P. G. Somerville, H. K. Thio, and J. R. Bayless (2015). "Broadband Strong Ground Motion Simulations of Large Subduction Earthquakes". *Bulletin of the Seismological Society of America* **105** (6), pp. 3050–3067. DOI: 10.1785/0120140322.

Somerville, P. G., K. Irikura, R. W. Graves, S. Sawada, D. J. Wald, N. A. Abrahamson, Y. Iwasaki, T. Kagawa, N. F. Smith, and A. Kowada (1999). "Characterizing Crustal Earthquake Slip Models for the Prediction of Strong Ground Motion". *Seismological Research Letters* **70** (1), pp. 59–80. DOI: 10.1785/gssrl.70.1.59.

Somerville, P. G., N. F. Smith, R. W. Graves, and N. A. Abrahamson (1997). "Modification of Empirical Strong Ground Motion Attenuation Relations to Include the Amplitude and Duration Effects of Rupture Directivity". *Seismological Research Letters* **68** (1), pp. 199–222. DOI: 10.1785/gssrl.68.1.199.

Sotelino, E. D. (2003). "Parallel Processing Techniques in Structural Engineering Applications". *Journal of Structural Engineering* **129** (12), pp. 1698–1706. DOI: 10.1061/(ASCE)0733-9445(2003)129:12(1698).

Spacone, E., F. C. Filippou, and F. F. Taucer (1996). "Fibre Beam-Column Model for Non-linear Analysis of R/C Frames: Part 1. Formulation". *Earthquake Engineering & Structural Dynamics* **25** (7), pp. 711–725. DOI: 10.1002/(SICI)1096-9845(199607)25:7<711::AID-EQE576>3.0.CO;2-9.

Stein, S. and M. Wysession (2003). *An Introduction to Seismology, Earthquakes, and Earth Structure*. Oxford, UK: Blackwell Publishing Ltd.

Sucuoğlu, H. and A. Nurtuğ (1995). "Earthquake ground motion characteristics and seismic energy dissipation". *Earthquake Engineering & Structural Dynamics* **24** (9), pp. 1195–1213. DOI: 10.1002/eqe.4290240903.

Taflampas, I. M., C. C. Spyrakos, and I. A. Koutromanos (2009). "A new definition of strong motion duration and related parameters affecting the response of medium–long period structures". *Soil Dynamics and Earthquake Engineering* **29** (4), pp. 752–763. DOI: 10.1016/j.soildyn.2008.08.005.

Takanashi, K. and M. Nakashima (1987). "Japanese Activities on On-Line Testing". *Journal of Engineering Mechanics* **113** (7), pp. 1014–1032. DOI: 10.1061/(ASCE)0733-9399(1987)113:7(1014).

Takemura, H. and K. Kawashima (1997). "Effect of loading hysteresis on ductility capacity of reinforced concrete bridge piers". *Journal of Structural Engineering* **43**, pp. 849–858.

Takizawa, H. and P. C. Jennings (1980). "Collapse of a model for ductile reinforced concrete frames under extreme earthquake motions". *Earthquake Engineering & Structural Dynamics* **8** (2), pp. 117–144. DOI: 10.1002/eqe.4290080204.

Tarbali, K. and B. A. Bradley (2016). "The effect of causal parameter bounds in PSHA-based ground motion selection". *Earthquake Engineering & Structural Dynamics* **45** (9), pp. 1515–1535. DOI: 10.1002/eqe.2721.

Teran-Gilmore, A. and R. Simon-Velazquez (2008). "Use of Cumulative Ductility Spectra Within a Deformation-Control Format for Seismic Design of Ductile Structures Subjected to Long Duration Motions". *Journal of Earthquake Engineering* **12** (1), pp. 136–151. DOI: 10.1080/13632460701364460.

Tesfamariam, S. and K. Goda (2015). "Loss estimation for non-ductile reinforced concrete building in Victoria, British Columbia, Canada: effects of mega-thrust

M w 9-class subduction earthquakes and aftershocks". *Earthquake Engineering & Structural Dynamics* **44** (13), pp. 2303–2320. DOI: 10.1002/eqe.2585.

Thatcher, W., G. Marshall, and M. Lisowski (1997). "Resolution of fault slip along the 470-km-long rupture of the great 1906 San Francisco earthquake and its implications". *Journal of Geophysical Research: Solid Earth* **102** (B3), pp. 5353–5367. DOI: 10.1029/96JB03486.

Tothong, P. and N. Luco (2007). "Probabilistic seismic demand analysis using advanced ground motion intensity measures". *Earthquake Engineering & Structural Dynamics* **36** (13), pp. 1837–1860. DOI: 10.1002/eqe.696.

Towns, J., T. Cockerill, M. Dahan, I. Foster, K. Gaither, A. Grimshaw, V. Hazlewood, S. Lathrop, D. Lifka, G. D. Peterson, R. Roskies, J. R. Scott, and N. Wilkens-Diehr (2014). "XSEDE: Accelerating Scientific Discovery". *Computing in Science & Engineering* **16** (5), pp. 62–74. DOI: 10.1109/MCSE.2014.80.

Travasarou, T., J. D. Bray, and A. D. Kiureghian (2004). "A probabilistic methodology for assessing seismic slope displacements". *13th World Conference on Earthquake Engineering*. Vancouver, Canada.

Tremblay, R. (1998). "Development of design spectra for long-duration ground motions from Cascadia subduction earthquakes". *Canadian Journal of Civil Engineering* **25** (6), pp. 1078–1090. DOI: 10.1139/198-028.

Trifunac, M. D. and A. G. Brady (1975). "A study on the duration of strong earthquake ground motion". *Bulletin of the Seismological Society of America* **65** (3), pp. 581–626.

Trifunac, M. D. and D. E. Hudson (1971). "Analysis of the Pacoima dam accelerogram—San Fernando, California, earthquake of 1971". *Bulletin of the Seismological Society of America* **61** (5), pp. 1393–1411.

Trifunac, M. D. and E. I. Novikova (1995). "Duration of earthquake fault motion in California". *Earthquake Engineering & Structural Dynamics* **24** (6), pp. 781–799. DOI: 10.1002/eqe.4290240602.

Trifunac, M. D. and B. D. Westermo (1977). "A note on the correlation of frequency-dependent duration of strong earthquake ground motion with the Modified Mercalli Intensity and the geologic conditions at the recording stations". *Bulletin of the Seismological Society of America* **67** (3), pp. 917–927.

Uriz, P. and S. A. Mahin (2008). *Toward Earthquake-Resistant Design of Concentrically Braced Steel-Frame Structures*. Tech. rep. PEER 2008/08. Berkeley, CA: Pacific Earthquake Engineering Research Center.

USGS (2008). *Interactive Deaggregations*. URL: http://geohazards.usgs.gov/deaggint/2008/ (visited on 2016-07-26).

Vamvatsikos, D. (2011). "Performing incremental dynamic analysis in parallel". *Computers & Structures* **89** (1-2), pp. 170–180. DOI: 10.1016/j.compstruc.2010.08.014.

— (2014). "Seismic Performance Uncertainty Estimation via IDA with Progressive Accelerogram-Wise Latin Hypercube Sampling". *Journal of Structural Engineering* **140** (8), A4014015. DOI: 10.1061/(ASCE)ST.1943-541X.0001030.

Vamvatsikos, D. and C. A. Cornell (2002). "Incremental dynamic analysis". *Earthquake Engineering & Structural Dynamics* **31** (3), pp. 491–514. DOI: 10.1002/eqe.141.

— (2004). "Applied Incremental Dynamic Analysis". *Earthquake Spectra* **20** (2), pp. 523–553. DOI: 10.1193/1.1737737.

— (2005). "Developing efficient scalar and vector intensity measures for IDA capacity estimation by incorporating elastic spectral shape information". *Earthquake Engineering & Structural Dynamics* **34** (13), pp. 1573–1600. DOI: 10.1002/eqe.496.

Vanmarcke, E. H. and S.-S. P. Lai (1980). "Strong-motion duration and RMS amplitude of earthquake records". *Bulletin of the Seismological Society of America* **70** (4), pp. 1293–1307.

Veletsos, A. S. and N. M. Newmark (1960). "Effect of inelastic behavior on the response of simple systems to earthquake motions". *2nd World Conference on Earthquake Engineering*. Tokyo and Kyoto, Japan, pp. 895–912.

Wald, D. J., H. Kanamori, D. V. Helmberger, and T. H. Heaton (1993). "Source study of the 1906 San Francisco earthquake". *Bulletin of the Seismological Society of America* **83** (4), pp. 981–1019.

Wang, G. (2011). "A ground motion selection and modification method capturing response spectrum characteristics and variability of scenario earthquakes". *Soil Dynamics and Earthquake Engineering* **31** (4), pp. 611–625. DOI: 10.1016/j.soildyn.2010.11.007.

Wang, G., Y. Wang, W. Lu, W. Zhou, and C. Zhou (2015). "Integrated duration effects on seismic performance of concrete gravity dams using linear and nonlinear evaluation methods". *Soil Dynamics and Earthquake Engineering* **79**, pp. 223–236. DOI: 10.1016/j.soildyn.2015.09.020.

Wick, M. and C. Boutreux (2016). *The GeoNames geographical database*. URL: http://www.geonames.org/ (visited on 2016-08-17).

Wilson, E. L. (1968). *A computer program for the dynamic stress analysis of underground structures*. Tech. rep. SEL-68-1. Berkeley, CA: Structural Engineering Laboratory, University of California.

Xie, L.-L. and X. Zhang (1988). "Engineering Duration of Strong Motion and its Effects on Seismic Damage". *9th World Conference on Earthquake Engineering*. Tokyo, Japan, pp. 307–312.

Xie, Y. M. (1996). "An assessment of time integration schemes for non-linear dynamic equations". *Journal of Sound and Vibration* **192** (1), pp. 321–331. DOI: 10.1006/jsvi.1996.0190.

Xu, C. and F. C. Lau (1997). *Load Balancing in Parallel Computers: Theory and Practice*. New York, NY: Springer Science & Business Media.

Youd, T. L., I. M. Idriss, R. D. Andrus, I. Arango, G. Castro, J. T. Christian, R. Dobry, W. D. L. Finn, L. F. Harder, M. E. Hynes, K. Ishihara, J. P. Koester, S. S. C. Liao, W. F. Marcuson, G. R. Martin, J. K. Mitchell, Y. Moriwaki, M. S. Power, P. K. Robertson, R. B. Seed, and K. H. Stokoe (2001). "Liquefaction Resistance of Soils: Summary Report from the 1996 NCEER and 1998 NCEER/NSF Workshops on Evaluation of Liquefaction Resistance of Soils". *Journal of Geotechnical*

and Geoenvironmental Engineering **127** (10), pp. 817–833. DOI: 10.1061/(ASCE)1090-0241(2001)127:10(817).

Zahrah, T. F. and W. J. Hall (1984). "Earthquake Energy Absorption in SDOF Structures". *Journal of Structural Engineering* **110** (8), pp. 1757–1772. DOI: 10.1061/(ASCE)0733-9445(1984)110:8(1757).

Zareian, F., D. G. Lignos, and H. Krawinkler (2010). "Evaluation of Seismic Collapse Performance of Steel Special Moment Resisting Frames Using FEMA P695 (ATC-63) Methodology". *Structures Congress 2010*. Reston, VA: American Society of Civil Engineers, pp. 1275–1286. DOI: 10.1061/41130(369)116.

Zembaty, Z. (1988). "A note on non-stationary stochastic response and strong motion duration". *Earthquake Engineering & Structural Dynamics* **16** (8), pp. 1189–1200. DOI: 10.1002/eqe.4290160807.

Zhao, J. X., J. Zhang, A. Asano, Y. Ohno, T. Oouchi, T. Takahashi, H. Ogawa, K. Irikura, H. K. Thio, P. G. Somerville, Y. Fukushima, and Y. Fukushima (2006). "Attenuation Relations of Strong Ground Motion in Japan Using Site Classification Based on Predominant Period". *Bulletin of the Seismological Society of America* **96** (3), pp. 898–913. DOI: 10.1785/0120050122.